Proceedings

# MEA Meeting 2008

**July 8–11, 2008, Reutlingen, Germany**

**6th International Meeting on Substrate-Integrated Micro Electrode Arrays**



**BIO PRO**
Baden-Württemberg GmbH

**NMI**
*Applied R & D*
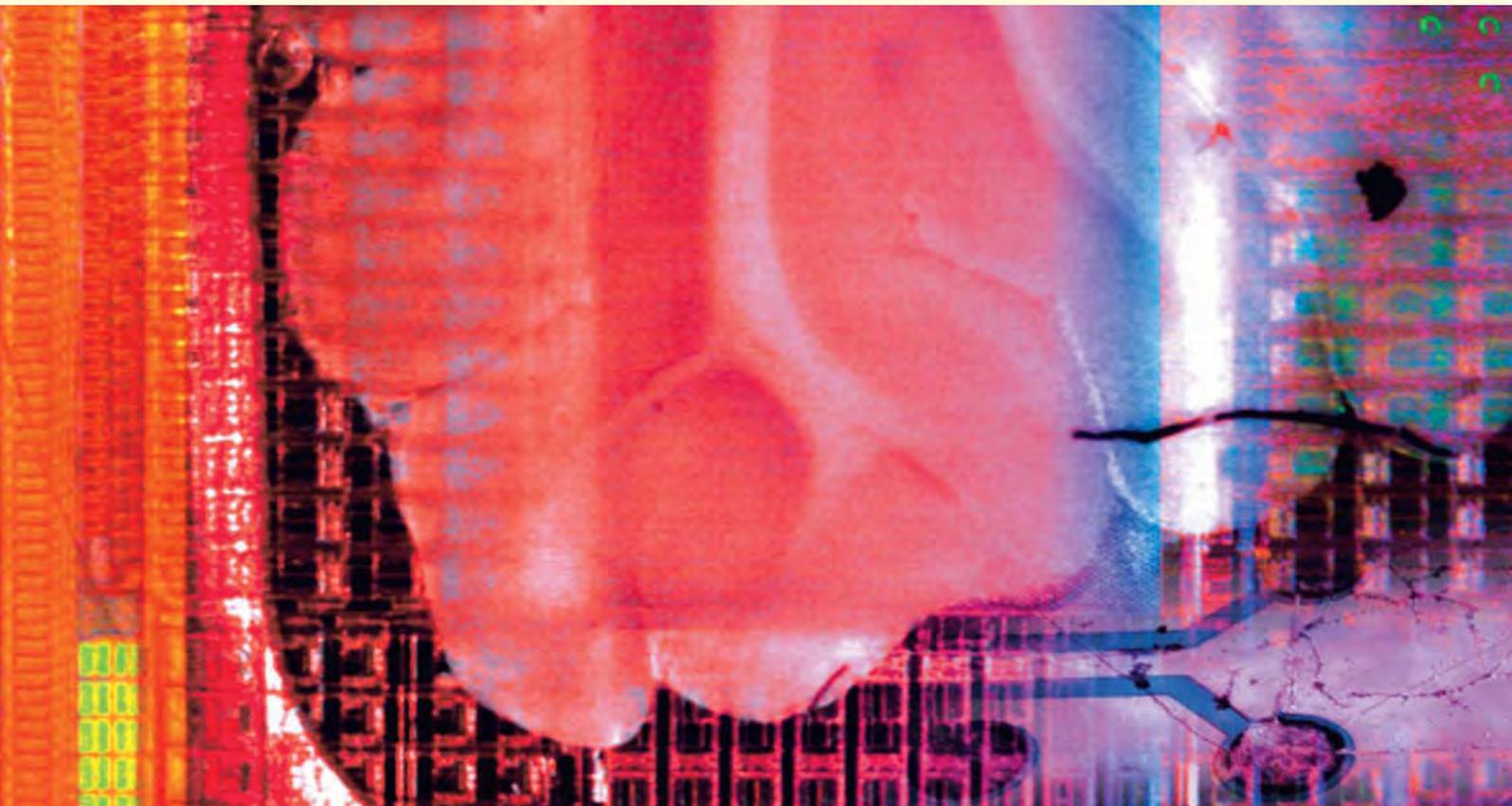
# Baden-Württemberg

## Where technology gets applied

Situated in the South-West of Germany, the state of Baden-Württemberg is home to one of the most exciting R&D infrastructures in the Life Sciences sector in Europe.

To get innovative technologies applied faster, BIOPRO works to develop novel concepts for translational research.

Baden-Württemberg

BIO PRO
Baden-Württemberg GmbH

Mannheim

Heidelberg

BioRegion
Rhein-Neckar-Dreieck

Heilbronn

Karlsruhe

BioRegio STERN

Stuttgart

Esslingen

Aalen

Offenburg

Nürtingen

Tübingen   Reutlingen

Ulm

Villingen-Schwenningen

BioRegionUlm

Furtwangen

Freiburg

Albstadt-Sigmaringen

Biberach

BioRegio
Freiburg

BIO VALLEY

BIO LAGO

Isny

Konstanz

■ **Universities***
▲ **Universities of Applied Sciences***
● **Research Institutes***
* with a focus on biotechnology

BIO PRO
Baden-Württemberg GmbH

Baden-Württemberg

Conference Proceedings of the
6th International Meeting on Substrate-Integrated Micro Electrode Arrays
July 8-11, 2008, Reutlingen, Germany

# Meeting Organisation

**Organiser**

NMI Natural and Medical Sciences Institute at the University of Tuebingen
Markwiesenstrasse 55, 72770 Reutlingen, Germany
Phone: +49 7121 - 51 530 -0 Fax: +49 7121 - 51 530 16; E-Mail: info@nmi.de
Internet: www.nmi.de

**Co-organiser**

BIOPRO Baden-Württemberg GmbH
Breitscheidstraße 10, 70174 Stuttgart, Germany
Phone: +49 711 218 185 00; Fax: +49 711 218 185 02; E-Mail: info@bio-pro.de
Internet: www.bio-pro.de

**Organisation Team**

Ira Digel, Nadja Gugeler, Priscilla Herrmann
E-Mail: meameeting@nmi.de
Internet: www.nmi.de/meameeting2008

**Scientific Programme Committee**

Prof. Ofer Binah, Faculty of Medicine, Technion, Haifa, Israel
PD Dr. Ulrich Egert, Bernstein Center for Computational Neuroscience, University of Freiburg, Germany
Prof. Lior Gepstein, Faculty of Medicine, Technion, Haifa, Israel
Prof. Elke Guenther, NMI Natural and Medical Sciences Institute, Reutlingen, Germany
Prof. Erik Herzog, Washington University, St. Louis, USA
Prof. Andreas Hierlemann, Physical Electronics Laboratory, ETH Zurich, Switzerland
Prof. Sung June Kim, Seoul National University, South Korea
Prof. Milena Koudelka-Hep, University of Neuchatel, Switzerland
Prof. Shimon Marom, Faculty of Medicine, Technion, Haifa, Israel
Dr. Thomas Meyer, Multi Channel Systems MCS GmbH, Germany
Prof. Wim L.C. Rutten, University of Twente, The Netherlands
Dr. Daniel Wagenaar, University of California, San Diego, USA
Prof. Dieter G. Weiss, University of Rostock, Germany
Prof. Bruce Wheeler, University of Illinois, Urbana, US

**Conference Chair**

Dr. Alfred Stett, NMI Natural and Medical Sciences Institute, Reutlingen, Germany

**Sponsor**

Multi Channel Systems MCS GmbH, Reutlingen, Germany (www.multichannelsystems.com)

NMI Natural and Medical Sciences Institute at the University of Tuebingen

BIOPRO Baden-Württemberg GmbH

Multi Channel Systems MCS GmbH

City of Reutlingen

# Foreword

**Substrate-Integrated Microelectrode Arrays:**
**Electrophysiological Tools for Neuroscience, Biotechnology and Biomedical Engineering**
6th International Meeting on Substrate-Integrated Microelectrode Arrays, July 8-11, 2008, Reutlingen, Germany

The response to our invitation to the sixth international meeting on substrate-integrated microelectrodes has been overwhelming: we expect about 200 participants from all over the world. About 490 authors and co-authors from 18 countries have submitted 147 contributions for oral and poster presentations.

The MEA user community has grown since our last meeting in Reutlingen in 2006. For the NMI it is again an honour to welcome many new participants and to greet the familiar faces of regular attendees. We are particularly delighted that the biannual meeting has become an established meeting place, attracting not only students but also senior researchers, MEA developers and new as well as experienced MEA users.
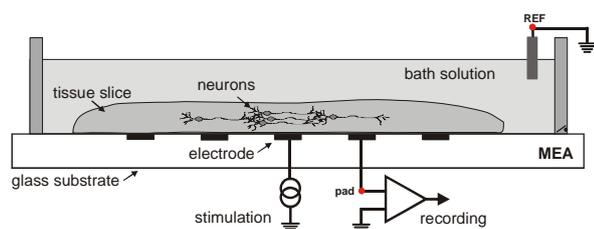


Stimulation and recording of electrical activity in tissue slices with a Microelectrode Array (MEA). The substrate-integrated electrodes can be used both for stimulation and recording.

Today's routinely-used MEAs are as simple as those introduced by Thomas et al. 36 years ago (Exp Cell Res 1972, 74:61-66). They consist of an array of extracellular electrodes that are embedded in a biocompatible glass substrate. At the NMI, it was Wilfried Nisch who began the development and fabrication of MEAs 20 years ago. Many different layouts and types of electrodes, optimized for a wide range of applications, are now manufactured by the NMI and delivered world-wide by Multi Channel Systems MCS to academic and industrial laboratories.

What is the fascination behind this tool that led to its acceptance in many fields of academic and industrial research? It is not only the development and engineering of new arrays involving thousands of electrodes or sophisticated microsystems or nanotechnology. It is rather the scientific urge to explore the fundamental physiological and pathophysiological brain functions. Cognitive functions such as associative learning, memory processes, emotions, visual perception and speech recognition depend on several neurons acting synchronically in space and time.

Moreover, pathophysiological conditions such as epilepsy, Alzheimer's disease, or other mental impairments have been shown to be associated with the disturbed function of the neuronal networks.

MEAs enable the repeated simultaneous electrical stimulation of and recording from multiple sites in cell and tissue cultures over extended periods of time, up to several months. Development, plasticity, circadian rhythms and neuronal regeneration are examples of applications that could particularly benefit from long-term monitoring of neuronal activity, as they involve processes that develop over extended periods of time.

In summary, MEAs are being used to address numerous questions in neuroscience, neurotechnology and cardiovascular research, and more than 300 publications are meanwhile available. MEAs are also increasingly being used for drug testing in the pharmaceutical industry. New fields of applications have arisen in neuronal and tissue engineering and stem cell research. On-going challenges are the long-term stable and multilocal feed-in of defined information into a distributed network (e.g. in neuroprosthetics) and the decoding and understanding of the activity of cell populations.

"A time to make friends" was the motto of the meeting in 2006 – and we, at the NMI, sincerely hope that this spirit prevails again. We welcome you heartily to Reutlingen and hope that the meeting will stimulate enthusiastic discussions, productive scientific exchange and trigger new answers to the ongoing challenges in the various fields of MEA technology and applications.

BIOPRO Baden-Württemberg GmbH, as the state agency for the promotion of modern biotechnology and the life sciences, is again supporting the publication of the results that will be presented at this year's MEA meeting. In addition BIOPRO will help to distribute these findings to companies in Baden-Württemberg in the pharmaceutical, biotechnology and medical technology industries.

Enjoy the meeting!

Alfred Stett
*Conference Chair;*
*Deputy Managing Director, NMI Reutlingen*

Dr. Ralf Kindervater
CEO, BIOPRO Baden-Württemberg GmbH

# Contents

# Signal Analysis and Data Mining................................................................ 107

**Retinal Signalling** ................................................................................................................**189**

**Pharmacology, Toxicology, Drug Screening** ........................................................................**209**

## CMOS-based array technology; Advances in culture, stimulaton and recording techniques ......................................................................................235

# Neuronal Dynamics and Plasticity

# Order-Based Representation in Networks of Cortical Neurons

Shimon Marom[1], Asaf Gal[2], Christof Zrenner[3],Vladimir Lyakhov[1], Goded Shahaf[1], Danny Eytan[1]

1 Technion - Israel Institute of Technology
2 Technion and Hebrew University, Israel
3 Tübingen University, Germany
* Corresponding author. E-mail address: pisa@web.it

## Opening Keynote Lecture

The wide range of time scales involved in neural excitability and synaptic transmission renders the temporal structure of responses to recurring stimulus presentations inherently variable on a trial-to-trial basis. This is probably the most severe biophysical constraint on putative time-based primitives of stimulus representation in neuronal networks.

Here we show that in spontaneously developing large-scale random networks of cortical neurons in-vitro, the order in which neurons are recruited following each stimulus is a naturally emerging representation primitive that is invariant to significant temporal changes in spike times. Using a small number of randomly sampled neurons, the information about stimulus position is fully retrievable from the recruitment order. The connectivity that makes order-based representation invariant to time warping is characterized by "bottlenecks" – stations through which activity is required to pass in order to propagate further into the network.

This study uncovers a simple and useful invariant in a noisy biological network.

# MEA recording as a screening tool: discovering mouse pheromones through recordings from the olfactory system

Tim Holy

Washington University School of Medicine in Saint Louis, Missouri, US
E-mail address: holy@wustl.edu

**Keynote Lecture**

Vomeronasal sensory neurons (VSNs), which detect chemical cues for social communication (pheromones), present a remarkable example of cellular diversity in the nervous system: each VSNs expresses just one receptor type, but collectively these neurons express approximately 250 different receptor types. Studying this sensory system, therefore, requires methods like multielectrode array (MEA) recording capable of observing activity in large numbers of sensory neurons simultaneously. This complexity is one of the reasons that little is known about the nature of sensory coding in this system or even the chemical identity of most mouse pheromones.

To identify the compounds that VSNs detect, we screened chromatographic fractions of female mouse urine for their ability to cause reproducible firing rate increases using MEA recording. Active compounds were found to be remarkably homogenous in their basic properties, with most being of low molecular weight, moderate hydrophobicity, low volatility, and possessing a negative electric charge. Purification and structural analysis of active compounds revealed multiple sulfated steroids, of which two were identified as sulfated glucocorticoids, including corticosterone 21-sulfate. Sulfatase-treated urine extracts lost more than 80% of their activity, indicating that sulfated compounds are the predominant VSN ligands in female mouse urine. As measured by MEA recording, a collection of 31 synthetic sulfated steroids triggered responses 30-fold more frequently than did a similarly-sized stimulus set containing the majority of all previously-reported VSN ligands.

Collectively, VSNs detected all major classes of sulfated steroids, but individual neurons were sensitive to small variations in chemical structure. VSNs from both males and females detected sulfated steroids, but knockouts for the sensory transduction channel TRPC2 did not detect these compounds. Urine concentrations of the two sulfated glucocorticoids increased many-fold in stressed animals, indicating that information about physiological status is encoded by the urine concentration of particular sulfated steroids. These results provide an unprecedented characterization of the signals available for chemical communication among mice.

# Spontaneous Cingulate Oscillation Modulated by Thalamic Inputs

Wei-Pang Chang[1], Jiaun-Shian Wu[2], Chia-Ming Lee[1], Kung-Po Chang[2] and Bai-Chuang Shyu[1*]

1 Institute of Biomedical Sciences, Academia Sinica, Taipei, Taiwan, R.O.C.
2 Institute of Zoology, National Taiwan University. Taipei, Taiwan, R.O.C.
* Corresponding author. E-mail address: bmbai@gate.sinica.edu.tw

A slice preparation preserving the functional connection between medial thalamus (MT) and anterior cingulate cortex (ACC) was developed recently from our lab. In the present study, we used potassium channel blocker, 4-aminopyridine, (4AP) and GABAA antagonist, bicuculline to induce oscillation in MT-ACC slice. The duration of oscillation is about $8.9 \pm 1.6$ s, and the amplitude of oscillation is about $121.4 \pm 11.6$ mV. Electrical stimulation in either cortex or thalamus induced cingulate oscillation in an all-or-none manner. And the duration and amplitude of oscillation evoked by thalamic stimulation were significantly lower than those evoked by cortex stimulation. To evaluate the role of thalamic inputs in oscillation, thalamic inputs were removed and the patterns of oscillation were examined. We found that oscillation was significantly augmented after removing the thalamic inputs. Gap junction blocker-carbenoxolone (CBX) was applied to investigate the role of gap junction involved in the oscillation, and found that oscillation could be block by 100 µM CBX. The neuronal network maintained in our MT-ACC slices is capable of generating spontaneous oscillation mediated by gap junction. Our results strongly suggested that the 4-AP+bicuculline induced oscillation was modulated by thalamic inputs. And the thalamic modulation of this cortical oscillation provides a useful model to further investigate the synaptic plasticity in the thalamocingulate pathway.

## 1 Thalamic inhibition of the cingulate oscillatory activities

### 1.1 Comparison of thalamic and direct cortical stimulation evoked oscillation in MT-ACC slice

Spontaneous oscillation could induce by the application of 4AP (100 µM) +bicuculline (5 µM). Duration of oscillation is about $8.9 \pm 0.6$ s, and amplitude of oscillation is about $121.4 \pm 11.6$ mV. Electrical stimulation applied in either thalamus or cingulate cortex (Fig. 1A) would invariably elicit the oscillatory activities in a fixed pattern. The amplitude of the cingulate oscillation evoked by various intensities of suprathreshold electrical stimulation in either thalamus or cortex is not significantly different. These results suggested that the electrical stimulation evoked cingulate cortical oscillation is an all-or-none event (Fig. 1B). Duration of oscillation is significantly longer in cortex evoked oscillation compared to that evoked by thalamic stimulation.
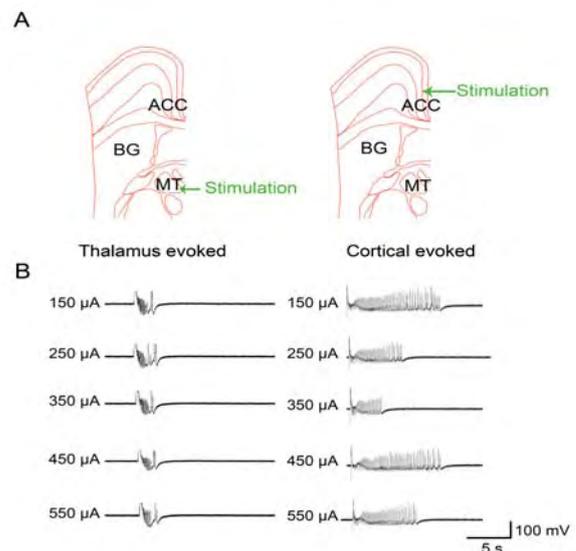


**Fig.1.** Comparison of the patterns of oscillation evoked by thalamic and direct cortical stimulation (A) Location of electrical stimulation site in thalamus and cortex. (B) Cingulate oscillation in response to thalamic and cortical stimulation. The duration of oscillation evoked by direct cortical stimulation (right panel) are significantly longer than those evoked by thalamic stimulation (left panel).

## 1.2 Thalamic modulation of the oscillation

In order to study the role of the thalamic inputs in the cingulate cortical oscillation, we performed field potential recordings from slices with intact thalamocingulate pathway and subsequent electrical recordings were performed from slices in which the thalamic inputs were removed (Fig. 2A). We compared the pattern of the oscillation with and without thalamocingulate pathway and found that the amplitude and duration of the oscillation was significantly higher after the pathway was removed (Fig. 2B). These results suggested that the overall effect of thalamic inputs in cingulate cortical oscillation is inhibitory. The distribution of the oscillation onset tended to be more dispersing without thalamic inputs.  The existence of multiple locations of the oscillation onsets when the thalamic inputs is removed indicated that there are many groups of neurons capable of generating oscillatory activities distributed in the cortex. However, when the thalamocingulate pathway is intact, Cg2 areas are highly regulated by thalamic inputs. And when the thalamus activities become silent, more neurons in the Cg2 fired in a synchronous manner to generate oscillation due to disinhibiting effect.
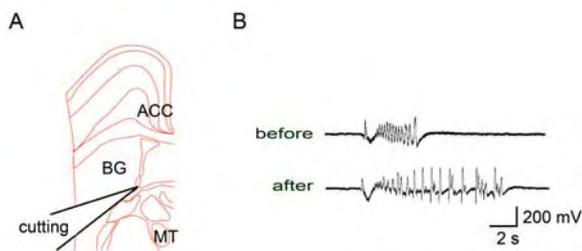


**Fig.2.** Thalamic modulation of the cingulate oscillation. (A) Thalamocingulate pathway was removed by a slight cut between the boundaries of basal ganglia and thalamus. (B) The duration and amplitude of cingulate oscillation were singificnatly higher after removing thalamic inputs.

## 2 Involvement of gap junction in cingulate oscillatory activities

### 2.1 The role of gap junction in the synchronization of the oscillation

The coherence of the oscillatory activities within GABAergic networks is thought to be mediated by the intercellular communication afforded by gap junctions, electrotonic transmission via gap junctions leading to a predisposition for synchronized firing be-

tween coupled cells. To investigate whether gap junctions are involved in the generation of cingulate cortical oscillation, a gap junction blocker, carbenoxolone (CBX) were added in the aCSF in the presence of 4-AP and bicuculline. Application of 50 µM CBX lower the amplitude and duration of the oscillatory activities, subsequent application of 100 µM CBX further lower the amplitude. Spiralnolactone (SPL, a mineralcorticoid receptor agonist) application did not restore the oscillatory activities indicated that CBX exert its effect via gap junction, but not through mineralcorticoid receptor agonist (Fig. 3A). Cross correlation index were used to study the time delay between signals (a measure of synchronization). We found that CBX 25µM significantly lower the cross correlation coefficient index (Fig. 3B), this result indicated that gap junction influence the synchronization of neuronal activities.
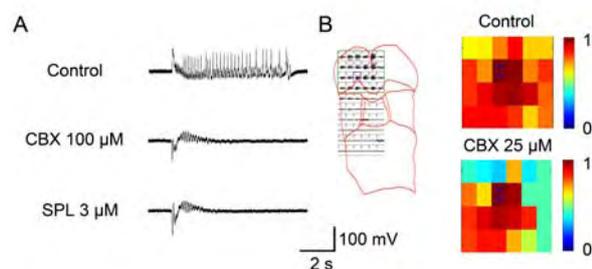


**Fig.3.** Gap junction blocker significantly lower the amplitude of oscillation. (A) The application of CBX 100 µM significantly attenuated the oscillation. And responses were not altered after application of SPL 3 µM. (B) Selected area were used for analysis of cross correlation index. The application of CBX 25 µM significantly lower the cross correlation index.

### Reference

[1] Albe-Fessard, D., Berkley, K. J., Kruger, L., Ralston, H. J. III & Willis, W. D. Jr. (1985) Diencephalic mechanisms of pain sensation. *Brain. Res.*, **356**, 217-296.
[2] Avoli, M., Rogawsk, M.A., Avanzini, G.. (2001) Generalized epileptic disorders: an update. *Epilepsia*, **42**, 445-457.
[3] Buonomano, D. V. & Merzenich, M. M.(1995) Temporal information transformed into a spatial code by a nural network with realistic properties. *Science*, **267**, 1028-1030.
[4] Lee, C. M., Chang, W. C., Chang, K. B. & Shyu, B. C. (2007) Synaptic organization and input-specific short-term plasticity in anterior cingulate cortical neurons with intact thalamic inputs. *Eur. J. Neurosci.*, **25**, 2847-2861
[5] Randy, M. B. & Daniel, J. S. (2002) Feedforward mechanisms of excitatory and inhibitory receptive fields. *J. Neurosci.*, **24**, 10966-10975

# How Should We Think About Bursts?

Steve M. Potter

Laboratory for Neuroengineering, Coulter Department of Biomedical Engineering,
  Georgia Institute of Technology, Atlanta, Georgia (America)
steve.potter@bme.gatech.edu

Population bursts of action potentials are the most prominent feature of activity recorded from mammalian neuronal networks grown on MEAs. In the intact brain or spinal cord, they are considered variously as motor patterns, sensory gates, sleep spindles, UP-states, developmental signals, epileptiform activity, or memories. I prefer to remain agnostic about what bursts "mean" in vitro, and to study them in whatever way suits the purpose at hand. In this talk, I summarize MEA work from my lab over the past decade, focusing on our continually changing perspectives on bursts, as new results and methods arrive.

Our overarching goal is to use MEAs and optics to study the basics of learning, memory, and information processing. Cultured networks are more easily accessed, imaged, controlled, and manipulated (physically, chemically, electrically, optically) than are any animal models, but it is important to keep in mind their many limitations and simplifications. To bring them closer to animal models, we developed the idea of embodying cultured networks, so they could interact with the world, express behavior and receive sensory input.[1,2] We developed ways to control bursting, and have recently verified that by doing so, one can more reliably study learning in vitro.

## 1 Introduction

Our first embodied cultured network consisted of a network of ~50,000 neurons and glia from rat cortex, grown on the 60-electrode MEA from Multichannel Systems, connected to a virtual rat in a virtual world.[20] The spiking activity produced by the cultured network, dominated by population bursts, was classified in real-time using an adaptive nearest-neighbor clustering algorithm.[2] The burst clusters were assigned to control behaviors of the simulated animal, or animat. We created the software and hardware necessary to make a closed-loop system, whereby the sensory input to the neurally-controlled animat was converted to electrical stimuli for the cultured network.[13-16] We observed that certain types of burst patterns, or more generally, spatio-temporal activity patterns (STAPs), tended to recur more often than others, and that sensory feedback created a greater diversity of STAPs expressed by the network.[2] Unfortunately, the neurally–controlled animat showed no lasting changes in behaviour as a result of interaction with its simulated environment.

## 2 Bursts are Bad!

We noticed early on that when a cultured network receives continuous input, e.g., from the sensory system of its embodiment, its tendency toward dish-wide bursts diminishes. This led to the view of bursts as pathological activity patterns resulting from deafferentation, or sensory deprivation. Probably due to large culture-to-culture differences in the level of spontaneous bursting,[19] we had a difficult time demonstrating reliable learning in cultured networks,[3] and were unable to replicate the in vitro learning results of others.[13] We hypothesized that perhaps bursts were erasing any memories we tried to encode in the networks via electrical stimuli. One can easily reduce or eliminate population bursts by pharmacological manipulations, such as high magnesium or excitatory synaptic blockers. But those produce an "anesthetized" culture, likely to have little capability for learning-related plasticity. Therefore, we developed a more natural means to prevent bursts. Artificial "sensory background" is delivered to the networks using distributed, low-frequency stimulation (~1 Hz/electrode across 10-20 electrodes).[4] This allows the networks to continue to respond to meaningful sensory input, and avoids interference with plasticity mechanisms that would occur with pharmacological manipulation. We have recently demonstrated that quieting bursts aids the induction and detection of lasting functional plasticity (see Madhavan poster). It was necessary to develop analytical tools to deal with the large ongoing drift in functional connectivity of cultured networks, to reveal changes induced by external stimuli.[10] This plasticity can be used to model *goal-directed* learning in embodied cultured networks[18] (see Chao poster). We conclude that *studies of learning in vitro should be carried out under conditions where the networks are not sensory deprived*.

Even if one takes the view that population bursting is bad, it may still be worth studying as a model for deafferentation syndromes such as chronic pain and epilepsy. This in vitro burst control work has resulted in a project to use closed-loop burst quieting to prevent seizures in epileptic rats, and eventually, humans (see Rolston poster).

## 3 Bursts are Good!

Although neuronal networks cultured from dissociated brain or spinal cord tissue are much less organized than in vivo, spontaneous bursts in MEA cultures are not random. Clustering the STAPs of many bursts revealed that each culture has fairly distinct patterns
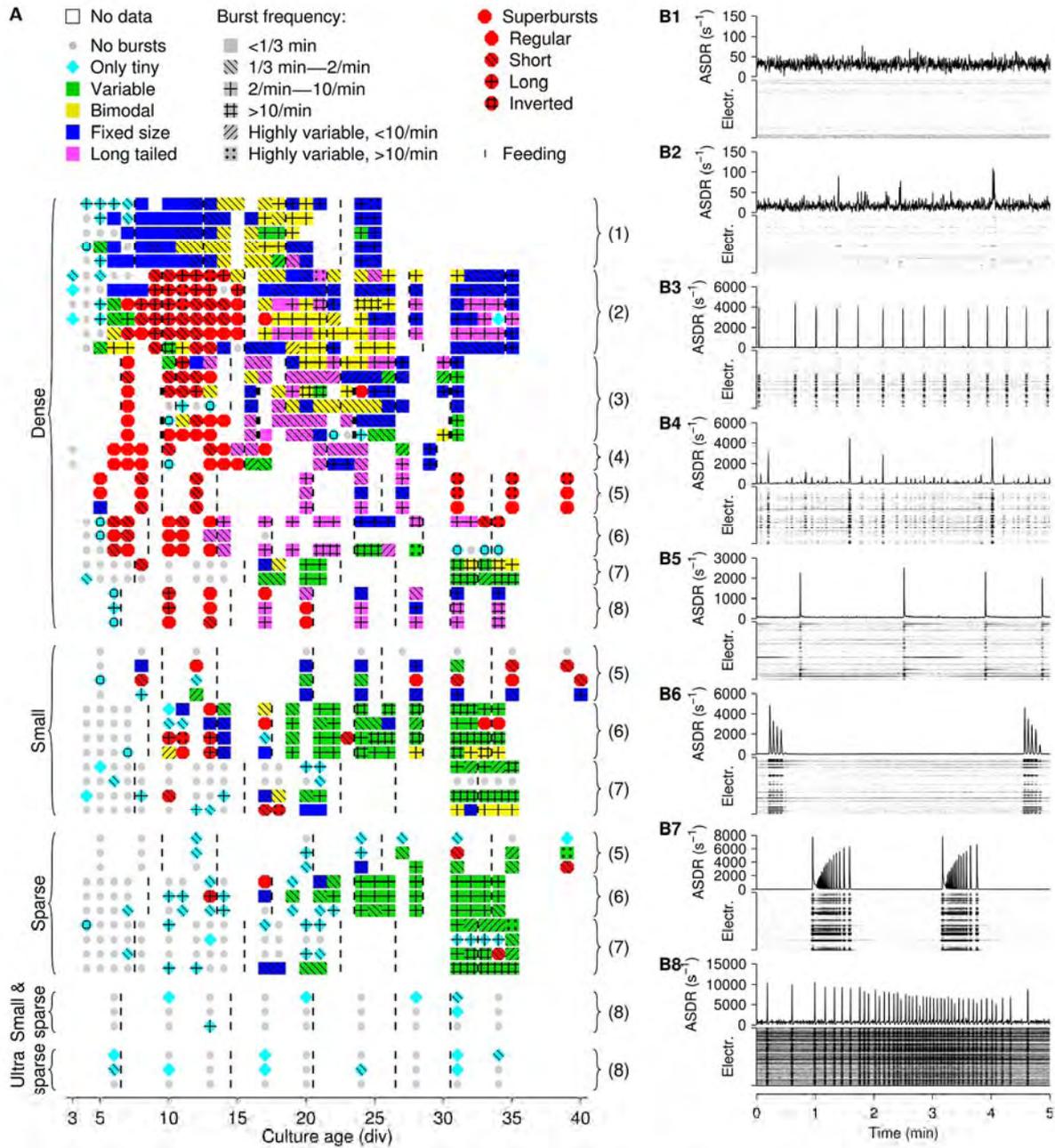


Figure 1. Classification of observed bursting behaviors. (A) Overview of the different classes of bursting behavior observed in our cultures. Numbers in parentheses indicate cell preparation number. Vertical bars indicate partial medium replacement times. Hash patterns indicate burst frequency for all types of burst patterns except superbursts. (B) Examples of burst pattern classes, with array-wide spike detection rates and gray-scale rasters for all electrodes, all taken from dense cultures. (B1) No bursting. (B2) Tiny bursts. (B3) Fixed size bursts. (B4) Variably sized bursts. (B5) Long-tailed bursts. (B6) Regular superbursts. (B7) Inverted superbursts. (B8) Dramatic burst rate variation.

that get repeated at irregular intervals.[5-8] We found both gross patterns, involving the entire network of thousands of neurons, as well as detailed sequences of action potentials propagating through a few neurons.[9] In this respect, MEA cultures replicated observations of recurring bursts or "avalanches" in brain slices,[8,22] although they do not usually exhibit a power-law distribution of burst sizes, but either involve a few electrodes or all active electrodes.[5] Since any given network expresses a diversity of bursts with non-random spatio-temporal structure, it is reasonable to think of bursts as information carriers, or the expressions of stored memories. We created new metrics to quantify these patterns, such as the Center of Activity Trajectory,[10] and have used them as reporters of changes induced in a network's input-output function by electrical (or chemical) stimuli. These functional changes can be thought of as learning. [5,11,12,21]

Bursts may serve as signals that the developing nervous system uses to form proper connections. Even in vitro, we found that certain types of bursts such as superbursts tend to occur most commonly at specific stages in a culture's development (Fig. 1).[19] We collected a large set of spontaneous and evoked activity from many cultures across the first month in vitro. These data[19] are available for others to study using their own burst analysis tools or other techniques.[24]

## 4 Bursting—What is next?

Along with the ability to control bursting by electrical stimulation comes the ability to evoke bursts at will. It is likely that the barrage of activity during a population burst engages a variety of plasticity mechanisms. Therefore, directed learning in cultured networks may be best effected by taking advantage of bursts by inducing them, rather than eliminating them completely. This may explain earlier successes at inducing functional plasticity in vitro using tetanic stimuli that repeatedly evoke bursts.[23] Through the use of a variety of electrodes and stimulus patterns to evoke different classes of bursts, perhaps different types of learning can be demonstrated.

The whole concept of "spontaneous activity" loses its meaning in vivo, where all neural events are initiated or greatly influenced by the continuous barrage of sensory inputs delivered by the millions of sensory axons leading to the brain. We often forget the unusual situation provided by cultured networks, of having zero input from the outside world — they are in "sensory deprivation". In cases where the network is interfaced using stimulating MEAs, this is no longer the case, and we have complete control of its inputs. We suggest that by delivering artificial sensory input continuously, cultured networks can serve as a more realistic model of brain processes in vivo. Whether bursts are bad or good, they provide a rich set of phenomena for studying learning, memory, and pathology in vitro and in vivo.

## References
(Our papers can be found online at neuro.gatech.edu)

[1] Potter, S. M. (2001). Distributed processing in cultured neuronal networks. *Progress In Brain Research Advances in Neural Population Coding*, 130, 49-62.

[2] DeMarse, T. B., Wagenaar, D. A., Blau, A. W., & Potter, S. M. (2001). The neurally controlled animat: Biological brains acting with simulated bodies. *Autonomous Robots*, 11, 305-310.

[3] Wagenaar, D. A., Pine, J., & Potter, S. M. (2006). Searching for plasticity in dissociated cortical cultures on multi-electrode arrays. *Journal of Negative Results in BioMedicine*, 5(16), 1-19.

[4] Wagenaar, D. A., Madhavan, R., Pine, J., & Potter, S. M. (2005). Controlling bursting in cortical cultures with closed-loop multi-electrode stimulation. *Journal of Neuroscience*, 25, 680-688.

[5] Madhavan, R., Chao, Z. C., & Potter, S. M. (2007). Plasticity of recurring spatiotemporal activity patterns in cortical networks. *Physical Biology*, 4, 181-193.

[6] Wagenaar, D. A., Nadasdy, Z., & Potter, S. M. (2006). Persistent dynamic attractors in activity patterns of cultured neuronal networks. *Physical Review E*, 73, 51907.1-51907.8.

[7] Segev, R., Baruchi, I., Hulata, E., & Ben-Jacob, E. (2004). Hidden neuronal correlations in cultured networks. *Physical Review Letters*, 92(11).

[8] Beggs, J. M. & Plenz, D. (2004). Neuronal avalanches are diverse and precise activity patterns that are stable for many hours in cortical slice cultures. *Journal of Neuroscience*, 24(22), 5216-5229.

[9] Rolston, J. D., Wagenaar, D. A., & Potter, S. M. (2007). Precisely timed spatiotemporal patterns of neural activity in dissociated cortical cultures. *Neuroscience*, 148, 294-303.

[10] Chao, Z. C., Bakkum, D. J., & Potter, S. M. (2007). Region-specific network plasticity in simulated and living cortical networks: Comparison of the center of activity trajectory (CAT) with other statistics. *Journal of Neural Engineering*, 4, 294-308.

[11] Chao, Z. C., Wagenaar, D. A., & Potter, S. M. (2005). Effects of random external background stimulation on network synaptic stability after tetanization: a modeling study. *Neuroinformatics*, 3, 263-280.

[12] Baruchi, I. & Ben-jacob, E. (2007). Towards neuro-memory chip: Imprinting multiple memories in cultured neural networks. *Physical Review E*, 75, 050901.

[13] Potter, S. M., Wagenaar, D. A., & DeMarse, T. B. (2006). Closing the Loop: Stimulation Feedback Systems for Embodied MEA Cultures. In M. Taketani & M. Baudry (Eds.), Advances in Network Electrophysiology using Multi-Electrode Arrays. (pp. 215-242). New York: Springer.

[14] Wagenaar, D. A., DeMarse, T. B., & Potter, S. M. (2005). MeaBench: A toolset for multi-electrode data acquisition and on-line analysis. 2nd Intl. IEEE EMBS Conference on Neural Engineering, 518-521.

[15] Wagenaar, D. A. & Potter, S. M. (2004). A versatile all-channel stimulator for electrode arrays, with real-time control. Journal of Neural Engineering, 1, 39-45.

[16] Wagenaar, D. A. & Potter, S. M. (2002). Real-time multi-channel stimulus artifact suppression by local curve fitting. J. Neurosci. Methods, 120, 113-120.

[17] Shahaf, G. & Marom, S. (2001). Learning in networks of cortical neurons. Journal of Neuroscience J. Neurosci, 21(22), 8782-8788.

[18] Chao, Z. C., Bakkum, D. J., & Potter, S. M. (2008). Shaping Embodied Neural Networks for Adaptive Goal-directed Behavior. PLoS Computational Biology, 4(3), e1000042.

[19] Wagenaar, D. A., Pine, J., & Potter, S. M. (2006). An extremely rich repertoire of bursting patterns during the development of cortical cultures. BMC Neuroscience, 7, 11.

[20] Potter, S. M., Fraser, S. E., & Pine, J. (1997). Animat in a Petri Dish: Cultured Neural Networks for Studying Neural Computation. Proc. 4th Joint Symposium on Neural Computation, UCSD, 167-174.

[21] Eytan, D., Minerbi, A., Ziv, N., & Marom, S. (2004). Dopamine-induced dispersion of correlations between action potentials in networks of cortical neurons. Journal of Neurophysiology, 92(3), 1817-1824.

[22] Ikegaya, Y., Aaron, G., Cossart, R., Aronov, D., Lampl, I., Ferster, D., et al. (2004). Synfire chains and cortical songs: Temporal modules of cortical activity. Science, 304(5670), 559-564.

[23] Jimbo, Y., Tateno, T., & Robinson, H. P. C. (1999). Simultaneous induction of pathway-specific potentiation and depression in networks of cortical neurons. Biophysical Journal, 76, 670-678.

[24] Eckmann, J.-P., Jacobi, S., Marom, S., Moses, E., & Zbinden, C. Leader neurons in population bursts of 2D living neural networks. New Journal of Physics, 10, 015011.

# Explaining burst profiles using models with realistic parameters and plastic synapses

T. Gritsun[1*], J. Stegenga[1], J. Le Feber[1] and W.L.C.Rutten[1]

1 Biomedical Signal and Systems group, Department of Electrical Engineering, Mathematics and Computer Science, University of Twente, Enschede, the Netherlands
* Corresponding author. E-mail address: t.gritsun@utwente.nl

One of the most prominent features of the electrical activity of dissociated cultured neural networks is the phenomenon of network bursts. Profiles of the instantaneous firing rate during bursts vary in shape and intensity during neuronal culture development. To shed some light on burst profile variability we constructed "pacemaker-driven" random recurrent neural network models with both static and frequency dependent synapses. We show variation of burst features by changing the network parameters of the models. The best agreement was found by including synapses with short-term plasticity.

## 1 Introduction

We studied neural network collective behavior in terms of synchronized network bursts (NB): namely the formation and characteristics of bursts in cortical neurons cultured on multi electrode arrays (MEAs). A NB can be characterized by its profile, which is calculated as a (smoothed) estimation of the array-wide firing frequency [1, 2]. In this work we focused on three NB profile shape parameters: half-widths of rising phase (Rp), falling (Fp) phase and maximum firing rate (mFr). A batch simulation of the artificial network was used to generate bursts. We studied how profile parameters depended upon network parameters, such as average number of connections per neuron (connectivity, C), excitatory fraction ratio (R) and the time delay between pre-synaptic spike and post - synapse response (transmission delay, D). The simulations produced NB features in ranges similar to experimental data. These simulations help to understand the development of the network structure throughout culture life-time. Several mechanisms that modulate synaptic transmission are active during bursts. These may change the spatio-temporal structure of bursts on large timescales through spike-timing dependent plasticity (including LTP and LTD). On small timescales, short-term plasticity (STP) (*e.g.* facilitation and depression phenomena) may affect firing rates during bursts. To test its influence, we used synapse models with and without STP.

## 2 Methods

We used spontaneous recordings previously used in [1]. Shortly, we obtained neocortical neurons from 1-day old Wistar rats. Cultures of dissociated neurons were grown on MEAs and 2 hour long recordings were made daily starting around 7 days *in vitro* (DIV).

We analyzed Rp, Fp and mFr as defined by van Pelt et al. [2] from experimental spontaneous bursting activity over a period from 9 to 36 DIV. In order to mimic these features we constructed several spiking models of a recurrent neural network with random sparse connectivity maps. In brief, we used the quadratic integrate and fire neuronal model by Izhikevich [3], and static and frequency dependent synapse models by Tsodyks et al. [4]. We approximated the ranges of C during culture development from experimental counting of van Huizen's et al. [5]. D was set in the range according to experimental findings of Muller et al. [6]. R was set in the range between 70% and 90% according to [7]. We ran batch simulation with normally distributed connectivity around C = {50, 100, …, 550}, transmission delays around D = {5, 10, 15, 20} msec and excitatory fraction ratio R = {70, 80, 90}%. Synaptic strengths were normally distributed between 0 and 1 mV. We introduced inhomogeneous distribution of synaptic strength (up to 12 mV) and intrinsic activation in small neuronal subsets (i.e. 'pacemakers') into network models. The total number of neurons was 5000.

Network simulations were performed using both modified CSIM simulator [8] and C programming language (in MEX-file) in a Matlab environment (the MathWorks, Inc) on a PC compatible platform. We used Euler's method to integrate neuronal and synaptic model equations with 1 ms simulation step.

The same NB parameters as in the experiments were calculated from the simulated spike trains and their sensitivity to variations of the network parameters C, R and D.

In this report we present several sensitivity plots of the mFr, Rp and Fp to variation of the connectivity C in order to compare simulated and experimental

data. The detailed results on the sensitivity analysis will be reported elsewhere.

## 3 Results

Figure 1 summarizes the development of three NB profile parameters acquired from 7 cortical cultures. In brief, mFr increases, Rp and Fp are more varied in first 3 weeks in vitro; mFr decreases, Rp and Fp are stabilized thereafter.
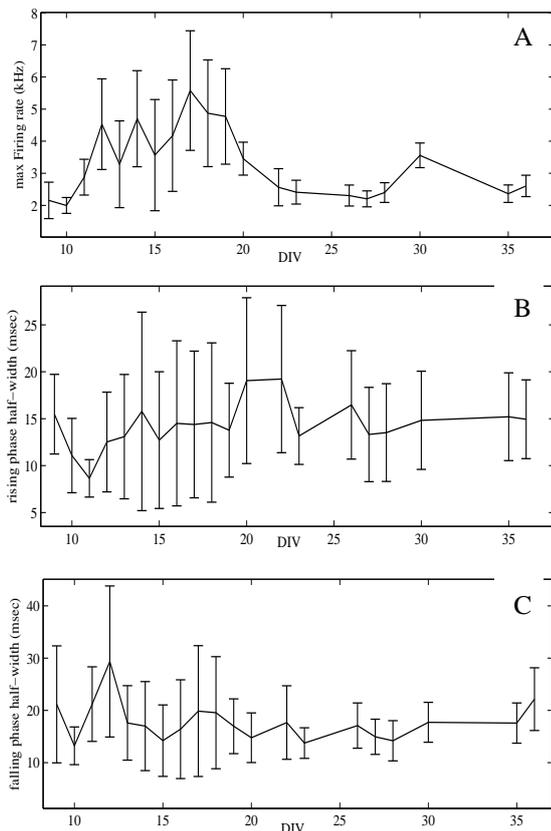


**Fig. 1.** Dynamics of three NB features: maximum firing rate (A), half-width of rising phase (B) and falling phase (C). Mean and standard deviation (SD) values were averaged from burst profiles on each day of recording from 7 neural cultures. In general, mFr rises in the first and second week in vitro and decays in the third week. Cultures older than 3 weeks show more or less constant value with smaller SD.

Figures 2a and b show sensitivity curves for NB profile parameters to the connectivity C in the network simulations with static synapses. Network activity increases with higher C (see fig 2a) and decreases with longer D and lower R (not shown here). Activity developed into NBs in the simulations with C ≥ 250. Networks with high C and R, and short D produced activity explosions as shown in figure 2a at C = 450. Except for these explosions, simulated NB features resemble those of experimental data in the networks when D ranges from 5 to 20 msec, R from 70 to 90% and C between 350 and 550 (not shown here).
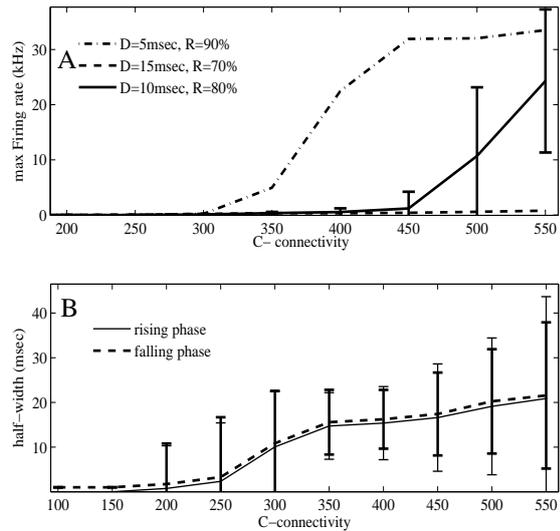


**Fig. 2.** Sensitivity curves for the connectivity; their effect on the NB profile in NN models with static synapses. A: Mean curves and standard deviation are plotted for the maximum firing rate, B: half-width rising and half-width falling phase, summary curves.

In the next simulation batch static synapses were substituted for dynamic modelled by Tsodyks et al. [4], in order to see the effect of STP on profiles. Figures 3a and 3b show changes in dynamics of the NB parameters after introducing the adaptive synapses. Here burst were detected in networks with smaller C (around 150 - 200). STP rules allowed simulating networks with higher C without mFr explosions and less varied Rp and Fp. These simulations mimic experimental data better than previous, mainly for older cultures, where Rp and Fp are stabilized around 15 msec.

## 4 Discussions

The highly connected networks with static synapses produce NBs with higher firing rate and more varied Rp and Fp values than the networks with dynamic synapses.

Following high variation of Rp and Fp values at C ≥ 400, simulated NB profiles generated using static synapse model resemble profiles found in cultures younger than 3 weeks in vitro. This corresponds to elevated range of mFr values that can be found in experimental data. In older cultures mFr drops to the values that correspond to values produced by network models with smaller connectivity. Experimental data acquired from cultures three weeks old, and older, are reproduced by models with frequency dependent synapses. Indeed, these findings are in agreement with experimental data reported by Van Huizen et al. (1985) [5]. They showed that average number of synapses increases during development and reaches a maximum at 3 weeks in vitro, after which it stabilizes at a lower value.
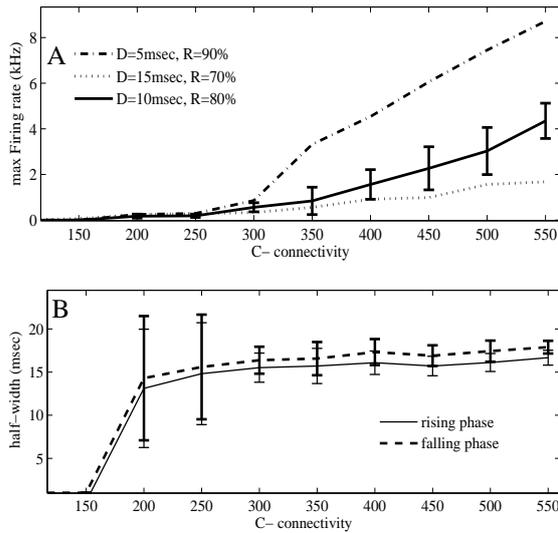
**Fig. 3.** Sensitivity curves for the connectivity; their effect on the NB profile in NN models with adaptive synapses. A: Mean curves and standard deviation are plotted for the maximum firing rate, B: half-width rising and half-width falling phase, summary curves.

We show the influence of STP on stability of the network activity through changes of network connectivity. First, STP prevented networks from activity explosions; next, it stabilizes Rp and Fp at shorter time values; and finally, it allows the networks to produce activity in smaller connectivity ranges. These shorter time ranges of Rp and Fp, which makes NB profiles narrower than profiles in the network models with static synapses, were caused by lower average firing rates.

**References**

[1] J. Stegenga, J. le Feber, E. Marani and W.L.C. Rutten, (2008) "Analysis of cultured neuronal networks using intra-burst firing characteristics," *IEEE Trans. Biomed. Eng.* Pp 1382-1390

[2] J. Van Pelt, P. Wolters, M.A. Corner, W.L.C. Rutten, G.J.A. Ramakers, (2004) *Long-term characterization of firing dynamics of spontaneous bursts in cultured neural networks*, IEEE trans. BioMed. Eng. 51, 11, pp2051-2062.

[3] Izhikevich E. M., (2003) "Simple model of spiking neurons," *IEEE Trans. Neural Networks*, vol. 14, pp. 1569–1572, Nov.

[4] Tsodyks M., Uziel A. and Markram H., (2000) Synchrony generation in recurrent networks with frequency-dependent synapses, J. Neurosci. 20 RC50, p. 1.

[5] F. van Huizen, H.J. Romijn and A.M.M.C. Habets, (1985) "Synaptogenesis in rat cerebral cortex is affected during chonic blockade of spontaneous bioelectric activity by tetrodotoxin," Dev. Brain Res., vol. 19, pp. 67–80, 1985

[6] T.H. Muller, D. Swandulla and H.U. Zeilhofer, (1997) "Synaptic connectivity in cultured hypothalamic neuronal networks," *J. Neurophysiol.* 77, pp. 3218–3225

[7] M. Toledo-Rodriguez, A. Gupta, Y. Wang, Cai Zhi Wu and H. Markram, "Neocortex: basic neuron types," in: M.A. Arbib, Editor, The Handbook of Brain Theory and Neural Networks (2nd edn ed.), MIT Press (2002) pp. 719-725

[8] T. Natschläger, H. Markram and W. Maass In: R. Kötter, Editor, *Neuroscience Databases. A Practical Guide*, Kluwer Academic Publishers, Boston, pp. 123–138, 2003

# Spontaneous coordinated activity in cultured networks: Analysis of multiple ignition sites, primary circuits, burst phase delay distributions and functional structures

Michael I. Ham[1,2*], Vadas Gintautas[1], Guenter W. Gross[2]

1 Los Alamos National Laboratory, CNLS and T-7, Los Alamos, New Mexico USA
2 Center for Network Neuroscience, University of North Texas, Denton, Texas
* Corresponding author. E-mail address: mih0001@t7.lanl.gov

All higher order central nervous systems exhibit spontaneous neural activity, though the purpose and mechanistic origin of such activity remains poorly understood. We explore the ignition and spread of collective spontaneous electrophysiological burst activity in networks of cultured cortical neurons growing on microelectrode arrays using information theory and first-spike-in-burst analysis methods. We show the presence of burst leader neurons, which form a mono-synaptically connected primary circuit, and initiate a majority of network bursts. Leader/follower firing delay times form temporally stable positively skewed distributions. Blocking inhibitory synapses usually results in shorter delay times with reduced variance. These distributions are generalized characterizations of internal network dynamics and provide estimates of pair-wise synaptic distances. We show that mutual information between neural nodes is a function of distance, which is maintained under disinhibition. The resulting analysis produces specific quantitative constraints and insights into the activation patterns of collective neuronal activity in self-organized cortical networks, which may prove useful for models emulating spontaneously active systems.

## 1 Introduction

Electrophysiological activity is aways present in neural systems. Such spontaneous activity plays putative roles ranging from synaptic development and maintenance [1,2,3] to anticipatory states [4] which assist animals in reaching rapid decisions with limited sensory input. Understanding the mechanisms of spontaneously generated activity and interaction patterns between neurons are, therefore, issues of substantial importance.

Over several decades, a large body of theoretical analysis and experimental data suggests cortical neuronal networks growing on microelectrode arrays (MEAs) *in vitro* are useful experimental models of neural assembly (e.g. [5,6,7]) though obvious limitations are inherent to extrapolations between *in vitro* and *in vivo* systems [8,9].

In this manuscript we present analysis of neuronal interactions during spontaneous burst activity *in vitro*. These collective high frequency action potential discharges are well documented features of such networks (e.g. [10]) and have been shown to influence learning and information processing by changing synaptic properties [11,12]. Previous research has shown that multiple ignition sites [10,13,14] recruit network neurons to create network bursts. Here, temporal relationships between leader (first neuron to fire in a network burst) and follower neurons are examined using a first-spike-in-burst analysis method to create response delay distributions (RDDs). Disinhibition with bicuculline reveales changes in ignition site statistics and follower responsiveness.

RDD features are found to provide estimates of the distance between leader and follower neurons during network activation. Similarly, mutual information between neuronal pairs is shown to be correlated with the distance between the two neurons in each pair.

Our approach reveals new insight into functional connectivity and network organization which may be useful for creating models of small to medium sized neural networks.

## 2 Methods

### 2.1 Microelectrode array fabrication

In-house MEA fabrication is described in previous publications [15]). Briefly, glass plates with a 100-nanometer layer of indium-tin-oxide (ITO, Applied Films Corp., Boulder, CO) were photo etched to create a recording matrix of 64 electrodes measuring 8-10 um in width and conductors leading to peripheral amplifier contacts on a 5 x 5 cm glass plate. Plates were spin-insulated with methyltrimethoxysilane resin, cured, and de-insulated at the electrode tips with single laser shots. Exposed electrode terminals were electroplated with colloidal gold to decrease imped-

ance at 1 kHz to approximately 0.8 MΩ. Butane flaming followed by application of poly-D-lysine and laminin helped cell adhesion. These microelectrode arrays, featuring substrate integrated thin film conductors allow long-term, extracellular microvolt recording of action potentials from 64 discrete sites in a neuronal network.

## 2.2 Cell culture

Frontal cortices were dissected from 16 to 17 day old mouse embryos. The tissue was mechanically minced, enzymatically dissociated, triturated, and combined with medium (Dulbecco's Modified Eagles Medium (DMEM) supplemented with 10% fetal bovine serum and 10% horse serum). Dissociated cells (100k / ml) were seeded on MEAs with medium addition after cells had adhered (usually 2-3 hrs). After 5 days, cultures were fed DMEM supplemented with 5% horse serum (DMEM-5). Greater detail is provided in earlier publications [16]. Cultures were incubated at 37 °C in a 10% CO2 atmosphere with 50% medium changes performed twice a week until used for experiments.

## 2.3 Electrophysiological Data Acquisition

For electrophysiological recordings, cultures were assembled into a recording apparatus on an inverted microscope connected to a two-stage, 64 channel amplification and signal processing system (Plexon Inc., Dallas). Cultures were maintained at a temperature of 37 °C, and pH of 7.4. The pH was maintained by a 10 ml / min flow of 10% CO2 in air into a cap on the chamber block featuring a heated ITO window to prevent condensation. Water evaporation was compensated by a syringe pump (Harvard Instruments) with the addition of 60 to 70 uL / hr sterile water. Details of chamber assembly and recording procedures can be found in previous papers [16]. Total system gain was set at 10k and action potential (AP) activity with a sampling resolution of 25 μs was recorded for later analysis.

## 2.4 Electrophysiological Data Acquisition

To identify network bursts, recordings are partitioned into 10 ms bins and number of spikes per bin is determined. An upper and lower threshold algorithm is used to identify network bursts. Upper threshold is selected as 20% of all recorded spikes. The lower threshold is found by rounding up the average bin count and is generally set at 1 or 2 spikes/bin.

The algorithm finds the first bin count at least equal to the lower threshold. Then, two possible scenarios are examined: (1) the number of spikes is greater than or equal to the upper threshold which indicates the start of a global burst. Bursts continue while consecutive bin counts are at or above the lower threshold. (2) Upper threshold is not reached. Bin is marked as the potential beginning of a burst. Consecutive 10 ms bins are searching for one that satisfies the upper threshold (a burst), or falls below the lower threshold (no burst).

All network bursts end when a consecutive bin falls below the lower threshold. Network bursts with activity gaps of less than 100 ms are combined. The first neuron in each burst (burst leader) to fire is recorded. The first spike each follower made in each network burst is used to determine response (phase) delays between leaders and followers.

## 2.5 Informational relationships

To quantify informational relaionships, neuronal time series are digitized into 10 ms bins. If a neuron fired within a bin, the bin is assigned a 1. If it did not fire, the bin is assigned a 0. Mutual information (MI) between neurons X and Y is calculated using $MI=\Sigma p(X,Y)*log2[p(X,Y)/p(X)p(Y)]$ where $p(X,Y)$ is the joint probability distribution and $p(X)$ and $p(Y)$ are the single variable marginals [17,18]. Normalized nutual information is found by dividing the MI by the smaller of the Shannon entropy of X or Y. Mutual information is 0 if and only if neurons X and Y are independent of each other.

## 3 Results

**Major burst leaders**

In 10 experimental networks, each recorded for at least three hours, all neurons led at least one network burst. However, only a small percentage, ( average 17%) are found to be major burst leaders (MBLs, Fig 1). Major burst leaders are defined as neurons that led at least 4% (arbitrarily chosen) of all network bursts. The set of MBLs are found to be relatively stable over many hours, though individual leadership rates fluctuated [19]. On average, MBLs led 84% of all network bursts (Fig 1).

Neuronal spike rates do not appear directly linked to burst leadership. In Fig 1, the percent spike activity (percent of total activity a neuron contributes) is compared to burst leadership under both native and biculline activity. It should be noted that MBLs are some of the most active recorded neurons, but that activity is not a good predictor of leadership.

**Response delay distributions**

For each MBL-follower pair, the aggregate of their response delays (time between MBL starting a burst, and follower responding) is represented as a response delay distribution (RDD, Fig2). RDDs are observed to be highly variable in nature and unique for each leader/follower pair. Three important features are extracted from a pair's RDD. (1) Minimum response

delay (MRD) values. These are identified as the intersection of the rising edge of the distribution with a value equal to 10% of the distributions peak. MRDs represent the minimum time it takes a signal to travel from a leader to a follower. Most MRDs are approximately 2 ms, but ranged up to 20 ms. (2) Peak delay. The most probable delay time between leader and follower onset. (3) Paired response correlation (PRC). A measure of how likely a follower is to respond to a given leader.
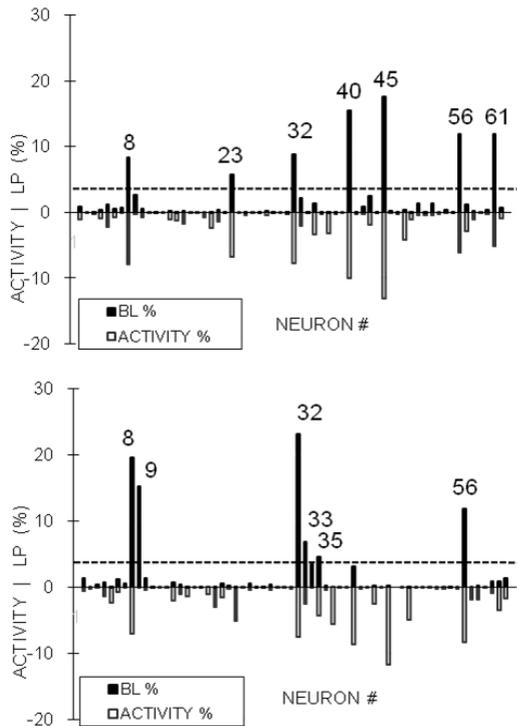


**Fig. 1.** Burst leadership (positive) and activity probability (negative) is shown for neurons recorded in native activity (top) and under 40 μM bicuculline (bottom). Neurons leading with rates above an arbitrarily chosen cutoff (dashed line) are considered major burst leaders. The addition of bicuculline changed the pool of major burst leaders which are stable during native activity.

## Primary circuit

All MBLs exhibit high PRC (>70%) values with respect to all other MBLs. Additionally MBLs have a PRC value > 90% with respect to at least one other MBL. Few non MBLs have PRC values of this magnitude. RDDs of MBL pairs show MRDs around 2 ms, which suggests that the shortest path between two MBLs is a single synapse [20]. Therefore, we conclude that MBLs form a highly connected 'primary circuit' responsible for initiating the majority of all network bursts and maintaining long term spontaneous activity.

## Disinhibition with bicuculline

Disinhibition with 40μM bicuculline changes the composition of MBL pools (Fig 1). In eight networks

where bicuculline was added, there are 52 MBLs during native activity and 48 after. Only 25 of the latter are MBLs during both time periods. Bicuculline also changes the nature of the response delay distributions. Four unique changes are observed. (1) increased responsiveness to the MBL, (2) overall shift of the distribution to shorter phase delays, (3) response by previously unresponsive neurons, (4) rarely, peak and MRD shift to higher phase delays. There are no observed cases in which a follower became less responsive to a burst leader. All four RDD changes could happen to followers of the same burst leader.
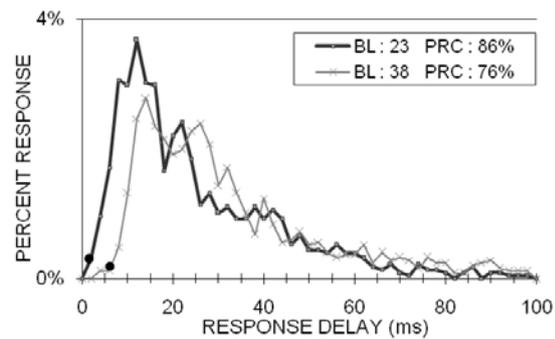


**Fig. 2.** Response delay distribution for a single follower and two burst leaders (2ms bins). Minimum response delays are depicted with filled circles. Followers have unique responses to different burst leaders.

## Mutual information and distance

Previously, we showed that RDD features are affected by distance from the burst leader [19]. Here we apply an information theoretic approach to examine whether all neuronal relationships are impacted by distance from one another. In Fig 3, the mutual information for all neural pairs is calculated first under native conditions, then after application of 40 μM bicuculline. Values are then averaged for all exact distances. The mean is plotted as a point and the standard error is indicated with error bars. We observe that, on average, mutual information between neuronal pairs drops as distance increases.

## 4 Discussion

We show that major burst leaders play an important role in network activation. Together, they dominate the initiation of spontaneous network firing pattens by exciting the network. However activity from a single MBL may not be enough to trigger the rest of the network. Our finding that MBLs are well connected to other MBLs through the primary circuit, suggests that leadership may be a shared property, requiring the combined activity of several highly connected neurons [21].

Response delay distributions (RDDs) between leader/follower pairs reveal the nature of the relationship between these two neurons. Small minimum re-

sponse delays correspond to the presence of short synaptic pathways between a pair. Peak delay times show the most probable path delay. Paired response correlation show how effective a particular leader is at activating a follower. These values can be very different for leaders of the same follower, suggesting that recruitment may depend heavily on which neruon leads a network burst.
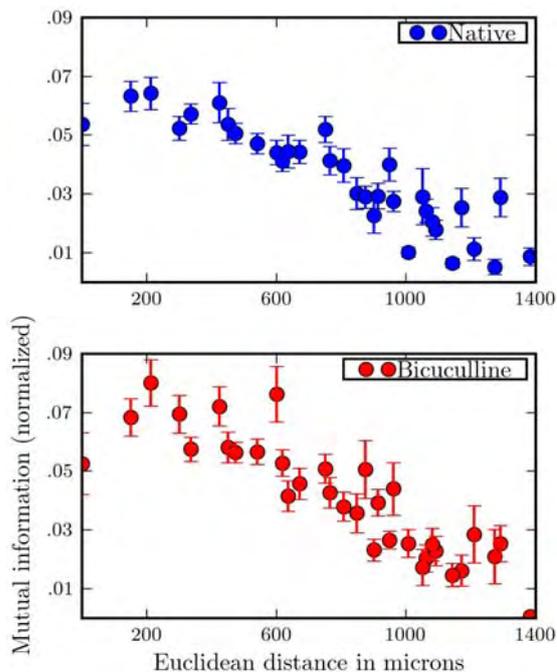


**Fig. 3.** Average mutual information values and the distance between neuronal pairs. The mutual information is measured before (top) and after (bottom) the addition of 40 μM bicuculline. Information decreases as a function of distance in both cases.

Blocking inhibition with bicuculline led to an immeadiate change in the burst leadership pool and response delay distributions. The abruptness of this change suggests that existing network circuitry remains unchanged while only computational activities are modified.

In a previous paper, we showed that RDD characteristics are a function of distance [19]. Here we show that mutal information between all neurons is also a function of distance. While not suprising, these two results show that burst propogation and mutual information are both proportional to distance.

Network bursts are well known features of natural nervous system activity. We hope that characterizations of collective activity patterns in these cultures will guide new models and lead to improved biologically accurate models of the computational abilities of the nervous system.

### Acknowledgement

gram. The authors also wish to thank Luis Bettencourt for providing invaluable insight and expertise.

### References

[1] R.R.Provine (1979) Wing-flapping develops in wingless chicks. Behav Neur Biol, 27:233–237.

[2] M. Meister, R.O.L. Wong, D.A. Baylor, and C.J. Shatz (1991) Synchronous bursts of action potentials in ganglion cells of the developing mammalian retina. Science, 252:939–943.

[3] N.C. Spitzer (2006) Electrical activity in early neuronal development. Nature, 444:707–712

[4] Y. Takikawa, R. Kawagoe, and O. Hikosaka (2002) Reward-dependent spatial selectivity of anticipatory activity in monkey caudate neurons. J Neurophysiol, 87:508–515.

[5] T. B. DeMarse, D. A. Wagenaar, A. W. Blau, and S. M. Potter (2001) The neurally controlled animat: Biological brains acting with simulated bodies. Auton. Rob., 11:305

[6] G. Shahaf and S. Marom (2001) Learning in networks of cortical neurons. J Neurosci, 21:8782–8788

[7] L. M. A. Bettencourt, G. J. Stephens, M. I. Ham, and G. W. Gross (2007) Functional structure of cortical neuronal networks grown in vitro. Phys Rev E, 75(2):021915

[8] M.A. Corner, J. Van Pelt, P.S. Wolters, R.E. Baker, and R.H. Nuytinck (2002) Physiological effects of sustained block-ade of excitatory synaptic transmission on spontaneously active developing neuronal networks?an inquiry into the reciprocal linkage between intrinsic biorhythms and neuroplasticity in early ontogeny. Neurosci Biobehav Rev, 26:127–185

[9] S. Marom and G. Shahaf (2002) Development, learning and memory in large random networks of cortical neurons: lessons beyond anatomy. Q. Rev. Biophys., 35:63

[10] E. Maeda, H. P. C. Robinson, and A. Kawana (1995) The mechanisms of generation and propogation of synchronized bursting in developing networks of cortical neurons. J Neurosci, 15:939

[11] T.V. Bliss and G.L.A Collingridge (1993). A synaptic model of memory: long-term potentiation in the hippocampus. Nature, 361:31–39

[12] A. Artola and W. Singer (1994) NMDA receptors and developmental plasticity in visual neocortex. In: The NMDA receptor. London: Oxford UP

[13] D. Eytan and S. Marom. (2006) Dynamics and effective topology underlying synchronization in networks of cortical neurons. J Neurosci, 26:8465–8476

[14] O. Feinerman, M. Segal, and E. Moses (2007) Identification and dynamics of spontaneous burst initiation zones in unidimensional neuronal cultures. J Neurophysiol, 97(4):2937–2948

[15] G.W. Gross, W.Y. Wen, and J.W. Lin (1985) Transparent indium-tin oxide electrode patterns for extracellular, multisite recording in neuronal cultures. Neurosci Methods, 15(3):243–252

[16] G.W. Gross (1994) Internal dynamics of randomized mammalianneuronal networks in culture. In: Enabling technologies for cultured neural networks. New York: Academic

[17] T. M. Cover, and J. A.. Thomas, Elements of Information Theory (Wiley, New York, 1991)

[18] L.M.A. Bettencourt, V. Gintautas and M.I. Ham (2008) Identification of functional information subgraphs in complex networks. to apear in Phys Rev Lett

[19] M.I. Ham, L.M.A. Bettencourt, F.D. McDaniels, G.W. Gross (2008) Spontaneous coordinated activity in cultured networks: analysis of multiple ignition sites, primary circuits, and burst phase delay distributions. J. Comp Neurosci 24(3) 346-357

[20] K. Nakanishi and F. Kukita (1998). Functional synapses insynchronized bursting of neocortical neurons in culture. Brain Res, 795:137–146.

[21] G.W. Gross and J.M. Kowalski (1999) Origins of Activity Patterns in Self-Organizing Neuronal Networks in Vitro. J Intel Mater Syst Struct 10(7) 558-564

# Neuronal responces to sensor inputs in the miniature neuro-robot hybrid

Suguru N. Kudoh[1]*, Minori Tokuda[2], Ai Kiyohara[1,3],Isao Hayashi[2], Chie Hosokawa[1] and Takahisa Taguchi[1,3,4]

1 Cell Engineering Research Institute, National Institute of Advanced Industrial Science and Technology (AIST)
2 Faculty of Informatics, Kansai University
3 Graduate School of Science, Osaka University
4 Neuroscience Research Institute, National Institute of Advanced Industrial Science and Technology (AIST)
* Corresponding author. E-mail address: s.n.kudoh@aist.go.jp

Rat hippocampal neurons were cultured on a dish with 64 micro planer electrodes. A complex network of neurons was formed and the network was able to distinguish patterns of action potentials evoked by different electrical current inputs. We integrated a living neuronal network and a Khepera II robot or robot made by LEGO mindstorm NX kit as a body for contacting to outside world. Using self-tuning fuzzy reasoning, we associated a distinct spatial pattern of evoked action potentials with a particular phenomenon in the outside of the culture dish. We succeeded in performing collision avoidance behaviour with premised control rule sets. During collision avoidance, the responding pattern of evoked action potentials was stable and robust against perturbation to spontaneous network activity. These results suggest that a cultured neuronal network can represent particular states as symbols corresponding to outside world.

## 1 Introduction

Rat hippocampal neurons reorganized a complex network on microelectrodes array dish and the spontaneous action potentials were frequently observed. The spontaneous activity was autonomous and was performed without any external stimulation, suggesting that interaction between neurons was fully active. In other words, the living neuronal network had autonomous internal state fluctuated by intaraction of mutually connected neurons. We think that internal state itself is main constituent of information processing in the network. We tried to "link" that internal state of the network and phenomenon in outside world. Our aim is to elucidate how to make the internal state be grounded on the real world.

For this purpose, we performed closed-loop interaction between the living neuronal network and outer world, using a neuro-robot hybrid system. The idea of integration of a moving robot and a living neuronal network providing for a closed-loop interaction between a neuronal network and outside world was firstly proposed by Potter's group as Hybrot [1]. In their recent papers, robot or simulated robot were controled by new statistic, the Center of neural activity (CA) of responses within 100 ms after each electrical stimulus. These responces were evoked by "prove" stimulus applied to the neural network every 5 seconds. "Prove stimuli" were mimicked sensory inputs of animals, which were continuously derived to the brain. They used well-designed stimulation protocols and paid attention to make the neuronal network be stable. Interestingly, they also succeeded in goal-directed learning.

Our approach in the neuro-robot is different from their original concept in following two points.

1) Instead of continuous prove stimuli, we stimulate the neuronal network only when actual sensors are activated.

2) We do not discriminate spontaneous activity and activity evoked by sensor inputs. We treat the spontaneous activity as representation of spontaneous behavior or "thinking".

Indeed, in our brain, it is difficult to find "pure" spontaneous activities because an animal brain continuously received numerous sensory inputs. Our small-scaled neuronal network has not so many inputs, which is not contradiction, if scaling factor is adequate. In addition, except for neurons directly connected to sensors, neurons cannnot distinguish between signals originated from sensory input and signals originated from spontanousl activity. Similarly, we does not discriminate spontaneous and sensory evoked activity. In these principles, our idea that internal state itself is main constituent of information processing in the network are reflected. We think a responce of neuronal network is not tightly coupled to an input from outer world. It seems that an input only recall a particular internal state to the network. The relationship between an object in outer world and an internal state is loose and fluctuated by network dynamics. The relationship of a particular object and an internal state of neuronal network linked to the object is defined only by reproducibility of such relationship

in experience of the cognitive system. This framework is same as definition of "qualia" in "Mind and the world order" by Lewis[2]. Neuronal network has history function of their activity, meaning the network is received from past. Internal state itself is autonomous but is influenced by inputs from past and sensors or other unit in the total network system. If this influenced internal state is loosely recalled reproducibly, there is a sort of universals. We think the fluctuation of such a sort of universals is resulted from" information processing" in the network, and it is, so to speak, a decision making process of neuronal network (Fig.1).
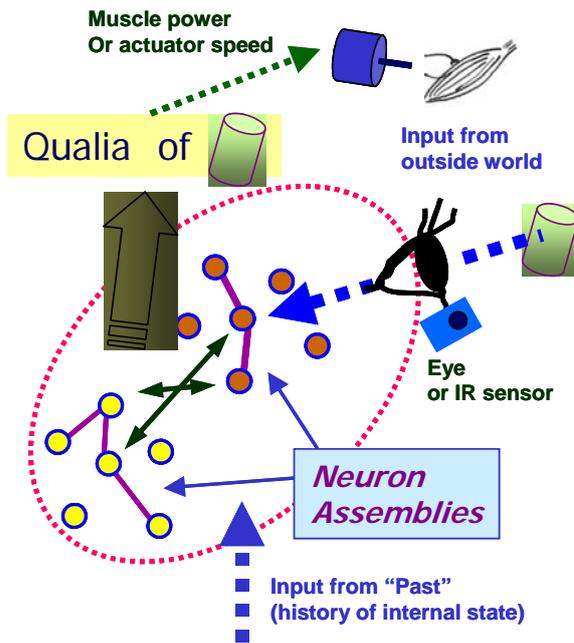


**Fig. 1**. A cognitive system and outside world.

In our paradigm, we do not perform conscious control of the living neuronal network. Instead of that, we tune interface between neurons and outer world. After that, the neuronal network tunes itself in self-organization manner. The direction of tuning is not always suitable for reasonable behavior, so we need to design the model for linking neurons with outer world, estimating of tuning manner of the neuronal network. Generally, the expectation is difficult and we have to find the model by exploratory methods. This point is resemble to the method for goal-directed learning of Potter's group.

We use a Khepera II robot for interfacing with a living neuronal network and the outer world and succeeded in performing collision avoidance behaviour with premised control rule sets. Using self-tuning fuzzy reasoning, we associated a distinct spatial pattern of electrical activity with a particular phenomenon in the outside of the culture dish.

## 2  System Integration for Vitroid

### 2.1 Main framework of Vitroid

**Vitroid concept**

We call our neuro-robot system as "Vitroid" with a direct coupling type of closed-loop interaction. The system is a sort of "test tube" for cognitive agent made by living component. A central processing unit of Vitroid is a living neuronal network (LNN), and all decision-making of the system is performed by the network of neurons. Because of that concept, we pay regard to LNN and perform no explicit manipulation to LNN.

**Living neuronal network (LNN)**

Method for preparing LNN of rat hippocampal neurons was described in previous papers. Our method is modified conventional Banker's method. Fig.2 indicates rat hippocampal neurons and glias cultured on a multi electrode array dish. Number of neurons was stable during culture days.
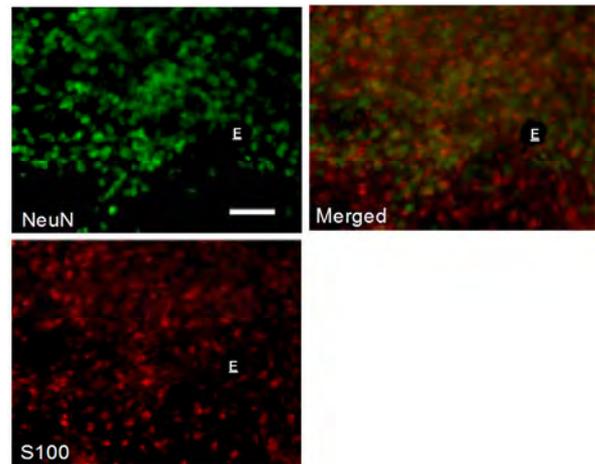


**Fig. 2**. An Example of LNN (E18D18). NeuN is a marker for nuclei of neuron and S100 is a marker for glia. "E" indicates an micro electrode. White bar indicates 50μm.

**Interpreters**

The system requires at least 2 interpreters; one is an "output interpreter" translating electrical activity patterns into behaviours of robot and another is an "input interpreter" translating outer phenomena into electrical stimulation. These interpreters consist of the coupling model for LNN and outside world. This requirement is essential for Vitroid system. The interpreters in Vitroid are essential for performing reasonable behaviours, because we can implement rules for reasonable behaviour only in these interpreters, just like couplings between actuator and sensor pairs in robot designed by embodied cognitive science.

### Robot Body

We use a Khepera II robot (K-Team) or Robot constructed by LEGO mindstorm NXT kit for body of Vitroid. In near future, we are also planning to implement cultivation equipments for LNN on a larger moving unit, then the system become to be "test tube" literally. In this paper we describe about Vitroid using Khepera II robot. C# and LabVIEW (National instruments) was adopted for the programming language for Vitroid. Values of 6 IR sensors of the Khepera II robot was translated into electrical stimulation pattern by an input interpreter.

### Closed-Loop Interaction

Electrical stimulation and detection of electrical activity of neurons were performed by multisite recording system for extracellular potentials (MED64 system, Alpha MED Science).

The current stimulation triggered certain internal state. The spatio-temporal patterns of action potentials evoked by different stimulations were not completely same as each other but fluctuated by each trials (fig.3). On the contrary, the patterns evoked by different electrodes were quite different. So we conclude that these different patterns were able to be used for determination of different actuator speeds.
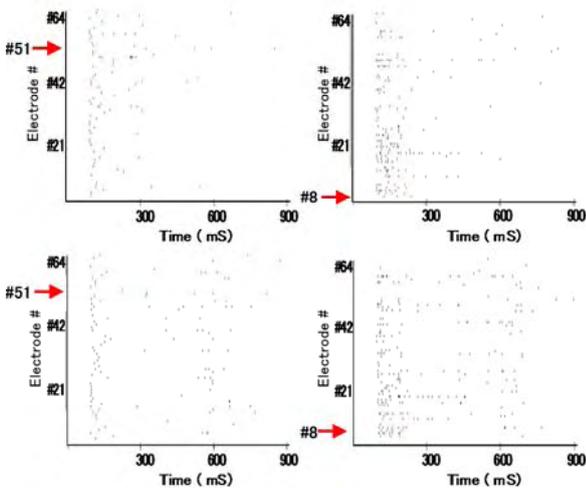


**Fig. 3.** An Example of spatio-temporal patterns of evoked action potentials. Graphs are raster plots of APs. Left panel shows patterns evoked by the stimulation to #51 electrode and Right shows patterns evoked by the stimulation to #8 electrode. Each response was recorded at different trials.

We designed Vitroid system to determine speeds of two actuators by output interpreter according to the spatial pattern of electrical activity of neurons. There are many candidate of such a translation algorithm. We currently adopted "self-tuning fuzzy reasoning" in this study. Fuzzy reasoning is not best much for the system because required function is a kind of a pattern recognition. We utilized a fuzzy reasoning unit as a generator of an in-between value of motor speed. The

system has two fuzzy reasoning units for input interpreters to determine stimulation patterns for two electrodes, and two parallel self-tuning simplified fuzzy reasoning units as output interpreters to control of the speed of Right and left actuators. The output interpreter received eight inputs from LNN. Each input is the number of detected action potentials per 50 ms time windows. These fuzzy controllers consist of 256 fuzzy rules with eight inputs (Fig.4). Each input has two types of fuzzy labels high-frequency and low-frequency. 256 fuzzy rules is too large and over spec for only two state recognition. But this large number of rules is in order to describe all classified patterns of action potentials in eight inputs. That is required rather for analysis of neuronal activity, not for control. The maximum frequency of the action potential in all electrodes is made the maximum of the horizontal axis of a membership function. The maximum membership function assigned to the high-frequency label is at three fourths of the points of maximum frequency, and the maximum of the membership function assigned to a low-frequency label was at one fourth of the points of maximum frequency. For simplification, each membership function for all 8 ch inputs is the same function currently.
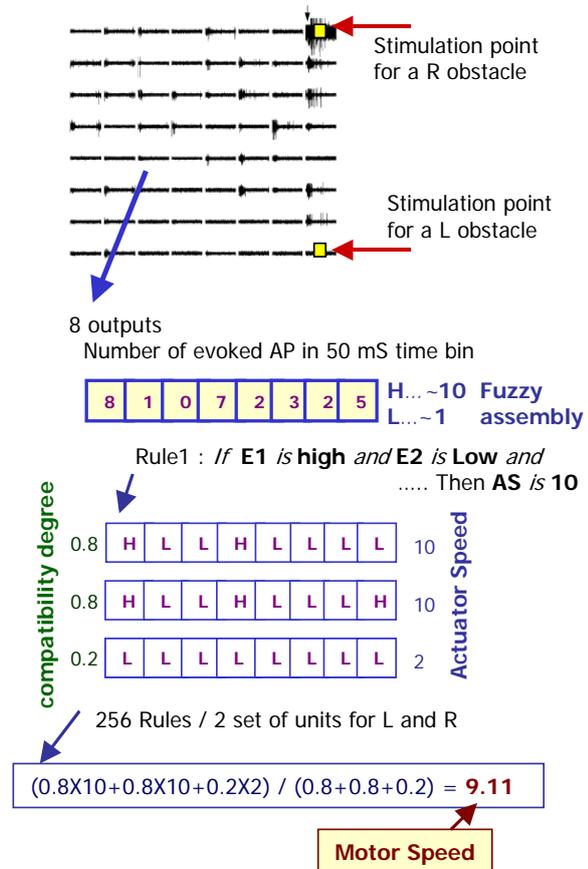


**Fig. 4.** Fuzzy reasoning used for pattern recognition.

Inputted pattern was compared to 256 pattern templates constructed by fuzzy rules. According to

similarity of inputted pattern to each template, compatibility degrees were calculated. Then a value of motor speed was decided as weighted average of value of consequent clause of each fuzzy rule.

Each value of consequent clause was tuned by supervised learning. The tuning is performed by minimization of differences between teacher signal and output value of output interpreter. Learning unit generates stimulation signals to a neuronal network and optimal speeds of actuators as a teacher signal. Then the system applied electrical stimulation to LNN and compared the output value of interpreter and teacher signal. This learning process make a coupling model of evoked pattern of action potentials in LNN and behavior of Vitroid in outside world.

**Implementation of Vitroid**

Vitroid was constructed by 5 independent programs and recording system for multiple-site extracellular potentials, and two computers (Fig. 5). The "Brain Server" program records electrical potentials and detects action potentials of neurons from 8 ch of electrodes. Fuzzy reasoning programs were implemented in an output and an input interpreter, respectively. The "Client" program controled the robot. The "multi Stimulator" program stimulates the neuronal network according to stimulation pattern command generated by an input interpreter. Programs exchange processing data information mediated by a datasocket transfer protocol (DSTP, National Instruments).
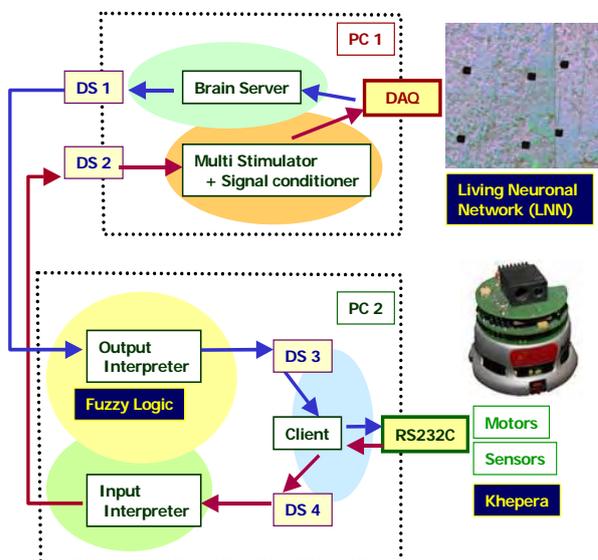


**Fig. 5.** Implementation of Vitroid.

## 2.2 Collision avoidance controlled by a LNN

Adequately tuned Vitroid succeeded in performing the zigzag run of between two walls arranged at parallel, without collision with a wall (Fig. 6). Inputs linked to "L-side obstacles" or "R-side obstacles" evoked reproducible pattern of electrical activity,

while spontaneous autonomous activity rather fluctuated during experiments. The spatiotemporal pattern of the network activity is determined not only by input stimulation but also spontaneous internal states of the network This is why the response of Vitroid was completely uniform.
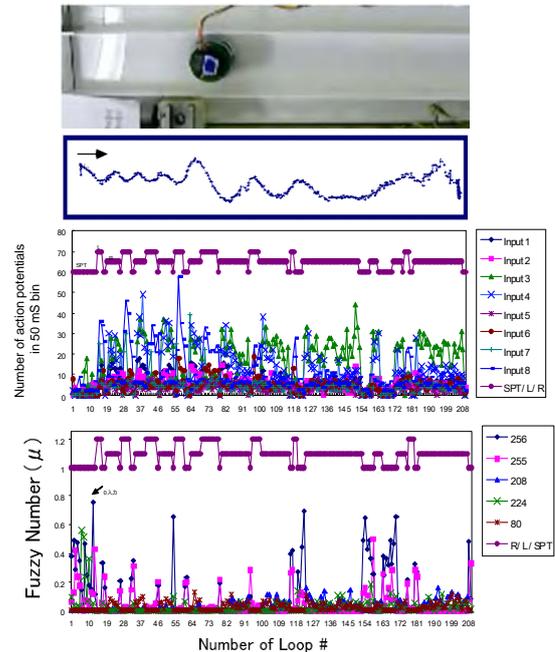


**Fig. 5.** Collision avoidance of Vitroid. Picture of experimental course, an example of trajectory of Vitroid, Number of action potentials evoked by sensory inputs and compatibility degrees (μ).

## 3 Conclusion

We integrated a LNN and a robot body using interpreters for a direct coupling type of closed-loop interaction. This cognitive system, Vitroid succeeded in performing collision avoidance. Vitroid is a good modelling system for novel synthetic intelligence.

**Acknowledgement**

**References**

[1] Bakkum D.J., Shkolnik A.C., Ben-Ary G., Gamblen P., DeMarse T.B. and Potter S.M. (2004) : Removing some 'A' from AI:Embodied Cultured Networks. In Embodied Artificial Intelligence.Edited by Iida F., Pfeifer R., Steels L. and Kuniyoshi, Y. New York, Springer. 3139 , 130–145

[2] R. Lewis C.I. (1929): Mind and the world order. C. Scribner's Sons., New York

[3] Kudoh S.N., Nagai R., Kiyosue K., and Taguchi T . (2001): PKC and CAMKII dependent synaptic potentiation in cultured cerebral neurons. Brain Research, 915(1), 79-87

# Long-term Activity-dependent Plasticity of Action Potential Propagation Delay and Amplitude in Cortical Networks

Douglas J. Bakkum[1], Zenas C. Chao[2], Steve M. Potter[3]*

1 University of Tokyo, Tokyo, Japan
2 RIKEN Brain Science Institute, Saitama, Japan
3 Laboratory for Neuroengineering, Coulter Department of Biomedical Engineering, Georgia Institute of Technology, Atlanta, Georgia, America
* Corresponding author. E-mail address: steve.potter@bme.gatech.edu

The precise temporal control of neuronal action potentials is essential for regulating many brain functions. From the viewpoint of a neuron, the specific timings of afferent input from the action potentials of its synaptic partners determines whether or not and when that neuron will fire its own action potential. Tuning such input would provide a powerful mechanism to adjust neuron function and in turn, that of the brain. However, axonal plasticity of action potential timing is counter to conventional notions of stable propagation and to the dominant theories of activity-dependent plasticity focusing on synaptic efficacies. Here, we used a multi-electrode array to induce, detect, and track changes in action potential propagation in multiple cortical neurons in vitro. We observed activity-dependent plasticity of propagation delays and amplitudes within minutes after applying patterned stimuli. The changes were activity-dependent because they did not occur when the same stimulation was repeated while blocking ionotropic GABAergic and glutamatergic receptors. Induced changes were stable because their expression persisted in the presence of the synaptic receptor blockers. We conclude that, along with changes in synaptic efficacy, propagation plasticity provides a cellular mechanism to tune neuronal network function in vitro, and potentially learning and memory in the brain.

## 1  Introduction

The precise temporal control of neuronal action potentials (APs) is essential for regulating many brain functions. It was recently shown in a detailed thalamo-cortical model that a single spike can alter activity across the entire cortex, within 2 seconds [1]. The specific timings and amplitudes of afferent input from the action potentials of a neuron's presynaptic partners determines whether or not and when that neuron will fire its own AP, and whether a synapse will strengthen or weaken, according to spike-timing dependent plasticity and other well-known synaptic mechanisms. We hypothesized that axonal plasticity of action potential propagation could vary how information is processed in the brain by regulating the timing and amplitude of synaptic input impinging on a neuron.

Axons in the mammalian cortex have traditionally been regarded as stable transmission cables. However, this view is more likely due to a lack of, rather than support from, experimental evidence [2] because their small diameter (<1 um) makes direct recordings at multiple sites difficult. Here we used cortical networks grown on MEAs to demonstrate AP propagation plasticity as an in vitro learning mechanism that may also be important in vivo. We observed the occurrence of activity-dependent plasticity of action potential propagation delays (up to 4 ms or 40% after

minutes and 13 ms or 74% after hours) and amplitudes (up to 87%) as they adapted to different patterns of stimulation. See also reference [3].

## 2  Methods

Dense cultures of neurons and glia were prepared and cultured from dissociated embryonic rat cortex as previously described [4]. We previously developed systems for stimulating and recording on any of an MEA's electrodes [5,6], and determined the types of pulses that are optimal for eliciting APs [7]. By adding synaptic blockers to the culture medium, we were able to track and quantify evoked APs that propagate non-synaptically through axons passing by two or more electrodes, which we call ***direct AP***s or dAPs. We used 3-4 week old cultures on 60-electrode arrays (MEA60, MultichannelSystems) and our MeaBench [6] software to induce, detect, and track for hours the changes in AP propagation in multiple neurons while different patterned stimuli were applied repetitively. The stimuli consisted of a probe pulse, delivered every 4 sec, preceded 2 sec by a "context" pulse. The location of the context electrode was varied every 40 min. The latencies of dAPs evoked by each probe were measured with ±10 μs precision, relative to the probe pulse. dAP amplitudes were measured to less than one μV by averaging. "Whole-dish probing"

(WDP) consisted of measuring responses to single pulses delivered to each electrode, in random order, at an aggregate rate of 10 Hz.

## 3 Results

In initial experiments done without blockers, we observed statistically significant changes of dAP propagation latencies and amplitudes when the context electrode was varied. There were no significant changes when the experiments were done with synaptic blockers present. In a second set of experiments (Fig. 1), we carried out WDP in the presence of blockers, after a 5 hr period of low-frequency patterned stimulation with blockers, then another WDP (with blockers) after a 5 hr period of the very same sequence of patterned stimulation with no blockers. Only the latter WDP showed statistically significant induced plasticity of latencies and amplitudes. These were up to ±13 ms or 74%, with dAP amplitude changes up to 87%. Thus, the induction of the observed plasticity required synaptic transmission, while its expression did not.

AP propagation plasticity provides a cellular mechanism to tune neuronal network function in vitro, and could be a hitherto unappreciated mechanism of learning and memory in the brain as important as changes in synaptic strength.
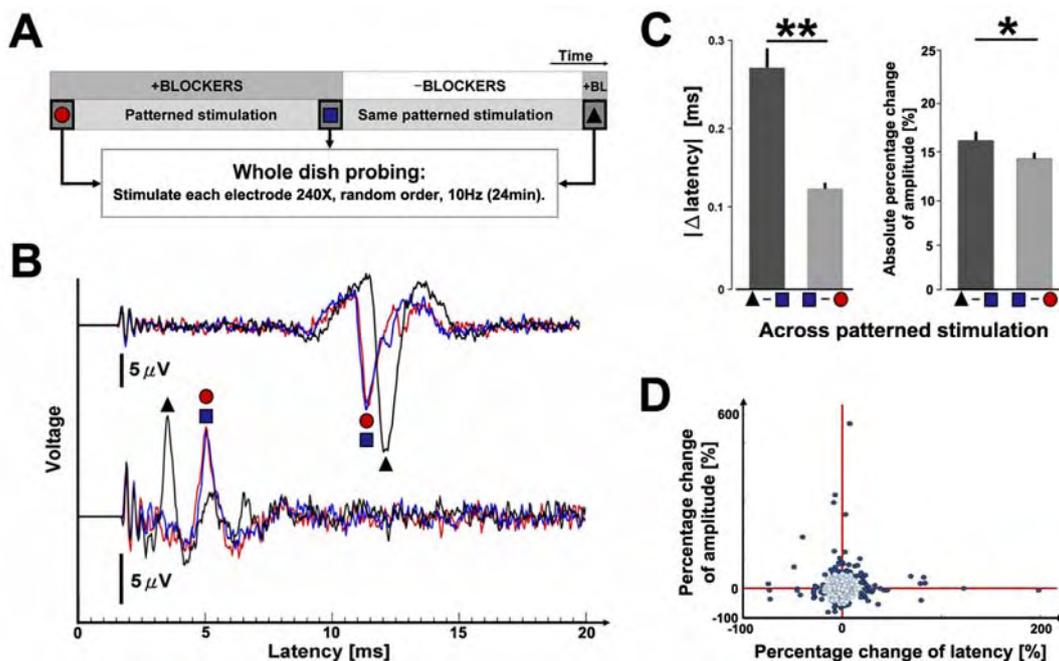


**Fig. 1.** Synaptic activity was needed to *induce* dAP latency and amplitude changes, while their *expression* was not dependent on synaptic transmission. (A) Experiment protocol. Synaptic APs were blocked to eliminate the influence of ongoing synaptic activity, and 3 identical periods of WDP (shape and color coded) were applied before and after the 5 hours and 20 minutes of patterned stimulation. (B) Example extracellular voltage traces for two separate dAPs during each whole-dish probing period (240 traces averaged). Changes that accrued during the patterned stimulation persisted (blue square to black triangle): they were not elastic reflections of ongoing synaptic activity. Changes were minimal during patterned stimulation in the presence of blockers (red circle to blue square): thus the significant changes were not artifacts from the electrical stimulation or from replacing media. (C) Statistics of dAP plasticity for all observations (mean + s.e.m. **P < 1e-6 and *P = 0.003. Wilcoxon signed rank test for paired samples. n = 904 dAP trains. 5 cultures from 3 dissociations). (D) Changes in latency were not monotonically correlated to changes in amplitude (P = 0.22, $\rho$ = 0.04; Spearman's rank correlation coefficient). The outlying data points, using an arbitrary cut-off at 10% of the distribution, were plotted with darker dots.

## References

[1] Izhikevich, E. M. & Edelman, G. M. (2008):. Large-scale model of mammalian thalamocortical systems. Proc Natl Acad Sci U S A, 105, 3593-3598..

[2] Debanne D (2004): Information processing in the axon. Nat Rev Neurosci 5: 304–316.

[3] Bakkum DJ, Chao ZC, Potter SM (2008): Long-Term Activity-Dependent Plasticity of Action Potential Propagation Delay and Amplitude in Cortical Networks. PLoS ONE 3(5): e2088

[4] Potter, S. M. & DeMarse, T. B. (2001): A new approach to neural cell culture for long-term studies. J. Neurosci. Methods, 110, 17-24.

[5] Wagenaar, D. A. & Potter, S. M. (2004): A versatile all-channel stimulator for electrode arrays, with real-time control. Journal of Neural Engineering, 1, 39-45.

[6] Potter, S. M., Wagenaar, D. A., & DeMarse, T. B. (2006): "Closing the Loop: Stimulation Feedback Systems for Embodied MEA Cultures." In M. Taketani & M. Baudry (Eds.), Advances in Network Electrophysiology using Multi-Electrode Arrays. (pp. 215-242). New York: Springer.

[7] Wagenaar, D. A., Pine, J., & Potter, S. M. (2004): Effective parameters for stimulation of dissociated cultures using multi-electrode arrays. Journal of Neuroscience Methods, 138, 27-37.

# Short-term plasticity in dissociated neuronal networks using paired-pulse stimulation

Pieter Laurens Baljon[1]*, Michela Chiappalone[2], Ildikó Vajda[3], Jaap van Pelt[3], Sergio Martinoia[1]

1 Department of Biophysical and Electronic Engineering, University of Genova, Genova, Italy
2 Department of Neuroscience and Brain Technology, Italian Institute of Technology, Genova, Italy
3 Department of Experimental Neurophysiology, Center for Neurogenomics and Cognitive Research, VU University, Amsterdam, the Netherlands
* Corresponding author. E-mail address: pieter.laurens@unige.it

To investigate the network response to trains of high-frequency stimulation, we started out with the shortest possible train: a pair of stimuli. We used networks of dissociated cortical neurons cultured on micro-electrode arrays. The research centred around the effects of one stimulus on the activity evoked by the other. Therefore we applied single stimuli as well as pairs, and compared the evoked activity. We investigated frequency dependence by modifying the distance between pulses in a pair in the range of 10-125ms (8-100Hz). In our protocols the two stimuli in the pair were applied from the same electrode, as well as from two separate electrodes.

## 1 Background

In this work we describe results from electrical-stimulation protocols consisting of pairs of pulses applied to cultured cortical networks. At the used inter-pulse intervals (IPI) we look for effects of the first pulse on the response to the second.

Such fast effects have received only limited attention at the network level, even though these effects presumably govern the frequency response of a network. As such, insight in these phenomena is important for understanding how networks respond to electrical stimulation.

We distinguish early and late responses using a window of 5-50 ms and 50-350 ms after the stimulus, respectively because the mechanisms governing short-term plasticity in immediately-evoked spikes may be different from those that govern short-term plasticity in evoked network bursts



**Fig. 1.** Stimulation protocols. The vertical grey bars indicate stimulus timing at the electrode indicated on the y-axis. Panel A and B show single and two-site protocols respectively. The horizontal axis also indicates IPI (IPI<10, 10<IPI<40 for the single-site protocol and IPI=66 and IPI=125ms for two-site) and the time between pairs T (T=5-10 seconds). The number N of pairs in a phase is 50 for the single-, and 300-400 for the two-site protocol.

## 2 Methods

### 2.1 Experimental Protocol

The experiments consisted of phases with spontaneous activity, phases with single test stimuli and phases with pairs of stimuli with identical parameters. The within-pair delay (IPI) was the variable of interest. The between-pair delay was 5 or 10 seconds; identical to the delay between test stimuli. We combined two datasets from experiments using networks of dissociated rat cortex cultured on micro-electrode arrays (MEAs). The two datasets comprised 14 and 8 experiments on 6 and 4 cultures respectively. For the first dataset the two pulses (biphasic pulses, 400$\mu$s per phase, 1V peak-to-peak) were applied at separate electrodes (two-site protocol, see Fig. 1B). In the second dataset, pulses (biphasic pulses, 250$\mu$s per phase, 1.5V peak-to-peak) were applied from a single electrode (single-site protocol, see Fig. 1A), and the protocol was repeated for 5 electrodes per experiment. In the first dataset we divided data in groups 'very short IPI' (IPI<10ms) and 'short IPI' (10<IPI<40ms). In the second dataset IPIs were 66 and 125ms.

### 2.2 Data analysis

We looked for an effect of the IPI on the size of the response. We quantified the response on an electrode by the average number of spikes after the test stimulus or second stimulus of the pair on that electrode. We excluded the stimulated electrode(s) and electrodes that showed no response. We made a distinction between the early and late response using a window of 5-50ms and 50-350ms after the stimulus respectively. The difference between the response to a

single stimulus, and to a pair was visualized in a scatter plot with the test response and the pair response on the horizontal and vertical axis respectively (see Figure 2). From this scatter plot we quantified the difference by counting the number of points above (suggesting potentiation) and below (suggesting depression) the diagonal. We assessed significance by testing whether the proportion of potentiation POP = #potentiated / (#potentiated + #depressed), differed from 0.5. Electrodes are either potentiated or depressed. That is, there is no 'no change' band around the diagonal.

## 3   Results

The panels in Figure 2 illustrate the response size at individual electrodes for both the paired-pulse protocol and the test stimulus for early- and late response (rows) at the four levels of IPI (columns). The loca-

tion of the point cloud with respect to the diagonal indicates whether an increase or decrease in the response size is more prominent. We did not test whether experiments were homogeneously distributed in the point clouds. Visual inspection indicated that there were no individual experiments greatly influencing overall outcomes. The early response (see Methods) is increased by IPIs up to 66ms; (IPI<10: POP=.68, n=93, p<.01, 10<IPI<40: POP= .67, NS, IPI=66ms: POP=.70, n=172, p<.01). This is presumably due to a de facto increased stimulation efficacy.

The effect for the late response goes two ways for increasing IPI. There is an increase (POP=.70, n=146, p<.01) for 10<IPI<40ms, but depression for IPI=125ms (POP=.24, n=242, p<.01). This is summarized in Figure 3.
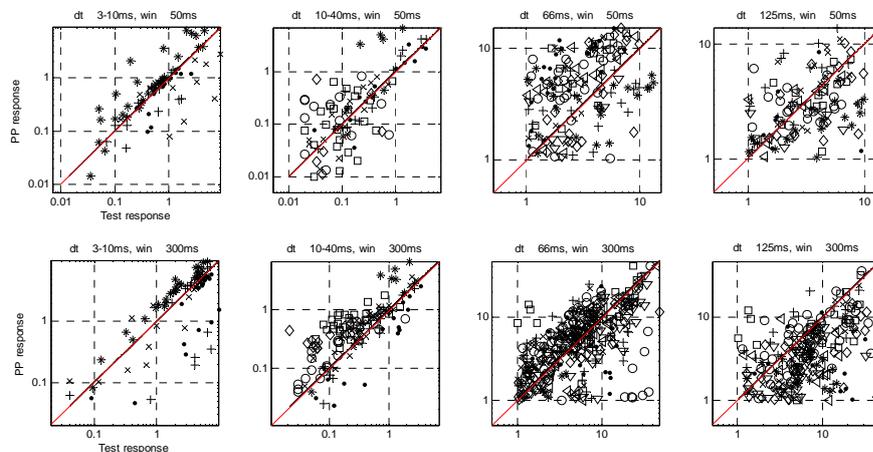


**Fig. 2.** Changes in the size of the response per electrode for different inter-pulse intervals. Symbols code for different experiments in a dataset. On the x-axis is the response size for the series of test stimuli and on the y-axis the response size for the paired-pulse protocol. The panels show results for different IPIs (columns) and early and late response (rows).
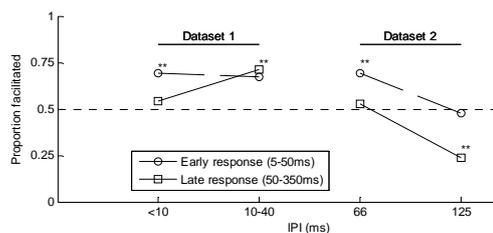


**Fig. 3.** Dependence on IPI of the facilitation in the early (dashed line) and late (solid line) response. The effect is expressed on the y-axis as the proportion of responses that increase with paired-pulse stimulation.

## 4   Conclusions

Our results confirm the frequency dependence of evoked activity, but they are new in that they describe higher frequencies (>100Hz). As might be expected, in general more stimulation yields more activity. But we also show that the potentiation effects are different for evoked spikes (early response) and evoked bursts

(late response). The data show the latter to have a strong frequency dependence exhibiting potentiation as well as depression when the second stimulus falls in the evoked burst. For the evoked spikes, potentiation seems to dissipate for an increasing inter-pulse interval; more similar to single-cell cell results [1].

At the same time, more work is necessary to separate neuronal mechanisms from changes in stimulus efficacy.

### References

[1]   R. S. Zucker and W. G. Regehr (2002): Short-term synaptic plasticity. *Annual Reviews Physiology, 64, 355-405*

# Synapsin knockout mice: an in vitro model of human epilepsy

Davide Boido[1], Pasqualina Farisello[1], Fabio Benfenati[1,2], Pietro Baldelli[2,1*]

1 Department of Neuroscience and Brain Technology, Italian Institute of Technology, Genova, Italy
2 Department of Experimental Medicine, Section of Physiology, University of Genova, Genova, Italy
* Corresponding author. E-mail address: pietro.baldelli@unige.it

Epilepsy has a strong genetic component [1] and mutant mice lacking synapsins (Syn), a family of abundant proteins of synaptic vesicles encoded by three genes (SYN I, II and III) implicated in the regulation of neurotransmitter release and synapse formation, are epileptic. The attacks appear in mice after the third month of age and their severity increases with age and with the number of inactivated SYN genes. We used micro-electrode arrays (MEAs) recordings to compare the neuronal network activity of hippocampal brain slices and primary neurons from wild-type (WT) and Syn knockout (KO) mice. We show the presence of sporadic spontaneous ictal discharges and a more intense electrically- or chemically-evoked epileptiform activity in KO mice with a clear age-dependent aggravation. Our results validate SynKO mice as an interesting experimental model of human genetic epilepsy in view of the recent identification of SYN genes mutations in patients with partial temporal lobe or frontal lobe epilepsy [2].

## 1 Introduction

Epilepsy is a neurological disorder that affects people in every country throughout the world. Up to 5% of the world's population may experience a seizure in their lives. About 40% of epilepsies have a genetic etiology. The dissection of the genetic basis of epilepsies has been so far very difficult due to the numerous genes involved [3]. Reports of epilepsy syndromes in humans that are associated with several nonsense and missense mutations in the synapsin (Syn) genes are increasing [2, 4]. In this scenario, in vitro models such as Syn knockout (KO) mice offer important clues on human epilepsy, representing one of the best approach to study neurophysiological mechanisms involved in the generation of spontaneous seizures and to test new antiepileptic drugs.

## 2 Materials and Methods

Horizontal cortical/hippocampal slices (0.3 mm thick) were obtained from 15 days-, 6 months- and 1 year-old WT and Syn KO mice. Slices were transferred over a planar MEA (500-30 TiN internal reference, Multi Channel System® - MCS, Reutlingen, Germany) coated with poly-ornithine (500μg/ml), and fixed by the use of a little platinum anchor. Experiments were performed at 34° C.

Hippocampal neurons extracted from embryos (E17) of both SynKO and WT mice, were cultured on planar MEAs (200-30 TiN, MCS) pre-treated with adhesion factors (Poli-L-Lysine and Laminin). Recordings were performed between 19 and 22 days *in vitro* (DIV) at 36.5° C.

### 2.1 Experimental Protocols

Network spontaneous activity were recorded and sampled at 10 kHz in both slices and cultured neurons for at least 20'. A 50' recordings, under treatment with the convulsant agent, 4-aminopyridine (4-AP; 200μM), was used to evaluate chemically-evoked epileptiform activity in both slices and cultures. To study electrically-evoked ictal discharges in hippocampal slices, a biphasic pulses (500μs @ ±4V) were delivered by MEAs micro-electrodes at the level of the entorhinal cortex by using a commercial general-purpose stimulus generator (MCS, STG 2008).

## 3 Results

SynKO cortical/hippocampal slices from 6 months old mice showed a clear epileptiform activity characterized by sporadic spontaneous interictal (I-IC) events and ictal (IC) discharges (Fig.1), which were absent in WT mice. An electrical stimulation applied at the level of the entorhinal cortex, completely ineffective in WT slices, elicited in most cases IC and I-IC waveforms in SynKO slices.

The application of the convulsant agent, 4-AP (200 μM) [5] to slices from young mice (15 days old) induced a sustained I-IC activity and rare IC discharges in both WT and SynKO slices (Fig.2). However, I-IC frequency recorded in SynKO (0.3 Hz) was higher than that recorded in the same region of WT (0.15 Hz) slices, while the analysis of IC incidence and frequency showed no marked changes comparing WT with SynKO slices.
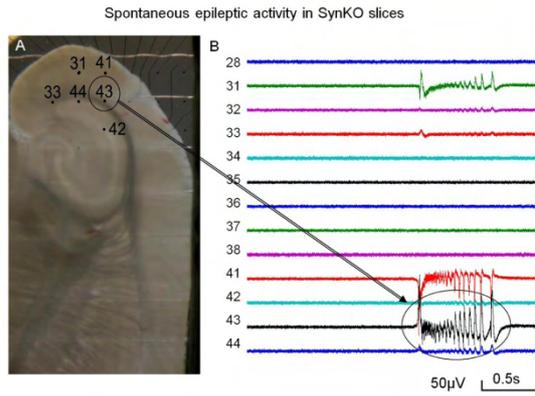
**Fig. 1.** Spontaneous IC discharges (B) recorded in acute horizontal brain slices (A) obtained from 3-months-old SynKO mice

The epileptiform activity of SynKO slices evoked by 4-AP stimulation, was also studied in slices obtained from older mice (1 year-old), revealing a clear age-related aggravation which paralleled the increase in the severity of the epileptic phenotype observed *in vivo*. The percentage of SynKO slices showing IC discharges further increased, while in WT slices IC were rarely observed. Interestingly, in 1 year old SynKO mice, IC events decreased their duration but maintained the same frequency observed in 15 days old animals.
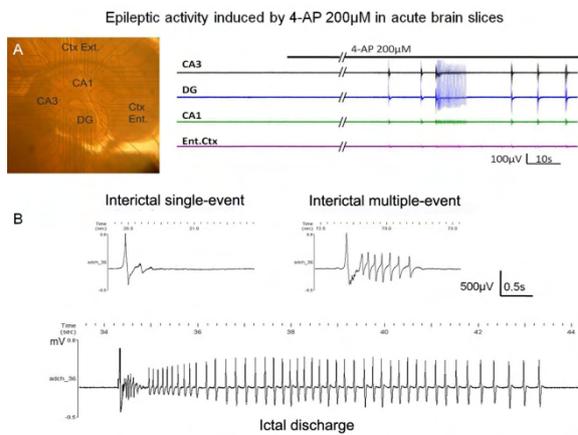


**Fig 2.** Pattern of electrical activity induced by 4-AP in different subfields of the brain slice: Entorhinal Cortex, DG. CA3 and CA1 (A) I-IC and IC events evoked by application of 4-AP 200 µM. (B) Some examples of the typical epileptic waveforms recorded from a brain slice in presence of 4-AP: I-IC single-event, I-IC multiple-event and an IC discharge.

The MEA approach was also used to study basal and 4-AP (100 µM) induced neuronal network activity in hippocampal primary cultures obtained from WT and SynKO mice embryos (Fig.3). Slow biphasic waveforms lasting 40-80 msec, similar to the I-IC events observed in slices, as well as sporadic, long-lasting (5-15 sec) IC discharges, were recorded in both WT and SynKO neuronal networks under 4-AP

treatment. The effect of the application of 4-AP 100 µM altered the electrical activity of SynKO cultures inducing a higher I-IC frequency in SynKO than in WT.
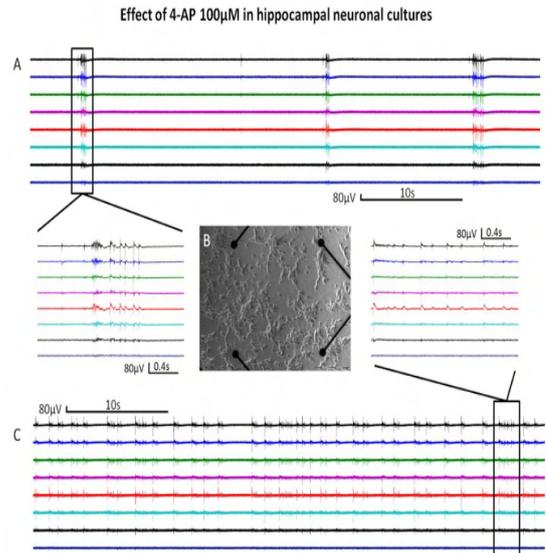


**Fig 3.** Pattern of electrical activity from (B) 20 DIV hippocampal neuronal cultures in control condition (A) and under treatment with 4-AP 100µM (C).

## 4   Conclusions

These preliminary results indicate that SynKO mice represent a reliable model of human epilepsy, useful to study how neuronal network hyperexcitabilty due to mutations in SV proteins leads to the development of epileptiform.

### References

[1] Noebels JL, (2003) The biology of epilepsy genes, Annual Review Neuroscience. 26: 599-625.
[2] C. C. Garcia, et al., (2004): Identification of a mutation in synapsin I, a synaptic vesicle protein, in a family with epilepsy *Journal of Medical Genetics, 41, 183-186.*
[3] O. K. Steinlein, (2004): Genetic mechanisms that underlie epilepsy. *Nature Reviews Neuroscience, 5, 400-408.*
[4] Cavalleri GL et al., (2007) Multicentre search for genetic susceptibility loci in sporadic epilepsy syndrome and seizure types: a case-control study. Lancet Neurol. 6:970-980.
[5] Avoli M, Louvel J, Kurcewicz I, Pumain R, Barbaroise M, (1996), Extracellular free potassium and calcium during synchronous activity induced by 4-aminopyridine in the juvenile rat hippocampus Journal Physiology 493.3: 707-717

# Constant Low Frequency Stimulation Shows Long-Term Response Changes in In-vitro Cortical Cultures During Development

Luca Leonardo Bologna[1,3*], Michela Chiappalone[1], Mariateresa Tedesco[2], Thierry Nieus[1], Sergio Martinoia[1,2]

1 Department of Neuroscience and Brain Technology, Italian Institute of Technology (IIT), Genoa, Italy
2 Neuroengineering and Bio-nanoTechnology Lab (NBT), Department of Biophysical and Electronic Engineering, University of Genoa, Genoa, Italy
3 Department of Communication, Computer and System Sciences, University of Genoa, Genoa (Italy)
* Corresponding author. E-mail address: luca.bologna@iit.it

Micro Electrode Arrays (MEAs) lend themselves to a careful investigation of the dynamics bound to the re-organization of cortical cells after dissociation. The analysis of electrophysiological activity changes during the in-vitro development gained an increasing interest in recent years [1][2]. Although a first study on the response to low-frequency stimulation has been carried out [3], a detailed analysis of how the long-term response to a low-frequency stimulus changes over weeks is still missing. Here, we present such a study by comparing the activity of the pre- and post-stimulus phase of five constantly stimulated cultures. As control study, we also report the spontaneous activity changes of one culture belonging to the same batch of the stimulated ones, which never underwent electrical stimulation.

## 1 Methods

### 1.1 Cell preparation

Cultures of dissociated cortical neurons were obtained from cerebral cortices of embryonic rats (E18), through enzymatic (0.125% trypsin solution for 25–30 min at 37 °C) and mechanical dissociation. Cells were plated onto 60-channel (one electrode used as internal reference) TiN-SiN MEAs (Multi Channel Systems, Reutlingen, Germany) at the final density of about 1600-2000 cells/mm$^2$.

### 1.2 Experimental protocol

Nine cultures from the same batch were monitored over four weeks in-vitro. The activity of the cultures was measured twice a week from 10 up to 28 days in vitro (div).

Four cultures were never stimulated and their only spontaneous activity was recorded for 30 minutes during every recording session. Five cultures were stimulated with a low frequency stimulus (0.2 Hz, biphasic pulse, 1.5V peak-to-peak amplitude), delivered sequentially from eight sites (three minutes per site). Thirty minutes of spontaneous activity were recorded before and after the stimulation phase during every recording session. The percentage increment of the Mean Firing Rate and the Mean Bursting Rate were observed in the phases preceding and following the stimulus.

## 2 Results

### 2.1 Stimulated and not-stimulated cultures show similar behavior over weeks

The Mean Bursting Rate (MBR) of cultures belonging to the same preparation undergoes similar changes over weeks. As representative examples we report in Fig. 1 and Fig. 3, the MBR changes of two cultures which were, respectively, never stimulated and constantly stimulated during their development (see Methods for further details).
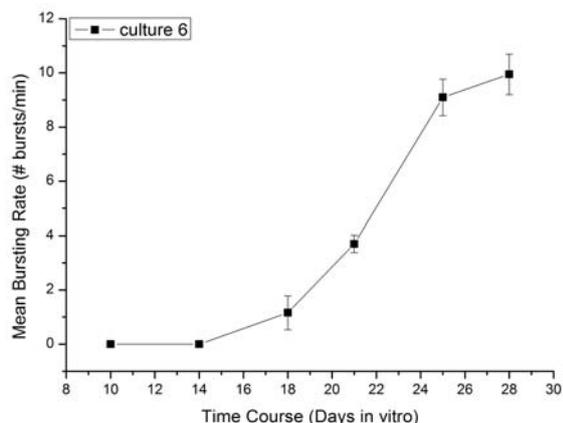


**Fig. 1.** Mean Bursting Rate changes of a never-stimulated culture over weeks
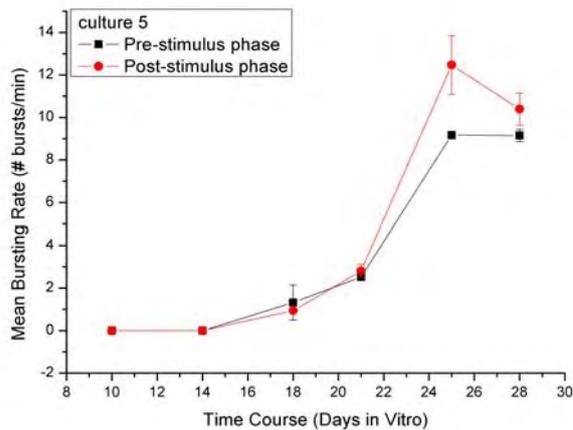
**Fig. 2.** Mean Bursting Rate changes of a constantly-stimulated culture over weeks. Both the values of the pre- and post-stimulus phases are shown

## 2.2 Low-frequency stimulation shows long-term activity changes over weeks

We stimulated five cultures during four weeks in vitro, twice a week, and observed the changes in the spontaneous activity before and after the application of the stimulation protocol (see Methods for further details).

Despite not all the cultures incremented their firing rate during all the developmental period after stimulation (see Fig. 3, cultures 1 and 4, div 25) we observed that, starting from the 21st div, the Mean Bursting Rate of all the observed cultures actually increased (see Fig. 4). Statistical tests confirmed that, after the 21st div, the differences between the pre- and post-stimulus Mean Bursting Rate were statistically significant (data not shown).
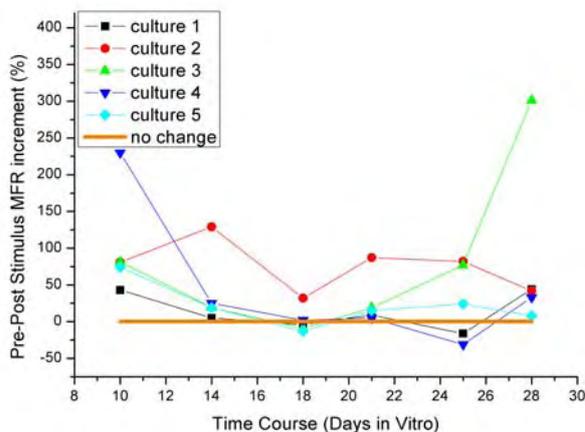


**Fig. 3.** Percentage increment of the Mean Firing Rate in the post-stimulus phase with respect to the pre-stimulus one.



**Fig. 4.** Percentage increment of the Mean Bursting Rate in the post-stimulus phase with respect to the pre-stimulus one.

## 3   Conclusions

Cultures of dissociated neurons develop over time by changing their patterns of activity. As an appropriate means to understand when the cultures themselves start to significantly respond to external stimulation in a stable way, we constantly applied a low-frequency stimulus twice a week starting from the second week in vitro. We observed that, although every cultures has its own behaviour during the first weeks, after the 21st day in vitro, the constant low-frequency stimulation drive the networks to increase their Mean Bursting Rate for at least 30 minutes.

### References
[1]   M. Chiappalone, M. Bove, A. Vato, M. Tedesco, S. Martinoia (2006): Dissociated cortical networks show spontaneously correlated activity patterns during in vitro development. Brain Research, 1093, 41-53
[2]   J. Van Pelt, I. Vajda, I., P.S. Wolters, M. Corner, G.J.A. Ramakers, G.J.A. (2005): Dynamics and plasticity in developing neural networks in vitro. Prog Brain Res, 147, 171-188.
[3]   I. Vajda, J. Van Pelt, P.S. Wolters, M. Chiappalone, S. Martinoia, E. J. W. van Someren, A. van Ooyen (2008): Low-frequency stimulation induces stable transitions in stereotypical activity in cortical networks. Biophys J, March, in press.

# Neuron Network Activity Scales Exponentially with Synapse Density

Brewer G[1, 2*], Boehler M[1], Pearson, R[1], DeMaris A[1], Wheeler B[3]

1 Medical Microbiology, Immunology and Cell Biology,
2 Neurology, Southern Illinois University School of Medicine, Springfield, IL USA
3 Bioengineering Department and Beckman Institute, University of Illinois at Urbana-Champaign, Beckman Institute, Urbana, IL USA
* Corresponding author. Email gbrewer@siumed.edu

In cortical brain networks, synaptic scaling appears to adjust the sum of synaptic inputs to produce a characteristic rate of synaptic output (1), especially important during a certain critical period of development (2). The output of a neuronal network as a function of synaptic inputs has not been explicitly determined during the course of development. Here we measured the development of synaptic density in cultured hippocampal neurons over a 3 week period in two serum-free media and correlated the expected increase in synapses with the increase in spontaneous spike rates to determine whether spike rates increase linearly or at a higher power in developing neuronal networks.

## 1 Methods

In order to increase synaptic development in the serum-free medium Neurobasal/B27™, we optimized three additional components previously shown to promote synaptic development: creatine (3), estrogen (4), and cholesterol (5). The primary hippocampal neurons were isolated from E18 rat embryos and cultured at 37°C in an atmosphere of 5% $CO_2$, 9% $O_2$ on substrates coated with poly-D-lysine. For measurement of electrical activity, neurons were cultured at 500 cells/mm$^2$ on multi-electrode arrays. Signals were acquired through an MEA 1060-BC amplifier (gain 1100, filtered at 8-3000Hz, sampled at 25 kHz) and MCRack software (Multichannel Systems). Signals were also analyzed with PCLAMP 9.0 software. At 1,2, and 3 weeks after plating, in the same culture conditions, spontaneous spike activity was detected in a one-minute recording period as the number of spikes with amplitude exceeding five times the standard deviation of the baseline noise. Cultures of E18 hippocampal neurons were plated at 160 cells/mm$^2$ on glass slips for immunostaining of synaptophysin, NR1, GLUR1 and GABA$_{AB}$ at synapses. One-half medium changes every 4 days were performed. Recordings and immunostains were collected at 1, 2, and 3 weeks.

## 2 Results

Once optimized, the resultant medium that we call NbActiv4™ (BrainBits LLC) produced higher spike rates earlier (2-fold after one week and two weeks) than the parent Neurobasal/B27™ (Fig. 1). At 3 weeks of development, spike rates were 8-fold higher in NbActiv4™ than Neurobasal/B27™ (Fig.

1). We immunostained separate cultures for the presynaptic protein synaptophysin and the postsynaptic AMPA receptor GluR1. Analysis of these puncta indicated that synaptic density increased with time in culture, and to higher levels in NbActiv4™ than Neurobasal/B27™ (data not shown). Similar increases were noted for NMDA receptor and GABA$_{A\beta}$ receptor puncta, but the increase in excitatory transmitter receptors (GluR1 and NR1) exceeded that for the inhibitory GABA receptor in NbActiv4™ compared to Neurobasal/B27™ (data not shown). We determined the efficacy of the developmental increase in synapses by correlating the increase in synaptic density to the increase in spike rates (Fig. 2). For neuronal networks in Neurobasal/B27™, spike rate scaled as a power function of synapses with a coefficient of 2.8. For networks cultured in NbActiv4™, the exponent was 75% larger at 4.9.

## 3 Conclusions

The higher exponent for neurons in NbActiv4™ indicates how important optimized nutrients are to biological function and that early development allows increases in characteristic rate. Many other factors such as ion channel densities and their control by kinases are integral to the process of transforming synaptic input into action potential information, but we used synapse density as a marker for a necessary early component on the input side of information processing. Although our cultures were seeded at a low density to more easily resolve synapses in a plane, the synapse density achieved varied with developmental time and nutrients up to 1500 synapses/neuron with

spike rates averaging 5 Hz. By comparison, development of the internet has continued to grow exponentially, while the volume of data transmitted has grown even faster (Gilder's Law), in support of Metcalfe's Law that the value of the network grows with the square of the connectivity (*6*). Since brain data transmitted as spikes scales at a higher exponent, as shown here in two-dimensional networks, the mammalian brain in 3 dimensions is likely to scale information transfer at an even higher function of synapses. In the mammalian brain, synapses per neuron are estimated at 8000 in the mouse cortex, 18,000 in the rat hippocampus and 50,000 in the human cortex (7). Even though our brain is slow by computer standards, a clear processing advantage is evident by raising the 50,000 connections/neuron to a higher power.

**Acknowledgement**

**References**

[1]   K. R. Leslie, S. B. Nelson, G. G. Turrigiano, *J. Neurosci* **21**, RC170 (2001).
[2]   T. K. Hensch, *Nat. Rev Neurosci* **6**, 877 (2005).
[3]   G. J. Brewer, T. W. Wallimann, *J Neurochem* **74**, 1968 (2000).
[4]   G. J. Brewer, J. D. Reichensperger, R. D. Brinton, *Neurobiol Aging* **27**, 306 (2006).
[5]   C. Goritz, D. H. Mauch, F. W. Pfrieger, *Mol. Cell Neurosci* **29**, 190 (2005).
[6]   http://www.jimpinto.com/writings/techlaws.html

[7]   V. Braitenberg, A. Schuz, in *Cortex: Statistics and geometry of neuronal connectivity*, Springer, Ed. Berlin, 2004), pp. 19-35
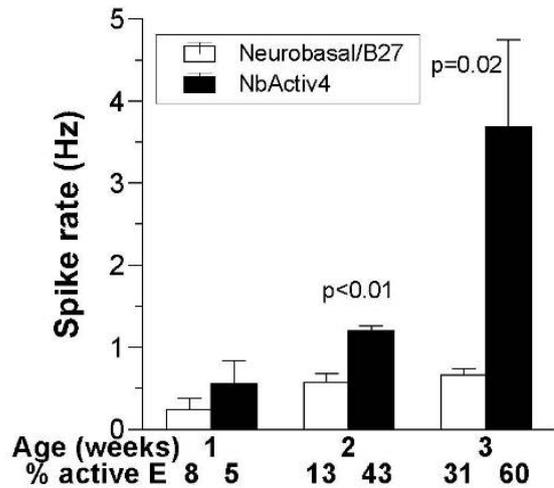


Fig. 1. Spontaneous activity of neurons cultured in Neurobasal/B27 (open bars, n=16) or NbActiv4 (closed bars, n=16) with activity over 0.03 Hz.
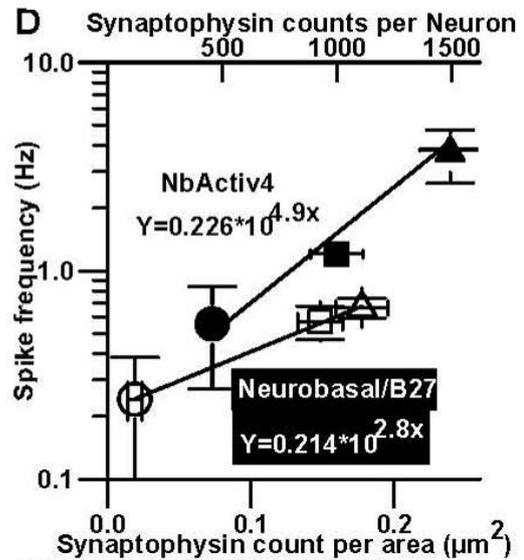


**Fig 2.** Action potential frequency per synaptophysin density increases at an exponential rate. Spike frequency for neurons cultured in NbActiv4 (closed point symbols, $R^2 = 0.983$, n=16) increases exponentially as a function of synapses 1.75 times that in Neurobasal/B27 (open point symbols, $R^2 = 0.999$, n=16). The data were collected at developmental day 7 (circles), 14 (squares), and 21 (triangles).

# Shaping Goal-directed Behaviour of Embodied Cultured Networks with Electrical Stimulation

Zenas C Chao[1], Douglas J Bakkum[2], Steve M Potter[3*]

1 RIKEN Brain Science Institute, Saitama, Japan
2 University of Tokyo, Tokyo, Japan
3 Laboratory for Neuroengineering, Coulter Department of Biomedical Engineering, Georgia Institute of Technology, Atlanta, Georgia, America
* Corresponding author. E-mail address: steve.potter@bme.gatech.edu

We developed an adaptive training algorithm, whereby an *in vitro* neocortical network learned to modulate its dynamics and achieve pre-determined activity states within tens of minutes through the application of patterned training stimuli using a multi-electrode array. *A priori* knowledge of functional connectivity was not necessary. Instead, effective training sequences were continuously discovered and refined based on real-time feedback of performance. The short-term dynamics in response to training became engraved in the network, requiring progressively fewer training stimuli to achieve the same results. Interestingly, a given sequence of stimuli did not induce the same plasticity, let alone desired activity, when replayed to the network and no longer contingent on feedback. The results suggest that even though a cultured network lacks the 3-D structure of the brain, it can learn, through shaping, to show meaningful behaviour.

## 1 Introduction

To study learning and memory *in vitro* promises to reveal basic mechanisms of network processing and information storage. Because MEA cultures are easily accessed and manipulated optically, physically, chemically, and electrically, they will allow links to be made between functional and morphological plasticity. We embodied dissociated cortical networks interfaced to computers with MEAs by allowing them to control the behaviour of a simulated animal (animat) or robot (hybrot) whose sensory system delivers electrical stimuli to the networks in a closed-loop fashion [1]. We developed a learning protocol in which desired animat behaviour is gradually shaped toward a goal criterion by delivery of spatio-temporally patterned stimuli. This low-frequency (~3Hz) training stimulation differs from most studies of cultured networks, where plasticity was induced by high frequency tetanic stimulation. Continuous low-frequency background stimulation (~3Hz) was applied to stabilize accumulated plasticity [2]. The shaping protocol was first tested in a simulated model network of leaky integrate-and-fire neurons with STDP and frequency-dependent synapses [3]. It was then validated in living MEA cultures.

## 2 Methods

Dense neuro-glial cultures were prepared and cultured from dissociated embryonic rat cortex as previously described [4]. The network simulation was the same one used in [2] and is described in detail in the supplement to [3]. The neurally-controlled animat moved in a round field according to the network response to a probe pulse that followed a *Context-control Probing Sequence* (CPS). If the movement was in the desired direction, *Shuffled Background Stimulation* (SBS) was delivered at an average of 3Hz. For incorrect behaviour, repeating spatiotemporal sequences of *Patterned Training Stimulation* (PTS) were delivered for 6 sec (also 3Hz average). PTSs were chosen from a large set of randomly generated sequences, with a probability that was updated according to how successful that PTS was at shaping correct behaviour (Fig. 1).

## 3 Results

The goal for the animat was to move toward the center of the field. In most cases, the animat learned to move correctly after a few minutes of closed-loop training (Fig. 2A). Failed learning proved to be due to poor choice of probe electrode location. With both the simulated and living networks, we showed that no successful learning resulted when the exact sequence of stimuli from a previously successful experiment were played back to the same network (Fig. 2B). Learning required closed-loop feedback that was contingent on the animat's moment-to-moment behaviour, and lasted over an hour.

# 4 Conclusion

Stimuli of a few pulses, chosen from a random set of spatiotemporal patterns, when delivered at the right time in the right context, can gradually shape
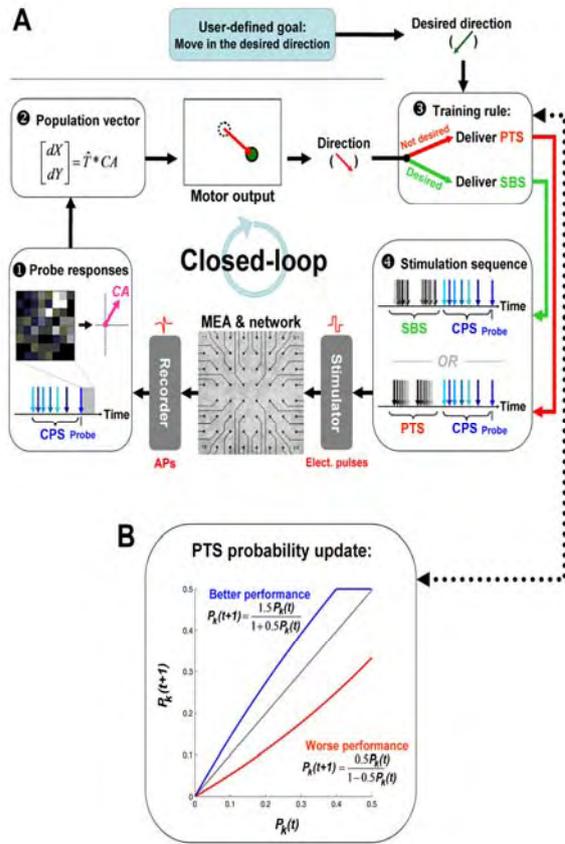


**Fig. 1. A**. ❶ A single probe electrode was repetitively stimulated every 6 seconds. After each stimulus, 100 msec of evoked responses were recorded to form the 2-D Center of Activity (CA) vector. ❷ The CA was transformed ($\hat{T}$) into incremental movement [$dX$, $dY$]. ❸ If movement was within ± 30º of the user-defined desired direction, a shuffled background stimulation (SBS) was delivered. Otherwise, a set of patterned training stimulation (PTS) was delivered. ❹ Context-control probing sequences (CPS) were delivered after SBS or PTS and before each probe. **B**. For unsuccessful movement, a PTS ($PTS_k$) was selected from a pool of 100 possibilities. The probability of each PTS ($P_k(t)$) being chosen later ($P_k(t+1)$) increased (blue) or decreased (red) depending on the success of the motor output.

behaviour of non-layered (dissociated) cortical networks. Short-term functional changes on which the sensory feedback is based are converted to long-term learning. Similar training algorithms may work in the human brain to help it adapt to artificial sensory input delivered to the cortex with an MEA, for example, proprioception signals from an artificial limb.

**Acknowledgement**
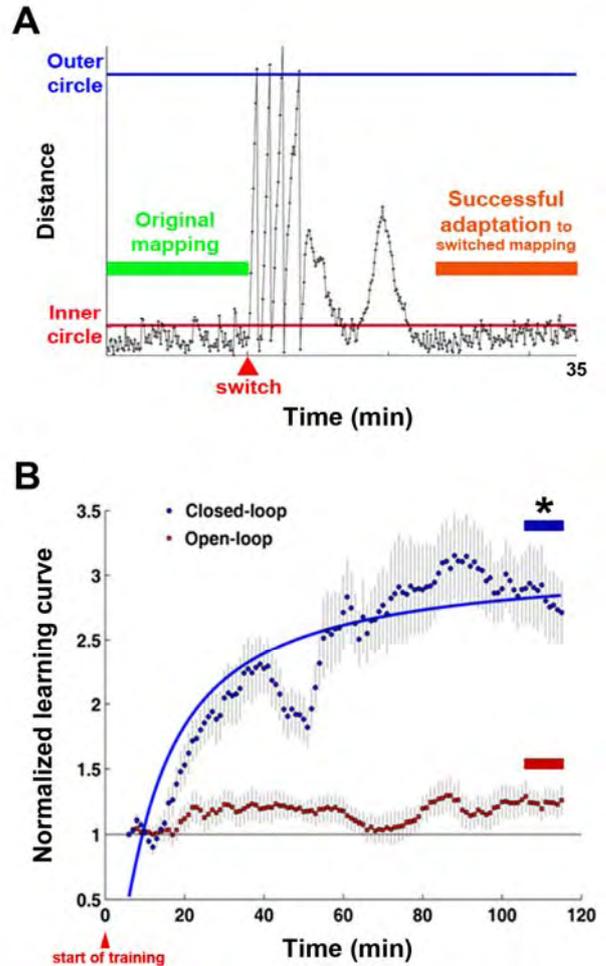
**Fig. 2. A.** Learning curve for animat controlled by simulated LIF network. At the "switch", the sensory mapping of location to desired direction was reversed, and the correct movement was re-learned in a few min. **B.** Average learning curve for 23 experiments on animats controlled by 6 living networks. When stimulation sequences were replayed to the networks (open-loop), independent of behaviour, no learning resulted.

## References

[1] Potter, S. M., Wagenaar, D. A., & DeMarse, T. B. (2006). Closing the Loop: Stimulation Feedback Systems for Embodied MEA Cultures. In M. Taketani & M. Baudry (Eds.), Advances in Network Electrophysiology using Multi-Electrode Arrays. (pp. 215-242). New York: Springer.R. da Pisa A. (1298): Le Livre des merveilles du monde. Poky Archive, 1, 1-99

[2] Chao, Z. C., Wagenaar, D. A., & Potter, S. M. (2005). Effects of random external background stimulation on network synaptic stability after tetanization: a modeling study. Neuroinformatics, 3, 263-280.

[3] Chao, Z. C., Bakkum, D. J., & Potter, S. M. (2008). Shaping Embodied Neural Networks for Adaptive Goal-directed Behavior. PLoS Computational Biology, 4(3): e1000042

[4] Potter, S. M. & DeMarse, T. B. (2001). A new approach to neural cell culture for long-term studies. J. Neurosci. Methods, 110, 17-24.

# Long term network plasticity in cortical assemblies

Michela Chiappalone[1,2*], Paolo Massobrio[2], Sergio Martinoia[2,1]

1 Department of Neuroscience and Brain Technology, Italian Institute of Technology, Genova (Italy)
2 Department of Biophysical and Electronic Engineering, University of Genova, Genova (Italy)
* Corresponding author. E-mail address: michela.chiappalone@unige.it

To investigate distributed synaptic plasticity at cell assembly level, we used dissociated cortical networks from embryonic rats grown on grids of 60 extracellular substrate-embedded electrodes (Micro-Electrode Arrays, MEAs). We developed a set of experimental plasticity protocols based on the pairing of tetanic bursts with low frequency stimuli (< 1Hz), delivered through two distinct channels of the array (i.e. associative tetanic stimulation In/Out Phase). We tested our protocols on a large dataset of stable cultures, selected on the basis of their initial level of spontaneous firing and their capability of evoking spikes as a consequence of low frequency test stimuli. We found that the associative protocol seems to produce more repeatable results and it is able to induce potentiation more than no change or depression in the majority of cultures.

## 1 Introduction

Experimental investigations on the electrophysiological behavior shown by neuronal assemblies represent a fundamental step towards understanding the universal mechanisms of brain coding, learning and memory. As recently reported [1, 2], to understand such universal basis, it is important to investigate how plasticity develops at network level. To address this issue, we used networks of dissociated cortical neurons directly grown onto Micro-Electrode Arrays (MEAs). After a few days in culture, neurons connect with each other with functionally active synapses and form a random network that displays spontaneous electrophysiological activity in the form of highly complex temporal patterns, ranging from isolated/random spiking to robust and rhythmic bursting behavior. The spontaneous activity changes spontaneously during the in vitro development [3] and can be modulated by chemical and electrical inputs [4], producing short and/or long-term effects in the in synaptic efficacy and network dynamics.

## 2 Materials and Methods

Cortical neurons extracted from rat embryos (E18) were cultured on planar arrays of 60 TiN/SiN electrodes (Multi Channel Systems® - MCS, Reutlingen, Germany), pre-treated with adhesion factors (Poli-L/D-Lysine and Laminin).

The experimental set-up is based on the MEA60 System (MultiChannelSystems, Reutlingen, Germany). Details about the methods can be found in [3].

### 2.1 Experimental protocol

We developed an experimental protocol based on four steps of stimulation:

1. Test stimulus 1. Delivery of a test stimulus from six-eight sites serially (50 biphasic pulses, 1.5V pp 250μsec single-phase duration, frequency 0.2Hz).
2. Test stimulus 2. Repetition of point 1 (stability).
3. Tetanic stimulation. Three types:
   a. Single tetanus, delivered from one channel, chosen among the ones used for the test stimulus.
   b. Associative tetanus In Phase. A tetanus and a train of pulses at 0.2 Hz (falling in the middle of the tetanic burst) were delivered simultaneously from two stimulation sites.
   c. Associative tetanus Out Phase. A tetanus and a train of pulses at 0.2 Hz (in correspondence of the silent period between two bursts of the tetanus) were delivered simultaneously from two stimulation sites.
4. Test stimulus3. Comparison of the evoke responses for each channel.

### 2.2 Processing technique

Extracellularly recorded spikes are usually embedded in biological and thermal noise and they can be detected using a threshold based algorithm [5]. To investigate the neural activity evoked by stimulation, we computed the post-stimulus time histogram (i.e. PSTH), which represents the impulse response of each site of the neural preparation to electrical stimulation. The PSTHs were calculated by taking 600-msec time windows from the recordings that follow each stimulus. We then counted the number of spikes occurring in a 2-4msec bin and divided this measure by the number of stimuli [6].

## 3 Results

Each cortical culture of our dataset was tested for stability, then the evoked responses before and after the application of the plasticity protocol were compared. The changes induced by the application of the plasticity protocol (Fig. 1) were evaluated by using both the Post Stimulus Time Histograms (i.e. PSTHs) and the map of the effective connections [7].
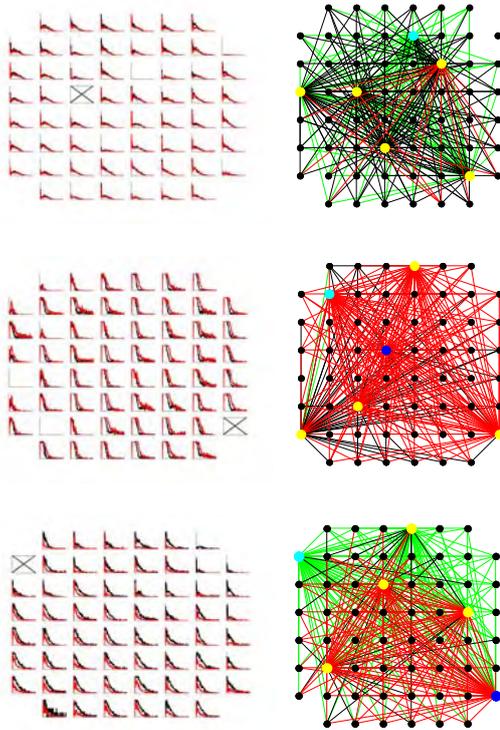


**Fig. 1.** PSTH 8x8 map and effective connectivity map for three representative experiments. Top: single tetanus. Center: In-phase. Bottom: Out-phase. Left: the PSTH map, reproducing the layout of a square MEA, reports the pre (black) and post-tetanus (red) histogram for each recording electrode. The 'X' indicates the stimulating electrodes. Right: the effective connectivity maps represents the amount of the changes in terms of evoked response induced by a specific plasticity protocol (green: depression, red: potentiation, black: no change). The coloured circle stand for the stimulating electrodes, the light blue is the electrode chosen for the tetanus delivery, the dark blue is the associative low-frequency stimulation electrode. Note that the in-phase protocol (center) is the one producing the highest level of potentiation.

The main results we obtained can be summarized as follows: (i) low frequency stimuli produce neither short nor long-term changes in the evoked response of the network; (ii) the associative tetanic stimulations are able to induce plasticity in terms of significant increase or decrease of the evoked activity in the whole network; (iii), the amount of the change (i.e. increase or decrease of the evoked firing) strongly depends upon the specific features of the applied protocols (Fig. 2); (iv) the potentiation induced by the in-phase associative protocol has long-term effects (i.e. hours).

## 4 Conclusions

The obtained results demonstrate that large *in vitro* cortical assemblies display Long Term Network Potentiation (LTNP), a mechanism supposed to be involved in the memory formation at cellular level. We think that this study could represent a first step towards understanding the plastic properties at neuronal population level [8].
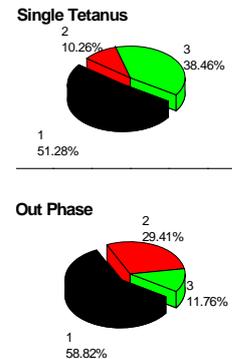


**Fig. 2.** Comparison of the three plasticity protocols applied to our entire dataset. The in-phase associative protocol is the only one producing the higher level of potentiation and no depression.

### References

[1] S. Marom and G. Shahaf, (2002): Development, learning and memory in large random networks of cortical neurons: lessons beyond anatomy. Quart Rev Biophys, 35, 63-87.

[2] S. Marom and D. Eytan, (2005): Learning in ex-vivo developing networks of cortical neurons. Prog Brain Res, 147, 189-199.

[3] M. Chiappalone, M. Bove, A. Vato, M. Tedesco, and S. Martinoia, (2006): Dissociated cortical networks show spontaneously correlated activity patterns during in vitro development. Brain Res, 1093, 41-53.

[4] M. Chiappalone, A. Vato, L. Berdondini, M. Koudelka-Hep, and S. Martinoia, (2007): Network dynamics and synchronous activity in cultured cortical neurons. Int J Neur Sys, 17, 87-103.

[5] A. Vato, L. Bonzano, M. Chiappalone, S. Cicero, F. Morabito, A. Novellino, and G. Stillo, (2004): Spike Manager: a new tool for spontaneous and evoked neuronal networks activity characterization. Neurocomputing, 58-60, 1153-1161.

[6] F. Rieke, D. Warland, R. de Ruyter van Steveninck, and W. Bialek, (1997): Spikes: exploring the neural code. Cambridge, Massachusetts: The MIT Press.

[7] O. Sporns, D. R. Chialvo, M. Kaiser, and C. C. Hilgetag, (2004): Organization, development and function of complex brain networks. Trends Cogn Sci, 8, 418-425.

[8] M. Chiappalone, P. Massobrio, and S. Martinoia, (2008): Network plasticity in cortical assemblies. Eur. J. Neurosci., in press.

# Measuring late phase LTP and imaging nuclear calcium signals in acute slices of genetically modified rats

Freitag HE[1*], Hofmann F[2], Bengtson CP[1], Weislogel J[1], Bading H[1]

1 Department of Neurobiology, Interdisciplinary Center for Neurosciences (IZN), University of Heidelberg, Heidelberg, Germany
2 Multi Channel Systems MCS GmbH, Aspenhaustrasse 21, D-72770, Reutlingen, Germany
* Corresponding author. E-mail address: freitag@nbio.uni-heidelberg.de

Long term potentiation (LTP) of the schaffer collateral pathway in the hippocampus is the most studied from of plasticity in the mammalian brain. To understand how information is stored in the brain requires more knowledge not only about the initiation of LTP but also about the criteria necessary for the establishment of the late phase of LTP. We made stable long term recordings (>5h) from acute hippocampal slices using microelectrode arrays (MEAs). In this study we demonstrate that acute hippocampal slices of genetically modified rats can be used to dissect signaling pathways important for the induction and maintenance phases of L-LTP.

## 1 Introduction

Since the discovery that central nervous system synapses have the ability to alter their synaptic strength as a response to changes in synaptic activity, the term synaptic plasticity has become one of the most studied concepts in neurophysiology. Long term potentiation (LTP) in schaffer collaterals of the hippocampus is NMDA receptor-dependent and, once initiated, persistent for hours to days and serves therefore as a model for learning and memory. Much interest is focused on the initiation of LTP but less is known about the mechanisms which make LTP persist for such extended time periods. This is partly due to the difficulty of maintaining stable recordings over several hours from acute slice preparations. Planar electrodes embedded into the surface of MEAs offer stable extracellular field recordings from up to 60 points on a brain slice [1]. In this study, we demonstrate that LTP recordings using MEAs provide a suitable technique to dissect the signalling pathways important for the induction and maintenance phases of LTP in acute slices of genetically modified animals.

## 2 Material and Methods

We established field EPSP recordings from acute hippocampal slices of rats (6 – 7 weeks old) on MEAs which remained stable for 5 hours and longer. Two different input pathways to CA1 cells were stimulated with alternating biphasic voltage pulses at one stimulus per minute for each pathway. The optimal stimulation strength (30-50% of the response maximum) was determined by an input/output (I/O) curve with pulses ranging from 500mV to 3V. After 40 minutes of baseline recording, either one or four tetanic stimulations (HFS, 100Hz, 1s) were applied to one pathway, the other one was used as an internal control. After the induction of LTP, the responses of the slices were recorded for an additional four hours or longer. After this period, the same I/O curve as before was acquired again. From these two I/O curves, the relationship between EPSP slope and population spike amplitudes for electrodes in the CA1 cell layer was determined.
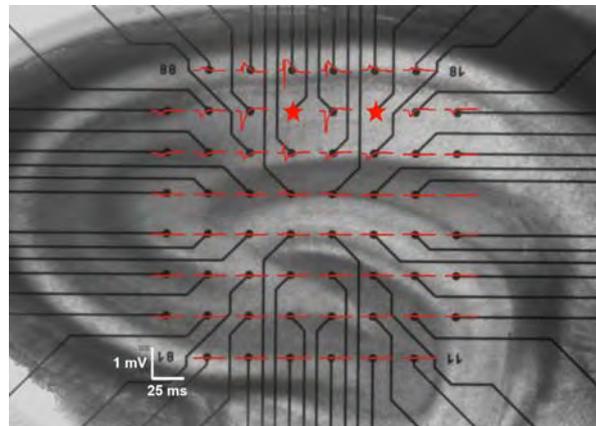


**Fig. 1** An acute hippocampal slice from a p37 rat positioned on a MEA. Shown in overlay (red traces) are signals recorded on all 60 electrodes in response to stimulation (100μs, 1.0 V) by electrode 57 (row, column coordinates relative to bottom right corner "11").

In some experiments acute slices were perfused with actinomycin D (25 μM) or anisomycin (25 μM) to block transcription or translation, respectively. Both blockers were bath-applied for at least 100 min including a baseline recording period of 40 min before LTP was induced.

To generate genetically modified rats, recombinant adeno-associated viruses (AAVs) were injected stereotaxically into the hippocampus of 22 day old animals. After an expression period of two weeks sev-

eral slices per hemisphere showed a large fraction of infected cells in the CA1 pyramidal cell layer and LTP experiments were performed.

Calcium imaging was done on an inverted microscope with a 40x oil objective using thin MEAs (180 µm thick). GCaMP2.0 fluorescence was excited with 470-490nm light from a monochromator (Polychrome II), detected with a CCD camera (Imago) and analysed using TILLvisION imaging software.

## 3 Results and Discussion

### 3.1 LTP recordings

We established two high frequency stimulation (HFS) paradigms which induced either a decaying form of LTP persisting only for about 2h (1x 100Hz, 1s, data not shown), or a long lasting LTP that was stable over the whole recording period (> 4h, late phase LTP (L-LTP), 4x 100Hz, 1s) in accordance with previously published results [1]. To further validate our protocols and to strengthen the power of our technique for late phase LTP recordings we tested anisomycin (25 µM) to block translation. Acute slices stimulated four times with 100Hz in the presence of anisomycin showed early-LTP (E-LTP) which declined back to baseline within 1 to 2h (Fig. 2). Thus late phase LTP recorded with MEAs requires translation, as reported previously [2]. These results serve to validate the MEA system for the induction and stable recording of late phase LTP.
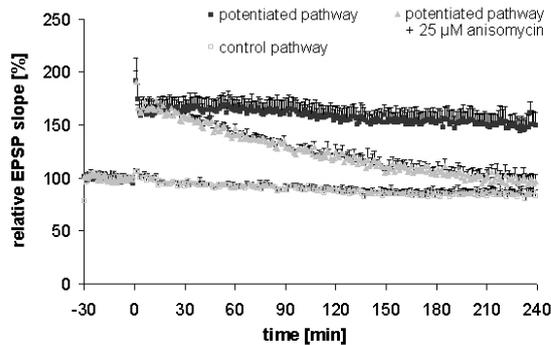


**Fig. 2** LTP recordings from MEAs. LTP was induced in the CA1 cell layer at time 0 with four high frequency stimulations (4x 100Hz, 1s) in the presence (grey) or absence (black) of the translational blocker anisomycin (25 µM).

### 3.2 Acute hippocampal slices of genetically modified animals

We generated genetically modified rats by stereotaxic injection of gene constructs designed to interfere with intracellular signalling pathways important for the establishment of L-LTP [3]. Target genes were

identified by gene chip analysis as being induced or repressed after the induction of LTP in culture [4]. Gain-of-function and loss-of-function experiments are currently underway to address the role of these genes in the maintenance phase of L-LTP.

In other experiments we are using the genetically encoded and nuclear localized $Ca^{2+}$ indicator GCaMP2.0-NLS to visualise and quantify nuclear calcium transients evoked during the induction of LTP by HFS. Parallel imaging and LTP recordings from the same slice revealed small nuclear $Ca^{2+}$ transients in response to single trains of HFS while subsequent HFS repetitions evoked much larger responses (data not shown).
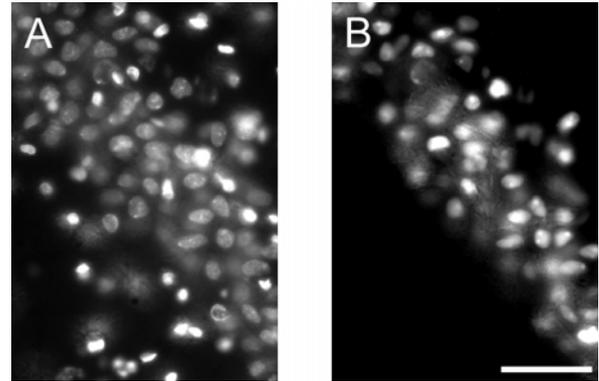


**Fig. 3** CA1 pyramidal cell layer of a 300 µm thick hippocampal slice of a p36 rat two weeks after stereotaxic injection of viruses expressing a nuclear localized GFP. A) Nuclear staining; B) GFP fluorescence; (bar: 70 µm).

## 4 Summary

We have previously shown that we are able to record LTP using MEAs for 5 h and longer. In this study we used the translational blocker anisomycin to inhibit L-LTP. This implicates *de novo* protein translation in the maintenance of LTP as previously demonstrated with traditional extracellular electrophysiological techniques. These results provide further evidence that MEA recording techniques are useful to explore especially the late phase of LTP.

To interfere with candidate proteins mediating the signalling pathways important for the maintenance phase of LTP we have established techniques for stereotaxic injections of adeno-associated viruses into the hippocampus. This method allows us to analyse late phase plasticity in acute hippocampal slices of genetically modified animals.

**References**
[1] F. Hofmann, H. Bading (2006); *J.Physiol Paris, 99, 125-132*
[2] U. Frey *et al.* (1988); *Brain Res, 452, 57-65*
[3] A. Cetin *et al.* (2006); *Nat Protoc., 6, 3166-3173*
[4] S. Zhang *et al.* (2007); *Neuron, 4, 549-62*

# Immunostaining for Identification of Neuronal-Impulse Pathway on Multielectrode Arrays

Daisuke Ito*, Hiroki Tamate, Masafumi Nagayama, Tsutomu Uchida, and Kazutoshi Gohara

Division of Applied Physics, Graduate School of Engineering, University of Hokkaido, Sapporo, Japan
* Corresponding author. E-mail address: ditoh@eng.hokudai.ac.jp

Immnuostaining of neurons cultured on Multi-electrode arrays (MEAs) is investigated on different dissociated density. Low density (< 500 cells/mm2) is effective to observe individually cell nuclei, dendrites, axons, etc. Even though low density cultured neurons show characteristic temporal activities such as spontaneous, synchronized, and bursting firings. The universal change of average firing rates is revealed regardless of different densities. Using both methods of imaging by immnuostaining and recording by MEAs, impulse pathways through neural networks might be identified. A preliminary experiment based on long term measurements more than one month is presented.

## 1 Introduction

Multi-electrode arrays (MEAs) are an optimal tool for identification of the pathways of neuronal networks. Using MEAs, the spatiotemporal dynamics of the networks have been measured. From the temporal point of view, it has been revealed that dissociated neurons have intrinsic features of impulses such as spontaneous firing and synchronized bursting [1, 2]. From the spatial point of view, the morphological changes of neurons on MEAs have been observed by 2-photon time-lapse microscopy [3]. However, there have been few studies about how the impulses visible on MEAs are transmitted in neuronal networks, especially in terms of spatial morphology. The aim of this study was to investigate how to clarify neuronal-impulse pathways on MEAs spatially.

## 2 Materials and Methods

To identify pathways, we developed a novel recording system of network dynamics. This system consists of MEAs for measurement of neuronal impulses and optical microscopy for time-lapse observation. For identification of the pathway in detail, we used immunostaining on MEAs with low-density cultivation to visualize neuronal connectivity clearly.

Primary neurons derived from rat cortex were plated on an MED probe (Alpha MED Science) at low densities (< 500 cells/mm$^2$). The MED probe was filled with glial conditioned medium and kept in a CO2 incubator. Spontaneous firings of neurons were recorded for more than one month (Fig.1). For time-lapse observation, the MED probe was filled with the medium and was then sealed with a sterile cover slip. The MED probe was kept on the microscope stage with an MED connector. After cultivation, cells were fixed and stained (Fig. 2).
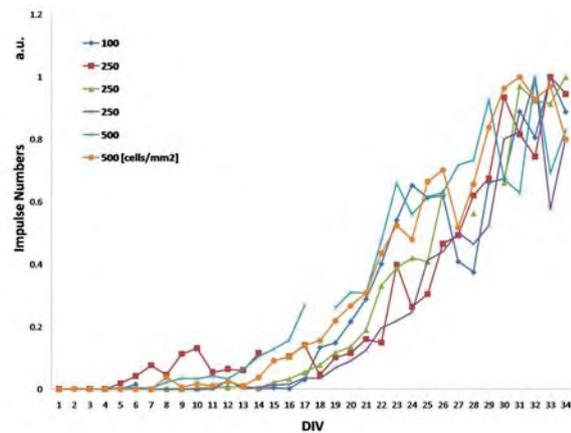


**Fig. 1.** Averaged impulse numbers in days in vitro measured during 5miniutes every day under different density of cultivation on 64 channel-MED probe. Each graph is normalized with each maximum. The universal change is shown in graphs regardless of densities.

## 3 Results and Discussion

At an early stage (about 5-10 DIV) of culture, spontaneous random firing was detected in some electrodes with the low-density culture. Then, average firing rates gradually increased, and synchronized bursting began to arise over many electrodes within several days (Fig. 1). These features of a neuronal network in a low-density culture resembled those in a high-density culture (see [4]). We revealed the universal changes in graphs regardless of densities. In such a low-density culturing condition, neuronal networks including cell bodies, dendrites (green) and axons (red) were clearly recognized with immunostaining (Fig. 2).
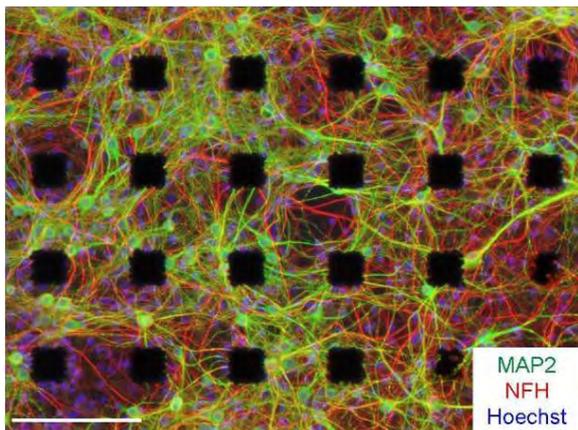
**Fig. 2**. An example of immunostaining micrograph of neuronal network cultured 34 DIV on MEAs. Neurons were stained with antibodies to MAP2 (green) and to NFH (red) to identify neuronal cell bodies, dendrites and axons, respectively. Cell nuclei were also stained with Hoechst 33342 (blue). Bar = 200 μm.
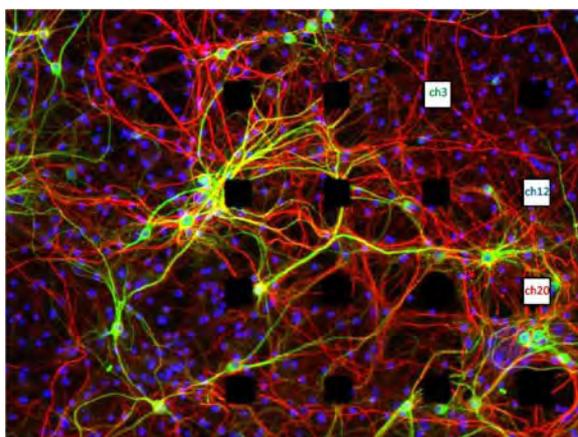


**Fig. 3.** Another example of immunostaining micrograph of neuronal network cultured 32 DIV on MEAs. This shows identified neuronal-impulse pathway. An axon mounted over three electrodes, ch3, ch12, and ch20.

Because the input and output of neuronal impulses was visible by immunostaining, the impulse pathways could be specified on MEAs to some extent using recorded firings from each electrode. For example, we recognized that an axon mounted over three electrodes (Fig. 3). In these electrodes, we detected repetitions of spontaneous neuronal impulse at a same time with a precision of 1 msec (Fig. 4). These results indicate the impulses detected at the three electrodes were derived from the axon mounted on the electrodes and suggest that how the impulses transmitting through the network could be identified [5].

Although, it cannot be denied that impulses were derived from another axon circuit to various directions, these results show that immunostaining in a low-density culture of neurons on MEAs is effective at identifying the neuronal-impulse pathways. Based on these preliminary results, we begun to develop further advanced system.
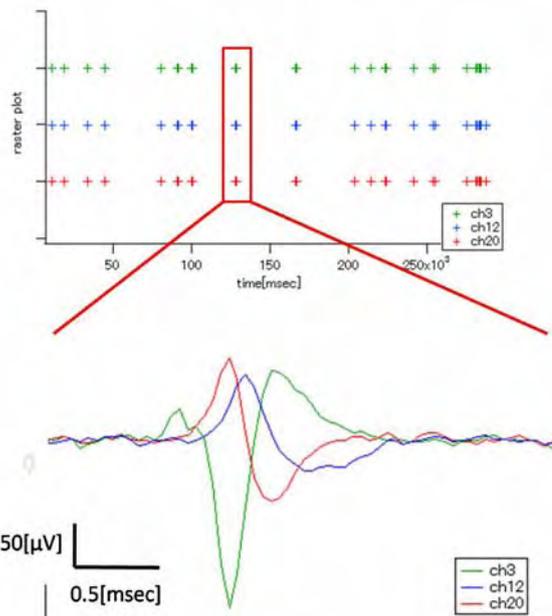


**Fig. 4.** Raster plot (above) shows synchronized temporal sequences at ch3, ch12, and ch20. The impulses were detected at three different positions at almost the same time. Law data (below) shows sequential response with high precision at 0.05ms.

## Acknowledgement

## References

[1]   H. Kamioka, E. Maeda, Y. Jimbo, H. P. C. Robinson, A. Kawana, (1996) : Spontaneous periodic synchronized bursting during formation of mature patterns of connections in cortical cultures. *Neurosci. Letters, 206, 109-112*

[2]   M. Chiappalone, M. Bove, A. Vato, M. Tedesco, S. Martinoia, (2006) : Dissociated cortical networks show spontaneously correlated activity patterns during in vitro development. *Brain Res., 1093, 41-53*

[3]   S. M. Potter, N. Lukina, K. J. Longmuir, Y. Wu, (2001) : Multi-site two-photon imaging of neurons on multi-electrode arrays. *Proc. SPIE, 4262, 104-110*

[4]   D. A. Wagenaar, J. Pine, S. M. Potter, (2006) : An extremely rich repertoire of bursting patterns during the development of cortical cultures. *BMC Neurosci. , 7, 11*

[5]   E. C. Tinture , J. Pine,(2002) : Extracellular potentials in low-density dissociated neuronal cultures. Journal of Neuroscience Methods, *117, 13-21*

# Structure-function relations in generic neuronal networks

S. Kandler[1,2*], A. Wörz[1,3], S. Okujeni[1,2], J. E. Mikkonen[4], J. Rühe[1,3], and U. Egert[1,5]

1 Bernstein Center for Computational Neuroscience, Albert-Ludwigs-University Freiburg, Germany
2 Neurobiology and Biophysics, Inst. of Biology III, Albert-Ludwigs-University Freiburg, Germany
3 Chemistry and Physics of Interfaces, Dept. of Microsystems Engineering, Albert-Ludwigs-University Freiburg, Germany
4 Department of Signal Processing, Tampere University of Technology, Tampere, Finland
5 Biomicrotechnology, Dept. of Microsystems Engineering, Albert-Ludwigs-University Freiburg, Germany
* Corresponding author. E-mail address: steffen.kandler@bccn.uni-freiburg.de

Higher brain functions depend on the transmission and integration of information within cortical networks. We are interested in how far such activity dynamics are affected by the structural features of the underlying neuronal circuitry and vice versa. To investigate this relation, we performed simultaneous microelectrode array and patch-clamp recordings in dissociated cortical cultures. This work shows details on how neurons are embedded into the dynamics and circuitry of larger generic networks.

## 1 Methods

Cortical tissue obtained from neonatal wistar rats was dissociated and cultured on polyethylene imine-coated microelectrode arrays (MEA) following standard procedures [1,2] (Fig. 1). After maturation, networks had an average neuron density of about 2,000 cells per $mm^2$. Cultures were maintained in MEM supplemented with heat-inactivated horse serum (HS, 5%), L-glutamine (0.5 mM), and glucose (20 mM) in a humidified atmosphere at 37°C and 5% CO2. Medium was partially replaced twice per week.
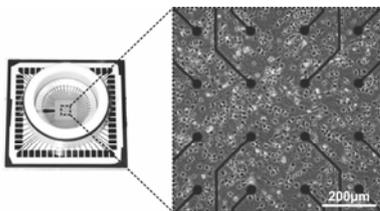


**Fig. 1.** Neuronal culture on MEA after 21 days in vitro.

Simultaneous MEA and paired patch-clamp recordings in whole-cell configuration were conducted outside the incubator at 35°C with a slow perfusion (100 µl/$min^{-1}$) of carbogenated (95% O2, 5% CO2) culture medium without HS supplement.

The neuron-to-neuron connectivity was analyzed based on subthreshold responses in a potential postsynaptic neuron to evoked action potentials (AP) in the potential pre-synaptic neuron. Array-wide burst detection was performed on all single MEA channel burst onset times. Participation in such network events was then detected in a window of max. 1 sec after network burst onset. Data was obtained from 21 cultures and 12 preparations. Analyses were performed with MATLAB using MEA-Tools [3] and FIND [4].

## 2 Results

Neuronal activity was almost exclusively comprised of synchronous network events. Individual cultures displayed subsets of bursts that had spatiotemporal patterns such as shorter bursts or phases of high-frequent bursting (Fig. 2).
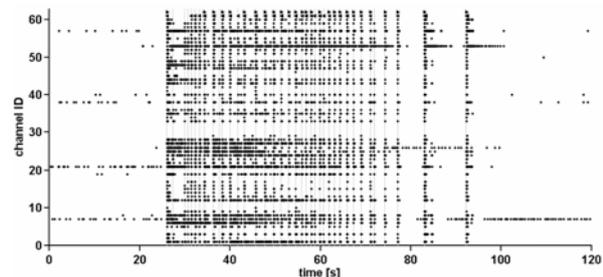


**Fig. 2.** Dot display of a characteristic network bursting phase in a simultaneous MEA and patch-clamp recording. (● APs on MEA channels (1-60), ◄ and ► APs on intracellular channels (61-62), | detected burst onsets).

The resting membrane potentials of the analyzed neurons (n=92) ranged from -46.2 mV to -78.3 mV (mean=-61.9 mV). A holding potential of -50 to -60 mV was applied to neurons with resting potential above -50 mV. The time constants ranged from 5.7 ms to 33.4 ms (mean=16.4 ms). Normal input-frequency properties were found for the analyzed neurons (data not shown).

Individual neuron pairs (n=10) were analyzed with respect to their embedding into network events (Fig. 3A). Activity was comprised of subthreshold responses to network input or single spikes and shorter bursts (Fig. 3B). No neurons were found to initiate network events. In general, activity was confined to network events only (mean=89%; mean MEA=81%; Fig. 3C). The first intracellular AP in network events had a mean delay of 43 ms (Fig. 3D). Mean rate of

burst participation was about 56%, but we also found neurons that participated in all detected network events or that had a high failure rate of 91% (Fig. 3E).

We tested pairs of neurons (n=46) for their inter-connectivity by detecting potential postsynaptic responses to evoked presynaptic AP (Fig. 4).

Of all neuron pairs, 54% were connected. 17% of the tested pairs had unidirectional excitatory connections, 9% unidirectional inhibitory ones. 28% had reciprocal connections. 46% of all pairs were not connected (Fig. 5).

Furthermore, we identified a high degree of connectivity on a range of lesser than 250 μm. Compared to the intact cortex, this indicates a high recurrent connectivity which might foster the synchronized bursting characteristic for such networks.
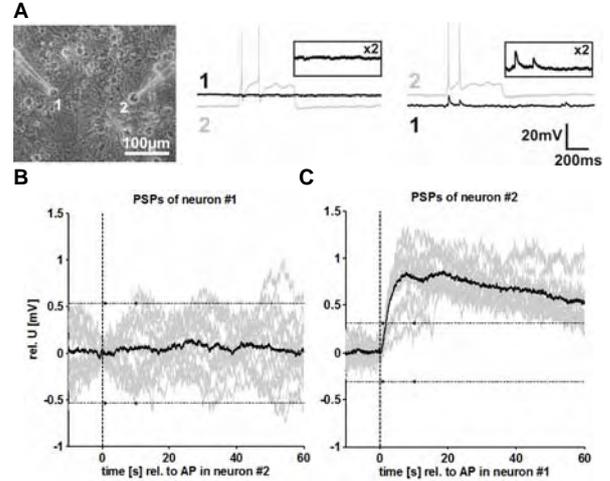


**Fig. 4. A.** Neuron-to-neuron connectivity of patched neuron pairs. Presynaptic APs were evoked by current stimulation (100-200 pA, 25-500 ms). After spike-triggered averaging, postsynaptic potentials (PSP) were detected based on a threshold criterion (5x SD of mean pre-AP signal amplitude; 1-11 ms after evoked AP). **B.** No PSP detection; neuron #2 did not synapse with neuron #1. **C.** PSP detection; neuron #1 had an excitatory connection with neuron #2.
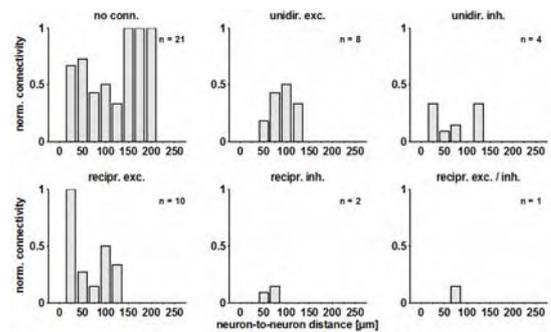


**Fig. 5.** Normalized unidirectional and reciprocal synaptic connections with respect to the linear distance between patched neuron pairs.



**Fig. 3. A.** Top: Burst profile of a patch-clamped neuron relative to network burst onset (black=mean). Mid: Normalized intracell. spike histogram. Bottom: Normalized extracellular rate profile. **B.** Participation of two neurons in network events. **C.** Ratio of spikes within network events for MEA (1-60) and two intracellular Channels (61-62). **D.** Delay distribution of intracellular APs relative to network event onset (black=median). **E.** Participation (i.e. min. 1 AP) in network events in intracellular recordings.

## 3 Conclusions

Our results show how neurons structurally and functionally integrate into larger generic networks. In particular, we found that individual neurons variably contribute to synchronized network events, which might explain the spatiotemporal patterns of bursting.

### References

[1]  Shahaf & Marom (2001), J. Neurosci. 21(22):8782-8788.
[2]  Potter & DeMarse (2001), J. Neurosci. Meth. 110(1-2):17-24.
[3]  Egert et al. (2002), J. Neurosci. Meth. 117(1):33-42.
[4]  Meier et al. (2007), Proc. 7th Ger. Neursci. Meeting, 1212.

# Effect of Short- and Long-term Electrical Stimulation on Network Behavior

David B. Khatami[1,2*], Gregory J. Brewer[4], Bruce C. Wheeler[1,2,3]

1 Department of Electrical and Computer Engineering, University of Illinois at Urbana-Champaign, Urbana, IL. USA
2 Beckman Institute, University of Illinois at Urbana-Champaign, Urbana, IL. USA
3 Department of Bioengineering, University of Illinois at Urbana-Champaign, Urbana, IL. USA
4 Department of Medical Microbiology and Immunology, Southern Illinois University, Springfield, IL. USA
* Corresponding author. e-mail address: khatami@uiuc.edu

Microelectrode array technology has been very useful in investigating the dynamics of neuronal networks as it provides a means of monitoring and manipulating many elements in the network simultaneously. This has lead to a great body of work in understanding the complex activity patterns that develop in primary neuronal cultures. In recent years however, more interest and effort has been placed on discovering the mechanisms responsible for learning and plasticity and the role that electrical stimulation plays in inducing such changes. This report highlights a number of experiments aimed at investigating the effect of short- and long-term electrical stimulation on network responsiveness. The frequency of stimulations has been found to greatly influence response desensitization on a short time scale while long-term stimulations are found to produce more rapid development and a higher level of activity in primary cultures of hippocampal neurons.

## 1  Introduction

The techniques for maintenance and manipulation of dissociated neuronal cultures have received much attention over the years as they provide good frameworks for the study of neuronal interaction and computation *in vitro*. The ability to create a well characterized interface between biological neuronal networks and electronics is highly desirable as this interface will not only pave the path to better understanding neuronal behavior but also has many practical applications in neural prosthetic and biosensor design. By combining knowledge and utilizing techniques from cell biology, electronics and microfabrication, our main goal is to investigate and contribute to the understanding of neuronal network dynamics and plasticity. Here, we report on experiments designed to study the influence of electrical stimulation on network dynamics. Patterned protein deposition on microelectrode surfaces allows us to engineer neural networks with a high degree of precision which in turn provides us with greater control over the complexity as well better ability to interface cells with electrodes. We have been able to demonstrate that neuronal networks can be patterned for extended periods of time and that a first order map of functional connectivity can be constructed and analyzed. This report primarily focuses on changes that occur in the activity and responsiveness of patterned neuronal networks as a result of: i) short-term electrical stimulation (minutes), ii) long-term (chronic) stimulation (days).

## 2  Methodology

A mixture (200 μg/ml) of poly-D-lysine and FITC conjugated poly-L-lysine is patterned onto silanized microelectrode array surfaces using microcontact printing (stamps are created by casting PDMS onto microfabricated SU8 molds). Primary E18 hippocampal neurons (BrainBits™) are plated at a density of 100-200 cells/mm$^2$ in serum-free neurobasal/B27 medium.

Short-term stimulation is achieved by applying 20 pulses ($\pm 25$ μA; 100 μs/phase) @ 20 Hz repeated 10 times every 5 s. Long-term stimulation involves stimulating the network for a period of 30 minutes everyday for 3 weeks starting at day 4 in vitro. Network dynamics is evaluated based on spike and burst rates, onset of activity (the day in which spontaneous activity is observed for the first time), as well as quality of responsiveness to a test stimuli (latency, jitter, reliability, etc.) Test stimuli are applied at a rate of 0.1 Hz to avoid accommodation and desensitization.

## 3  Results

The improvements made in patterning techniques and our efforts in optimizing dimensions for long-term pattern integrity and recordability has resulted in our ability to maintain relatively low density cultures of primary neurons on patterns for over 90 days (Figure 1). We have also found these patterned networks to be superior in localizing cells to electrodes thus providing a more reliable electrical interface for recording and stimulation (Figure 2). Our experiments have sug-

gested that the frequency chosen for stimulation has a dramatic effect on network responsiveness. While low frequencies (0.1-0.2 Hz) did not show much desensitization, higher frequencies (5-10 Hz) resulted in rapid response suppression (Figure 3). Chronic stimulations applied for 30 minutes daily staring at day 4 in vitro produced spontaneous activity at an earlier age compared to networks that did not receive stimulations. Chronically stimulated cultures were also observed to have a much higher number of active units (Figure 4).
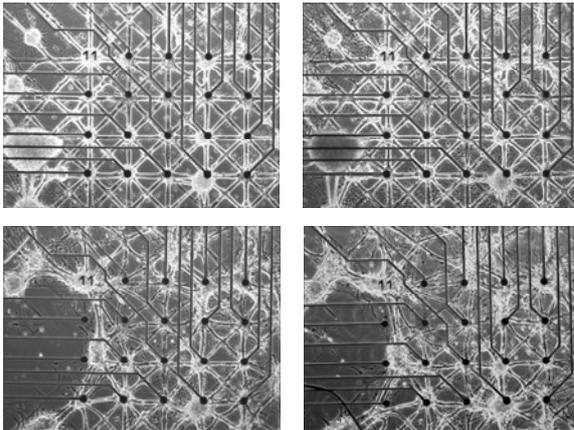


**Fig. 1.** Phase contrast Images of patterned cultures are shown at 14, 30, 60 and 90 days in vitro (from left to right and top to bottom starting at the top left corner). At day 40, a portion of the left side of the culture was disrupted, lost adhesion and came off during a media change. Design features: Node size = 80 um Line width = 20 um

**Percentage of Active Electrodes**
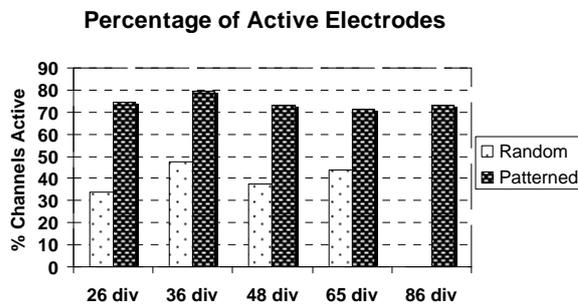


**Fig. 2.** Design enhanced localization of networks to electrodes such that the number of active electrodes was consistently greater than 70% in Patterned Networks as compared to less than 50% in Random cultures.
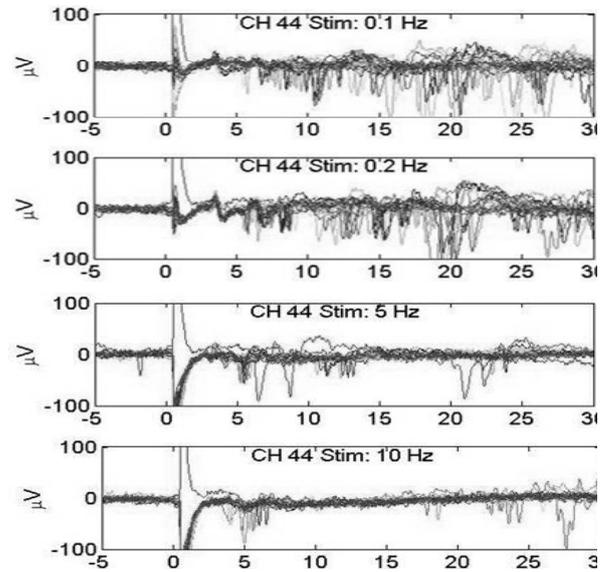


**Fig. 3.** Response traces overlaid. Groups of 20 test pulses were applied at 4 different frequencies (0.1 - 10 Hz) in random order. Higher frequencies result in response suppression while low frequencies did not show desensitization.

**Percentage of Electrode Registering Activity in Each Group**
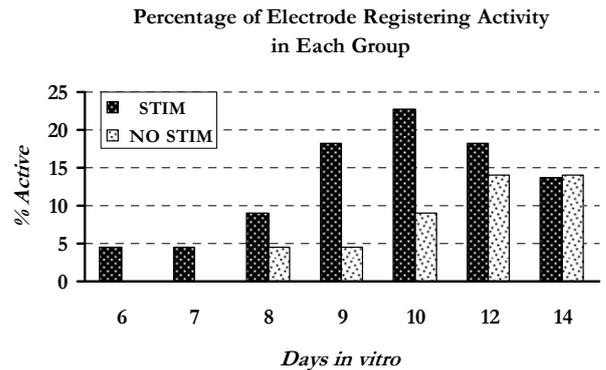


**Fig. 4.** STIM: Network received daily stimulations (30 min.) starting at 4 days in vitro. Spontaneous activity was recorded at the beginning of each stimulation session. (No spontaneous activity on 4 and 5 div). NO STIM: built-in control. Network did not receive any stimulation.

### Acknowledgement

# The Autonomic Regulation of Spontaneous Activity in Living Neuronal Network

Ai Kiyohara[1,2] , Takahisa Taguchi[1] and Suguru N. Kudoh[1*]

1 Cell Engineering Research Institute (RICE), National Institute of Advanced Industrial Science and Technology (AIST)
2 Graduate School of Science Osaka University
* Corresponding author. E-mail address: s.n.kudoh@aist.go.jp

We analyzed spontaneous action potentials from rat hippocampal neurons by multi-electrode array system. Frequency and spatial distribution between the electrodes of spontaneous activity were investigated during the culture days, and we focused in their dependency on the culture day. Spontaneous action potential was observed without any electrical stimulation. Spatio-temporal pattern became to be complex day by day. There was a transient state with high frequency bursts (HFB) in a particular stage, then the burst activity terminated. The heterogeneity of the spatial distribution of the action potential increased after the termination of the high frequency burst. These results suggest that functional network were autonomously reconstructed by network activity.

## 1  Introduction

Spontaneous electrical activity was frequently observed in dissociated rat hippocampal neurons cultured on a multi-electrodes-array and we can estimate functional structure in the network from spatio-temporal pattern of such activity. We developed reconstructed networks of dissociated rat hippocampal neurons, in which we can precisely analyse the mechanisms of the network for responding to an environment.

Using the multi-electrodes-array system, we previously investigated the spatio-temporal pattern of spontaneous action potentials. Interestingly, each culture contained hub-like neurons with many functional connections. The neuronal networks cultured on the dish were not random networks but heterogeneously reconstructed networks. In addition, after the transient stage with high-frequency-bursting activity of action potential (HFB), it increased gradually that variance in frequency of spontaneous action potential between each electrode. These results suggest that dissociated rat hippocampal neurons formed a particular self-assembled neuronal network, and synaptic plasticity induced by HFB was critical for the formation of the network structure.
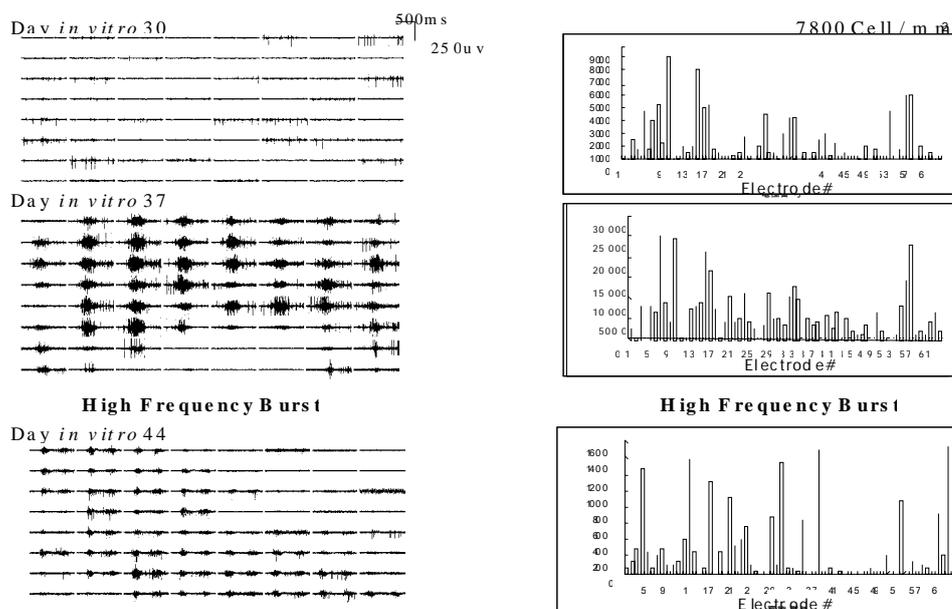


**Fig. 1.** Observation of the high frequency burst period.

## 2 Methods

We isolated a rat hippocampus and cultured hippocampal neurons on the multi-electrodes array dish. The hippocampal region was cut off from Wistar rats on embryonic day 18, and neurons were dissociated by 0.175% trypsin in $Ca^{2+}$- and $Mg^{2+}$- free phosphate-buffered saline (PBS-minus) supplemented with 10 mM glucose at 37oC for 10 min. Neurons were plated on a MED probe, having 64 planar microelectrodes in the center of the culture dish at 37oC in 5% CO2 / 95% air at saturating humidity. Spontaneous extracellular action potential was recorded for 10 minutes in normal culture medium at 10-120 days in vitro. Extracellular potential were collected through 64 electrodes simultaneously with the integrated MED64 system (Alpha MED Science, Japan) at a sampling rate of10 kHz. We observed a change of spontaneous action potentials during culture days.

## 3 Results

We analysed developmental change of the pattern of spontaneous action potential in the cultured neuronal network. We found a particular transient period with high frequency burst lasting for about a week at about 20-50 days. After termination of a high fre-

quency burst period, the spatio-temporal patterns of the spontaneous activity drastically changed (fig.1).

In addition, we also found cultures resisting to the inhibition of N-methyl-D-aspartate receptors (NMDA-Rs) appeared after the high frequency burst period (fig.2). The result suggested that NMDA-Rs contribute to modification of dynamics of neuronal network in early stages, but not after high frequency burst period.

## 4 Conclusion/Summary

We found a characteristic transient high-frequency burst activity. The activity plays an important role in the autonomous modification of the neuronal connections in the network. Heterogeneous distribution of connection in the network after the high frequency burst period seems to be suitable for information processing. Appearance of APV resistant network suggested that NMDA-Rs dependent network structure was changed after a high frequency burst period.
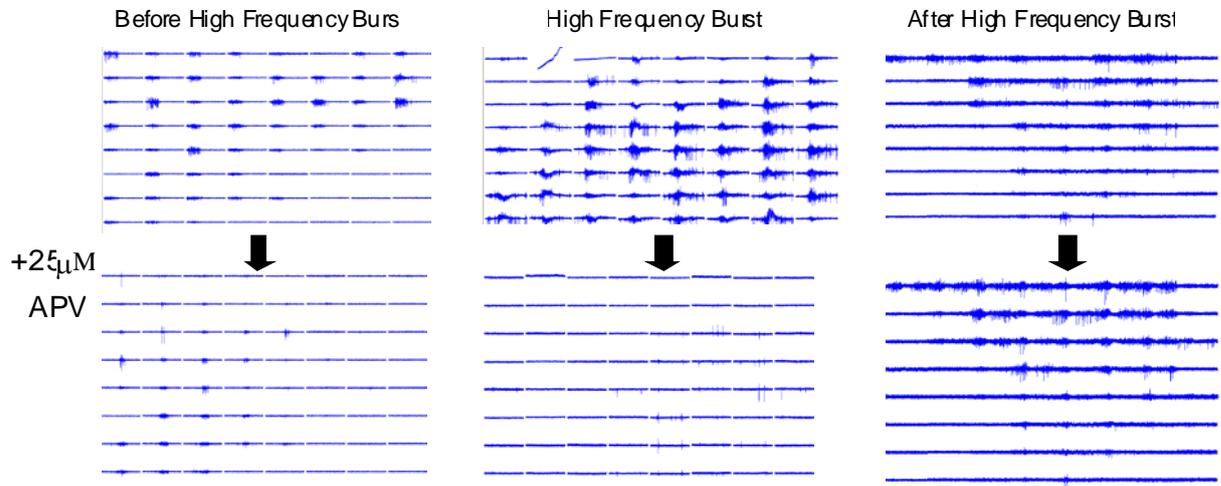
**Fig. 2.** Change of the pattern of the action potential during inhibition of the NMDA-Rs.

# Synchronization of Firing Rhythms in Cultured Hypothalamic Neurons

Klisch C[1], Inyushkin AN[2], Pévet P[2,3], Meissl H[1,2*]

1 Dept. of Neuroanatomy, Max Planck Institute for Brain Research, Frankfurt, Germany
2 European Laboratory for Circadian Research, Strasbourg and Frankfurt
3 Institute for Cellular and Integrative Neurosciences, CNRS, Strasbourg, France
* Corresponding author. E-mail address: meissl@mpih-frankfurt.mpg.de

## 1 Background

Individual neurons of the suprachiasmatic nucleus (SCN) express circadian rhythms in their firing rate when cultured on multielectrode arrays (MEA). In this work, we have used SCN cultures grown on MEAs to investigate the recruitment of neurons during time in culture and to determine the role of orexin, a neuropeptide involved in the regulation of sleep-wake cycles and food intake, on network properties.

## 2 Methods

SCN, obtained from 1- to 5-day old rats, were dissociated using papain. Viable cells were plated at different densities on MEAs and maintained for several days in DMEM/F12 medium supplemented with 10% fetal calf serum and antibiotics before recording. Long-term recordings of firing rate were carried out using a MEA-system (Multichannel Systems, Reutlingen). Spikes from individual neurons were discriminated offline using Spike 2-software (Cambridge Electronic Design).

For whole-cell patch clamp recordings of SCN neurons acute brain slices of 3 week old rats or cell cultures of 1-5 day old rats were used.

## 3 Results

SCN neurons cultured on multielectrode arrays show fast voltage transients which correspond to single action potentials. These fast voltage transients appear in isolated single events or in clusters or bursts and can exhibit highly synchronized activity. Network activity increases with time in culture and shows a recruitment of an increasing number of neurons. Network properties are altered through the application of neurotransmitter agonists and antagonists, like GABA and bicuculline, and neuropeptides, eg. orexin A. This neuropeptide modulates the firing rate of SCN cells being either inhibitory or excitatory. Furthermore, orexin A changes the temporal dependencies between neurons as established in a cross-correlation analysis; as a result the synchronisation between individual neurons is enhanced, abolished or even reversed. A transient application of orexin A has a relatively sustained influence on network dynamics and connectivity. Injection of bicuculline multiplied the number of detectable correlations near to the theoretical limit.

In whole-cell patch clamp experiments on slices orexin A (0.25-250 nM), applied by local superfusion through a multibarrel, pressure-driven system (DAD12, ALA Scientific Instruments), caused significant changes in the frequency of spontaneous inhibitory postsynaptic currents (IPSCs) in a reversible manner with no effect on the mean amplitude or decay time constant. Different concentrations of orexin A altered the frequency of IPSCs in 40% to 67% of the SCN cells recorded; the effects were widespread throughout the SCN and observed in all regions of the nucleus. At low concentrations (0.25-2.5 nM) orexin A more readily induced an increase in frequency of IPSCs whereas at higher concentrations (25-250 nM) the predominant effect of orexin A was a reduction in IPSCs frequency. A negative Spearman's rank correlation between the change in IPSCs frequency and the concentration of orexin A was found (r = -0.358, P <0.001). Both the increasing and the decreasing effects of orexin A were reproducible in whole-cell patch clamp experiments on cell cultures (n=21). The effects of 2.5, 25 nM and 250 nM orexin A on the frequency of IPSCs were likely to be postsynaptic, since the responses were reproducible in the presence of tetrodotoxin (0.5 μM). In contrast, the ability of 0.25 nM orexin A to induce an increase in frequency of IPSCs was significantly reduced in the presence of tetrodotoxin (P=0.005, $\chi^2$-test), indicating that the effect was mediated by a frequency increase of presynaptic action potentials. Application of the $GABA_A$ receptor antagonist gabazine (5 mM) completely (63%) or partially (31%) blocked spontaneous IPSCs generation suggesting a GABAergic nature of IPSCs.

## 4 Conclusions

Our data show that dispersed SCN neurons form a complex network that develops gradually with time in culture. Orexin A may have a direct effect on SCN neurons and modulates inhibitory synaptic transmission between SCN neurons. It is therefore likely that orexin A has a direct influence on the SCN network, potentially as a substance providing a feedback signal of lateral hypothalamic nuclei involved in regulation of sleep/wake cycles or feeding to the circadian timekeeping system.
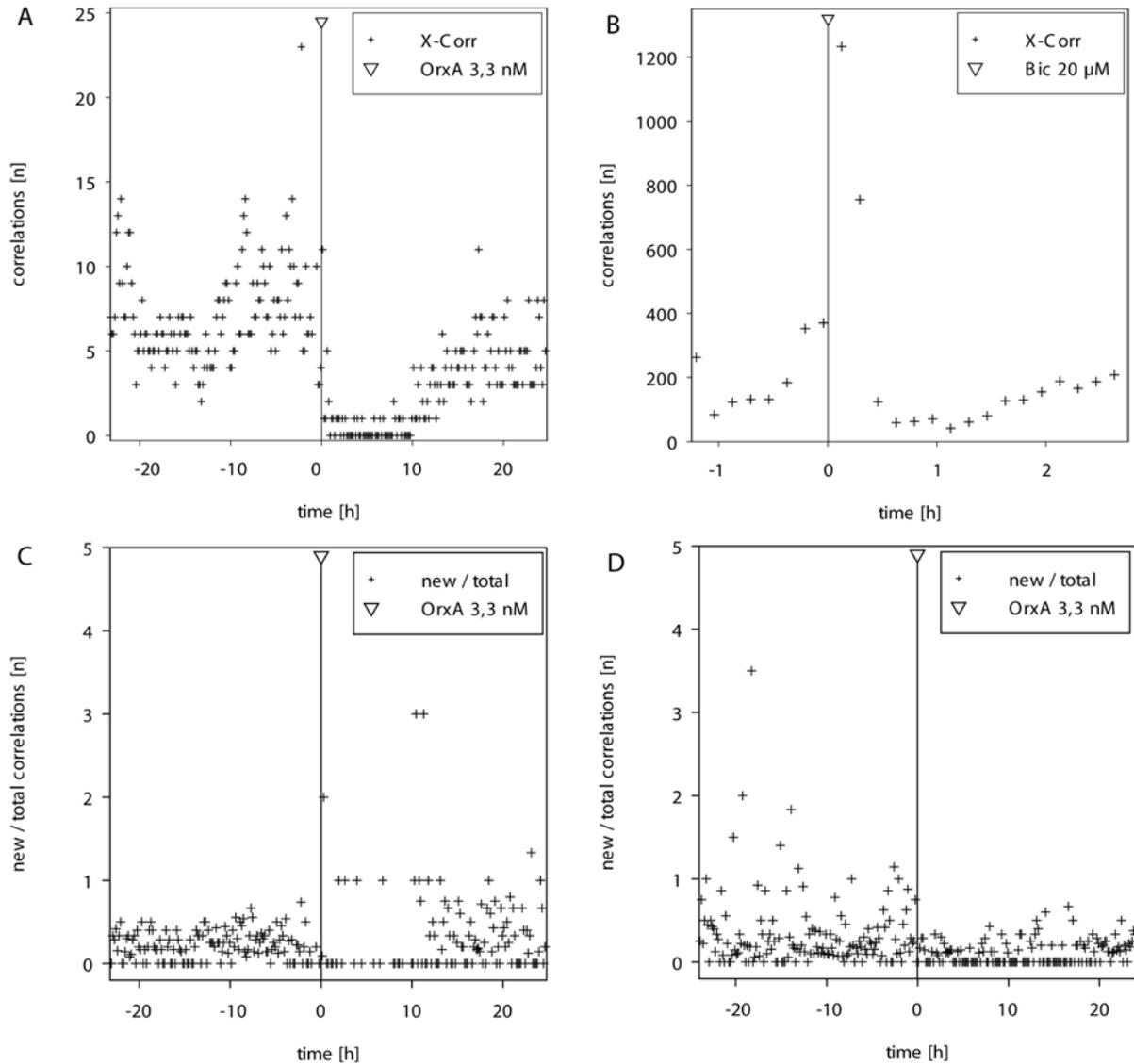


**Fig. 1** The number of crosscorrelations between all electrodes found during 600 s bins change after neurotransmitter/neuropeptide application. While orexin A application diminish synchronized activity for long times (A), bicuculline transiently increase the number of correlations revealing the full connectivity of the culture (B). Orexin A has a long lasting effect on the dynamics in the network shown by a lowered quotient of new correlations versus their total number (C, D).

# The neurophonic potential in nucleus laminaris of birds

Nico Lautemann[1*], Paula T. Kuokkanen[2], Richard Kempter[2,3], Hermann Wagner[1]

1 Institute for Biology II, RWTH Aachen, Germany
2 Institute for Theoretical Biology, HU Berlin, Germany
3 Bernstein Center for Computational Neuroscience, Berlin, Germany
* Corresponding author. E-mail address: nico@bio2.rwth-aachen.de

The auditory system of birds can be used as a model system for signal processing in the sub-microsecond time range. In nucleus laminaris (NL), the interaural time differences are detected and a neurophonic potential with a high signal-to-noise ratio can be measured. We use microelectrode arrays to analyse the neurophonic potential as well as to measure the delay lines proposed by an early model by Jeffress. Here we present the first direct evidence of delay lines in the barn owl.

## 1  Introduction

Although action potentials in the nervous system have typical durations of at least 1 ms, events can be encoded in the sub-microsecond range, for example in the auditory system.

To subserve the detection of interaural time difference, which is used to localize the azimuthal position of a sound source, the Jeffress-model [1] has suggested three levels of processing: frequency specificity, delay lines and coincidence detection. This system is realized in birds in the third-order nucleus laminaris, the first nucleus where binaural signals are processed and coincidence detection takes place.

We use the auditory system of birds (chicken, barn owl) to study the neurophonic potential (NP), a frequency-following potential with a temporal precision of some 10 µs, occurring in the network formed by nucleus magnocellularis (NM) and nucleus laminaris in the brainstem. Through our studies, we expect to find out more about the origin of the NP (Fig. 1). We hypothesise that NM axons are the origin of the high-frequency component of the NP, whereas the spike-activity of NL neurons is the source of the low-frequency component.

## 2  Materials & Methods

Acute coronal slices of the brainstem (300 µm thick) were prepared from barn owls (*Tyto alba*, P2-P8). Recordings were made on perforated 8x8 MEAs (Multichannel Systems, Reutlingen, Germany) while stimulating extracellularly at different loci (Fig.2). The latencies of the averaged response (n=20) were determined by calculating the time difference between corresponding extrema to show the progression of the signals within NL (Fig. 3 B). TTX was used to show the neuronal origin of the response.
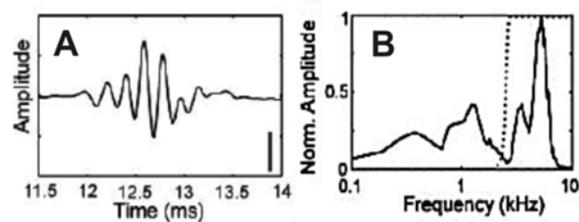


Fig. 1: Neurophonic potential (mean of n=128 trials) evoked by an acoustic click stimulus applied at 10 ms (A, scale bar: 2,5 mV) and the normalized amplitude of the Fourier transform showing 3 major peaks (B) [2]. The question is whether those peaks can be correlated to the different field sources (axons, synapses, somata).
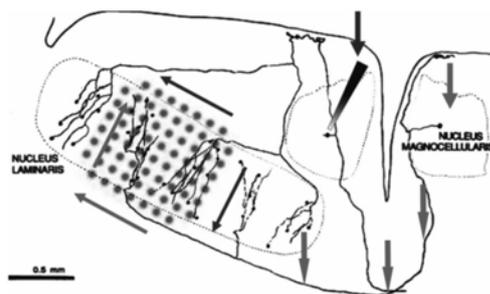


Fig. 2: Schematic drawing of the recording situation (anatomy: [3]): Acute slices of the brainstem are placed on the MEA as shown. This orientation allows the recording along the projections from NM while stimulating with tungsten electrodes (3-5 MΩ, bipolar pulses, 100-4000 mV) at different positions (vertical arrows). With this arrangement, the delay lines proposed by the Jeffress-model can be measured.
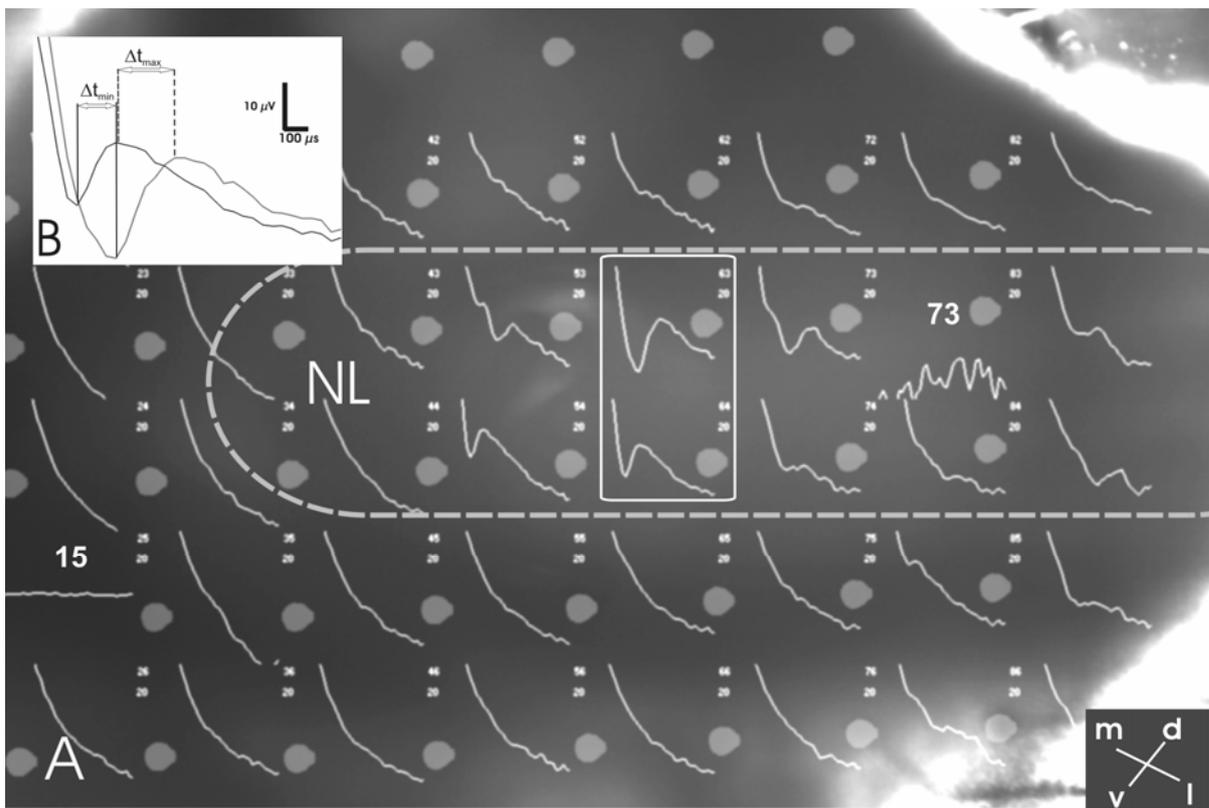
Fig. 3: **A** Cutout (5x8 electrodes) of the averaged (n=20) stimulus-triggered response in the NL of the barn owl (orientation is indicated by the crosshairs). Here, bipolar stimulation pulses (100 µs, ± 2400 mV) were used and applied in the medial region (on the left side, not shown). The projections of the contralateral NM run from medial to lateral outside of NL (border indicated by dashed line), and within the NL from ventral to dorsal (see also Fig. 2). Accordingly, the latencies of the response increase from medial to lateral and from ventral to dorsal. Electrode 73 is defective, electrode 15 is the internal ground electrode. **B** shows a superposition of the responses of the marked electrodes in (A). The time differences between the extrema indicate the latencies along the dorso-ventral extension of the NL.

## 3 Results

Latencies changed within the NL of the barn owl from medial to lateral as well as in the dorso-ventral direction in response to contralateral stimulation. Averaged signal amplitudes ranged from 10 to 50 µV. Latencies between two neighbouring electrodes (interelectrode distance: 200 µm) were about 34 to 250 µs corresponding to propagation velocities between 0,8 – 5,9 m/s at 35 °C (Fig.3 A). The responses vanished after application of TTX.

## 4 Summary

Because MEAs allow the simultaneous measurement of the neuronal response with a high temporal and spatial resolution, the signal propagation within NL can be accessed. Our data provide direct evidence for delay lines in NL thereby indicating the realisation of the Jeffress-model. In future experiments, we will use Ca-free medium to separate axonal (projections from NM) from somatic responses. These data will be used to simulate the NP.

**References**
[1] Jeffress LA (1948) A place theory of sound localization. J. Comp. Physiol. Psychol. 4, 35-39.
[2] Wagner H., Brill S., Kempter R., and Carr C.E. (2005) Microsecond precision of phase delay in the auditory system of the barn owl. J Neurophysiol 94, 1655-1658.
[3] Carr C.E., Soares D., Parameshwaran S., and Perney T. (2001) Evolution and development of time coding systems. Curr. Opin. Neurobiol. 11, 727-733.

# Learning in Live Neuronal Cultures: a Training Protocol Evaluated

Joost le Feber[*], Jan Stegenga, and Wim L.C. Rutten

Biomedical Signals and Systems, University of Twente, Enschede, Netherlands
* Corresponding author. E-mail address: j.lefeber@utwente.nl

We applied a training protocol to cultured cortical networks, adapted from Shahaf and Marom [1]. Like they did, *on average* we found an improved response to input stimuli. However, not all experiments were successful, and the shapes of our learning curves differed from theirs. Furthermore, we investigated connectivity changes in the whole network. We concluded that not only a selected connection could be altered, but that connectivity in the rest of the networks also changed. Connectivity changes may go undetected if general parameters like network wide firing rate are used to analyze connectivity.

## 1 Introduction

Several studies investigated plasticity in cultured neuronal networks, but only one protocol [1] aimed to train a culture to produce a predefined response upon stimulation. Although quite successful, the results were never reproduced elsewhere and they did not serve as a basis for wider exploration yet. Furthermore, the protocol observed only one selected connection in the network. We extended that study by looking at induced connectivity changes in other connections as well, and we used longer periods of observation to study the induced changes.

## 2 Methods

Experiments consisted of: *I. spontaneous measurement. II. Select electrodes:* all electrodes were stimulated at various amplitudes. We selected a stimulation electrode that frequently induced a network burst and (following the original training protocol) an evaluation electrode that responded to these stimuli at a ratio of ~0.1. *III. spontaneous measurement; IV. Training protocol:* stimulate the selected electrode until ≥2 responses to the last 10 stimuli (max 10 min) followed by 5 minutes of no stimulation. Repeat cycle until network wide response drops below threshold; *V. spontaneous measurement.* We used spontaneous activity measurements to assess connectivity changes induced during *II* or *IV*. We divided all spontaneous measurements into data blocks and used conditional firing probability analysis to calculate connectivity matrices in each block. Connectivity matrices describe all functional connections between pairs of electrodes in terms of strength and latency. To watch new connections appear or old ones disappear, we calculated similarity indices (SI) between all data block pairs (*A,B*), such that SI(*A,B*)=1 if all connections in *A* are

also found in *B* and vice versa. SI(*A,B*)=0 if there are no connections that are found in *A* and *B*.

## 3 Results
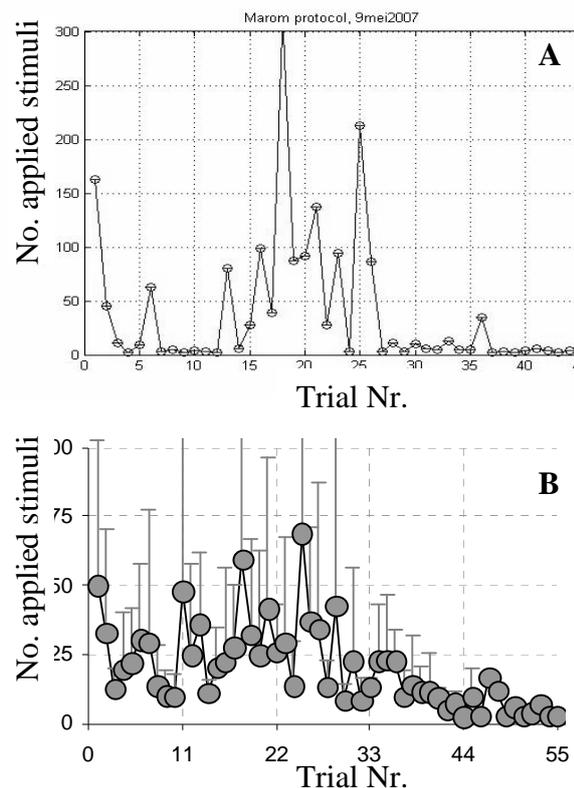


**Fig. 1.** Learning curves during training protocol. A shows a typical example of an individual learning curve, as observed in 5 of 10 experiments. B depicts average learning curve of all 10 experiments. No. applied stimuli decreases significantly with trial Nr. (Kendall's tau: Correlation coefficient: -0.33; P<0.01).

1. *Training effect.* In 5 of 10 experiments (8 cultures; 26±14 DIV) we found a learning curve as in

Figure 1a, characterized by an initial decline, followed by a rise, roughly centered around trial Nr 20, to finally reach a stable low level. Three cultures reached a stable low level immediately, and two others showed wild fluctuations without a clear trend. The average learning curve of all cultures is shown in Fig.1b. Strikingly, the first 10 trials often yielded results very similar to the original results published by Shahaf and Marom.
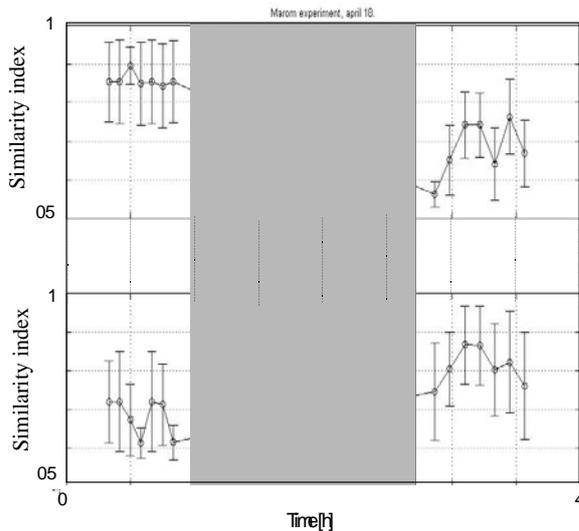


**Fig 2.** Example of similarity of connectivity matrices before and after training protocol. Gray bar indicates duration of training protocol. Before and after the protocol we measured spontaneous activity. Recordings were divided into data blocks and we calculated connectivity matrices for each data block. Upper panel shows mean similarity index (for explanation see text) to all data blocks before the traing protocol. Lower panel depicts mean SI to all data blocks after the protocol. Similarity decreased significantly across the training protocol in 7 of 8 experiments (ANOVA: p<0.01).

*2. Plasticity.* Newly appearing or disappearing connections were studied by calculating mean SI to all data blocks before, or after the training protocol (example in Fig.2). Similarity decreased significantly (ANOVA, p<0.01) in 7 of 8 experiments (2 experiments were excluded because no spontaneous activity was recorded after the training protocol). Furthermore, the strength of 64% of all persisting connections was significantly affected by the protocol, either up or down. Although the average strength did not change (example in Fig 3), the mean *absolute* change was 52±26%, clearly exceeding the spontaneous fluctuation during a comparable time span (~30% standard deviation).
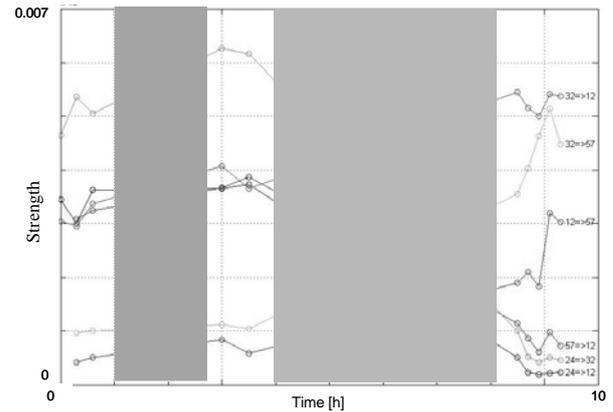


**Fig 3.** Strengths of persisting connections during one of our experiments. The experiment consisted of 5 steps (see text). White areas: spontaneous activity recordings (I, III, and V). First gray bar: II, Select electrodes. Second gray bar: IV:training protocol. The graphs illustrate that the strength of most individual connections was affected by the protocol; either strengthened or weakened. In total, the strength of 64% of all persisting connections was significantly changed. The figure also suggests that global paramers like mean strength may not be affected by the protocol.

## 4 Discussion

Our results show that the training protocol did induce connectivity changes in all cultures. However, it was not always possible to train a selected connection in the predefined manner. This may be caused by the new balance that must be established between network activity and connectivity, which may or may not include the predefined alteration of the selected connection. This search for a new balance may also explain the connectivity changes in the rest of the network. We found that the strength of many individual connections changed either up or down (by 52% on average), but that the mean strength remained unchanged. Thus, it may be difficult, if not impossible, to analyze the induced connectivity changes using global parameters like array wide firing rate.

On average, however, we did find a significantly 'improved' response to electrical stimuli after the training protocol.

### Acknowledgement

### References

[1]    Shahaf, G. and S. Marom, Learning in networks of cortical neurons. J Neurosci, 2001. 21(22): p. 8782-8788

# Developmental Characteristics of Ultra-slow Oscillations in the Hippocampal Networks on Multi-Electrode Array

Xiangning Li, Wei Zhou, Shaoqun Zeng, Qingming Luo

Britton Chance Center for Biomedical Photonics, Wuhan National Laboratory for Optoelectronics, Huazhong University of Science and Technology, Wuhan, Hubei, China, 430074

## 1   Background/Aims

Spontaneous neural oscillations have been found in many types of neural tissues ranging from the hippocampus to the spinal cord in vivo and in vitro. These activities are believed to play a pivotal role in many physiological functions, including the network formation, signal processing, learning and so on. Various forms of neuronal oscillations present in the hippocampal networks, including rhythms in the delta, theta, beta, gamma and ultra-fast bands. Recently, the hippocampal slow oscillation characterized by a slow frequency ($\leq 1$ Hz) rhythm was observed in some studies.

## 2   Methods/Statistic

To explore the mechanism underlying the appearance and maintaining of these firing patterns, the hippocampal neurons were cultured on the multi-microelectrode array dish for over 9 months and the spontaneous activity was recorded successively.

## 3   Results

Random firing was observed in the high density cultured neuronal network in the 1st week *in vitro* and transformed into synchronized activity after two weeks *in vitro*. Then an ultra-slow oscillation (~0.004 Hz) of the tightly burst was observed during the spontaneous development. These oscillations consisted with regular episodes, which persisted about 70 s each, recurred every approximately 240 s and were synchronized array-widely. In each episode, there was a decreased tendency of burst rates from 4.6 Hz to 0.2 Hz, while the spike rate decreased from around 100 Hz to zero. When expose to bicuculline, the block of GABAA receptors, these episodes were supplanted by regular burs.

These spontaneous oscillations could maintain from one month to six months after plating. During the spontaneous development of the network, the number and duration of burst in the episode decreased while the interval between the episode increased. Before no activity could be recorded from the network, the firing pattern transform from the slow oscillation into random activities, and the latter firing pattern kept for more than 2 months.

## 4   Conclusion/Summary

These indicate the presence of an ultra-slow oscillation in a certain stage during the development of hippocampal neuronal network. The firing patterns were an important symbol of the spontaneous development. The emergence of this pattern was frequency- and-temporal dependent and controlled by the balancing of excited and inhibited neural networks.

# Artificial Background Sensory Input Aids Functional Plasticity in Cultured Cortical Networks

Radhika Madhavan[1], Zenas C. Chao[2], Steve M. Potter[3*]

1 National Center for Biological Sciences (TIFR), Bangalore, India
2 RIKEN Brain Science Institute, Saitama, Japan
3 Laboratory for Neuroengineering, Coulter Department of Biomedical Engineering, Georgia Institute of Technology, Atlanta, GA (America)
* Corresponding author. E-mail address: steve.potter@bme.gatech.edu

Some bursting disorders, such as epilepsy, may result from partial deafferentation of cortical tissue. We hypothesized that population bursting is responsible for the variability that we and others observed when inducing functional plasticity in cultured cortical networks using extracellular electrical stimulation delivered via MEAs. We artificially reafferented cultures of dissociated rat cortical neurons and glia by delivering distributed low-frequency (1-2 Hz per electrode) stimulation, which we previously showed controls population bursting.[1] Here, we demonstrate a strong correlation between the level of burst quieting or desynchronization, and functional plasticity induced by tetanic stimulation. Burst control also reduced variability of network responses to probe stimuli, enhancing *detection* of induced plasticity. Reafferented networks provide a more realistic in vitro model of learning and memory than do isolated cultured networks. A better understanding of the relations between bursting and network plasticity may offer useful clues for treating learning disorders in juvenile epilepsy.

## 1 Introduction

Dissociated cortical cultures provide an accessible and controllable model of the brain, while preserving the essential molecular and structural properties of the individual neurons in the cortex. One of the major disadvantages of *in vitro* models is that they lack the rich spatiotemporal sensory inputs that the brain continuously receives. Multi-electrode stimulation protocols provide artificial sensory background to dissociated cortical networks[1] and make their activity patterns more like those recorded *in vivo* by eliminating synchronous population bursts, while preserving the ability of the network to fire action potentials. We propose that cultured networks receiving continuous multisite stimulation might be more suitable, than isolated networks, for the study of learning and long term plasticity *in vitro*.

## 2 Methods

Dense neuro-glial cultures were prepared and cultured from dissociated embryonic rat cortex as previously described.[2] Between 21 and 35 days in vitro, cultures that exhibited robust spiking and population bursts across at least 45 of 59 electrodes (MEA60, Multichannel Systems) were chosen for this study. 20 or 25 electrodes in each culture were stimulated cyclically at 0Hz (no quieting stimulation), an aggregate of 20Hz (1 stimulation/sec) or an aggregate 50 Hz (2 stimuli/second) to produce varied amounts of burst quieting. 4-6 "probe" electrodes were stimulated every 4-18 seconds, 50 ms after the beginning of a 250 ms pause in the background input, and the network responses were measured using the Center of Activity Trajectory (CAT) statistic, which we previously showed was an effective and efficient way to measure functional plasticity.[3] After 3 hours of quieting, probing, and CAT monitoring, tetanic stimulation was delivered for 15 min. Then quieting, probing, and CAT monitoring continued for 3 hours. "Detectability" of plasticity was based on the statistical significance (Wilcoxon rank sum test) of the difference of CAT across the tetanus (change), as compared to across an equal interval in the middle of the initial 3-hour period (drift).

## 3 Results

We were able to produce a wide range of bursting (~1 per hr to ~1 per 10 sec), with varying amounts of background stimulation, in 14 networks. Strong tetanic stimulation produced functional change easily detectable over the intrinsic drift only in well-quieted cultures (Fig. 1). Higher levels of ongoing bursting activity reduced the ability to detect plastic changes due to the fluctuating pre-tetanus baseline response.

Previous studies on dissociated cultures have demonstrated network-level changes in response to tetanic stimulation that lasted for a maximum period of 30 minutes post-tetanus[4]. We investigated the long term stability of tetanus-induced changes by comparing the changes in the periods before and after the

tetanus. Induced functional changes persisted for at least 2 hours post-tetanus in burst-controlled cultures.

## 4 Conclusion

Intrinsic population bursts are an inevitable consequence of deafferentation in cultured networks. By restoring background activity with mild, distributed stimulation, they can be reduced or prevented. They activate undesired plasticity mechanisms in cortical networks, causing synaptic drift that makes studies of learning in vitro difficult. By controlling bursts, one can allow salient artificial sensory input or external stimulation to produce more reliable, more easily detected functional changes in the networks.

### References

[1] D.A. Wagenaar, R. Madhavan, J. Pine and S.M. Potter (2005). Controlling bursting in cortical cultures with closed-loop multi-electrode stimulation. *J. Neuroscience*, 25, 680-688.

[2] S.M. Potter and T B. DeMarse (2001). A new approach to neural cell culture for long-term studies. *J. Neurosci. Methods,* 110, 17-24.

[3] Z. C. Chao, D J. Bakkum and S.M. Potter (2007). Region-specific network plasticity in simulated and living cortical networks: Comparison of the center of activity trajectory (CAT) with other statistics. *Journal of Neural Engineering*, 4, 294-308.

[4] Y. Jimbo, T. Tateno and H.P. Robinson (1999). Simultaneous induction of pathway-specific potentiation and depression in networks of cortical neurons. Biophys J *76*, 670-678.
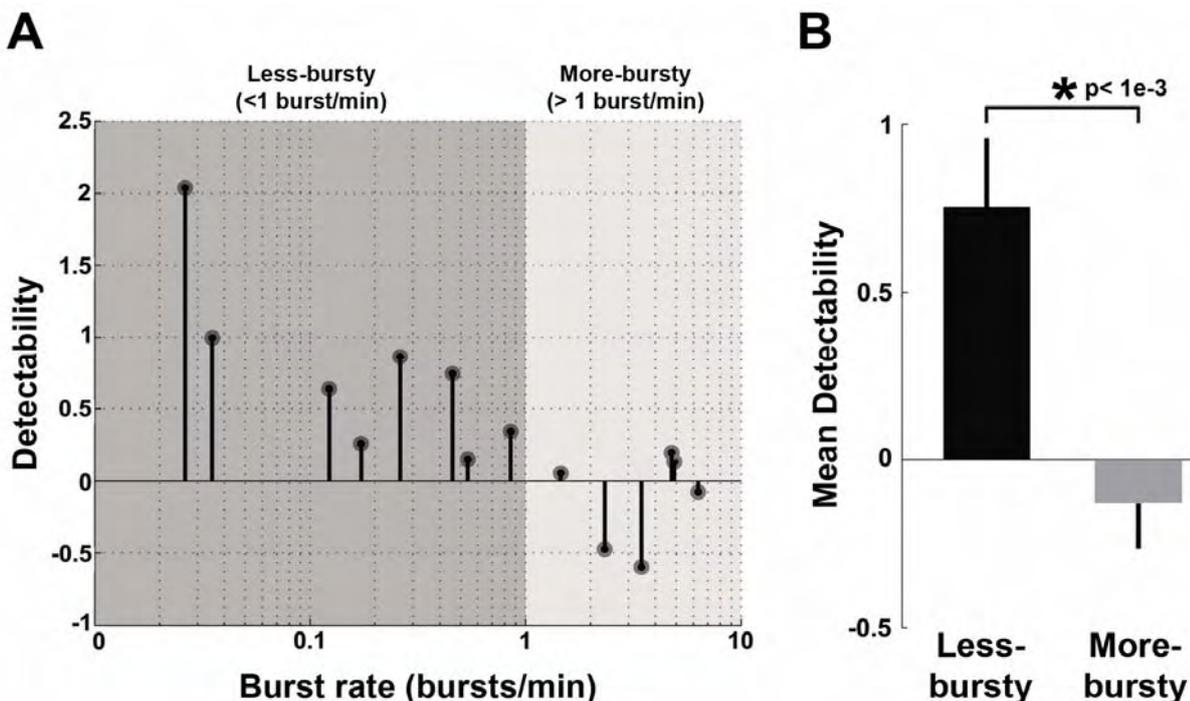
**Fig. 1.** By controlling the bursting rate of cortical cultures using low-frequency distributed electrical stimulation (artificial reafferentation) over a wide range, we showed that tetanus-induced plasticity becomes harder to detect the more bursts the culture expresses. The best induction and detection of plasticity was observed in cultures with few or no bursts (A). When experiments were divided into "less bursty" (<1/min) and "more bursty" (>1/min) groups, the detectability difference between them was statistically significant (p<0.001) (B).

# Microelectrode array (MEA) analysis of ion channels controlling spontaneous chromaffin cells electrical activity

A. Marcantoni, V. Carabelli, V. Comunanza, D. Gavello, J. Rojo-Ruiz, E. Carbone*

Department of Neuroscience; NIS Center, CNISM Research Unit, University of Torino, I-10125 Torino (Italy)
* Corresponding author. E-mail address: emilio.carbone@unito.it

A 60 MEA system (MCS GmbH, Reutlingen, Germany) was used for recording spontaneous action potentials from rat chromaffin cells (RCCs). The results obtained were compared with the intracellular action potential recorded in perforated patch clamp experiments with the aim of: 1) monitoring the spontaneous electrical activity by means of extracellular recording and, 2) identifying the role of ion channels controlling action potential firings by analyzing the changes of extracellular recordings induced by selective ion channel blockers. Preliminary analysis of spontaneously active RCCs revealed the existence of strict correspondence between extracellular MEA signals and intracellular action potential recordings, making the MEA system a valuable tool for studying the functional role of ion channels in cell excitability.

## 1 Introduction

Adrenal chromaffin cells represent an ideal system for studying the biophysics of voltage-gated Ca2+ channels and their role on neurotransmitter release. Chromaffin cells express mainly high-threshold Ca2+ channels (L, N, P/Q and R-types) and under chronic hypoxic conditions (3% O2) or following long-term β-adrenergic stimulation they also express low-threshold T-type channels [1]. Moreover, rat chromaffin cells (RCCs) have high access resistance at rest and possess sufficient high densities of Na+ and K+ channels to generate all-or-none action potential spikes when injecting small amounts of current (3-5 pA) through the cell membrane. In normal culture conditions, RCCs preserve a round spherical shape and do not develop neuronal processes even after several days in culture. Moreover, these cells express a homogeneous distribution of voltage-gated ion channels which are involved in the generation of the action potential. This is at variance to that occurring on neurons where ion channels distribution varies greatly from the soma to the dendrites or axons, increasing the number of possible extracellular waveforms that can be detected with MEAs. These peculiar properties make the chromaffin cells an interesting model for studying single extracellular action potentials. Considering the different role of Na+, Ca2+ and K+ channels in the generation of action potentials we initiated a detailed study of the spontaneous (autorhythmic) electrical activity of RCCs using a 60 MEA system made of 30 μm electrode diameter separated by 200 μm distance (MCS GmbH, Reutlingen, Germany). The purpose of the study was dual: 1) to monitor the spontaneous electrical activity by means of extracellular recordings which leave unaltered the intracellular medium and preserve the cells near physiological conditions; 2) to identify the role of ion channels controlling action potential firings by analyzing the changes of extracellular recordings induced by selective ion channel blockers.
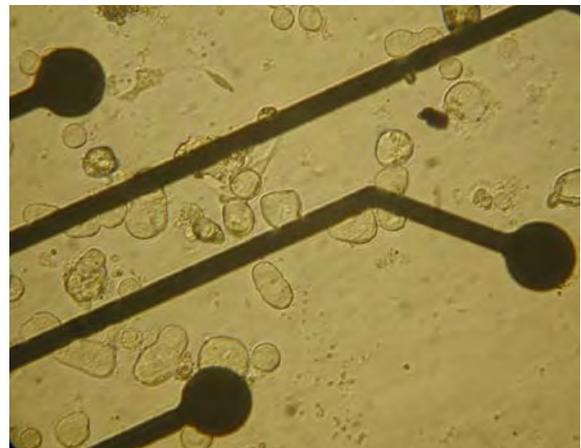


**Fig.1.** Isolated chromaffin cells plated on a standard MEA

## 2 Materials and Methods

Isolated RCCs were plated on a MEA culture chamber and kept in a $CO_2$ incubator for 2-5 days before recordings. RCCs ready for recordings appeared as round spherical cells inter-dispersed within the 60 MEA (Fig.1). The standard extracellular solution contained (mM) 135 NaCl, 4 KCl, 2 $Ca_2Cl$, 2 $MgCl_2$, 10 Hepes, 10 Glucose (pH 7.4). All the drugs where directly injected in the MEA chamber and the signal where recorded 10 minutes after the administration. For perforated patch clamp experiments performed in

current clamp mode we used the same extracellular solution used for the MEA recordings and the intracellular solution contained (mM): 135 KAsp, 8 NaCl, 20 HEPES, 2 MgCl$_2$, 5 EGTA.
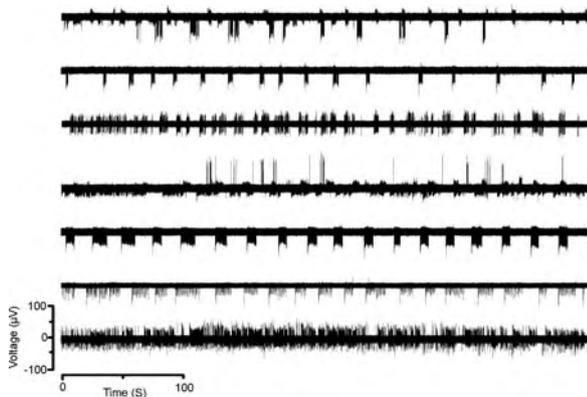


**Fig.2.** Trains of spontaneous action potentials recorded with a MEA system from cultured RCCs

## 3 Results and Discussion

Preliminary analysis of spontaneously active RCCs revealed the existence of two distinct modes of autorhythmic activity (Fig.2): a bursting mode interrupted by periods of quiescence and a continuous mode of firing with mean frequency of 2-3 Hz. This proves that under physiological conditions, RCCs possess an intrinsic autorhythmic activity due to the proper expression of pace-making and action potential-generating ion channels at the cell membrane. The autorhythmic activity was clearly resolved as biphasic signals characterized by an early fast negative component of 40-100 μV amplitude lasting less than 1 ms followed by a delayed component of opposite sign of 10-20 μV, lasting 2-3 ms. The biphasic signals could have opposite sign and were proportional to the positive or negative first derivative of the intracellularly recorded action potential. The two types of responses accounted for more than 90% of the MEA recordings. Since a signal proportional to the negative first derivative is usually associated to electrical responses of cells expressing high densities of voltage-gated ion channels at the cell-electrode interface [3, 4] we focused our analysis on the RCCs which produced this type of response. We found that low doses of TTX (3-10 nM) decreased the early negative component of extracellular signals (Fig.3) and 300 nM TTX fully blocked the spikes, suggesting that TTX-sensitive Na+ channels contribute to the generation of the fast negative component of MEA recordings. Increasing doses of TEA (1-20 mM) had, on the contrary, little effects to the fast component but reduced and prolonged the delayed positive phase of MEA recordings (Fig.3), in good agreement with the observation that TEA prolonged the duration of intracellular action potentials by blocking voltage-gated and Ca2+-

dependent K+ channels [2]. Ca2+ channels were found to contribute to both the depolarization and repolarization phase of the action potential as well as to the firing frequency. Removal of Ca2+ from the bath or addition of 500 μM Cd2+ blocked the spontaneous firing while addition of the L-type channel blocker, nifedipine (3 μM), produced a net reduction of the delayed positive phase and reduced the frequency of firing, suggesting strict coupling between L-type and Ca2+-dependent K+ channels and a specific role of L-type channels in pace-making chromaffin cells activity [2].
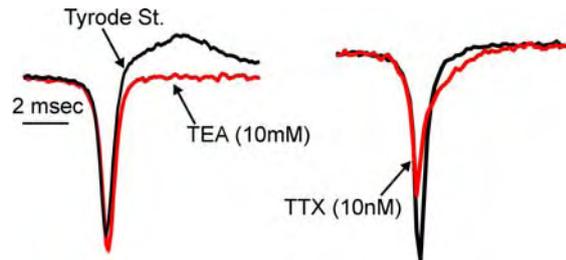


**Fig.3.** Effects of TEA and TTX on the shape of single extracellular action potentials (average of 20 traces)

Our preliminary experiments demonstrate that MEA is a promising tool for studying RCCs excitability, allowing the detection of spontaneous action potentials without altering the cell membrane and the intracellular environment as in patch-clamp experiments. Here we show the spontaneous electrical activity of RCCs plated on a standard MEA, revealing the presence of two different pattern of activity (bursts or continuous) that could be related to different physiological cell functions. Preliminary experiments performed comparing the effects of different drugs on the shape of the extracellular and intracellular action potentials reveal a strict correspondence between extracellular MEA signals and intracellular action potential recordings and makes the MEA system a valuable tool for studying the functional role of ion channels in cell excitability.

**References**
[1] Carbone E. et al. (2006) Pflugers Archiv **453**: 373-383
[2] Marcantoni A. et al. (2007) Cell Calcium **42**: 397-408
[3] Schätzthauer R. & Fromherz P. (1998) Europ J. Neurosci. **10**: 1956-1962
[4] Fromherz P. (2003) In: *Nanoelectronics and Information Technology*. Ed Waser R., Wiley-VCH, Berlin p. 781-810.

# *In vitro* dynamics of small engineered networks of *helix* neurons coupled to Micro-Electrode Arrays

Paolo Massobrio[1]\*, Mariateresa Tedesco[1], Mirella Ghirardi[2], Carlo Giachello[2], Sergio Martinoia[1]

1 Neuroengineering and Bio-nano Technology Group (NBT), Department of Biophysical and Electronic Engineering (DIBE), University of Genova, Genova (Italy)
2 Department of Neuroscience, University of Torino, Torino, (Italy)
\* Corresponding author. E-mail address: paolo.massobrio@unige.it

Aim of this work is the implementation and characterization of small-engineered cultured neuronal invertebrate networks coupled to Micro-Electrode Arrays (MEAs). In particular a one-to-one correspondence between neurons and microelectrodes was obtained in order to investigate the basic electrophysiological properties of *Helix aspersa* circuits.

## 1 Introduction

Micro-Electrode Array technology constitutes a valid and well recognized methodology to investigate the basic dynamical properties of neuronal networks coming from different biological preparations. In this work, we reported preliminary studies about the possibility to couple big neurons of invertebrates (*Helix aspersa*) to the microelectrodes in a one-to one ratio. In this way, it is possible to build well defined and engineered neuronal circuits that can be characterized by means of cross-correlation based algorithms.

## 2 Materials and Methods

### 2.1 Cell Culture

Neurons of *Helix aspersa* snails were individually identified by their position and their size in the ganglia, removed by sharp glass microelectrodes and transferred to MEA pretreated with poly-L-lysine (0.5 mg/ml in sodium tetraborate 0.1 M, pH 8.2) and *Aplysia* hemolymph. In particular in this work, we considered the *in vitro* circuits that originate among C1, B2 and buccal (B1 and B3, not distinguished by their shape) neurons. Fig. 1 shows an example of network made up of *Helix* neurons. It is evident the sizes of such neurons with respect to the microelectrode dimension: this makes easy a one-to-one coupling even with manual positioning.

### 2.2 Experimental setup

*Helix* cells were plated over 8 x 8 MEA (30 μm diameter, 200 μm inter-electrode distance), purchased by Multi Channel Systems (Reutlingen, Germany). Electrical activity was evoked by means of voltage pulses released by a glass microelectrode placed over the cells and controlled by a mechanical micromanipulator.
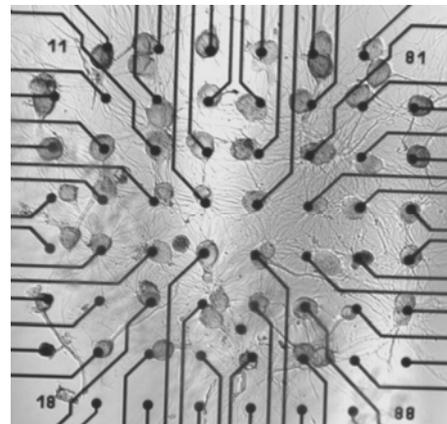


**Fig. 1.** Differential Interference Contrast image of a network of *helix* neurons coupled to a MEA.

### 2.3 Data analysis

Spikes were detected by means of a previously developed differential threshold spike detection algorithm [1] adapted for longer and larger signals. From the generated spike train, we evaluated the cross-correlation function between the pairs of spike trains. Then, we built the functional connectivity map, by taking into account the latencies of the picks of the cross-correlation function, and we evaluated the more probable connections among the three kinds of neurons.

## 3 Results

*Helix* neurons are generally silent, i.e., no spontaneous activity appears [2]. Thus, by means of a glass microelectrode, we first delivered voltage pulses to trigger the action potentials. Once this process starts, it lives on for several hours. All the performed analysis concerns these phases of electrophysiological activity after the stimulation.

### 3.1 Neuronal dynamics exhibited by *Helix* neurons

The principal feature of *Helix*'s neuron signals is the slow dynamics, both in terms of shape and frequency [3]. However, the three aforementioned classes of cells (C1, B2, and buccal), show small differences in the timing and frequency, as highlighted in the raster plot of Fig. 2 and by Inter-Spike Interval analysis (not shown). We found that the mean firing rate for buccal, C1 and B2 cells assumes values equal to $5.14 \pm 2.63$, $1.86 \pm 0.85$ and, $2.43 \pm 1.45$ spikes/s (mean $\pm$ standard deviation).
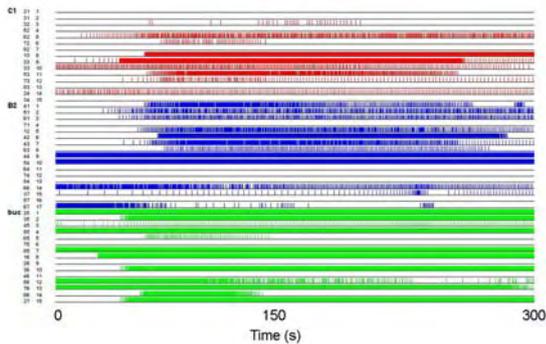


**Fig. 2.** Raster plot of 1 min of electrophysiological activity of C1 (red), B2 (blue), and buccal (green) cells.

### 3.2 Identification of synaptic pathways

Several studies concerning the *Helix aspersa* neurons are devoted to study the local circuits that can be established.

Up to know these features were investigated by using patch clamp techniques which allows to record only from few neurons. This limitation can be overcome by plating a neuron for each microelectrode of a MEA. In this way, several connections take place and a more complex network arises. Thus, we reconstruct the connectivity map (Fig. 3) by evaluating the latency of the peaks of the cross-correlation. We applied a threshold to the latency in a range between 5 and 10 ms: this choice guarantees that we take into account only physiological synaptic delays [2]. In Fig. 4, we quantified the percentage of detected connections among all the kind of neurons.

## 4 Discussion and Conclusions

The use of big neurons of invertebrates (in this work, neurons of *Helix aspersa*) coupled to MEA offers the possibility to recreate well defined networks with peculiar dynamics and connectivity properties, that were investigated by applying cross-correlation based algorithms. However, the level of precision regarding the connectivity could also be increased if the

growth of the neurites is driven by using engineered methods such as micro-patterning techniques [4, 5]. Thus, the natural next step will be the implementation of an *ad hoc* set-up able to release drops of adhesion molecules to allow a spatial-confined outgrowth of the neurite and a more specific connectivity.
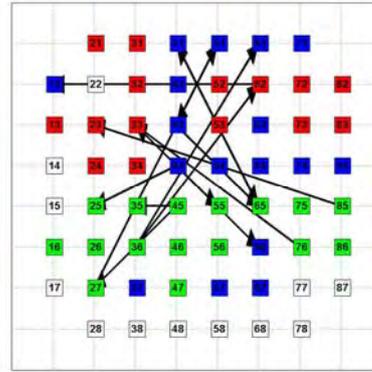


**Fig. 3.** Functional connectivity map of the neuronal network shown in Fig.1. Red, blue and green squares state for C1, B2 and buccal neurons, respectively.
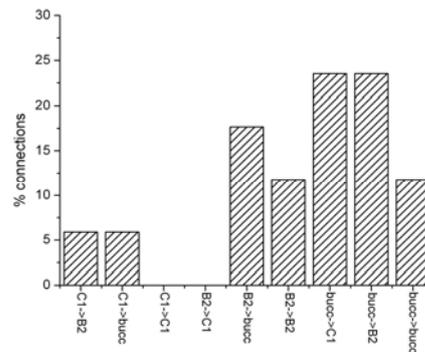


**Fig. 4.** Percentage of the detected connections among C1, B2 and buccal neurons.

## References

[1] A. Novellino, A. Maccione, M. Gandolfo, M. Chiappalone, P. Massobrio, and S. Martinoia, "A novel spike detection algorithm for real-time applications," in Mea Meeting 2006, Reutlingen, 2006, pp. 73-74.

[2] F. Fiumara, G. Leitinger, C. Milanese, P. G. Montarolo, and M. Ghirardi, "In vitro formation and activity-dependent plasticity of synapses between helix neurons involved in the neural control of feeding and withdrawal behaviors," Neuroscience, vol. 134, pp. 1133-1151, 2005.

[3] S. Antic and D. Zecevic, "Optical signals from neurons with internally applied voltage-sensitive dyes," The Journal of Neuroscience, vol. 15, pp. 1392-1405, 1995.

[4] E. Claverol-Tinturé, M. Ghirardi, F. Fiumara, X. Rossel, and J. Cabestany, "Multielectrode arrays with elastometric microstructured overlays for extracellular recordings from patterned neurons," Journal of Neural Engineering, vol. 2, pp. L1-L7, 2005.

[5] E. Macis, M. Tedesco, P. Massobrio, R. Raiteri, and S. Martinoia, "An automated microdrop delivery system for neuronal network patterning on microelectrode arrays," Journal of Neuroscience Methods vol. 161, pp. 88-95, 2007

# Homeostatic regulation of activity in cortical networks

Samora Okujeni[1,2*] Steffen Kandler[1,2], and Ulrich Egert[1,3]

1 Bernstein Center for Computational Neuroscience Freiburg, Germany
2 Neurobiology and Biophysics, Institute of Biology III, University Freiburg, Germany
3 Biomicrotechnology, Department of Microsystems Engineering, University Freiburg, Germany
* Corresponding author. E-mail address: okujeni@biologie.uni-freiburg.de

In absence of complex architecture, central parameters of connectivity in neuronal networks are the size of dendrites and axons in conjunction with the spatial distribution of cell bodies. We study the effects of connectivity on activity dynamics in cultures of dissociated cortex by pharmacologically manipulating neuronal differentiation processes. This work shows that neurons developing under inhibited PKC activity display enhanced neurite outgrowth and decreased cell migration and pruning. Despite of changes in the connectivity statistics we found no profound changes in level and structure of activity of single neurons indicating homeostatic regulation mechanisms. Effects on network dynamics that are currently investigated however indicate functional consequences of altered connectivity statistics.

## 1 Background

Central parameters of connectivity in random neuronal networks are the spatial distribution of neurons in conjunction with the size and branching complexity of axonal and dendritic fields. We investigate these features and their functional consequences in cultures of dissociated cortical neurons. These generic random networks display a self-regulated maturation process characterized by cell migration, neurite outgrowth and pruning, similar to the critical period in developing cortex. Within this period we modulated neuronal connectivity by pharmacologically interfering with structural differentiation processes. Previous studies demonstrated that inhibition of the protein kinase C (PKC) prevented cell migration in granule cell cultures (Kobayashi, 1995), increased dendritic arborization of Purkinje cells in organotypic cerebellar slices (Metzger, 2001) and impaired pruning in climbing fibers of the cerebellum (Kano, 1995). Following these findings, cortical cell cultures were chronically treated with PKC inhibitors and morphological effects investigated and correlated to the activity dynamics in the developing networks.

## 2 Methods

Primary cell cultures were prepared from newborn rat cortices following a standard protocol adapted from S. Marom. Cells were plated at densities ranging between 1000-9000 cells per mm$^2$ onto PEI coated MEAs and coverslips. Cultures were incubated at 5% $CO_2$ and 37°C. One third of medium was replaced twice a week. PKC inhibitors (Goe6976 0.3 & 1 μM, K252a 0.15 μM; Sigma-Aldrich) were applied with the first medium exchange at DIV1. For morphological characterization, cultures were stained against microtubule-associated protein 2 (Abcam). Recordings were performed under culture conditions (MEA1600-BC system, MCS, Germany).
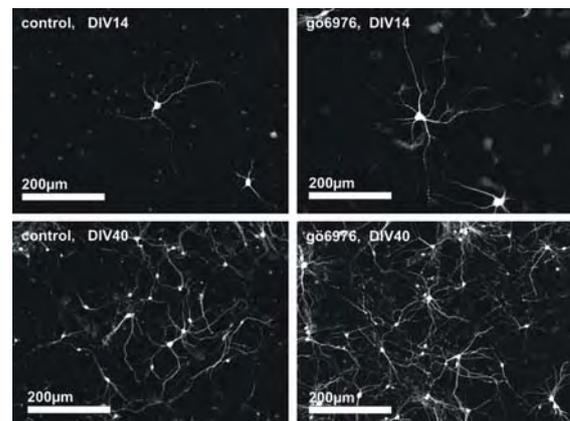


**Fig. 1.** Visualization of the dendritic network. Immunohistochemical staining against MAP2 expressed in dendrites and cell bodies. Chronic treatment with the PKC inhibitor Goe6976 resulted in enhanced neurite outgrowth in isolated neurons and in neurons embedded in a network

## 3 Results

Dendritic fields were characterized with a modified Scholl analysis (Scholl, 1953) describing the radial dendritic field density of neurons. To account for the overlap of dendritic fields of spatially non-uniformly distributed neurons and for the influence of neuronal neighborhood relations on neuritic differentiation, neurons were grouped into classes of comparable local neuron density. For this we determined the number of neighboring neurons within a range of

100μm according to a measure for spatial clustering (Prodanov, 2007). Blocking PKC activity significantly enhanced maximal radial dendritic arborization up to +20% at intermediate (DIV14) and about +75% at later stages (DIV40) of development (Fig. 3). Typically, neurite density decreased in untreated cultures but slightly increased with PKC inhibition between DIV14 and DIV40. This suggests that blocking PKC activity prevents pruning and prolongs the neurite elongation phase. Neurons in sparse cultures with negligible dendrite field overlap were traced manually and likewise showed significantly enhanced dendritic field extents under PKC inhibition at DIV14 (Fig .2).

Although the overall neuron density revealed no differences across conditions (data not shown), control cultures had a higher proportion of neurons in regions with higher local neuron density. This indicates that cell migration was inhibited under PKC inhibition, resulting in the persistence of the homogenous initial spatial distribution of neurons. Comparable neuron distributions within one condition after DIV14 indicate that neuronal migration is largely accomplished in the initial phase of network maturation.

Electrophysiological recordings performed in the course of development revealed no significant changes in global level of activity, firing rates of single neurons or regularity of spiking. Changes in the size distribution of neuronal avalanches (Beggs, 2003) during development, however, followed the course predicted by a model of homeostatic network maturation and revealed an accelerated development of the network under PKC inhibition consistently with the prediction of a model for enhanced neurite outgrowth (Tetzlaff et al., Cosyne 2008).

## 4  Summary

Our work shows that pharmacological inhibition of PKC activity enhances neurite outgrowth and prevents cell migration and pruning in cortical cell cultures. This establishes modified connectivity statistics in the developing networks. The lack of profound changes in level and structure of activity of single neurons points towards homeostatic mechanisms that regulate these dynamics independent of neuronal connectivity statistics. Changes in the network dynamics that are currently investigated, however, indicate functional consequences of altered connectivity statistics.
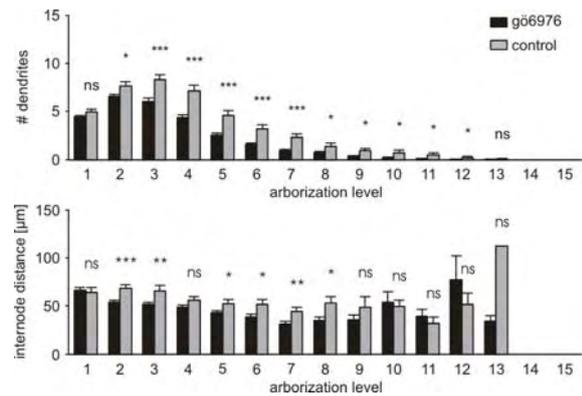
**Fig. 2.** Dendrite characteristics of single neurons. Dendrites of neurons in sparse cultures at DIV14 were traced manually and internode characteristics determined in dependence of the arborization level. Cultures chronically treated with the PKC inhibitor Goe6976 (1muM) revealed significantly more dendrites and slightly longer internode distances at intermediate arborization levels revealing enhanced bifurcation probabilities and neurite elongation. Bars depict mean values ±SEM. Significance levels were determined using student's t-test (5, 1, and 0.1 %)
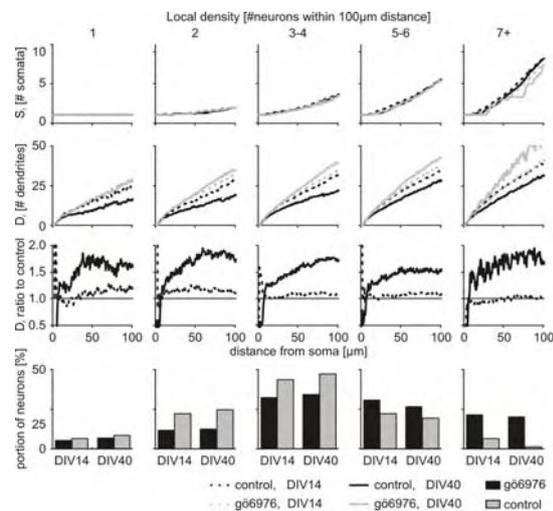


**Fig. 3.** Modified Scholl analysis. Neurons were grouped according to their local neuron density (columns) and the radial dendritic density ($D_r$) determined for these groups (2nd row). The ratio of $D_r$ between treatment and control cultures emphasizes that PKC inhibition results in a higher radial dendrite density. This effect is markedly increased in older cultures. The number of somata within a certain distance from the soma ($S_r$) (1st row) shows that grouping according to local neuron density results in similar neuronal neighborhood relations in the comparison across pharmacological conditions. The bottom row depicts the percentage of neurons in a density class. Control cultures show a tendency towards denser classes indicating stronger clustering due to cell migration.

**References**

[1]  Kobayashi S (1995). *Brain Res Dev Brain Res 90 122-128.*
[2]  Metzger F (2000). *Eur J Neurosci 12 1993-2005.*
[3]  Kano M (1995). *Cell 83 1223-1231.*
[4]  Scholl DA (1953). *Journal of Anatomy 87 387-406.*
[5]  Prodanov D (2007) *J Neurosci Methods 160 93-108.*
[6]  Beggs JM (2003). *J Neurosci 23 11167-11177.*

# Neuronal Avalanches In Networks Of Neurons Cultured In Vitro

Valentina Pasquale[1*], Paolo Massobrio[2], Luca Leonardo Bologna[1], Michela Chiappalone[1], Sergio Martinoia[1,2]

1 Department of Neuroscience and Brain Technology, Italian Institute of Technology (IIT), Genova, Italy
2 Neuroengineering and Bio-nanoTechnology Lab (NBT), Department of Biophysical and Electronic Engineering, University of Genova, Genova, Italy
* Corresponding author. E-mail address: valentina.pasquale@iit.it

Periods of synchronized bursting activity are usually generated by different *in vitro* models for the study of neural dynamics (acute and cultured brain slices, cultures of dissociated neurons): in 2003, Beggs and Plenz [1] demonstrated that within these synchronous epochs there exists a more sophisticated embedded form of dynamics, called *neuronal avalanche*. In this work, we analyzed the electrophysiological activity produced by networks of dissociated cortical neurons cultured onto MEAs by considering the approach proposed by Beggs and Plenz [1] and we asked whether and how neuronal avalanches are intrinsic to the network formation and stabilization, trying to understand the phenomenon of self-organization in cortical networks. We found that criticality is related both to the development of networks and balance between synchronization and variability in the bursting activity.

## 1 Methods

### 1.1 Cell preparation

Dissociated neuronal cultures were obtained from cerebral cortices of embryonic rats (E18), through enzymatic (0.125% trypsin solution for 25–30 min at 37 °C) and mechanical dissociation. Cells were then plated onto 60-channel TiN-SiN MEAs (Multi Channel Systems, Reutlingen, Germany) pre-treated with adhesion promoting molecules (poly-L-lysine and laminin) at the final density of about 1500 cells/mm$^2$. For more details about cell culture technique, see [2].

### 1.2 Processing technique

A *neuronal avalanche* is defined as an event of widespread spontaneous electrical activity over the MEA, preceded and followed by a silent period: from the spike-detected signals, we identified neuronal avalanches as sequences of consecutive time bins of width $\Delta t$, which contain at least one spike on one electrode of the array. Then, the *avalanche size* is defined as the number of electrodes being active at least once inside an avalanche, while the duration of an avalanche is usually called *avalanche lifetime* and is expressed in number of bins $\Delta t$. We derived the relative histograms of avalanche sizes and lifetimes and reported the results in bilogarithmic plots.

The time scale of the phenomenon is different as it is referred to spiking activity and not to LFPs (as for slices): thus, the time window used to bin the spiking activity has to be considerably reduced (range $0.2 - 1$ ms) with respect to other *in vitro* preparations.

### 1.3 Dataset

We considered several recordings of spontaneous activity, both in mature cultures (3 cultures, 4th week *in vitro*) and during development (6 cultures, recorded twice a week from 7 to 42 days *in vitro*), as well as a large-scale network computational model, developed to interpret the experimental results (see [2] for details).

Some cultures were treated with specific drugs affecting the bursting dynamics of *in vitro* cortical networks: we tested acetylcholine (ACh) in concentration 10 μM on 3 cultures and bicuculline (BIC) in concentration 30 μM on other 3 cultures [3].

## 2 Results

### 2.1 Mature cortical networks display different avalanche distributions

We observed different distributions of avalanche sizes and durations, i.e. sub-critical, critical or super-critical, depending on both the age and the development of cultures (Fig. 1).

The number of avalanches detected per minute is low until the 3rd week *in vitro*; then, it increases and generally reaches a stable state that is maintained during the whole mature phase. Once a culture had reached the mature stage, it showed a preferred behavior (critical, subcritical or supercritical), even if some deviations are possible.

In fact, there is variability among cultures, showing that every network develops in a different way ac-

cording to some factors, such as the actual plating density, the cellular composition and the coupling with the electrodes.

## 2.2 Avalanche distribution is correlated with balance between synchronization and variability in the bursting activity

These behaviors correlate with the level of synchronization among bursts and the ratio between bursting and random spiking activity. In particular, criticality was found in correspondence to medium synchronization among bursts and poor random spiking activity (Fig. 2).

We confirmed these results through the application of specific drugs affecting the balance between coherence and variability in the network's activity (i.e. ACh and BIC). These hypotheses were also confirmed by the computational model, in which we mimicked both the spontaneous activity and the effect of these substances on cultures and we found the same results as in the experiments (data not shown). In particular, simulated results support the plausibility of a scale-free network topology underlying the critical state.

## 3 Conclusions

Cortical neurons preserve their capability of self-organizing in an effective network also when dissociated and cultured *in vitro*. The distribution of avalanche features seems to be critical in those cultures displaying medium synchronization among bursts and poor random spiking activity, as confirmed by chemical manipulation experiments and modeling studies.

**References**
[1] J. M. Beggs and D. Plenz (2003): Neuronal avalanches in neocortical circuits. The Journal of Neuroscience, 23, 11167-11177.
[2] V. Pasquale, P. Massobrio, L. L. Bologna, M. Chiappalone, and S. Martinoia (2008): Self-organization and neuronal avalanches in networks of dissociated cortical neurons. Neuroscience, 153, 1354-1369.
[3] G. W. Gross, H. M. E. Azzazy, M. C. Wu, and B. K. Rhodes (1995): The use of neuronal networks on multielectrode arrays as biosensors. Biosensors & Bioelectronics, 10, 553-567.
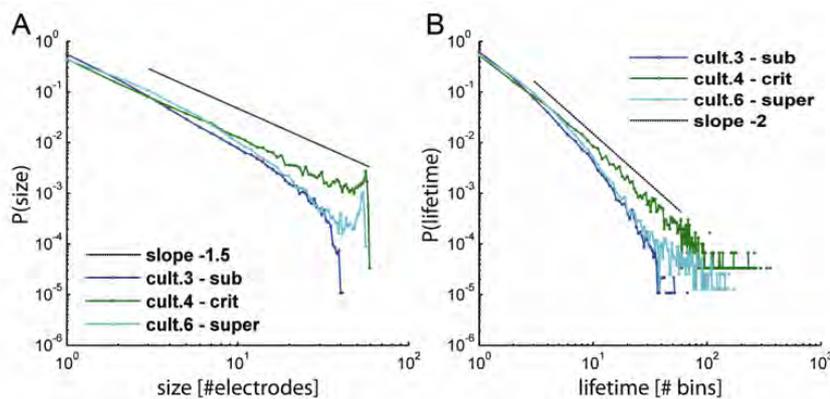


**Fig. 1.** In mature cultures we can observe different dynamic behaviors, exemplified by three selected cultures. A, Avalanche size distributions. B, Avalanche lifetime distributions. Both histograms are compared with power laws whose exponents are -1.5 and -2, for the size and for the lifetime respectively.
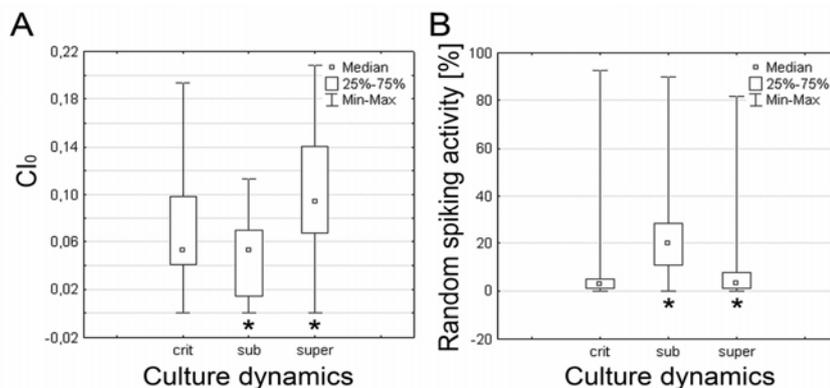


**Fig. 2.** Different avalanche distributions correspond to different global activities, both in the synchronization level and the proportion between random spikes and bursts. A, Box plots of CI0 distributions for critical, subcritical and supercritical cultures. B, Box plots of percentage of random spiking activity distributions for the same groups of cultures

# Dynamics of Spontaneous Activity in Long-Term Measurements

Pettinen, A[1*], Mikkonen JE[1,2*], Teppola H[1], Linne M-L[1], Egert U[2]

1 Department of Signal Processing, Tampere University of Technology, Finland
2 Bernstein Center for Computational Neuroscience, Albert-Ludwigs-University Fre burg, Germany
* Equal contribution

The focus of the experiments done using MEAs has traditionally been in repeated short-term measurements. However, in this study we utilize a specific setup to measure the activity of cell cultures over a longer term, in order to develop new methods for analysis of quantitative changes in the measurements and to provide insight on the dynamic shifts in baseline during long-term measurements.

## 1 Background and Aims

Microelectrode arrays (MEAs) have well established themselves as a dextrous tool for measuring the behaviour of networks consisting of electrically active cells. The focus of the experiments done using MEAs has traditionally been in repeated short-term measurements (see, e.g. [1]). However, in this study we utilize a specific setup to measure the activity of cell cultures over a longer term. The aim of this study with long-term measurements of cultured neurons and neuron-like cells is both to develop new methods for analysis of quantitative changes in the measurements and to provide insight on the dynamic shifts in baseline during long-term measurements. The former provides new points of comparison for such long-term measurements where the cells are stimulated, either electrically or chemically, while the latter is beneficial in extracting new information considering baseline changes over a longer period of time.

## 2 Methods

Cells were obtained from Wistar rat prefrontal cortex within 24 hr after birth (P0) and mechanically and enzymatically dissociated using standard cell biology protocol modified from [2]. $10^6$ cells were plated on substrate-integrated MEAs coated with polyethylene imine. The cultures were maintained in an atmosphere of 37°C, 5% CO2 and 95% air in an incubator. Quarter of the medium was exchanged twice per week. The basic measurement system was an MCS microelectrode array (MEA) system. This system was modified to enable uninterrupted measurements over extended periods of time, ranging from days to weeks (with an additional perfusion system). The utilization of long recordings prevented the involuntary stimuli, and enabled the monitoring of changes in the baseline. Thereafter, the spontaneous activity was recorded for at least 12 hours, and the instances of activity were saved for offline analysis with Matlab®.

## 3 Results

During the long-term measurements conducted in this study, the baseline was monitored for spontaneous changes in temporal and spatial activation patterns. Recordings with the presented setup demonstrated that the neuronal cultures have increased activity for up to 10 minutes after mechanical disturbances. Furthermore, overnight experiments demonstrated changes in the baseline activity with emerging high activity states and turn-over of active channels. Our results demonstrate the need for more detailed questions on the interpretation of "control" or "baseline" analysis and their possible consequences on the interpretation of the experimental results.

## 4 Conclusion

We report that there are clear changes in the baseline over a long-term measurement. Thus, it becomes evident that when analyzing long-term measurements, the above-mentioned baseline changes must be taken into account. This requires further development of the analysis methodology for long-term cultures. The methods used here for analyzing the long-term measurement data provide new assets for future development of possible online analysis tools.

## References

[1]  Wagenaar et al (2006): Searching for plasticity in dissociated cortical cultures on multi-electrode arrays, Journal of Negative Results in BioMedicine,  5:16

[2]  Shahaf and Marom (2001): Learning in Networks of Cortical Neurons, The Journal of Neuroscience,  21(22):8782-8788
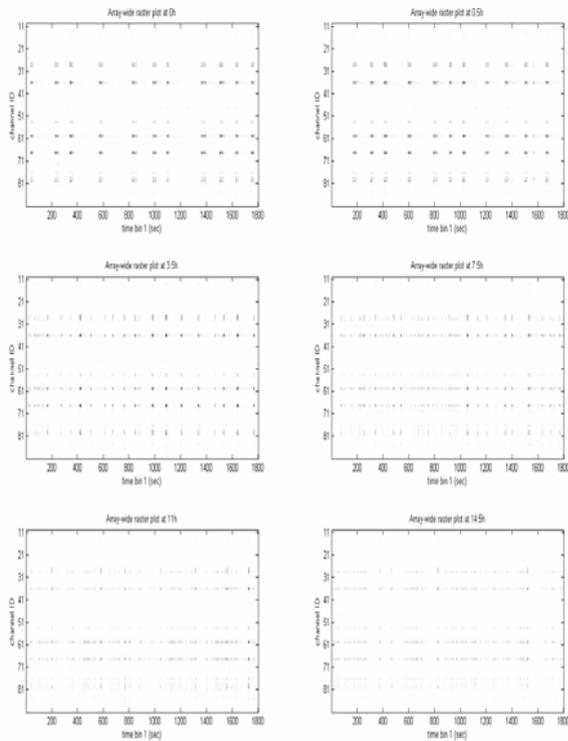
**Fig. 1:** Array-wide raster plots at different timepoints during one measurement.
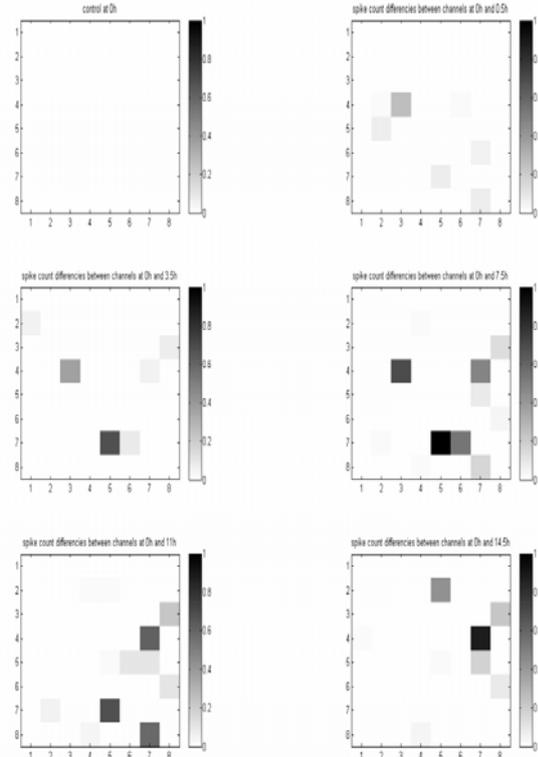


**Fig. 2.** Normalized spike count differencies between channels at different timepoints during one measurement

# Large Neuronal Networks Are Needed for Burst Formation in Cortical Cultures *in Vitro*

Andrea Rabosio[1], Katia Laganá[2*] Elisabetta Menna[3], Michele Matteoli[3] Philippe Kern[4], Alessandro Spinelli[5], Gytis Baranauskas[156*]

1 Department of Material Chemistry and Chemical Engineering, Politecnico di Milano, Italy
2 Laboratory of Biological Structure Mechanics, Department of Structural Engineering, Politecnico di Milano, Milan, Italy
3 Department of Medical Pharmacology and Consiglio Nazionale delle Ricerche- Institute of Neuroscience, University of Milan, Italy
4 EMPA – Materials Science and Technology, Micro/Nano-Patterning group, Thun, Switzerland
5 Electronics and Information Department, Politecnico di Milano, Milan, Italy
6 Department of Robotics, Brain and Cognitive Sciences, Italian Institute of Technology
* Corresponding author. E-mail address: baranauskas.gytis@iit.it

It has been shown that cortical cultures develop regular bursting activity after two weeks in culture *in vitro*. It is not clear whether such a type of neuronal activity can be modulated by network size and architecture. To address this question, neuronal cultures patterned in narrow 40 μm strips have been grown in vitro for 2-3 weeks. No bursting activity has been observed in patterned cultures for 2 weeks while the appearance of irregular burst during the 3d week in vitro coincided with the establishment of connections between the stripes. We conclude that a large network of neurons is required for the generation of regular bursts.

## 1 Introduction

It is well established that in cortical cultures *in vitro* bursting of action potentials develops during the first two weeks in culture [1, 2]. Since no such continous regular bursting is observed *in vivo* [3], we asked whether large, apparently chaotically interconnected networks of neurons that form in *in vitro* cultures could be a reason for such a phenomenon. To test this hypothesis, we employed cortical cultures patterned on MEA electrode arrays .

## 2 Methods

Neurons were derived from E18-E19 rat embryos and grown in a standard serum free medium. For polylysine pattern micro-printing, PDMS stamps were obtained from matrices fabricated employing maskless UV lithography. Before micro-printing MEAs were washed with acid solution (pH = 2) to remove any absorbed polylysine and left overnight with pluronic acid (1 %) to reduce non-specific protein adhesion. A single type of pattern of approximately 1300 μm long, 40 μm wide strips separated by 60 μm gaps was used (Fig. 1). In addition, all surrounding area of approximately 3 $cm^2$ was stamped with un-patterned polylysine. For control experiments, cultures were seeded on non-patterned MEAs. Multichannel Systems (Reutlingen, Germany) set-up was used to record cultures while ClustaKwik and IgorPro (Wavemetrics) software was used for data analysis. Regular bursting activity was defined by the presence of a clear peak in the inter-spike interval distribution histogram (Fig. 2) that corresponded to the intervals within a burst (<0.5 s). In addition, a coefficient of variation (CV) was used as an indicator of the presence of bursts (CV > 1.5).

## 3 Results

Initially, all neurons adhered only to the area containing stamped polylysine that is the strips and the surrounding non-patterned area (Fig. 1). In non-patterned networks a clear bursting activity could be detected, on average, after 9 days *in vitro* (DIV9, n = 8). Such distinct bursts were always present at DIV10 (n = 8). In contrast, during the first 13 days, no such bursting activity could be detected in any patterned cultures (n = 11). In a fraction of patterned cultures (4/11), a regular firing without bursts could be observed for several days in a row after 9-11 days in vitro (Fig. 2). In non-patterned cultures, such a regular firing without bursts could be observed only on 2/70 electrodes (2 out of 8 cultures) and it lasted only a single day. During further development of cultures, occasional axons would grow across non-stamped, polylysine free areas thus connecting several stripes into a single network. The establishment of this connectivity between several stripes coincided with the appearance of irregular bursting (n = 4/11) during the late stages of development in vitro (> 13 days in vitro). However, no regular bursting could be detected in patterned neuronal cultures even after 20 days in vitro.
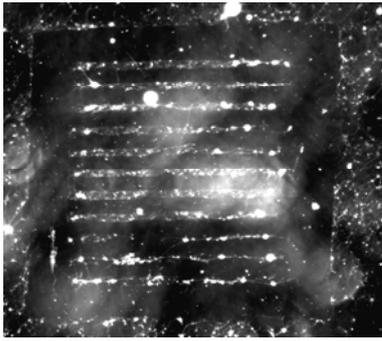
**Fig. 1.** A photo of an example of a neuronal pattern after 5 days in vitro. The pattern size is 1.3 mm X 1.3 mm.

## 4   Conclusions

Our data show that no bursting could be detected in neurons that grew in separate stripes and only an occasional regular firing without bursts of action potentials could be observed in such cultures. The occurrence of bursts seems to require the presence of large interconnected neuronal networks as the appearance of the first bursts coincided with the development of connections between stripes. However, because of the distance between stripes, such connections were established at late stages of development (> 13 days *in vitro*). Thus, the occurrence of bursts was much delayed in patterned cortical cultures. However, even in the presence of these interstripe connections in patterned cultures, no regular bursting could be detected for at least 3 weeks. We conclude that large interconnected neuronal networks are required for the appearance of continous, regular action potential burst firing. It is likely that fine tuning of network connections that occur during the development *in vivo* [4] suppresses the generation of such continous regular burst firing in neurons of adult brain.

**Acknowledgement**

**References**

[1] Chiappalone M., Bove M., Vato A., Tedesco M. & Martinoia S. (2006): Dissociated cortical networks show spontaneously correlated activity patterns during in vitro development. *Brain Res 109, 41-53*.

[2] Wagenaar D.A., Pine J & Potter SM (2006): An extremely rich repertoire of bursting patterns during the development of cortical cultures. *BMC Neuroscience, 7, 147*.

[3] Wagenaar DA, Nadasdy Z & Potter SM (2006): Persistent dynamic attractors in activity patterns of cultured neuronal networks. *Phys Rev E Stat Nonlin Soft Matter Phys 7, 051907*.

[4] Khazipov R, Sirota A, Leinekugel X, Holmes GL, Ben-Ari Y & Buzsaki G (2004): Early motor activity drives spindle bursts in the developing somatosensory cortex. *Nature, 43, 758-61*.
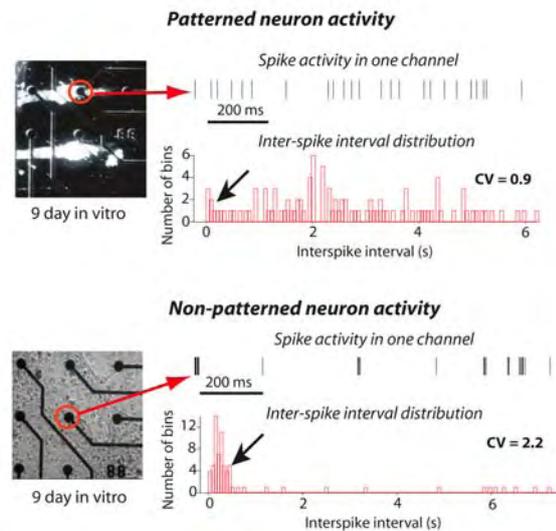
**Fig. 2.** No bursting activity is detected in patterned cortical cultures for at least 13 days *in vitro*. *Top row*, a photo of an example two neuronal stripes grown on MEA (left panel) and of activity recorded from the red-circled electrode (right top panel). Only spikes denoted as bars are shown. An interspike interval histogram shows no peak (the arrow indicates the expected location of the peak) indicating the absence of bursts while a low coefficient of variance (0.9) indicates the absence of any pattern in the neuronal activity. *Bottom row*, in contrast, in non-patterned cultures of the same age (a photo of an example culture grown on MEA shown in the left panel) clear bursts could be detected (top right, spike arrival bar plot) that is confirmed by a high coefficient of variation (2.2) and the presence of peak in the interspike interval histogram (right bottom panel).

# Impairment of synaptic plasticity in STOP null mouse: a multi-electrode array study

Ruiz Geoffrey [1, 2], Andrieux Annie [2], Job Didier [2], Roucard Corinne [1], Bressand Karine [1*]

1 SynapCell SAS, Biopolis, 5 avenue du Grand Sablon, 38700 La Tronche, France
2 INSERM U836 Equipe 1 Grenoble Institut des Neurosciences, 38700 La Tronche, France
* corresponding author. E-mail address : kbressand@synapcell.fr

The STOP null mouse is an animal model which presents synaptic and behavioral deficits imitating features of schizophrenia. These deficits can be alleviated by neuroleptic treatment, providing an attractive model to test news antipsychotic drugs. In this study, we explored bioelectrical activity within hippocampal slices of STOP null mice using MEA tool. The aim of the study was to define relevant bioelectrical criteria for STOP null mice. We examined evoked electrical activity in basic conditions, and after paired-pulse and theta burst stimulation in order to study short and long term plasticity (LTP), respectively. The results confirm that only LTP is impaired in STOP null mice and show for the first time that heterozygous STOP mice present a partial LTP impairment.

## 1 The STOP null mouse: an attractive model to test new antipsychotic drugs

STOP null mouse is a genetically modified mouse lacking the STOP gene coding for a protein called Stable Tubule Only Polypeptide (STOP). The STOP protein belongs to the family of microtubule-associated proteins (MAPs). The STOP null mice present hyper-dopaminergy, severe behavioral disorders and synaptic defects in glutamatergic neurons imitating features of Schizophrenia. These deficits can be alleviated by antipsychotic treatment. As synaptic defects were considered as important factor in schizophrenia, this model is very attractive to test new antipsychotic drugs. Andrieux *et al.* (1) found that they present an impairment of long term potentiation in hippocampal neuronal network using usual electrophysiology techniques (glass micropipettes and patch-clamp). The aim of this study was to find relevant bioelectrical criteria which characterize STOP null mice using an efficient and fast technology: Multi-Electrode Array (MEA).

## 2 MEA: an efficient and fast electro-physiological technology

MEA used in this study is the Panasonic's MED64 which allows to record up to 64 electrodes simultaneously. Our biological material consisted in acute hippocampal slices from STOP +/+, +/- and -/- adults BalbC/SV129 mice. Only slices without visible damage were placed on the MEA, and then electrically stimulated within the CA3 area. Evoked responses were recorded within the CA1 area (cf. Fig.

1). An input/output curve is recorded, allowing the selection of stimulation intensity (inducing 50% of maximal amplitude), and a paired pulse test is realized. The paired pulse test consists in a double stimulation spaced by 50ms. After that, evoked responses were recorded for twenty minutes (baseline), and high frequency stimulation (theta burst, TB, 100Hz, 1sec) is applied. Evoked responses were recorded for one hour post TB.
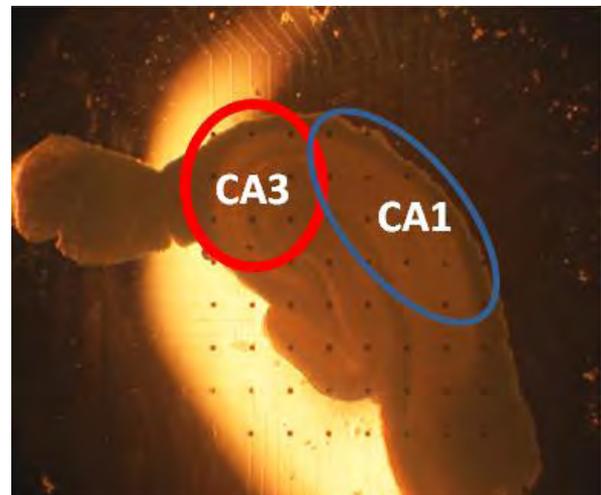


**Fig. 1.** Photograph of a STOP mouse hippocampal slice on MEA showing stimulation (red) and recording (blue) areas.

For each slice, we analyzed the amplitude of evoked responses:
i) During baseline: mean amplitude of evoked responses during the 10 minutes preceding TB.
ii) After paired pulse: mean percentage of increase. Data shown here are only paired pulse facilitation

that is to say increase amplitude after the second pulse compared to the first.

iii) After theta burst: mean percentage of increase between 30 and 60 min after theta burst referred to baseline amplitude.

LTP is defined as a sustained increase of evoked response amplitude after theta burst lasting more than 30 minutes (Fig 2 and 3). Only slices presenting a stable baseline ($\pm$ 20%) and an abrupt increase of evoked response amplitude after TB are taken into account.
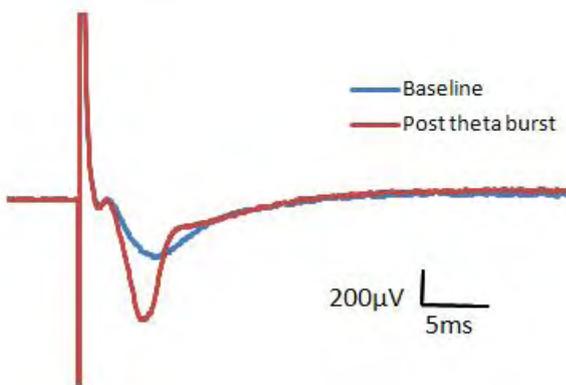


**Fig. 2.** Example of typical evoked responses recorded from a STOP +/+ mouse before and after theta burst. Amplitude is increased after theta burst which is characteristic of LTP.

## 3 LTP impairment as a relevant criterion of STOP null mice

Concerning bioelectrical activity during baseline and paired pulse facilitation, no differences were observed between the three genotypes of STOP mice.

Concerning LTP, we found an increase of 60 $\pm$ 3.6% (n=8 slices) compared to the baseline for +/+ mice. For the -/- mice, the response is only increased by 22 $\pm$ 1% (n=9 slices) following the TB. This result is significantly different from the +/+ result (P<0,001). Heterozygous mice presented an increase of 42 $\pm$ 1.3%

(n=17 slices), intermediate between the +/+ and -/- mice.
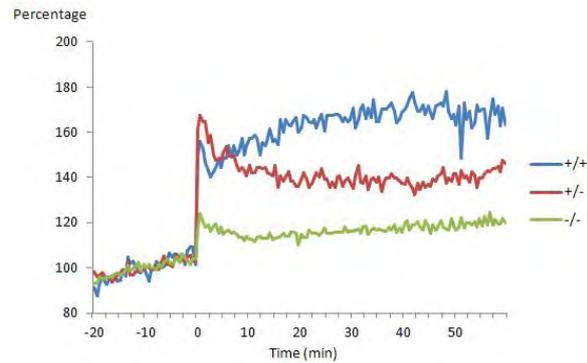


**Fig. 3.** LTP is defined as a sustained increase of evoked response amplitude after application of theta burst. Typical example of one slice for each STOP mouse genotype.

## 4 Conclusion

This study confirms that STOP null mice present an impairment of LTP and shows for the first time that heterozygous STOP mice have an intermediate impairment of LTP probably due to the presence of one allele instead of two. This suggests that the deletion of one allele is sufficient to induce synaptic plasticity's impairment. These results also strongly support the importance of the cytosqueleton and associated proteins such as STOP in the generation and maintenance of LTP. This study confirms the efficacy of the MEA to make easy-to-use and reproducible electrophysiological measurements. MEA represents a relevant tool to explore biomarkers in transgenic mice. This technology will also be used to evaluate antipsychotics drugs effects on LTP mice.

**References**

[1] Andrieux, A., Salin, P., Vernet, M., Kujala, P., Baratier, J., Gory-Fauré, S., Bosc, C., Pointu, H., Proietto, D., Schweitzer, A., Denarier, E., Klumperman, J. & Job, D. (2002) The suppression of brain cold-stable microtubules in mice induces synaptic defects associated with neuroleptic-sensitive behavioral disorders. *Genes Dev*, 16. 2350-2364.

# The Role of Highly-Active Neurons in Developing Networks

Mark Shein[1,2,*], Vladislav Volman[3,4], Nadav Raichman[1], Yael Hanein[2] and Eshel Ben-Jacob[1,3]

1 School of physics and astronomy, Raymond & Beverly Sackler Faculty of exact Sciences, Tel-Aviv University, Tel-Aviv 69978, Israel
2 Department of Physical Electronics, School of Electrical Engineering, Tel Aviv University, Tel Aviv 69978, Israel
3 Center for Theoretical Biological Physics, University of California at San Diego, La Jolla, CA 92093-0319, USA
4 Computational Neurobiology Laboratory, The Salk Institute for Biological Studies, La Jolla, CA 92037, USA
* Corresponding author. E-mail address: markshei@post.tau.ac.il

Recently, there has been a growing interest in spontaneous brain activity following evidence that it may have a functional role. Consequently, considerable effort was directed towards understanding how neuronal spontaneous activity is maintained and regulated. The activity of most neurons in the network is characterized by firing in synchronized bursting events (SBEs), however, a subset of highly active neurons shows rapid activity which persists between SBEs. Here we investigated the dynamical properties and putative role of these highly active neurons (HA-neurons) in cortical cultured networks grown on Multi-Electrode-Arrays (MEA). By using statistical and time-series analysis, we found that the activity patterns of HA-neurons are marked by special firing properties that may be associated with the regulation of the SBEs. We also show that during the course of network development, its activity follows a transition period in which mostly HA-neurons are active. A similar effect was observed in the recovery of the network's activity from intense chemical inhibition of excitatory synapses. Finally, we studied the time order of neuronal activation during SBEs in networks with engineered geometry and found that HA-neurons are typically the first to fire and are more responsive to electrical stimulations.

## 1 Introduction

Electrical activity in the brain is comprised of evoked activity (induced by external stimuli), and spontaneous (internally-generated) activity [1]. Recently, increasing research efforts have been directed to the investigation of spontaneous activity and to studying the physiological mechanisms underlying the generation and regulation of this activity. These studies are motivated by an accumulating body of experimental evidence, which suggests that spontaneous activity may play a decisive role in shaping neural cell assemblies [2]. If so, it consequently implies that some innate, yet unknown, mechanisms of activity maintenance, initiation and regulation should exist.

Cultured networks that exhibit spontaneous activity in the absence of any external electrical stimulations or chemical cues are commonly used as a valuable model system for studying spontaneous neuronal activity [3, 4]. The spontaneous activity in cultured neuronal networks is often marked by the existence of synchronized bursting events (SBEs) - relatively short time windows of several hundreds of milliseconds during which a large fraction of the cells is engaged in intense firing [3, 4]. This mode of collective behavior has been observed across many different brain structures and preparations [5, 6]. However, while the majority of cells fire exclusively during SBEs, a small fraction of the cells appear to fire between SBEs.

In this work, we investigated the dynamics of such cells identified in the spontaneously activity of cortical neuronal networks. In order to investigate the putative regulatory role played by these highly active neurons (HA-neurons), we investigated their dynamics in early developing networks, during recovery from intense chemical inhibition and in response to electrical stimulations.

## 2 Methods

We used micro-electrode arrays (MEA-chip, Multi Channel Systems) to monitor the electrical activity of in-vitro embryonic (18-19 day) rat cortical cultured networks with confined geometry. These networks were restricted (using PDMS stripes) to grow only in the area covered by the electrodes, thus, allowing uniform sampling of all the network area. Recordings and stimulations were performed using MEA-1060B amplifier and STG-1008 stimulator, respectively.

We identified HA-neurons according to their inter spike interval (ISI) profiles; regular neurons, in contrast to the HA-neurons, rarely exhibit ISIs in the interval of $[10^2, 10^4]$ milliseconds. Consequently, we defined HA-neurons to be those with significantly high fraction ($>0.1$) of ISIs in the interval $[10^2, 10^4]$. Such neurons were also found to fire a large fraction of their spikes between SBEs.

# 3 Results

We confirm previous results [7] by showing that while most of the neurons fire during the SBEs, there is a small subset of highly-active neurons (~10% in our cortical cultures) whose activity persists between the SBEs. We found that the activity patterns of these neurons are marked by distinctive firing characteristics - unimodal distribution (vs. bimodal of the rest of the neurons) in the inter spike intervals and by significantly higher power spectral density at low frequencies. Such spectral profile may be indicative of long range auto-correlations, and may suggest the existence of some innate mechanisms which regulate the firing of the HA-neurons during the networks silent states.
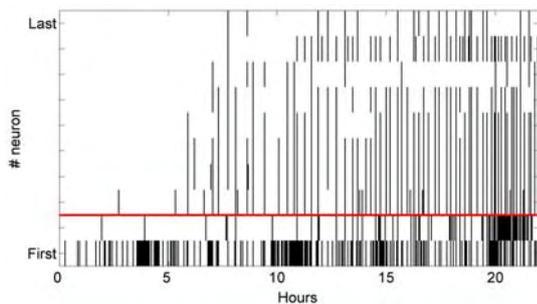


**Fig. 1**. Initiation of electrical activity in developing networks. We show here the activity raster plot of 22 neurons taken at 5th day in vitro. For clarity of presentation, the individual neuronal traces are rearranged according to the time of their first spike (bottom row for the earliest). During the five first hours, mostly HA-like neurons (below the red line) were active. The collective activity emerged later as short time windows of rapid neuronal firings (the SBEs) which were separated by longer intervals of quiescence state.

We next investigated whether HA-neurons have a putative role in the maintenance and regulation of the spontaneous activity of the cultured networks during their development from a collection of isolated cells into mature wired networks of interconnected neurons (figure 1). Our results show that the early network development is marked by a transient period, during which a large fraction of neurons are classified as HA-neurons (figure 2). This fraction gradually decreases during the course of the network's maturation as additional neurons, which fire exclusively during SBEs, begin to fire spikes. A similar effect was observed in the recovery of networks from intense chemical inhibition of glutamatergic synapses. The fraction of HA-neurons gradually increased following the complete abolishment of spontaneous activity in the network.

In addition, we found that in developing networks, HA-neurons act as headers or precursors of the activation of SBEs, in the sense that they are typically the first to fire during a synchronized bursting event.

To further understand this effect we investigated the response of regular neurons and HA-neurons to electrical stimulations. We found that HA-neurons are more excitable in the sense that they responded with a higher fidelity to electrical stimulations regardless of the stimulation location.
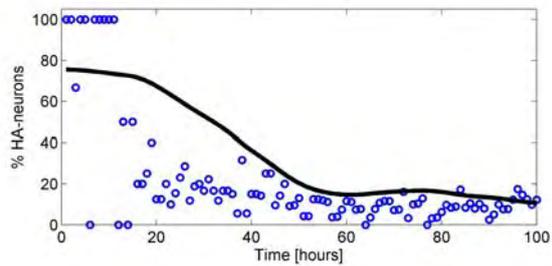


**Fig. 2.** The activity of HA-neurons is correlated with the homeostatic regulation of developing cultured networks. HA-neurons were identified (see methods) in consecutive, non-overlapping, one hour windows. The fraction of HA-neurons in respect to the number of identified active cells (blue circles) is initially high, and decreases gradually during the course of the networks development. The black line is the smoothed average over data from several experiments (N=7).

# 4 Conclusions

Overall, the results presented here suggest that HA-neurons may be recruited by the network to initiate its activity and maintain its activity homeostasis. In this view, HA-neurons can be regarded as highly excitable neurons, which are more sensitive than other neurons to fluctuations in the network's activity. This sensitivity may be regulated in a "network dependent" manner, by a biophysical mechanism yet to be discovered.

**References**

[1] Kandel, E.R., S J. H., and T.M. Jessell, Principles of Neural Science. 4th Ed. ed. Vol. 1. 2000, New York: McGraw-Hill Education.

[2] Yuste, R., Introduction: spontaneous activity in the developing central nervous system. Semin Cell Dev Biol, 1997. 8(1): p. 1-4.

[3] Maeda, E., H.P. Robinson, and A. Kawana, The mechanisms of generation and propagation of synchronized bursting in developing networks of cortical neurons. J Neurosci, 1995. 15(10): p. 6834-45.

[4] Segev, R., et al., Long term behavior of lithographically prepared in vitro neuronal networks. Phys Rev Lett, 2002. 88(11): p. 118102.

[5] Spitzer, N.C., Spontaneous activity: functions of calcium transients in neuronal differentiation. Perspect Dev Neurobiol, 1995. 2(4): p. 379-86.

[6] Ben-Ari, Y., Developing networks play a similar melody. Trends Neurosci, 2001. 24(6): p. 353-60.

[7] Sipila, S.T., et al., Depolarizing GABA acts on intrinsically bursting pyramidal neurons to drive giant depolarizing potentials in the immature hippocampus. J Neurosci, 2005. 25(22): p. 5280-9.

# Study of Spatiotemporal Signal Activity Change after Long-Term Potentiation in Rat Hippocampus using MEA

Shin JA, Son MS, Yang SR and Park JH

Department of Medical Science Graduate School of East-West Medical Science, Kyung Hee University, Yong-In, Korea

## 1 Background

Changes in synaptic efficacy have been hypothesized to be an important process for the memory formation in the central nervous system (CNS). Understanding the mechanisms of LTP is important, not only in the study of neuroscience but also in the study of the pathophysiology of neurological disorders.

## 2 Methods

A stimulation was applied to in the stratum radiatum of the CA1 region to stimulate the SC/commissural pathway from cultured hippocampal slice. LTP induction was made by single point theta bust stimulation (TBS) and several points corresponding recording in a conventional LTP experiment. Moreover, this effect was mediated by activation of a NMDAR and AMPAR, because it was shared by a NMDA and AMPA agonist, and was blocked by its selective antagonist.

## 3 Results

As the results, LTP induction and recording of LTP had extremely obstinate. It had been shown that the induced LTP was blocked by NMDAR antagonist treatment. LTP is regulated by phosphorylation of the AMPAR. It had been shown that AMPAR antagonist also blocked the induced LTP however the reduced LTP amount was smaller than NMDAR antagonist treatment. Moreover, it had been shown that AMPAR antagonist also blocked the induced LTP however the reduced LTP amount was smaller than NMDAR antagonist treatment). Under experimental conditions, application of concentrations of Cassia t. (100 μg/ml) resulted in a significant increase in LTP magnitude. Furthermore, NMDAR and AMPAR antagonist could block increased LTP by Cassia t. treatment. For these reasons, it was assumed that Cassia t. might influence the NMDAR and AMPAR activities. Nevertheless, Cassia t. did not completely blocked by the antagonists. It was shown that Cassia t. would go through other pathway such as metabotropic glutamate receptor (mGluR). Hence, it may need more investigation to understand the action mechanism of mGluRs, and the relationship under induced LTP condition with Cassia t.

## 4 Conclusion/Summary

In this study, two technologies were adapted; organotypic hippocampal slice culture and LTP induction techniques. In this experimental, it was clearly demonstrated that the LTP amount was controlled by it and the controlled LTP used for chemical treatment effects. As the result, it had been shown that the induced LTP was blocked by NMDAR antagonist, MK-801 10 μM and AMPAR antagonist, NBQX 10 μM as others reports. Under this experimental conditions, treatment of concentrations of Cassia t. (100 μg/ml) resulted in a significant increase in LTP magnitude. This tool would be very useful for understanding the mechanism of LTP and effect of drug as using a closer model system to in vivo.

# Changes in bursting caused by learning

Jan Stegenga[*], Joost le Feber, Enrico Marani, Wim L C Rutten

Biomedical Signal and Systems, Institute for Biomedical Technology, Enschede, the Netherlands
* Corresponding author. E-mail address: j.stegenga@utwente.nl

The localization of learning in dissociated cultures to the stimulation-evaluation electrode pair was studied. The cultures were trained using the Conditional Repetitive Stimulation (CRS) algorithm, in which repetitive focal stimulation is ended when a preset ratio of desired responses is achieved. We found that CRS can be used to strengthen an initially weak stimulus-response relationship. We used estimations of the instantaneous firing frequencies per electrode during spontaneous network bursts (NBs), called phase profiles, to determine the spatial extent of the changes required to establish a new stimulus-response relationship in the network. We found significant changes in the profiles, both on the stimulated and observed electrode pair, but also at numerous other sites. The results indicate that most of the changes are uncontrolled and that the whole network is involved during learning.

## 1   Introduction

Multi electrode arrays (MEAs) are an important tool in studying the processing of information in networks of neurons. Central to this research are the neural code and the mechanisms underlying learning and memory. The neural code allows the network to sense its environment and act on it. Learning represents modifications to the networks' connectivity as a consequence of experience. Various stimulation paradigms aiming to change network connectivity, measured by action potential firings in reaction to test stimuli, have been introduced [1-3]. Most of these were open-loop, in that stimulation did not depend on network activity. These showed that, under certain conditions, changes lasting for $\geq 30$ min could be induced. A certain amount of control over the changes that were induced came with the introduction of the conditional repetitive stimulation (CRS) algorithm by Shahaf et al [4]. This was the first successful closed-loop algorithm, as stimulation was stopped when the network response fulfilled a predefined goal. The network could thus be trained to incorporate a new input-output relationship defined between a stimulation electrode and an evaluation electrode. However, the role of the rest of the network has not been investigated. We investigated the influence of learning on spontaneous bursting, with emphasis on the per electrode contributions. To this end, we made profiles of the firing rate during bursts. A profile of summed activity was called a burst profile (BP), and profiles of single electrode activity were called phase profiles (PPs). The size and shape of the profiles was highly dependent on culture and age, and changed on a time-scale of several hours [5]. The relative stability of the profiles during spontaneous development allowed the comparison between profiles before and after CRS with normal development.

## 2   Methods

We used cultures of newborn rat neocortical cells, as described elsewhere [5]. The training procedure was based on that developed by Shahaf et al [4]. Shortly, low frequency stimulation (ISI: 1 to 5 s) was applied to a single electrode as long as a predefined desired response at an evaluation electrode was observed in less than 2 out of the 10 last stimuli. A response was defined as the presence of one or more spikes in a certain time window after stimulation (e.g. 50 to 80 ms) at a non-stimulated electrode. Only electrodes with a small initial response ratio (<0.1) within the response window were chosen for evaluation.

Spontaneous NBs before and after CRS experiment were detected by analyzing the Array-Wide Spiking Rate (AWSR, the sum of activity over all electrodes). Next, we estimated the instantaneous AWSR during a burst by convolving spike-occurrences with a Gaussian function (standard deviation 5-10 ms). We followed the same procedure for each electrode site as well. When bursts were less intense, we used time-averages of several bursts by aligning them to peak AWSR, in order to get a more stable estimation of the per site firing frequency.

Similarity between two profiles was calculated by the mean squared value of their difference. We used t-tests with $\alpha=0.05$ for determining significant changes between sets of profiles (i.e. before-set and after-set). In 4 experiments, the spontaneous activity before a CRS experiment was longer than the CRS experiment. These, and the associated CRS experiments were used to determine any changes that occurred spontaneously (control) and during CRS, respectively.

# 3 Results

## 3.1 Training

Typical learning curves showed a fast initial decrease in the number of stimuli required to elicit the desired response with a responsiveness >0.2 (*N*, see figure 1). Often, a period with higher *N* was observed, before settling on a low value. In many cases we found a decrease in array wide response to stimuli during the learning experiment.
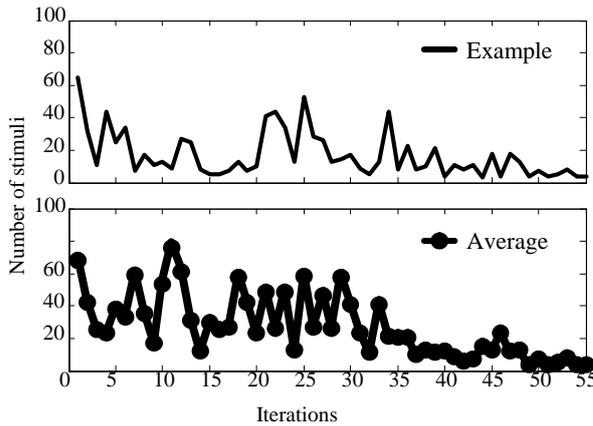


**Fig. 1.** Learning curves. Top) Learning curve of one experiment. Bottom) Average learning curve (12 experiments; 9 cultures).

## 3.2 Profile changes

All BPs changed significantly during CRS, while 2 out of 4 changed significantly also during control. Figure 2 shows how the BPs in one experiment changed shape.
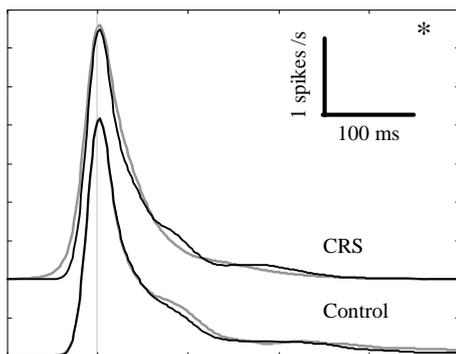


**Fig. 2.** : Change in burst profiles immediately before and after CRS (top two traces, black equals before, gray after). The lower two traces are immediately before and after an equal period of spontaneous development. All curves are 45 minute averages. The single asterisk in the upper right corner indicates that changes were significant only during CRS.

The percentage of PPs that changed significantly increased from 46% during control to 57% during CRS. On average there were 13 active electrodes. Figure 3 shows the changes in PPs in the same experiment as in figure 2.
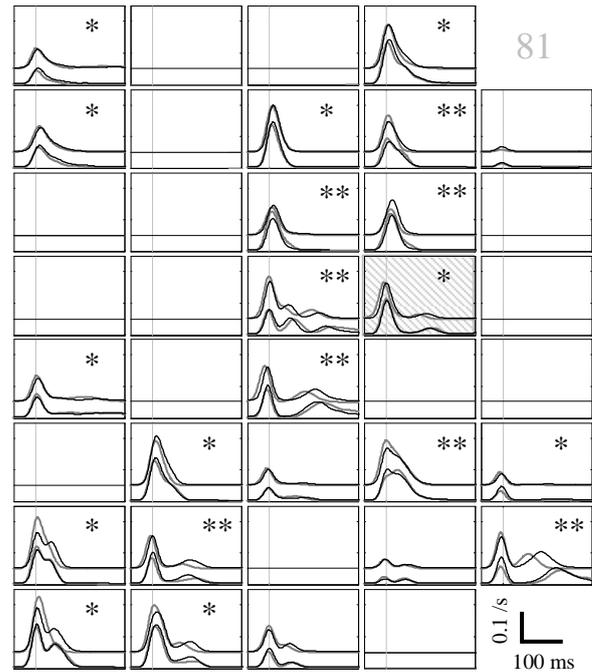


**Fig. 3.** Phase profiles of the most active part of the MEA shown in the same layout as the electrodes. The shaded plot is at the location of the stimulus electrode (*i.e.* 74), evaluation was at electrode 73. Double asterisks denote profiles that changed both during CRS and control; single stars only changed significantly during CRS.

# 3 Discussion

Application of CRS learning resulted in an increased number of profile changes. The CRS protocol, although it evaluated only one (effective) connection, thus resulted or required the change of PPs on many electrodes. This should be taken into consideration if one were to train multiple connections using the CRS algorithm.

**References**
[1] Jimbo, Y., H.P. Robinson, and A. Kawana, Strengthening of synchronized activity by tetanic stimulation in cortical cultures: application of planar electrode arrays. IEEE Trans Biomed Eng, 1998. 45(11): p. 1297-304.
[2] Madhavan, R., Z.C. Chao, and S.M. Potter, Plasticity of recurring spatiotemporal activity patterns in cortical networks. Phys Biol, 2007. 4(3): p. 181-93.
[3] Ruaro, M.E., P. Bonifazi, and V. Torre, Toward the neurocomputer: image processing and pattern recognition with neuronal cultures. IEEE Trans Biomed Eng, 2005. 52(3): p. 371-83.
[4] Shahaf, G. and S. Marom, Learning in networks of cortical neurons. J Neurosci, 2001. 21(22): p. 8782-8.
[5] Stegenga, J., et al., Analysis of cultured neuronal networks using intraburst firing characteristics. IEEE Trans Biomed Eng, 2008. 55(4): p. 1382-90.

# Detection of spontaneous firing pattern in cultured single neuron: application of a multi-electrode array chip combined with agarose microstructures

Ikurou Suzuki[*], Junko Hayashi, Kenji Yasuda

Department of Biomedical Information, Division of Biosystems,
  Institute of Biomaterials and Bioengineering, Tokyo Medical and Dental University
  Tokyo, JAPAN
* Corresponding author. E-mail address: suzuki.bmi@tmd.ac.jp

## 1  Introduction

Neural dynamics depends on spatial factors such as the network's topography as well as on temporal factors such as activity-dependent modifications. One of the best approaches to understanding the mechanism of neuronal dynamics is to characterize the neuronal network system by monitoring and stimulating individual neurons in a topologically defined network at single cell level and doing this for extended periods of time.

We therefore previously developed an on-chip multi-electrode array (MEA) system combined with an array of agarose microchambers (AMCs). It is possible to record the firing at multiple cells simultaneously for long term and topographically control the cells position and their connections [1-3]. However, not showing neuron on the electrode because of the Pt/Pt-black coated electrodes was problem. As a result, the number of the survived neurons and the detail of connections between a neuron to neighbour could not be identified.

In our present study, to overcome this problem, we developed thin pt/pt-black coated electrode for visualizing the neuron on the electrode. We detected spontaneous firing pattern of cultured single neuron on the electrode and the firing of two neurons for long term.

## 2  Methods

Multi-electrode arrays (MEAs) were formed on the glass slide comprised 64 50x50-μm electrodes. The surface of each of the recording terminals was thinly coated with Pt/Pt-black to reduce the impedance. The layer of agarose 10μm thick were coated on the MEA. Microchambers to fix cell positions were created using photothermal etching methods as shown in Fig. 1. The 1480-nm infrared laser was focused on the agar layer on the electrode, causing the agar at the focal point to melt.

Rat hippocampi were obtained from 18-day-old rat embryo. The cells were used to place neurons one by one into separate agarose microchambers using glass micropipette. Cultures were incubated at 37°C with 5% $CO_2$ at saturated humidity. Quarter-culture medium was exchanged twice a week by the medium, which was conditioned for two days in an astroglial cell culture.

The experimental set-up is based on previously developed system. Details about the measurement system can be found in [4].

## 3  Results

Fig. 2 shows the conventional electrode and developed thin pt/pt-black coated electrode. It is possible to optically observe the neuron on the electrode. Using this MEA, we succeeded to record spontaneous firing of cultured single neuron over 2 weeks and have detected three firing pattern of cultured single neuron. In many neurons, burst spiking was observed (Fig. 3A). In a few neurons, high frequency firing (about 5Hz) at single spike and the spiking pattern containing burst spike and single spike were observed (Fig. 3B, C). These firing patterns were preserved during measurement time over 2 weeks.

Fig. 4 shows the spontaneous firing of cultured two neurons on the electrode. One was fast spiking neuron and the other was bursting neuron. Magnified waveform shows evoked firings of fast spiking neuron by the firing of burst neuron.

## 4  Summary

In this work we detected spontaneous activity pattern of cultured single neuron and two neurons on the MEA. These results suggest that cultured single neuron have individual firing pattern. The results also show the advantage of our AMC/MEA cultivation and measurements methods and suggest they will be useful for investigating the mechanism of neural dynamics depending on network size and on combination of individual firing pattern.
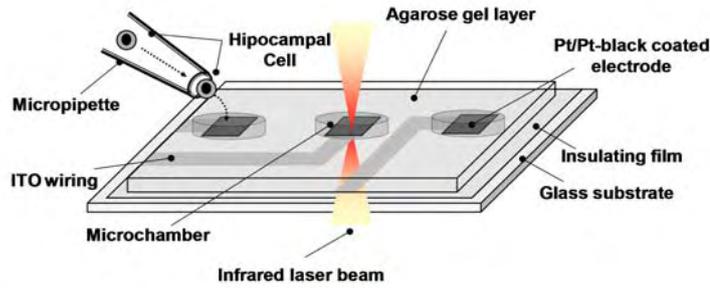
**Fig. 1.** Schematic drawing of agarose microchamber (AMC)/multi-electrode array (MEA) cell cultivation method. Microchambers to array cells are formed on the electrodes by spot heating agarose gel. Rat hippocampal cells are placed one by one into a different agarose microchamber using a glass micropipette.
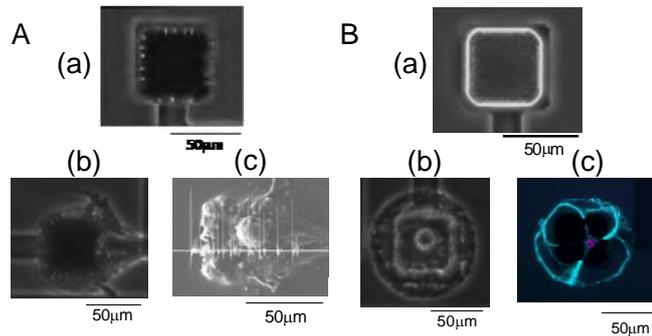


**Fig. 2.** Thin pt/pt-black coated electrode for optical imaging the neuron on the electrode. (A) Conventional pt/pt-black electrode. (a) Phase contrast Image of electrode 50μm in diameter. (b)Phase contrast image of cultured single neuron on the electrode. (c) Scanning electron microscopy imaging of (b). (B) Thin pt/pt-black coated electrode. (a) Phase contrast image. (b) Phase contrast image of cultured single neuron on the electrode. (c) Fluorescent image of cultured single neuron on the electrode.
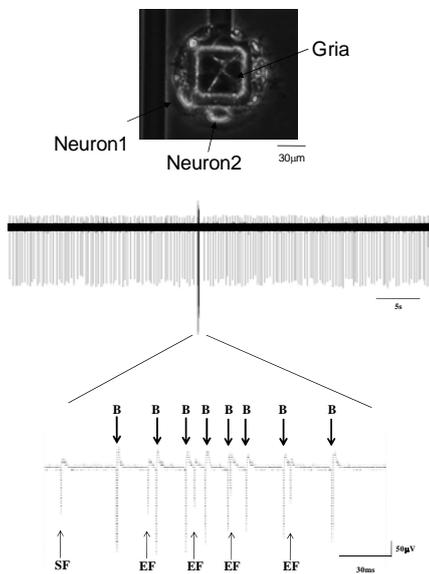


**Fig. 3.** Spontaneous firing pattern of cultured single neuron. (A) Burst spiking neuron. (B) Fast spiking neuron. (C) Mix spiking neuron.
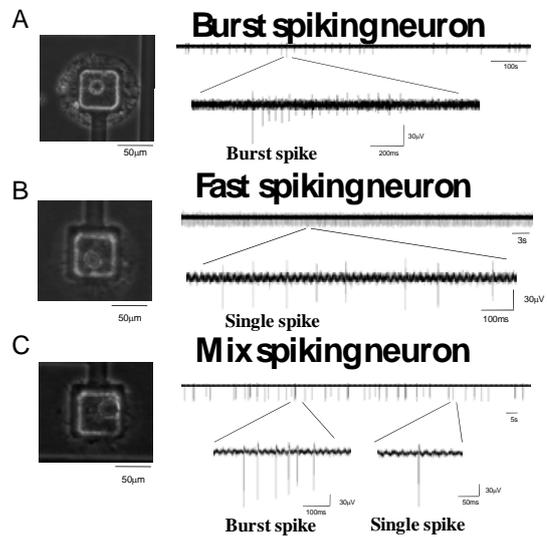


**Fig. 4.** Spontaneous activities of cultured two neurons in an agarose microchamber. B: Firing of bursting neuron. SF: Spontaneous activity of fast spiking neuron. EF: Evoked firing of fast spiking neuron.

### References

[1] I. Suzuki, Y. Sugio, Y. Jimbo, K. Yasuda. *Lab Chip* .5, 3, 241-247,2005

[2] I. Suzuki, K. Yasuda. *Biochem. Biophys. Res. Commun.*356, 470-475,2007

[3] I. Suzuki, K. Yasuda. *Jpn. J. Appl. Phys.*,46,9B,6398-6403,2007.

[4] I. Suzuki. A. Hattori, K. Yasuda. *Jpn. J. Appl. Phys.*,46,42,L1028-L1031,2007.

# Mapping The Impact Of Long-Term Electrical Stimulation To Organotypical Hen Embryonic Brain (HEB) Spheroids On Their Spiking Activity. Part I

Uroukov I S[1*], Bull L[2]

1 Faculty of Applied Sciences, University of the West of England, Bristol, U.K.,
2 Faculty of Computing, Engineering, and Mathematical Sciences, University of the West of England, Bristol, U.K.,
* Corresponding author: Ivan.Uroukov@uwe.ac.uk

A comprehensive dataset of multi-electrode array recordings was collected from three-dimensional hen embryo brain cell cultures, termed spheroids, under long-term electrical stimulation. The aim is to understand the ongoing changes in the spiking activity under electrical stimulation within the lifetime of 14-72DIV of the neuronal networks contained therein. The spiking dynamics were analyzed and behavioral characteristics derived. Some effects on spiking patterns and exhaustion were followed in culture lifetime. With respect to the culture development, two main types of spiking exhaustion were found: one which materializes in the form of a drop in the sporadic (tonic) spiking frequency at the later experimental stages; and another associated with decreasing spiking train appearance throughout the study period.

## 1 Study design and results

### 1.1 Background.

The majority of the work which test the electrical response, at the network level utilises dispersed monolayer cultures but recently was suggested denser monolayer cultures should be used. We undertook the first MEA measurements of three-dimensional hen embryo brain cell cultures called 'spheroids', finding complex spiking activity development during their maturation [1]. We are particularly interested in the computational behaviour of such aggregate cultures, i.e., their capacity to exhibit memory and learning [2]. Long-term teaching stimulation-recordings are required to undertake such studies and herein we describe a long-term study on the effect of electrical stimulation to begin exploring the spiking behaviour under stimulation over time.

### 1.2 Materials and methods.

Typically, a preparation utilizes 12 brains resulting in several thousands spheroids after two weeks *in vitro*. Each sample consists of 10-30 spheroids with unique and originally insulated networks. Ten MEAs were used and kept for recordings for two and halve months. The Stimulation recordings are illustrated on Fig. 1.

## 2 Results

The Fst/Fsp ratio Fig.2 is ranging between1.8-2 when close to 14 DIV, which is gradually decreased to 1.6-1.7 within the next 10 DIV. The spiking was a mixture type comprised by some sporadic activity and transferring to patterned spiking trains. Those formations varied in length and were changing according to the DIV. Figure 3 shows the persistence of the train sizes during the experiments where in 14 to18 DIV they vary and hide in the dominant sporadic activity. As a result of the subsequently reduced sporadic activity, more organized and persistent trains were observed at 22-27 DIV. At 28-31 DIV, the activity undergoes a major behavioral change into clean trains with vanishing sporadicity. At 30-31 DIV a grouping in massive train clusters were observed with mute periods in between. In 40-72 DIV, the activity is characterized with a transition between trains to sporadic spiking. In both, where trains and sporadic spiking occurred, exhaustion was observed in terms of decreased spiking frequency Fig. 3C, with Fsp/Fst dynamically adapting & shifting depend on exhaustion Fig. 3A, were all significant Fig. 3B.

## 3 Conclusions

The change in the spiking frequency with respect to the spike organization was analyzed and associated to spiking exhaustion of the cell culture in 14-72DIV. Two types of spiking exhaustion were described: one encounters the drop of the sporadic spiking frequency at the latest experimental stages and another associated with decreasing the spiking train's appearance.
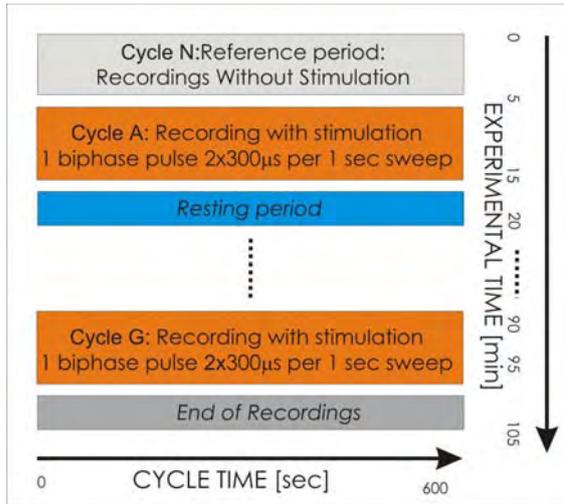
**Fig 1.** Stimulation-recording protocol



**Fig 2.** Frequency ration Fst/Fsp



**Fig 3:** Data analysis. **A** - Frequency distributions and fits. **B** - CDF function blue- *A* vs *BCDEFG*, **C** - Frequency ration *Fst/Fsp*

## References

[1]  Electrophysiological measurements in three-dimensional in vivo-mimetic organotypic cell cultures: Preliminary studies with hen embryo brain spheroids, *Neuroscience Letters 404 (2006) 33–38*

[2]  Towards Neuronal Computing: Simple Creation of Two Logic Functions in 3D Cell Cultures using Multi-Electrode Arrays, *Unconventional Computing, 2007*

**Fig. 2.** Spiking Frequency plots for 14-72DIV

# Mapping The Impact Of Long-Term Electrical Stimulation To Organotypical Hen Embryonic Brain (HEB) Spheroids On Their Spiking Activity. Part II

Uroukov I S[1*], Bull L[2]

1 Faculty of Applied Sciences, University of the West of England, Bristol, U.K.,
2 Faculty of Computing, Engineering, and Mathematical Sciences, University of the West of England, Bristol, U.K.,
* Corresponding author: Ivan.Uroukov@uwe.ac.uk

A comprehensive dataset of multi-electrode array recordings was collected from three-dimensional hen embryo brain cell cultures, termed spheroids, under long-term electrical stimulation. The aim of this study is to show the classified networks with a distinguished spiking behavior as result of long term electrical stimulation within the lifetime of 14-72DIV of the neuronal networks contained therein. Four main types of spiking behavior were mapped during long term electrical stimulation. Two main classified and known as excitatory and inhibitory classes were found. As a complimentary part, two more were distinguished and termed 'Flat Liner' and 'Up-Down' which were associated with a superpositioning of  the first two – excitatory and inhibitory.

## 1    Study design and results

### 1.1 Background.

As we undertook the first MEA based investigation of the dynamic of the 3D cell cultures called 'spheroids', we realize their variety of the network response to the electrical stimulation shown as excitatory and/or inhibitory reaction to the stimulation. The network behaviour and its dynamic is an important issue when the computational behaviour of such aggregate cultures, i.e., their capacity to exhibit memory and learning are subject to interest. As we previously described, the long term electrical stimulation was required to understand the ability of the network [1] to perform simple computing [2]. In line of those experimentations the network activity and its characteristics were derived and classified.

### 1.2 Materials and methods.

Typically, a preparation utilizes 12 brains resulting in several thousands spheroids after two weeks *in vitro*. Each sample consists of 10-30 spheroids with unique and originally insulated networks. Ten MEAs were used and kept for recordings for two and halve months. The Stimulation recordings are illustrated on Fig. 1.

## 2    Results

The reaction of the network is counted by the behavior of spiking frequency ration –F-*stimulated* over F-*spontaneous*, taken as mean value per cycle A to G in respect to spontaneous spiking frequency in cycle N. Analyzing Fig.2, the Fst/Fsp ratio, we found two main classes of networks in the spheroids – excitatory (Fig.2B) and inhibitory (Fig.2D).  Two more classes were described as no reaction or 'flat liners', (shown Fig. 2C) and 'Up-Down' (shown Fig. 2A). The spiking frequency data was computed and analyzed and the distributions were plotted and fitted. Their behavior is illustrated on Figure3 and indicated with pointing arrows to show their shift when electrical stimulation is applied during the time course of an experiment. Those classes were found to be well pronounced after 31DIV when the spiking frequency ratio Fst/Fsp was maximally rising in respect to other DIV.

## 3    Conclusions

In the major network responses in the spheroids, to electrical stimuli, titled excitatory and inhibitory, two more subclasses were found. They were associated with the superposition and interaction of the two main types networks in the spheroids.  The spiking frequency ratio plots and the spiking frequency distributions showed a quantitatively and qualitatively change in the reaction of neuronal networks to the electrical stimuli in the spheroids. All those changes were observed in the networks of the spheroids by the age close to the real hatching of hens, when the chick come up with developed sight and able to walk.
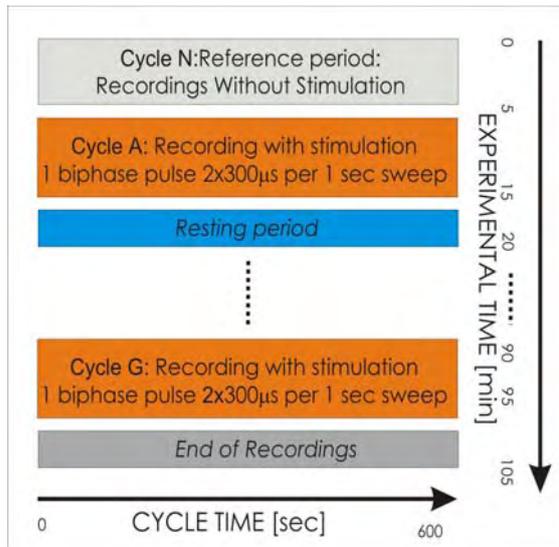
**Fig 1.** Stimulation-recording protocol
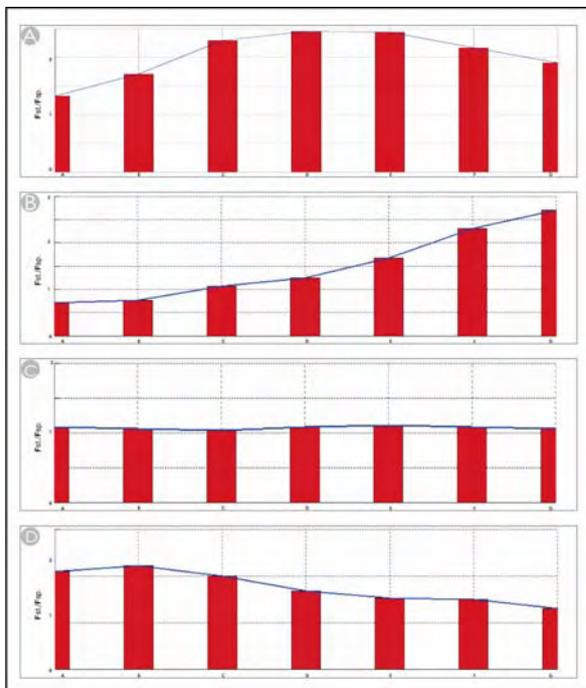


**Fig. 2**. Fst/Fsp ratio for distinguished network behaviour **A** – 'Up-Down'. **B** – 'Excitatory behaviour', **C** – 'flat liner' , **C** – 'Inhibitory behaviour' ,
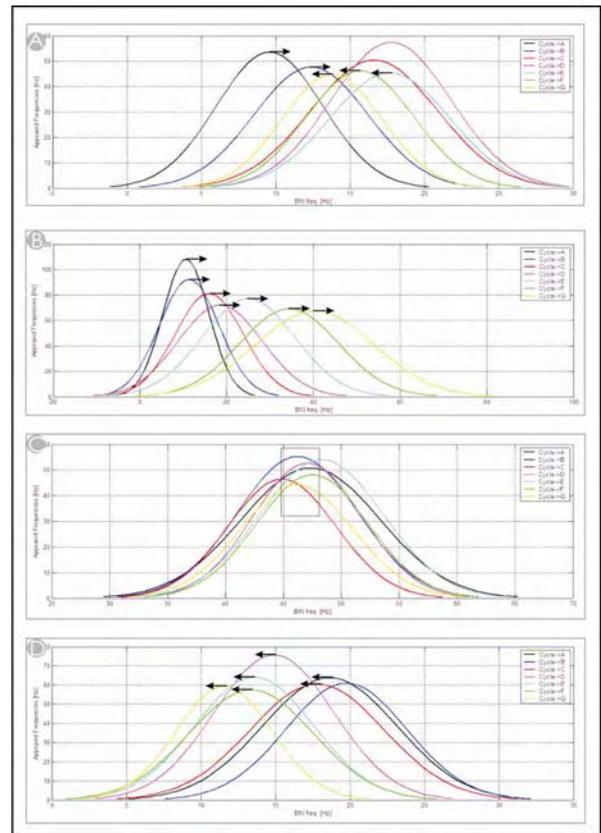


**Fig 3.** Spiking Frequency Distribution for distinguished network behaviours. **A** – 'Up-Down'. **B** – 'Excitatory behaviour', **C** – 'flat liner', **C** – 'Inhibitory behaviour',

## Acknowledgement

## References

[1] Initial Results from the use of Learning Classifier Systems to Control *In Vitro* Neuronal Networks, Gecco'07, July 7-11, 2007, London, England, United Kingdom. Copyright 2007, ISBN:978-1-59593-697-4.

[2] Towards Unconventional Computing through Simulated Evolution: Learning Classifier System Control of Non-Linear Media. *Artificial Life,* 2007

# Structural Organization of Cultured Brain Slices of Mice on Silicon Chips

M. Wiemhöfer, Peter Fromherz[*]

Max Planck Institute of Biochemistry, Department of Membrane and Neurophysics
* Corresponding author. E-mail address: fromherz@biochem.mpg.de

Recently organotypic hippocampal slices were coupled to Multi-Transistor-Arrays (MTA) fabricated by an extended CMOS technology [1]. Time-resolved maps of field potentials were observed with a spatial resolution of 7.8 μm on an area of one squaremillimeter. The approach gives insight into correlations of neuronal activity in space and time that is a key to understand the dynamics of complex neuronal networks. For a quantitative interpretation of transistor recording as well as of capacitive stimulation [2], knowledge of the microscopic structure of the tissue in contact to the silicon chips is essential. We have analyzed the three dimensional cellular structure of organotypic hippocampal slices from mice on silicon chips by two-photon microscopy. With this method the density of neuronal cells on the chips and their distance to the substrate can be visualized. These are important parameters for an improved theoretical description in terms of the volume conductor model [3]. Chambers of perspex were glued on silicon chips with an oxide surface. Hippocampal slices from newborn BL57/6 mices were cultured for 2-3 weeks by a Gähwiler-type technique and compared with slices that were cultured by the original roller tube technique [4]. The cultures on the chips developed normally as compared to the roller tube technique. The stratum pyramidale showed the wide broadening known from the roller-tube cultures without increased neuronal degeneration shown by the uptake of propidium iodide and by electrophysiology. The measurements help for a quantitative interpretation of transistor recordings that map the dynamics of the neuronal networks in cultured slices.

## References

[1] M. Hutzler, A. Lambacher et al. (2006) J. Neurophysiol., 96, 1638-1645.
[2] M. Hutzler and P. Fromherz (2004) Eur. J. Neurisci. 19, 2231-2238.
[3] P. Fromherz (2002) Eur. Biophys. J. 31, 228-231.
[4] B.H. Gähwiler (1981) J. Neurosci. Meth. 4, 329-342.

# Neuronal Engineering

# Cortical network hyperexcitability in Synapsin I KO mice

Michela Chiappalone[1,3*], Silvia Casagrande[2], Mariateresa Tedesco[3], Flavia Valtorta[4], Pietro Baldelli[1,2] Sergio Martinoia[1,3] and Fabio Benfenati[1,2]

1 Department of Neuroscience and Brain Technology, Italian Institute of Technology, Genova (Italy)
2 Department of Experimental Medicine, Section of Physiology, University of Genova, Genova (Italy)
3 Department of Biophysical and Electronic Engineering, University of Genova, Genova (Italy)
4 S. Raffaele Scientific Institute, Vita-Salute University, Milano (Italy)
* Corresponding author. E-mail address: michela.chiappalone@iit.it

Synapsins (Syns) are synaptic vesicle phosphoproteins that play a role in synaptic transmission and plasticity by acting at multiple steps of exocytosis. Mutation of *SYN1* gene results in an epileptic phenotype in mouse and man, implicating SynI in the control of network excitability. We used microelectrode array recordings to study the spontaneous and evoked network activity in embryonic primary cortical neurons from wild-type (WT) or SynI knockout (KO) mice. Our results demonstrate that the ablation of the *SYN1* gene is associated with a highly increased spontaneous activity with more frequent and sustained bursts of action potentials and a high degree of synchronization in the network. A set of electrical stimulation experiments performed on the two genotypes show that the evoked activity is more intense in KO networks, characterized by a sustained enhanced spiking probability after the stimulus.

## 1 Introduction

Epilepsy syndromes have a large genetic component. In addition to mutations in specific subunits of voltage- and ligand-gated ion channels, a number of other potential genes whose mutation may underlie epilepsy have been identified, including genes involved in neural development, synaptogenesis, neurotransmitter release and synaptic plasticity [1, 2]. Although a large number of these genes have been inactivated in animal models, only few mutants exhibit an epileptic phenotype, such as knockout (KO) mice lacking members of the synapsin (Syn). Synapsins (Syns) are synaptic vesicle phosphoproteins that play a role in synaptic transmission and plasticity by acting at a multiple steps of exocytosis. Recently, a form of familial epilepsy characterized by a non-sense mutation in the SYN1 gene that was present in all affected family members was reported [3].

## 2 Materials and Methods

SynI KO mice were generated by homologous recombination [4]. Cortical neurons extracted from embryos (E17) of both WT and KO mice were cultured on planar arrays of 60 TiN/SiN electrodes (Multi Channel Systems® - MCS, Reutlingen, Germany), pre-treated with adhesion factors (Poli-L/D-Lysine and Laminin). Experiments were performed at various ages of *in vitro* development, ranging from the second to the fifth week after plating.

### 2.1 Experimental protocols

For developmental studies, the spontaneous activity was monitored and recorded for 20-30 minutes at various ages, namely at 12-15, 18-20, 24-26 and 31-35 DIV.

Electrical stimulation experiments were conducted on the basis of the following protocol. Four of the 60 electrodes of the array were probed with test stimuli for 20 min. Test stimuli were sent sequentially to each selected electrode at 0.2 Hz frequency [5]. Recordings of evoked activity were performed on 27-33 DIV cultures.

## 3 Results

To study the cellular bases of the high susceptibility to epileptic seizures of mice lacking SynI, we first analyzed the spontaneous electrical activity of networks of cortical E17 primary neurons prepared from WT and SynI KO embryos and plated onto MEAs. The spontaneous activity of the cultures from both genotypes was characterized by a balanced presence of random spikes and bursts of action potentials. However, SynI KO networks displayed a much higher spiking and bursting activity than WT networks (Fig. 1, left).

The cross-correlograms of the bursting activity recorded by all the possible pairs of electrodes (59x59, excluding autocorrelation) show that, under basal conditions, the SynI KO preparation presents a

higher number of synchronized channels. In addition, the level of synchronization reaches its maximum values in most of the bursting channels and the correlation peak is much sharper.

During development, the mean values of firing rate, bursting rate and burst duration were significantly higher in SynI KO networks than in WT cultures (data not shown). Moreover, these activity parameters progressively increased with network development only in SynI KO cultures.
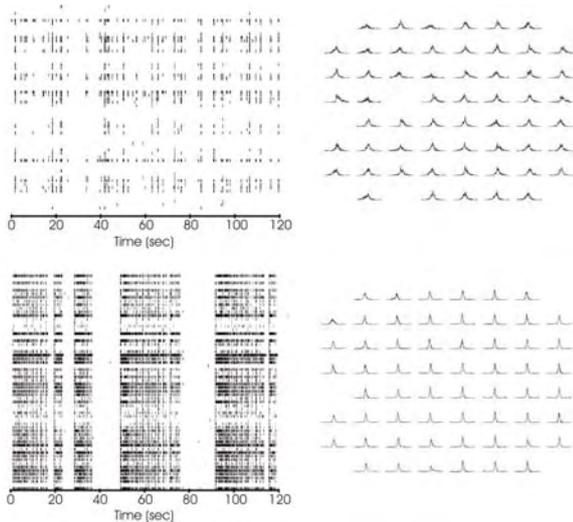


**Fig. 1.** Raster plot and mean cross-correlograms of the 60 MEA channel for one representative WT (top) and Syn I KO (bottom) culture.

We next analyzed the response over time of WT and SynI KO networks to a train of low-frequency, localized extracellular stimulations applied through a single electrode of the array.
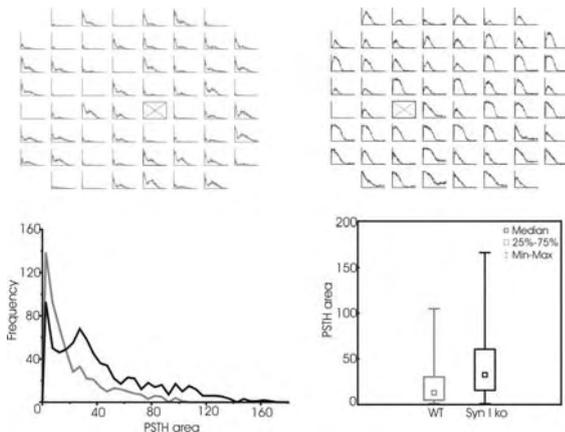


**Fig. 2.** Electrical stimulation of WT and KO culture. Top: 8x8 PSTH maps reproducing the layout of the MEA: the histograms of the responses of a representative WT (left) and KO (right) networks are reported. Time scale [0, 600] msec. The 'x' indicates the stimulating electrode. Bottom: histogram of the PSTH areas calculated for each recording channel in a dataset of 7 cultures (3 WT and 4 KO, age range 27-33 DIV): the area of the evoked response in KO cultures is statistically higher than in WT networks, as also proven by the box plot on the right. Color code: grey (WT) and black (KO).

The number of spikes generated by the active channels of the MEA in response to the 50 stimuli were summated over time (bin = 4 msec, T = 600 msec) and used to generate the corresponding post-stimulus time histogram (PSTH, Fig. 2, top panels) which expresses the change of the firing probability as a function of time after the stimulus. The PSTHs generated from each channel of the entire MEA showed a very homogeneous pattern within the whole network and clear-cut differences in the spiking probability between WT and SynI KO cultures (Fig. 2, bottom), which further emphasize the diffuse hyperexcitability of the mutant networks. Given the spontaneous activity of SynI KO networks, characterized by prolonged bursts and high firing rates, it is not surprising that focal electrical stimulation elicits such a network-wide bursting behavior.

## 4 Conclusions

By using MEAs, we studied the spontaneous as well as stimulus-evoked activity of primary cultures from WT and SynI KO mice. The presented results could suggest an explanation for the high susceptibility of SynI KO mice to epileptic seizures.

**References**
[1]  J. L. Noebels, (2003): The biology of epilepsy genes. Annual Review of Neuroscience, 26, 599-625.
[2]  O. K. Steinlein, (2004): Genetic mechanisms that underlie epilepsy. Nature Reviews Neuroscience, 5, 400-408.
[3]  C. C. Garcia, H. J. Blair, M. Seager, A. Coulthard, S. Tennant, M. Buddles, A. Curtis, and J. A. Goodship, (2004): Identification of a mutation in synapsin I, a synaptic vesicle protein, in a family with epilepsy Journal of Medical Genetics, 41, 183-186.
[4]  L. S. Chin, L. Li, A. Ferreira, K. S. Kosik, and P. Greengard, (1995): Impairment of axonal development and of synaptogenesis in hippocampal neurons of synapsin I-deficient mice. Proc Natl Acad Sci USA 92:9230-9234.
[5]  D. A. Wagenaar, J. Pine, and S. M. Potter (2004): Effective parameters for stimulation of dissociated cultures using multi-electrode arrays. J Neurosci Meth 138:27-37.

# Culturing and Measuring of Human Embryonic Stem Cell-Derived Neuronal Cells on MEA

Heikkilä Teemu[1]*, Tanskanen Jarno[1], Ylä-Outinen Laura[2], Lappalainen Riikka[2], Suuronen Riitta[1,2,3], Skottman Heli[2], Narkilahti Susanna[2], and Hyttinen Jari[1]

1 Department of Biomedical Engineering, Tampere University of Technology, Tampere, Finland
2 Regea – Institute for Regenerative Medicine, University of Tampere, and Tampere University Hospital, Tampere, Finland
3 Department of Eye, Ear and Oral Diseases, Tampere University Hospital, Tampere, Finland
* Corresponding author. E-mail address: teemu.heikkila@tut.fi

One of the major application areas for human embryonic stem cells (hESC) is the differentiation into neuronal cells for therapeutic purposes. This requires production of neurons that can form functional neuronal networks. We utilized the multi-electrode array (MEA) technology to study the electrical activity of hESC-derived neuronal cultures. Our aim was to set up a MEA measurement system for recording of hESC-derived neurons. The coating of MEA dishes, culturing of neurons, and measurement parameters were optimized. We followed the functional development of the neuronal networks towards synchronized activity as well as determined their response to specific synaptic receptors targeting drugs.

## 1  Introduction

Functional neuronal cells are needed in large amounts for treatment of neurodegenerative disorders [1]. So far, there are no reported studies about measuring the functionality of neuronal networks derived from hESCs that are one of the most reasonable sources for neuronal cell transplantations. Thus, a lot more functional *in vitro* information is needed of the characteristics of hESC-derived neuronal cells in order the make the most suitable cell grafts.

MEA technology allows simultaneous monitoring of spatial and temporal distribution of the electrical activity exhibited by neuronal populations over weeks or months. Analysis of multi-channel recordings on dissociated rodent mouse cortical or hippocampal slices [2-5] or embryonic stem cell derived neurons [6-7] have been carried out in recent years. hESC-derived neuronal cell populations are, however, still to be studied.

Here, our aim was to set up a MEA measurement system (MEA60, Multi Channel Systems MCS GmbH, Reutlingen, Germany) for recording of hESC-derived neurons. The MEA dishes (200/30-Ti-gr, MCS) were coated with polyethyleneimine (0.1% PEI) and laminin (10 μg/ml) [8]. The cell viability and neuronal differentiation was assessed. The MEA cultures were measured one to three times a week, each recording lasting 5 to 10 min.

Pharmacological responses of the neuronal cultures were tested with synaptically acting antagonists for glutamate receptors AMPA/kainate (6-cyano-7-nitroquinoxaline-2,3-dione, CNQX) and NMDA (D(-)-2-Amino-5-phosphonopentanoic acid, D-AP5). In addition, the effects of GABA and GABA-A receptor antagonist (-)-bicuculline methiodide were studied.

## 2  Results and discussion

**PEI/laminin coating supported cell survival and differentiation**

PEI/laminin supported long-term culturing of neurons on MEA dishes (Fig. 1). The LIVE/DEAD assay showed that using either laminin, PEI, or PEI/laminin as a coating substrate did not affect the cell viability (Fig. 2). PEI coating caused, however, a decreased process growth compared to PEI/laminin coated MEA dishes. The neuronal processes grew equally well in laminin and PEI/laminin coated wells.
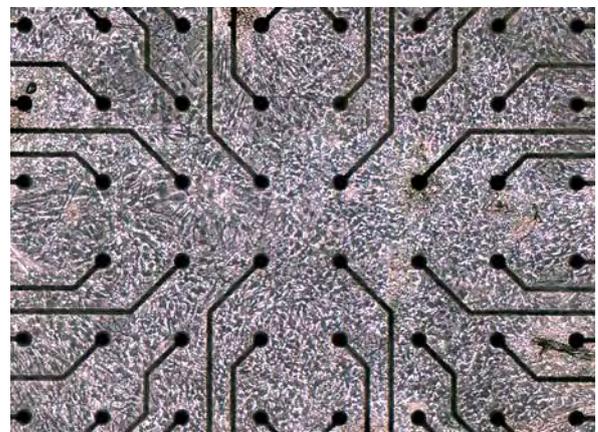


**Fig. 1.** A neuronal network on a PEI/laminin coated MEA dish after 33 d of culturing. Electrode interdistance = 200 μm.
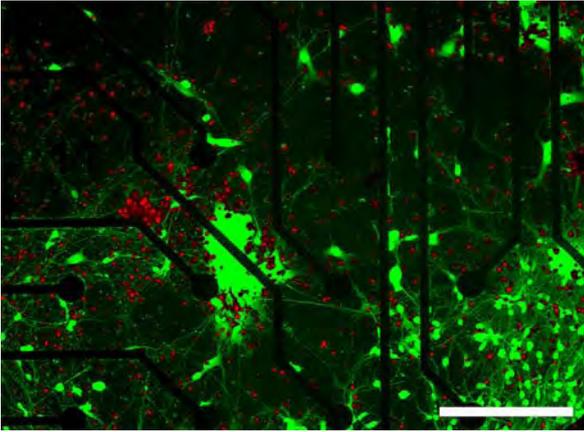
**Fig. 2**. A cell viability assay after 6 weeks of culturing on a MEA dish. Live cells are shown in green and dead cells in red color. Scale bar = 200 μm.

**Developing neuronal networks showed spontaneous synchronized activity**

hESC-derived neuronal cultures formed functional networks that could be sustained for months without any contaminations. Both asynchronous and synchronous activity was observed depending on the maturation stage of the network. The dependence of neural networks' activity on sodium-ion channels was examined with tetrodotoxin (TTX). The activity became completely blocked in the presence of TTX and reappeared after its wash out.

We detected wide variety of spontaneous activity from hESC-derived neuronal networks. We recorded same kind of synchronous bursts (Fig. 3) appearing typically after a month of culturing on hESC-derived neuronal networks as described for mouse ES-derived [7] neuronal networks.
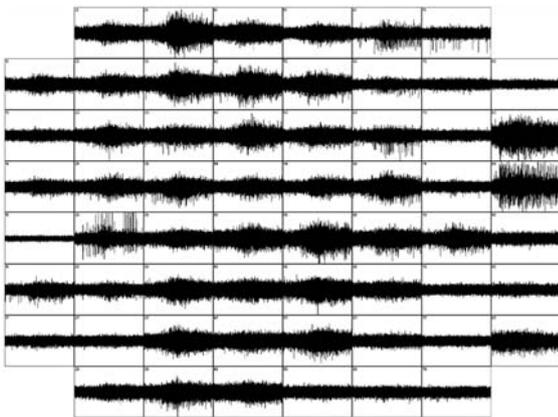


**Fig. 3.** Activity during 2 s interval in 60 channels. The synchronous signal bursts occurred over the network at the same time.

**Neuronal networks were susceptible to pharmacological modulation**

Our pharmacological investigation demonstrated that hESC-derived neuronal network activity can be modulated by synaptically acting drugs. Antagonizing AMPA/kainate and NMDA receptors by CNQX and D-AP5 application resulted in suppression of all activity. The effect of CNQX+D-AP5 was reversible and the activity returned after a wash-out. GABA suppressed the activity in dose dependent manner. Addition of bicuculline returned the GABA inhibited activity, increased the amount of signals over the baseline level as well as induced synchronous bursting.

## 3 Summary

Here, we showed the generation of functional networks of hESC-derived neuronal cells *in vitro*. To our knowledge, no studies have described that before. Our results show that these networks are spontaneously active and develop similar synchronous bursting activity described for rodent embryonic stem cell - derived neuronal networks [7] and cortical cultures [2-5]. Furthermore, the network activity is sensitive to synaptically acting drugs indicating that the typical excitatory and inhibitory receptors are involved in the functional activity of the networks. Thus, MEA technology is useful tool for utilizing hESC-derived neuronal cells for developmental and drug screening studies as well as for regenerative medicine.

**References**

[1] Hess, D.C., Borlongan, C.V. (2008): Stem cells and neurological diseases. *Cell Proliferation*, 41(1): 94-114.

[2] Otto, F., Görtz, P., Fleischer, W., Siebler, M. (2003): Cryopreserved rat cortical cells develop functional neuronal networks on microelectrode arrays. *Jounal of Neuroscience Methods* 128: 173-181.

[3] Wagenaar, D.A., Pine, J., Potter, S.M. (2006): An extremely rich repertoire of bursting patterns during the development of cortical cultures. *BMC Neuroscience*, 7:11.

[4] Chiappalone, M., Vato, A., Berdonini, L., Koudelka-Hep, M., Martinoia, S., 2007. Network dynamics and synchronous activity in cultured cortical neurons. International Journal of Network Systems 17(2):87-103.

[5] Madhavan, R., Chao, Z., Potter, S. (2007): Plasticity of recurring spatiotemporal activity patterns in cortical networks, *Physical Biology*, 4:181-193.

[6] Ban, J., Bonifazi, P., Pinato, G., Broccard, F., Studer, L., Torre, V., Ruaro, M.E., (2006): ES-derived neurons form functional networks in vitro, Stem Cells 25(3): 738-749.

[7] Illes, S., Fleischer, W., Siebler, M., Hartung, H-P., Dihné, M. (2007): Development and pharmacological modulation of embryonic stem cell-derived neuronal network activity, *Experimental Neurology* , 207: 171-176

[8] Multi Channel Systems MCS GmbH (2005): Microelectrode Array (MEA) User Manual. Reutlingen, Germany, pp. 20–21.

# Pharmacological Modulation Of Murine Embryonic Stem Cell-derived Neuronal Network Activity Is Similar To Primary Tissue-derived Neuronal Network Activity

S. Illes, F. Otto, J.Opatz , P.Görtz, C.Lange-Asschenfeldt, M.Siebler, M.Dihne

Department of Neurology, University Hospital Düsseldorf, Heinrich-Heine University

## 1 Background

Recently, we demonstrated that murine embryonic stem (ES) cell-derived neural cells are able to generate functional neuronal networks on microelectrode arrays (MEA). The development of ES cell-derived neuronal networks is characterized by distinct electrophysiological stages. In early stages of neuronal maturation (1-2 weeks) only single spikes and nonsynchronous bursts of spikes were detected, whereas at later stages of maturation (>3 weeks), network activity was characterized by synchronously oscillating bursts of spikes. This electrophysiological maturation was paralleled by morphological changes including increased numbers of neuronal processes and presynaptic vesicles. Formerly, in vitro generated neuronal networks were typically derived from primary brain tissue and used to characterize neuronal network activity with respect to their modulation by pharmacologically acting drugs. To clarify if ES cell-derived neuronal networks behave similar to primary neuronal networks we compared the effects of different glutamatergic and GABAergic substances on the modulation of network activity.

## 2 Methods

Undifferentiated ES cells were expanded in the presence of leukemia inhibitory factor (LIF). After formation of embryoid bodies in the absence of LIF, neural differentiation was induced with a mixture of DMEM/F12 and neurobasal medium supplemented with N2, B27 and glutamine for 6 days resulting in neural-induced serum-free, floating culture of embryoid-body-like aggregates (SFEBs). Neural-induced SFEBs where then propagated by adding fibroblast growth factor-2 (FGF-2) for further 6 days. Neural-induced SFEBs were seeded either on poly-L-ornithine and laminin-coated microelectrode arrays or coverslips. Three weeks after seeding and neuronal maturation, ES cell-derived neurons developed synchronously oscillating networks which were subjected to pharmacological investigations.

## 3 Results

We observed that low concentrations of glutamatergic substances result in increased network activity whereas high concentrations result in decreased network activity. This effect could be demonstrated for both N-methyl-D-aspartate (NMDA) and alpha-amino-3-hydroxy-5-methyl-4-isoxazolepropionic acid (AMPA)/kainate receptors. The inhibition of glutamatergic transmission by the specific NMDA-receptor antagonist (2R)-amino-5-phosphonovaleric acid (AP5) or the specific AMPA/kainate receptor antagonist 6-cyano-7-nitroquinoxaline-2,3-dione (CNQX) decreased neuronal network activity. Application of gamma-aminobutyric acid (GABA) inhibited synchronously oscillating network activity, whereas the inhibition of GABA-A-receptors by bicuculline or picrotoxine increased the synchronously oscillating network activity

## 4 Conclusion

We demonstrated that inhibition or activation of glutamatergic and GABAergic receptors results in a modification of ES cell-derived neuronal network activity similar to primary neuronal networks. Thus, the MEA technology represents a powerful tool to describe the temporal progression of stem cell-derived neural populations towards mature, functional neuronal networks that can be applied to investigate pharmacological

# Neurons derived from P19 embryonal carcinoma cells establish functional neuronal network properties

Yuzo Takayama[*], Hiroyuki Moriguchi, Atushi Saito, Kiyoshi Kotani, Yasuhiko Jimbo

Graduate School of Frontier Sciences, University of Tokyo, Japan
* Corresponding author. E-mail address: y-taka@bmpe.k.u-tokyo.ac.jp

P19 embryonal carcinoma cells were differentiated into neurons by retinoic acid application and were cultured on micro-electrode arrays. We showed that P19-derived neuronal networks had quite similar network properties to those of primary neurons. This will provide the novel capability of MEA system, such as monitoring differentiation processes of stem cells.

## 1 Introduction

Regeneration of the damaged central nerve system (CNS) is one of the most important research themes in neuroscience and neuroengineering. It is essential to replenish the lost neurons and to establish appropriate functional network using pluripotent stem cells. Little is known, however, about the properties of stem cell-derived neuronal network, particularly under the differentiation and developmental processes.

In this work, we cultured P19 embryonal carcinoma cells on micro-electrode array (MEA)[1]. P19 cells were differentiated into neurons by retinoic acid application and formed densely connected networks. The P19 is pluripotent cell line that serves as a flexible model system for CNS neurons [2], and is thus suitable for studying the network-wide dynamics of neurons derived from stem cells. Here, spontaneous electrical activity of P19-derived neurons was recorded and analysed.

## 2 Methods

To initiate differentiation, P19 cells were plated into bacteria culture dishes, which allow cells to aggregate, and cultured in the presence of $1 \times 10^{-6}$ M all-trans retinoic acid. After 4 days, cells were dispersed with 0.25 % trypsin-EDTA and plated on MEA coated with 0.1% polyethyleneimine and Laminin. The plated cell density was $1 \sim 2 \times 10^5$ cells/cm$^2$. After 4 days *in vitro*, medium was replaced with Neurobasal medium supplemented with B27, L-glutamine. One-half of the medium volume was changed every 2 days.

The MEA substrate consists of 64 indium-tin-oxide (ITO) electrodes coated with platinum-black. The electrical signals obtained through each electrode were amplified 5000 times with 64-channel amplifier (NF). The recording bandwidth was 100 Hz to 5 kHz and the sampling rate was 25 kHz.

## 3 Results

P19 cells treated with retinoic acid strated extending neurites within 3 days after plating and formed densely connected network after 2 weeks cultures (Fig.1).
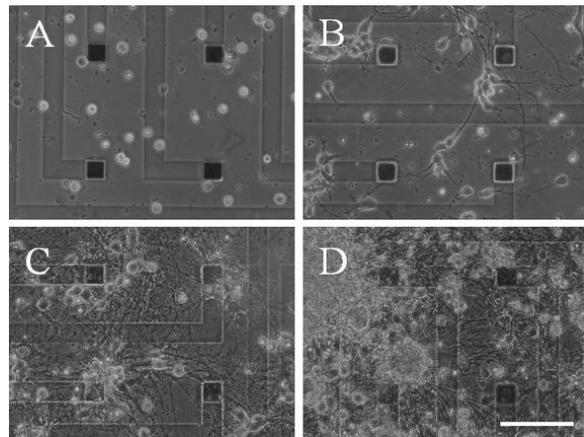


**Fig.1.** Phase-contrast images of P19-derived neurons cultured on MEA substrate (A) immediately, (B) 3 DIV, (C) 15 DIV, (D) 26 DIV after plating. Scale bar; 100 μm.

After 2 weeks *in vitro*, it was possible to record the spontaneous synchronized periodic bursts, which were the characteristic features in primary CNS neurons (Fig.2). These synchronized bursts were separated by silent periods where only occasional spikes were observed. Furthermore, addition of NMDA receptor blocker APV (50 μM) almost inhibited the spontaneous synchronized burting. In contrast, addition of GABA-A receptor bicuculline-methiodide (BMI; 1,10 μM) substantially increased the occurrence of periodic synchronized bursting. These results demonstrated that the glutamatergic excitatory synapses and the GABAergic inhibitory synapses were active in these P19-derived neuronal networks.

We concluded that MEA-based recording was useful for monitoring differentiation processes of stem cells. P19-derived neuronal networks had quite similar network properties to those of primary neurons, and thus provide a novel model system to investigate stem cell-based neuronal regeneration.

### References

[1] Y. Jimbo, T. Tateno, H. P. C. Robinson : "Simultaneous induction of pathway-specific potentiation and depression in networks of cortical neurons", Biophys. J. , Vol. 76, pp. 670-678 (1999)

[2] M. W. McBurney : "P19 embryonal carcinoma cells", Int. J. Dev. Biol. , Vol. 37, pp. 135-140 (1993)
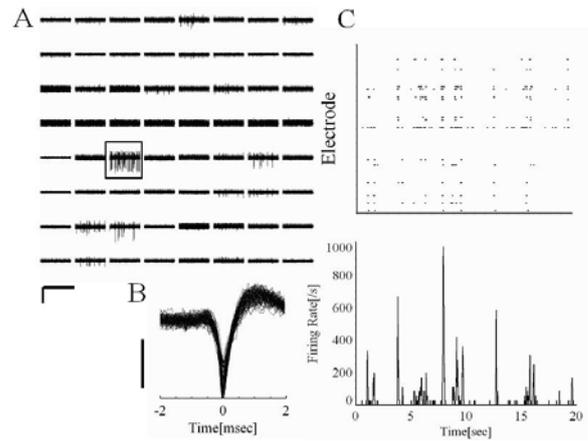
**Fig.2**. Spontaneous electrical activity in P19-derived neuronal networks at 22 DIV. (A) Extracellular voltage traces obtained through 64 substrate electrodes. Scale bar; 20 sec × 100 µV. (B) Superimposition of 100 spikes obtained at single recording site indicated in (A). Scale bar; 100 µV (C) Temporal characteristics of 20 sec of spontaneous activity. Upper panel: Raster plots of spontaneous activity for 64 electrodes. Lower panel: Firing rate of spontaneous activity recorded by all electrodes.

# The Effects of Different MEA Coating Agents on Growth and Differentiation of Human SH-SY5Y Neuroblastoma Cells

Heidi Teppola[1]*, Jertta-Riina Sarkanen[2], Jyrki Selinummi[1], Antti Pettinen[1], Tuula O. Jalonen[3], Marja-Leena Linne[1]

1 Department of Signal Processing, Tampere University of Technology, Tampere, Finland
2 Cell Research Center, Faculty of Medicine, University of Tampere, Finland
3 Department of Biological and Environmental Science, University of Jyväskylä, Finland
* Corresponding author. E-mail address: heidi.teppola@tut.fi

Human SH-SY5Y neuroblastoma cells were cultured on microelectrode array (MEA) plates treated with following coating agents: poly-D-lysine (PDL), poly-L-lysine (PLL), polyethyleneimine (PEI) with laminin, and laminin alone. The cells were also treated with all-*trans* retinoic acid (RA) and cholesterol (CHOL), and their growth, morphology, and differentiation, as well as the presence of synaptic vesicles in synaptic contacts was studied. The aim is to develop electrically active long-term networks of human neuronal cells.

## 1 Introduction

In order to form functional, long-term neuronal networks of human SH-SY5Y neuroblastoma cells, the first important step is to optimize the cell growth on MEA plates with different coating alternatives. The SH-SY5Y cell line was selected as test application because of its neuron-like phenotype and easy maintenance [1]. It has previously been shown that RA+CHOL treatment induces differentiation and synaptic vesicle recycling in SH-SH5Y cells [2].

In this work the SH-SY5Y cells were first either allowed to differentiate spontaneously or were treated with RA+CHOL, in order to make the cells electrically excitable on MEA plates. The effects of the treatments on differentiation and the cells' capability to communicate with each other on MEA plates were verified with AM1-43 staining of the synaptic vesicle recycling. The ultimate goal of this work was to find the best alternative amongst the various coating agents by following the cell growth, morphology and level of differentiation. Specifically developed automated image processing algorithms were used to analyze the cell growth.

## 2 Materials and Methods

**Cell culture and differentiation**

The SH-SY5Y neuroblastoma cells (CRL-2266; ATCC, Manassas, VA, USA) were cultured and differentiated together with RA and CHOL as described by Sarkanen et al. 2007 [2]. The passage 33 cells were plated with the density of 5000 cells/cm$^2$ on MEA-plates (standard 100/10-Ti-gr, MCS GmbH, Reut-lingen, Germany). The success of differentiation, and the responses of synaptic vesicles on high-K$^+$ induced depolarization, were verified with 4μM AM1-43 fluorescence staining [2].

**Coating agents**

➢ PDL 0.05% with laminin 0.002%
➢ PLL 0.05% with laminin 0.002%
➢ PEI 0.1% with laminin 0.002%
➢ Laminin 0.002%
➢ No coating

All coating agents were diluted in sterile water, except PEI, which was diluted in borate buffer. First, the plates coated with PDL, PLL, and PEI, were incubated over night at +4$^\circ$C, after which they were rinsed with sterile water. Finally, laminin was added for one hour.

**Automated analysis of cell growth**

To estimate the speed of cell growth, the area occupied by cells was automatically detected from each of the microscopy images. First, the image was segmented into small regions using Quad-tree segmentation [3]. These regions were then labelled, and based on the intensities and size of the regions, divided into four classes: electrodes, cells, background, and stains. The analysis procedure was implemented in the eCognition 5.0 image analysis platform by Definiens AG, München, Germany.

## 3 Results and Discussion

The results show that cells attach on MEA plates with all of the used coating agents. However, auto-

mated analysis of the cell density confirms that there is less cell growth when PEI+laminin coating or no coating is used (Fig. 1).
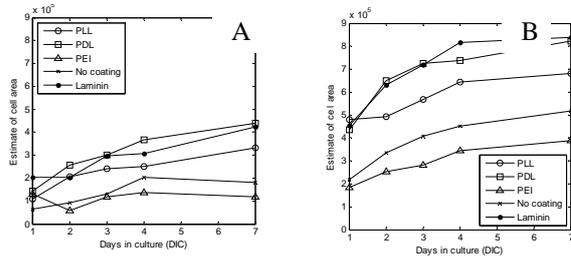


**Fig. 1.** Presentation of cell growth for up to seven days using different MEA surface coatings. Each measurement point represents the median of cell areas from nine images. In both experiments, A) and B), there is less cell growth when the MEA plates are coated with PEI+laminin or are without coating.

The maturation, morphology, and distribution of the cells are more neuron-like with PEI+laminin than with any of the other treatments. Preliminary results indicate that PEI alone is not sufficient for optimal growth of the SH-SY5Y cells, but PEI+laminin seems to be a promising coating. PLL and PDL with laminin, as well as laminin alone, induce more glial-type cells than does PEI+laminin (Fig. 2).
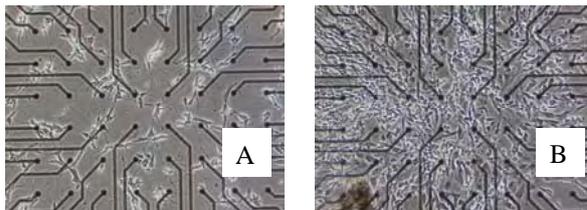


**Fig. 2.** Images of MEA plates coated with A) PEI+laminin B) PLL+laminin. The RA+CHOL treated human SH-SY5Y cells were grown for 7 days in culture.

The results indicate that the morphology and distribution of the SH-SY5Y cells are very similar on MEA plates coated with PLL/PDL with laminin or laminin alone (data not shown). Uneven distribution of cells is mostly detected when no surface coating has been used (Fig. 3). The RA+CHOL differentiated and high-$K^+$ depolarized cells express more AM1-43 positive dots on MEA plates than the non-differentiated cells (Fig. 4), indicating synaptic vesicle recycling similar to what has been shown previously in cells grown on normal culture dishes [2].
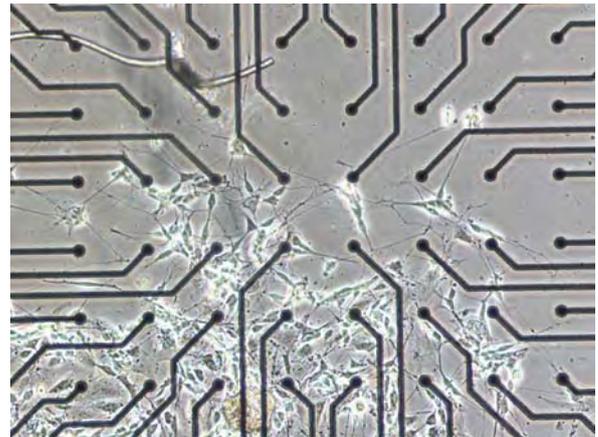


**Fig. 3.** Image of a MEA plate without coating at day 7. The SH-SY5Y cells are unevenly distributed.
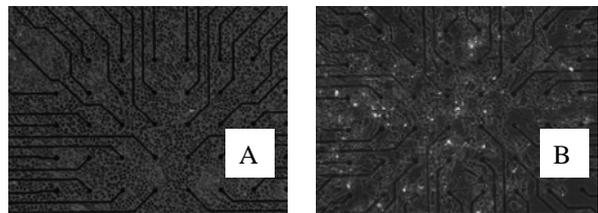


**Fig. 4.** Images of AM1-43 stained high-$K^+$ depolarized human SH-SY5Y cells A) without treatments and B) treated with RA+CHOL. White dots indicate areas containing actively recycling synaptic vesicles. Cells were cultured for 7 days on the MEA plates coated with PLL+laminin.

## 4  Conclusions

The MEA coating agents seem to have a strong impact on cell morphology, growth, and viability. Based on our results, more emphasis should be put on the impact of coating agents on the structure, function, and electrophysiological properties of the created neuronal networks. In future, the presented human neuroblastoma cell networks may be used to replace primary animal cell cultures in various electrophysiological experiments, for example as a tool for toxicity and drug testing.

**References**
[1] Shenai MB. et al. IEEE Trans Nanobiosci. 3(2): 111-7, 2004
[2] Sarkanen J.-R. et al. J. Neurochem.102: 1941-1952, 2007
[3] Jain R., Kasturi R., and Schunck B.G., Machine Vision, McGraw-Hill, Inc., New York, NY, 1995

# Signal Analysis and Data Mining

# High throughput brain slice EEG recording of oscillating hippocampus: technical standards, analysis and data-mining

Arjen B. Brussaard

Department of Experimental Neurophysiology Center for Neurogenomics and Cognitive Research, VU University Amsterdam, The Netherlands

**Keynote Lecture**

# Long-term Memory Statistical Structure In MEA Dissociated Cortical Neuron Recordings

Federico Esposti[.*], Jacopo Lamanna, Maria Gabriella Signorini

Dipartimento di Bioingegneria, Politecnico di Milano, Milano, Italy
* Corresponding author. E-mail address: federico.esposti@polimi.it

The study of nonlinear long term correlations in neuronal signals is a central topic for advanced MEA signal processing. In particular, the existence of long-term memory in such a signal could provide interesting information about changes in inter-neuron communications, e.g. long-term potentiation (LTP) or long-term depression (LTD). In this study we propose a new method for long-term correlation analysis of neuronal burst activity based on the analysis of the Periodogram slope of the MEA signal studied through recordings of dissociated cortical neurons. Moreover we show the effectiveness of the method in analyzing the activity changes that take place during the development of such cultures.

## 1 Introduction

In last decade the mammalian cortex has been deeply studied *in vitro* in the form of dissociated neuro-glial cultures implanted on multi-electrode arrays (MEA). Spontaneous activity [1-3] is one of the neuronal network fundamental aspect deeply investigated through MEA devices. It refers to the activity that the network shows in absence of any external stimulation. It is well-known that this behavior, also reported in *in-vivo* studies, is characterized by periodic synchronization episodes, usually called bursts (as reported e.g. in [4-7]). Moreover it was reported that both single electrode [9] and multi-electrode [10-11] neuronal recordings exhibit long-term memory characteristics [8].

The study of nonlinear long term correlations in neuronal signals is a central topic for advanced MEA signal processing. In particular, the existence of long-term memory in such a signal could provide interesting information about changes in inter-neuron communications (e.g. LTP or LTD) correlated with the administration of neuroactive drugs or with the development of the network itself.

In this study we propose a new method for long-term correlation analysis of neuronal burst activity of dissociated cortical neurons studied through MEA recordings.

## 2 Materials and Methods

### 2.1 Cell cultures, MEA recordings and spike sorting

For the present study we employed MEA data kindly provided by professor Steve Martin Potter and colleagues in [7]. In particular, we employed the 12 thirty minute-long recordings classified as "small" in [7]. In brief, these recordings were performed on cultures of E18 rat cortical neurons (plus glia) with a density of $1.6 \pm 0.6 \cdot 10^3$ cells/mm$^2$, recorded longitudinally from the 6th to the 35th *day in vitro* (div) with 59 electrode MEAs with a diameter of 30 μm, purchased from MultiChannel Systems (Reutlingen, Germany). The electrodes were organized in a square grid with the corners missing, spaced 200 μm center-to-center. Spike sorting was performed with the MEABench software [12], as described in [7].

For any detail about cultures, recordings and spike sorting, please refer to [7].

### 2.2 Analysis procedure

As expected, we noticed on data the presence of spontaneous activity characterized by periodic synchronization episodes, usually called bursts. So, in order to approach a intra-burst analysis, we developed an original frequency-based burst detector algorithm.

Fig.1 represents how the algorithm works: all MEA channels are merged forming a single series, showing on the x axis the recording time and on the y axis the spiking activity of all channels. Along this series the starting point of a burst is detected comparing the obtained series with a frequency threshold fixed at 10 Hz. Frequency is computed as the inverse of the inter-spike interval (ISI) of the merged series. The reference duration of a burst is chosen in 200ms.

Some controls are implemented in order to verify the presence of a real burst. First, the number of channels involved has to be more than the 15% of the total channel number. A channel is considered as "firing" if it spikes at least three times in the 200ms time window. Moreover, two detected bursts can not be closer than 600ms. These arbitrary values were chosen by training the algorithm on 3 experimental series and comparing results with data in [7].
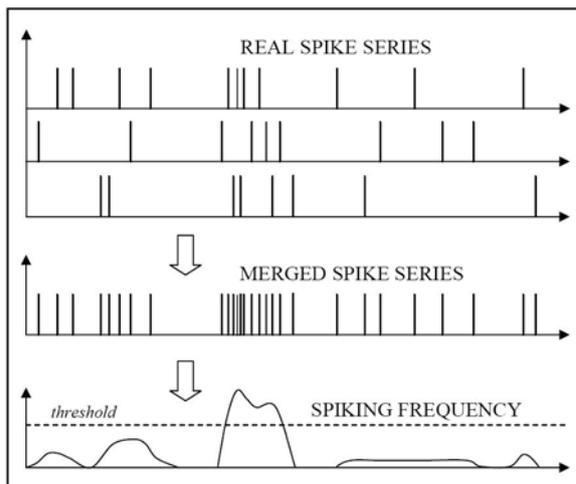
**Fig. 1.** graphical depiction of the burst detection algorithm (for simplicity just three channels are represented here).

The application of complex nonlinear signal processing methods for long-term memory estimation requires to work with one-dimensional data. For this reason we processed MEA recording (in particular bursting epochs of the MEA raster plots) in order to obtain 1D signals.

We applied the Space Amplitude Transform (SAT), originally introduced in our paper [13], in order to perform such a conversion.
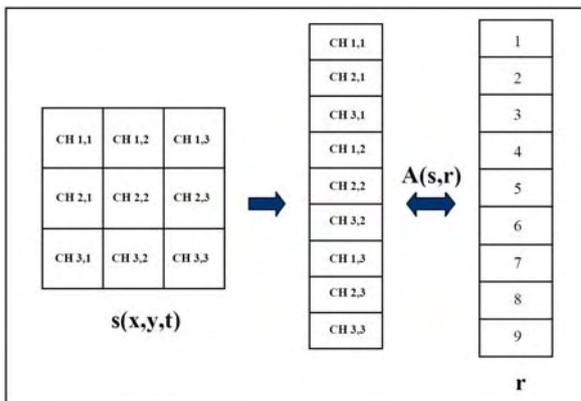


**Fig.2.** Graphical example of the role of the arrangement algorithm R and the Space-Amplitude Transform A(s,r) with a 3x3 domain matrix. See text for details.

The Space-Amplitude Transform, A(s(·),r), is a geometric transform that executes a projection from a 2D domain set s(x,y,t), e.g. the usual Raster plot, to a 1D image set I(r,t), exploiting an Arrangement table r as Fig.2 represents. SAT produces a one-dimensional signal in which every sample represent a spike of the original raster plot in terms of time (on the x axis) and position (on the y axis), associating to each MEA channel a discrete value. In this way, the topological information of the raster plot (i.e. the channel position) is transformed in the amplitude for the Space

Amplitude Transformed signal (CH-AMPL, Fig.2 and Fig.3).

This association between position and amplitude is done according to an arrangement algorithm. This simple operation allows to represent a bidimensional value, i.e. the MEA coordinates pair, through a single parameter (amplitude) with no information loss. In a graphic representation, the output of the *Space-Amplitude Transform* can be seen as the interpolating function of the Raster plot that locally assumes a value assigned on the basis of the Arrangement algorithm (Fig.2).

This method allows to approach an intrinsically 2D plus time signal, i.e. time recordings from a 2D electrode array, as a 1D plus time signal in order to speed up and make simpler the data analysis.
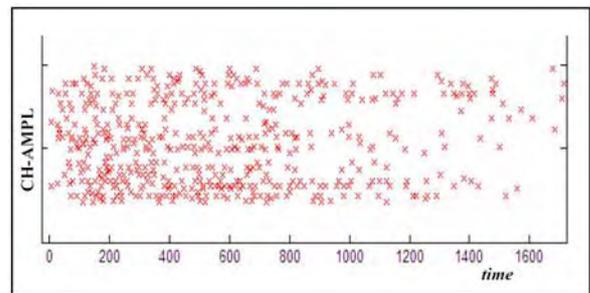


**Fig.3.** Example of a 170ms long burst transformed according to the SAT analyzed at 0.1ms resolution. No information loss is introduced.

## 2.3 Long-term memory estimation

A signal displaying a power law spectral density near the origin is called "one-over-*f*" or "pink" noise. Such signals are commonly observed in many different systems, including physical, biological, physiological, economic, technological and sociological ones [8]. When $P(f) \approx 1/f^{\alpha}$, with $P(f)$ the signal power spectral density, for $f \to 0$ and some $\alpha > 0$, it is often possible to define some sort of generalized correlation function which is found to decay very slowly (hyperbolically).

The slow decay signifies that the current value of the series is affected not only by its most recent values but also by its past values. For this reason, such processes are often referred to as "long-memory" or "long-range dependence" processes [8]. In this specific case, we are interested in evaluating the presence of long-term correlations in the global activity of the network. The SAT signal, representing with no distortion the spatial and temporal information of the raster plot, is a very good candidate in showing long-term memory correlations, as reported with different methods, in [10][11].

For long-term correlated signals, $\alpha$ ranges between 0 and 3 (Fig.4). Alpha near 0 indicates the presence of a stationary process with zero correlation, i.e. a white noise. Alpha between 0 and 1 indicates a long-

range positively correlated stationary signal. Alpha between 1 and 2 indicates a long-range negatively correlated non-stationary signal and, finally, alpha between 2 and 3 indicates a long-range positively correlated non-stationary signal. If α = 2, the process is classified as Brownian motion.
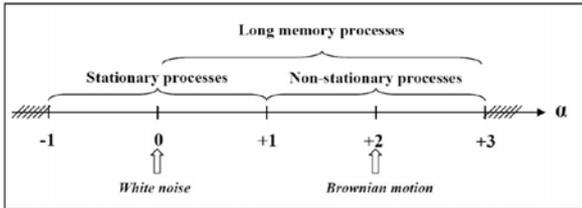


**Fig.4.** Graphical representation of the physical meaning of α parameter.

One of the most simplest method for α estimation is the Periodogram [8][14-15]. Fig.5 shows an example of the α coefficient estimation in the Periodogram of a burst. The method estimates α as the linear slope of the periodogram, in a log-log plot, close to the zero frequency axis. As a matter of fact, being $P(f) \approx 1/f^{\alpha}$, for $f \to 0$ and some $\alpha > 0$, $\log(P(f)) \approx -\alpha \cdot \log(f)$. The range of Periodogram plot interpolation was chosen in the two lowest decades of frequencies ($10^{-4}$-$10^{-2}$ Hz).

We applied the above described methods (burst detection, SAT and Periodogram analysis) to 12 longitudinal recordings from [7], ranging from (usually) 6 to 35 div. Each recording contained hundreds of bursts.
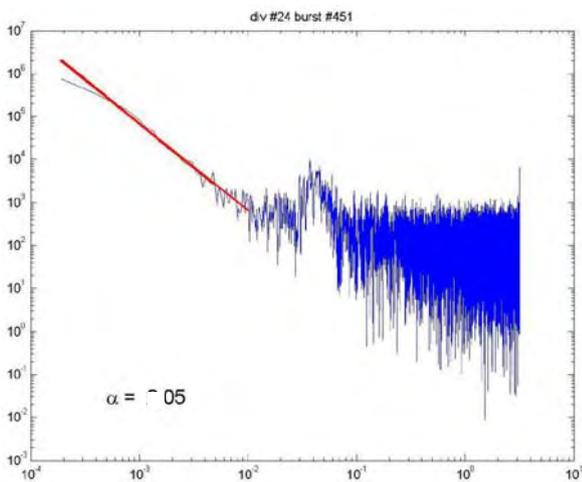


**Fig.5.** Example of a α estimation from a 24-div burst Periodogram. The straight line represents the interpolation used for the α parameter estimation. (Periodogram estimated on N=400 samples).

## 3 Results

We obtained 12 plots showing, on the y axis, the mean α value (± std) of all bursts vs. the number of *days in vitro* (on the x axis). All plots showed a similar trend, exemplified in Fig.6. We found that the α coefficient is close to 0.5 in the first two *weeks in vitro*, wiv (indicating a positive long-term correlation in

a non-stationary time series). α suddenly grows to 1.5 circa around the 17 div (± 2div) and then irregularly grows till 2 in the following 20 days.

## 4 Discussion

The behavior of the α exponent across the culture development can be divided in three stages. The first stage essentially coincides with the first two wiv. In this period α is ≤ 0.5 representing a condition in which the signal is stationary and presents a positive correlation. It is known that in the first one or two wiv the network is poorly bursting and the spiking activity can be classified as Global, i.e., bursts usually involve almost the whole neuronal network [7][16-18].
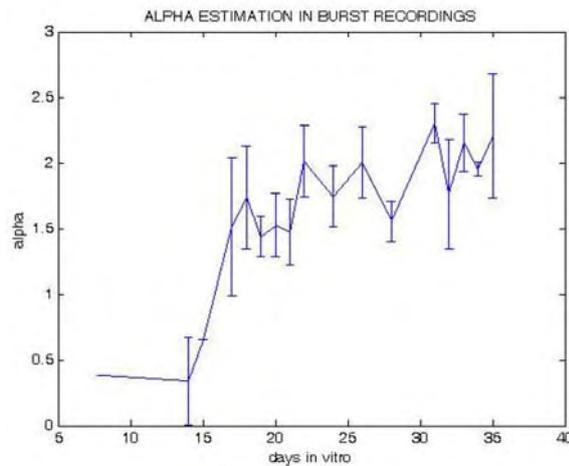


**Fig. 6.** example of α estimation results in a longitudinal cortical murine neuronal MEA recording.

The signal positive correlation, that derives from the presence of lasting trends in the SAT-transformed signal, accounts for this topological characteristic.

The second stage is represented by a sudden change in the α exponent around the 17th div. As known from literature, in a period comprised between the 6th and the 18th div, the network reorganizes its synaptic connectivity through a process called "pruning" [7][17][19-20]. Through this remodeling, the network sacrifices useless synapses. At the same time, from the spiking activity viewpoint, the network starts to produce an higher number of bursts characterized by a localized activity (i.e., bursts involve a limited number of neurons). This is a typical sign of the creation of sub-networks [17][20]. In this stage, α suddenly raises to a value close to 1.5 and so remains for 2 – 4 div. Such an α indicates the presence of a non-stationary signal with a strong negative correlation. The presence of localized activity produces pronounced discontinuities in the SAT signal, confirming the signal as a non-stationary negatively correlated.

The last stage involves (at least) the 15 div following the previous stage. This period is characterized by a slow α increment toward α ≈ 2. This condition corresponds to a non-stationary signal that exhibits oscil-

lations similar to a Brownian motion. This state testifies an energetically stable system; probably for this reason the activity of sub-networks repeats in a semi-random way. This considerations are supported by the morphological and temporal considerations done in [7] through the direct observation of pressing and regular bursts.

The kind of analysis we employed here for the first time seems to be able to highlight activity modifications that involve the whole neuronal network. The future development of our work is to show the usefulness of this kind of approach in analyzing other aspects of neuronal networks, e.g. in presence of chemical or electrical stimulations.

# 5 Conclusions

The results presented in this work suggest a new method for the analysis of the statistical characteristics of neuronal network activity. This approach has the advantage to allow the use of well-characterized non-linear signal processing methods, such as Periodogram, for the analysis of the whole network activity. Up to date, the whole-network-activity nonlinear analyses required the creation of *ad hoc* laborious methods.

Concerning the used MEA series, we were able to divide the network development in three stages. A first stage (between the $6^{th}$ and the $16^{th}$ div *circa*) was characterized by a signal stationarity together with a positive long-term correlation. The second stage, corresponding to the network pruning, was characterized by a sudden $\alpha$ increment as a sign of a non-stationarity characterized by a negatively long-memory correlated condition. This could be probably the consequence of sub-networks creation, which is a typical of developing self-assembling neuronal networks. Finally, network maturity came together a progressive $\alpha$ increment toward $\alpha \approx 2$, i.e. toward a Brownian motion-like processes.

**Acknowledgement**

**References**

[1] A.M.M.C. Habets et al. (1987), Spontaneous neuronal firing patterns in fetal rat cortical networks during development in vitro: A quantitative analysis. Exp. Brain Res., vol. 69, pp. 43-52.

[2] M.A. Corner and G.J.A. Ramakers (1991), Spontaneous bio-electric activity as both dependent and independent variable in cortical maturation: Chronic tetrodotoxin versus picrotoxin effects on spike-train patterns in developing rat neocortex neurons during long-term culture. Ann. N. Y. Acad. Sci., vol. 627, pp. 349-353.

[3] T.A. Basarsky, V. Parpura and P.G. Haydon (1994), Hippocampal synaptogenesis in cell culture: Developmental time course of synapse formation, calcium influx, and synaptic protein distribution J. of Neurosc., vol. 14, pp. 6402-6411.

[4] T.H. Murphy et al. (1992), Spontaneous synchronous synaptic calcium transients in cultured cortical neurons. J.l of Neurosc., vol. 12, pp. 4834-4845.

[5] H. Kamioka et al. (1996), Spontaneous periodic synchronized bursting during formation of mature patterns of connections in cortical cultures. Neurosci. Lett., vol. 206, pp. 109-112.

[6] R. Segev, Y. Shapira, M. Benveniste and E. Ben-Jacob (2001), Observations and modeling of synchronized bursting in two-dimensional neural networks. Phys. Rev..E vol. 64, pp. 011920.

[7] D.A. Wagenaar, J. Pine and S.M. Potter (2006), An extremely rich repertoire of bursting patterns during the development of cortical cultures. BMC Neuroscience, vol. 7, pp. 11.

[8] . Beran (1994), Statistics for Long Memory Processes, Chapman & Hall, N.Y.

[9] M.C. Teich, C. Heneghan, S.B. Lowen, T. Ozaki, E. Kaplan (1997), Fractal character of the neural spike train in the visual system of the cat. J Opt. Soc. Am. A, vol. 14, 3, pp. 529-546.

[10] J.M. Beggs, D. Plenz (2003), Neuronal avalanches in neocortical circuits. The J. of neurosc., 23(35): 11167-11177.

[11] R. Segev, M. Benveniste, E. Hulata, N. Cohen, A. Palevski, E. Kapon, Y. Shapira, E. Ben-Jacob (2002), Long-term behavior of lithographically prepared in vitro neuronal networks. Phys. Rev. Lett., 88(11).

[12] D.A. Wagenaar, T.B. DeMarse, S.M. Potter (2005), MEA-Bench: A toolset for multi-electrode data acquisition and on-line analysis. Proc 2nd IEEE EMBS Conf on Neural Eng, 518–521.

[13] F. Esposti, J. Lamanna, M.G. Signorini (2007), A new approach to the spatio-temporal patter identification in neuronal multi-electrode registrations. Proc of Neuroscience Today '07, 21-24. Available free online from Nature Procedings <http://dx.doi.org/10.1038/ npre.2007.1306.1>

[14] P. Flandrin (1989), On the spectrum of fractional Brownian motions. IEEE trans. on inf. theory, vol. 35, N 1: 197-199.

[15] M.S. Taqqu, V. Teverovsky, W. Willinger (1995), Estimators for long-range dependence: an empirical study. Fractals, 3(4), pp: 785-798.

[16] E. Maeda, H. P. C. Robinson and A. Kawana (1995), The mechanisms of generation and propagation of synchronized bursting in developing networks of cortical neurons. J. of Neuros., vol. 15, pp. 6834-6845.

[17] F. Esposti, M.G. Signorini (2008), Synchronization of MEA neuronal networks. European Physical Journal Special Topics, in press.

[18] F. Esposti, M.G. Signorini, J. Lamanna, F. Gullo, E. Wanke (2007), How do TTX and AP5 affect the post-recovery neuronal network activity synchronization? Proc. of IEEE EMBC'07, pp. 3012-3015.

[19] O. Shefi (2002), Growth morphology of two-dimensional insect neural networks. Neurocomputing, vol. 44, pp. 635.

[20] J. Van Pelt, P. S. Wolters, M. A. Corner, W. L. C. Rutten and G. J. A. Ramakers (2004), Long-term characterization of firing dynamics of spontaneous bursts in cultured neural networks. IEEE Trans. on Biomed. Eng. vol. 51, pp. 2051-2062.

# Spike train data analysis of substance-specific network activity: Application to functional screening in preclinical drug development

Olaf H.-U. Schroeder[1*], Alexandra Gramowski[1,2], Konstantin Jügelt[1], Christiane Teichmann[1], Dieter G. Weiss[2]

1 NeuroProof GmbH, Rostock, Germany
2 Institute of Biological Sciences, University of Rostock, Rostock, Germany
* Corresponding author. E-mail address: olaf.schroeder@neuroproof.com

Neuronal networks grown on microelectrode arrays from primary dissociated cell cultures are an interesting alternative for substance screening in drug development and safety pharmacology. The activity patterns obtained following chemical stimulation of these networks are reproducible, so that they are applicable as a new read-out system in cell-based drug screening. This report is going to present results about the system's possibilities and limits for the use in drug screening, taking into account that efficient data analysis is of crucial importance. This article describes data analysis and classification methods of activity patterns of neuronal network cultures on MEA neurochips. The spike train parameters required to describe the activity patterns of these spontaneously active neuronal cell cultures are different from those needed for stimulation experiments of brain-slice cultures. The evaluation of which parameters are more or less suitable can be made by performing classification experiments for which an activity pattern data base of 21 substances was built up. Since the substance effects depend on the concentration, it is being investigated whether a classification approach with different concentrations is possible.

## 1 Background/Aims

Cultured neuronal networks grown on microelectrode arrays from primary dissociated brain cells are a powerful addition to the battery of screening assays in drug development and safety pharmacology. The activity pattern changes observed after chemical stimulation of these networks are reproducible, so that the system is applicable as an innovative read-out system in drug screening. Here we describe the system's possibilities and limits for its use in drug screening. First, data analysis and classification methods for analyzing activity patterns on MEA neurochips of primary dissociated cell cultures were standardized by SOPs. The required spike train features describing the activity patterns of these spontaneously active cell cultures are found to be different from those needed for analyzing electrically stimulated brain-slice cultures. Evaluation and selection of the most suitable parameters are performed as an intrinsic part of the classification experiments. Meanwhile, a data base consisting of the concentration-dependent changes of a large number of quantitative parameters for 21 reference substances with known mode of action (primarily anticonvulsants, anesthetics and antidepressants) was established. As the substances' effects depend on substance concentration, it is being investigated how a classification approach with different concentrations is possible.
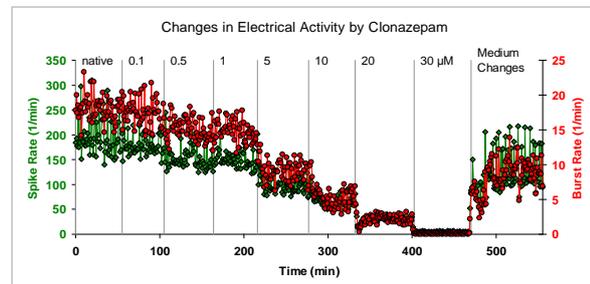


**Fig. 1.** Spike and burst rate response curve for a standard experiment

## 2 Methods

### 2.1 Neuronal Network Cultures

Primary neuronal cells from NMRI mice were cultured on MEA neurochips. The spike train data were recorded with a standard setup (Gramowski et al. 2004). We used the microelectrode array (MEA) neurochip technology consisting of the MEAs (CNNS, UNT, Denton Texas, USA), the MEA workstation (Plexon, Inc., Dallas, TX, USA), and analyzing software (Plexon, Inc., and NeuroProof GmbH, Rostock, Germany). The results shown here originate from frontal cortex tissue. Preliminary tests were run to estimate the optimal range of the concentration–response curve. In doing so, preliminary EC10, EC50,

and EC90 were determined if possible. Subsequently, at least 8 more tests with defined increasing concentrations were conducted. A stable activity phase of at least 30 minutes was analysed for every application phase (Fig. 1). For this study we tested the following substances: Agmatine (AGM), Baclofen (BAC), Biculculline (BCC), Clonacepam (CLO), Dermorphine (DER), Diazepam (DIA), DPDPE (DPD), Fluvoxamine (FLV), Fluoxetine (FLX), Gabapentin (GBP), Ketamin(KET), Levetiracetam (LEV), Naloxone (NLX), Octanol (OCT), Phenobarbital (PHB), Phenytoin (PHT), Pregnanolone (PRE), SCH50911 (SCH), Substance P (SUB), Topiramate (TPM) and Valproate (VPA).

## 2.2 Data Analysis

Chemically stimulated networks require a specific data analysis approach due to their spontaneous and complex network behaviour (Fig. 2). Certain spike train parameters such as peri-stimulus histograms are not suited in this case. We work with a parameter-free non-classical statistical classification approach. A good starting point for investigating network behaviour is to classify substance-specific network responses independent of the individual network culture specificity. Since substance-specific responses are concentration-dependent one has to decide for which concentrations a comparison of substance-specific activity patterns should be performed. This is especially important since substances often act via different modes of action at different concentrations. For this reasons we try to classify substance-specific activity patterns at different concentrations to reflect the full dynamic range of a substance.

## 2.3 Spike Train Features

For each of these substances' addition phases, spike train features were calculated for stable activity. Computation of spike train features should characterize effects such as general activity, burst structure, regularity of oscillation and synchronicity. We constructed spike train features known from literature (see Brown et. al. 2004 and Gramowski et. al. 2004) and also heuristic ones (Tab. 1). Since it is very difficult to assess the significance and relevance of features in advance, we have constructed spike train features in a gun-shot manner. Some spike train features are parameter-dependent. For example CV-Net and CV-Time spike train features (see Gramowski et al. 2004) are strongly parameter dependent, since the so-called bin parameter is crucial for the values of these features. Another important spike train feature is the so-called contrast, which is the absolute value of the difference of the number of spikes of two consecutive intervals divided by the number of spikes in both intervals. This spike train feature also depends strongly

on the length of the bin intervals. Since this parameter is continuous, one can construct an infinite number of such contrast features. In conclusion, it becomes obvious that the most important step in data mining of spike train data is the assessment of spike train features, which we performed by feature selection. All parameters have to be normalized to the native situation as baseline of activity.
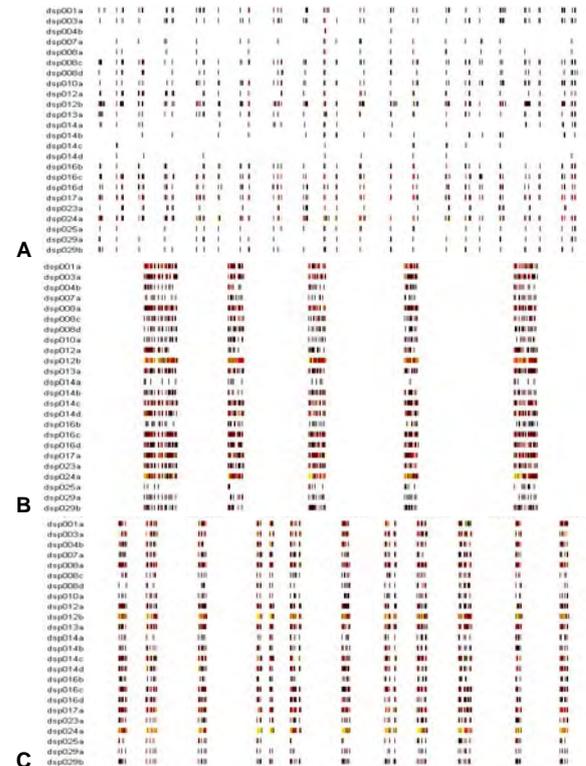


**Fig. 2.** Example of different spike train pattern responses; A: native; B: application of substance I; C: additional application of substance II.

## 2.4 Feature Selection

Feature selection is a widely accepted method in bioinformatics and a wide range of different approaches have been proposed (Gyon et. al 2003). One method of feature selection can be performed by measuring the significance of a feature by a so-called feature score. We calculated rankings of features by different feature scores. Different scores were assessed with classification experiments. The 40 most suitable parameters were selected and their total correct predictions were compared. In this manner we obtained the best results for a MDL (minimal description length) modified algorithm.

**Table 1:** Example of a classification experiment with 4 substances, each inner cell represents the class assignment for one substance in %, the sum column and row indicate the number of datarecords.

|     | BAC | BCC | CLO | DIA | sum |
|-----|-----|-----|-----|-----|-----|
| BAC | 90  | 1   | 9   | 0   | 78  |
| BCC | 3   | 84  | 7   | 7   | 91  |
| CLO | 4   | 4   | 70  | 23  | 79  |
| DIA | 2   | 7   | 18  | 73  | 101 |
| sum | 78  | 87  | 86  | 98  | 349 |

**Table 2:** Example of a classification experiment with 10 substances

|     | BAC | BCC | CLO | DIA | DPD | FLX | LEV | PHT | PRE | SCH | sum |
|-----|-----|-----|-----|-----|-----|-----|-----|-----|-----|-----|-----|
| BAC | 73  |     |     |     | 10  | 5   | 4   | 8   |     |     | 78  |
| BCC | 1   | 74  |     | 4   | 10  | 3   |     | 7   | 1   |     | 91  |
| CLO |     | 1   | 61  |     |     | 10  | 9   | 4   |     | 15  | 79  |
| DIA |     | 4   | 12  | 58  | 3   |     | 12  | 2   | 9   |     | 101 |
| DPD | 7   | 7   |     |     | 44  | 27  | 6   | 5   | 1   | 1   | 81  |
| FLX | 4   |     |     | 1   | 13  | 58  | 7   | 1   |     | 16  | 77  |
| LEV |     |     | 9   | 8   | 4   | 13  | 59  | 2   |     | 4   | 90  |
| PHT | 3   | 2   | 2   | 2   |     | 3   | 10  | 72  | 2   | 5   | 60  |
| PRE |     |     | 6   | 13  | 13  | 3   |     | 6   | 59  |     | 32  |
| SCH | 2   |     | 6   | 1   | 3   | 23  | 9   | 9   | 7   | 42  | 115 |
| sum | 71  | 79  | 78  | 77  | 77  | 123 | 101 | 79  | 39  | 80  | 804 |

**Table 3:** Example of a classification experiment with 21 substances

| %   | AGM | BAC | BCC | CLO | DER | DIA | DPD | FLV | FLX | GBP | KET | LEV | NLX | OCT | PHB | PHT | PRE | SCH | SUB | TPM | VPA | sum |
|-----|-----|-----|-----|-----|-----|-----|-----|-----|-----|-----|-----|-----|-----|-----|-----|-----|-----|-----|-----|-----|-----|-----|
| AGM | 21  | 1   |     | 1   | 6   |     | 1   | 4   | 8   | 3   | 1   | 3   | 1   | 3   | 6   | 11  | 6   | 7   | 3   | 8   | 8   | 143 |
| BAC | 5   | 67  |     |     | 3   |     | 5   | 4   | 5   | 8   |     |     |     |     |     | 1   |     |     |     | 3   |     | 78  |
| BCC |     |     | 62  |     | 3   | 1   | 11  | 10  | 2   | 2   |     |     | 9   |     |     |     |     |     |     |     |     | 91  |
| CLO |     |     |     | 43  | 1   | 3   | 1   |     | 3   |     | 3   | 13  |     | 11  |     | 3   | 6   | 1   | 8   | 5   |     | 79  |
| DER |     |     |     |     | 36  |     | 17  | 4   | 3   | 4   |     | 1   | 7   |     | 4   |     |     | 10  | 10  | 5   |     | 81  |
| DIA |     |     | 4   | 8   | 3   | 51  |     |     |     |     | 3   | 9   | 8   | 3   |     | 1   | 10  |     | 1   |     |     | 101 |
| DPD |     | 4   | 3   |     | 16  |     | 32  | 17  | 1   | 16  |     |     |     |     |     | 3   |     | 7   |     |     | 1   | 81  |
| FLV | 5   | 13  | 6   |     | 19  | 1   | 5   | 23  | 3   | 9   | 1   | 2   | 2   | 2   | 2   | 2   | 1   | 4   |     |     | 3   | 108 |
| FLX |     | 1   |     | 10  | 1   | 1   | 7   |     | 49  | 4   |     | 1   |     | 8   | 3   | 3   |     | 1   | 9   | 1   |     | 77  |
| GBP | 2   | 10  | 8   |     | 7   |     | 11  | 16  | 16  | 16  |     |     |     |     | 11  | 1   |     | 3   | 1   |     |     | 110 |
| KET | 2   |     |     |     | 12  | 12  | 2   |     | 3   |     | 30  | 2   | 15  | 5   | 2   | 5   |     |     | 5   |     | 7   | 60  |
| LEV | 3   |     |     | 8   | 19  | 6   |     | 1   | 1   |     | 4   | 36  |     | 4   | 3   | 1   |     | 3   | 2   | 2   | 6   | 90  |
| NLX |     |     | 3   |     | 10  | 10  | 7   |     | 12  |     | 7   |     | 14  | 12  | 1   | 5   | 3   | 7   | 10  | 1   |     | 74  |
| OCT | 1   |     |     | 3   | 11  |     | 9   | 2   | 9   |     | 5   | 1   | 11  | 19  | 2   | 1   | 7   | 5   | 7   | 1   | 8   | 135 |
| PHB | 11  |     |     | 17  | 12  |     |     | 21  |     |     |     |     | 2   | 8   | 15  | 2   |     |     | 3   | 3   | 8   | 66  |
| PHT | 8   | 2   |     |     | 7   |     | 2   |     | 13  | 8   | 2   |     |     |     |     | 43  |     |     | 5   | 10  |     | 60  |
| PRE | 3   |     |     | 3   | 6   | 19  | 9   |     |     |     | 3   |     |     | 3   | 9   |     | 44  |     |     |     |     | 32  |
| SCH | 3   | 1   |     | 4   | 15  | 2   | 1   |     | 11  | 3   |     |     | 4   | 5   | 2   |     |     | 28  | 17  | 6   |     | 115 |
| SUB | 3   | 1   | 1   |     | 13  |     | 2   |     | 6   | 3   | 3   | 6   | 18  | 8   | 4   |     | 14  |     | 10  | 3   | 3   | 116 |
| TPM | 1   |     |     | 2   | 20  |     | 4   | 1   | 9   | 6   | 1   | 9   | 5   |     | 11  | 10  |     | 7   |     | 15  | 2   | 130 |
| VPA | 1   |     |     |     | 26  |     | 3   | 7   | 6   | 1   | 1   | 4   |     | 7   | 3   | 7   | 1   |     | 3   | 6   | 22  | 69  |
| sum | 67  | 85  | 80  | 74  | 232 | 83  | 106 | 91  | 154 | 82  | 53  | 78  | 68  | 98  | 85  | 87  | 49  | 103 | 84  | 67  | 70  | 1896 |

**Table 4**: Example of the classification experiment with 21 substances and the concentration used as feature

| %   | AGM | BAC | BCC | CLO | DER | DIA | DPD | FLV | FLX | GBP | KET | LEV | NLX | OCT | PHB | PHT | PRE | SCH | SUB | TPM | VPA | sum |
|-----|-----|-----|-----|-----|-----|-----|-----|-----|-----|-----|-----|-----|-----|-----|-----|-----|-----|-----|-----|-----|-----|-----|
| AGM | 19  | 2   |     | 1   | 8   |     | 4   | 6   | 8   | 1   |     | 1   |     | 5   | 7   | 15  | 4   | 6   | 4   | 8   |     | 143 |
| BAC | 4   | 69  |     |     | 1   |     | 9   | 6   | 5   |     |     |     |     |     | 1   | 1   |     | 3   |     |     |     | 78  |
| BCC |     | 3   | 57  |     | 6   | 1   | 7   | 9   | 2   | 6   |     | 9   |     |     |     | 1   |     |     |     |     |     | 91  |
| CLO |     |     | 1   | 54  | 6   | 1   | 1   |     | 3   |     | 1   | 4   | 1   | 10  |     |     |     | 8   | 4   | 5   |     | 79  |
| DER |     |     | 1   |     | 37  |     | 14  |     | 11  |     |     | 1   | 5   | 3   | 5   | 1   | 9   | 10  | 4   |     |     | 81  |
| DIA |     |     | 5   | 10  | 3   | 52  |     |     |     |     | 3   | 2   | 9   | 3   |     | 1   | 11  |     | 2   |     |     | 101 |
| DPD |     | 16  | 4   |     | 21  |     | 37  | 4   | 1   |     |     |     | 1   |     | 1   | 1   | 3   |     | 9   | 3   |     | 81  |
| FLV | 4   | 19  | 7   |     | 17  | 1   | 7   | 25  | 9   |     |     |     |     | 2   | 1   | 1   | 1   | 3   | 3   |     |     | 108 |
| FLX | 1   |     |     |     | 16  | 1   | 4   | 10  | 48  |     |     | 1   |     | 7   |     | 4   |     | 3   | 5   |     |     | 77  |
| GBP | 2   | 3   | 2   |     | 10  |     | 5   | 2   | 10  | 56  |     |     |     | 1   | 5   |     |     | 4   | 1   |     | 1   | 110 |
| KET | 3   |     |     | 2   | 15  | 17  |     |     | 3   |     | 35  |     | 8   | 2   | 5   | 3   | 2   |     | 3   | 2   |     | 60  |
| LEV | 3   |     |     | 2   | 11  | 1   |     | 1   | 8   |     | 1   | 39  | 2   | 4   | 6   |     | 1   | 2   | 4   | 8   | 6   | 90  |
| NLX |     |     | 3   |     | 11  | 10  | 7   |     | 15  | 1   | 4   |     | 14  | 8   |     | 3   | 5   | 7   | 11  | 3   |     | 74  |
| OCT |     |     |     | 1   | 18  | 1   | 8   | 2   | 7   | 1   | 2   | 4   | 9   | 21  | 2   | 5   | 3   | 6   | 11  |     | 2   | 135 |
| PHB | 6   |     |     | 12  | 18  |     |     | 2   | 17  |     |     |     |     | 6   | 21  | 2   |     | 3   | 2   | 12  |     | 66  |
| PHT | 3   |     | 3   |     | 10  |     | 5   |     |     | 7   | 15  | 2   |     | 2   |     | 47  |     |     | 2   | 5   |     | 60  |
| PRE |     |     |     |     | 6   | 13  | 9   |     |     |     |     |     |     |     | 13  |     | 53  | 3   | 3   |     |     | 32  |
| SCH | 3   |     |     | 4   | 13  |     | 4   |     | 17  | 1   |     | 1   | 2   | 7   | 2   | 1   |     | 23  | 18  | 5   |     | 115 |
| SUB | 3   | 1   | 2   | 2   | 18  |     | 6   | 3   | 2   |     | 2   | 1   | 6   | 12  | 8   | 7   | 10  |     | 17  | 1   |     | 116 |
| TPM | 2   | 1   |     | 4   | 16  |     | 9   | 1   | 5   |     |     | 2   | 5   | 2   | 7   | 11  |     | 12  | 9   | 15  |     | 130 |
| VPA |     |     |     |     | 32  |     | 1   | 6   |     | 4   |     | 10  |     | 6   | 3   |     |     |     | 4   |     | 33  | 69  |
| sum | 57  | 99  | 78  | 78  | 264 | 79  | 120 | 78  | 156 | 74  | 47  | 59  | 64  | 88  | 84  | 97  | 50  | 102 | 119 | 72  | 31  | 1896 |

## 2.5 Machine Learning and Cross Validation

Data records were trained with an artificial network algorithm called resilient backpropagation. Then, cross-validation was conducted where in each test the concentration datasets from one experiment were excluded as a whole. The best features of the categories general activity, oscillation, synchronicity, and burst structure were analysed separately.

## 3 Results

Our classification results deliver a total of correct prediction rates from 79% for a classification of 4 substances to 44% for 21 substances (Tables 2, 3, 4).

The total correct prediction rate can be improved significantly if the concentration is used also as a feature for training and testing of the artificial neuronal network (Tables 4 and 5).

We computed the best 40 features with a MDL-like score. The best feature is the length of the so-called burst plateau. This feature has a higher ranking than the concentration feature. The spike rate, feature 2041, appears at the end of the ranking list. The feature 1151 describes the burst amplitude computed by integration of an approximation curve. This parameter quantifies also the peak frequency of the spike rate within a burst. However, peak frequency does not appear in the 40 bests list. In this manner the construction of spike train features is presently further assessed.

## 4 Conclusion/Summary

The classification results prove that the neuronal network cultures provide reproducible results. This means in particular that the neuronal networks organize themselves reproducibly. It is possible to draw conclusions from the classification results on the mode of action. It remains open if the different concentration-dependent modes of action of multiple mechanisms can be generally taken into consideration. Feature recognition can be used to determine the most significant spike train parameters, making it an indispensable tool for the development and evaluation of new spike train parameters.

Based on our substance data base, optimal functional parameters can be chosen for special indicators and, combined with the appropriate choice of a specific tissue, models for the test of substances for various applications are being developed.

**Table 5:** Feature scores of 40 best features with the feature descriptions of the NeuroProof Software Squid

| Feature | L-Score |
|---|---|
| 1231burstsBrstPlatMean | 0.181 |
| concentration | 0.172 |
| 1152burstsBrstAmplSD | 0.171 |
| 1282burstsBrstSpMaxRateSD | 0.170 |
| 1151burstsBrstAmplMean | 0.168 |
| 1181burstsBrstSpNmbrMean | 0.167 |
| 1281burstsBrstSpMaxRateMean | 0.166 |
| 1232burstsBrstPlatSD | 0.164 |
| 1131burstsBrstPercSpinBrstMean | 0.160 |
| 1161burstsBrstAreaMean | 0.157 |
| 1241burstsBrstPlatPosMean | 0.157 |
| 1272burstsBrstSpRateSD | 0.155 |
| 1491burstsSynShareMean | 0.155 |
| 1414burstsShY3/Y1CVnet | 0.148 |
| 1171BurstsSummeBrstDurMean | 0.148 |
| 1191burstsBrstSpDensMean | 0.146 |
| 1182burstsBrstSpNmbrSD | 0.145 |
| 1324burstsShDist1CVnet | 0.145 |
| 1374burstsShCount3CVnet | 0.145 |
| 1444burstsShFastCVnet | 0.143 |
| 1354burstsShCount1CVnet | 0.142 |
| 1162burstsBrstAreaSD | 0.141 |
| 1271burstsBrstSpRateMean | 0.141 |
| 1334burstsShDist2CVnet | 0.141 |
| 1421burstsShY1Mean | 0.141 |
| 1192burstsBrstSpDensSD | 0.140 |
| 1201burstsBrstSrprMean | 0.140 |
| 1214burstsBrstPeakFrqCVnet | 0.140 |
| 1364burstsShCount2CVnet | 0.140 |
| 2051SimplexSpSimplexMean | 0.140 |
| 1144burstsBrstRateCVnet | 0.139 |
| 1344burstsShDist3CVnet | 0.139 |
| 1422burstsShY1SD | 0.139 |
| 1424burstsShY1CVnet | 0.138 |
| 2041spikesSpRateMean | 0.137 |
| 1202burstsBrstSrprSD | 0.137 |
| 1222burstsBrstPeakFrqPosSD | 0.137 |
| 3115gaborY1Gbr | 0.136 |
| 1161BurstsSummeBrstAreaMean | 0.136 |
| 1171burstsBrstDurMean | 0.135 |

**References**

[1] Brown, E. N., Kass, R. E., Mitra, P. P. Multiple neural spike train data analysis: state-of-the-art and future challenges. *Nature Neuroscience 7, (2004), 46-461*

[2] Gramowski, A., Jügelt, K., Weiss, D. G. and Gross, G. W. Substance identification by quantitative characterization of oscillatory activity in murine spinal cord networks on microelectrode arrays. *Eur J. Neurosci. 19,* (2004). *2815-2825*

[3] Guyon I., Elisseeff A., An introduction to variable and feature selection. *J. Machine Learning Research 3, (2003), 1157-1182*

# The CARMEN Virtual Laboratory: Web-Based Paradigms for Collaboration in Neurophysiology

Frank Gibson[1*], Jim Austin[2], Colin Ingram[3], Martyn Fletcher[2], Tom Jackson[2], Mark Jessop[2], Alastair Knowles[1], Bojian Liang[2], Phillip Lord[1], Georgios Pitsilis[1], Panayiotis Periorellis[1], Jennifer Simonotto[1], Paul Watson[1], Leslie Smith[4].

1 School of Computer Science, Newcastle University, Newcastle upon Tyne, NE1 7RU, UK.
2 Department of Computer Science, University of York, Heslington, York, YO10 5DD, UK
3 School of Neurology, Neurobiology and Psychiatry, Newcastle University, Newcastle upon Tyne, NE1 7RU, UK.
4 Department of Computing Science and Mathematics, University of Stirling, Stirling FK9 4LA, UK.
* Corresponding author. E-mail address: Frank.Gibson@ncl.ac.uk

Dissemination, reuse and sharing of digital resources is technically and culturally challenging in neuroscience – particularly in the area of Multi-Electrode Array (MEA) recording. Large, complex datasets are typical, with a heterogeneous range of data and code formats. The CARMEN project (http://www.carmen.org.uk/) aims to enable broad sharing or resources, through provision of a secure, online environment for data analysis, and curation of data, analysis code and experimental protocols.

## 1 Introduction

Multi-electrode array (MEA) based neuroscience research has matured to the point where integrated hardware and software systems for recording and stimulation can be bought off the shelf. Alongside commercial acquisition software, many neuroscientists develop custom analysis code.

Dissemination, reuse and sharing of digital resources are both technically and socially challenging. Large, complex datasets are common place with, heterogeneous range of data and code formats. Significantly, deeply ingrained social precedents impede resource sharing, despite the obvious potential for advancement both in neuroscience, and for society as a whole[1]. The CARMEN project aims to addresses these challenges, through provision of a secure environment for resource sharing, online data analysis, and precise description and curation of experimental protocols.

The benefits of sharing life-science data resources to maximise knowledge discovery are well known and documented [2]. Sharing resources can leverage community expertise, allowing others to perform different analyses on the same dataset or to perform the same analyses on different datasets, e.g. as in comparative studies across the same target animal or CNS structure.

There are several barriers to the efficient and effective sharing of resources: (a) datasets are large and complex, with no widely accepted community standards for data formats such as electrophysiology recordings; (b) experiments are not always reported consistently, or in sufficient detail to enable to third party interpretation and evaluation. Re-use of resources – datasets, analysis code or experimental protocols – is predicated on precise knowledge of exactly what these resources represent, i.e. knowledge of the study subject(s), equipment and protocols describing how the data was generated and/or processed. This is commonly referred to as metadata; data about data.

In the absence of accurate and detailed metadata resources are effectively meaningless. Annotation, the process of ascribing metadata to resources to enable future reuse, requires effort. Further, scientists may as a consequence of annotation be obliged to publish details of their protocols. Some may not wish to do this.

Ownership and accreditation are highly important. Resources, currently withheld by small groups and individuals, are globally scarce, and therefore of high perceived value. Some neuroscientists worry that they may not be appropriately credited for new results obtained using their datasets, while others are concerned that errors in their analyses may be uncovered, while others feel that resources represent competitive advantage and simply should not be dispensed to others [3].

It is recognised that the neurophysiology community is large, disparate, and global. Groups vary in size and capability, from independent researchers to highly parallel data production lines in pharmaceutical companies and research institutes. CARMEN aims to provide the basis for these diverse groups to share and repurpose resources across organisational boundaries, potentially within a single, seamless virtual marketplace. A web based platform is being developed to meet this brief.

In this paper we describe the CARMEN system and technical progress to date. We outline future work and discuss potential impact and applications.

## 2 Technical Progress

Initial requirements for CARMEN have been collected through extensive, iterative discussion with the project members. In summary, these requirements are: Allow "experimenter" users to describe, store and analyse data (time and image series) from various electrophysiology acquisition systems – in various proprietary and bespoke formats. Allow "analyst" users to describe, store and browse code (source and executable) for data analysis. Allow execution of code in Matlab, R, Java, Python and C/C++ languages, including parallel processes. Allow "simulation" users to describe, store and analyse data generated by simulation tools, including the NEURON and GENESIS simulators. Allow data derived from the results of analyses to be stored and bound to source data for further analysis. Allow users to specify and apply access control rights to their resources. Allow both web and client based software tools to connect to the environment securely for data analysis and visualisation. Enable data translation between different proprietary and bespoke data formats, retaining source data at all stages in translation. Support a user community that is distributed and growing, with varying data preservation capabilities and requirements.

These requirements drive the design and development of the CARMEN system.

### 2.1 The CARMEN Architecture

CARMEN is a Three Tier Web architecture [4], consisting of server deployments at different scales, e.g. from desktop to data warehouse. The data tier is shared between databases and a distributed (i.e. virtual) file system called the Storage Request Broker (SRB) [5]. Databases are used to store user accounts, metadata, system states and links between resources and users. Physical files, (e.g. data recordings and analysis code), are stored in the SRB. CARMEN server nodes support storage and invocation of both data and analysis services. Analysis operations may take place adjacent to data, minimising the need to transport high volume datasets. The ability to describe, search and navigate resources is provided by common frameworks for representation of data and metadata. A security framework provides the basis for groups to control access to resources, so as to enable secure collaborations, and productive competition between these collaborations. Single point access to the system is delivered via an interactive Web portal.

### 2.2 Representation of Metadata

Poor or insufficient metadata impedes resource interpretation, evaluation and reuse. The CARMEN consortium has defined what information and level of detail must be ascribed to a dataset that is submitted to CARMEN. This reporting consensus is called the Minimum Information about a Neuroscience Investigation (MINI) [6]. The document is separated into the following sections: contact and context, study subject, task, stimulus, behavioural event, recording, time series data. This reporting consensus is structured within the FuGE data model [7]. FuGE models common aspects of life-science experiments such as protocols, equipment and materials and is being implemented by domains such as genomics, proteomics and metabolomics. By using FuGE, CARMEN datasets can be combined with this type of information, providing a framework for integrative or system level investigation, from biological processes to neural function.

The terminology used for metadata descriptions must be associated with meaning or semantics to allow consistent description and interpretation not only for neurophysiology experiments but also analysis code and data produced. To achieve this, CARMEN aims to develop and contribute to the Ontology for Biomedical Investigations (OBI) [8]. OBI is an ontology providing consistent terminology and descriptions for life-science investigations. In this way, it is envisaged that terminology used to describe CARMEN data will be consistent and interpretable across the life sciences.

### 2.3 Representation of Data

A standard representation for metadata supports an environment where different experiments can be characterised in a way that is amenable to both users and computers. Raw electrophysiology recordings use a multitude of data formats – both vendor-specific and bespoke. Raw data is often unreadable without the original software or detailed knowledge of the format. This situation presents a serious barrier to collaborative neuroscience. Valuable research time is wasted decoding formats and writing data converters. To attempt to overcome these restrictions, CARMEN is developing an intermediate data format for neurophysiology recordings. The Neurophysiology Data Translation Format (NDTF) [9], provides a standard for sharing data, specifically for inter-application and data communication between analysis software developed within the CARMEN project. It provides improvements over and above existing translation formats such as NeuroShare [10], such as the ability to encode static files. Further, it is optimised for dynamic access operations such as streaming and search, allowing client tools developed in conjunction with CARMEN to support high performance visualisation and pattern searching. NDTF is a wrapped data set consisting of a configuration file and one or more ('host') data files. The configuration file is an XML [11] document which contains metadata and manages associated data. The use of NDTF provides a common mechanism for programs to interpret the semantics of data. It allows systems to 'know' which programs can be used on which datasets, and provides a format for encoding output data.

## 2.4 Running Analysis Code

MEA datasets can run into terabytes presenting storage challenges and pushing desktop processing and analysis power beyond its current limits. CARMEN will help to overcome these issues by enacting analysis on the system that holds the data. Data transfers can thereby be confined to closely connected cluster machines on server nodes, enabling faster computation and shorter analysis times.

To benefit from the processing capability in CARMEN, analysis code will be uploaded and wrapped to form Web Services [12]. Web Services provide a common means of communicating with different languages and data types. Curating analysis code as Web Services facilitates the re-running and re-use of code. Early stage support has been developed for services based on MatLab, Java and R, with C/C++ and FORTRAN to be addressed in the near future.

It will be possible to enact services residing in CARMEN automatically, in user defined sequences. For example, typical MEA analyses may involve thresholding, then spike detection, and then graphical presentation of the results. Within CARMEN, the source data may be connected to the threshold service, the output of the threshold service may be connected to the spike detection service. The spike times produced form this service may form the input to the graphical presentation service, which displays the results to the user. This process of connecting services and invoking sequences by way of single commands is termed 'workflow'. A workflow is a programmatic depiction of a sequence of operations and provides a mechanism to visualize and enact processes, such as complex data analyses. Building workflows encourages users to provide modular components, rather than monolithic programs that offer less flexible opportunities for re-use. Analyses may be re-enacted by other users, by launching appropriate workflows. Moreover, the same workflow may be run on different datasets. In addition to data, code and services, workflows are valuable resources that can be shared between researchers. It will be possible to construct workflows consisting of data and services within CARMEN using a workflow editing environment, such as Taverna [13].

## 2.5 Security

Security and usability can be contradictory concerns. CARMEN aims be usable, intuitive and user friendly, promoting collaboration and the development of research ideas. Security (as a non functional property and also in terms of implementation) can influence the usability of a system as recent examples have demonstrated [14]. We have avoided developing a framework that compromises system usability to provide security.

Authentication and authorization are critical issues in CARMEN. Access to system resources is carried out by authenticated users in possession of appropriate authorization tokens. We are building on top of established research work [15] in the areas of Web Services to accommodate our access control and authorization requirements. Our custom security mechanisms are deployed and act as mediators between the users and system resources. We can control access and usage of resources held in CARMEN, resources deployed as web services, as well as safeguard the process of uploading and downloading data. We are exploring additional functionality such as the ability to create audit records by keeping track of access to certain resources, delegating access rights and revoking rights granted to users. Typical users will interact with the security system via the Web-based portal.

## 2.6 Portal

CARMEN can be accessed via a Web Portal allowing users to upload, download, view, annotate and share resources, based on the security permissions ascribed to each resource. The CARMEN portal is written in Java using the Google Web Toolkit [12], which converts the Java code to Ajax. This allows rapid prototyping, generating modern interfaces which give CARMEN the look and feel of a desktop environment. Ajax can perform asynchronous communication between browser and the Application Tier, without the need to refresh the user interface. This allows large datasets to be viewed rapidly without impacting heavily on browser performance or user experience.

## 3   Future Work

**Provenance:** Provenance provides an audit trail of analysis; what services were run, when, and what results were produced. This is similar to transcribing the process in a lab-book, except that it happens automatically. Provenance tracing mechanisms allow the derivation of resources to be captured, both for subsequent scrutiny, and to ensure appropriate accreditation and acknowledgement of originators.

**Ownership:** At both social and technical application levels, the CARMEN consortium are exploring new mechanisms for publication and accreditation that truncate the resource dissemination cycle, and addressing the issues of expression and control of ownership. One proposal is the assignment of licenses to data, such as the Protocol for Implementing Open Access Data [16], or Creative Commons Zero (CC0) waiver [17].

**Networking:** A Social Networking platform constructed around data and resources may facilitate researchers' discovery of new resources and collaborations in a manner that evokes current working practices, which would not have been possible though the traditional laboratory based working environment.

**Availability:** The project aims to release a stable system to consortium members in October 2008.

## 4  Discussion and Conclusion

The Central Nervous System (CNS) is arguably the most complex and extensively studied biological organ. As with other complex systems, the ability to share observational resources such as data and analysis code, to chart complex dependencies, is imperative to our ability to understand its behaviour. CARMEN is disseminating descriptive frameworks for neurophysiology data and metadata, allowing resources in many different forms to be semantically linked and compared. A software system is being developed as a pilot implementation of these frameworks, allowing distributed neuroscience groups to share resources within a virtual marketplace. In future, it is hoped that CARMEN like systems may be integrated with other neuroscience databases. Globally, resource sharing initiatives like CARMEN are gaining momentum, with the FIND project (Germany), JNode activities (Japan) and emerging NSF data sharing programmes (US) spearheading advances that are highly complementary. Building on the work of these national initiatives, there is an opportunity to address global, communal metadata standards, allowing resources embedded in many different systems to be utilised in an integrative manner. The potential benefits to MEA research and the neuroscience domain are transformational; a semantic, worldwide web of data, analysis services, and collaboration and exploitation opportunities navigable from a desktop internet browser.

**References**

[1]  G.A. Ascoli, "Mobilizing the base of neuroscience data: the case of neuronal morphologies," Nat Rev Neurosci, vol. 7, Apr. 2006, pp. 318-324.

[2]  M.W. Foster and R.R. Sharp, "Share and share alike: deciding how to distribute the scientific and social benefits of genomic data," Nat Rev Genet, vol. 8, 2007, pp. 633-639.

[3]  J. Teeters et al., "Data Sharing for Computational Neuroscience," Neuroinformatics, Feb. 2008.

[4]  W.W. Eckerson, "Three Tier Client/Server Architecture: Achieving Scalability, Performance, and Efficiency in Client Server Applications.," Open Information Systems, vol. 10, Jan. 1995.

[5]  "Storage Request Broker"; http://www.sdsc.edu/srb/index.php/Main_Page.

[6]  Frank Gibson et al., "Minimum Information about a Neuroscience Investigation (MINI) Electrophysiology," Mar. 2008; http://hdl.handle.net/10101/npre.2008.1720.1.

[7]  A.R. Jones et al., "The Functional Genomics Experiment model (FuGE): an extensible framework for standards in functional genomics," Nat Biotech, vol. 25, Oct. 2007, pp. 1127-1133.

[8]  "Ontology of Biomedical Investigations"; http://purl.obofoundry.org/obo/obi.

[9]  "The Neurophysiology Data Translation Format (NDTF) "; http://purl.org/net/carmen/ndtf.

[10]  "Neuroshare"; http://neuroshare.sourceforge.net/.

[11]  "Extensible Markup Language (XML)"; http://www.w3.org/XML/.

[12]  "Web Services"; http://www.w3.org/2002/ws/.

[13]  T. Oinn et al., "Taverna: a tool for the composition and enactment of bioinformatics workflows," Bioinformatics (Oxford, England), vol. 20, Nov. 2004, pp. 3045-54.

[14]  J. Wu and P. Periorellis, "Authorization-Authentication Using XACML and SAML," Newcastle University Technical Reports, vol. CS-TR No 907, Feb. 2005; http://www.cs.ncl.ac.uk/research/pubs/trs/papers/907.pdf.

[15]  P. Periorellis, "GOLD Infrastructure for Virtual Organisations," e-Science All Hands Meeting, vol. Proceedings 2006; http://www.cs.ncl.ac.uk/research/pubs/inproceedings/papers/970.pdf.

[16]  "Protocol for Implementing Open Access Data"; http://sciencecommons.org/projects/publishing/open-access-data-protocol/.

[17]  "Creative Commons Zero (CC0) waiver."; http://labs.creativecommons.org/license/zero/.

# Real-Time Embedded Signal Processing for MEA-based Neurobiological Recording Systems

Jean-François Bêche*, Timothée Lévi, Stéphane Bonnet, Ricardo Escolá, Antoine Defontaine, Régis Guillemaud

CEA-LETI, DTBS/STD/LE2S, 17 rue des Martyrs, Grenoble, France
* Corresponding author. E-mail address: jfbeche@cea.fr

This paper presents a real-time embedded processing algorithm for MEA-based neurobiological recording systems. Its different modules have been successfully validated through extensive simulations with simulated and real datasets. The algorithm's architecture is hardware-oriented for implementation on an FPGA test platform and for portability to a full-custom ASIC.

## 1 Introduction

Real-time embedded signal processing is a challenging yet mandatory step in the development of multi-electrode array (MEA) instrumentation [1]. The data flow generated by large arrays must be compressed to envision compact data acquisition systems with wireless transmission for body implantation. Our approach is to match and adapt the mathematical signal processing tools developed within our research team to hardware description language algorithms.

Those algorithms are applied to neural spike sorting [2] [3] [8], which consist in identifying the neurons that contribute to the signal recorded by each electrode, their number and their firing rate.

The identified basic functions are (1) bandwidth reduction for selective band amplification and noise reduction, (2) discrimination threshold computation, (3) extraction and alignment of neurobiological spike signals, (4) data dimension reduction using principal component analysis (PCA) and finally (5) online spike clustering [4]. Those real-time functions are depicted in Fig. 1. The intended goal is to perform all these operations in an on-chip fashion in order to integrate them with the analog processor (analog front-end stages, analog multiplexers and analog-to-digital converters) and to minimize the data flux while maximizing the data content.

## 2 Methods

### 2.1 FTDA method

The FTDA (Filter, Threshold, Detection, and Alignment) method allows automatic alignment of spikes from MEA recordings, real datasets [5] or simulated data from Simone software [6] (Fig. 2).



**Fig. 2.** Dataset generated by the SIMONE software for a 3-neuron network.

The filtering stage is required to optimize the signal to noise ratio of the application. The selective



**Fig. 1.** Complete signal channel processing for MEA-recorded data.

digital filter's coefficients are chosen according to the wavelet-based analysis performed in the downstream processing [7]. The Finite Impulse Response (FIR) type was selected for its inherent stability and weak requirement on the coefficients' precision.
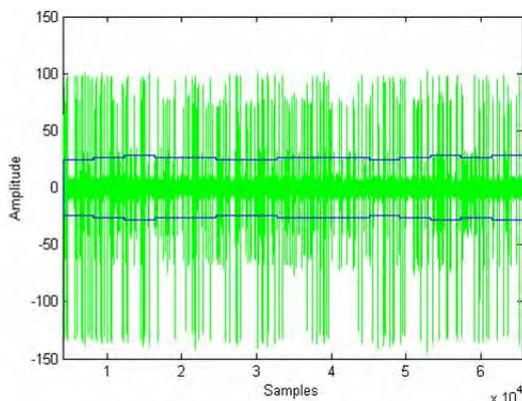


**Fig. 3.** Filtered data and estimated detection threshold

The discrimination threshold is required for the detection of the action potentials above the noise background. The threshold computation rests on the statistical properties of the noise distribution and is set between three and five times the estimated standard deviation. The result of the algorithm provides a real-time adaptive threshold value (Fig. 3).

The detection and alignment are simultaneously performed. The alignment criterion is selectable. Here, we present data with the absolute maximum criterion, where the extracted spikes' records are all centered on the absolute maximum of the signal and last 2.5ms (Fig. 4).
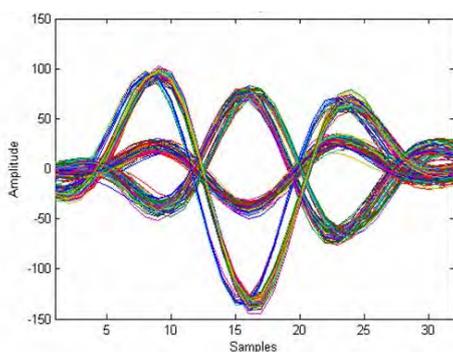


**Fig. 4.** Extracted and aligned spikes (32 samples= 2.5ms)

## 2.2 Spike sorting and classification

Additional data dimension reduction is achieved through PCA analysis. The extracted signals are used to find an ordered set of basis vectors that capture the directions of largest variation in the data. These computing operations take place offline. After loading the coefficients into the digital processor, the PCA operations are performed online. Finally, an online cluster analysis is performed to identify clusters in multidimensional datasets and to sort the data in the principal components' space (Fig. 5). Our algorithm is a real-time evolving clustering method intended to perform embedded spike sorting.
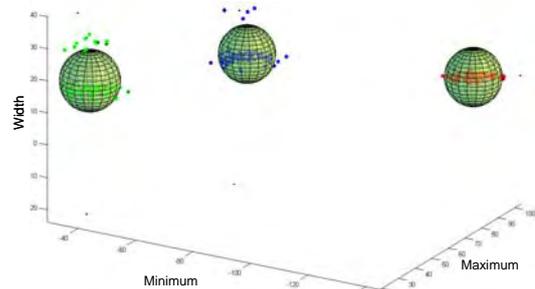


**Fig. 5.** Clustering results, identification of 3 different neurons

## 3. Conclusion

We have fully developed our processing algorithm with MATLAB and transcribed the architecture into a hardware description language (VHDL). The results of both implementations have been successfully compared and validated through simulations with real and generated datasets as illustrated from Fig. 2 to Fig. 5. The VHDL script is now ready for hardware implementation on a dedicated test platform currently under development.

**References**

[1] A. Stett, New-generation MEA technology: improving the interface to physiological function, *3rd Int. Conference on Substrate integrated Microelectrode Arrays*, Denton, USA, 2003

[2] A. Zviagintsev, Y. Perelman, R. Ginosar, Low–power architectures for spike sorting, *2nd International IEEE EMBS Conference on Neural Engineering*, vol. 1, pp. 162–165, Viginia, 2005

[3] M. S. Lewicki, A review of methods for spike sorting: the detection and classification of neural action potentials, *Computation in Neural Systems*, vol. 9, no. 4, pp. R53–R78, 1998

[4] M. Salganicoff, M. Sarna, L., Sax, and al., Unsupervised waveform classification for multi-neuron recordings: a real-time, software-based system. i. algorithms and implementation., *Journal of Neuroscience Methods*, vol. 25, no. 3, pp. 181–187, 1988

[5] G. Charvet, O. Billoint, L. Rousseau, and al., Biomea : a 256-channel mea system with integrated electronics, *29th International Conference of the IEEE Engineering in Medicine and Biology Society*, Lyon, 2007

[6] R. Escolá, C. Pouzat, B. Chaffiol, A. Yvert and al., SIMONE: A realistic neural network simulator to reproduce mea-based recordings, *Transactions of Neural Systems and Rehabilitation Engineering,* vol. 16, no. 2, pp. 149–160, 2008

[7] R. Escolá, S. Bonnet, I. Magnin, and al., Wavelet-based scale-dependent detection of neurological action potentials, *29th International Conference of the IEEE Engineering in Medicine and Biology Society*, Lyon, 2007

[8] P. M. Horton, A. U. Nicol, K. M. Kendrick, and al., Spike sorting based upon machine learning algorithms (soma), *Journal of Neuroscience Methods*, vol. 160, no. 1, pp. 52–68, 2007

# Recording and simulation of hippocampal neural networks

Elisa Diaz Bellostas[1,2], Ricardo Escola[2], Pascale Pham[2], Régis Guillemaud[2*], Guillaume Becq[3], Pierre-Olivier Amblard[3], Catherine Villard[1]

1 Institut Néel, Université Joseph Fourier CNRS, Grenoble, France
2 CEA/LETI/DTBS - Direction de la Recherche Technologique, Grenoble, France
3 Department Image and Signal, Gipsa-lab CNRS, Grenoble, France
* Corresponding author. E-mail address: regis.guillemaud@cea.fr

In order to simulate the spiking activity of in-vitro neuron networks recorded by MEA, the engine SIMONE (Statistical sIMulation Of Neuronal networks Engine) has been updated and used. SIMONE has been originally designed to produce realistic extracellular signals used as input data for the validation of spike detection and sorting algorithms. The aim of this study is to compare simulated with measured spikes trains. We present different simulations based on the architecture of a real network composed by 14 neurons grown around one electrode. The comparison between real and simulated data is quantitatively performed using different spike detection tools based on thresholding or wavelet analysis. A careful adjustment of SIMONE parameters allows to reproduce the spontaneous bursting pattern of this real network while further investigations emphasize the role of synaptic noise in network activity.

## 1 Methods

For experimental measurements, neurons from mice embryo hippocampus are grown on a MEA covered by polylysine and observed 24 days after plating.

The code SIMONE [1] simulates the spiking activity of a neuronal network measured by a MEA. It is built using the R environment, an open source version of the well-known S language [2]. SIMONE's dynamic model is based on two coupled stages : (i) each neuron is represented by the leaky integrate-and-fire (LIF) model [3], with spike waveforms generated from templates, (ii) the extracellular detection is modeled via an electrode gain while the neural signal attenuation versus the distance to the electrode is described by a pseudo-monopole of current in the extracellular medium.

The user can define different distributions, functions and parameters to describe the desired neural network and the associated electrodes (an unique electrode in our case, with a distribution of surrounding cells similar to the real case). Three types of currents are taken into account here to feed the LIF model: synaptic current, noise current and self-induced current. The last one models the recovery dynamics, not included in the classical LIF model, and shape the bursting regime [4]. The overall model may be fully parametrized using stochastic functions.

## 2 Results

Real and simulated networks are shown in Fig. 1. The so-called simulated network 1 is made from random connections while network 4 is built from uni-directional connections. The small population (6%) of inhibitory compared to excitatory neurons in the hippocampus [5] yields the presence of only one inhibitory neuron in the center of network 1. Three neurons are within the detection range of the electrode while the remaining eleven cells compose the surrounding network.
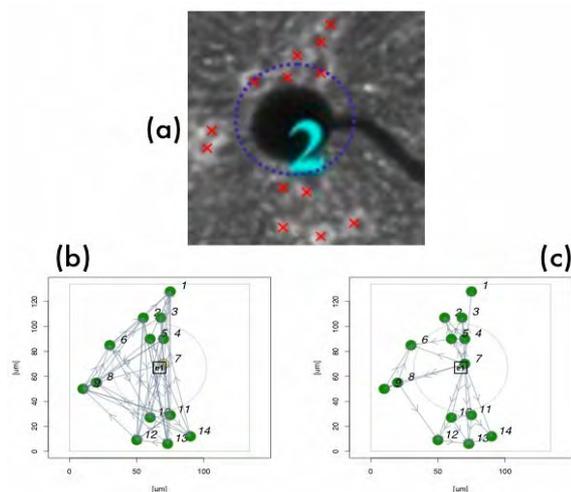


**Fig. 1.** (a) real network geometry; (b) simulated network 1; (c) simulated network 4. The centre of the electrode is represented by the square label "e1". Green (yellow) spots represent excitatory (inhibitory) neurons. The blue circle in a) and the grey circles in b) and c) represent the range of electrode detection (70µm). They enclose three neurons actually detected by this particular electrode "e1".

Activity of these networks with a $I_{noise}$ contributing to only 8% of the total current is given in Fig.2. $I_{noise}$ variations control both the amount of spike and the

delay between the start of the simulation and the beginning of the spiking activity, showing an oscillating behaviour (Fig.3). The mean spiking rate is typically multiplied by a factor of 3.5 between the values 5% and 15% of $I_{noise}$ (network 4).
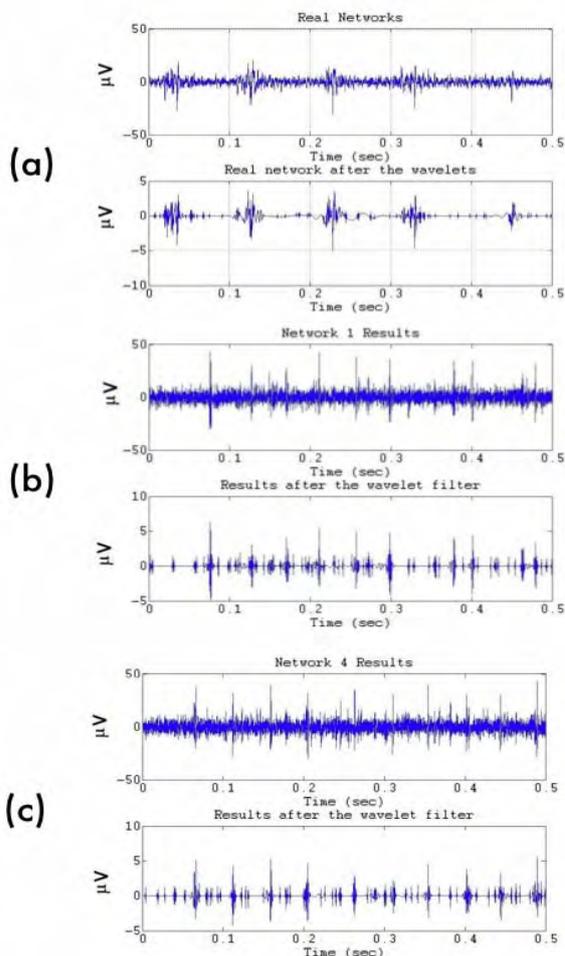


**Fig. 2.** Signals before and after a wavelet filtering are shown with $I_{noise}$=8% of the synaptic current and $I_{self}$=0. (a) Real network; (b) network 1; (c) network 4.



**Fig. 3.** Spiking activity of networks 1 and 4 with different $I_{noise}$ during 50 ms (500 samples).

Tuning Iself and adjusting Inoise yields a remarkable similarity between the simulated and the real networks (Fig.4).
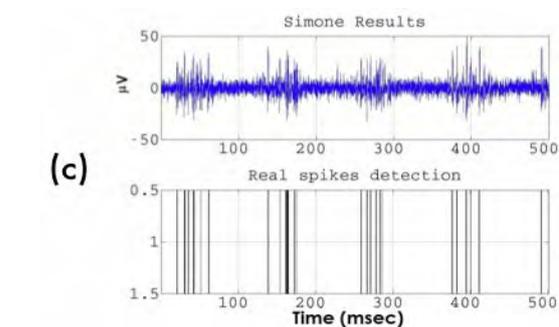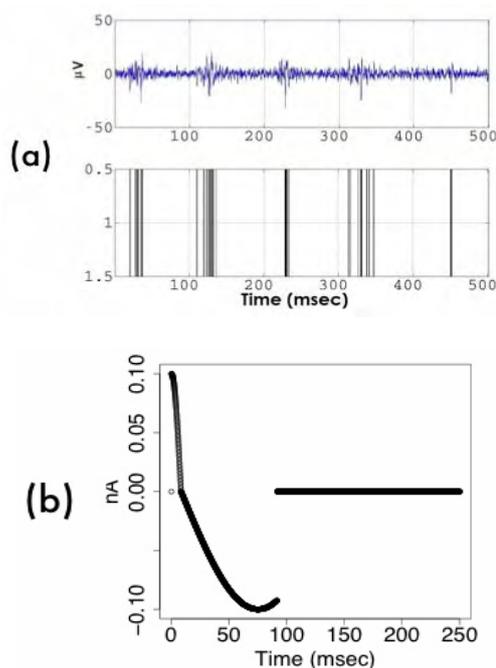


**Fig. 4.** (a) Real signal with the spike detection. Many burst can be noticed; (b) $I_{self}$ used for the simulation of the real signal (a); (c) Results of the simulation on network 4 with $I_{noise}$ =15 %.

## References

[1] R. Escolà, C. Pouzat, A. Chaffiol, B. Yvert, I. E. Magnin, R. Guillemaud (2008), SIMONE : A Realistic Neural Network Simulator to Reproduce MEA-based Recordings, *IEEE transactions on neural and rehabilitation engineering*, *16(2),149-60*

[2]

[3] W. Gerstner W. Kistler (2002), Spiking neurons models, *Cambridge University Press*.

[4] L. Paninski, J. W. Pillow, E. P. Simoncelli (2004), Maximum likelihood estimation of a stochastic integrate-and-fire neural encoding model, *Neural Comput. 16, 2533-2561*.

[5] D.L. Benson, F.H. Watkins, O. Steward, and G. Banker (1994), Characterization of GABAergic neurons in hippocampal cell cultures, *J. Neurocytol. 23, 279-295*.

# Estimating functional connectivity in networks of dissociated cortical neurons

Matteo Garofalo[1*], Alessandro Noriaki Ide[2], Thierry Nieus[1], Paolo Massobrio[2], Michela Chiappalone[1,2], Sergio Martionia[1,2]

1 Department of Neuroscience and Brain Technology, Italian Institute of Technology, Genova, Italy
2 Department of Biophysical and Electronic Engineering, University of Genova, Genova, Italy
* Corresponding author. E-mail address: matteo.garofalo@iit.it

In this paper we compare statistical methods to estimate functional connectivity in populations of dissociated cultured neurons. We discuss results obtained by using cross-correlation and information theory based methods. They are all validated through a neuronal network model and then applied to experimental data acquired by microelectrode arrays. Our results show that information theory based methods improve the performances of correlation based methods.

## 1 Introduction

In vitro cultured neuronal networks coupled to microelectrode arrays (MEAs) constitute a valuable experimental model to study its electrophysiological properties. After a few days in culture, neurons start to grow and connect each other with functionally active synapses, forming a random network and displaying spontaneous activity. Identification of causal relationships between pairs of neurons plays an important role in the study of synaptic interactions at population level. To investigate functional connectivity in cortical networks we used cross-correlation [1], mutual information and entropy [2].

## 2 Materials and Methods

Dissociated cortical neurons were extracted from rat embryos and plated into microelectrode arrays (MEAs). Functional connectivity for each pair of electrodes or neuron was estimated by using (i) cross-correlation, (ii) mutual information (MI) and (iii) entropy. These methods were validated through a neuronal network model proposed by Izhikevich [3].

**(i)** The connection strength between two electrodes was defined based on the maximum peak of the cross-correlogram function and its direction, by the peak latency from the center of the cross-correlogram.
**(ii)** MI was estimated between each pair of electrodes considering two different approaches: spike count and time code.
**(iii)** Joint inter spike interval (J-ISI) entropy was evaluated to assess causality between two channels.

All the methods were validated on neural networks characterized by different connectivities. Performances were measured in terms of ROC (Receiver Operating Characteristic), in particular by using the AUC parameter (area under curve) [4].

## 3 Results

MI proved to detect efficiently the connectivity maps in networks characterized by bidirectional connections. However since MI computed on a couple of spike trains is symmetric its performances break down in more realistic networks characterized by many unidirectional connections. Average ROCs (Fig.1), computed over eight different neural network models are shown. The joint entropy method displays (Fig.1) higher performances (AUC=0.94) compared to the correlation method (AUC=0.87). Nevertheless the performances are comparable, the differences in the connectivity maps inferred using method (i) and (iii) on real data are evident, as shown in Fig.2.

## 4 Discussion

Entropy and cross-correlation have shown good results in terms of AUC and ROC in relation to model data. However, they predict different connectivity maps (Fig.2, on real data). Despite MI cannot recover unidirectional connections it correlates better, compared to entropy and correlation, with the synaptic strength. Moreover an asymmetric MI function can be defined by computing the mutual information of shifted spike trains. Similarly to the correlation function, maximal values of the MI function yield direction and strength of the connections. Preliminary tests on few neurons models confirm that information theory based methods improve the performances of correlation based methods.

**References**

[1] Chiappalone M, Bove M, Vato A, Tedesco M, Martinoia S. (2006). Dissociated cortical networks show spontaneously correlated activity patterns during in vitro development. *Brain Res* 1093:41–53.

[2] Borst A, Theunissen F, (1999). Information theory and neural code. *Nature*. Vol.2(11): 947-957.

[3] Izhikevich, E. (2003). Simple model of spiking neurons. *Neural Networks, IEEE Transactions on*, 14(6): 1569-1572.

[4] Fawcett, T. (2006). An introduction to ROC analysis. *Pattern recognition letters*, 27:861-874.
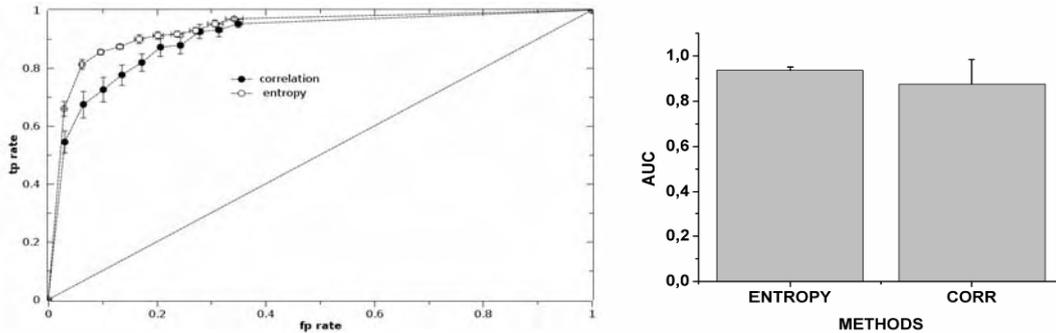


**Fig. 1.** Comparison of entropy and cross-correlation ROCs (left). AUC relative to the ROCs obtained with eight different computational models.
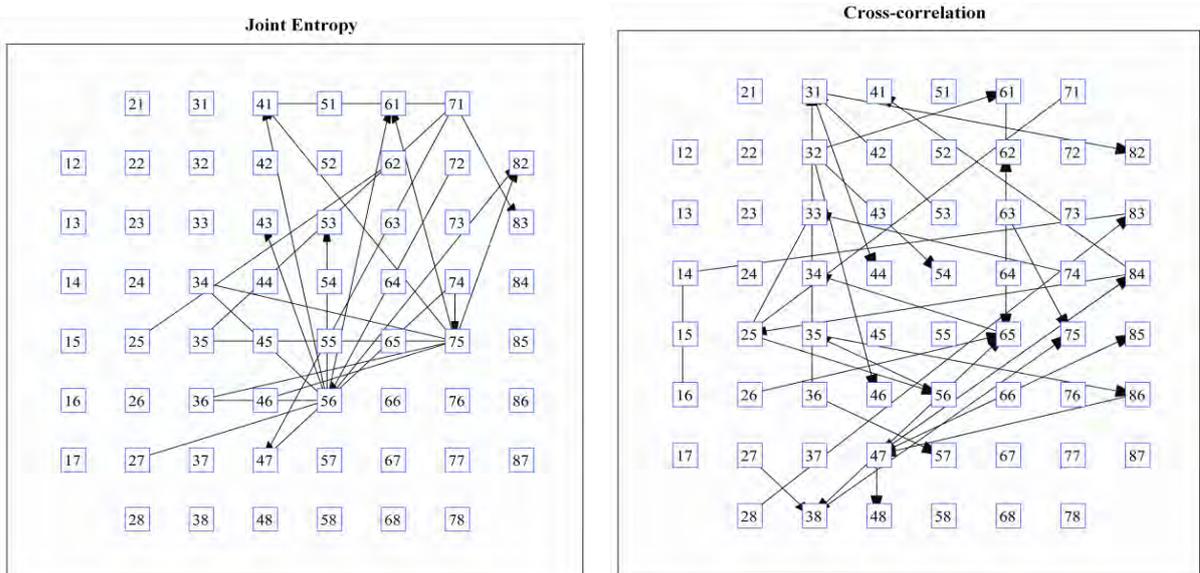


**Fig. 2.** Different maps inferred by entropy (left) and cross-correlation (right) method related to the same experiment (real data).

# A new, robust and multi-purpose approach to Burst Detection based on mono-dimensional MEA spiking activity series.

Jacopo Lamanna[1], Federico Esposti[1], Maria Gabriella Signorini[1]

1 Dipartimento di Bioingegneria, Politecnico di Milano, Milano, Italy
* Corresponding author. E-mail address: Jacopo.lamanna@mail.polimi.it

This work presents a fast and reliable algorithm for burst detection on MEA recordings, based on the analysis of a mono-dimensional signal representing the whole network activity. By using a matrix transform, the signal is extracted from the usual raster plot as a single series of spikes from all the channels of the MEA. The ISI length is compared with an opportune threshold for a first extraction of the high frequency intervals of the recording. On this signal bursts are signed out through the analysis of the derivative. Regardless of the variability in culturing methods and conditions, as well as noisy activity corruption, the signal we generated clearly evidences the occurrence of bursts, confirming the reliability of this new method despite of great changes in network firing activity features.

## 1 Introduction

One of the most interesting evidences in the activity of MEA neuronal cultures is the synchronization of action potentials across the network. Time series constituted by these synchronization occurrences (bursts) are usually extracted for a variety of applications [1-2]. Traditional burst detection algorithms present some difficulties in general purpose applications, due to the great number of parameters that are considered for the detection of a burst. These approaches limit the choice of the researcher concerning classification of burst shapes. Burst features, in fact, can vary a lot across the same recording. In addition, detection parameters need a specific setting when applied to cultures that present different ages, densities and chemical environments. We present a simple and reliable method for burst detection, which aims at reducing these limits and is characterized by a low computational weight.

## 2 The method

Neuronal activity recordings are usually represented as a raster plot, i.e. a matrix of spike series as function of MEA channels. In our method, the representation of the whole-network activity is obtained by extracting a one-dimensional signal from the standard raster-plot and by processing it for burst detection. The number of the channel in which each spike takes place, which represents the spatial information of the activity, is stored in a separated series.
The method can be summarized as follow:

i) The n channels of the raster plot are merged into a single series of spikes. Only spikes separated by an ISI (inter-spike interval) shorter than 0.1 *s* are added to the sequence (Fig.1).
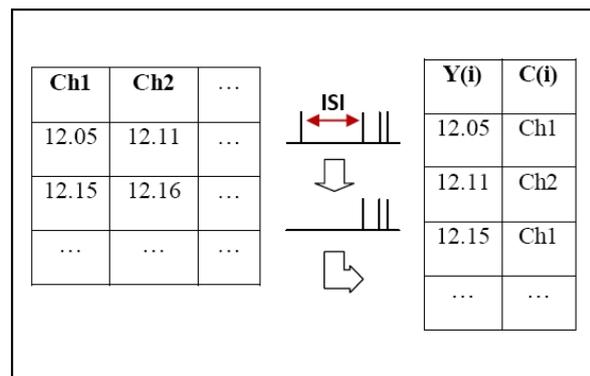


**Fig. 1.** Single channel spikes series are merged into a 1D signal. The sequence of channel numbers is stored for further analysis.

ii) Fig.2 presents a plot of the signal: the y axis reports the values of time at which spikes occur while the x axis reports the index of the series. As can be noticed in Fig.2, burst events are characterized by a step-like shape that we will refer to as *burst step*. The detection of burst events is done through the imposition of a threshold on the derivative of this spikes series: spikes related to a derivative which is lower than a threshold fixed at 2 [s/au] are considered to form a burst. A simple digital filter implementing incremental ratio with twenty coefficients can be applied to evaluate the derivate (Fig.3).

iii) Spike events extracted as burst activity (Fig.4) and the associated channels are then fast processed to satisfy specific application purposes (e.g. the extraction of bursts spatial patterns for statistical analysis).
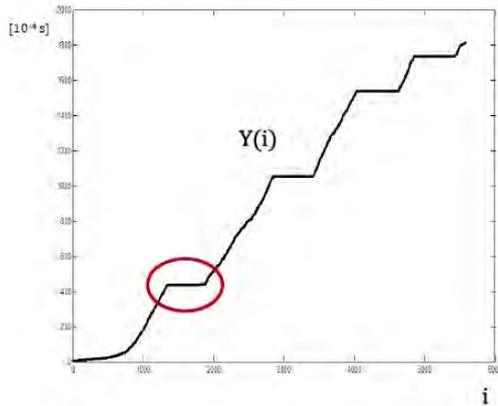
**Fig. 2.** The series of spikes from all channels evidences burst events through a sequence of easily detectable steps.



**Fig. 3.** A threshold is imposed upon the derivative of the signal, which is evaluated through a 20 coefficient high pass filter. For the entire length of the burst, the derivative remains strictly slow.

Should be noticed that the *burst step* is present and well detectable despite of the number of channels involved into the burst and the total number of spikes produced. Therefore, no conditions on bursts shape are needed. The spatial information associated to the spikes series is stored for further processing.

## 3  Discussion

The application of this method to the wide and well documented database of MEA recordings provided by [3] allowed us to confirm the high robustness and low computational weight of this approach. A first implementation of the algorithm appeared to be efficient through the large variety of culture conditions and protocols we faced; in particular, recordings from [3] where different in terms of cultivation density and div (i.e. days in vitro). The comparison with operative mode extraction shows that the algorithm is reliable and precise, thanks to further customization of burst time boundaries detection.



**Fig. 4.** An example of burst extraction: starting and ending spike times are clearly defined.

## 4  Conclusions

The detection of multi-channel synchronizations in MEA cultures (bursts) is a central task for several purposes: from burst rate statistical analysis to burst features longitudinal analysis, the automation of burst time series extraction is essential. The method presented has two main features: the first is the low computational effort guaranteed by the one-dimensional representation of the whole network firing activity; the second is the robustness of burst extraction. This feature had proved to be independent from network firing dynamics, as a consequence of the easy-computable one-dimensional signal representation.

**References**

[1] A.M.M.C. Habets et al. (1987), Spontaneous neuronal firing patterns in fetal rat cortical networks during development in vitro: A quantitative analysis. Exp. Brain Res., vol. 69, pp. 43-52.

[2] T.A. Basarsky, V. Parpura and P.G. Haydon (1994), Hippocampal synaptogenesis in cell culture: Developmental time course of synapse formation, calcium influx, and synaptic protein distribution J. of Neurosc., vol. 14, pp. 6402-6411.

[3] Wagenaar DA, Pine J, Potter SM, An extremely rich repertoire of bursting patterns during the development of cortical cultures, BMC neuroscience, 2006;7:11.

# A New Software Analysis Tool for Managing High Density MEA Systems

Alessandro Maccione[1*], Mauro Gandolfo[1], Marcello Mulas[1], Luca Berdondini[2], Kilian Imfeld[3], Sergio Martinoia[1] and Milena Koudelka-Hep[3]

1 Department of Biophysical and Electronic Engineering, University of Genova, Genova (Italy)
2 Department of Neuroscience and Brain Technology, Italian Institute of Technology (IIT), Genova (Italy)
3 Institute of Microtechnology (IMT), Université de Neuchâtel, Neuchâtel (Switzerland)
* Corresponding author. E-mail address: alessandro.maccione@unige.it

To unravel the electrical circuitry of neural network, innovative technologies providing higher number of recording electrodes have been developed. The amount of recorded data (several GByte) became a problem for conventional analysis software tool commercially available or reported in literature. Here we present a new software tool able to manage huge amount of data in a convenient way.

## 1   Introduction

To explore the local propagation patterns and the overall network activity of dissociated cultures, in the last few years innovative technologies have been developed to obtain high density multi electrode arrays [1, 2]. These systems provide thousands of channels and data streams of several GByte, which make impossible conventional approaches to data analysis. Moreover visualization tools such as raw data plot are not efficient in monitoring thousand of channels. The aim of this work is to present a new software tool able to manage huge amount of data in a convenient way.

## 2   Methods

The software has been developed under the Visual Studio 2006 environment which allows portable code, different languages implementation (C, C++, C#), and easy integration of COM and dll.

The software provides classical analysis algorithms, such as spike or burst detection [3], and integrates imaging techniques for data visualization.

## 3   Results

The software handles different file format (e.g. .dat, .mcd) organized in any recording layout from few to thousand of electrodes. More specifically, it provides a re-player window (i) and an off-line analysis window (ii).

### 3.1 Re-player window

By using the re-player (Fig. 1), the recordings can be run forward and backward. Two kinds of visualization modes, presenting the whole activity as a slow-motion movie and integrating the activity over a defined time window, were developed: electrical activity level in false colour (Fig. 2 left) and difference between max and min value of the electrical activity (Fig. 2 right).



**Fig. 1.** Re-player window. The global activity of 4096 channels, visualized in false colour (bottom left), and the raw data plots of 100ms from 6 different selected electrodes are shown (right).
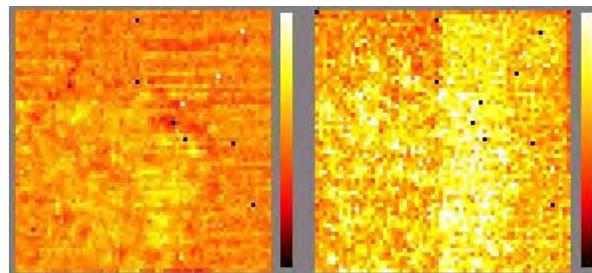


**Fig. 2.** (Left) False colour representation of one frame of the whole recording area of 64 by 64 channels; (right) representation of the same frame by using the 'max-min' visualization.

By clicking on a single pixel (or by dragging and dropping) on the activity display, the raw data plot of one or more channels can be visualized.

## 3.1 The off-line analysis window

The off-line analysis window shows the analysis results organized in tabs, one for each algorithm (Fig. 3). In order to select only the active electrodes without visualizing the not significant ones, a specific tab called "Spike Statistics" has been developed (Fig. 4), including a false colour map of the Mean Firing Rate for each channel. In this way it is possible to highlight the active areas, and the list of active electrodes can be conveniently stored for further analysis.
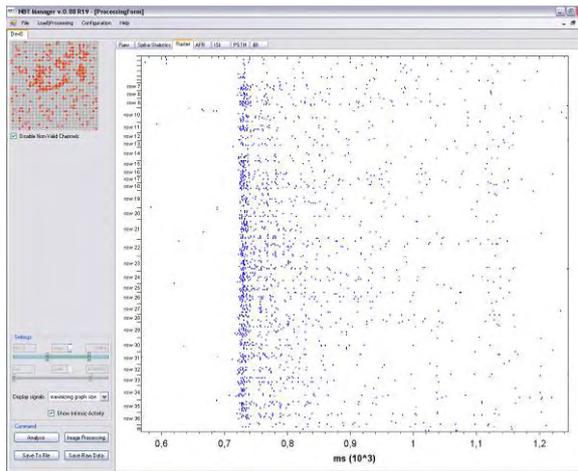


**Fig. 3.** Off-line analysis window: signals recorded from a hippocampal culture of 31 DIV. The off-line analysis window is organized in tabs (top). The recording layout of 4096 channels (i.e. 64 x 64) is reported on the top left of the panel. On the right, the raster plot of 400 selected channels (the red pixel on the left) is visualized, for a time frame of 1.2 s.

The developed software tool was used to analyse data coming from hippocampal networks of 31DIV, cultured over high density MEAs (4096 channels).
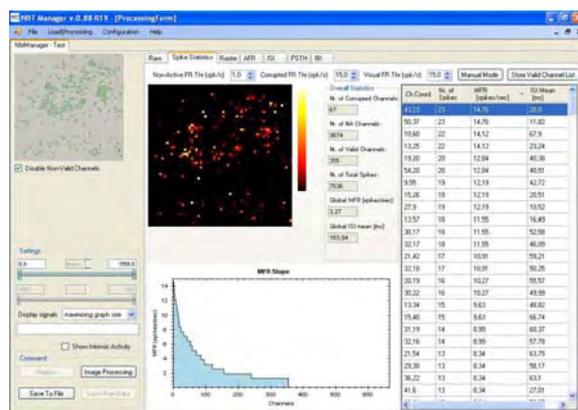


**Fig. 4.** The "Spike Statistics" tab provides a summary of the activity recorded on the whole active area. The false colour map shows the Mean Firing Rate of each channel calculated over the whole recording period. The graph at the bottom represents the mean firing rate intensity for each electrode ordered from the higher to the lower value.

The raster plot of the active channels computed by using the "Spike Statistics" tab shows a high synchronous network burst lasting about 130ms (Fig. 3). On the left panel (Fig. 4), together with the MFR map, the list of active channels, sorted according to their MFR value, is also visualized and reported as a graph at the bottom of the screen.

## 4 Conclusion

We presented an innovative software tool to process a huge amount of data recorded from high density devices. We developed methods that combine classical imaging techniques and electrophysiological signal processing, integrating data mining techniques and innovative approaches to data visualization. We do believe that this tool is a suitable and powerful tool for the neuroscientific community.

**References**

[1] K. Imfeld, S. Neukom, A. Maccione, Y. Bornat, S. Martinoia, P. A. Farine, M. Koudelka-Hep, and L. Berdondini (2007) Large-scale, high-resolution data acquisition system for extracellular recording of electrophysiological activity, IEEE Transactions on Biomedical Engineering,.

[2] B. Eversmann, M. Jenkner, F. Hofmann, C. Paulus, R. Brederlow, B. Holzapfl, P. Fromherz, M. Merz, M. Brenner, M. Schreiter, R. Gabl, K. Plehnert, M. Steinhauser, G. Eckstein, D. Schmitt-Landsiedel, and R. Thewes (2003) A 128x128 CMOS biosensor array for extracellular recording of neural activity, IEEE Journal of Solid-State Circuits, vol. 38, pp. 2306-2317.

[3] D. H. Perkel, G. L. Gerstein, and G. P. Moore, (1967) Neuronal spike train and stochastic point processes I. The single spike train, Biophysical Journal, vol. 7, pp. 391-418.

# Detection of intrinsically different clusters of firing neurons in long-term mice cortical networks

Andrea Maffezzoli, Francesca Gullo and Enzo Wanke

Department of Biotechnologies and Biosciences, University of Milano-Bicocca, Milan, Italy.

## 1 Background/Aims

Spontaneous activity is present *in vivo* during CNS development, and *in vitro* in neocortex slices and networks of cultured neurons. To investigate how neuronal firing governs synaptic transmission in such a way as to maintain regenerative synchronised bursting without inputs or anatomical specifications, we used the multi-electrode array (MEA) technique to record action potentials from post-natal cortical neurons. Contrary to the widespread rule of averaging activity, we concentrated on the activity of each neuron and a novel method of analysis showed that two or more classes of cells in all the experiments could be described on the basis of similarities in statistically-defined variables, such as burst duration, number of spikes per burst, etc. Such cluster-specific features were defined under control conditions, but responded differently when ligand- or voltage-gated ion channels were blocked or potentiated. We showed that the technique could be used iteratively in cascade, thus suggesting the presence of a heterogeneity of functioning, and confirming the existence of families or sub-families of excitatory/inhibitory cells. Our method, open to advanced implementations, could become a highly sensitive means of developing therapeutic drugs and investigating knock-in/knock-out mouse models of human channelopathies or degenerative syndromes.

## 2 Methods/Statistics

The primary cultures of cortical neurons were prepared as described by others [Wagenaar et al. 2005; Li et al. 2005]. The cultures were covered with gas permeable covers (MEA-MEM, Ala Scientific Instruments, Inc., USA) after four days *in vitro* (DIV) until the end of the culture period. The raw analogue signals sampled at 40 kHz were recorded at 36°C in $CO_2$-controlled incubators from MEA-1060BC pre-amplifiers (bandwidth 1-8000 Hz, Multi Channel Systems, Germany) connected to an MEAWorkstation (bandwidth 120-8000 Hz, Plexon Inc. USA), sorted to timestamp files by the MEAWorkstation Sorter software, and subsequently cleaned of artefacts using the OFFLine Sorter program (Plexon Inc., USA). The timestamps were directly read into MATLAB and computation of the other variables mentioned in the text was done in this language [Gullo et al., 2006; Maffezzoli et al., 2007].

## 3 Results

Depending on the different strategies used to define a burst, it should be remembered that spike rate (SR) is linearly related to burst rate (BR) and the number of spikes (SN) in each burst by SR = BR * SN. BR and SN are physiological variables that are most certainly governed by different mechanisms because they involve processes whose time scales differ by at least one order of magnitude (5-15 s and 0.1-1 s). Furthermore, SN is proportional to burst duration (BD) and the intra-burst spike rate (IBSR: the average spike rate observed in the burst, although IBSR can markedly depend on how the recorded neurons fire (accomodating or fast-spiking cells) and therefore on how the data are evaluated. In order to detect and cluster groups of "similar" neurons (with respect to one individual feature), we fixed two threshold values (between the minimum and the maximum) and asked the program to average the neurons in which that variable was lower (or higher) than the two fixed thresholds (see Fig. 1B. This analysis was made over a previously defined time interval (usually not less than 2-3 minutes), and revealed groups of neurons that behaved differently in terms of each feature under control conditions and after drug treatment; we could then calculate all of the other variables and investigate whether these groups had different performances.

At right are shown the rasters of the timestamps of seven neurons selected from the experiment shown in Figure 1. The timestamps were selected from the time records obtained under control conditions, during treatment with bicuculline 10 µM, AP5, and CNQX 1, 3 and 10 µM, and during washout. The insets show one burst on a 1 s time scale in which almost every spike can be seen. The rows in each inset (from bottom to top) represent the timestamps originating from three short-BD neurons (black, red and green) and four long-BD neurons (blue, cyan, magenta and navy). The data are time-aligned.
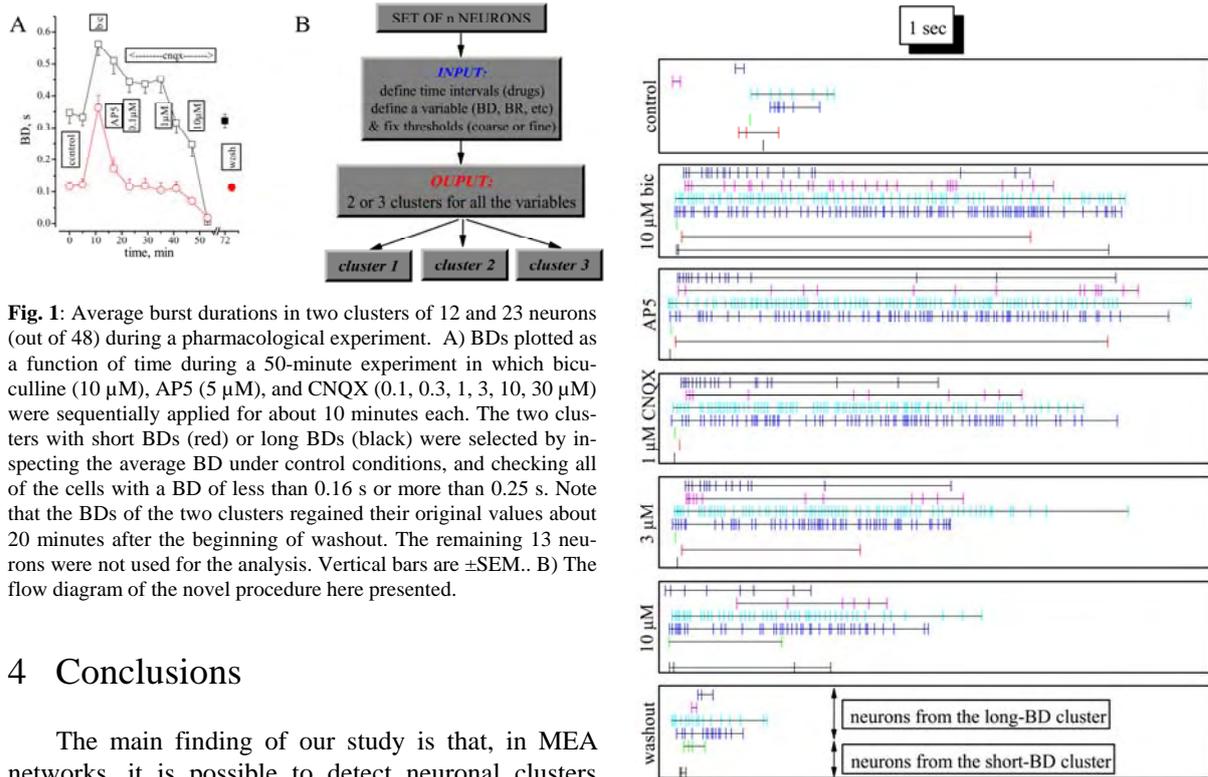
**Fig. 1**: Average burst durations in two clusters of 12 and 23 neurons (out of 48) during a pharmacological experiment. A) BDs plotted as a function of time during a 50-minute experiment in which bicuculline (10 µM), AP5 (5 µM), and CNQX (0.1, 0.3, 1, 3, 10, 30 µM) were sequentially applied for about 10 minutes each. The two clusters with short BDs (red) or long BDs (black) were selected by inspecting the average BD under control conditions, and checking all of the cells with a BD of less than 0.16 s or more than 0.25 s. Note that the BDs of the two clusters regained their original values about 20 minutes after the beginning of washout. The remaining 13 neurons were not used for the analysis. Vertical bars are ±SEM.. B) The flow diagram of the novel procedure here presented.

## 4  Conclusions

The main finding of our study is that, in MEA networks, it is possible to detect neuronal clusters with intrinsically different characteristics under control conditions as well as during the action of any modifier of neuronal activity. This can be done by computing physiologically relevant variables and then using defined time intervals to average all of the data coming from the cells that satisfy threshold criteria.

# Assessing New Techniques for Spike Detection on MEA Data

Shahjahan Shahid[*], Leslie S Smith

Dept. of Computing Science and Mathematics University of Stirling, Stirling, Scotland, UK
* Corresponding author. E-mail address: ssh@cs.stir.ac.uk

Spike detection and sorting on electrophysiological signals from MEA electrodes is demanding because noise levels are high, and many neurons may be simultaneously recorded by each electrode. In such data, there are always detection failures (false negatives and false positives). We present a new spike detection technique based on Cepstrum of Bispectrum (CoB) and assess it on real neural data. The technique is compared with four established techniques using simultaneously recorded intracellular and extracellular signals. The new technique outperforms existing techniques on detecting spikes in the extracellular signal which are due to recorded intracellular spikes.

## 1 Introduction

Detecting spike events (action potentials) in extracellularly recorded signals is a challenging task: there is a high probability of the presence of more than one dominant spike train, spikes appear randomly in the signal (due to natural behaviour), different shapes of spikes are present (due to additive neural noise), different phases of spike signal are found (due to different geometries of detector and neuron), neural noise is of high amplitude (the electrode is far from the target neuron), and others. Further, sometimes only spikes from distant neurons are present which can confuse spike detection algorithms.

Simple, popular detection techniques (e.g., plain amplitude thresholding *pln*) are applied directly to the signal after high pass filtering. But high pass filtering alone is not enough for noise treatment. Some algorithms (e.g., wavelet (*wav*) or nonlinear energy (*neo*) based techniques) use a denoising technique or use forms of noise suppression relying on spike signal characteristics. These techniques work well on a restricted range of signals, such as signals with high signal to noise ratio or signals where the spike shape is close to the predefined wavelet. The choice of signal conditioning technique is not optimal for processing general extracellular signals with spikes.

We propose a new algorithm (*cob*), based on Cepstrum of Bispectrum (CoB) [1] a new technique based on higher order statistics (HOS). This performs well on synthesized signals [2]. Here, we apply the new technique to real MEA data and compare the performance with other established techniques.

## 2 Spike Detection Techniques

*pln* employs no pre-processing. Amplitude thresholds (positive and negative) are applied to the signal. The threshold value is a function of the signal median and standard deviation.

*wav* [3] uses wavelet based signal processing. A predefined wavelet type (e.g. db2, bior1.3, bior1.5, haar, sym2, etc) is used for finding the wavelet coefficients which are relatively immune from noise effects.

*mor* [4] uses a structuring element based filter to enhance spike peaks and suppress noise. Amplitude thresholding is used to discriminate spike events.

*neo* [5] uses the product of the instantaneous amplitude and frequency of the signal to highlight spike events. Amplitude thresholding is used to discriminate spike events.

**New Spike Detection Technique**

The *cob* applies a technique based on blind deconvolution theory to the signal and estimates the spike events as a impulse sequence. Deconvolution needs an inverse filter which is estimated using CoB. Since CoB is based on HOS, it is immune to Gaussian noise. In addition CoB uses averaging in its estimation thus providing an average inverse filter. An error term is generated due to noise in the signal and/or estimation error. This error term can be suppressed by wavelet (coiflet) denoising and amplitude thresholding improving performance.

## 3 Results and Analysis

To observe the performance of *cob*, we apply it to real signals recorded from hippocampus [6] by the Buszaki Lab. Our first test signal is an intracellular signal recorded from dendrites (Fig.1: Top). This signal contains the neuron's internal spike trains plus some other secondary spike (spikelet) trains. There is a high level of noise due to the spikelets. We apply *cob* to this signal and show its pre-threshold output in Fig. 1 (bottom). Clearly, the algorithm suppresses the noise (spikelets) and at the same time it highlights the impulse train. Setting the threshold for this processed signal is relatively easy. Hence, it is possible to detect

spike events from this type of noisy signal with very few errors (either false positive or false negative).

*cob* performance is also observed from a pair of signals simultaneously recorded intracellularly and extracellularly (Fig. 2: top and second top) from Buzsaki's group [6]. Our aim is to observe the intracellular spike in an extracellular signal. The spikes are clearly visible in both signals because the noise level is low. We find that the extracellular signal records more than one spike train. We apply *cob* to the extracellular signal and show the output before applying a threshold (third top plot of Fig. 2), and after a suitably chosen threshold (bottom plot of Fig. 2). All visually observable spikes in the extracellular signal are detected by *cob*. All spike events in intracellular signal are found in *cob* detected spike events. In addition, it detects all other spike events even although they have different shapes.

| | *cob* | *wav* | *mor* | *pln* | *neo* |
|---|---|---|---|---|---|
| **True +ve** | 30 | 16 | 27 | 29 | 30 |
| **False –ve** | 0 | 14 | 3 | 1 | 0 |
| **False +ve** | 15 | 29 | 5779 | 189 | 139 |

**Table 1.** Confusion table. We show the number of correctly matched and missed spikes (with respect to the spikes in the intracellular signal (Fig. 2 top) for five algorithms applied to the real extracellular signal (Fig. 2 second from top).

To compare the performance of *cob* with other established techniques we use the same extracellular signal (Fig.2). We adjust the parameters of the respective techniques so that the maximum numbers of the intracellular spikes are matched (true positive) at minimum false positive (relative to the intracellular spike train). Table 1 shows the results from these techniques.

Since our all observations are relative to the intracellular spike train, the spikes from other neurons are counted as false positives. Visually 30 intracellular

and 45 extracellular spikes are detectable. *cob* and *neo* detect all intracellular spikes in extracellular signal while *wav* detects only 15 matched spikes. Since spike templates in this signal do not completely match with the available single wavelet, *wav* performs badly. On the other hand, the different techniques produce different number of false positives: *cob* produces fewest followed by *wav,* and *mor* produces most. Hence we conclude that *cob* detects spikes with fewest errors. Reducing the minimum inter-spike interval and spike timing accuracy from 0.5 to 1ms improves the performance of the other techniques.

## 5 Conclusion

*cob* is developed from HOS which extracts non-Gaussian terms from a distribution. The extracellular signal has a non-Gaussian distribution. Hence traditional techniques do not work as well. Thus the *cob* technique outperforms the others.

**References**

[1] S. Shahid and J. Walker (2008) Signal Processing, 88(1):19–32.
[2] L. S. Smith et. al. (2007) Poster presented at SFN Meeting. http://www.cs.stir.ac.uk/~lss/recentpapers/sfnposter2007.pdf
[3] Z. Nenadic and J. Burdick (2005) IEEE Trans Biomed Eng, 52(1):74–87.
[4] E. E. Zelniker et. al. (2008) accepted to J. Neurosci Methods.
[5] K. Kim and S. Kim (2000) IEEE Trans. Biomed. Eng., 47(10):1406–1411.
[6] http://crcns.org/data-sets/hc
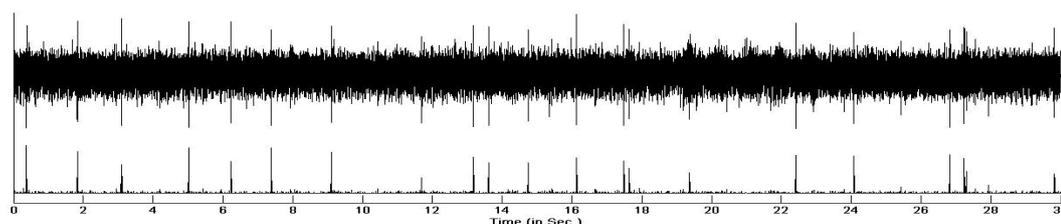


**Fig. 1.** Noisy intracellular signal (top) and noisy spike event train detected by *cob* (bottom)
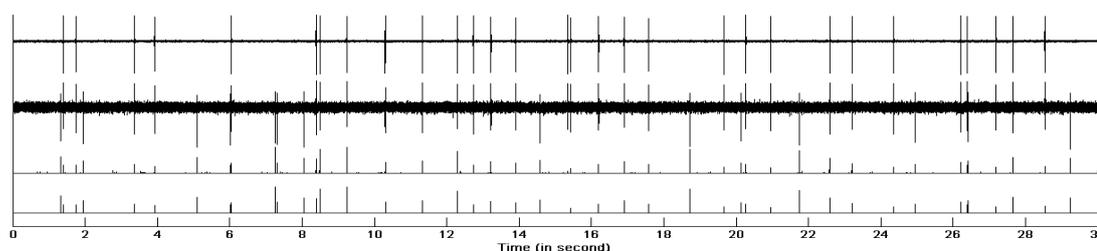


**Fig. 2.** Simultaneously recorded intracellular and extracellular signal (top 2 plots) and *cob* detected spike train: before and after threshold (bottom 2 plots).

# Leveraging CARMEN Resources for Multi-modal Analysis of MEA Data

Simonotto J[1,2*], Eglen S[3], Echtermeyer C[4], Adams C[2], Kaiser M[1,2], Sernagor E[2]

1 School of Computing Sciences, Newcastle University, Newcastle upon Tyne, UK
2 Institute of Neuroscience, Medical School, Newcastle University, Newcastle upon Tyne, UK
3 Department of Applied Mathematics and Theoretical Physics, University of Cambridge, Cambridge, UK
4 School of Biology, University of St. Andrews, St. Andrews, UK.
* Corresponding author. E-mail address: jennifer.simonotto@ncl.ac.uk

Using data from multi-electrode array recordings from developing murine retina, we showcase using CARMEN as a resource for multi-modal analysis of data, development of new analysis techniques, and adaptation of techniques from other areas to MEA data. The pooling of knowledge, data, and algorithms allows one to make multi-species/multi-developmental stage/multi-phenotype comparisons rapidly, and using the same code for easiest comparison, and can make it simple to test new algorithms. These tools and methods can be then used in and for a variety of types of data.

## 1 Introduction

For experimentalists, the development and use of customised analysis algorithms to analyse data has historically been on a laboratory-to-laboratory basis. New methods could be picked up by reading about different techniques and implementing code oneself, or by collaborating with a different group, but one did not necessarily obtain comparable results due to different parameter settings (window length, threshold, etc). For algorithm developers, the lack is typically in

an understanding of assumptions implicit in data (recording location, tissue/animal type, sampling rate, filter parameters, etc). CARMEN (Code, Analysis Repository and Modeling for E-Neuroscience) provides an interface for 1) collaboration between people/labs (experimentalists and algorithm developers), and 2) facilitates comparison across developmental period/laboratory-specific recording techniques/species by means of providing a common standard for both algorithms and data.
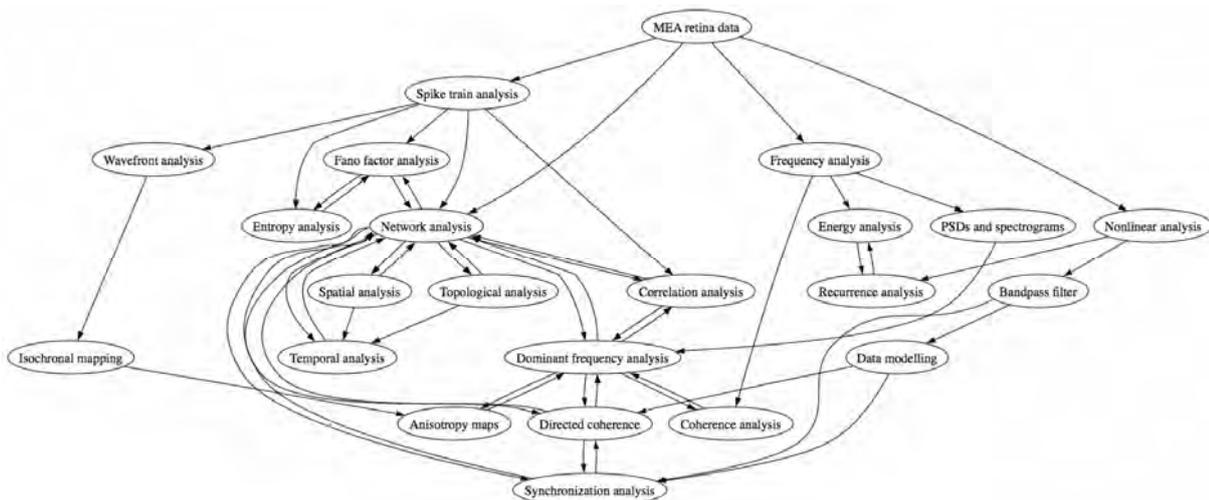


**Fig. 1.** Analysis Tools and Result Comparison Chart for MEA Data.

## 2 Aims

Our interest is to unravel dynamics and characteristics of small-scale neural networks using MEAs; thus, our aim is to develop tools to characterize and quantify these properties. We use recordings of spontaneous activity in the retina to refine our analysis

tools, which are also useful outside of retinal research (such as in epileptogenesis, cardiac dynamics, etc). In many cases, MEA data processing focuses on linear and frequency-based analysis of extracted spikes; these methods are good in general for determining changes in firing rate, etc, but do not necessarily detect subtle network communication differences.

Nonlinear dynamics in conjunction with linear and frequency-based analysis methods can resolve these issues: applying them to both raw data and spike times can reveal more information about underlying changes. Such investigations have previously been limited in scope and practicability due to the large-scale nature of some of the more relevant calculations as well as availability of data; however, through inter-action with the CARMEN Consortium, infrastructure for collaborations as well as data storage and analysis is gained, yielding better, faster, and more relevant results.

## 3 Methods

CARMEN offers a global platform for collabora-tors to share algorithms, computing power and data. Our Work Package within CARMEN aims to under-take a large-scale analysis of spontaneous retinal ac-tivity during different stages of development. This in-volves two aspects: first, we are collecting existing MEA recordings from various investigators covering a range of developmental ages, species and genetic backgrounds. Second, we are developing algorithms to analyse the recordings with various techniques automatically. Pooling the data from various sources (varying in MEA platforms, lab protocols, species, ages) is one of the advantages of CARMEN enabling us to cross-compare results using consistent tech-niques.

## 4 Results and Conclusions

Dominant frequency analysis, spatial correlation, burst analysis, network spikes, dynamic Bayesian net-work analysis, entropy measure calculation, correla-tion network analysis, wave spatiotemporal character-istic measures, and inter-spike-interval statistical measures were used to extract information from both raw and spike-time data; results were combined and compared. It is anticipated that more analysis methods will be implemented and compared with existing re-sults in the near future, with the final aim to correlate and compare many result 'frames' with each other (see Fig. 1).

# Visualization of Pacemaker-Switching in Cultures of Cardiac Myocytes Growing on MEAs

Frank Sommerhage[1], Chi-Kong Yeung[2], Andreas Offenhäusser[1], Sven Ingebrandt[1*]

1 Institute of Bio- and Nanosystems (IBN2) and CNI - Center of Nanoelectronic Systems for Information Technology, Forschungszentrum Jülich GmbH, D-52425 Jülich, Germany
2 Department of Pharmacology, Faculty of Medicine, The Chinese University of Hong Kong (CUHK), Shatin, Hong Kong
* Corresponding author. E-mail address: s.ingebrandt@fz-juelich.de

The shapes of action potentials recorded from cardiac myocytes tend to change periodically in some cultures. Action potentials in primary cardiac cell cultures from embryonic rats were recorded extracellularly with a custom-made 8x8 microelectrode array system. A software program was implemented including a spike detection algorithm as well as temporal and special data processing to visualize switching of pacemakers in cardiac myocyte cultures.

## 1 Background and Motivation

Monitoring the electrical activity of cardiac myocyte cultures became a vital field in basic and drug research [1, 2]. Extracellular recordings with microelectrode arrays (MEAs) enable non-invasive, long-term measurements of beating cardiac myocyte cultures.

During several experiments with primary embryonic rat cell cultures of 4-5 DIV, we noticed periodical changes in excitation size (Fig. 1) and shape (Fig. 2) of action potentials (APs). These variations occurred without the application of drugs or cause of lesions. Once such variation occurred on a chip, shape variations were very obvious in recordings of about 30% of the 64 available electrodes. Recordings from the remaining electrodes showed changes as well, but they were less apparent.
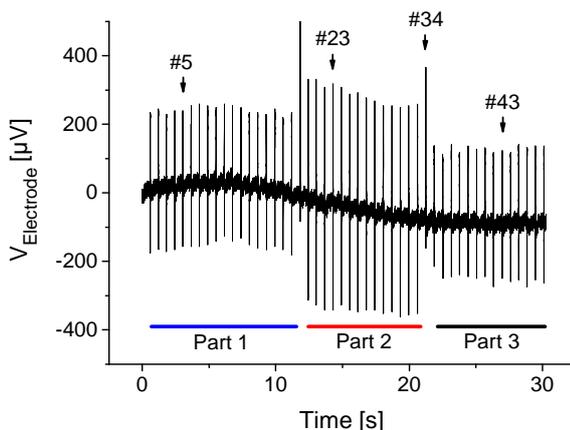


**Fig. 1.** 48 cardiac action potentials recorded with a 10 µm electrode (Position: horizontal 7, vertical 5) in an 8x8 array over 30 seconds. Variations in action potential shapes are grouped in intervals (Part 1 to 3). In the transmissions between the parts, APs showed additional differences in shape.
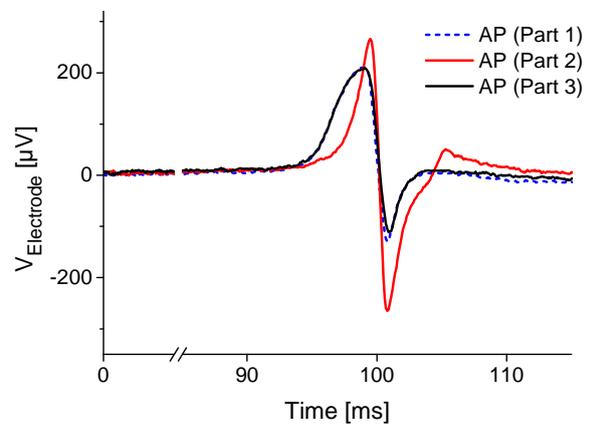


**Fig. 2.** Superposition of averaged (n = 12 to 18) action potentials of 3 sequentially following time intervals (Part 1 to 3) in Fig. 1. AP shapes from part 1 and 3 are very similar, while the AP shape in part 2 is different with larger amplitude.

## 2 Materials and Methods

For extracellular recordings of cardiac APs, a custom-made MEA system was used, consisting of 64 planar gold electrodes with diameters of 10 µm. The electrodes were arranged in an 8x8 matrix with a pitch of 200 µm [3].

To investigate the phenomenon of signal shape variations more closely, we imported the recorded data into Matlab (Matlab Version 7.0 from The MathWorks Inc., Germany). We used a (yet unpublished) custom-made program to evaluate the recordings. The program included a spike detection algorithm to find cardiac APs in very noisy recordings. Subsequently, the time stamps of detected APs in the recordings were used to calculate beat frequencies, average AP propagation speeds, as well as average AP propagation directions.
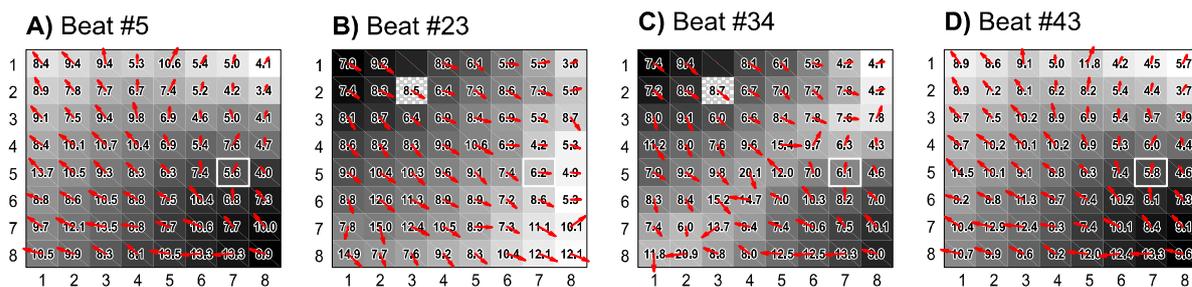
**Fig. 3.** Beat propagations in a primary cardiac myocytes culture. Beat numbers correspond to AP numbers in Fig. 1 (white bordered electrode). Arrows represent directions and speed (encoded in length), while shades represent the order in which APs occurred (darker = earlier, brighter = later). Numbers indicate the propagation speed, given in cm/s. The electrode pitch was 200 µm.

In order to visualize all recorded APs of a single beat, the chronological occurrence of APs was plotted in shades of grey over an 8x8 grid. Arrows indicate propagation directions and propagation speeds in the respective grid position. Eventually, all beats were visualized in animations and could be interpreted easily.

## 3  Results

To elucidate the rhythmic appearance of different AP shapes on one electrode, 4 selected beats out of 48 in a video file (see supplements) were depicted in Fig. 3. The visualized beats corresponded to APs marked in Fig. 1. In Fig. 3A, APs propagated from the lower right to the upper left corner with an average conduction speed of 7.9±0.6 cm/s. About 14 seconds later, the propagation direction was rotated by approximately 180°, while the average conduction speed increased to 8.6±0.4 cm/s as depicted in Fig 3B. The 34th beat (Fig. 3C) showed the collision of two excitation fronts in the middle of the 8x8 recording grid. This resulted in large excitation sizes as depicted in Fig. 1 (APs #19 and #34). A few beats later, the direction of excitation pointed from bottom right to top left and had a conduction speed of 7.9±0.3 cm/s again (Fig. 3D). AP shape, excitation size, propagation direction and speed were completely restored to the values already observed before the temporary change to another pace maker region.

During the experiment, APs occurred with an average frequency of 1.59±0.02 per second (95.6±1.4 bpm). Small variations in the beat frequency did not correlate directly with the changes in AP shape in Fig. 1. In fact, the beat frequency decreased slightly in the transitions just from one shape to another. During the following beats, the frequency recovered and decreased again in the next transition.

## 4  Conclusions

In our experiments we were able to observe changes in cardiac AP propagation caused by at least two different pace maker regions on a MEA. Two pace makers, located in different places on the MEA, caused variations in AP propagation speeds and propagation directions in cardiac cell layers. These variations were neither obviously apparent in amplitudes or shapes of AP recorded by about 70% of 48 available electrodes, nor identified by small changes in the beat frequency. Furthermore, only about 30% of the available electrodes recorded differences in signal shapes and excitation amplitudes, which indicated unusual or unexpected anomalies in the cardiac cultures.

The influence of different pace maker regions may distort the results of measurements performed with only a few electrodes, which can not provide information of propagation directions and speeds. Such de-localized pacemaker situations are known for the heart organ as cardiac fibrillations. Therefore, our tool could be very helpful for drug screening and should be considered to serve in a test system for medical prevention of damages based on cardiac fibrillation.

**Supplemental Material**

A video file, containing the here described results and clearly showing the switching of AP propagation directions is available for download:

http://www.Sommerhage.de/science/fzj/ibn2/cardiac/

**References**

[1]  Stett A., Egert U., Guenther E., Hofmann F., Meyer T., Nisch W., Haemmerle H. (2003): Biological application of micro-electrode arrays in drug discovery and basic research. *Analytical and Bioanalytical Chemistry*, 377, 486-495.

[2]  Yeung C.-K., Sommerhage F., Wrobel G., Offenhäusser A., Chan M., Ingebrandt S (2007): Drug profiling with cultured cardiac myocytes using planar microelectrode arrays. *Analytical and Bioanalytical Chemistry*, 378, 2673-2680.

[3]  Wrobel G., Zhang Y., Krause H.-J., Wolters N., Sommerhage F., Offenhäusser A., Ingebrandt S. (2007): Influence of the first amplifier stage in MEA systems on extracellular signal shapes. *Biosensors and Bioelectronics*, 22, 1092-1096.

# Electromagnetic Simulation of Contracting Cardio-myocyte Cultures on MEA

Jarno M. A. Tanskanen[1*], Juho Väisänen[1], Mari Pekkanen-Mattila[2], Jari A. K. Hyttinen[1]

1 Department of Biomedical Engineering, Tampere University of Technology, Tampere, Finland
2 Regea Institute for Regenerative Medicine, University of Tampere, Tampere, Finland
* Corresponding author. E-mail address: jarno.m.tanskanen@tut.fi

In this abstract we consider electromagnetic simulations of cardiomyocyte cultures on MEAs to address the effects of contraction on the measured electric field potential signal. MEAs are widely employed in studying cardiomyocyte action. Cardiomyocyte properties are sometimes interpreted from the recorded signal shapes (waveforms), or the recorded waveforms may be associated with similar looking electrocardiogram signal waveforms. Cardiomyocyte movement has not been considered in such analysis. Our simulations show that cardiomyocyte contraction movement contributes to the measured signal. In this abstract, exemplary preliminary simulation results are shown.

## 1 Introduction

Microelectrode arrays (MEAs) are widely employed in studying cardiomyocytes [1,2]. In this abstract, we address the effects of cardiomyocyte contraction to the MEA measurements. To the best of our knowledge, prior to our work, cardiomyocyte movement has not been considered as a factor affecting the measurements. Our reasoning is based on the fact that cardiomyocyte action potentials are recordable relatively near the microelectrodes (MEs), e.g., within a few tens or 100 µm, and the distance the cardiomyocytes move when a piece of tissue contracts, may well be of the same order of magnitude. Thus, it is expected that the moment may have fundamental effects on the measured signals.

To address the effects of the movement, we simulated a standard MEA well with a contracting and non-contracting cardiomyocyte slab model. Simulations were made with Comsol Multiphysics (Comsol AB, Stockholm, Sweden), which based on finite element modeling (FEM). FEM and Comsol Multiphysics have also been used, e.g., in modeling interactions between neurons and MEs, [3] and [4], respectively.

## 2 Methods

A 2D model of a MEA well with a ground/reference electrode, 59 microelectrodes, culture medium, and a contracting cardiomyocyte tissue slab was constructed in Comsol Multiphysics (Figs. 1A and 1B), with material conductivities and dimensions set as shown in Table 1. Although the model is 2D, also the heights of the components are defined in the model. It is to be noted that it is difficult to simulate very thin structures with Comsol Multiphysics, thus the electrode material is overly thick in the simulator. An over all view to the simulated system is also seen in Fig. 3A. A real MEA signal from a cardiomyocyte culture (Fig. 1C) was used to modulate the surface potential of the slab, which varied between –68 mV and 41 mV. The surface potential varied sinusoidally in the vertical direction in the lower half of the slab, while the potential of the upper half of the slab was zero. The sinusoidal amplitude was then made time dependent by modulating it with the measured signal. Slab displacement (Fig. 1C) was simulated by lowpass filtering and delaying the MEA measurement (Fig. 1C). Maximum displacement was of 24 µm upwards. Field potentials produced by the tissue slab were measured by a probe seen in Fig. 1B between the slab and the nearest ME.

## 3 Results

In Fig. 2, are shown the field potential simulations with and without contraction, i.e., slab movement, as observed at the field potential probe location seen in Fig. 1B.

**Tab. 1.** Dimensions and conductivities of the components of the model (diameter ∅).

| Component | Dimensions | Simulated Material | Conductivity |
|---|---|---|---|
| Ground/reference electrode | 2 mm x 5 mm, height 1 µm | Titanium | $7.4 \cdot 10^5$ S/m |
| Microelectrodes | ∅ 30 µm, height 1 µm | Titanium | $7.4 \cdot 10^5$ S/m |
| Active tissue slab | ∅ 400 µm, height 100 µm | Clump of cardiomyocytes | 20 S/m |
| Culture medium | ∅ 19 mm, height 500 mm | Liquid | 1.5 S/m |
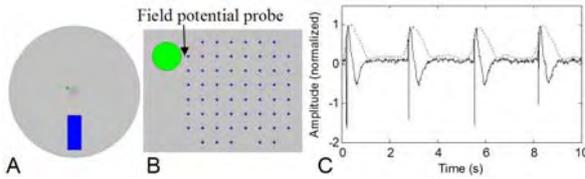
**Fig. 1**. (A) Simulated MEA geometry.The ground/reference electrode blue and tissue slab green. (B) Layout of the MEs and the tissue slab. Distance from the rim of the slab to the edge of the nearest ME is 85 µm. Field potential measurement probe is at the small dot between the tissue slab and the ME closest to it. (C) Normalized MEA measurement of a cardiomyocyte culture (solid) used to modulate the surface potential of the slab in time, and the normalized displacement of the slab (dashed).
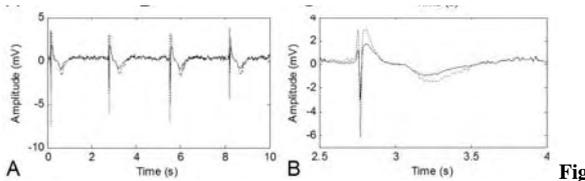


**Fig**. 2. (A) Field potential at the probe location seen in Fig. 1B with (solid) and without slab contraction (dashed). (B) Detail of the field potential curve seen in (A).

From Fig. 2, it is seen that the simulated contraction with the given slab surface potentials affects mostly the amplitude of the field potential at the probe, although some slight signal shape differences are also observable. An overall view to the electric field potential at the time 3.28 s (at time of the local minimum of the negative peak of the dashed line in Fig. 2B) without tissue contraction is shown in Fig. 3A. In Figs. 3B and 3C, field potentials at the time 0.281 s (at the time of the maximum of the second peak in Fig. 2B) are shown for non-contracting and contracting tissue slabs, respectively. Comparing Figs. 2B and 2C, it is seen that while the contraction has a clear effect on the field potential distribution close to the edge of the slab (observable at the lower rim of the slab in this simulation), the effect at the MEs is not as pronounced.

## 4   Conclusions and Discussion

From our preliminary simulations, we can conclude that the contracting movement may have an ef-fect on the measured signals, and thus, in interpretation of the measured waveforms, also the movement of the active cells should be considered. The fact that the distance, which the electrically active cells may move, may well be of the same order than the maximum distance from an electrode over which an action potential may still be measured, suggests that movement artifact should be taken into account, although this cannot be definitely demonstrated by the simulations shown in this abstract. It is not unimaginable that such cell aggregate acceleration, speed, movement distance, and especially movement relative to the tissue surface potential change could take place that also the measured signal shape could change profoundly due to the moment.

The presented simulator is not an accurate presentation of the reality; the model of the surface potential of the tissue slab used in this abstract is preliminary, and will be redesigned based on knowledge on actual cellular membrane currents and tissue surface potential distributions. Thereafter, numerous tissue slab geometries and contraction directions and speeds must be simulated with respect to the MEA layout geometries, in order to find the cases in which tissue movement has the greatest effects on the measured field potentials.

## References

[1]   M. Reppel, F. Pillekamp, Z. J. Lu, M. Halbach, K. Brockmeier, B. K. Fleischmann, and J. Hescheler, Microelectrode arrays: A new tool to measure embryonic heart activity. *Journal of Electrocardiology, 37 Suppl. 1, 104-109.*

[2]   J. Hescheler, M. Halbach, U. Egert, Z. J. Lu, H. Bohlen, B. K. Fleischmann, and M. Reppel, Determination of electrical properties of ES cell-derived cardiomyocytes using MEAs. *Journal of Electrocardiology, 37, Suppl. 1, 110-116.*

[3]   J. R. Buitenweg, W. L. C. Rutten, and E. Marani, Geometry-based finite-element modeling of the electrical contact between a cultured neuron and a microelectrode. *IEEE Transactions on Biomedical Engineering, 50(4), 501-509.*

[4]   C. Moulin, A. Gliere, D. Barbier, S. Joucla, B. Yvert, P. Mailley, and R. Guillemaud, New 3-D finite-element model based on thin-film approximation for microelectrode array recording of extracellular action potential. *IEEE Transactions on Biomedical Engineering, 55(2), 683-692.*

**Fig. 3.** (A) Overall view to the electric potentials in the MEA at time 3.28 s (c.f., Fig. 2B). (B)–(C) Simulated electric field potentials at time 0.281 s (at the time of the maximum amplitude of the second peak in Fig. 2B) for the (B) non-contracting and (C) contracting tissue slab, respectively. Axis distances are in meters, and color scale is in volts. Note that only the original (non-contracted) position of the tissue slab is shown both in (B) and (C).

# Thermal Noise As A Probe For Cell Adhesion

Zeitler R, Fromherz P

Max Planck Institute for Biochemistry, Department of Membrane and Neurophysics, Martinsried / München, Germany

Cells that are cultured on substrates show a gap of several 10nm between the substrate surface and the cell membrane. That cleft is filled with aqueous electrolyte. Sheet resistances on the order of 10-100 MOhm per square are expected. Knowledge of exact values for the sheet resistance is mandatory to understand the electrical interfacing of cells and chips, and it provides information on adhesion properties of cells. Suitable methods are an application of ac voltages and a recording of the response by measurements of current, of transistor voltage or fluorescence dyes.

An alternative approach relies on the Fluctuation-Dissipation-Theorem that implies that every dissipative process also causes fluctuations. It was previously shown that the recording of voltage fluctuations that are recorded with individual transistors provided information on the sheet resistance [1].

The application of a Multi-Transistor Array with a spatial resolution of 7.8µm [2] with reduced noise and improved time resolution enabled us to record two-dimensional maps of the noise in the area of cell adhesion. A theoretical model for the thermal noise in the two-dimensional core-coat conductor of a cell-chip system was developed. It was used to evaluate noise maps and to determine the profile of the It was used to evaluate noise maps and to determine the profile of the sheet resistance.

## References

[[1] M. Voelker and P. Fromherz (2006) Phys. Rev. Lett, 96:228102.
[2] A. Lambacher et al. (2004), Applied Physics A 79:1607.

# Neurostimulation and Neuroprosthetics

# Subretinal stimulation with hyperpolarising and depolarising voltage steps

Matthias Gerhardt, Alfred Stett*

NMI Natural and Medical Sciences Institute at the University of Tuebingen, Reutlingen, Germany
* Corresponding author. E-mail address: stett@nmi.de

We calculated the membrane potential of the pre-synaptic terminals (psT) of the bipolar cells in the bipolar cell layer in response to stimulation with rectangular pulses. We find out, that both depolarisation and hyperpolarisation occur in a temporal shift. To analyse the effect of depolarisation and hyperpolarisation separately we have developed the TriState Stimulation. From subretinal stimulation experiments with TriState we find out that a depolarisation of the psT gives with significant lower threshold an retinal response then a hyperpolarisation. Further we compared TriState to rectangular subretinal stimulation. From that experiments we conclude that the rising edge of rectangular pulses make the significant stimulation effect.

## 1 Introduction

In subretinal implants, monophasic rectangular voltage impulses are applied to the photoreceptor side for electrical stimulation of degenerated retinas. It has been shown that anodic voltage impulses have a lower stimulation threshold than cathodic impulses [1].

Application of voltage to stimulation electrodes charges the capacity of the electrical double-layer of the metal/electrolyte interface. Application of monophasic voltage impulses leads to biphasic current impulses with fast, strong but transient capacitive currents with opposite sign at the rising and falling edges of the voltage impulse. Hence, the rising edge of anodic rectangular impulses generates a retinal inward current (from photoreceptor to ganglion cell side) followed by a retinal outward current. It has been shown by simulations that an inward current results in a depolarisation of the presynaptic end of the bipolar cells [2]. Depolarsiation of the presynaptic terminals results in $Ca^{2+}$ influx into presynaptic terminals and exocytosis, wheras the $Ca^{2+}$ channels are closed at hyperpolarizing membrane voltages [3].

To analyse the step response to fast membrane hyperpolarisation and depolarisation separately, we applied monophasic current impulses to explanted retinas. To generate current impulses with low rise time, we developed a new tri-state circuit. The results were plotted as Chronaxie curves.

## 2 Methods

**Tri-State generator**

Monophasic current impulses were realized by a TriState generator. In addition to the OFF and ON state of a regular voltage source, it has a third state (OPEN) with a very high source resistance ( ~ 1 GΩ).

The functionality of the TriState generator is shown in Fig. 1. During OFF and ON phase the output impedance is 50 Ω. After the ON phase of duration $t_1$ the output resistance of the generator increases to 1 GΩ (OPEN) and the current drops to zero. This prevents discharging of the load. After $t_2$ the voltage is set to 0 V and the output impedance to 50 Ω. For comparing TriState stimulation with voltage impulse stimulation, in the following the output of the Tristate generator is given by the output voltage.
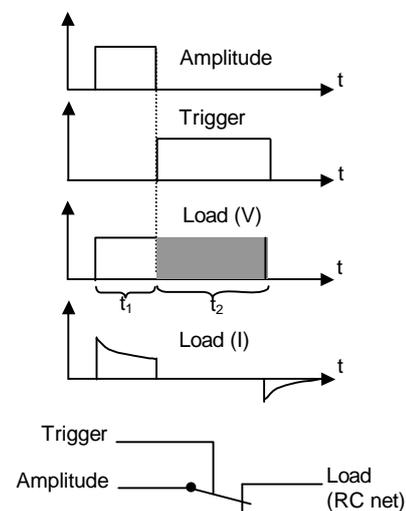


**Fig. 1**: The TriState generator. $t_1$: impulse duration (up to 400 µs), and $t_2$: response measuring interval with high-impedance load.

**Simulation**

To simulate the effect of a temporal stimulation pattern on the membrane potential of a bipolar cell we simulated a cable model (length: 70 µm, diameter 1.4 µm, specific membrane resistance $r_m$=0.8 kΩcm², specific membrane capacity $c_m$=1 µF/cm², intracellular

and extracellular resistance $r_e = r_i = 70\ \Omega cm$). The response of the cell membrane to external stimulation was calculated in the frequency domain and the step response in the time domain was obtained by numerical inverse Laplace transformation. The external field was obtained from finite element simulation of monopolar stimulation (Fig. 2).
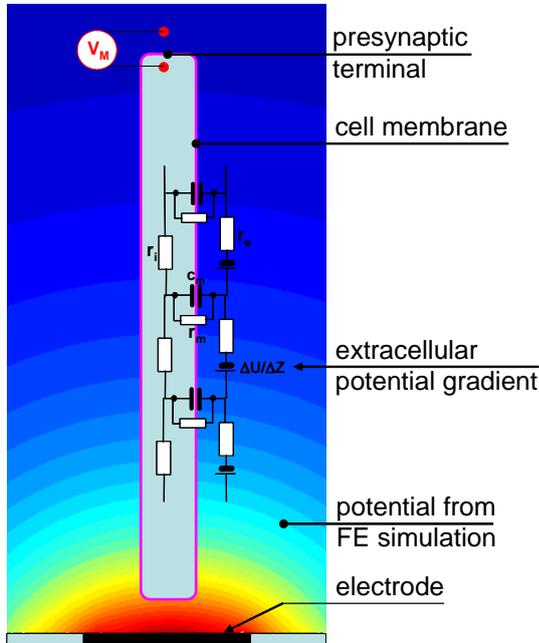


**Fig. 2**: Model of a bipolar cell, connected to the simulated extracellular potential generated by a stimulation microelectrode.

**Stimulation experiments**

Experiments were carried out as described in [1]. Briefly, retinas were explanted from eyes from blind RCS rats (age $100 \pm 10$ days) and placed on the electrode array of a MEA with the ganglion cell side up (Fig. 3). The retinas were perfused by modified Ringer's solution (120 NaCl, 5 KCl, 2 CaCl$_2$ 1 MgCl$_2$, 30 NaHCO$_3$ 15 glucose, 0.2 L-glu, 1.4 NaH$_2$PO$_4$ in mM). One MEA electrode was connected to the TriState generator.
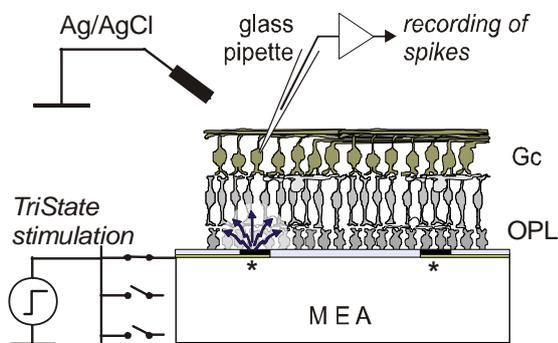


**Fig. 3**: Electrical stimulation of explanted retinas placed on a microelectrode array (MEA). Recording was done by the means of a glass pipette attached to the cell body of a ganglion cell (Gc). OPL: outer plexiform layer of the retina.

To collect data for chronaxie curves, the stimulation was applied in two subsequent cascades to vary amplitude (6 values) and duration (6 values) of TriState impulses, respectively, with 12 - fold application of both cascades.

**Data analysis**

To analyse the ganglion cell response, for all 36 stimulation parameter sets a $m \times n$ raw data matrix were constructed. The matrix contained the post stimulus spike counts per 50 ms time bins in $m$ columns from all $n$ trials of the experiment with a given parameter set.

From all raw data matrices the singular values S were calculated by singular value decomposition [4]. The singular value with the largest amount ($S_{11}$) is linked to the most significant component of the raw data matrix and reflects the efficacy of the stimulation. The singular values were plotted against duration and amplitude of TriState stimulation. This resulted in a set of tuning curves for each ganglion cell, which then have been fitted to a set of sigmoidal model functions (Fig.7) by multi curve fitting. The inflection points of that curves were used to assemble a chronaxie curve (Fig.8) for each stimulation experiment.

# 3 Results

**TriState stimulation**

With the TriState generator set to a certain voltage, a monophasic current impulse is generated as shown in Fig. 4. and given by Eq. 1 ($t_1$ = start time; $t_2$ = end time), where $\tau$ is the time constant of the electrode/tissue interface.

$$I(t) = I_0 e^{-\frac{t-t_1}{\tau}} \left( \theta(t - t_1) - \theta(t - t_2) \right) \tag{1}$$
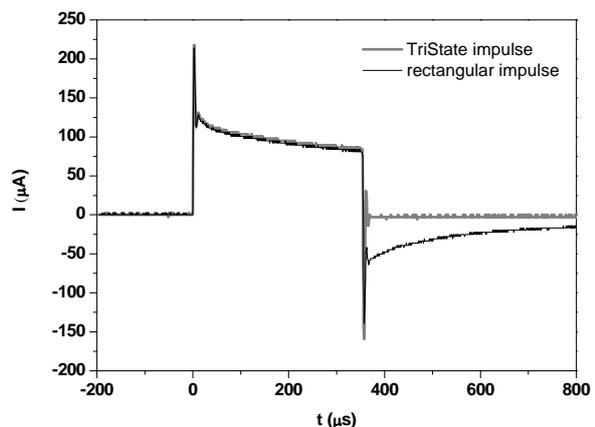


Fig. **4**: Electrode current resulting from a TriState impulse and a rectangular voltage impulse.

Using this impulse shape for the time course of the extracelluar voltage, the membrane voltage at the presynaptic terminal was simulated. In contrast to rec-

tangular voltage impulses, with TriState stimulation no hyperpolarisation occurs at the presynaptic terminal (Fig. 5.)
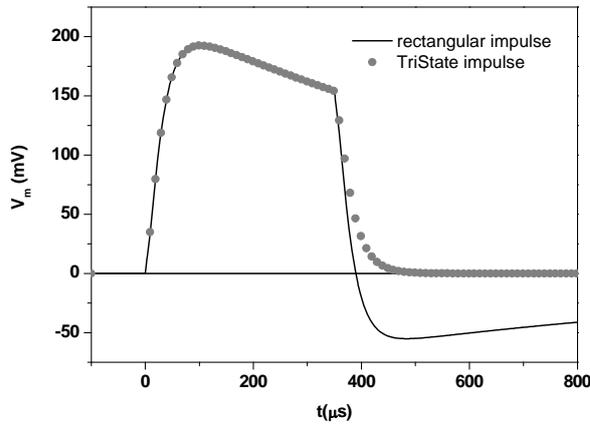


**Fig. 5:** Simulated membrane voltage $V_m$ at the presynaptic terminal of the bipolar cell model as a response to a rectangular voltage impulse (1 V) and a monophasic current impulse (TriState stimulation, 1 V).

### Chronaxie curves

From 13 ganglion cells a set of tuning curves for depolarising TriState stimulation were obtained (Fig. 6). The resulting chronaxie curves are shown in Fig. 7. Eleven curves could be fitted using the Lapicque model [5] with a chronaxie in the range between 0.2 ms and 0.5 ms. For hyperpolarising stimulation only one chronaxie curve could be assembled but was incompatible with the Lapicque model. The other 12 cells displayed no or very small reactions to the hyperpolarising stimulation in the tested parameter window.

For 6 other cells chronaxie curves for depolarising TriState stimulation and anodic rectangular stimulation could be assembled, respectively (Fig. 8). The voltage threshold for TriState stimulation was lower than for stimulation with monophasic voltage impulses.

## 4 Discussion

We showed that electrical stimulation of degenerated retinas from blind RCS rats was more efficient with retinal inward current impulses than with outward current impulses. Furthermore we showed that thresholds for short anodic rectangular voltage impulses (duration < 350 µs) were higher than for depolarising steps. This is in agreement with the simulation of the membrane voltage at the presynaptic terminal in response to voltage gradients along the axis of the bipolar cells and the voltage-dependend gating characteristic of $Ca^{2+}$ channels in bipolar cells. We conclude that the rising edge is the dominant component in voltage impulses to trigger exocytosis.
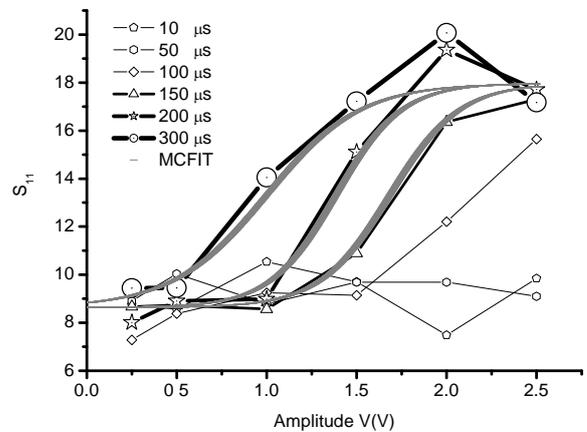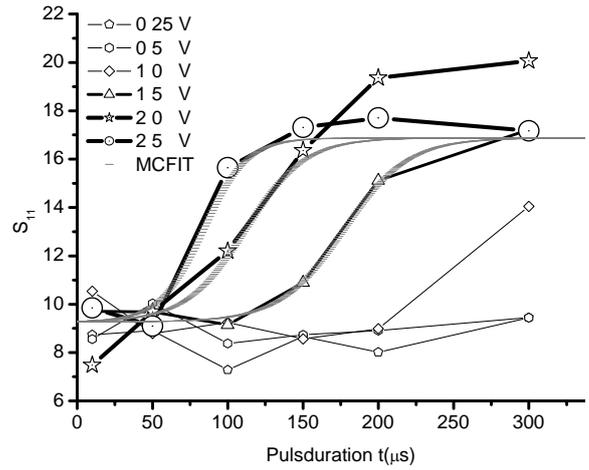




Fig. 6: Set of tuning curves compiled from spike recordings from one ganglion cell. The retina has been stimulated (TriState stimulation) with different durations (top) and amplitudes (below). $S_{11}$ denotes the highest singular value determined from a set of 12 experiments with the same stimulation parametrisation. The curves where $S_{11}$ reached saturation had been fitted by multi curve fitting.
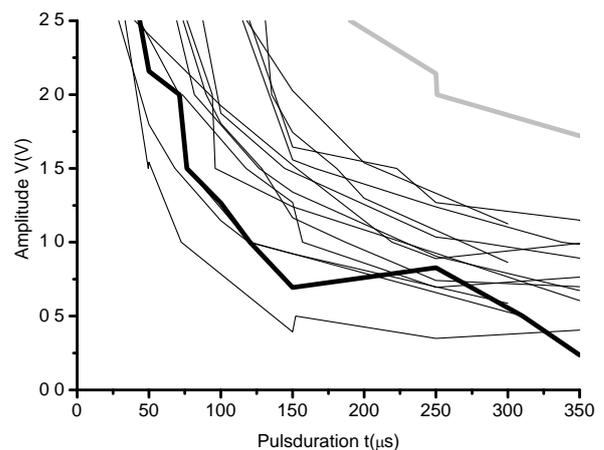


Fig. 7: Chronaxie curves of 13 ganglion cells. Each retina was stimulated by depolarising and hyperpolarising TriState impulses, Only one cell responded both to hyperpolarizing (bold grey curve) and for depolarizing (bold black curve) impulses.
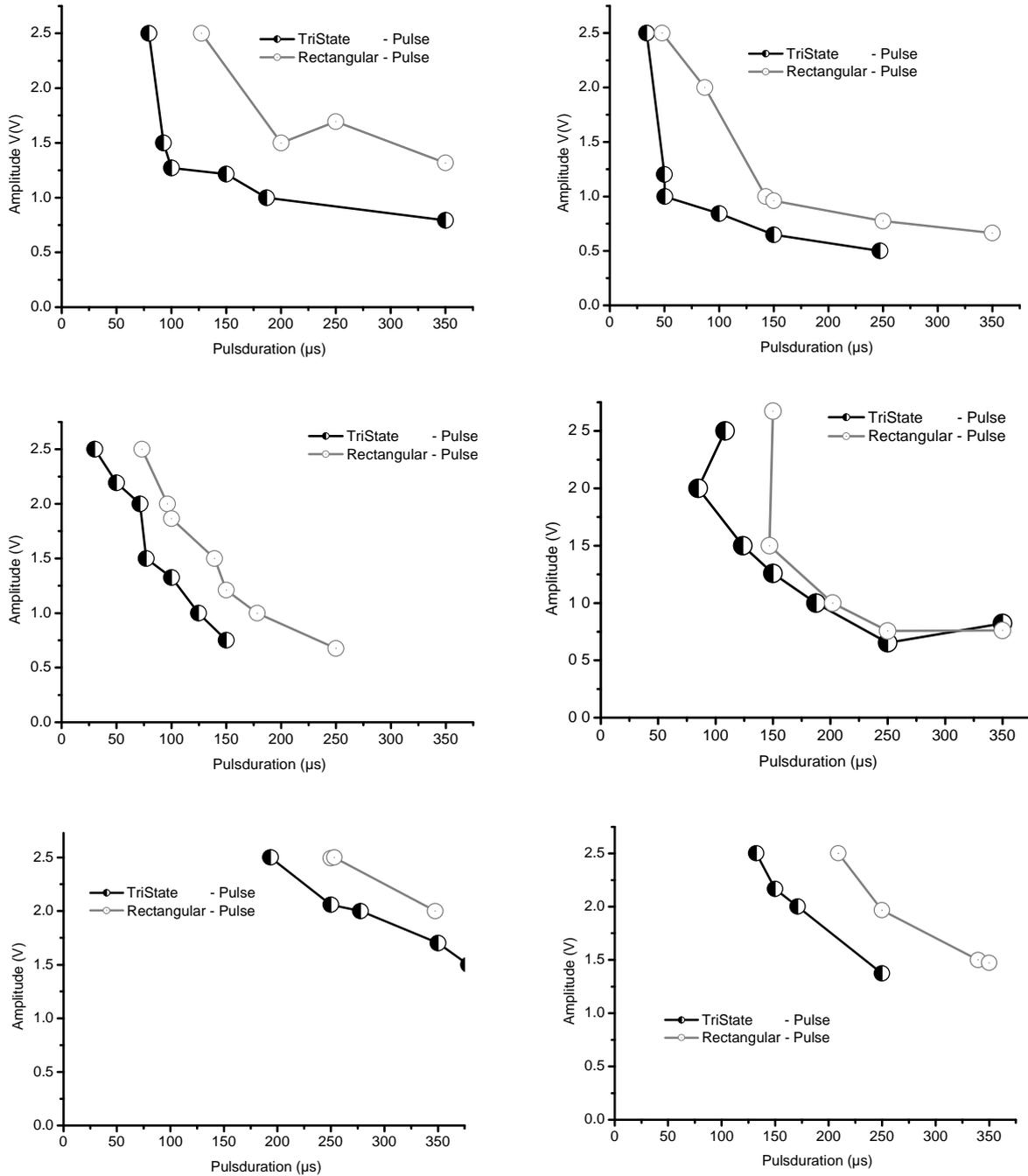
Fig. **8**: Chronaxie curves of 6 ganglion cells obtained from stimulation experiments both with TriState and rectangular voltage impulses.

## References

[1] Stett A., Mai A., Herrmann T. (2007). Retinal charge sensitivity and spatial discrimination obtainable by subretinal implants: key lessons learned from isolated chicken retina. *Journal of Neural Engineering 4*, S7-S16

[2] Gerhardt M., Stett A. (2006). Simulation of extracellular stimulation of bipolar cells with monopolar and dipolar electrode configurations. In: Stett A. (ed): *Proceedings MEA Meeting 2006*. BIOPRO edition Vol. 3, p. 93-94. BIOPRO Baden-Wuerttemberg GmbH, Stuttgart, 2006. ISBN: 3-938345-02-0

[3] Pan ZH, Hu HJ, Perring P, Andrade R. (2001). T-type Ca(2+) channels mediate neurotransmitter release in retinal bipolar cells. Neuron. 2001 Oct 11;32(1):89-98.

[4] Mallinowsky ER. (1980). Factor Analysis in Chemistry. John Wiley & Sons, New York.

[5] Lapicque, L.(1907), Researches quantiatives sur I'excitation èlectrique des nerfs traitèe comme une polarization. J. Physiol, Paris 9:620-635

# Extracellular Stimulation of Mammalian Neurons on Silicon Chips: Design of a Safe Protocol By Repetitive Activation of Na+ Channels

Ingmar Schoen, Peter Fromherz*

Max Planck Institute for Biochemistry, Department of Membrane and Neurophysics, D-82152 Martinsried / Munich, Germany
* Corresponding author. E-mail address: fromherz@biochem.mpg.de

We present an electrophysiological study of capacitive stimulation of mammalian cells on planar insulated electrodes. Particular emphasis is laid on the derivation of the primary polarizations, the local activation of sodium channels and on a safe protocol that excludes cell damage by electrochemistry or electroporation.

## 1  Background & Aims

Reliable extracellular stimulation of neuronal activity is the prerequisite for electrical interfacing of cultured networks and brain slices, as well as for neural implants. Safe stimulation must be achieved without a damage of the cells by irreversible electroporation or electrochemical byproducts. With respect to a future application of highly integrated semiconductor chips, we present an electrophysiological study of capacitive stimulation of mammalian cells in the geometry of adhesion on an insulated titanium dioxide/silicon electrode [1].

## 2  Methods

We used HEK293 cells with overexpressed NaV1.4 channels and neurons from rat hippocampus. Weak biphasic stimuli of falling and rising voltage ramps were applied in the absence of Faradayic current and electroporation. We recorded the response of the intra and extracellular voltage and evaluated the concomitant polarization of the attached and free cell membrane.

## 3  Results

Falling ramps efficiently depolarized the central area of the attached membrane. A transient sodium inward current was activated that gave rise to a weak depolarization of the cell in the order of 1 mV. The depolarization could be enhanced step by step by a train of biphasic stimuli until self-excitation of sodium channels set in. We applied the same protocol to cultured rat neurons and found that pulse trains of weak capacitive stimuli were able to elicit action potentials.

## 4  Conclusion & Outlook

Our results provide a basis for safe extracellular stimulation not only for cultured neurons on insulated semiconductor electrodes, but also more generally for metal electrodes in cell culture and brain tissue.

**References**

[1]  I. Schoen and P. Fromherz. 2008. Extracellular stimulation of mammalian neurons through repetitive activation of Na+ channels by weak capacitive currents on a silicon chip. *J. Neurophysiol.* in press. doi:10.1152/jn.90287.2008.

# Network-state Dependent Stimulation Efficacy and Interaction with Bursting Activity in Neuronal Networks *in vitro*

Oliver Weihberger[1,2], Jarno Ellis Mikkonen[1,3], Samora Okujeni[1,2], Steffen Kandler[1,2], Ulrich Egert[1,4]

1 Bernstein Center for Computational Neuroscience Fre burg, Albert-Ludwigs-University Freiburg, Freiburg Germany
2 Institute of Biology III, Neurobiology and Biophysics, Albert-Ludwigs-University Fre burg, Fre burg Germany
3 Department of Signal Processing, Tampere University of Technology, Tampere Finland
4 Biomicrotechnology, Department of Microsystems Engineering, A bert-Ludwigs-University Freiburg, Freiburg Germany

An understanding of the mechanisms that underlie information processing and storage in neuronal networks is largely missing. Dynamical interactions on a wide range of spatial and temporal scales are involved, but it is unclear how they arise and by which mechanisms they are governed. We are interested in how neuronal networks respond to incoming stimuli, which interactions arise and how this enables the processing and storage of information. We electrically stimulated cortical cell cultures grown on microelectrode arrays (MEAs) and characterized network responses during different activity states. Stimulation at fixed intervals without defined relation to an activity state ('random') resulted in decreasing response length with decreasing time since last synchronous network activity (*network burst*) and vice versa. Stimulation during spontaneously occurring, 20 - 60 second long periods of elevated network-wide bursting (*Superbursts)* yielded the longest responses. During the following refractory period, responses were shortest and stimulation even failed to induce spikes. Stimulation during burst-onsets ('intraburst') could either temporarily induce or inhibit spiking, but it could neither terminate nor shorten the burst progression. Stimulation during periods of no activity ('post-burst'), induced short- ($\leq$ 50 − 100 ms post stimulus) and long-term ($\geq$ 100 ms post stimulus) response components and increased response reproducibility. Different stimulation sites elicited distinguishable short-term response dynamics. Finally, low-frequency stimulation (0.1 − 0.4 Hz) at selected sites with any of the paradigms interfered with the bursting activity and reversibly suppressed Superbursts.

## 1 Introduction

Cortical cell cultures grown on MEAs give the possibility to study neuronal functions such as learning, memory, information processing and storage under controlled, easily accessible and experimentally manipulable conditions. Under the assumption that basic neuronal properties are maintained *in vitro*, various research groups in recent years were interested in revealing mechanisms that may underlie those functions. Shahaf *et al.* [1] for the first time showed learning and memory capabilities in *ex - vivo* networks by imprinting advanced stimulus/response associations. Eytan *et al.* [2] demonstrated stimulus-specific adaptation properties, possibly resulting from a selective gain control. Beggs & Plenz [3] investigated neuronal avalanches, i.e. network-wide propagating activity patterns, as a means for information transfer and storage. Bonifazi *et al.* [4*]* found fast and reliable stimulus decoding from *ensembles* of neurons along with a critical dependency on the network's balance between excitation and inhibition. Almost all those studies used electrical stimulation as network-input and the re-

sponse was interpreted as the 'processed' output. Network responses are inherently variable, with large spatio-temporal fluctuations, reminiscent of chaotic systems [5]. Averaging over many trials and networks, or pooling different neurons [4] is necessary to reduce the noise in order to reliably conclude about the network's processing properties. In our work, we want to describe dynamic input/output relationships for neuronal networks *in vitro*. We aim at predictive models that allow a tight interaction with and control of neuronal activity by electrical stimulation.

Here, we show that electrical stimulation efficacy and spontaneous activity in neuronal networks *in vitro* are interdependent. The timing of stimulation with respect to oscillatory activity states determined over response lengths and stimulation could in turn interfere with spontaneous busting activity. Phase-coupled stimulation during always the same, predefined state of network activity had the advantage of a clearly defined and controlled stimulation environment. We obtained reproducible and stable responses, yielding a

more unique description of network input/output relationships.

## 2 Materials & Methods

### 2.1 Culture preparation

Cells from prefrontal cortical tissue of neonatal wistar rats were cultured on polyethylene imine-coated MEAs. Cultures were maintained in MEM supplemented with heat-inactivated horse serum (5%), L-glutamine (0.5 mM), and glucose (20 mM) at 37° C and 5% $CO_2$. Medium was partially replaced twice per week.

### 2.2 Recording and stimulation

A Multi Channel Systems MEA1060BC amplifier, STG2008 stimulus generator and meabench [6] were used for recording and stimulation inside the incubator. The criteria for single-electrode bursts were a minimum of three spikes, inter spike intervals $\leq 75$ ms, with maximal one interval $\leq 150$ ms allowed. Network burst criteria were burst onsets within $\leq 150$ ms on at least three electrodes. For Superburts, global activity-periods clearly above baseline were manually extracted and network bursts and their respective on- and offsets assigned. Monophasic negative voltage pulses, width 400 μs, amplitudes $\geq 0.4$ Volt were used for stimulation. Three stimulation paradigms were applied: 'Random' stimulation at fixed intervals (typically 20 sec), without relation to network activity. For 'intraburst' stimulation, the firing rate of a preselected electrode was calculated online by single-trial rate estimation [7]. Whenever a given threshold was crossed, a stimulus was triggered (Fig. 1a). In 'post-burst' stimulation, whenever a minimum period without spikes on pre selected electrode(s) passed, a stimulus was triggered (Fig. 1b).
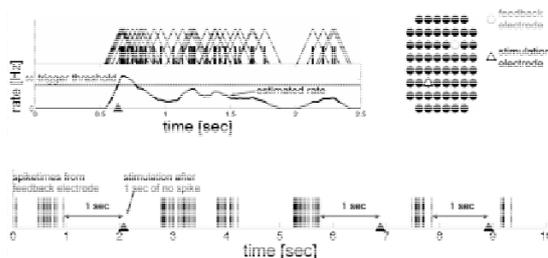


**Fig. 1. a)** left: Intraburst stimulation: online convolution of spike times and triangle kernel function yielded instantaneous rate estimate. Crossing of a threshold triggered a stimulus (marker). right: 8x8 MEA, with feedback (for phase-coupling) and stimulation electrode b) post-burst stimulation: feedback electrode's spike times were continuously monitored, after a fixed period without spikes, a stimulus was triggered (marker)

## 3 Results

### 3.1 Spontaneous activity modulates stimulation efficacy

**Modulation by network bursts**

After 'random' stimulation, responses were extracted according to the criteria for single-electrode bursts. Stimulation trials were sorted for increasing response length (in seconds). Pre-stimulus activity and response lengths were inversely correlated: high bursting activity immediately preceded short responses, periods of no or low bursting activity preceded long responses (Fig. 2a). Quantitative analysis, including examples from different networks shown in Fig. 2b. This effect was most clearly observed when stimulation elicited long- *and* short-term responses, as well as when the activity did not (yet) develop into Superbursts.

**Modulation by Superbursts**

During superbursting activity, stimulation elicited the longest responses. After the end of Superbursts, responses were shorter or stimulation even failed to elicit spikes (Fig. 3a). Response length distribution was broadest during Superbursts, distributions after Superbursts and during other activity phases were similar. Response reliability, however, was clearly diminished just after Superbursts.
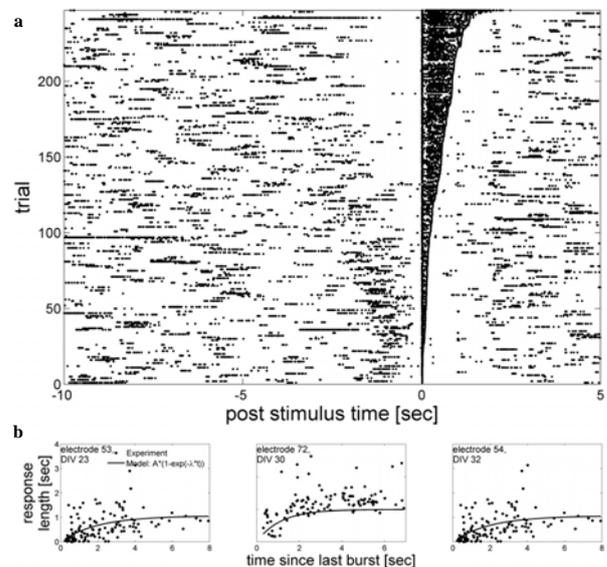


**Fig. 2.** a) raster plot, electrode 54, -10 to 5 seconds post stimulus, applied at electrodes 16 and 43. Trials sorted for response length. Note the increasing response length with decreasing pre-stimulus activity. b) Response length vs. time since last burst before stimulation for three electrodes, different networks. Experimental data (dots) and model A*(1-exp(-λ*t)) describe a saturating response length.
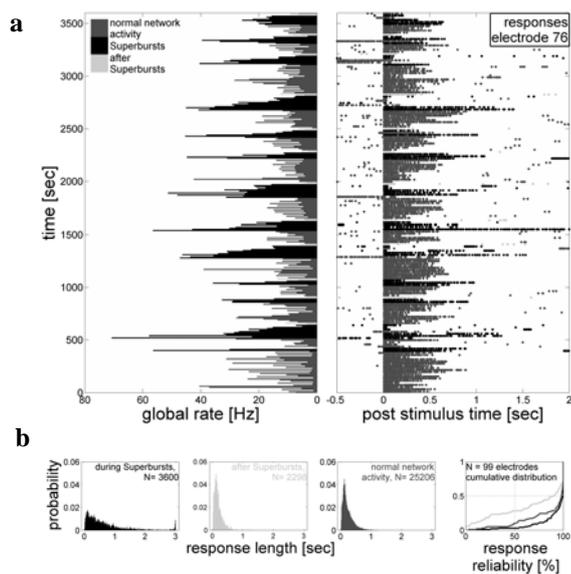
**Fig. 3.** a) left: 1-hr. global firing-rate, bin width 10 sec. right: responses from electrode 76 to 180 stimulation trials, applied at electrode 57, during the same period. Repeated increase and reset of response length, correlated with spontaneous Superbursts. b) response length distributions (99 electrodes). right: response reliability = (#responses)/(#stimuli)

## 3.2 Phase-coupled stimulation

**Intraburst stimulation**

Stimulation was triggered within 50 -100 ms after burst onset on the feedback electrode. The impact of stimulation on the burst dynamics was analyzed by comparing stimulation trials with control trials in which the trigger criterion was fulfilled, but no stimulus was applied. Stimulation could induce additional spikes on top of the ongoing burst or it could temporarily inhibit spiking during the burst (Fig. 4). Short-term responses were induced even when the ongoing spiking was inhibited. In general, intraburst stimulation could not terminate or curtail burst progression. A reduction of average burst length was observed only when stimulation suppressed superbursting activity (section 3.3).

**Post-burst stimulation**

Stimulation induced clearly separable short-and long-term response components. Stimulation at different sites elicited distinguishable delays in the reliable short-term response. Comparable dynamics could be reproduced 24 hrs. later, showing the stability of this effect (Fig. 5a).
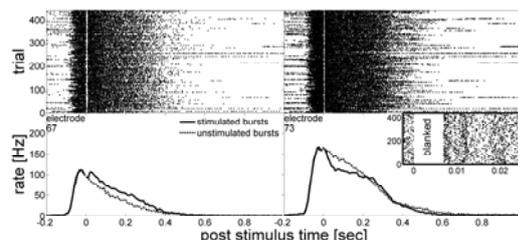


**Fig. 4.** top: raster plots, electrodes 67 (left) and 73 (right), 450 trials intraburst stimulation at electrode 64. Bursts started before stimulation. Burst progression did not markedly change during the experiment. inset: 7 ms blanking period that minimized artifacts, followed by short-term response spikes. bottom: corresponding PSTHs, including those for control trials (dashed). Additional spikes were induced (left), or spiking was temporarily inhibited (right).
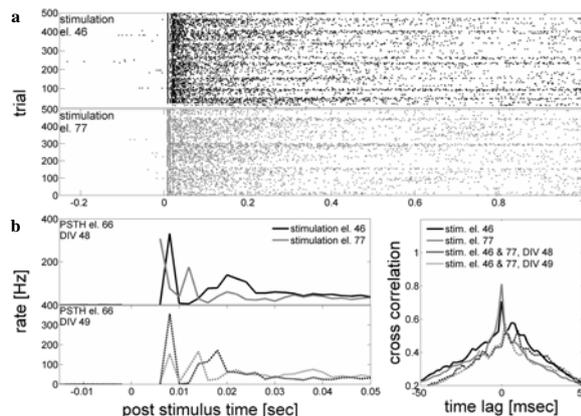


**Fig. 5.** a) raster plots, electrode 66, 500 post-burst stimulation trials at electrodes 46 (black) and 77 (gray). bottom left: corresponding PSTHs for -15 to 50 ms post stimulus at DIV 48 (solid lines) and for DIV 49 (dashed lines). Response-delays changed with different input sites, but were comparable for identical input sites at successive days (compare different colors vs. solid and dashed lines of same color). **b)** PSTH cross-correlation, normalized and averaged over 11 electrodes.

Different input sites (stimulation electrodes) could be distinguished by means of their induced short-term response. In cross-correlations between PSTHs, the normalized and averaged peak was higher and closer to 0-lag for same input sites compared to different input sites.

## 3.3 Interfering with Superbursting activity

Oscillatory superbursting activity with distinctive global rate fluctuations was terminated either directly or a few minutes after stimulation start. After the end of stimulation, Superbursts could reappear (Fig. 6). This effect was independent of the stimulation paradigm. Furthermore, effective stimulation electrodes consistently had early network burst onsets during spontaneous activity (Fig. 6 insets). The probability for very long network bursts was decreased during Superburst suppression. This means, from an initial bursting state, including abnormally long bursts during Superbursts, the network's activity was shifted to more regular burst firing without episodic Superburst patterns.
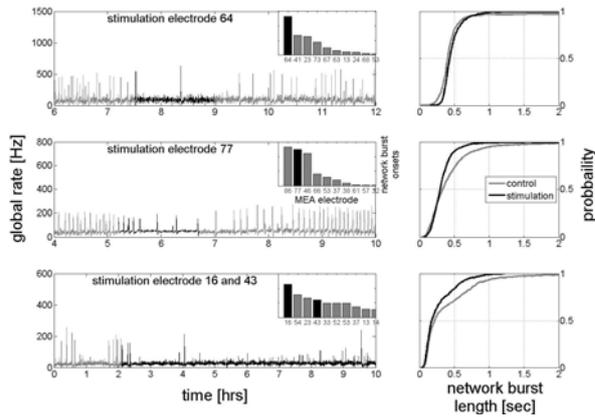
**Fig. 6.** left: global rate profiles, three different networks. 'intraburst' (top), 'post-burst' (middle) and 'random' (bottom) stimulation periods in black, control in gray. bottom: Superbursts reappeared during stimulation. insets: ranking of electrodes starting network bursts, used for stimulation electrode selection. right: cumulative distributions of network burst length. Probability for very long bursts decreased during stimulation.

## 4 Conclusions

Electrical stimulation efficacy and spontaneous bursting activity in neuronal networks *in vitro* are interdependent. Effective electrical stimulation does not merely need defined stimulus properties, e.g. amplitude, width or type, but also a consideration of the phase when the stimulus is applied. Phase-coupled stimulation places the stimulus into the same context of network activity, resulting in more reproducible and predictive responses. Furthermore, it enables a detailed assessment of the network's transfer function with reduced influence of interfering effects. Input/output relationships are defined for separate activity states, rather than for a grand average of different states. This would aid in the understanding how information imposed by electrical input patterns is processed by neuronal networks *in vitro* and physiologically realistic systems in general.

## References

[1] G. Shahaf and S. Marom, "Learning in networks of cortical neurons," *J. Neurosci.*, vol. 21, no. 22, pp. 8782-8788, Nov.2001.

[2] D. Eytan, N. Brenner, and S. Marom, "Selective adaptation in networks of cortical neurons," *J. Neurosci.*, vol. 23, no. 28, pp. 9349-9356, Oct.2003.

[3] J. M. Beggs and D. Plenz, "Neuronal avalanches in neocortical circuits," *J. Neurosci.*, vol. 23, no. 35, pp. 11167-11177, Dec.2003.

[4] P. Bonifazi, M. E. Ruaro, and V. Torre, "Statistical properties of information processing in neuronal networks," *Eur. J. Neurosci.*, vol. 22, no. 11, pp. 2953-2964, Dec.2005.

[5] Y. Jimbo, A. Kawana, P. Parodi, and V. Torre, "The dynamics of a neuronal culture of dissociated cortical neurons of neonatal rats," *Biol. Cybern.*, vol. 83, no. 1, pp. 1-20, July2000.

[6] D. Wagenaar, D. Wagenaar, T. B. DeMarse, and S. M. Potter, "MeaBench: A toolset for multi-electrode data acquisition and on-line analysis,". T. B. DeMarse, Ed. 2005, pp. 518-521.

[7] M. Nawrot, A. Aertsen, and S. Rotter, "Single-trial estimation of neuronal firing rates: from single-neuron spike trains to population activity," *J. Neurosci. Methods*, vol. 94, no. 1, pp. 81-92, Dec.1999.

# Analysis of Light Induced Activity in Defined Neural Networks

Boris Hofmann[1], Stefan Eick[1], Simone Meffert[1], Sven Ingebrandt[1], Ernst Bamberg[2], Andreas Offenhäusser[1]*

1 Institute of Bio- and Nanosystems (IBN2) and CNI - Center of Nanoelectronic Systems for Information Technology, Forschungszentrum Jülich GmbH, D-52425 Jülich, Germany
2 Max-Planck-Institute for Biophysics, Max-von-Laue-Strasse 3, D-60438 Frankfurt, Germany
* Corresponding author. E-mail address: a.offenhaeusser@fz-juelich.de

In this work we show a way to use light in combination with MEAs to stimulate and record single neurons and small networks of neurons. Channelrhodopsin (ChR2), a blue-light gated ion channel is used to trigger membrane currents via a light pulse that can evoke action potentials, depending on the cellular system used. We introduce a convenient way to illuminate a single spot of about 10μm in diameter with laser light (λ=473nm). Furthermore we show the combination of defined neural networks grown on microelectronic devices and light stimulation. We use aligned μ-contact printing to create single, yet interconnected cells on recording sites. For transfection of the cells with a ChR2 containing plasmide electropermeabilisation can be used. Advantages are a high transfection efficiency and stable expression of the protein for at least 21 days.

## 1 Introduction

Neural network analysis is one of the major applications for microelectrode arrays or FET devices. Whereas recording of slices and tissue is commonly used, interfacing single neurons and defined neural networks still is very challenging. The formation of defined neural networks could be shown many times in literature [11], whereas alignment of these networks to recording devices is still uncommon. Several techniques like homogenous coating and subsequent protein ablation by a laser [13] or photolithographic patterning [5] exist but are either time consuming or may damage the chip as well as the adhesion proteins used. Aligned μ-contact printing proved to be very promising [6] but also has some drawbacks as two non-transparent surfaces have to be aligned in respect to each other. Furthermore, different coupling methods exist; proteins can either be physisorbed to the surface [3] or covalently attached to it [9]. Once a stable and reliable cell culture is established on chip the lack of possible stimulation techniques for cells have to be overcome. Current or voltage [12] stimulation are possibilities for reliable stimulation but the cells have to be situated either on an electrode or a FET with stimulation possibilities [7]. Although the techniques allow the interfacing of single cells these still have to be situated on a stimulation site. Furthermore electrical stimulation may also lead to permeabilisation of the cells what subsequently might also trigger an action potential but in the same time damage the cell and do not lead to the desired long term monitoring of the network. This lack of possible stimulation techniques can be overcome by using genetically engineered Channelrhodopsin 2(ChR2) expressing neurons. ChR2 is a blue-light-gated cation channel with a retinal as gating mechanism. It can be used to depolarize cells via a light pulse and subsequently stimulate genetically engineered neurons. The stimulation of the cells is reproducibly, rapidly, non-invasively [8] and independent of their position on the device. For transfection of the cells with the channel genes different transfection techniques exist. Commonly used are viral systems, e.g. lenti-virus [1], or chemical transfection. Both techniques provide transfection efficiencies that are not sufficient for application on neural networks on microelectronic recording devices. Electrofection seems to be a powerful tool to raise transfection efficiencies to useable values and therefore gives access to the combination of defined neural networks on MEAs and light stimulation of cells. Until now no one has, to our knowledge, shown a combination of these techniques.

## 2 Materials and Methods

### 2.1 Setup

**Laser stimulation**

Activation of ChR2 was achieved using a 473nm diode laser that was coupled to the optical path of the microscope via an optical fibre and a dichroic mirror. Epifluorescent illumination was still possible. Spot diameter of the laser was about 10μm, depending on

fibre and objective. The laser was controlled using TTL pulses. Stimulation times down to about 1ms could be achieved
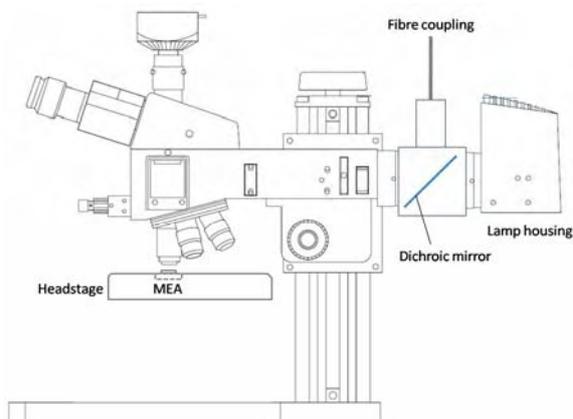


**Fig. 1.** Schematic drawing of the setup. The laser can be coupled to the optical path of the microscope via a fibre and a dichroic mirror (picture adapted from http://www.zeiss.de).

### Recording setup

We used a custom-made, 64-channel amplifier system in which microelectrodes were coupled directly to the inputs of high-impedance operational amplifiers (preamplifier gain 10.22), then coupled to a main amplifier (gain 100) providing an overall gain of 1022. The high-pass performance of the recording system was only dependent on the size, material, surface condition, and cleanliness of the microelectrodes providing a large bandwidth recording system. As a result of this ultimate high-impedance input, the bandwidth of our MEA system was enhanced to 0.4 Hz–3.9 kHz for electrodes with a diameter of 20 μm. This performance enables reliable recordings of distinct signal shapes of extracellularly recorded action potentials originating from individual cells. Most importantly, recordings with our current setup can be done with cheap-to fabricate, reusable, planar gold microelectrodes, which can be designed in sizes smaller than the soma of individual cells [4]. Data were sampled at 10 kHz per channel, with simultaneous acquisition across all channels using the MED64 conductor 3.1 software (Alpha MED Sciences, Japan). An extracellular Ag/AgCl electrode, which was set to ground potential, served as a reference electrode. A more detailed description of the data acquisition has been published previously [4].

### Microelectrade arrays

The MEAs were manufactured on glass wafers using standard silicon technology. The planar 64-channel gold MEAs (8×8) were designed with diameters of 6, 8, 10 or 20 μm at a pitch of 100 or 200 μm. The chips were passivated by an oxide–nitride–oxide layer deposited by plasma-enhanced chemical vapour deposition consisting of 500 nm $SiO_2$, 500 nm $Si_3N_4$, and 100 nm $SiO_2$. Details of the fabrication and encapsulation processes have been previously described [4]. The MEAs were additionally platinised according to [10]. Briefly, a 3 electrode CV setup with the short-cutted MEA as working electrode was used. The MEA was filled with platinum 3745 solution and after a 10s holding potential of -0.2V the voltage was swept between -0.9 and -0.2 V for up to 40 times with a sweeping speed of 100mV/s. Afterwards the MEAs were gently rinsed using bidest and could then be used for further preparation like protein coating. Finally cell culture was done as described in 2.2 and 2.3.

### 2.2 HEK 293-ChR2

We used the human embryonic kidney cell line 293, which was stably transfected with channelrhodopsin coupled to eYFP as a model system. In short, cells were grown in DMEM supplemented with 10% (v/v) fetal calf serum, 1ml 100x penicillin/streptomycin, 200 μg/ml zeocin (Invitrogen) and 5 μg/ml blasticidin (Invitrogen). The expression of ChR2 was activated by adding Tetracyclin (Sigma) and could be visualized by fluorescence. The HEK 293 cells were plated onto poly(L)lysine-coated MEAs at densities of 4500-6000 cells per chip (effective chip surface: 6.2 mm2). The chips were incubated at 37 °C and 5% $CO_2$ for 3-5 days before recordings.

### 2.3 Neurons

**Isolation of embryonic neurons**

Cortical neurons were obtained as previously described [2]. Briefly, embryos were recovered from pregnant CD rats at 18 days gestation. Cortices were dissected from the embryonic brains; cells were mechanically dissociated by trituration in Hank's Balanced Salt Solution (without Ca2+ and Mg2+), 0.035% sodium bicarbonate, 1 mM sodium pyruvate, 10 mM HEPES, 20 mM glucose, pH 7.4 with a fire polished siliconized Pasteur pipet. Two volumes HBSS 0.035% sodium bicarbonate, 1 mM pyruvate, 10 mM HEPES, 20 mM glucose, pH 7.4 were added. For 3 min, nondispersed tissue was allowed to settle; the supernatant was centrifuged at 200g for 2 min.

**Transfection of the cells**

The pellet was re-suspended in 0.1ml transfection solution and 3-5μg of plasmid (eYFP coupled ChR2 under CMV promotor) was added. After transferring the solution to a transfection cuvette the transfection of the cells was achieved using the AMAXA nucleofector device. Afterwards, the cell solution was extended with 0.5ml of RPMI solution (+0.5 mM Lglutamine, + 10% FCS v/v). Cells were plated on our custom-made 64 electrodes MEAs /16 FET chips,

which were previously patterned with polylysine or a mixture of polylysine and extracellular matrix gel (PECM). Cell density was about 12000 cells/cm². After one hour of adhesion, excessive exchange of medium was done in order to remove dead cells and debris. After 4h the medium was exchanged by Neurobasal Medium (+ 1xB27, 0.5 mM Lglutamine). Half of the medium was changed every 3-4 days (Publication in preparation).

**Patterning of the cells**

Patterning of the substrates was done by covalently binding PLL or PECM to an epoxy silane layer [9]. Substrates were activated using oxygen plasma and the activation was confirmed by contact angle measurements. After activation the substrate were brought into a preheated desiccator and about 100µl of epoxy silane was added. Silanization was performed at 5mbars of pressure for 1h. The epoxy group of the silanes was activated by treatment of the chips with phosphate buffer at pH 8.2. The buffer was removed shortly before stamping. Aligned µ-contact printing of proteins was achieved using a fine-placer [6] with redesigned micro stamps that can be released while still in contact to the substrate. The stamps were designed to fit the layout of our devices and additionally providing the best basis for the neural networks. The nodes, where the cell bodies can adhere, have a diameter of 12 µm and the interconnecting lines have a width of 4 µm. Pitch of the nodes is, same as for the pitch of the microelectronic structures, 200µm. For better stability during the printing process stabilizing cross connections were designed. Diameter of the stamp was about 2mm to fit the inner diameter of our encapsulation which is 2.8mm in diameter. After successful alignment, the stamp was brought into contact with the device surface by means of a high-precision lever and the applied pressure was measured with a balance that was mounted to the device. Applied pressure was between 5-10g which corresponds to an overall pressure of 160-320 g/cm2.
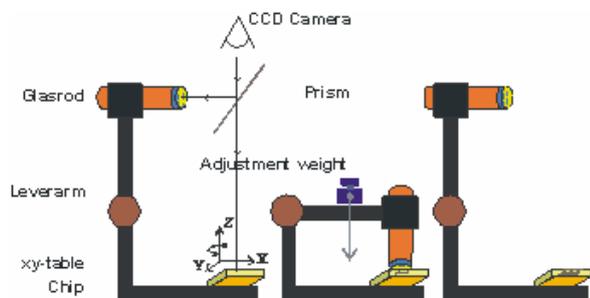


**Fig. 2.** Schematic drawing of the aligned-µCP device. Printing is basically done in three steps: alignment, stamping and releasing of the stamp.

# 3   Results

## 3.1 Prerequisites

**Cell transfection**

For the transfection of the neurons we achieved a final yield of up to 65% transfected cells. The cells were stably transfected for more than 21 days in culture.

**Stimulation**

The laser stimulation system gives us the possibility to locally interface cells expressing ChR2. We achieved a spot diameter of about 10µm which matches the size of the cell body of a rat cortical neuron. However, with rising laser power also the stray light and thereby the total area illuminated, increased.

## 3.2 HEK 293-ChR2

First analysis was performed on a model system. We used HEK 293 cells that stably expressed channelrhodopsin. By patching the cells in the whole cell voltage clamp mode we were able to measure light dependent inward currents as shown in Fig.3.
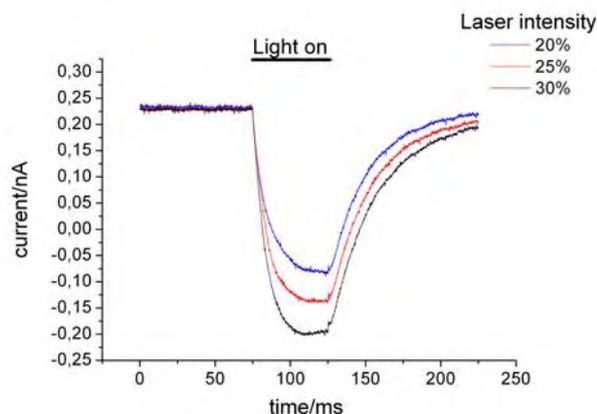


**Fig. 3.** Light evoked currents in a whole cell voltage clamp patched HEK ChR2 cell.

## 3.3 Neurons

**Cell patterning**

Aligned patterning of proteins was successfully performed with a precision of a few µm. We were able to form a precise and homogenous pattern over the whole chip surface for either physisorbed or covalently coupled proteins. Adaption of cell culture conditions lead to a high amount of single, yet interconnected, cells on electrodes.
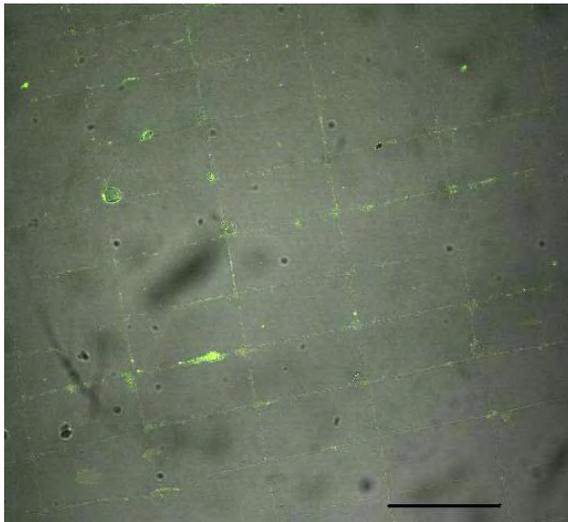
**Fig. 4.** Expression of ChR2 in a patterned cortical culture after 17 DIV. Picture is a merged image of a fluorescence (eYFP -coupled to ChR2) and a DIC picture. Scale bar corresponds to 100μm.

## Stimulation of neurons

Using our stimulation set up we were able to depolarize transfected cells. Upon adjustment of extracellular medium we were also able to depolarize the cells above threshold potential and evoke single action potentials in cortical rat neurons.

## 4 Discussion

In this work we show that interfacing single cells is possible by using genetically engineered ChR2 expressing neurons. We introduced a stimulation setup that is useable with any kind of chip as it works with the microscope optics and is compatible with upright microscopes. Properties of the setup were determined using a model system, namely ChR2 expressing HEK cells. We could clearly show light induced inward currents and a dependency of the current to the laser power due to further channels opening. Saturation was not reached at lower intensities what might be explained by increased stray light effects that activate a bigger area of the cell. After first properties of light stimulation were determined, the setup is to be used with defined neural networks that are positioned using aligned μ-contact printing of adhesion proteins. These proteins can either be physisorbed to the surface or covalently coupled to an epoxy silane layer. The silane layer can be coupled to the surface of our chips prior to stamping. The covalently coupled layer proved to support the cells for a longer time as no stripping of the layer was observed. A high yield of single yet interconnected cells could be achieved after adaption of cell number and culture conditions. This gives access to really studying single cells and networks consisting of single but interconnected cells. Furthermore we showed that high transfection efficiencies are possible using the nucleofector even there is a big loss of cells during electropermeabilisation. Combining the two techniques one can study single cells as well as cellular networks even there is no electrode in close proximity to the cell that shall be stimulated. Possible applications are the analysis of long term potentiation in dissociated cultures as well as coincidence detection.

## References

[1] E.S. Boyden, F. Zhang, E. Bamberg, G. Nagel, and K. Deisseroth (2005): Millisecond-timescale, genetically targeted optical control of neural activity. Nat Neurosci, 8(9):1263–1268

[2] G. J. Brewer, J. R. Torricelli, E. K. Evege, and P. J. Price (1993): Optimized survival of hippocampal neurons in b27-supplemented neurobasal, a new serum-free medium combination. J. Neurosci. Res., 35(5):567–576

[3] J.C. Chang, G.J. Brewer, and B.C. Wheeler (2003): A modified microstamping technique enhances polylysine transfer and neuronal cell patterning. Biomaterials, 24(17):2863–2870

[4] H. Ecken, S. Ingebrandt, M. Krause, D. Richter, M. Hara, and A. Offenhausser (2003): 64-channel extended gate electrode arrays for extracellular signal recording. Electrochim. Acta, 48(20-22):3355–3362

[5] C.D. James, A.J.H. Spence, N.M. Dowell-Mesfin, R.J. Hussain, K.L. Smith, H.G. Craighead, M.S. Isaacson, W. Shain, and J.N. Turner (2004): Extracellular recordings from patterned neuronal networks using planar microelectrode arrays. IEEE Trans Biomed Eng, 51(9):1640–1648

[6] L. Lauer, S. Ingebrandt, M. Scholl, and A. Offenhäusser (2001): Aligned microcontact printing of biomolecules on microelectronic device surfaces. IEEE Trans Biomed Eng, 48(7):838–842

[7] S Meyburg (2005): Transistor arrays for the direct interfacing with electrogenic cells. PhD thesis, 01 Fakultät für Mathematik, Informatik und Naturwissenschaften

[8] G Nagel, T Szellas, W Huhn, S Kateriya, N Adeishvili, P Berthold, D Ollig, P Hegemann, and E Bamberg (2003): Channelrhodopsin-2, a directly light-gated cation-selective membrane channel. Proc. Natl. Acad. Sci. U. S. A., 100(24):13940–13945

[9] Y. Nam, D.W. Branch, and B.C. Wheeler (2006): Epoxysilane linking of biomolecules is simple and effective for patterning neuronal cultures. Biosens Bioelectron, 22(5):589–597, Dec 2006.

[10] P. Thiébaud, N. F. de Rooij, M. Koudelka-Hep, and L. Stoppini (1997): Microelectrode arrays for electrophysiological monitoring of hippocampal organotypic slice cultures. IEEE Trans Biomed Eng, 44(11):1159–1163

[11] A.K. Vogt, L. Lauer, W. Knoll, and A. Offenhäusser (2003): Micropatterned substrates for the growth of functional neuronal networks of defined geometry. Biotechnol Prog, 19(5):1562–1568

[12] D.A. Wagenaar, J. Pine, and S.M. Potter (2004): Effective parameters for stimulation of dissociated cultures using multi-electrode arrays. J Neurosci Methods, 138(1-2):27–37

[13] M. Yamato, C. Konno, S. Koike, Y. Isoi, T. Shimizu, A. Kikuchi, K. Makino, and T. Okano (2003): Nanofabrication for micropatterned cell arrays by combining electron beam-irradiated polymer grafting and localized laser ablation. Journal Of Biomedical Materials Research Part A, 67A(4):1065–1071

# Real-time and Batch Control of MEA Channel Selection and Stimulation

Downes J.H.[1*], Hammond M.W.[1,2], Xydas D.[1], Whalley B.J.[2], Becerra V.M.[1], Warwick K.[1], Nasuto S.J.[1]

1 Cybernetics, School of Systems Engineering,
2 School of Pharmacy, University of Reading, England
* Corresponding author. E-mail: j.downes@reading.ac.uk

We present software tools allowing near real-time control of electrical stimulation on Multi Electrode Arrays (MCS hardware: MEA1060BC plus STG2004), with fast switching between electrodes and the application of custom stimulus waveforms. These Linux-based tools are designed to work with MEABench, but could be easily used with other acquisition systems. Benefits include rapid stimulus modulation in response to neuronal activity (closed loop) and batch processing of stimulation protocols.

## 1   Introduction

A key element in recent investigations of cultured neuronal networks on MEAs is the ability to apply electrical stimuli to a culture using standard hardware such as the MEA1060BC plus STG 2004 (MCS, Reutlingen, Germany). However, the MS Windows-based electrode selection and stimulus waveform tools commonly used offer limited flexibility of stimulation control. Constraining factors include the need for manual switching between active electrodes, separately from creating / loading and executing stimulus waveforms; lack of automated protocol execution; and significant delays imposed if MS Windows (non-real time) batch processing is used. As a consequence, investigations that rely upon rapid stimulus modulation in response to neuronal activity recorded via MEAs are severely limited. Whilst stimulus control has been improved using custom hardware [1], such control for off-the-shelf stimulators is not presently available. Consequently, we have developed software tools allowing precise, near real-time control of MCS hardware from a single interface. These Linux-based tools are presently designed to work with MEABench [2] but could easily be used with other acquisition systems.

### Purpose of Stimulation Control

Stimulation control has three main applications: (i) testing neuronal responsiveness to different stimulation patterns (to establish appropriate stimulus); (ii) training a substrate in order to elicit plasticity (learning); and (iii) stimulating within a 'live' closed-loop system such as an Animat ('embodied culture') whereby continual stimulus modulation by culture activity is mediated via robotic embodiment in the external environment.

To achieve (i & ii), an easy to configure 'interactive' interface is required, affording safe yet flexible experimentation with different stimulation patterns across rapidly switching electrodes. The ability to store and batch protocols (with minimal manual input) is invaluable in saving time and ensuring experimental consistency, whilst a graphical user interface provides an easy and safe way to work within the hardware and biological constraints. To achieve (iii), speed and efficiency are the most important factors - ensuring that real time constraints are met as closely as possible. Here, the software must wait for an automatically delivered choice of electrode(s) and waveform(s) (based on robot sensor data), before triggering stimulation.
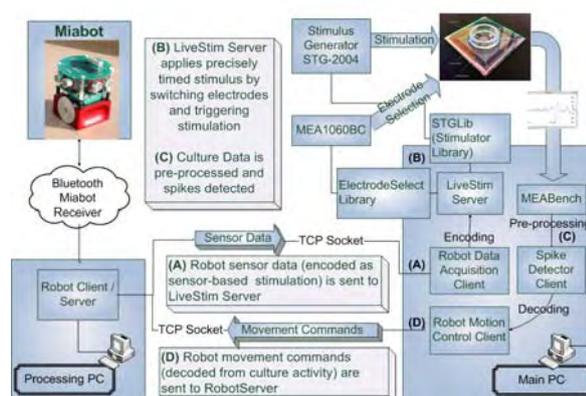


**Fig. 1.** Tools within a closed loop system: top left: robot embodiment, top right: MEA + hardware and software, bottom: client-server architecture.

Our software interface to the MEA1060BC and STG 2004 stimulus generator provides all of the above functionality in an Open Source, easily extensible set of libraries and command line/GUI interfaces.

The title figure shows a screenshot of the application, with stimulus output shown on the scope (inset).

## 2 Methods

Software was written in C and C++ with libraries interfacing to the underlying hardware via the STG2004 and MEA1060BC driver software. The STG2004 driver was ported from Linux kernel 2.4 to 2.6.1 A Python and TKinter wrapper was written to provide the Graphical User Interface (GUI).

**Software Configuration and Testing**

Software installation scripts were created to ensure correct configuration. The software was tested using a combination of low-level function, and high-level functionality testing. System performance was evaluated with timed C tests (gettime()).

## 3 Results

We achieved a closed loop time of 34 ms +/- 6 ms (n = 10) for the culture closed loop: from stimulation, to culture response based stimulation (see Table 1). The time for a robot closed loop (from sensory based culture stimulation to new sensory input stimulation following robot action), depends on frequency and speed of robot sensors, actuators and communications.

| Action | Time (ms) | |
|---|---|---|
| (1) Select or switch electrode/s | 16 | +/- 1 |
| (2) Stimulus request to observed stimulus receipt | 35 | +/-6 |
| (3) Stimulate pre-selected electrode (repeat) | 2 | +/- 1 |
| (4) Stimulate different electrode | 19 | +/- 3 |
| (5) Load and apply new stimulus waveform | 24 | +/- 2 |
| (6) Apply 2 different waveforms (same elec.) | 7 | +/- 2 |
| (7) Apply 2 waveforms (different elecs.) | 19 | +/- 2 |
| (8) Stimulate, observe response (different elec.) | 32 | +/- 5 |
| Complete closed loop (3) + (8) | **34** | **+/- 6** |

**Table 1:** Software performance (n = 10)

### 3.1 Functionality and Flexibility

- Rapid switching of electrodes and precise control over timing of stimulation.
- ASCII waveform files (MC_Stimulus type 4).
- Ability to store and batch experiments from file.
- Client-server configuration accepts electrodes and waveform choice, providing near real-time control of culture stimulation from external sources (e.g. sensory input from robot).

There are two modes of operation; Test Mode (for evaluating stimulus patterns and executing protocols – e.g. to induce plasticity), and Live Mode (for closed loop experiments). Test Mode runs with a GUI, whilst Live Mode uses a client-server architecture.

| Parameter | Min | Max | Resolution |
|---|---|---|---|
| Amplitude (mV) | -7500 | 7500 | 1-2 |
| Duration (µs) | 20 | ?* | 20 |
| Electrode | 1 | 60 | - |
| #Electrodes Sel-d | 0 | 60 | 1 Electrode |
| Channel | 1 (A) | 2 (B) | - |

**Table 2:** Bounds of stimulus and electrode parameters. * Limited only by waveform file size and STG Memory

## 4 Discussion

The new tools facilitate experiments requiring automated fast electrode switching and precisely timed application of stimuli; including execution of traditional protocols such as electrode cycling (applying a pulse on each), and stimulating with trains of tetanic pulses at various frequencies (inc. the simultaneous application of different frequency trains on different electrodes). This level of flexibility and control cannot presently be achieved with the MS Windows-based tools, which require manual interaction between two non-communicating programs for electrode selection and stimulation.

**Applications**

The precise timing and automated control lend themselves to closed loop Animat experiments; facilitating easy modification of the methods for decoding culture activity and encoding robot sensor data as stimulation. The client-server architecture allows closed loop components to run on separate machines. The efficacy of different stimulation types can be evaluated using the Test Mode and associated GUI.

## 5 Conclusion and Future Work

Our software affords flexible stimulation control using standard hardware, thus opening the door for users wishing to conduct previously impractical closed loop neuronal network investigations. It is planned to release the software tools in the near future under the GPL**Acknowledgement**

**References**

[1] Wagenaar D.A., Potter S.M. (2004) « A versatile all-channel stimulator for electrode arrays, with real-time control. Journal of Neural Engineering 1 : 39-44.

[2] Wagenaar D.A., DeMarse T.B., Potter S.M. (2005) Mea-Bench : A toolset for multi-electrode data acquisition and on-line analysis. 2nd International IEEE EMBS Conference on Nerual Engineering, 16-19 March 2005 : pp.518-521.

# Extracellular Stimulation Of Individual Rat Cortical Neurons With Sputtered Iridium Oxide Microelectrodes

Stefan Eick[1], Jens Wallys[1], Sven Ingebrandt[1], Boris Hofmann[1], André van Ooyen[2], Uwe Schnakenberg[2], Andreas Offenhäusser[1]*

1 Institute of Bio- and Nanosystems (IBN2) and CNI - Center of Nanoelectronic Systems for Information Technology, Forschungszentrum Jülich GmbH, D-52425 Jülich, Germany
2 Institute of Materials in Electrical Engineering (IWE1), RWTH Aachen, D-52074 Aachen, Germany
* Corresponding author. E-mail address: a.offenhaeusser@fz-juelich.de

We present the successful electrical stimulation of action potentials in individual rat cortical neurons by micro-scaled gold electrodes with sputtered iridium oxide films. The non-invasive stimulation has simultaneously been monitored by intracellular recording of the membrane potential using the patch-clamp technique. An investigation of the influence of stimulation pulse parameters on stimulation efficacy and action potential (AP) parameters has been conducted.

## 1  Introduction

Extracellular stimulation is crucial to the development of hybrid neuroelectronic systems as well as for studies of cultured neuronal networks and brain tissue. Applications like prosthetics require materials and devices for stable long-term interfacing without damaging cells and devices by electrochemical reactions. Insulated planar electrodes can be utilized for the purely capacitive stimulation [1]. For multi-electrode arrays (MEAs), cell and electrode damage must be prevented by using controlled electrode voltages below the used material's threshold for electrochemical reactions [2]. A promising material for neurostimulation is iridium oxide (IrOx) due to its low impedance in the relevant frequency range and very high charge delivery capacity compared to other electrode materials. This is caused by the porous structure of IrOx and its electrochemical characteristics [3, 4]. It can handle up to 10 times higher charge injection before faradaic currents flow and lead to electrolysis. Furthermore, IrOx proved to be highly biocompatible and very stable in electrolyte solutions [5]. The aim of this work was to examine the extracellular stimulation of individual neurons with a novel type of planar MEAs with sputtered IrOx films (SIROFs).

## 2  Chip fabrication

MEAs with arrays of 8x8 electrodes were manufactured on glass wafers with electrodes, contact lines and bond pads consisting of a 300nm gold layer sandwiched by two 30nm titanium adhesive layers (Fig. 1). The chip passivation was achieved by a stack of 500nm $SiO_2$, 500nm $Si_3N_4$ and 100nm $SiO_2$ [6]. Microelectrodes with sizes as small as 10 µm additionally carried 300nm SIROF for improved stimulation

capabilities (Fig. 2). The chips were flip-chipped to custom-made 68-pin PCB carriers and encapsulated with underfill, glass rings and silicon glue to protect the bond pads from the electrolyte and to form a Petri dish for cell culture [6].
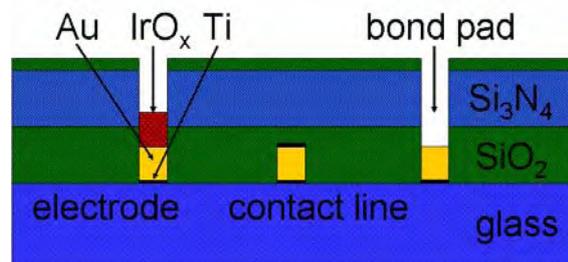


**Fig. 1:** Stack sequence and structure of the MEA chips (not to scale).
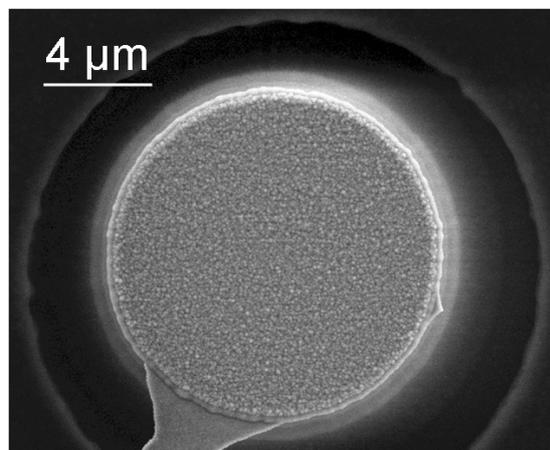


**Fig. 2:** Scanning electron micrograph of a SIROF electrode. The grainy surface structure of the $IrO_x$ film can be clearly seen.
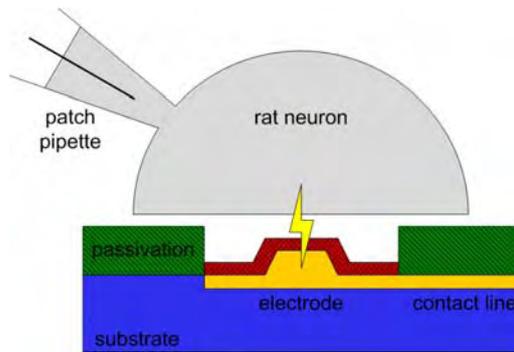
**Fig. 3:** Experimental situation for the single cell stimulation experiments. A rat cortical neuron, which was grown on the microelectrode was additionally attached by a patch-clamp pipette in whole-cell configuration.

## 2 Experimental Setup

CD Rat embryonic cortical neurons (E18) [7] were used for stimulation experiments at five to seven days in vitro. Extracellular stimulation of individual cells grown on microelectrodes was achieved using trains of biphasic voltage pulses with varying pulse amplitude, frequency, number and phase sequence (first positive or negative), which were applied to the electrodes using a custom amplifier system. The stimulated cell's membrane potential was simultaneously recorded intracellularly with a standard patch-clamp setup in the current-clamp mode (Fig. 3). This allowed for the monitoring of stimulation success and the 'health condition' of the cell during the experiment.

## 3 Results

Extracellular stimulation of individual neurons was successfully achieved with our SIROF MEAs. The influence of different stimulation pulse parameters on
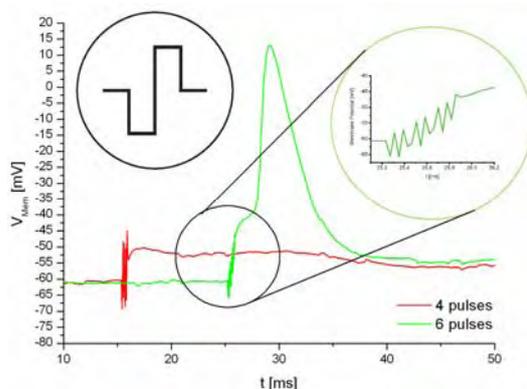


**Fig. 4:** Extracellular stimulation with trains of four and six biphasic pulses with amplitudes of 600mV recorded intracellularly in the current-clamp mode. While a train of four pulses was not sufficient, it was possible to excite an AP with six pulses instead. The right inset shows a magnification of how the six pulses raise the membrane potential step by step above the threshold for AP excitation.

the success of AP excitation and health parameters like AP amplitude and latency was examined. To give an example, higher amplitudes increased the probability of an AP and reduced the response latency, but were limited to values below 1V to prevent electrochemical reactions at the electrode. Instead of exceeding this voltage limit, another way to significantly improve the AP probability is to increase the number of stimulation pulses. The pulses add up, raising the membrane potential step by step above the threshold for AP excitation (Fig. 4). Furthermore, an influence of the phase sequence of the stimulation pulse on the stimulation success and AP latency was found. With first negative biphasic pulses (left inset of Fig. 4) we achieved the highest stimulation success. The positive rising flanks of these pulses were identified to be responsible for the membrane depolarization.

## 4 Conclusion

Planar SIROF MEAs promise to be a feasible tool for long term neurostimulation for network studies and prosthetics. By careful examination of the influence of pulse parameters it is possible to get rid of damaging electrochemical processes at the electrode surface without losing stimulation efficacy.

**References**

[1] Schoen I, Fromherz P. (2007): The mechanism of extracellular stimulation of nerve cells on an electrolyte-oxide-semiconductor capacitor. Biophys. J., 92, 1096-1111.

[2] Wagenaar DA, Pine J, Potter SM. (2004): Effective parameters for stimulation of dissociated cultures using multi-electrode arrays. J. Neurosci. Methods., 138, 27-37.

[3] Slavcheva E, Vitushinsky R, Mokwa W, Schnakenberg U. (2004): Sputtered iridium oxide films as charge injection material for functional electrostimulation. J. Electrochem. Soc., 151, E226-E237.

[4] Slavcheva E, Schnakenberg U, Mokwa W. (2006): Deposition of sputtered iridium oxide - Influence of oxygen flow in the reactor on the film properties. Appl. Surf. Sci., 253, 1964-1969.

[5] Lee IS, Whang CN, Park JC, Lee DH, Seo WS. (2003): Biocompatibility and charge injection property of iridium film formed by ion beam assisted deposition. Biomaterials, 24, 2225-2231.

[6] Ecken H, Ingebrandt S, Krause M, Richter D, Hara M, Offenhäusser A. (2003): 64-Channel extended gate electrode arrays for extracellular signal recording. Electrochim. Acta., 48, 3355-3362.

[7] Brewer GJ, Torricelli JR, Evege EK, Price PJ. (1993): Optimized Survival Of Hippocampal-Neurons In B27-Supplemented Neurobasal(Tm), A New Serum-Free Medium Combination. J. Neurosci. Res., 35, 567-576.

# Capacitive stimulation of rabbit ganglion cells in epiretinal configuration

Max Eickenscheidt[1], Günther Zeck[2], Peter Fromherz[1]

1 Max Planck Institute for Biochemistry, Department of Membrane and Neurophysics, Martinsried, Germany
2 Max Planck Institute of Neurobiology, Department of Computational and Systems Neurobiology, Martinsried, Germany

An important goal in neuroprosthetic research is safe stimulation that avoids a damage of the cells by Faraday current and irreversible electroporation. We have interfaced mammalian retina with biocompatible silicon chips with electrolyte-oxide-semiconductor (EOS) capacitors insulated with Hafnium dioxide [1]. We studied an epiretinal configuration where the ganglion cells can be brought in close contact to the capacitor.

## 1  Methods

This study utilized retinal tissue from adult rabbits as described in [2]. After removal of the eyes, the stump of the optic nerve was injected with Rhodamine dextran, which labels the ganglion cells. After 2-4 hours the retina was isolated and placed ganglion cell side down on the silicon chips. Individual ganglion cells were targeted under a fluorescence microscope and their electrical response was recorded with a tungsten electrode.

## 2  Results

We applied falling and rising voltage ramps with varying height (0 - 5 V) and duration (0.05 – 20 ms) that resulted in a purely capacitive current without Faradayic component. Depending on the strength and duration of the current, we recorded single action potentials and burst patterns that resembled the response observed with light stimulation. Falling ramps were far more efficient than rising ramps. The threshold could be described by a rheobase of about 0.45 mA/cm² and a chronaxie of about 4 ms.

## 3  Conclusion

The asymmetry of stimulation efficiency and the low threshold current suggest that the capacitive stimulation has to be attributed to a close adhesion of the ganglion cells with a high seal resistance between the capacitor and a lower attached membrane (part of the somatic membrane, initial segment of the axon). Within that geometry, falling voltage ramps may depolarize the attached membrane such that voltage-gated channels are activated there, whereas the effect on the upper free membrane (part of somatic membrane, dendritic tree) is low, in analogy to experiments with individual snail neurons on EOS capacitors [3].

**References**
[1]  Wallrapp F., Fromherz P. (2006). $TiO_2$ and $HfO_2$ in electrolyte-oxide-silicon configuration for applications in bioelectronics. *J. Appl. Phys. 99*, 114103
[2]  Zeck G., Masland R. (2007). Spike train signatures of retinal ganglion cells types. *Eur. J. Neurosci. 26*, 367-380
[3]  Schoen I., Fromherz P.(2007). The mechanism of extracellular stimulation of nerve cells on an electrolyte-oxide-semiconductor capacitor. *Biophys. J., 92*, 1096-1111

# Mi-Besan – development of neuronal biohybrid systems

Katrin Göbbels[1*], Thomas Künzel[1], André van Ooyen[2], Jens Wallys[3], Anna Reska[3], Werner Baumgartner[1], Sven Ingebrandt[3], Uwe Schnakenberg[2], Andreas Offenhäusser[3], Peter Bräunig[1]

1 Institute of Biology II, RWTH Aachen University, 52070 Aachen, Germany
2 Institute of Materials in Electrical Engineering (IWE 1), RWTH Aachen University, 52070 Aachen, Germany
3 Institute of Bio- and Nanosystems (IBN-2), Forschungszentrum Jülich, 52425 Jülich, Germany
* Corresponding author. E-mail address: goebbels@bio2.rwth-aachen.de

In the project Mi-Besan the possibility is investigated to generate a biohybrid system of networks of locust neurons cultured at low-density and a semiconductor chip. The chip will consist of sputtered iridium oxide film (SIROF) - electrodes for stimulation of, and field-effect transistors (FETs) for recording from cells. Investigations are presented that address the biocompatibility and material properties of IrOx as cell culture substrate. Two different biological test systems are used. The main focus of this work is to develop new tools for single cell analyses in neuronal networks.

## 1   Introduction

The project Mi-Besan concentrates on the development of biohybrid systems composed of defined neuron populations and semiconductor chips, which allow for simultaneous extracellular stimulation of neurons and the non-invasive recording of their activity *in vitro*. We integrate sputtered iridium oxide film (SIROF)-electrodes for stimulation [1] and field-effect transistors (FET) for recording [2] on one chip. It is essential to advance and miniaturise these micro-electronic devices. Therefore insect neurons are used as biological test system. Insect neurons have a size range of 10-120 μm enabling us to choose appropriate cell sizes for the gradual miniaturisation process of the electrodes (Fig.2a). The use of IrOx electrodes, in con-trast to established electrode materials like gold or platinum, allows for small electrode sizes and high stimulation currents in a range where no cell damage occurs. The main goal of this project is the bidirectional coupling between stimulation system, neuron, and recording system. In the long run, this will result in a new approach for the investigation of synaptic connections and analysis of communication patterns in simple neuronal networks. One prerequisite to achieve this goal is the investigation of the bio-com-patibility of the electrode material. In addition to neu-rons from locusts we used chicken neurons as second biological test system in this part of the study. Both were incubated on different IrOx [1] and evaluated with respect to cell survival and neurite outgrowth. Additionally, we investigated surface coating of IrOx. Coating could be able to shield a possible cytotoxicity effect of IrOx or generally improve neuronal growth. First stimulation experiments were done with simple, planar IrOx electrodes (Fig.1e), whereas different de-signs are planned in interaction with FETs

(Fig.1f). However, independent from chip layout, simultaneous stimulation and recording from single cells require exact positioning of cells on the electrodes in low den-sity cell culture.
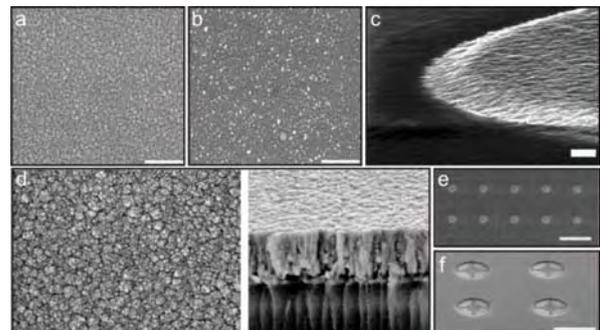


**Fig. 1.** SEM images of iridium oxide. a) Sputtered IrOx with 6.5 sccm oxygen supply to the chamber (IrO 3). b) Sputtered IrOx with oxygen supply of 13 sccm (IrO 4). c) IrOx on $SiO_2$. d) top view (left) and cross section (right) of IrOx. e) Planar IrOx electrodes. f) Planar Quad-IrOx electrodes. Scale bars: a), b), c) 500 nm; e) 100 μm; f) 100 nm.

## 2   Materials and Methods

Locust and chicken neuron cultures were prepared on different IrOx surfaces, which differ in their degree of roughness (Fig.1). Biocompatibility parameters like cell viability and neuronal growth were analysed quan-titatively by counting of living as well as fixated, im-munostained cells. Neuron-specific immu-nocytoche-mical stainings were done with antibodies against horseradish peroxidase (HRP [3]) for locust and mi-crotubuli associated protein 2 (MAP2 [4]) for chicken cells. The morphology of locust and chicken neurons was analysed qualitatively (Fig.2). Vitality of locust neurons was shown by intracellular recordings. In ad-dition, the influence of Concanavalin A (Con

A)- and Poly-D-lysine (PDL)-coating of the IrOx surfaces was investigated. Contact angle, atomic force microscopy (AFM) and enzyme kinetics measurements [5] were done to evaluate the quality of coating. Furthermore, first stimulation experiments with locust neurons on IrOx electrodes integrated on a semiconductor chip were done. Changes in the membrane potential of sti-mulated neurons were recorded via patch clamp tech-nique or intracellular recordings with sharp electrodes.
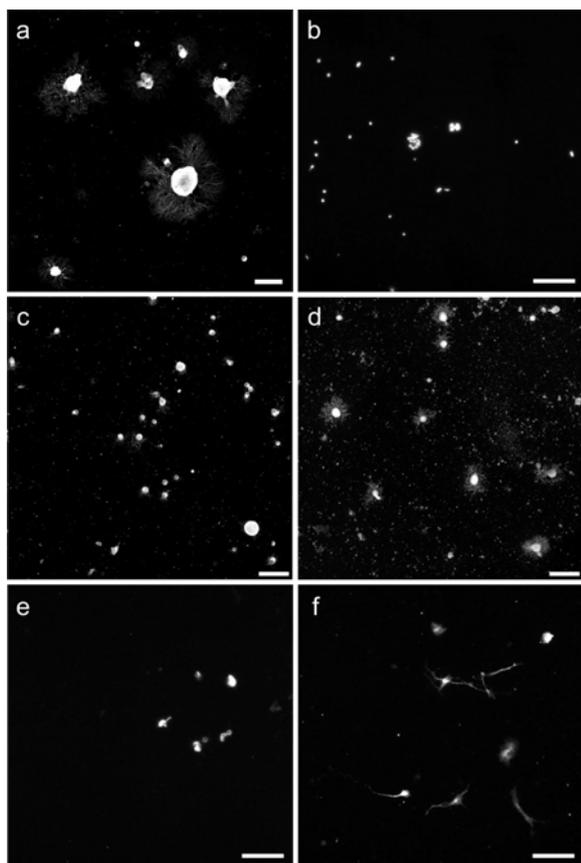


**Fig. 2.** a) Anti-HRP stained locust neurons grown on glass. b) DAPI stained nuclei of chicken cells grown on IrO 3. c) Anti-HRP stained locust neurons grown on IrO 3. d) Anti-HRP stained locust neurons grown on Con A-coated IrO 3. e) MAP2 stained chicken neurons grown on IrO 3. f) MAP2 stained chicken neurons cultured on PDL-coated IrO 3. Scale bars: a) 80μm; b), e), f) 50 μm; c), d) 40 μm.

## 3   Results and Discussion

The quantitative and qualitative analysis of the expe-riments shows IrOx to be biocompatible to locust neu-rons (Fig.2c,d). It is possible to culture chicken cells on non-modified IrOx surfaces. But compared with control experiments, the growth of chicken neurons on IrOx surfaces is inhibited (Fig.2e,f). This was shown quantitatively but also qualitatively. Cell clusters (Fig.2b) provide an indication of impaired cell adhe-sion. Furthermore, the formation of neurites was dis-turbed. Thus uncoated IrOx

shows distinctly limited biocompatibility to chicken neurons. To improve the growth of neurons from chicken, PDL-coating of IrOx surfaces was tested. A clear improvement in the overall numbers of neurons as well as neuronal outgrowth could be shown (Fig.2). The coating experiments show PDL-coated IrOx to be biocompatible to chicken neurons. Con A-coating of IrOx slightly improved growth of locust neurons (Fig.2). To summarize, insect cells are less demanding regarding the substrates they grow on. In a more de-tailed view on the coating, AFM recordings show that the amorphous structure of IrOx is undisturbed by the coating process. Contact angle measurements result in values of 90° for water on IrOx. Coating leads to more hydrophilic surfaces; Con A-coating produces contact angles of around 60° and PDL-coating results in val-ues around 80°. The enzyme marker assay provides the opportunity to produce direct evidence of the presence of Con A and PDL molecules on the IrOx surfaces, respectively. We supplied evidence for coat-ing of all test materials. Because of the rougher sur-face of IrOx in comparison to glass, more coating molecules can be found on IrOx surfaces. The bio-compatibility of locust neurons and IrOx leads to the opportunity to culture these neurons on non-modified MEAs with IrOx electrodes. Recent results show the possibility to do single cell stimulations of locust neu-rons with IrOx electrodes *in vitro*. Subsequent investi-gations concentrate on the precise positioning of lo-cust cells.

## References

[1]   B. Wessling, W. Mokwa, U. Schnakenberg (2006): RF-sputtering of iridium oxide to be used as stimulation material in functional medical implants. *J. Micromech. Microeng.*, 16, S142-S148

[2]   C. Sprössler, M. Denyer, S. Britland, W. Knoll, A. Offen-häusser (1999): Electrical recordings from rat cardiac muscle cells using field effect transistors. *Phys. Rev. E*, 60, 2171-2176

[3]   R. Loesel, S. Weigel, P. Bräunig (2006): A simple fluorescent double staining method for distinguishing neuronal from non-neuronal cells in the insect central nervous system. *J. Neurosci.. Methods*, 155, 202-206

[4]   T. Kuenzel, B. Mönig, H. Wagner, J. Mey, H. Luksch (2007): Neuronal differentiation of the early embryonic auditory hind-brain of the chicken in primary culture. *Eur. J. Neurosci.*, 25, 974-984

[5]   P. Hinterdorfer, K. Schilcher, W. Baumgartner, H.J. Gruber, H. Schindler (1998): A mechanistic study of dissociation of individual antibody-antigen pairs by atomic force microscopy. *Nanobiology*, 4, 177-188

# Modeling The Potential Field Generated By Electrical MEA Stimulations: Towards Focal CNS Stimulation

Sébastien Joucla[1,2*], Lionel Rousseau[3], Blaise Yvert[1,2]

1 CNRS, UMR5228, Bordeaux, F-33000, France
2 Université de Bordeaux, UMR5228, Bordeaux, F-33000, France
3 Université Paris EST, ESIEE, Noisy-le-Grand, France
* Corresponding author. E-mail address: sebastien.joucla@univ-paris5.fr

A nice advantage of microelectrode arrays (MEAs) is their ability to both record the activity of large neuronal populations and to deliver electrical stimulations on a high number of sites. An important issue remains to be able to control the spatial extent of microstimulations throughout the tissue. Here, we propose a new MEA design leading to an improved focalization of the potential field and its second derivatives (activating function). We first developed a finite element model to compute the extracellular potential generated in the tissue, and validated this model using experimental recordings of the potential field. We show that only current – and not voltage – stimulations allow to control the potential field irrespective of the electrode impedance. Second, using this model, we tested the field focality for different electrode configurations. While bi- and tri-polar stimulations are more focal than monopolar stimulations, these approaches generate anisotropic potential fields. This can be overcome by using concentric bipolar pairs of electrodes. However, in this case, the amount of current needed to achieve potential amplitudes comparable to the monopolar case is several tens higher. To overcome these limitations, we propose a new stimulation configuration made of a ground surface surrounding all electrodes of the array. We show that focal stimulations can be achieved with this configuration with currents comparable to the monopolar case, and that the focality of the field strongly depends on the impedance of the interface between this surface and the medium. Finally, we present a microfabricated prototype of a 60-channel MEA incorporating this new configuration.

## 1  Introduction

Extracellular electrical stimulation (EES) of the central nervous system (CNS) has been used empirically for decades, both with fundamental and clinical goals. Nowadays, microstimulation has been gaining increasing interest with the development of microelectrode arrays (MEAs), which provide an efficient tool to deliver electrical stimulations to large neural networks on many different sites, either in vivo or in vitro. Because many regions of the CNS are topographically organized (e.g., sensory and motor cortical areas or spinal motoneuronal pools), precise MEA microstimulations will benefit from a pixel-like independent addressing of focal stimulations around each given microelectrode of an array without overlapping across other electrodes. However, controlling the spatial extent of EES still remains a challenging stake.

The goal of this work is threefold. First, we validate a finite element model (FEM) to compute accurately the potential field (PF) generated by EES throughout the medium. Second, we evaluate the PF focality for different electrode configurations, and propose a new configuration to improve this focality [1]. Finally, we present the process of microfabrication and a 60-channel prototype of such an array.

## 2  Validation of FEM calculation of the potential field

We experimentally delivered monopolar stimulations between one electrode of a MEA and an external ground electrode, both in presence and in absence of neural tissue, and recorded the PF generated within the medium, with 60 other electrodes of the array (Fig. 1). We then modelled this PF using a finite element (FE) resolution of the Poisson equation ($-\mathrm{div}(\sigma\nabla V)=0$) equipped with Dirichlet ($V=V0$) or Robin ($\sigma\nabla V\cdot n+qV=qV0$) boundary conditions (BCs) on the stimulation and the ground electrodes. The first type of BCs is widely used [2] and assumes that the voltage V0 in the medium in front of an electrode is uniform. When this voltage was set to the measured metal voltage of the electrode (typically several 100 mV), the PF generated in the medium was several orders of magnitude stronger than the actual one. This was due to the fact that the electrode impedance was not taken into account. We thus adjusted the voltage of the stimulation electrode so as to best explain the experimentally recorded PF. However, such condition did not allow a perfect fit between the modeled and experimental PF (Fig. 1B, red curve). We further used Robin BCs, which take into account the surface conductance q of the electrodes and allow the potential in the medium to be non uniform in front of the electrodes. The conductances of both ground and

stimulation electrodes were optimized to best fit the experimental data. Such modeling allowed a perfect fit of the experimental recordings of the potential field (Fig. 1B, black curve).
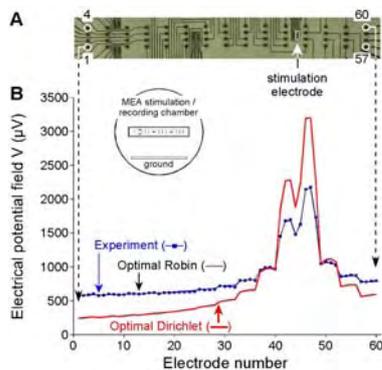


**Fig. 1.** Modeling of the potential field generated by a monopolar stimulation, using different types of boundary conditions.

## 3 New stimulation configuration

Using the FE model equipped with Robin BCs, we compared the focality of the potential field for different electrode configurations. Classical bipolar (B) and tripolar (T) stimulations focalize the PF more than monopolar (M) stimulations, but in a non-isotropic way, presenting "blind areas" near the SEs (Fig. 2A). This is overcome with a concentric bipolar (CB) configuration [3], leading to an isotropic focalization of the field. However, in this case, (1) the amount of current necessary to achieve comparable potential levels is much higher than in M, and (2) the focalization stagnates for distances beyond 100 μm.
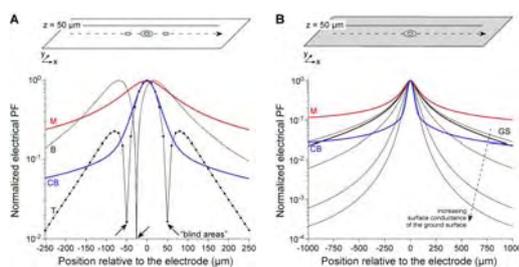


**Fig. 2.** The use of a ground surface surrounding the electrodes of the array improves the PF spatial focality better than classical multipolar configurations do.

To overcome these drawbacks, we introduce a ground surface (GS) surrounding all electrodes of the array (Fig. 2B). This configuration generates an isotropic PF whose focality is greater than in M and CB, and does not require much higher currents than in M. Moreover, by varying the surface conductance of the GS, we found that the more conductive the GS, the more focal the potential field. Especially, a strong focality would be obtained with porous materials (such as black Pt).

Similar focality results were obtained with the PF spatial second derivatives, which are the source term

of the cable equation driving the response of a neurone to an extracellular field [4].

## 4 MEA fabrication

We developed a new technology dedicated to the fabrication MEAs including a ground surface surrounding the electrodes (either a plane or a grid). Classically, the process to made MEAs is composed of 3 masking levels for the definition of: 1) the 3D microelectrodes (useless in case of 2D microelectrodes), 2) the leads connecting each microelectrode, and 3) the passivation layer, with an opening above each electrode [5]. The additionnal GS configuration only requires one supplementary masking level on which we deposit a second metallic layer above the passivation. A realization of such a Pt MEA is presented in Fig. 3. The GS is a grid to leave enough transparency.
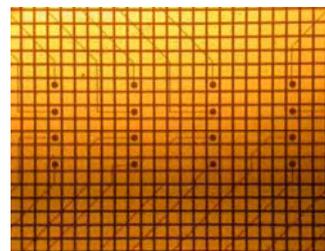


**Fig. 3.** Part of a 4×15 MEA with a grid-like ground surface surrounding all the electrodes to improve the focality of extracellular stimulations.

## 5 Conclusion

This work aimed at modeling and improving the focality of MEA stimulations. We validated a model for the computation of the potential field, and developed a new electrode configuration, which can easily be integrated on current MEA devices to stimulate neural networks with increased spatial selectivity.

**References**

[1] Joucla, S., Rousseau, L., and Yvert, B. (2007), Dispositif de stimulation d'un tissu vivant par microélectrodes, ses module amovible et utilisation. French Patent deposit No. 07-07369

[2] Mc Intyre, C.C. et al. (2004), Electrical field and stimulating influence generated by deep brain stimualltion of the subthalamic nucleus. Clinical Neurophysiology 115:589-595

[3] Edell, D.J., Wyatt, J.L. Jr., and Rizzo, J.F. 3rd (1995), Method and apparatus for preferential neuron stimulation. United States Patent 5,411,540

[4] Rattay, F. (1986), Analysis of models for external stimulation of axons. IEEE Trans Biomed Eng 33(10):974-977

[5] Rousseau, L., Perrais, V., Charvet, G., Guillemaud, R., Lissorgues, G., Meyrand, P., and Yvert, B. (2007), New high density 3D MEAs associated with an integrated electronics acquisition system (BioMEATM). Micro TAS, Paris, Poster 0481

# In vitro neuronal activity change induced by thermal effects of near-infrared laser stimulation

Gyumin Kang, Yoonkey Nam[*]

Department of Bio and Brain Engineering, KAIST, Daejeon, Korea
* Corresponding author. E-mail address: ynam@kaist.ac.kr

It has been reported that the near-infrared (NIR) optical stimulation elicited compound action potential in peripheral nervous system of rat *in vivo* and this was proposed as a new way of modulating neural activity. To test the feasibility of optical stimulation of neural networks in vitro, we flood-exposed the cultured hippocampal neuronal networks on MEAs to the continuous wave near-infrared (NIR) laser and investigated the change of spontaneous and electrically stimulated network responses. We found significant decrease of spontaneous spike rates, the change of isolated single unit spike waveforms and time-shift of evoked spikes. This is the first time to investigate the effect of NIR laser stimulation on live neural circuits *in vitro*.

## 1 Introduction

Electrical or chemical stimulation is often used to modulate the electrical activity of neuronal circuits *in vivo* or *in vitro*. Recently, infrared ($\lambda$ = 1800 nm ~ 6100 nm) based optical nerve stimulation methods have been reported as an alternative to electrical stimulation for the purpose of high resolution neural prosthetic interface designs [1]. These studies demonstrated the effect of optical stimulation by measuring evoked compound action potentials (CAP) from rat sciatic nerve or cochlear nerve [2, 3]. Here, we investigated the neural modulation effect of optical stimulation by exposing dissociated hippocampal neuronal networks on microelectrode arrays (MEAs) to near-infrared laser ($\lambda$ = 785 nm) and measuring spontaneous and evoked electrical activities [4].

## 2 Methods

Hippocampal neurons from E-18 Sprague-Dawley rat embryos were cultured in Neurobasal/B27 medium (Invitrogen) supplemented with 2 mM L-glutamine (Invitrogen), 12.5 $\mu$M glutamate (Sigma-Aldrich) and Penicillin-Streptomycin (Invitrogen). Neurons were seeded at the density of 600 cells/mm$^2$ on MEAs (200/30-ITO, MultiChannelSystems (MCS)) which were precoated with poly-D-lysine (0.1 mg/ml, Sigma-Aldrich). Cultures were maintained in an incubator with 5 % $CO_2$ and 37 °C and the half of media was replaced with fresh media every 3 ~ 4 days. Experiments took place at 24 ~ 45 DIV.

Each experiment was composed of 5 sessions each of which lasted for 10 minutes (Fig. 1). A fiber-coupled diode NIR laser ($\lambda$ = 785 nm, 1.9×10$^6$ mJ/cm$^2$, BWF1, B&WTEK) was used as a light source and it was coupled to the MEAs from the bot-

tom (Fig. 1). Spikes were detected from the high-pass filtered (200 Hz) data stream using the threshold level of – 8 times the standard deviation of the background noise. Only active channels showing firing rates over 0.1 Hz during the first baseline session were used for statistical tests. Unpaired t-tests were performed between two sets of spike rates (bin = 1 min) with and without NIR laser stimulation. P-value 0.05 was used as a significance level. To compare evoked responses, negative-positive biphasic current pulses (pulse amplitude: 12 $\mu$A, pulse width: 200 $\mu$s, stimulator STG 2004 from MCS) were applied to cultures at 1 Hz with and without NIR laser stimulation. All data are expressed as mean ± S.D..



| Session | baseline1 | NIR1 | baseline2 | NIR2 | baseline3 |
|---------|-----------|------|-----------|------|-----------|
| Laser | OFF | ON | OFF | ON | OFF |
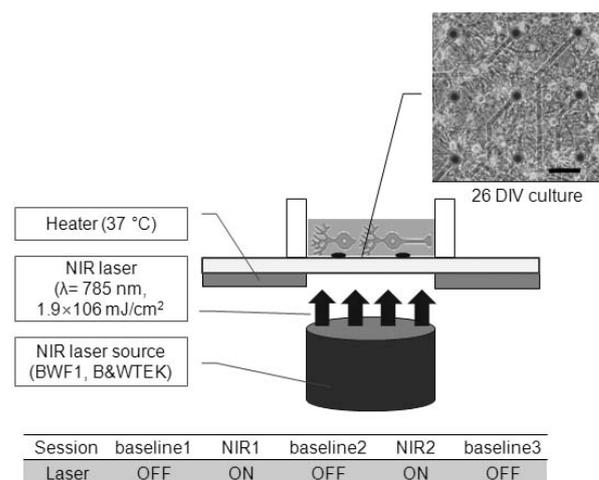
**Fig. 1.** Experimental setup of NIR laser stimulation. NIR laser covered whole culture from the bottom of the MEAs. Scale bar = 100 $\mu$m.
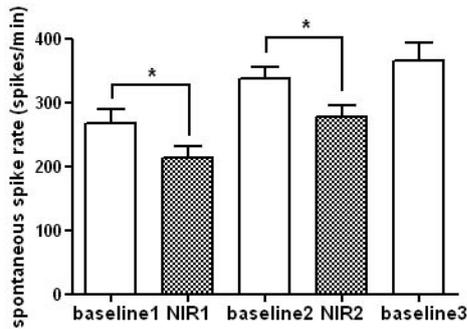
**Fig. 2.** One example of 5 consecutive sessions with and without NIR laser stimulation. Spontaneous spike rate was significantly decreased (n = 12 electrodes from 1 culture, * p<0.05).

## 3   Results

During the two NIR laser stimulation sessions, spontaneous spike rate was significantly decreased in

72.1 % (n = 204 channels from 5 cultures) and significantly increased in 4.9 % from the previous baselines consistently. After NIR laser stimulation was over, 72.1 % of channels, whose spike rate had been significantly decreased by NIR laser stimulation, showed that their spike rate turned back to the previous baseline and 27.9% showed that spike rate increased more than the previous baseline.

Spikes from active channels were sorted using principal components analysis (PCA) from Offline-Sorter (Plexon) based on their spike waveform. Among them, four single unit spikes from two cultures changed their spike waveform with NIR laser stimulation and those were significantly classified from the spike waveforms without NIR laser stimulation (p<0.05). The time for repolarization in the waveform from the group of spikes with NIR laser stimulation was shortened by 80 ~ 175 μs from the one without NIR laser and the change were quiet reversible.
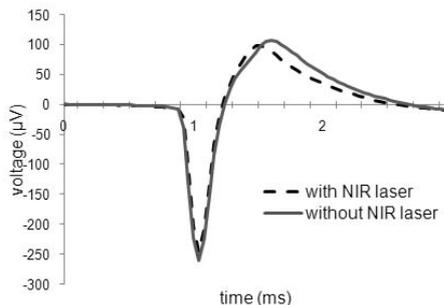


**Fig. 3.** Spike waveform change with NIR laser stimulation. Repolarization peak was shifted by 80μs. (average of 2829 spikes for with NIR laser and 2570 for without NIR laser)

The effect of NIR laser stimulation on spike timings by electrical stimulations was measured by continuous stimulation on a channel by current pulse at 1 Hz and comparing the PSTHs with and without NIR laser. From two different cultures, the first spikes that was precisely timed to the stimuli was shifted closer to the stimuli by 0.20 ± 0.19 ms (n = 38 channels) with NIR laser stimulation.

## 4   Conclusion

In vitro NIR laser stimulation induced several changes in neural activity of cultured neuronal networks. First, many active channels showed decreased firing rates during while the whole culture was exposed to NIR laser. Second, we detected a reversible consistent change of spike waveforms from some channels implying the NIR laser effect at the level of action potential generation. Third, there was the shift of spike timing of the electrically evoked action potentials due to NIR laser. We were able to reproduce these effects by raising the culture plate temperature by 4 °C, which strongly suggests that the thermal energy of NIR laser was dominant in our experiment. However, NIR laser stimulation was reversible and seemed not to affect the viability of the neuronal network. We expect that a NIR stimulus can serve as one method to suppress neuronal activity and also to go side by side with an electrical pulse to modulating neuronal activity.

**References**

[1]   J. Wells, C. Kao, E.D. Jansen, P. Konrad, and A. Mahadevan-Jansen (2005): Application of infrared light of in vivo neural stimulation, J. Biomed. Opt., vol. 20, no. 6, 064003

[2]   A. D. Izzo, J. T. Walsh, E. D. Jansen, M. Bendett, J. Webb, H. Ralph, C. P. Richter (2007): Optical parameter variability in laser nerve stimulation: a study of pulse duration, repetition rate, and wavelength, *Biomedical Engineering, IEEE Transactions on* , vol.54, no.6, 1108-1114

[3]   J. Wells, C. Kao, P. Konrad, T. Milner, J. Kim, A. Mahadevan-Jansen, and E. D. Jansen (2007): Biophysical mechanism of transient of optical stimulation of peripheral nerve, Biophys. J., vol. 93, 2567-2580

[4]   D. A. Wagenaar, J. Pine, and S. M. Potter (2004) : Effective parameters for stimulation of dissociated cultures using multi-electrode arrays, J Neurosci Methods, 138, 27-37

# Coil design optimization for magnetic stimulation of neural tissue cultures on MEAs

Michele Nicoletti[1], Jochen F. Meyer[1*], Thomas Weyh[2], Tiffany N. Kinney[1],
Florian Ilchmann[2], Guenter W. Gross[3], Bernhard Wolf[1,2],

1 Technische Universität München, Zentralinstitut für Medizintechnik Imetum, Garching, Germany
2 Technische Universität München, Heinz Nixdorf-Lehrstuhl für medizinische Elektronik, Munich, Germany
3 University of North Texas, Department of Biological Sciences, Denton, TX, USA
* Corresponding author. E-mail address: meyer@tum.de

New therapeutic approaches involving transcranial magnetic stimulation (TMS), e. g. in pain management, are currently being investigated. Using electrophysiological recording technology on multielectrode-arrays (MEAs), the responses of spinal cord and frontal cortex neuronal networks to pulsed magnetic fields were investigated. So far, we have shown that certain stimulation patterns can cause a significant shift in activity. The field strengths used are sub-threshold and do not elicit action potentials directly, which renders the effects unexplainable by the standard neuron model. A new stimulation coil was developed and miniaturized to enable simultaneous fluorescence microscopy of the cell cultures grown on MEA-glass chips. For this purpose, the coil design was optimized for a maximum electrical field gradient. The axonal morphology was taken into consideration in the simulations. The new coil will be used to analyze the effects of pulsed magnetic fields in depth.

## 1 Introduction

### 1.1 TMS

Transcranial magnetic stimulation (TMS) is a non-invasive medical technique that was first utilized by Barker in 1985 [1]. In recent years, it has contributed considerably to research trying to elucidate certain mechanisms in the human brain. As an instrument in diagnostics, it has been gaining importance in clinical and scientific studies. In addition, its therapeutic applications are becoming increasingly popular, while traditional, often painful electrical stimulation techniques are losing their appeal. In particular, the non-invasive, selective modulation of brain activity is a promising, new approach with high potential for future applications.

### 1.2 Physical and technical basics

Basser & Roth [2] introduced the first models for the electromagnetically induced neuronal stimulation. They were derived from the cable equation and are based on the assumption that only the field components parallel (axial) to the axon [4] (~$10^7$ V/m) are responsible for the innervation in TMS. The radial field components (ca. ~$10^3$ V/m) do not play a significant role. According to the model of Hodgkin & Huxley, an axon follows a differential relation.

### 1.3 Constraints of construction

Limited space on the stage of a fluorescence microscope does not allow conventional, large coils to be used. Thus, a ferrite core coil had to be optimized

to meet the requirements for the electromagnetic field characteristics.

## 2 Materials and methods

### 2.1 Adjustment of the field geometry

To improve the field characteristics, the model was broken down into its functional parts and treated as a magnetic circuit. The optimal parameters were deter-mined through a numerical FEM (finite elements method) simulation.

After reviewing the magnetic circuit, the magnetic resistance was reduced by incorporating a field guiding core. Since the field required for the stimulation is really the stray field from the ferrite apex, guiding the field additionally amplifies the field gradient and limits the dispersion of the field. A handy side effect of this limitation is the protection of the neighbouring electronic measuring equipment.

### 2.2 Enhancing the magnetic flux density

A high magnetic flux density at the location of the cell culture is essential for a sufficiently strong electric field. The second Maxwell-equation states that the magnetic flux density B [T] is proportional to the induced electric field E [V/m]. Thus, two parameters of the coil design became most important: The apex radius which determines the penetration depth of the B-field, and the apex angle which influences the focusing of the field. In figure 4, both parameters are plotted against each other. The increment is the respective production tolerance. Obviously, the

magnetic flux density B possesses a local maximum, which determines the optimal parameters for this coil geometry (r = 2,5 mm; α = 52°). The next optimization step was to create a field gradient that grows along the ferrite structure and remains that way up to the tip of the apex. For this purpose, a surrounding gradient coil was incorporated (see fig. 1, left).
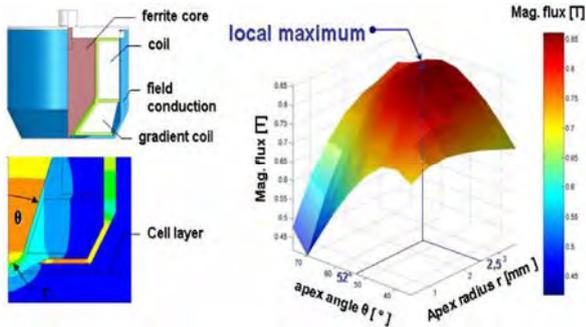


**Fig. 1.** The maximum flux density B [T] at a distance of 1 mm from the ferrite core as a function of the apex angle and the apex radius.

## 2.3 Field gradients of the coil

The fields determined by the simulations were implemented in a neuron model. Consequently, the results from the FEM analysis were transformed into field sizes decisive for the stimulation (see fig. 2).
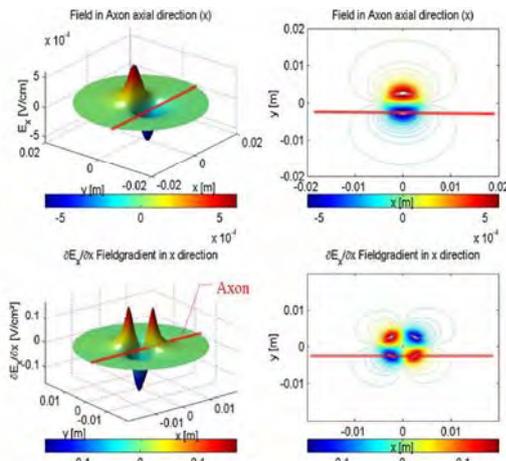


**Fig. 2.** Axial (x-direction) field component of the induced E-field (red line: axon, 3D and contour plot) and respective field gradients.

## 2.4 Field gradients from the axonal morphology

To estimate the influence of the axonal morphology on the generation of an action potential, the field gradient was computed with relation to the curvature of an axon. The maximum E-field created by the coil was assumed to be constant in the vicinity of the curvature. Figure 4 shows that the maximum field gradient is achieved at a curvature of 90°.
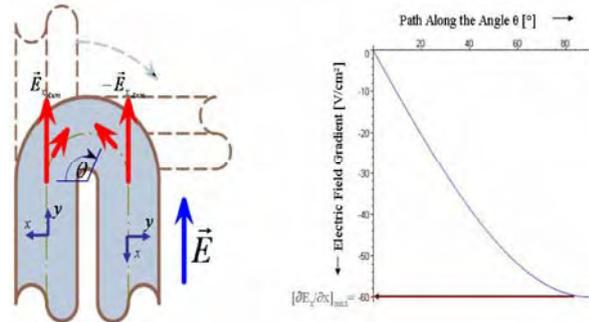


**Fig. 3.** The field gradient depends on the curvature angle.

## 3 Results

The investigations on the model imply that the morphology of the cells plays a much greater role in eliciting an action potential than the field geometry of the stimulation coil in the case of the coil investigated here by a factor of ~100. This is explained by the different dimensions of the structures creating the field gradient. While the coil's crucial parameter is the curvature of the ferrite apex [mm], the axonal morphology is determined by the curvature of the axon [$10^{-2}$mm]. The field gradients simulated here can be excluded from being capable of directly eliciting action potentials. However, sub-threshold inhibitory effects of the applied fields on cell cultures were measured. This effect was shown to be repeatable at burst frequencies between 1 and 5 Hz.

## 4 Discussion

We have shown that a stimulation coil miniaturized to our requirements cannot elicit action potentials directly. However, the therapeutic possibilities that are emerging from magnetically induced sub-threshold activity modulation seem worth pursuing. The research on cell cultures is an important first step towards understanding the relation between certain stimulation sequences and the resulting neural activity shifts. Possible applications of a non-invasive activity modulation include treatment of epileptic seizures as well as pain management.

**References**
[1]  A. T. Barker, R. Jalinous (1995): Non invasive magnetic stimulation of human motor cortex. Lancet, 1, 1106 – 1107
[2]  P. J. Basser, B. J. Roth (1991): Stimulation of a myelinated axon by Electromagnetic Induction. Med & Biomed Eng & Comput., 29(3), 261 – 268
[3]  L. G. Cohen, S. Bandinelli (1988): Noninvasive mapping of human motor cortex with magnetic stimulation. Neurology. 38, 386 - 387

# Interfacing Networks Of Insect Neurons With Electronic Devices

Anna Reska[1], Jens Wallys[1], Peter Gasteier[2], Katrin Göbbels[3], Petra Schulte[1], Peter Bräunig[3], Martin Möller[2], Jürgen Groll[2], Andreas Offenhäusser[1*]

1 Juelich Research Center, Juelich, Germany
2 DWI e.V. and Institute of Technical and Macromolecular Chemistry, RWTH Aachen, Aachen, Germany
3 Institute of Biology II, RWTH Aachen University, 52070 Aachen, Germany
* Corresponding author. E-mail address: a.offenhaeusser@fz-juelich.de

Sensory mechanisms of insects use highly specific and complex neuronal information processing. These systems are extraordinarily efficient. Therefore, mimicking these processes in biohybrid sensors by coupling a neuronal network of interest onto an electronic device could enhance the function of these devices. For such applications, these biological systems have to be well characterized. Monitoring developmental events like recovery of axonal growth and synaptogenesis is best performed non-invasively and over a large time-scale. Therefore, using extracellular recording devices such as MEAs is particularly suitable for these studies. To rebuild a simplified copy of a neuronal circuit *in vitro*, an artificial environment was designed to control precisely the neuronal adherence and growth. The MEA surfaces were coated with a six-armed star-shaped poly (ethylene glycol)-based polymer layer as an aversive background combined with the cell adhesive lectin concanavalin A (con A). Primary insect neuronal cells were cultured up to two weeks onto these surfaces building defined networks on the prepared patterns. Preliminary extracellular stimulations of single neurons were successfully achieved with locust neurons seeded onto uncoated MEAs.

## 1  Introduction

Within the animal kingdom, insects have evolved a particularly well-adapted sensory system based on straight-forward neuronal circuits consisting of only a few specialized neuron types. The locust jump, for instance, is controlled by tens of neurons within the neuronal network in the metathoracic ganglion. Another example is a specialized circuit of neurons in the terminal abdominal ganglion of the cricket that controls its highly sensitive, hair-based wind-evoked escape reaction. Because of the highly efficient information processing within this circuit, the cricket is able to detect air movements as small as thermal noise [1]. Investigating this network is part of the EU project CILIA (Customized Intelligent Life-inspired Arrays).

To rebuild a simplified copy of a neuronal circuit *in vitro*, the presented artificial environment should be designed to control precisely the neuronal adherence and growth. One of the core challenges in the design of biosensors and biohybrid devices is developing universal strategies for covalently attaching biomolecules to solid-state components [2]. For this purpose, a special surface coating of adherent binding sites in spatially controlled, non-fouling background has been developed on glass surfaces yielding geometrically-confined cellular networks on artificial surfaces [3]. Two-neuron functional networks of cricket neurons were generated on such pre-patterned networks on glass slides. The synaptic connectivity was proven by double patch-clamp recordings. The surface coating procedure was then transferred to standard glass MEAs with gold electrodes [4] for extracellular recording of insect neuronal networks to allow for non invasive network investigation.

## 2  Materials & Methods

### 2.1 Star PEG /conA coating

The MEA devices were cleaned with isopropanol, activated with methanol and hydrochloric acid (ratio 1:1). The six-armed star-shaped poly(ethylene glycol)-based pre-polymers terminated with isocyanate functional groups (star-PEG) were diluted in tetrahydrofuran (100mg/ml) and a tenfold volume of MilliQ water. After pre-crosslinking of 5 minutes, about 100 µl of solution was pipetted onto the MEA chip fixed to a custom built retainer. The substrates were spun for 40 seconds at 2500 rpm. The star PEG layer was crosslinked for another 90 minutes before a pattern of concanavalin A, a cell adhesive lectin protein, was coupled by microcontact printing with PDMS stamps using a fine-placer for pattern alignment to the MEA electrodes [5].

### 2.2 Neuronal preparation and recordings

For our experiments, neurons from the metathoraic ganglion of locusts and from the terminal abdominal ganglion of crickets were isolated by mechanical and

enzymatic dissociation and then cultivated in modified L15 medium on MEAs. After three to five days of *in vitro* culture, single neurons were extracellularly stimulated by biphasic pulses produced by a single electrode of the array while the cellular response was simultaneously recorded by means of standard patch-clamp technique.

# 3  Results and Discussion

Successful transfer of the patterning procedure to the MEA surface (fig.1) allows for better control of neuron position and identification of neuronal connection during stimulation and recording experiments.
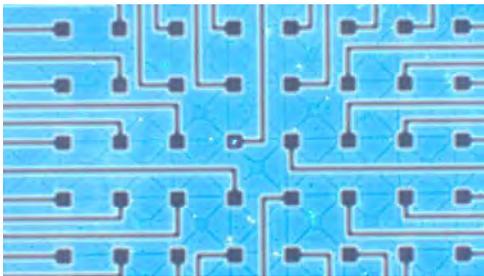


**Fig. 1.** Concanavalin A aligned printed pattern on star PEG precoated MEA device (electrode distance 100μm, patterns of 20-30μm node diameters with 2-8μm line widths have been used).

Although the alignment of the pattern nodes to the electrodes on the array has an accuracy less than 1μm  (fig.1), it remains problematic that the neuron cell bodies are attached only via a small area of the cell membrane (as shown with TIRF experiments), and thus the cell bodies often attach not only to the node areas prepared on the electrodes but also to the connecting lines meant for axon pathfinding (fig.2).
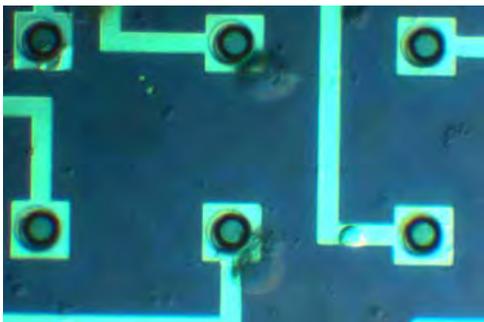


**Fig. 2.** Cricket neurons seeded on prepatterned MEA surface after 6 days in vitro (electrode distance 100μm).

In future experiments, we will investigate whether this finding could be used as an advantage to stimulate the neurons in the area of the axon hillock, which is the region of the neuron where the action potential is formed *in vivo*.

As seen in the recording shown in fig.3, locust neurons have been successfully stimulated extracellularly via a MEA electrode. Two rectangular bi-phasic voltage pulses (amplitude of 1 V and frequency of 10 kHz) were applied to the respective microelectrode. The stimulation led to high capacitive transients of the neuron membrane voltage directly after the stimulation pulse. The amplitude of the capacitive transients is higher than the amplitude of the action potential; however, a clear action potential due to extracellular stimulation can be seen. Further characterization of this stimulation system is necessary.
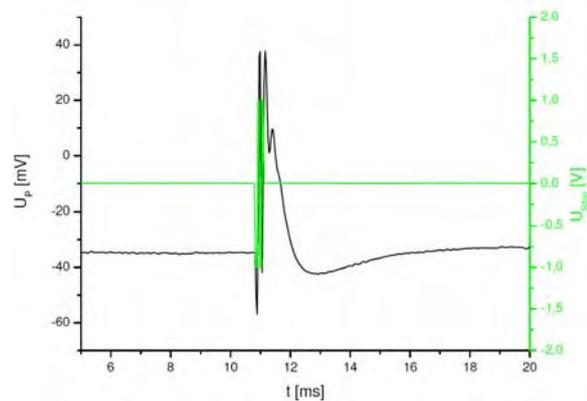


**Fig. 3.** Extracellular stimulation pulse (green) with the evoked action potential from a locust neuron (black).

Stefan Eick is currently working on intergrating stimulation and recording within a single device. In future insect neuronal networks will be applied to these devices and incorporated with artificial sensory systems, such as photolithographic hair arrays, leading to the development of novel biosensor devices.

## References

[1] Shimozawa 2003, Wien NewYork. p. 145-157.
[2] Medintz, I. et al. Nat. Mat. 5, 842 (2006)
[3] Reska A. Gaste,ier P., Schulte P., Moeller M., Offenhäusser A., and Groll J., Adv. Mat 2008, accepted
[4] Ecken, H., Ingebrandt, S., Krause, M., Richter, D., Hara, M., and Offenhäusser, A. Electrochim. Acta 48 (20-22), 3355–3362 (2003).
[5] Lauer, L., Ingebrandt, S., Scholl, M., and Offenhäusser, A. IEEE Trans Biomed Eng 48(7), (2001) 838–842.

# Opening of Ca$^{2+}$ channels by repetitive extracellular stimulation from capacitors to control intracellular Ca$^{2+}$ levels.

Kerstin Scheidt, Peter Fromherz*

Max Planck Institute of Biochemistry, Department of Membrane and Neurophysics
* Corresponding author. E-mail address: fromherz@biochem.mpg.de

Hybrid systems of neuronal networks and micro-electronic chips may be used to elu-cidate network processes like learning and memory. A prerequisite is a well defined and controlled outgrowth of the neu-rons that constitute the network. We want to im-plement this control electrically from a silicon chip: opening of voltage dependent Ca2+ channels (VDCCs) by extracellular capacitive stimulation is our tool to manipu-late the intracellular Ca2+ level that is known to play a decisive role in neuronal out-growth. The basic requirement for this approach is the feasibil-ity of capacitive open-ing of VDCCs. As a model sys-tem, we used HEK293 cells transfected with L-type Ca2+ channel Cav1.2. Capacitive gating of Cav1.2 channels was studied by whole cell voltage clamp and current clamp recordings. In addition we detected the incom-ing Ca2+ ions by Fura-2 fluorescence micros-copy and showed that the intracellular Ca2+ concen-tration of the cells was greatly enhanced by repetitive capacitive chip stimulation. The results provide the basis for work on neuronal outgrowth.

# Heart

# Progress in stem-cell based therapy and tissue engineering strategies for the treatment of cardiac dysfunction

Lior Gepstein

Faculty of Medicine, Technion, Haifa, Israel

**Keynote Lecture**

# Modulation of Cardiomyocyte Electrical Properties by Regulated BMP-2 Expression

Carlota Diaz[1,2], Urs Frey[1], Jens Kelm[3], Andreas Hierlemann[1*], Martin Fussenegger[2*]

[1] ETH Zurich, Department of Biosystems, Science and Engineering, Basel, Switzerland
[2] ETH Zurich, Institute for Chemical and Bioengineering, Zurich, Switzerland
[3] Clinic of Cardiovascular Surgery, Zurich University Hospital, Zurich, Switzerland
* Corresponding authors. E-mail address: fussenegger@chem.ethz.ch

Since cardiomyocytes lose their ability to divide after birth, any subsequent cell loss or dysfunction results in pathologic cardiac rhythm initiation or impulse conduction. Strategies to restore and control the electrophysiological activity of the heart may, therefore, have a great impact upon the regeneration of cardiac tissue functionality. Using lentivirus-derived particles to regulate the bone morphogenetic protein-2 (BMP-2) gene expression in a pristinamycin-inducible manner, we demonstrated the adjustment of cardiomyocyte electrophysiological characteristics. CMOS-based high-density microelectrode arrays (HD-MEAs) were used to monitor the electrophysiological activity of neonatal rat cardiomyocytes (NRCs) cultured either as monolayers (NRCml) or as microtissues (NRCmt).

## 1 Background/Aims

Cardiomyocytes are responsible for heart contractions and are the dominant cell type in the normal heart with respect to volume. Irregularities in the heartbeat, due to cardiac electrical dysfunction, are one of the most frequent causes of mortality and morbidity in today's industrialized society. There is, accordingly, a compelling need to move clinical studies toward cardiac regenerative strategies aimed at improving cardiac functionality. This will require more complex *in vitro* models that enable the study and assessment of how potent therapeutic genes, related to heart functionality, impact cardiac electrophysiological irregularities [1].

## 2 Methods/Statistics

A CMOS (complementary metal oxide semiconductor)-based high-density microelectrode array (HD-MEA) [2], featuring a reconfigurable routing for an almost arbitrary set of 126 from a total of 11'000 electrodes was used to record electrical cardiomyocyte activity in real time. In order to modulate the electrogenic properties of cardiomyocytes we selected lentivirus-derived particles to regulate the bone morphogenetic protein-2 (BMP-2) gene expression. BMP-2 was originally identified as a molecule that induces bone and cartilage formation, but today it is considered a multifunctional cytokine also involved in cardiac differentiation and functionality [3].
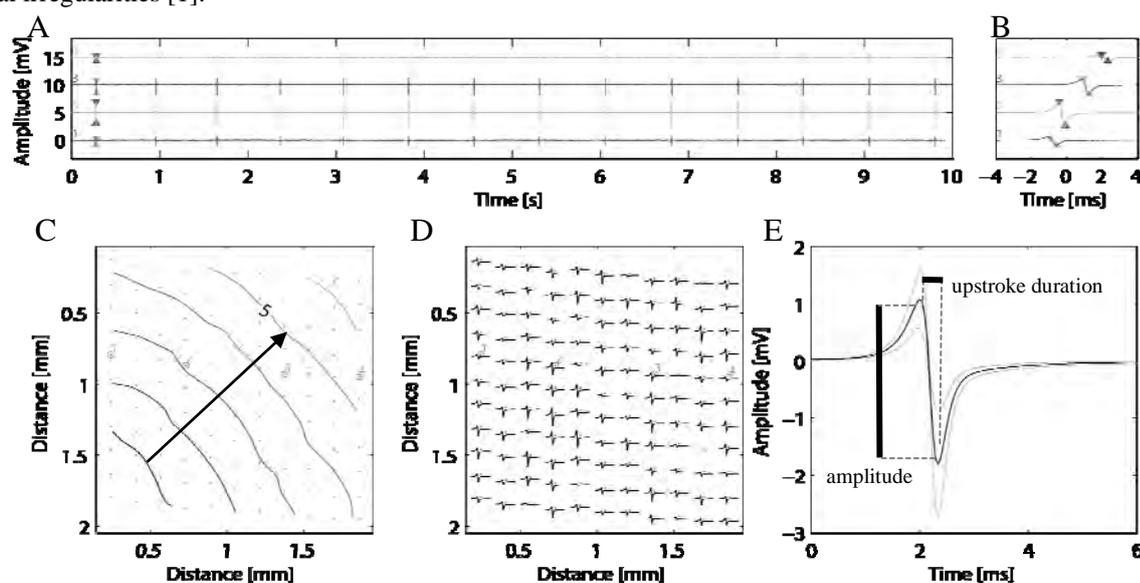


**Fig. 1.** Electric activity recordings of cardiomyocytes cultured for 5 days on HD-MEAs

Statistical significance of the recorded data was assessed by one-way analysis of variance (ANOVA) followed by a Tukey post-hoc test (Software: Systat 12 for Windows).

## 3 Results

A typical HD-MEA-based electrogram plot, generated during the spontaneous activity of contracting cardiomyocytes, shows a frequency of $1.4 \pm 0.05$ Hz (Fig. 1A). Activation maps show the direction of the excitation spread and indicate the propagation velocity ($322 \pm 8$ mm/s) within the cultures (Fig. 1C). Figure 1D shows the average signal shape per channel aligned in time. The average peak-to-peak amplitude was $2.8 \pm 1.3$ mV, and the duration of the AP upstroke (depolarization time), which is the time from maximum to minimum peak, was assessed to be $0.35 \pm 0.05$ ms (Fig. 1E). Additionally, the origin of the excitation can be determined (Fig.2). While the origin of the excitation shows a waveform with only a negative peak, (asterisk in Fig. 2B) action potentials with a negative peak preceded by a positive one indicate subsequently excited cells. We genetically modified cardiomyocytes and cardiac-like microtissues (Fig. 3), recorded the associated changes in the electrophysiological characteristics, and validated this system for gene/cell therapeutic applications.
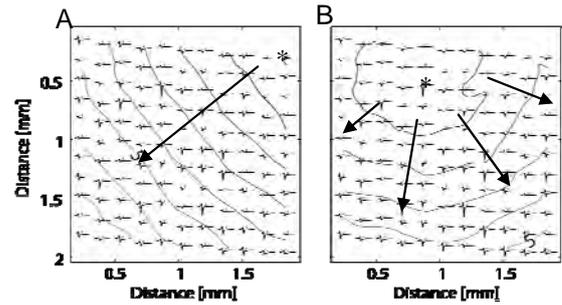


**Fig. 2.** Electrical potential shapes at the origin of excitation and in adjacent areas.
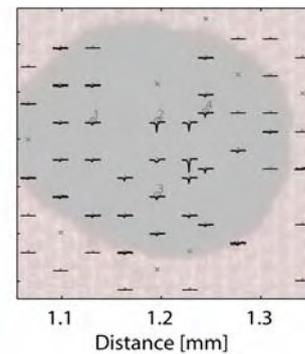


**Fig. 3.** Average signal shape from each electrode adjacent to cardiac-like microtissue.
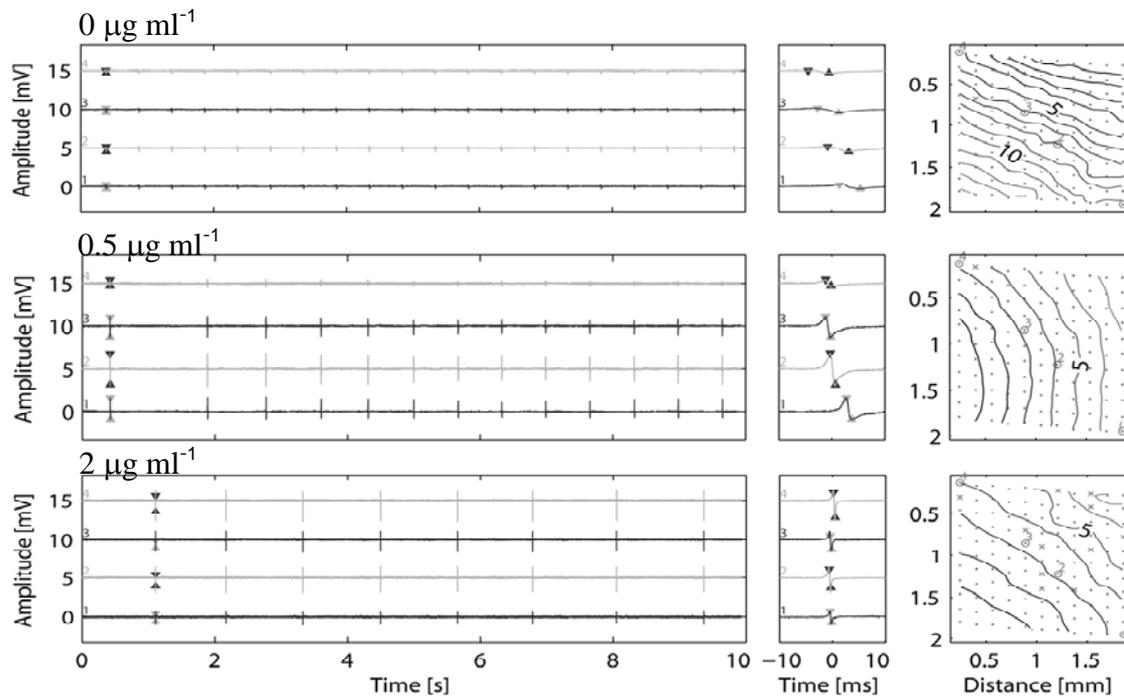


**Fig. 4.** Tuneable electrophysiological properties through BMP-2 regulation at different PI concentrations.

We used an antibiotic (pristinamycin I, [PI]) regulation system to modulate the expression of BMP-2 and thus to control the respective cardiac electrophysiology (Fig.4).

## 4. Conclusions/Summary

To date, proof of electrophysiological control of cells through heterologous synthetic regulation systems was lacking. The electrophysiological control of cardiac cells in HD-MEAs offers the possibility to measure functional effects in real time, thus providing insights and a ready-to-use tool for gene-function studies and for the future discovery and preclinical evaluation of novel genes with potential therapeutic effects. In this case, modulation of cardiac electrogenic activity by regulated BMP-2 expression has been demonstrated, which may represent an important therapeutic avenue in the future treatment of heart failure when insuficient beating frequency compromises cardiac function.

### References

[1]   Stett, A., Egert, U., Günther, E., Hofmann, F., Meyer, T., Nisch, W. and Hämmerle, H. (2003): Biological application of microelectrode arrays in drug discovery and basic research. *Analytical and Bioanalytical Chemistry 377, 486.*

[2]   Frey, U., Sanchez-Bustamante, C.D., Ugniwenko, T., Heer, F., Sedivy, J., Hafizovic, S., Roscic, B., Fussenegger, M., Blau, A., Egert, U. and Hierlemann, A. (2007): Cell recordings with a CMOS high-density microelectrode array. *Conf. Proc. IEEE EMBS Meeting, Lyon, France, 167.*

[3]   Wang, Y.X., Qian, L.X., Liu, D., Yao, L.L., Jiang, Q., Yu, Z., Gui, Y.H., Zhong, T.P. and Song, H.Y. (2007): Bone morphogenetic protein-2 acts upstream of myocyte-specific enhancer factor 2a to control embryonic cardiac contractility. *Cardiovascular Research 74, 290.*

# An *In Vitro* Method For Detecting Potential Proarrhythmic Properties Of New Chemical Entities: A Novel Analytical Approach For Characterising Cardioactive Drug Effects

Bryant S*, Broadbent S, Wyllie C, Kotiadis W, Palmer R, Parsons A, Heal R, Demmon J, Nicol S.

VivoMedica (UK) Ltd, Sittingbourne, UK
* Corresponding author. E-mail address: simon.bryant@vivomedica.com

Existing assays that screen for hERG activity are often used for predicting QT prolongation but may not be predictive of proarrhythmic risk. The use of cultured cardiac myocytes in conjunction with microelectrode array (MEA) technology and a proprietary waveform analysis methodology is a novel in vitro screening tool for detecting drug-induced changes in cardiac electrophysiology. The aim of this study was to investigate the novel DrugPrint® analysis method for quantifying drug-induced changes in the spontaneous field action potentials (sfAP) recorded from cardiac myocytes. IKr blockers increased the duration of the sfAP waveform causing a rightward shift in the centre of gravity. In contrast, ICa blockers decreased duration and profile area of the sfAP waveform causing a leftward shift in the centre of gravity. However INa blockers such as lidocaine primarily decreased spike amplitude without significantly effecting sfAP duration. Proarrhythmic compounds such as astemizole disrupted the normal rhythmic beating activity observed under control conditions. These data demonstrate that DrugPrint® was able to discriminate between different modes of drug action and identify potential proarrhythmic activity. As such we propose that the system is a suitable model for in vitro screening providing a more integrated approach to the assessment of drug effects on cardiac physiology.

## 1 Introduction

DrugPrint® is an integrated system for testing pharmaceutical lead compounds at an early stage of their development lifecycle for potential cardiotoxic side effects, in particular harmful delays in ventricular repolarisation.

Using a combination of whole-cell biology, microelectrode array technology (MEA) and sophisticated waveform analysis, DrugPrint® provides a poweful experimental / analysis package that can identify potential drug-induced changes in cardiac function across the full range of native cardiac ion channels.

The use of cultured cardiac myocytes in conjunction with microelectrode array (MEA) technology is a novel *in vitro* screening tool for detecting drug-induced changes in cardiac electrophysiology which provides a more integrated approach to the assessment of drug effects on cardiac physiology [1,2].

## 2 Materials and Methods

### Myocyte preparation: Cell Culture

Embryonic (d19) rat cardiomyocytes were isolated using standard enzymatic techniques and seeded onto MEAs at a concentration of $\sim.0.5 \times 10^6$ cells/ml. Cardiomyocytes were grown to confluence in Ham's F10 (435ml nutrient mix supplemented with 10% Foetal Bovine Serum (FBS)). Cells were kept in a standard incubator with an air:5% $CO_2$ mix at 37°C.

### Electrophysiology

Microelectrode arrays of a standard 8x8 configuration and composition (indium tin oxide, 30µM diameter and 200µM spacing, Scientifica 200/30iR-ITO-gr) were used in conjunction with a 60 channel amplifier (Scientifica MEA-1060-BC). Extracellular voltage measurements were digitised at 10 kHz and recorded using DrugPrint® proprietary software.

For the duration of the experimental recordings MEAs were covered with a gas permeable membrane (fluorinated ethylene-propylene, ALA Scientific Instrument MEA-MEM) secured by a Teflon bath housing and housed in an environmentally controlled chamber (Plas-Lab 850-LCS) saturated with an air:5%

$CO_2$ mix and maintained at $36\pm1°C$. The MEAs were covered with 1ml Ham's F10 with 10% FBS, under static flow conditions.

Electrical activity of normal cardiac function is recorded in the form of a spontaneous field action potential (sfAP), an extracellular recording that represents the transmembrane action potential. The analysis algorithms of DrugPrint® have been optimised to compare the profile characteristics of the sfAP waveform recorded under control conditions to that recorded in the presence of the test substance.
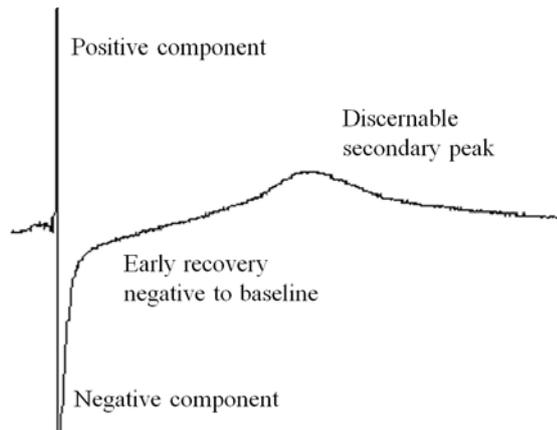


**Fig 1.** Characteristics of the profile of a typical sfAP waveform.

Specific baseline characteristics of a normal sfAP are shown above [2,3]

## 3 Results

### 3.1 Effect of Dofetilide and Nifedipine on sfAP

In contrast to adult rats, experimental studies indicate that $I_{Kr}$ is functional in the rat embryo; class III antiarrhythmics have been demonstrated to elicit concentration-dependent prolongation of the foetal action potential duration [4]. We report that dofetilide increased sfAP duration in a does-dependent manner. In the presence of 60 nM dofetilide sfAP duration was increased by $68\pm11\%$ from $118\pm4$ ms to $199\pm13$ ms (red trace, n=4, $P<0.001$). A similar prolongation of sfAP was induced by the application of other $I_{Kr}$ blockers astemizole ($73\pm15\%$), E-4031 ($31\pm7\%$) and sotalol ($54\pm12\%$).

In contrast nifedipine caused a dose-dependent shortening the duration of the sfAP waveform. In the presence of 300 nM nifedipine sfAP duration was shortened by $28\pm1\%$ from $125\pm12$ ms to $90\pm8$ ms (red trace, n=4, $P<0.05$). A similar shortening of sfAP was induced by the application of other $I_{Ca}$ blockers verapamil ($33\pm3\%$), amlodipine ($32\pm7\%$) and diltiazem ($40\pm3\%$).
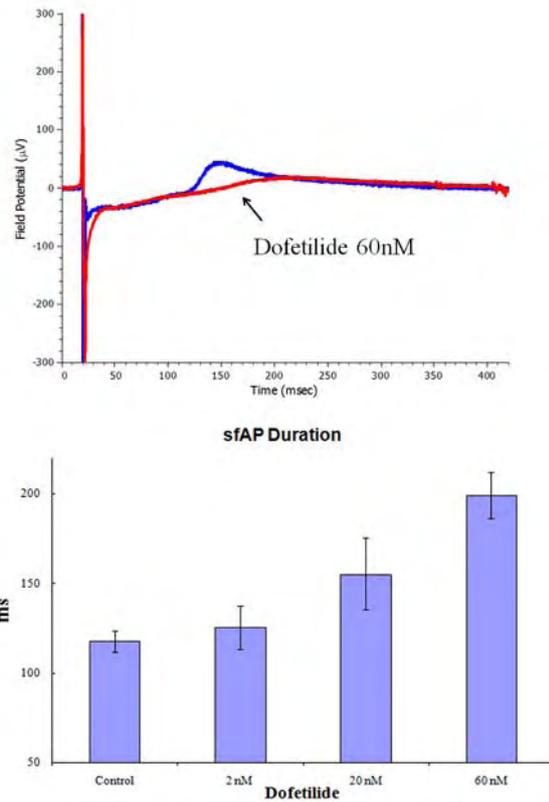


**Fig.2** The effect of dofetilide on the profile of the sfAP waveform.
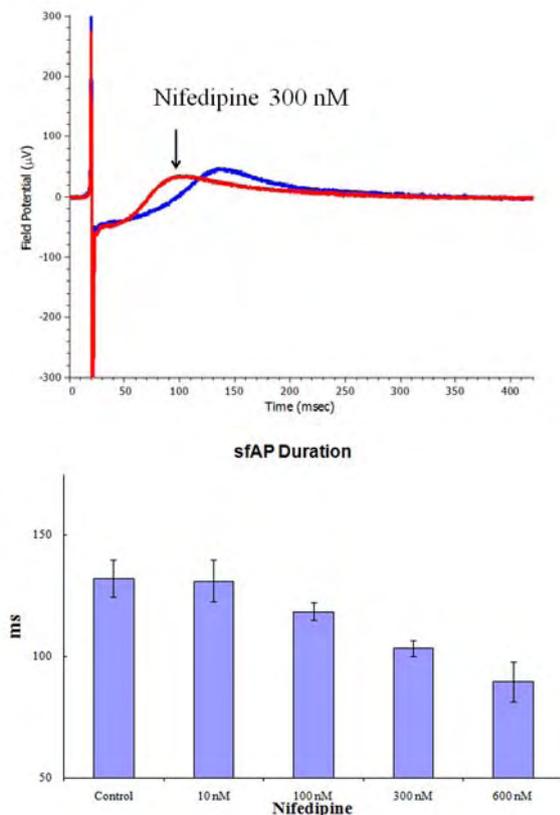


**Fig.3** The effect of nifedipine on the profile of the sfAP waveform.

## 3.2 Effects of $I_{Kr}$, $I_{Ca}$, $I_{Na}$ and $I_{to}$ blockers on sfAP

We have examined the effects of an initial data set of specific ion channel blockers, with well defined actions on cardiac electrophysiology, on the profiles of the sfAP. Mean data for the effects of these compounds on sfAP duration are summarised in figure 4.

These data show that the $I_{Kr}$ blockers prolonged sfAP and the $I_{Ca}$ blockers shortened sfAP duration. sfAP duration was prolonged by the class 1a antiarrhythmics and not significantly altered by the class 1b anitarrhytmics. The $I_{to}$ blocker 4AP prolonged sfAP duration.
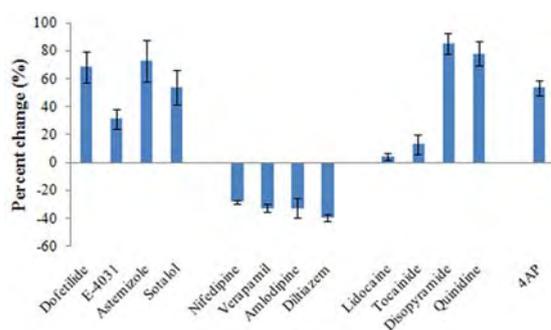


**Fig 4.** Effects of specific ion channels blockers on sfAP duration.

## 3.3 DrugPrint® feature changes

The analysis algorithms of DrugPrint®, have been designed to compare the profile of the sfAP waveform recorded under control conditions to that recorded in the presence of the test substance. The algorithms compare the information contained within the profiles of the sfAP waveforms in a number of different ways that include: measurements of specific individual components of the waveform profile such as spike amplitudes and profile areas; changes in the whole of the waveform that are given a directional polarity such as radius of gyration; and changes over the total waveform that are unidirectional such as wavelet analysis. An example of each is shown below.

**Effects of the compound data set on spike amplitude**

An example of a measure of a specific component of the sfAP waveform profile would be the effects of the ion channel blockers on the peak amplitude of positive component of the initial spike complex. The four $I_{Na}$ blockers caused a significant decrease in this parameter, with the decrease being most pronounced with the class 1b antiarrhythmics. $I_{Ca}$ blockers also caused a reduction in this parameter suggesting that both sodium and calcium channel activity contribute to this feature.
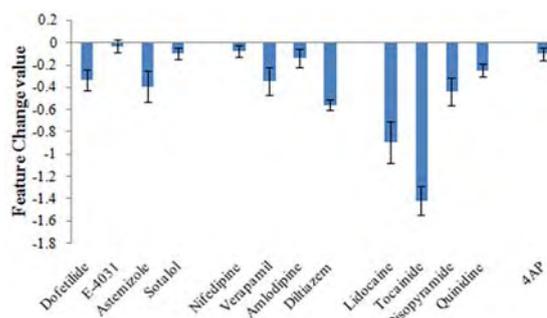


Fig 5. Feature change values for parameter 3 Peak level.

**Effects of the compound data set on absolute profile recovery area**
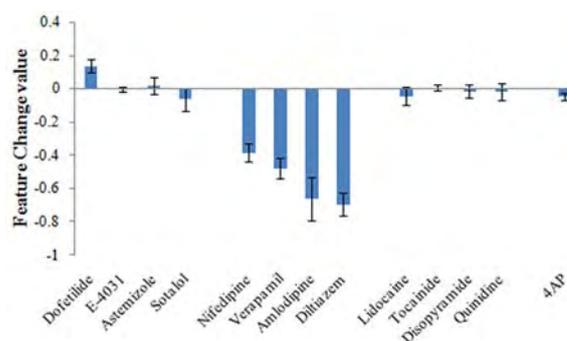


**Fig 6.** Feature change values for absolute profile recovery area.

Another example of a measure of a specific component of the sfAP waveform profile would be absolute profile recovery area. Figure 6 shows that this parameter is significantly reduced by the $I_{Ca}$ blockers but unaffected by the application of either $I_{Kr}$ or $I_{Na}$ blockers.

**Effects of the compound data set on Centre of gravity of absolute profile**
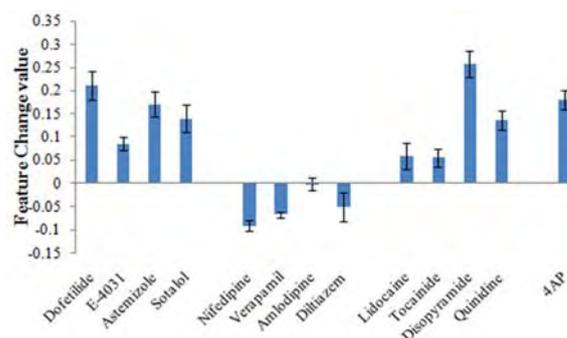


**Fig 7.** Feature change values for centre of gravity of absolute profile.

Centre of gravity of absolute profile is an example of a measure of change over the whole of the sfAP waveform profile that has polarity. This parameter was increased by class III and class 1b antiarrhythmics and reduced by application of $I_{Ca}$ blockers.

**Effects of the compound data set on amplitude variance**

Amplitude variance is an example of a measure of change over the whole of the sfAP waveform profile that is unidirectional. Thus any drug-induced change in the profile of the sfAP will elicit an increase in this parameter. Thus application of $I_{Ca}$, $I_{Kr}$ or $I_{Na}$ blockers all increase this parameter.
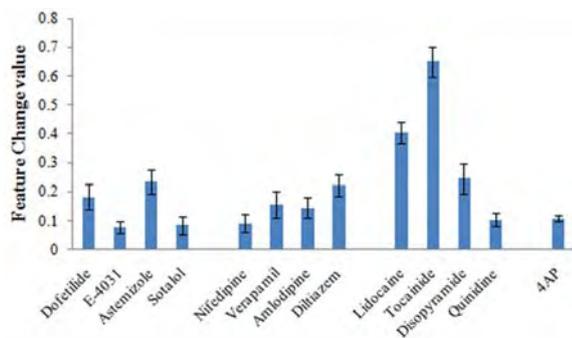


**Fig 8.** Feature change values for amplitude variance.

## 3.4 Discriminatory power of DrugPrint®

Individual feature changes are descriptive when viewed singly, but when the data from all the features are combined the discriminatory power of DrugPrint® is increased considerably. Data from 13 compounds was subjected to a blind "k-means" analysis. The data presented in figure 9 shows that these data separate into 3 sub-groups that correspond to the class 1b, class IV, and class III and 1a antiarrhythmics.
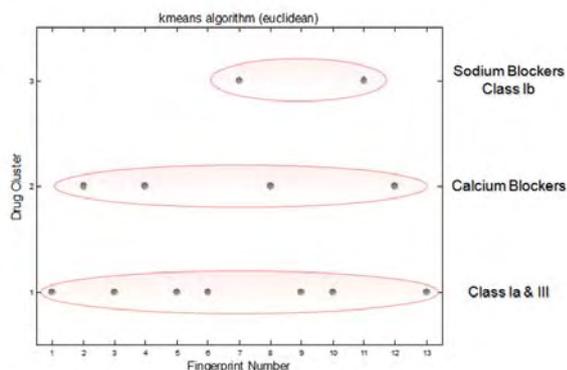


**Fig 9.** DrugPrint® discriminates between differentiate classes of drugs

## 3.5 Effect of compounds on rhythmic activity
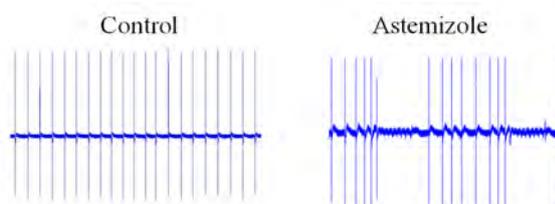


**Fig. 10.** Effect of astemizole on rhythmic activity

Under control conditions spontaneous beating is stable showing a low variability in interspike interval. Application of astemizole (100nM) destabilised beat rate. The drug-induced increase in interspike interval variability is quantified by DrugPrint® in a number of parameters that include the coefficient of variance.
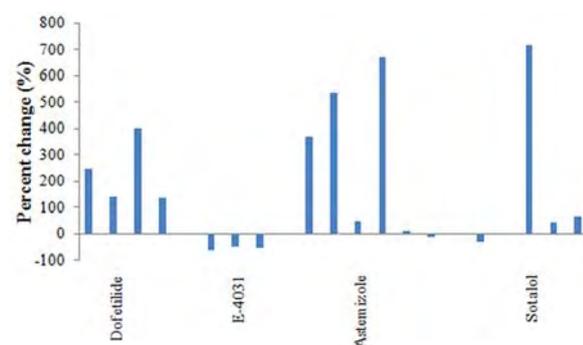


**Fig 11.** Effect of $I_{Kr}$ blockers on ISI properties. Application of several $I_{Kr}$ blockers increased the coefficient of variance of interspike interval, indicative of a disruption to normal rhythmic activity.

## 4 Conclusion

These data demonstrate that the use of cultured cardiac myocytes in conjunction with microelectrode array (MEA) technology is a novel *in vitro* screening tool that can be used for the detection of drug-induced changes in cardiac electrophysiology. The specific mathematical descriptors used by the DrugPrint® analysis software was able to discriminate between different modes of drug action e.g. between drug classes such as $I_{Ca}$ and $I_K$ blockers.

Moreover, the more integrated nature of this preparation enabled the DrugPrint® analysis software to identify disruptions to normal rhythmic activity making it a suitable model to identify drug-induced arrhythmias.

These data suggest that the DrugPrint® analysis approach is a unique and potentially powerful tool for the *in vitro* screening of cardioactive drugs

Heart

## References

[1] T. Meyer, P. Sartipy, F. Blind,.C. Leisgen & E. Guenther. (2007): New cell models and assays in cardiac safety profi ling. *Expert Opin. Drug Metab. Toxicol. 3(4) 507-517*

[2] C. Yeung, F. Sommerhage, G. Wrobel, A. Offenhäusser, M. Chan, S. Ingebrandt. (2007): Drug profiling using planar microelectrode arrays. *Anal Bioanal Chem 387 2673–2680*

[3] G. Meiry, Y. Reisner, Y. Feld, S. Goldberg, M. Rosen, N. Ziv, O. Binah. (2001): Evolution of Action Potential Propagation and Repolarization in Cultured Neonatal Rat Ventricular Myocytes. *(J Cardiovasc Electrophysiol, 12, 1269-1277*

[4] C. Abrahamsson, M. Palmer, B. Ljung, G. Duker,C. Bäärnhielm, L. Carlsson, B. Danielsson, B. (1994)): Induction of rhythm abnormalities in the fetal rat heart. A tentative mechanism for the embryotoxic effect of the class III antiarrhythmic agent almokalant. *Cardiovascular Research. 28, 337-344*

# Effect of dofetilide on field action potential of ventricular myocardium in intact guinea pig heart

Hou Yuemei, Na Jina, Li Jie, Zhang Xiaoqing, Song Jianguo, Fan Ping, Huang Yan, Wang Linpeng, Guo YuJun

Cardiovascular Research Institute, First Teaching Hospital, Xinjiang Medical University, Urumuqi, Xinjiang, China

## 1  Objective

Dofetilide is one of the newly marketed antiarrhythmic agents. It is a pure class III agent which can rapidly blocks component of delayed rectifier potassium current (Ikr). The effect of dofetilide on dose-dependent prolonging field action potential duration (fAPD) changing conduction sequence and field action potential shapes at local myocardium in intact guinea-pigs heart will be detected by a new technique of microeletrode arrays (MEA).

## 2  Methods

Thirty guinea pigs of both sexes weighting $280\pm20$g were randomly divided into three groups: control group dofetilide group ($10-6$mol/L) and dofetilide group ($10-7$mol/ l). The animals were anesthetized with chlorine hydrate 0.3 ml/100mg, then the hearts were quickly isolated, perfused with Tyrode's solution, and recorded the heart rate, field action potential duration (fAPD), conduction sequence and field action potential shapes at local myocardium with MEA.

## 3  Results

The MEA recorded clearly fAPD prolongation and hear rate reduction with both $10^{-6}$ mol/L and $10^{-7}$ mol/ L Dofetilide groups, but dispersion of fAPD no increase. The $10^{-6}$ mol/L Dofetilide group more prolonged fAPD and decreased heart rate than $10^{-7}$mol/L Dofetilide group.

## 4  Conclusion

MEA is a sensitive, low noise, long time and stable and local tissue action potential multiple-channel recording mapping system in small animal whole heart. Dofetilide has a sensitive, dose-dependent effect on reducing heart rate, prolonging fAPD, change fe-field action potential shapes, but not increasing dispersion of fAPD at local myocardium in intact guinea-pigs heart group.

# Investigating concentration gradient effects of dofetilide on FPs of cultured ventricular myocytes

Hou Yuemei, Rayile Aisa, Ma Yan

Laboratory of Cardiac Electrophysiology, First Affiliated Hospital, Xiniang Medical University, Urumqi, China

## 1 Objective

Investigting the morphologic characteristics of cultured ventricular myocytes' field potentials(FPs). Analyse the effects of Dofetilide in different concentration on FPs of cultured ventricular myocytes of suckling mice by MEAs.

## 2 Methods

The preparations of cultured vntricular mocytes with spontaneous impulse which placed in MEAs pads were obtained by the technique of primary myocardial cell culture. In order to investigate the effect of Dofetilide in different concentration on FPs of cultured vntricular mocytes, control group (n=10), 0.005μmol/L Dofetilide group(n=10), 0.01μmol/L Dofetilide group(n=10), 0.1μmol/L Dofetilide group(n=10) and 1μmol/L Dofetilide group(n=10) were performed in our research. FPs recordings by means of microelectrode arrays(MEAs) were performed to investigate both FPdur and impulse rate.

## 3 Results

Our results show that FPdur prolongation and impulse rate decrease become more and more conspicuous by using Dofetilide from concentration of 0.005 μmol/L to 1μmol/L compared with the control group (FPdur: F=124.610, P<0.01. Impulse rate: F=50.340, P<0.01).

## 4 Conclusion

Dofetilide presents its antiarrhythmic function by prolonging FPdur. FPdur prolongation shows a concentration gradient effect by using Dofetilide from concentration of 0.005 μmol/L to 1μmol/L on cultured ventricular myocytes. It is effective and safe for cultured vntricular mocytes of suckling mice to prolong FPdur by using Dofetilide in concentration of 0.01μmol/L. The risk of proarrhythmia can be increased by using Dofetilide in concentration beyond 0.01μmol/L. Therefore, MEAs mapping technique offers a versatile and powerful platform to study the concentration gradient effects of drugs and the proarrhythmic effects of antiarrhythmic drugs.

# Electrophysiological studies on ventricular myocardium of guinea pig heart by microelectrode arrays

Hou Yuemei, Na Jina, Ma Li, Li Jie, Zhang Xiaoqing, Song Jianguo

Cardiovascular Research Institute, First Teaching Hospital, Xinjiang Medical University, Urumuqi, Xinjiang, China

## 1 Objective

The morphology of field potentials(FPs) was studied by microelectrode arrays (MEAs) mapping technique. The effect of amiodarone and dofetilide on ventricular myocardial field action potential duration (fAPD) and heart rate was mapped by MEAs in guinea pigs.

## 2 Methods

The morphology of field potentials(FPs) was mapped by a microelectrode arrays (MEAs) mapping techniques in sixty guinea-pig. The sixty guinea-pigs were randomly divided into three groups: control group, amiodarone group, dofetilide group. Both ventricular muscle field potential(FPs), autorhythmicity of Guinea Pig Heart and fAPD were observed by MEAs.

.

## 3 Results

These results showed that MEAs could record sixty different shapes of fAPDs, autorhythmicity of Guinea Pig Heart and ventricular activation sequence. The fAPD of ventricular myocytes was remarkably prolonged and the heart rate was reduced in both amiodarone and dofetilide group (P<0.001).

## 4 Conclusion

MEAs was a reliable 60 sites tissue potential mapping system in Langendorff perfused guinea pig's heart with Thyrode in 86 minutes means. MEA proved the prolongation of fAPD and reduction of heart rate by both amiodarone and dofetilide, Thus MEA is an idea tool in investigating new antiarrhythmia drugs and proarrhythmia mechanism of antiarrhythmia drugs.

# Inhomogeneity of Cell Properties In The Cardiomyocyte Derived HL-1 Cell Line

Udo Kraushaar[1*], Julia Nagel[1], Thomas Meyer[2], Elke Guenther[1]

1 NMI Natural and Medical Sciences Institute, Reutlingen, Germany
2 Multi Channel Systems MCS GmbH, Reutlingen, Germany
* Corresponding author. E-mail address: udo.kraushaar@nmi.de

The murine atrial cardiomyocyte-derived cell line HL-1 is a widely accepted tool to investigate cardiomyocte activity. It is assumed that this cell line consists of a homogeneous cell type which allows using them for drug screening experiments. Here we show evidence that there are at least two different cell types. These were grouped into regular cardiomyocytes as well as into pacemaker cells based on their electrophysiological behaviour. Stimulation of the cell layer led to a uniform excitation spread always starting in the pacemaking area, independent of the stimulation location. This indicates that the pacemaker cells are the primary voltage sensing cells.

## 1 Introduction

The HL-1 cell line, derived from murine atrial cardiomyocytes, is often used as a model for investigations of cardiomyocyte activity. These cells combine several advantages: they can be kept easily in culture, divide continuously, organize in a spontaneously active syncytium and maintain their cardiac phenotype over culturing time. Optionally they can be electrically stimulated via extracellular electrodes, providing the opportunity to investigate fibrillation effects etc. Homogeneity of the specimen is a must for drug testing and the investigation of signal propagation mechanisms. To test for the homogeneity of HL-1 cells these were plated on a 60-well multielectrode array (MEA) to investigate possible variability in the excitability of the syncytium by stimulating different locations of the electrode field.

## 2 Methods

HL-1 cells (generous gift of Dr. Claycomb [1]) were cultured and proliferated in special Claycomb medium. Parts of the cells were plated on 60-electrode glass coated with bacto-gelatine and allowed to recover for a minimum of 24 h, resulting in a cell monolayer. Only MEAs with cells spontaneously beating between 1 and 3 Hz were used for further investigation. Extracellular field potentials were obtained in the medium using a MEA1060 amplifier attached to a computer running MCRack. The amplifier included an integrated blanking circuit which allowed minimizing of the stimulus artifact when used with a STG2004 stimulator MEAs (All Multi Channel Systems, MCS, Germany). The amplifier was heat controlled by a TC01 (MCS) set to 37°C. Stimuli were applied monopolar or bipolar via the MEA electrodes.

## 3 Results

Figure 1 shows field action potentials (fAP) simultaneously recorded from all 60 MEA electrodes.



**Fig. 1**: Multielectrode array (MEA) recording of a field potential in a HL-1 cell culture. Each window represents the signal from a single electrode.

The time of the fAP occurrence on the single electrodes varied depending on the distance between the electrode and the location of the initial excitation. In Fig. 2A the excitation originated at the upper right (blue) and propagated to the lower left (red) of the MEA.

Occasionally in the very same experiment a second pacemaker located on the upper left took over spontaneously, resulting in an excitation wave from upper left to lower right (Fig. 2B).

This switching between the pacemaker areas could be prevented by electrical stimulation adjacent to either the one or other pacemaker. Interestingly,

stimulation of more distant electrodes did not result in an excitation spread from this respective point but from the nearest of the two pacemakers. This behaviour was seen in every MEA recording investigated.

## 4 Conclusion:

Our finding indicates that the HL-1 cells can be at least separated into two cell types, namely into "regular" cardiomyocytes and pacemaker cells that may differ in their ion channel patterns. Further studies will show if this inhomogeneity will have an impact on the validity of drug screening experiments on these cells.
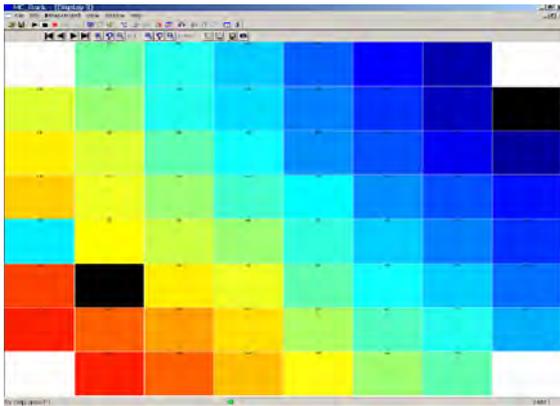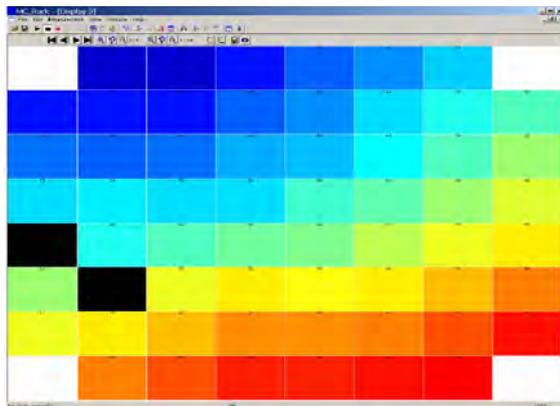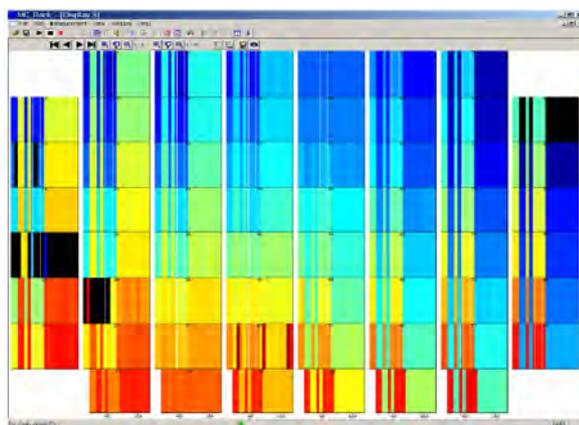
**References**

[1] Claycomb et al. Proc. Natl. Acad. Sci. USA, 2979-2984(95), 1998

**A**



**B**



**C**



**Fig. 2:** False colour mapping of the excitation spread on HL-1 cells on a single MEA. Blue indicates an early detection whereas red indicates a later detection compared to a reference time. A displays an excitation wave spreading from the pacemaker in the upper right to the lower left of the MEA. Each colour block represents a single MEA electrode. In B a second pacemaker took over indicated by the excitation originating now in the upper left and propagating to the lower right of the MEA. C: spontaneous switching between pacemaker areas, illustrated in a colour-vs.-time plot. Transitions of the origin of the excitation are displayed as changes of the colour within the same block.

Heart

# Retinal Signalling

# Classification of Velocity Changes by the Activity Patterns of Retinal Ganglion Cell Ensembles

León M. Juárez Paz[*], Jutta Kretzberg

Carl von Ossietzky University Oldenburg, Oldenburg, Germany
* Corresponding author. E-mail address: l.m.juarez.paz@uni-oldenburg.de

Light responses of retinal ganglion cells (RGC) to a moving stimulus were recorded extracellularly in the isolated turtle retina using a 10 x 10 Utah array. In order to test the capability of RGC to encode velocity changes of the moving stimulus, we analysed the simultaneous activity of all recorded RGC using Principal Components Analysis (PCA). Our results show that not only the firing rate of the RGC activity, but also its temporal structure carries information about the stimulus parameters. Furthermore, it was found that the transient response of the RGC in the first milliseconds after a velocity transition carries the most information about stimulus parameters such as speed and direction.

## 1 Introduction

All the visual information available to the brain originates from the activity of ensembles of retinal ganglion cell (RGC) ensembles. Therefore, responses of RGC to a moving stimulus are the basis for visually guided behaviour e.g. the optokinetic nystagmus (OKN), a reflex behaviour in which animals use head and/or eye movements to compensate for large-field continuous movement [1]. In lower vertebrates like e.g. turtle, the detection of moving objects is already done at the retinal level [2].

For the turtle retina, it was shown that speed, direction and acceleration of moving stimuli could be decoded reliably from RGC activity using Bayesian stimulus reconstruction based on spike rates of individual ganglion cells [3]. In this study, we want to qualitatively test if the temporal structure of the RGC population firing rate also contains enough information to decode these properties of motion stimuli.

## 2 Methods

### 2.1 Electrophysiology

The responses of RGC to a moving stimulus were recorded extracellularly in the isolated turtle (*Pseudemys scripta elegans*) retina. Action potentials were registered using a 10 x 10 Electrode silicon array (Cyberkinetics, Foxborough, MA). The array was introduced from the pigment epithelium side of the retina until it reached the RGC layer. Signals were amplified, pre-processed and stored using the Bionic 100-channel acquisition system (Cyberkinetics). Not all electrodes on the array registered activity of RGC. Nevertheless, there were cases in which one electrode registered the activity of more than one cell.
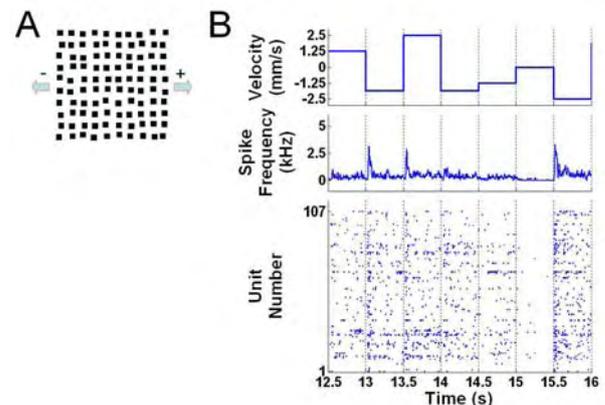


**Fig. 1. Experiment A.** Pattern of dark squares on a bright background. Movements to the left were considered as negative and movements to the right as positive velocities. **B.** Sequence of different moving velocities of the squares pattern (top). Spike firing rate of the whole population of recorded RGC (n=107) (middle). Raster plot of the RGC responses to the different velocities (bottom).

### 2.2 Stimulus

The stimulus consisted of a moving pattern of dark squares on a bright background (Fig. 1A). The position of each square in the pattern was shifted relative to its position in a regular grid, setting the average distance between squares centres to 400 μm. The pattern moved in a pseudo-random sequence of velocities, which were held constant for periods of 500 ms and instantaneously changed to a new velocity at the end of each period. For the experiment, nine different velocities were used. These velocities were obtained by combining five different speeds between 0 mm/s and 2.5 mm/s (with increments of 0.625 mm/s) and two motion directions. Negative velocity values correspond to movements to the left and positive values to movements to the right. Each of the 72 possible velocity transitions was projected on the turtle retina 70

times. For more details about the experiment refer to [3].

## 2.3 Pre-analysis

Although for the present study it was not critical to know the cell of origin of each spike, off-line spike-sorting was applied to the recorded activity of RGC using the supervised k-means clustering software SpikeSorter (Cyberkinetics). After this procedure, the instantaneous firing rate was calculated considering the whole population of recorded RGC. The instantaneous rate was determined using bins of 1 ms and then smoothed with a sliding window of 12.5 ms (Fig. 1B, middle).

## 2.4 Principal Component Analysis

Principal Component Analysis (PCA) is a standard method to reduce the number of variables of an original space with the minimal loss of information [4]. This analysis has already been used to optimally characterise different waveforms based on their principal components e.g. in the field of spike sorting [5]. In this study, PCA was used to evaluate the time dependent firing rate of the responses of the population of RGC. With this approach we wanted to test qualitatively:

If stimulus velocity transitions can be discriminated based on the instantaneous firing rate of a population of RGC.

The relevance of different time scales of the RGC responses for velocity transition discrimination.

If different segments of the RGC responses are equally suited for the discrimination of velocity transitions.

Thus, PCA was applied to the time course of the instantaneous firing rate of the RGC population considering response periods of different lengths and different timing related to the onset of the velocity transition.

## 3   Results

The instantaneous firing rate of the RGC population showed in most of the cases a transient change during the initial response period after velocity transitions. These transient responses occurred with a certain characteristic latency of 10 to 50 ms after each stimulus transition. Moreover, the latency, duration and magnitude of this response transient were reproducible for defined velocity transitions (Fig. 2).

### 3.1 Classification of velocity transitions

To find out if the time structure of the instantaneous population firing rate is characteristic enough to reliably estimate the stimulus velocity transitions, we analysed the RGC responses using PCA.
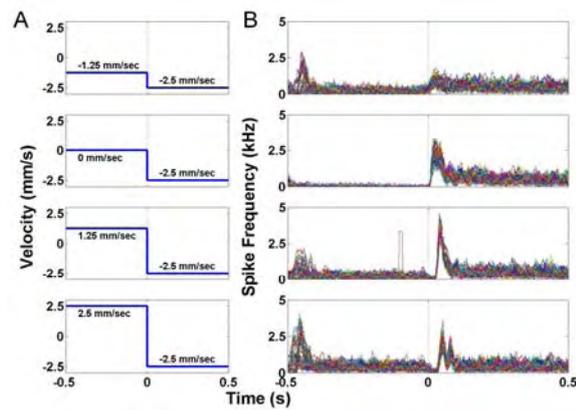


**Fig. 2. Responses of the population of RGC to a moving stimulus A.** Different velocity transitions with same after-transition velocity. **B.** Time course, for all 70 trials, of the RGC population instantaneous firing rate obtained using a sliding window of 12.5 ms and steps of 1 ms. Time 0 is the time of velocity transition.

In most of the cases, the first two principal components of the RGC responses were found to form clusters representing the different velocity transitions (Fig. 3). When the whole period (500 ms) of the RGC responses to the after-transition velocity was considered for PCA, it was observed that different transitions cluster differently well depending on the before-transition velocity (Fig. 3). Clusters representing different after-transition velocities are separated best if before-transition velocity was lower (Fig. 3, centre). When no motion was present previous to velocity transition (Fig. 3, right), the speed of the after-transition velocity (represented by different colours) can be well separated, but not the direction of movement (represented by different symbol directions). For velocity transitions with high before-transition velocity values, it is almost impossible to estimate the after-transition velocity based on the RGC responses (Fig. 3, left).
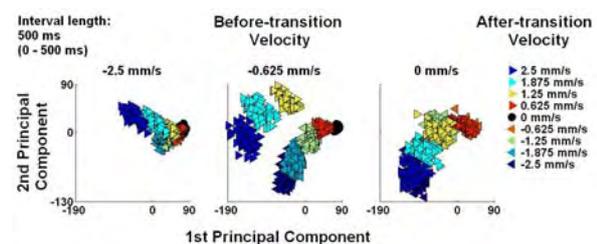


**Fig. 3. First two principal components for the whole period (500 ms) of the RGC population responses to the after-transition stimulus velocity. Symbol colours represent different speeds, symbol direction represents motion direction.**

## 3.2 Effects of response period length

To investigate the effects of the response period length on the discrimination of different velocity transitions, we varied the duration of the interval used for the PCA. As first step, we used the initial response period after the velocity transition (Fig. 4). Here, for a time period of 12.5 ms no clustering was present,

while for longer time periods clusters were more clearly observable. It was found that already with time periods of 50 ms length, the formation of clusters representing different velocity transitions was qualitatively similar to the results when the whole period of the RGC responses was considered (compare Figs. 3 and 4).
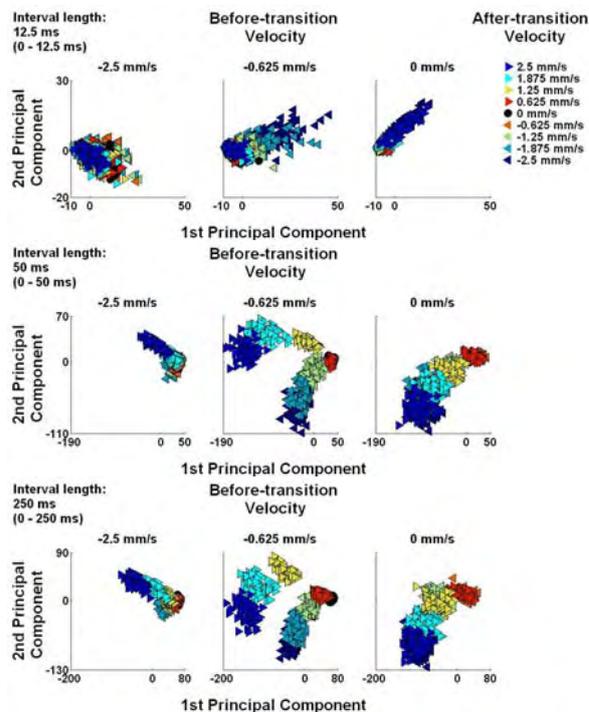


**Fig. 4.** First two principal components for different initial periods of the RGC responses to the after-transition stimulus velocity, at the onset of velocity transition.

To test if specific segments of the RGC responses are equally informative about the motion parameters of the stimulus, we compared the results obtained for the initial periods of the responses (Fig. 4) with PCA results obtained considering periods of the same lengths as before but located at the end of the responses of RGC to the after-transition velocity presentation. Again, clustering depended on the length of the time periods (Fig. 5). Compared to PCA based on the initial periods of RGC responses, longer time periods were necessary to obtain cluster e.g. 50 ms were not long enough to obtain separate clusters (Fig. 5). Moreover, in contrast to the results obtained with the initial response periods, the clusters obtained with the final response periods did not correspond to the different velocity transitions, but to the after-transition speed, independent of the motion direction and the before-transition velocity (compare Figs. 4 and 5).

## 3.3 Effect of response period timing

To systematically analyze which parts of the responses allow best classification of the different features of the moving stimulus, we varied the timing of

the evaluated response period (steps of 5 ms) relative to the occurrence of a velocity transition in combination with the period length. To quantify the effects of these two parameters for the classification performance, we calculated the variance contribution of the first two principal components (Fig. 6).
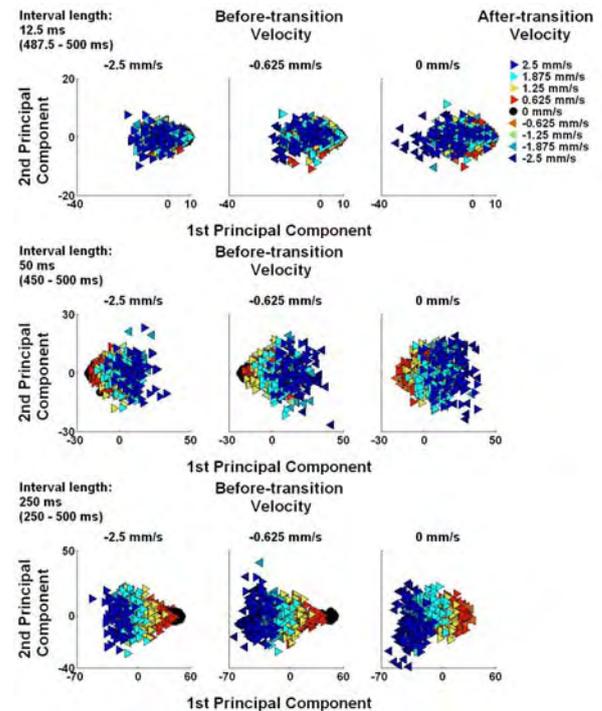


**Fig. 5.** First two principal components for different final periods of the RGC responses to the after-transition stimulus velocity, at the end of actual velocity presentation.

For all interval lengths except 500 ms the variance contribution reached its highest values when the evaluated response period ended 40 ms to 60 ms after velocity transitions. Moreover, for time windows longer than 12.5 ms but shorter than 500 ms, a second peak of variance contribution was found. The two peaks were separated by a time interval similar to the length of the time period considered for PCA.

Please note that segments of the response to the before-transition velocity are evaluated together with initial response segments after transition, if the interval length is bigger than the interval upper limit relative to the occurrence of the velocity transition (e.g. an interval of 500 ms length and an upper limit of 200 ms covers the final 300 ms of the response to the before-transition velocity and the initial 200 ms of the responses to the after-transition). This is the reason for the low variance contributions when the evaluated interval is placed earlier than 40 ms after velocity transition. Most probably, the different shape of the curve for the longest intervals of 500 ms is also due to the strong impact of the before-transition velocity.
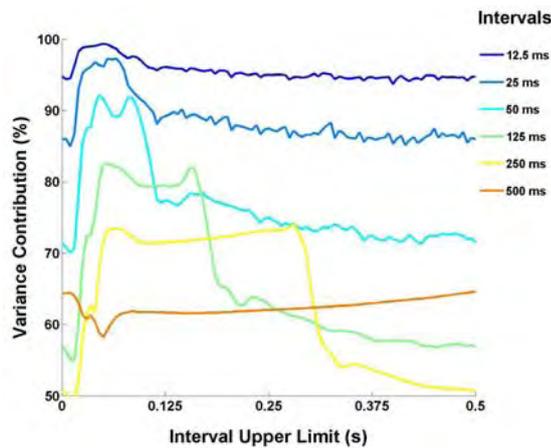
**Fig. 6.** Variance contribution of the first two principal components considering time periods of different lengths and different timing relative to the occurrence of velocity transition.

Intuitively, one would expect that the formation of clusters is better for parameter combinations leading to higher values of variance contribution. In order to test this hypothesis, a further analysis was carried out considering the timing of response periods for which the variance contribution reached its maximum for the interval periods of different lengths (Fig. 7). Comparing the clustering performance when the evaluation interval started at the time of the velocity transition (Fig. 4) with this analysis (Fig. 7), it was found that optimal timing improves the clustering performance. Here, short response periods of only 12.5 ms already led to clustering of some velocity transitions (compare upper rows of Figs. 4 and 7). In this case, separation of clusters is particularly good for transitions which include a change in direction or the increase of speed in the same direction. For longer time windows (50 ms and 250 ms), the effect of optimal timing is not evident.

This suggests that the combination of the length and the timing of the considered response period needs to be optimized to obtain best clustering performance.

## 4 Conclusions and Outlook

Our results let us conclude that PCA is a useful method to evaluate qualitatively how well velocity transitions of a moving stimulus are encoded by the time structure of a RGC population instantaneous firing rate. In the present study, we found that not only the overall instantaneous firing rate of turtle RGC, but also its temporal structure carries information about the moving stimulus parameters, namely speed and direction. Furthermore, the transient response of the RGC in the first milliseconds after a velocity transition is most informative about this transition. The sustained response after this initial period still encodes stimulus speed, but the information about movement direction is lost.
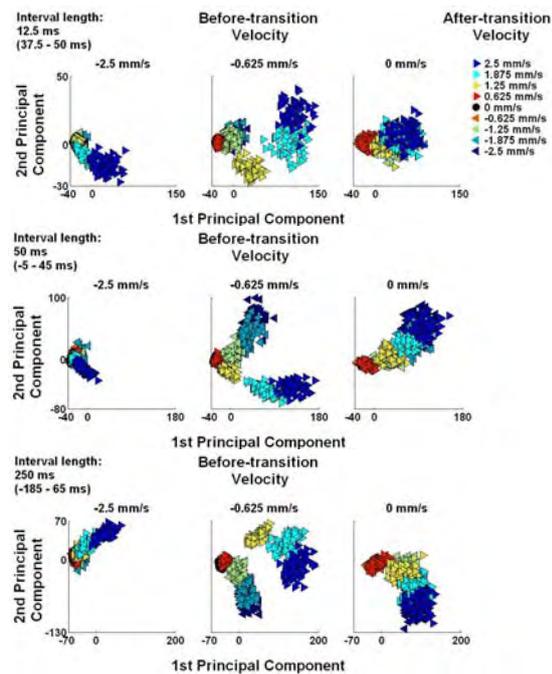


**Fig. 7.** First two principal components for the responses of RGC at the end of velocity presentation.

This suggests that transient changes in firing rate simultaneously encode changes in motion speed and direction, while sustained responses of the RGC population allow the decoding of the actual speed of the moving stimulus when long time windows are used for integration. Future work will consider methods to quantify the classification performance of the different velocity transitions based on the PCA results e.g. discriminant analysis.

## References

[1]  B. Cohen, V. Matsuo, and T. Raphan. *Quantitative Analysis of the Velocity Characteristics of Optokinetic Nystagmus and Optokinetic After-Nystagmus.* Journal of Physiology, Vol. 270, [321-344], 1977.

[2]  H. Kolb. *How the Retina works.* American Scientist, Vol. 91, [28-35], 2003.

[3]  A. Thiel, M. Greschner, C. W. Eurich, J. Ammermueler, and J. Kretzberg. *Contribution of individual retinal ganglion cell responses to velocity an acceleration encoding.* Journal of Neurophysiology, Vol. 98, [2285-2296], 2007.

[4]  Jolliffe I.T. *Principal Component Analysis, Springer Series in Statistics, 2nd ed.*, Springer, NY, 2002.

[5]  M. Lewicki. *A review of methods for spike sorting  the detection and classification of neural action potentials.* Network: Computation in Neural Systems, Vol. 9, [53-78], 1998.

# Electrical image of a patch of the retinal ganglion cell layer

Günther Zeck[1], Armin Lambacher[2], Peter Fromherz[2]

1 Max Planck Institute of Neurobiology, Department of Computational and Systems Neurobiology, Martinsried, Germany
2 Max Planck Institute for Biochemistry, Department of Membrane and Neurophysics, Martinsried, Germany

To understand the processing of visual information by the parallel channels in the retina recording of many output neurons at high spatial and temporal resolution is required. Many types of output neurons (ganglion cells) in the rabbit retina can be characterized by their activity patterns that are defined by the (averaged) timing of successive inter-spike intervals [1]. It is unclear how these activity patterns are transmitted from the action potential initiation sites towards the optic nerve head. Here we used a newly developed multi-transistor array [2] to image the propagation of a population of action potentials in response to simple visual stimuli.

## 1 Methodology and Results

We projected visual stimuli (moving gratings flashed or flickered spots) on a flat-mount adult rabbit retina. We measured the electrical activity in a 1 mm$^2$ patch of the ganglion cell layer. The spatial sampling was 8 x 16 μm$^2$ with a temporal resolution of 0.12 milliseconds. The transistor density of this array is higher than the ganglion cell density in the rabbit retina. Therefore every action potential was picked up simultaneously by several transistors. For a given transistor we considered the spatial activity patterns during a one millisecond epoch following the spike initiation. The spatial activity patterns for all spikes on this transistor were averaged. Only transistors that were active in more than 50% of the activity epochs were considered. The resulting templates could be grouped either in axons of passage (biphasic extracellular waveform with amplitudes of ~ 0.4 mV) or cell somata (extracellular waveform amplitude often exceeding 1 mV). In many cases we measured not only the somatic signal but also the corresponding propagating axonal signal. Duplicate templates were removed.

We calculated the action potential conduction velocity for axons of an identified ganglion cell or axons of passage. The velocity was constant independent of the visual stimulus. Furthermore, the propagation of spike patterns was not altered by the extracellular potentials of close parallel axons or cell bodies (no ephaptic interaction). However, in the same retinal patch different ganglion cells transmitted their signals at different velocities (range between 1 – 2 m/s).

## 2 Conclusion

In summary, the multi-transistor array provides a unique opportunity to study signal processing and propagation in the ganglion cell layer. We could show that the stimulus representation by the combined spike patterns of a population of ganglion cells is different from the combined pattern when it leaves the eye.

**References**
[1] G.M. Zeck , R.H. Masland (2007). *Eur. J. Neurosci. 26*, 367-380
[2] A. Lambacher, M. Jenkner, M. Merz, B. Eversmann, R.A. Kaul, F. Hofmann, R. Thewes and P. Fromherz (2004) *Applied Physics 79, 1607-1611*

# Multielectrode Array Recordings Of Neural Activity Patterns In The Developing Retina Of The Cone Rod Homeobox Knockout (*Crx-/-*) Mouse

Adams C[1], Simonotto J[1,2], Eglen SJ[3], Sernagor E[1*]

1 Institute of Neuroscience, Medical School, Newcastle University, Newcastle upon Tyne, UK
2 School of Computing Sciences, Newcastle University, Newcastle upon Tyne, UK
3 DAMTP, Centre for Mathematical Sciences, University of Cambridge, Cambridge, UK
* Corresponding author. E-mail address: evelyne.sernagor@ncl.ac.uk

Using multielectrode array recordings from developing retinal ganglion cells, we show that in the dystrophic cone-rod homeobox (Crx) knockout retina where photoreceptors degenerate between 1 and 5 months postnatal, ganglion cells have developed strong compensatory physiological mechanisms to overcome the lack of visually-evoked activity. Indeed, they exhibit strong spontaneous bursting activity and slow oscillations. In addition, a large proportion of ganglion cells are intrinsically photosensitive, responding to blue light stimulation. These results show that the Crx retina is capable of developing compensatory mechanisms to counteract visual experience impairment during the critical wiring period of visual connections.

## 1 Introduction

The *Crx-/-* mouse is a model for retinal dystrophy. *Crx-/-* photoreceptors lack outer segments from the onset, resulting in complete absence of vision through the photoreceptor/bipolar/ganglion cell pathway from birth [1]. However, all other retinal layers appear intact at birth and start degenerating from one month postnatal, when wiring of visual connections have matured [2,3]. The degeneration process lasts 3-4 months, ultimately resulting in a retina lacking outer nuclear and plexiform layers whilst the inner retina remains mostly intact, with retinal ganglion cells (RGCs) still sending impulses to the visual centres of the brain via the optic nerve. As immature retinal neural activity, both in the form of spontaneous waves and early visual experience, is important for the development of visual connections, the *Crx* retina offers an interesting scenario to study early neural activity patterns in the absence of visual experience during the critical period for establishing visual connections.

## 2 Methods

We have used a 60 channel microelectrode array (MEA, 30 μm electrode diameter, 200 μm separation) (Multi Channel Systems MCS GmbH) to record firing patterns from the RGC layer of *Crx-/-* and wild-type (wt) retinas during the first postnatal month, before the onset of degeneration. Signals were acquired at 25 kHz without filtering. In addition to spontaneous activity, retinas were also stimulated with diffuse blue light (480 nm wavelength) to evaluate RGC intrinsic photosensitivity, a phenomenon normally encountered

in ~3% of all murine RGCs (projecting to the circadian clock in the hypothalamus) [4,5]. Spikes were amplitude threshold-detected using MC_Rack to calculate total firing rates on each electrode. To evaluate global activity and propagation patterns, we have computed firing rates for each electrode as well as correlation indices as a function of distance between electrodes. To estimate local field responses we have also measured all intrinsic signal frequencies.
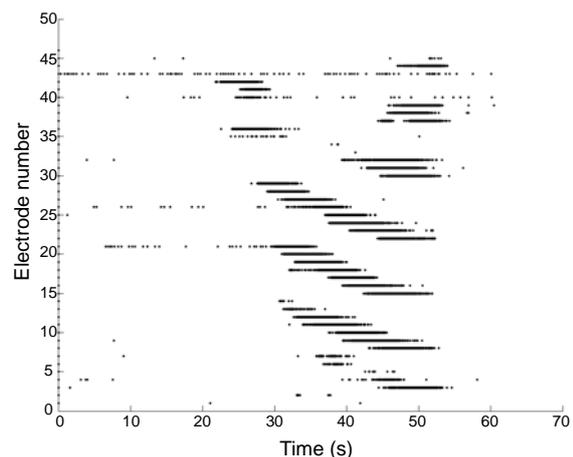


**Fig. 1**: Raster plot of a spontaneous wave sweeping across the RGC layer of a P7 *Crx-/-* retina.

## 3 Results

Spontaneous waves of activity normally sweep across the RGC layer in wt mouse until postnatal day 14 (P14), after which they break down and disappear by P20 [6]. In the *Crx-/-* retina, propagating waves

(Figure 1) disappear earlier, around P10, switching to strong random bursting.

Slow oscillations (4-15Hz) (Figure 2), mediated by glutamatergic connections and intrinsic membrane properties, become conspicuous at P14, increasing in power over time. We were able to record such oscillations up to 2 months postnatal, the oldest age studied (and well into the period of degeneration). We also found that correlation indices were 3 times higher in the *Crx-/-* retina than in wt for all ages investigated (Figure 3). Finally, we found a striking increase in responsiveness to blue light in *Crx-/-* retinas, with 12-93% of all electrodes on the array showing a significant response when compared with <4% in wt.
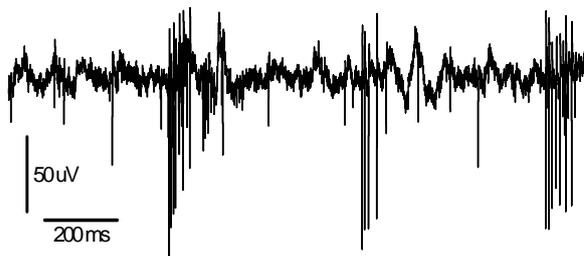


**Fig. 2:** bursting and oscillations recorded on one electrode from a P26 *Crx-/-* retina.
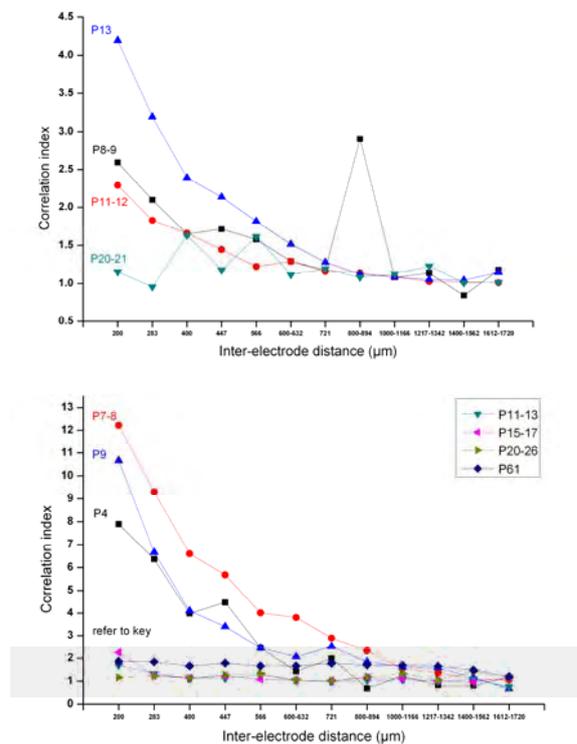




**Fig. 3:** Correlation index plots as a function of distance between electrodes for *Crx-/-* versus wt retinas. Each data point represents average values for a certain age and distance.

.

## 4 Conclusions

These results demonstrate that the Crx-/- retina is capable of developing compensatory mechanisms to counteract visual experience impairment during the critical wiring period of visual connections.

**References**
[1] Furukawa T, Morrow EM, Cepko CL (1997) Crx, a novel otx-like homeobox gene, shows photoreceptor-specific expression and regulates photoreceptor differentiation. *Cell 91 531-541.*
[2] Pignatelli V, Cepko CL, Strettoi E (2004) Inner retinal abnormalities in a mouse model of Leber's congenital amaurosis. *J Comp Neurol 469 351-9.*
[3] Morrow EM, Furukawa T, Raviola E, Cepko CL (2005) Synaptogenesis and outer segment formation are *perturbed* in the neural retina of Crx mutant mice. *BMC Neurosci 6 , 5.*
[4] Berson, DM, Dunn, FA, Takao M (2002) Phototransduction by retinal ganglion cells that set the circadian clock. *Science 295 1065-1070.*
[5] Berson, DM (2003) Strange vision: ganglion cells as circadian photoreceptors. *TINS 26 314-320.*
[6] Demas J, Eglen SJ, Wong RO (2003) Developmental loss of synchronous spontaneous activity in the mouse retina is independent of visual experience. *J Neurosci 23 2851-2860*

# Correlations and the Structure of the Population Code in a Dense Patch of Retina

Dario Amodei[1], Greg Schwartz[2], Michael Berry[2*]

1 Department of Physics, Princeton University, Princeton, NJ, 08540
2 Department of Molecular Biology, Princeton University, Princeton, NJ, 08540
* Corresponding author. E-mail address: berry@princeton.edu

We have fabricated a 60 channel multielectrode array and a 252 channel multielectrode array (both with 30 micron interelectrode spacing) to study collective firing patterns in salamander retinal ganglion cells. Using data from the 60 channel array, we construct Ising models of the retinal population code and use them to classify retinal responses to stimuli. We show that our classifications are robust and repeatable.

## 1   Multielectrode Arrays

Recent work (e.g. Schneidman *et al* 2006, Tkacik *et al* 2006) has shown that the collective spike patterns of small groups of ganglion cells in the retina can be represented to high accuracy by a maximum entropy Ising model constructed from the pairwise correlations of the cells' spikes. Extending this work, we investigate the accuracy of fully-connected Ising models for groups of more than 30 densely clustered retinal ganglion cells in salamander. We construct Ising models for each of three types of stimuli: natural scenes, random checkerboards, and geometric shapes.
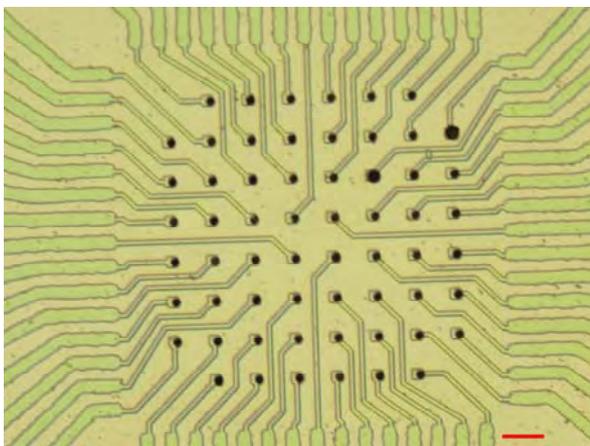


**Fig. 1.**  Completed 60 channel array (scale bar = 30 μm)

To make these measurements we have fabricated a multielectrode array with 60 channels in a square pattern and a 30 μm interelectrode spacing (figure 1). The array has features down to 2 μm and is fabricated using a combination of photolithography, electron beam lithography, lift-off, and dry etching. The fabrication process is a modified version of that of Gunning *et al* 2005. We have also successfully fabricated a 252 channel array (also with 30 μm spacing; central region shown in figure 2), which will be used to con-struct even larger Ising models and to test the hypothesis (Tkacik *et al* 2006) that dense patches of ~200 correlated cells can be approximated by an Ising model poised near a critical point.

## 2   Ising Models

We explore the probability landscape of our Ising model and compare it with the probability landscape of Ising models from simulated networks. To test the idea that the energy basins of large Ising models represent feature classifications by the retina, we compute the average stimulus triggering each basin. We show that the basin structure is highly repeatable across successive presentations of the same video, and robust to removal of a large fraction of the data. Finally, we measure the relative strength of noise correlations as compared to stimulus correlations and explore the role played by both types of correlation in forming the population code. We find small but strongly statistically significant noise correlations that contribute meaningfully to the dynamics of the Ising model.
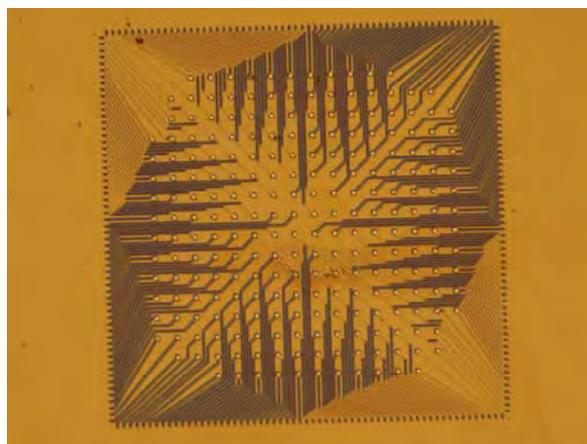


**Fig. 2.** Central region of 252 channel array

## Acknowledgement

## References

[1] D. Gunning, C. Adams, W. Cunningham, K. Mathieson, V. O'Shea, K.M. Smith, E.J. Chichilnisky, A.M. Litke, and M. Rahman, *Nuclear Instruments and Methods in Physics Research A* **546,** 148 (2005)

[2] E. Schneidman, M.J. Berry, R. Segev, and W. Bialek, *Nature* **440,** 1007 (2006)

[3] G. Tkacik, E. Schneidman, M.J. Berry, and W. Bialek, arXiv :q-bio/0611072v1 (2006)

# LED-based illumination system for the MEA60 system for full field stimulation of explanted retinas

Herrmann, T.[1], Krause, T.[1], Gerhardt, M.[1], Hesse, M.[2], Boven, K-H.[2], Stett, A.[1*]

1 NMI Natural and Medical Sciences Institute, Reutlingen, Germany
2 Multi Channel Systems MCS GmbH, Reutlingen, Germany
* Corresponding author. E-mail address: stett@nmi.de

For full field light stimulation without the need of optics we developed a LED-based illumination system. In order to perform ERG experiments with explanted retinas the illumination system was integrated to a MEA setup. Using this assembly with different LEDs we took recordings from retinas. The obtained I-O curves enabled the choice of a suitable LED for light stimulation. As it is easy to control, the illumination system could be simply adapted to a parallel recording setup.

## 1 Background

Electroretinogram (ERG) and ganglion cell recordings with MEAs from explanted retinas [1] are used to investigate retinal function and effects of pharmacological compounds on retinal activity [2]. For full field light stimulation we developed a LED-based illumination unit for the MEA60 system. The peak wavelength of the emission spectrum of the LED corresponded to the peak wavelength of the spectral sensitivity curve of the retina from Long Evans rats. We validated the system with ERG recordings from explanted retinas.

## 2 Methods

We measured the emission spectrum of LEDs with a microspectrometer. The LEDs were driven by voltage-controlled circuits with temperature compensation and the voltage output of a stimulus generator (STG).

Segments from explanted rat retinas (adult Long Evans) were placed ganglion cell site down on MEAs (Fig. 1). The preparation and handling of rat retina for MEA recordings is described in an application note and can be downloaded from

http://www.multichannelsystems.com/application s/applicationnotes/applicationnotes.htm.

To examine the wavelength selectivity of the rat retina we projected monochromatic (FWHM = 15 nm) light flashes (5 ms duration, 350 $\mu W/cm^2$) through the objective of an inverted microscope onto the retinal sample. The ERGs (Fig. 2) were recorded with a MEA-amplifier (bandwidth 0.5 – 2800 Hz) and the amplitude of the b-wave was analysed.
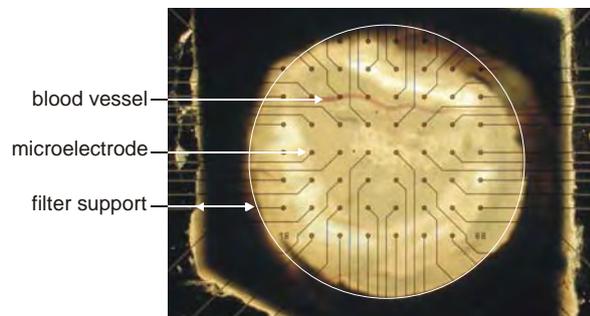


**Fig. 1.** Segment of a rat retina on a MEA. The retinal sample is placed to a nitrocellulose filter with punched opening to enable proper handling of the sample.
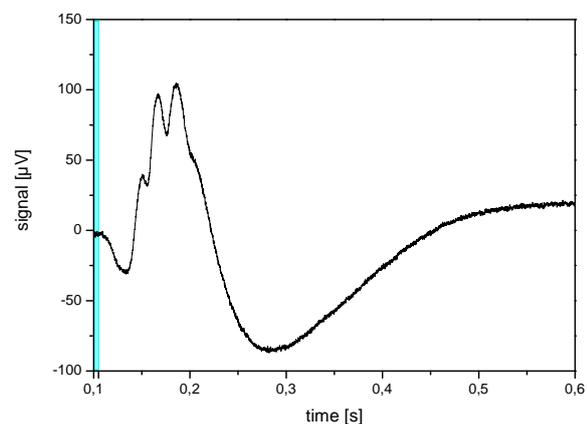


**Fig. 2.** Flash-ERG of explanted Long Evans retina after full field stimulation (illumination: 3600 lx, duration: 5 ms) with a Luxeon LED.

## 3 Results

The spectral sensitivity curve of the retina from Long Evans rats (Fig. 3) showed peaks at 361 nm and at 502 nm. The later corresponds with the peak wavelength of the Luxeon LED (Typ Star/0, 1W, cyan) at 505 nm (Fig. 4).

We embedded the LED in a housing with a distance of 1.8 cm to the bottom side of the MEA. Using the voltage controlled driver circuit we obtained a retinal illuminance in the range from 1 to 100000 lx (Fig. 5). Fig. 6 shows the I-O curves obtained under these conditions with different LEDs. The b-wave amplitudes were stable up to one hour. The driver unit for the LEDs is designed to control four LEDs in parallel.



**Fig. 5.** Performance of the Luxeon LED.



**Fig. 3.** Spectral sensitivity curve of rat retina (Long Evans).
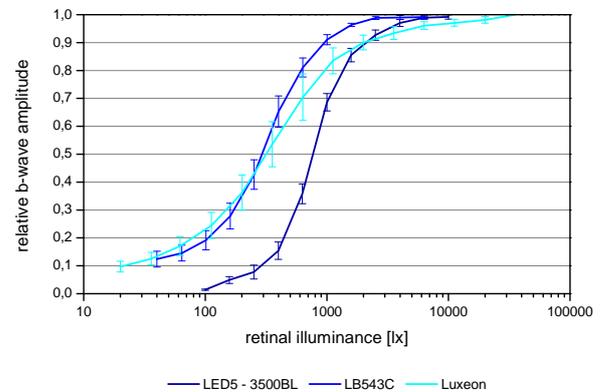


**Fig. 6.** I-O-curves obtained with the tested LEDs.

## 4 Conclusion

With the LED-based illumination system no optics are needed for retina stimulation and ERG recording with MEA setups. It allows homogeneous full-field stimulation with fast temporal modulation. The retinal illumination is easy to control without altering the spectrum of the emitted light when changing the emission power. Further work aims at parallelisation of the recording system to increase the throughput of examined retinas.

**Fig. 4.** Emission spectras of the tested LEDs.

**References**

[1] Kraft A., Herrmann T., Stett A. (2006). Electroretinogram recordings with MEAs from explanted rat retina (rat µERG). In: Stett A. (ed): *Proceedings MEA Meeting 2006*. BIOPRO edition Vol. 3, p. 97-98. BIOPRO Baden-Wuerttemberg GmbH, Stuttgart, 2006. ISBN: 3-938345-02-0

[2] Guenther E., Herrmann T., Stett A. The Retinasensor: An In vitro Tool to Study Drug Effects on Retinal Signaling. In: Taketani M., Baudry M. (eds): *Advances in Network Electrophysiology Using Multi Electrode Arrays*; p. 321-331. Springer, Berlin 2006

# Simultaneous Recordings of Electroretinogram and Ganglion Cell Activity from Explanted Retinae of Wildtype and Bassoon-knockout Mice

Diana Karnas [1,2], Hilmar Meissl [1]

1 Dept. of Neuroanatomy, Max Planck Institute for Brain Research, Frankfurt, Germany
2 Dept. of Neurophysiology and Chronobiology, Jagiellonian University, Krakow, Poland

Multimicroelectrode array (MEA) technology is now frequently used to record extracellular signals from electrogenic cells in primary cell cultures or from brain slices. In the present study, we used MEA technology to perform multisite recordings of local electroretinograms ($\mu$ERG) simultaneously with extracellular recordings from ganglion cells in the isolated mouse retina. The aim of the study was to develop an in vitro test of the mouse visual system for comparing wildtype mice and mouse mutants with impaired visual function.

## 1 Background/Aims

The protein Bassoon is an integral component of the photoreceptor ribbon synapse. In mouse retinae deficient of functional Bassoon protein (*Bsn-/-*) photoreceptor ribbons are not anchored to the presynaptic active zones resulting in an impaired photoreceptor synaptic transmission, and the formation of ectopic synapses (Dick et al., 2003). To investigate the functional role of Bassoon we performed multielectrode array (MEA) recordings from explanted retinae of *Bsn-/-* mice and C57/Bl6 mice (as a *wildtype* control). MEA technology enables multisite recordings of local electroretinograms ($\mu$ERG) simultaneously with extracellular recordings from ganglion cells in the isolated retina.

## 2 Methods

Pieces of retinae of C57/Bl6 and *Bsn-/-* mouse were mounted with the ganglion cell side down on MEAs. Full field light stimulation was provided by a LED with peak wavelength of 505 nm and an intensity range of about 4.6 log units. Micro ERGs and responses of retinal ganglion cells were recorded on 60 electrodes simultaneously and stored on hard disk using the software MC_Rack (MCS, Reutlingen) for off-line analysis. Data analysis included the measurement of a- and b-wave amplitudes and implicit time of $\mu$ERGs, as well as the analysis of spike rate and response duration.

## 3 Results

With increasing light intensity, a- and b-wave amplitudes increase and the implicit time diminishes in the *wt* ERG. Stimulation with prolonged pulse duration results in a clear separation of ON- and OFF-components of the ERG. The metabotropic glutamate receptor agonist APB (20 $\mu$M) causes a disappearance of the b-wave by blocking the ON retinal pathway. NBQX (20$\mu$M), a selective AMPA/ Kainate receptor antagonist, partially reduces the a- and d-wave and slightly enhances the b-wave. The implicit time of the a-wave of *Bsn-/-* retinae is comparable with the *wt* a-wave. However, the amplitude of the *Bsn-/-* a-wave is enlarged and the response curve shows a steeper rise of the V/log I-function. The b-wave in *Bsn-/-* ERGs is not clearly distinguishable (Fig. 1). In retinal ganglion cells (RGC) of *wt* mice the spike rate and response duration increases with stimulus intensity and the implicit time of spike bursts decreases. RGCs of *Bsn-/-* mice show a nearly normal response pattern (Fig. 2). However the duration of spike bursts and their implicit time are strongly prolonged in comparison to *wt* mice.

## 4 Conclusion

These results demonstrate that Bassoon deficient mice possess a well developed signal transduction pathway despite an altered synaptic transmission and clear changes in ERG responses.

**References:**
[1] Dick O. et al.: The presynaptic active zone protein Bassoon is essential for photoreceptor ribbon synapse formation in the retina. Neuron 37, 775-786 (2003)
[2] Lars van Ahrens et al.: Application of multielectrode recording to the retina of a genetically engineered Bassoon-knockout mouse. 4th International Meeting on Substrate-Integrated Microelectrode Arrays, Reutlingen (2004)
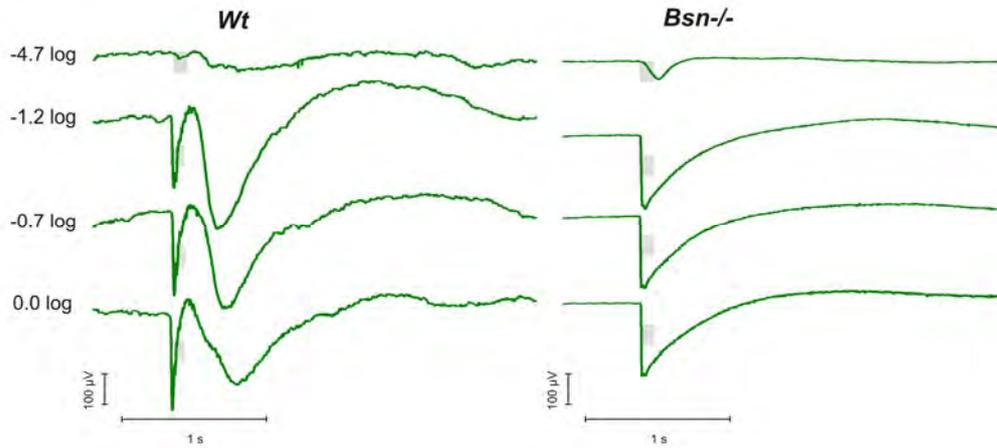
**Fig. 1.** Micro-ERG recorded from the *Bsn-/-* retina in comparison to *wt* μ-ERG. Light intensities are shown on the left side of the picture; grey areas indicate the stimulus duration (100 ms).
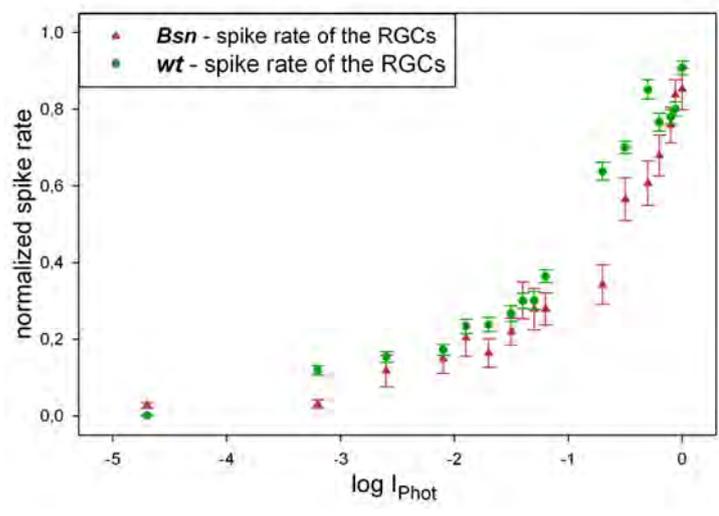


**Fig. 2.** Summary of responses of retinal ganglion cells from both mouse strains; spike rate as a function of stimulus intensity (log I Phot).

# Functional Properties of Retinal Ganglion Cells in P23H Homozygote Rat Model of Retinitis Pigmentosa During Photoreceptor Degeneration.

Kolomiets B[1,2], Simonutti M [1], Sahel JA [1,2], and Picaud S [1,2]

1 Institute of Vision, Université P et M Curie, Paris, France
2 Fondation Ophtalmologique A. de Rothschild

The P23H transgenic albino rat was generated to provide an animal model of retinitis pigmentosa, inherited retinal disorder with progressive loss of retinal function leading to blindness. In contrast to P23H heterozygote line, the P23H homozygote rats are characterized by very rapid decline in rod and cone function at P21 – P60 days. At these ages profound morphological changes also start to occur in inner retina (Cuenca et al., 2004). In an attempt to clarify whether these morphological changes affect the visual and electrically evoked responses in retinal ganglion cells (RGCs), we focus here on recordings from isolated retina of P23H homozygote rat. Initial *in vivo* ERG recordings were performed in transgenic rats and confirmed that later in development (P90, P130) principal components of the full-field electroretinogram are already significantly reduced in amplitude. Subsequently, using extracellular multielectrode array recording technique (MEA60 setup, MCS, Germany) from RGCs in *ex vivo* isolated retinas we demonstrate that in such transgenic animals with severely depressed ERG at P90 and P130, basic mechanism for visual information processing remains largely preserved. Multielectrode array recordings obtained with 3DMEA60 biochips (8x8 layout, 200 µm spacing, Ayanda Biosystems) from retinas of transgenic rats clearly demonstrate that comparable to age-matched wild type animals number of RGCs in P23H rats were spontaneously active and evenly spaced across the retinal area in MEA dish. The RGCs in transgenic rats presented routine (irregular or bursting) discharge patterns and typical mean firing rates. At least 70% of RGCs tested in 1.5x1.5 mm retinal area could respond to uniform light of photopic intensities, mainly with sustained ON- responses while OFF-responses were not found. Number of cross-correlation patterns (mutual or due to shared input activation) between nearby RGCs revealed. Single electrical stimuli (monophasic square pulses (0.1 – 300 µA), 200-500 µs duration, presented at 0.5Hz) were applied to RGCs layer through the pairs of nearby multielectrode array recording electrodes, dedicated to current stimulation. Direct local stimulation of RGCs layer evoked typical one-two-spike responses occurring at 10 – 300 µA thresholds and short (1.8 – 8 ms) latencies in limited number of RGCs located in vicinity to stimulation electrodes. However, considerably larger proportion of short-latent responses might be also present in other RGCs although obscured by artefact lasting for more than 1-2 ms period at higher (>100 µA) current intensities. Together, present results suggest that in the progress of retinal degeneration despite well documented morphological changes in outer and inner retina, the functional state of rescued RGCs in P23H homozygote rats after substantial loss of photoreceptors remain light sensitive, maintain their basic network properties and can be driven by local electrical stimulation.

## References

[1] Cuenca N, Pinilla I, Sauvé Y, Lu B, Wang S, Lund RD (2004) Regressive and reactive changes in the connectivity patterns of rod and cone pathways of P23H transgenic rat retina. Neuroscience. 2004;127:301-317.

# Processing of Directional Information from Neural Output of Rabbit Retina

Martiniuc A[1], Stürzl W[1,2], Knoll A[1] , Zeck G[3]

1 Computer Science Department VI, Technical University Munich, Garching (Germany)
2 Department of Neurobiology and Center of Excellence `Cognitive Interaction Technology', Bielefeld University, Bielefeld (Germany)
3 Department of Systems and Computational Neuroscience, Max Planck Institute of Neurobiology, Martinsried (Germany)

The estimation of motion direction from time varying retinal images is a fundamental task of visual systems. Neurons that selectively respond to directional visual motion are found in almost all species. A prominent example of the processing of directional information has been found in the rabbit, where direction selective neurons in lateral geniculate nucleus (LGN) signal movement-direction more precisely than their retinal counterparts [1]. However, the mechanism how this may be achieved remains unclear.

Here we propose a simple model that can explain sharpening of directional selectivity taking into account synaptic input from direction selective retinal ganglion cells (DSRGCs) only. We further suggest a model to account for other than the four cardinal directions encoded by the retina.

## 1 Methods

We recorded retinal ganglion cell activity from the adult isolated rabbit retina using a 60 channel multi-electrode array (Multichannelsystems, Reutlingen). Moving gratings in eight different directions were used to identify direction selective cells [2]. Directional tuning was determined by means of the index of directional selectivity ($DSi$).

After spike sorting the timestamps were passed to computational models mimicking a cell postsynaptic to the DSRGCs. We applied two models recently proposed to describe retinogeniculate transmission: a voltage-based model [3] that assumes linear summation of excitatory postsynaptic potentials (EPSPs), and an "integrate-and-fire" (I&F) neuron with conductance-based synapses [4]. We investigated the effect of EPSP summation and spike threshold in two different scenarios: (1) synaptic input from a single DSRGC, (2) input from two DS RGCs with different directional tuning.

## 2 Results and Discussions

### 2.1 Results

For single retinal input we found that the $DSi$ of the LGN neuron increased for all EPSP amplitudes tested (blue traces in Fig 1). While single EPSPs on their own do not reach threshold, rapid spiking activity in the DSRGC can trigger LGN spikes. The maintained firing rate is significantly reduced in our simulations. This effect is more pronounced for lower EPSP amplitudes. These findings were verified by the conductance-based I&F model (red trace in Fig. 1).

The combination of differently tuned ganglion cells often leads to an asymmetric tuning curve. Adjusting the synaptic strength of two inputs leads to symmetrically tuned postsynaptic neurons with intermediate directional tuning (Fig. 2).
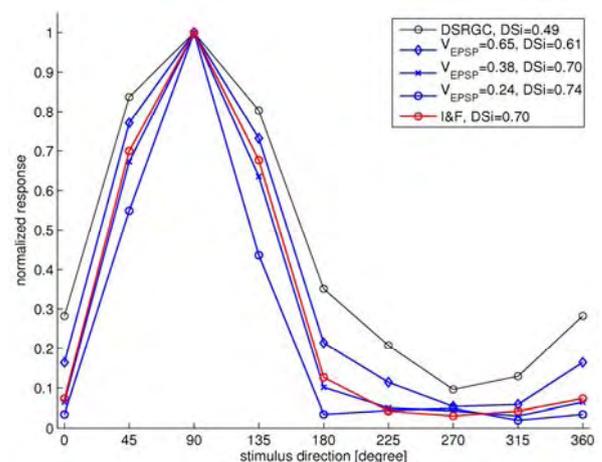


**Fig. 1. Sharpening of directional tuning**: Normalized response of a direction selective retinal ganglion cell (DSRGC, black trace), and of simulated LGN cells using the voltage based model (blue) or the I&F model (red). LGN cells with smaller EPSP amplitudes ($V_{EPSP}$ given in fractions of the spike threshold) achieve higher index of directional selectivity ($DSi$). The DS index is 1 for cells responsive for a single direction of movement and is 0 for non-tuned cells.
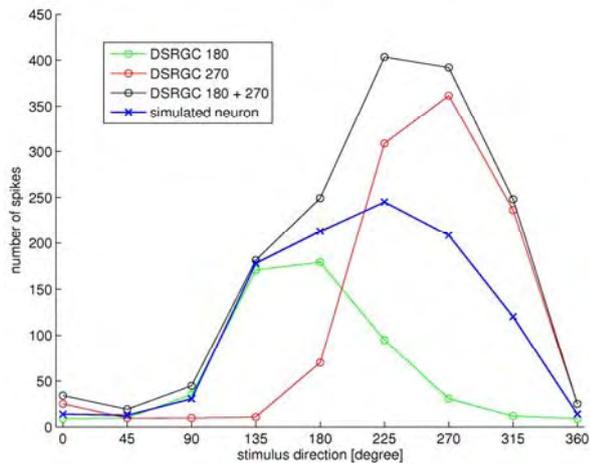
**Fig. 2.** Simulation of a post-synaptic neuron tuned to an intermediary direction (blue) by combining input of two DSRGCs, tuned to 180° (green) and 270° (red), respectively. Summation of the responses of the two DSRGCs leads to an asymmetric tuning (black).

## 2.2 Conclusions

Our simulations with realistic synaptic input based on extracellular recordings from retinal gan-glion cells can explain the sharpening of directional selectivity found in LGN neurons [1]. The sharpening is a result of the intrinsic spiking pattern of the DSRGCs combined with EPSP summation and spike threshold. As exemplified by the combination of two DSRGCs sharp directional information may provide the basis for fast estimation of local movement across the retina.

### References

[1] Levick WR, Oyster CW, Takahashi E. Rabbit lateral geniculate nucleus: Sharpener of directional information. *Science* 165: 712-714, 1969.
[2] Zeck GM, Masland RH. Spike train signatures of retinal ganglion cell types. *European Journal of Neuroscience* 26: 367-380, 2007.
[3] Carandini M, Horton JC, Sincich LC. Thalamic filtering of retinal spike trains by postsynaptic summation. *Journal of Vision* 7(14): 20, 1–11, 2008.
[4] Casti A, Hayot F, Xiao Y, Kaplan E. A simple model of retina-LGN transmission. *Journal of Computational Neuroscience* 25(47): 11003-11013, 2007.

# Optimization of Stimulation Parameters in Degenerate Mouse Retina by Using Glutamate Blocker

Jang Hee Ye and Yong Sook Goo*

Department of Physiology, Chungbuk National University School of Medicine, Cheongju, South Korea.
* Corresponding author. E-mail address: ysgoo@chungbuk.ac.kr

As a part of Korean retinal prosthesis project, we investigated the stimulation parameter in degenerate retina for the long term goal of acquiring the optimal stimulation parameters for the upcoming prosthesis. For animal model of degenerate retina, *rd/rd* mice were used for this study. From previous study, we identified the slow wave component originated from glutamatergic synapse in *rd/rd* mouse retina. In this study, we blocked the slow wave component with specific glutamatergic synapse blocker, and compared the differences in evoked responses before and after the drug treatment in degenerate retina.

## 1 Introduction

Photoreceptor loss as a result of retinal degenerative diseases, such as retinitis pigmentosa (RP) and age related macular degeneration (ARMD) are the leading causes of blindness in adults [1]. By electrical stimulation of the remaining retinal neurons, retinal prosthesis could be a feasible treatment which could restore useful vision in blind individuals. One of the prerequisites for the retinal prosthesis to succeed is optimization of electrical stimuli applied through prosthesis [2]. rd/rd mice was used for the animal model of RP. From previous study, we identified that in rd/rd mice retina, about 10 Hz slow wave component (Fig. 1) originated from glutamatergic synapse appeared along with ganglion cell spikes [3]. This slow wave component blocked any significant electrically evoked response peak in poststimulus time histogram (PSTH).

Therefore, in this study we blocked the slow wave component with specific glutamatergic synapse blocker and compared the differences in evoked response before and after the drug treatment for the long term goal of acquiring optimal stimulation parameters for the upcoming retinal prosthesis.

## 2 Material and Methods

### 2.1 Recording of retinal ganglion cell activity

C3H/HeJ (rd/rd mouse, postnatal 8 weeks) strain was used for RP model. From isolated mouse retina, retinal patch (~5 X 5 mm) was attached with the ganglion cell side on the surface of the multi-electrode array (MEA).



**A. Raw data**

**B. Filtered data: spike**

**C. Filtered data: slow wave component**

200 ms    40 µV
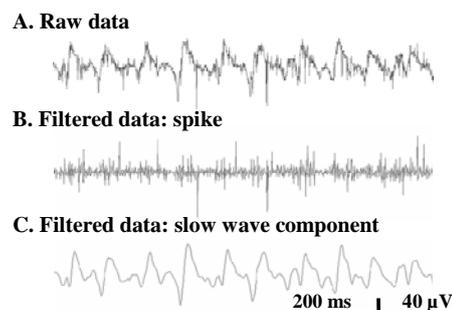
**Fig. 1.** Isolation of slow wave component in rd/rd mouse retina. Bandwidth: (A) 10 Hz ~ 3kHz. (B) 200 Hz ~ 3 kHz and (C) 10 Hz ~ 50 Hz. In raw data, slow wave component appeared along with the spikes.

### 2.1 Electrical stimulation & data analysis

8 X 8 grid layout MEA (electrode diameter: 30 µm, electrode spacing: 200 µm, and impedance: 50 kΩ at 1 kHz) was used for stimulation and recording the ganglion cell activity. Monopolar current stimulation wasapplied through one of 60 channel, and remaining channels were used for recording. 20 trains of biphasic pulse were randomly applied at the rate of 0.25 Hz. Phase width and current intensity changed from 60 ~ 1000 µs, from 2 ~ 50 µA, respectively. Electrically-evoked responses were observed during 1 ~ 25 ms time span after the stimulation. Evoked response was compared before and after CNQX and AP7 (100 µM) treatment. Charge density was calculated with Coulomb's law.

## 3 Results

The slow wave component in rd/rd mouse disappeared with CNQX and AP7 treatment (Fig. 2). There are two peaks of electrically-evoked responses (Fig.

3); very early (latency of 1 ~ 3 ms) and early (latency of ~5 ms) response. Before the CNQX and AP7 treatment, the amplitude of very early and early response was 108.16 ± 33.80 µV and 79.16 ± 21.62 µV, respectively (n=4). With CNQX and AP7 treatment, the amplitude of very early response was significantly increased (243.56 ± 20.93 µV, p<0.05), while that of early response was significantly decreased (33.12 ± 25.79 µV, p<0.01) (Fig. 3 B).

We acquired the strength-duration curve (SD curve) in rd/rd mouse. There is no significant change in SD curve with application of CNQX and AP7. The rheobase and chronaxie was about 2 µA and 600 µs, regardless of treatment of CNQX and AP7 (Fig. 4).

**A. Control**
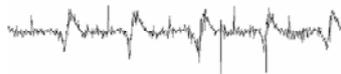
**B. CNQX + AP7**

200 ms | 40 µV

**Fig. 2.** Treatment of glutamatergic synapse blocker in *rd/rd* mouse retina.

**A. Electrically-Evoked Responses**
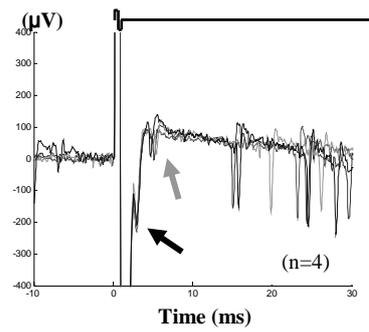


*(Figure continued)*

**B. Electrically-Evoked Responses with Perfusion of CNQX + AP7**
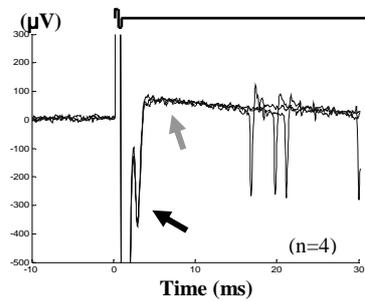


**Fig. 3.** Example of electrically-evoked responses of ganglion cells before (A) and after (B) glutamatergic synapse blocker treatment in rd/rd mouse retina (with 500 µs duration, 20 µA intensity current stimulus). Black and gray arrows indicate the evoked very early and early responses, respectively. n=number of traces.
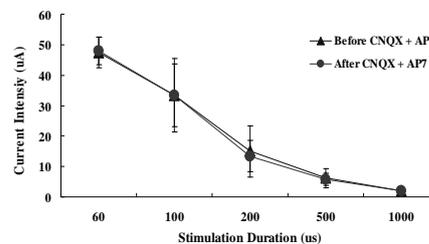


**Fig. 4.** Strength-Duration curve in *rd/rd* mice retina (n=6: No. of ganglion cells).

## 3  Summary & Discussion

The result showed that the amplitude of very early response was significantly increased with the application of glutamate blocker, CNQX and AP7, while that of early response was significantly decreased. For further study we will do artifact subtraction to clearly isolate two responses and to see if the two responses originate from the same unit. Because of the limited number of experiment (n=3 preparations), we should do more experiments to have solid conclusion regarding the question if the presence of slow wave component is a major obstacle in providing electrical stimulation through the prosthesis in degenerate retina.

**References**

[1]   L. Hyman. (1987): Epidermiology of eye in the elderly. *Eye, 1 pt 2, 330-341*

[2]   I. J. Lowenstein, S. R. Montezuma, J. F. Rizzo III. (2002): Outer retinal degeneration : An electronic retinal prosthesis as a teratment strategy. *Arch. Ophthalmology, 47. 588-596.*

[3]   J. H. Ye and Y. S. Goo. (2007): The slow wave component of retinal activity in *rd/rd* mice recorded with multi-electrode array. *Physiol. Measurement, 46. 3198-3204.*

# Pharmacology, Toxicology, Drug Screening

# Potential of MEA Based Neurotoxicity Assays for Regulatory Hazard Assessment of Chemicals

Tomasz Sobanski

European Commission- Joint Research Centre, Italy

# Tissue-specific neurotoxicity of cytostatic and anaesthetic drugs

Jochen F. Meyer[1*], Tiffany N. Kinney[1], Florian Ilchmann[2], Bernhard Wolf[1,2]

1 Technische Universität München, Zentralinstitut f. Medizintechnik Imetum, Garching, Germany
2 Technische Universität München, Heinz Nixdorf-Lehrstuhl für Medizinische Elektronik, München, Germany
* Corresponding author. E-mail address: meyer@tum.de

MEA-supported primary neuronal cell cultures have become a reliable, efficient, yet highly involved tool in pharmacological research. We have used frontal cortex (FC) and substantia nigra (SN) tissue to quantify the acute neurotoxic effects of cisplatin, a common chemotherapeutic agent, and lidocaine, a local narcotic which has also been shown to inhibit mitosis in several cell lines in vitro. Both substances caused dose-dependent activity suppression in both tissues, with FC cultures generally being more susceptible to both substances than SN. In addition to the changes in overall action potential production, internal activity pattern changes were analyzed in FC cultures.

## 1 Background

### 1.1 Neurological side-effects

Many cytostatic drugs as well as local and systemic anaesthetics have been shown to exhibit neurological side effects. These rare but serious effects are difficult to diagnose. While complications involving parts of the peripheral nervous system are well recognized, the attention given to acute side effects to the central nervous system does not match the severity of the problem. We propose a novel approach to quantifying the neurotoxicity of these drugs by measuring the changes in total action potential production as well as effects on the internal activity patterns.

## 2 Methods

### 2.1 Electrophysiology

We used an electrophysiological experimental setup similar to the one introduced by GW Gross et. al. [1] with custom made MEA glass plates (CNNS, University of North Texas, Denton, USA), a Plexon MEA-WS/64 Workstation (Plexon Inc., Dallas, USA) and data analysis software Neuroexplorer (Nex Technologies, Littleton, USA) as well as iBurst and Autoplots (CNNS).

### 2.2 Cranial tissue culture

Frontal cortex (FC) and substantia nigra (SN) were the tissue types chosen for this study. Because of physiological and cell biological differences of these areas, different forms of neurotoxicity may point towards possible mechanisms of action of the compounds under investigation. FC and SN tissue was iso-lated from Balb/C embryonic mice (gestation: day 15). Networks reached maturity and produced spontaneous electrical activity after 3 weeks incubation time. Morphological differences between FC and SN were seen and are depicted in figures 1 and 2. FC neuronal cell bodies were generally larger than SN neurons and had a greater number of cell processes.
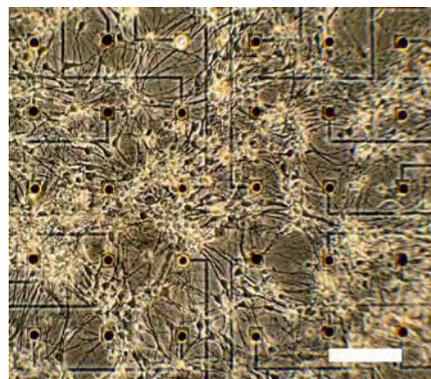


**Fig. 1.** FC cells grown on PDL/Laminin coated MEA plate. White bar: 150 µM
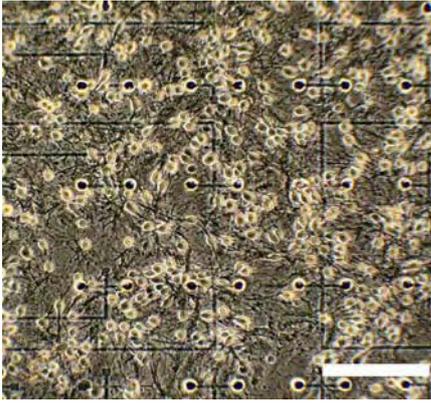
**Fig. 2.** SN cells grown on PDL/Laminin coated MEA plate. White bar: 150 μm

## 2.3 Typical activity patterns

FC network activity consisted of bursts, i. e. short sequences of at least 5 action potentials with repetition frequencies of typically 100-500 Hz and strong coordination of the majority of active cells (Fig. 3). For burst parameter definitions see figure 5. SN cultures had more complex activity patterns comprised of seemingly random firing and only occasional embedded coordinated bursting, making analysis of burst parameter changes difficult (Fig. 4).
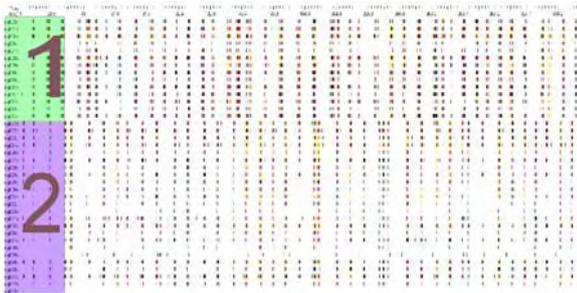


**Fig. 3.** Typical FC activity pattern; Data from a two-network recording: Upper part from network 1, lower from network 2. Time period shown: 200 sec. Each row represents one active unit, which can be signals from a cell body, an axon or a dendrite.
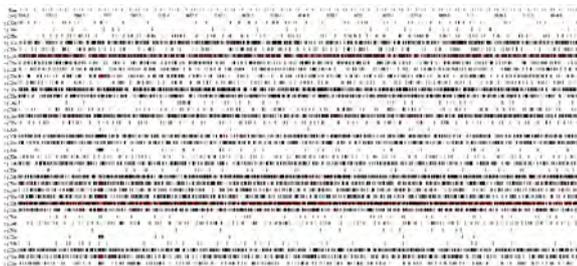


**Fig. 4.** Typical SN activity pattern. Time period shown: 360 sec.
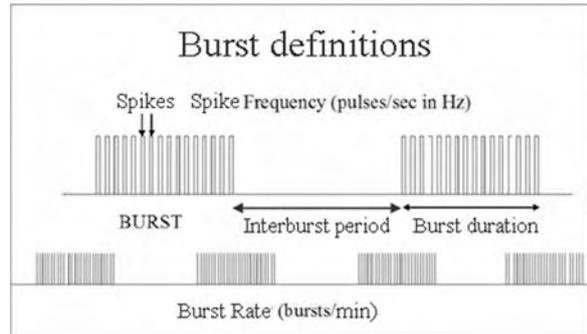


**Fig. 5.** Definitions of important burst variables in coordinated activity

## 3 Results

### 3.1 Dose-dependent activity decay

The 23 cultures (14 FC, 9 SN) we have recorded from so far exhibited a dose-dependent decrease in action potential production. The obtained data show that FC tissue was much more susceptible to both drugs, with IC50s of 18 μM (CisPt) and 2 μM (lidocaine), while the SN cultures were less affected by them (IC50, CisPt: 130 μM; IC50, lidocaine: 65 μM). Figures 7-10 illustrate the observations from a total of 14 FC cultures and 9 SN cultures. Sigmoidal curve fittings were performed using Origin software (OriginLabs, Northhampton, USA). Figure 6 shows an example of a single experiment with increasing doses of lidocaine on FC cells. Activity suppression was generally reversible via 1-2 medium changes.

Cisplatin suppressed action potential production by interfering with the activity pattern; only at very high concentrations were neurons entirely silenced. Lidocaine acted differently; at moderate concentrations many neurons had already dropped out from network activity (see figures 11 and 12).
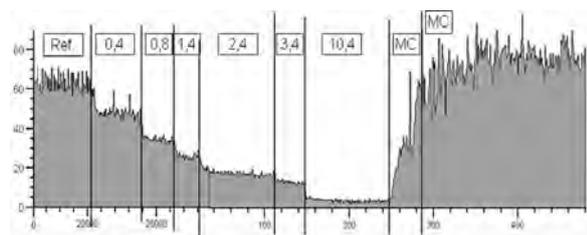


**Fig. 6.** Responses of an FC network to increasing doses of lidocaine. Concentrations in μM. Two medium changes (MC) caused the activity to return to even higher values than before the first compound addition. This was most likely due to accumulation of metabolites in the one day old reference medium and the partial nutrient depletion of it.
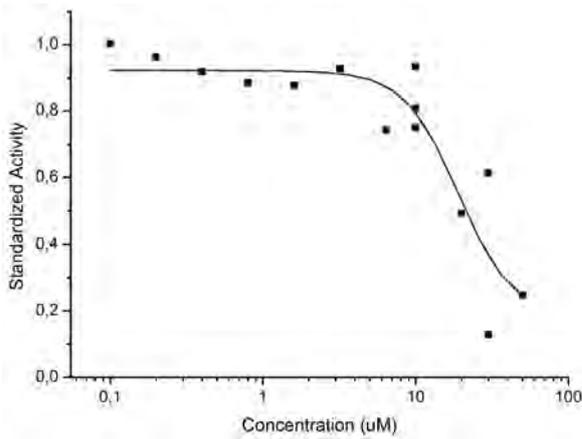
**Fig. 7.** Dose-dependent spike reduction due to cisplatin; Data from 4 FC cultures. Activity values here and all of the following diagrams were standardized with respect to the initial reference value.



**Fig. 9.** Activity decay from lidocaine administration in 7 SN networks

## 3.2 Burst pattern changes

Internal activity pattern changes in terms of average burst duration, average interburst period, and spike frequency within the bursts were measured in FC cultures. They require further analysis and may then point towards possible mechanisms of action. Figs. 11-12 summarize the data on the variables burst duration, interburst period, spike frequency in bursts ("Spike Hz") and the number of active and bursting neurons in the data set.



**Fig. 10.** Decrease in action potential production under lidocaine; data from 10 FC cultures

## 3.3 Additional observations

An initial increase of activity at very low lidocaine concentrations was seen in 80% of the cultures. Onset times for effects to be apparent were usually in the range of 3-5 minutes. Inhibition of spike production did not recover on its own within a time range of up to 12 hours but was generally reversible (80-100%) via one or two consecutive medium changes. Acute morphological changes of individual cells, such as swelling or shrinking, were not observed.



**Fig. 8.** Cisplatin-induced activity reduction; data from 2 SN cultures.
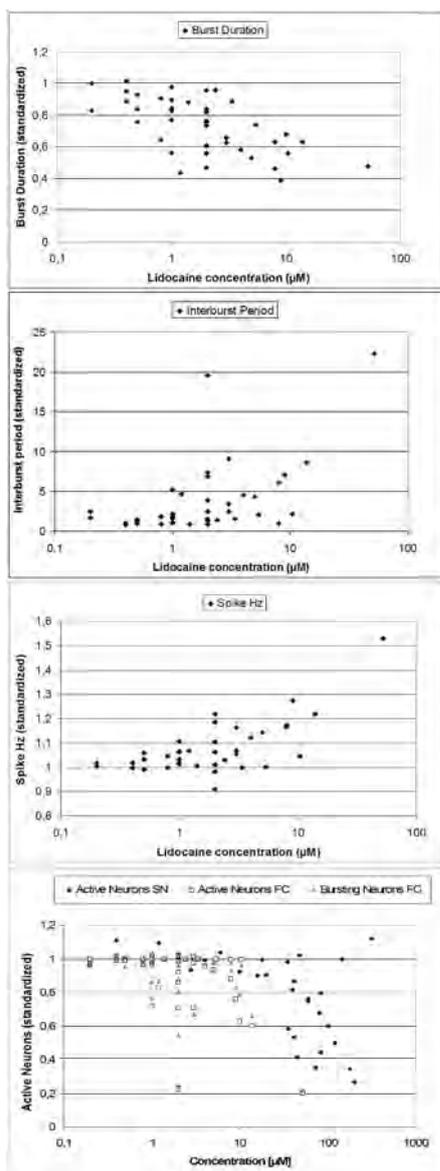
**Fig. 11.** Effects of Lidocaine on burst duration, interburst period, Spike frequency in bursts and active neurons (from top to bottom)
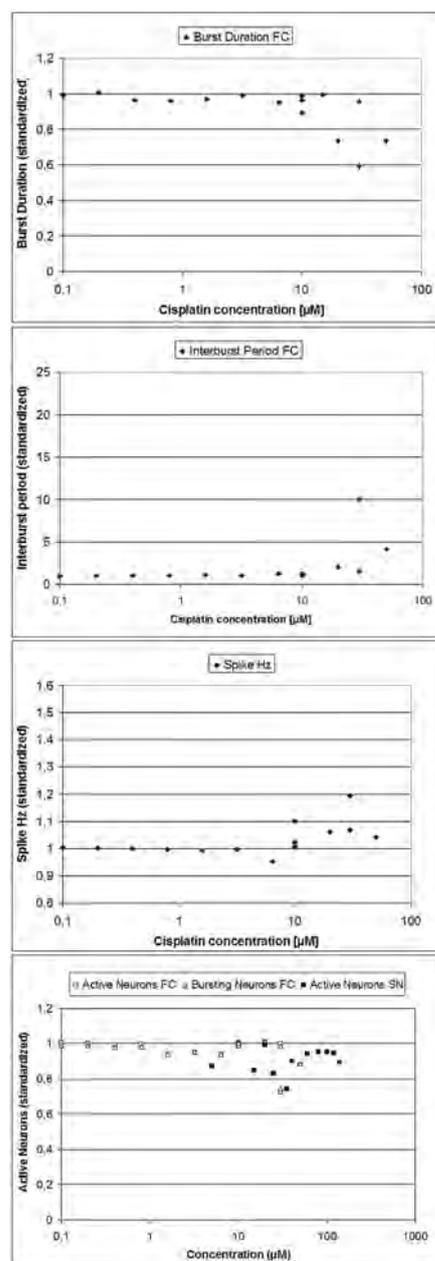


**Fig. 12.** Effects of CisPt on burst duration, interburst period, Spike frequency in bursts and active neurons (from top to bottom)

## 4 Discussion

Lidocaine and cisplatin inhibited the electrical activity of primary neuronal cell cultures in a dose-dependent manner. The effects were tissue-specific, which manifested in different IC50 values (FC: 2 µM/Lidoaicne, 18 µM/CisPt; SN: 65 µM/Lidocaine, 130 µM/CisPt), as well as in burst pattern changes. These pattern changes were only quantified in FC cultures, since native SN activity does not consist of highly coordinated bursts. Under the influence of lidocaine, bursts became shorter and sparser in a dose-dependent manner. The repetition rate of the individual action potentials inside the bursts rose as well. In both tissue types, the number of active neurons

dropped significantly at concentrations beyond 1 μM (FC) and 30 μM (SN). In some instances, some of the neurons remained active but lost the coordination of their activity. Under Cisplatin, similar observations were made. However, the onset of these effects was at considerably higher concentrations. Conversion of bursting activity into random firing was not observed under Cisplatin.

# 5 Outlook

With proceeding automation, the experimental setup presented here will become an efficient screening tool for neurotoxic side-effects of a broad variety of medical compounds. Members of our department have designed a new multi-site recording system [2]. It contains 24 separate 32 channel-MEA plates and is designed to fit any standard liquid handling system. The MEA plates are equipped with optical fluorescent pH and oxygen sensor spots and a Pt-1000 temperature sensor. The modular design enables the user to incubate the bottom plate with the cell cultures as one unit before assembly of the upper board that contains preamplifier and sensor signal processing electronics.
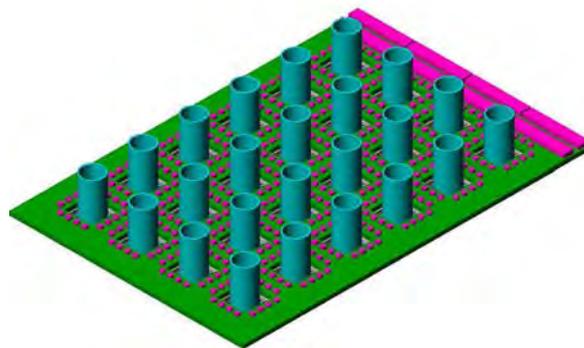


**Fig. 13.** Design study of a 24-well recording platform with disposable 32 channel MEA plates

**References**

[1] G. W. Gross, B. K. Rhoades, D. L. Reust, F. U. Schwalm (1993): Stimulation of monolayer networks in culture through thin-film indium-tin oxide recording electrodes. *J. Neuroscience Methods, 50(2) 131-43*

[2] F. Ilchmann, V. Lob, J. Wiest, B. Wolf (2008): Automated Cell Analytics, Application on Sensor Chips. Screening - trends in drug discovery, Volume 9, 21-23

# Drug development of new synthetic peptides for cancer pain treatment: Electrophysiological profiling of the opioid receptor system

Alexandra Gramowski[1,2,*], Olaf Schröder[2], Konstantin Jügelt[2], Andrzej Lipkowski[3], Aleksandra Misicka-Kesik[4], Dieter G. Weiss[1]

1 Institute of Biological Sciences, University of Rostock, Rostock, Germany;
2 NeuroProof GmbH, Rostock, Germany
3 Polish Academy of Science, Medical Research Centre, Warsaw, Poland
4 Faculty of Chemistry Warsaw University, Warsaw, Poland
* Corresponding author. E-mail address: alexandra.gramowski@neuroproof.com

Progressive pain associated with advanced stages of cancer is the major factor that destructs last span of life of patients. Here more potent analgesics are needed. The focus of the EU project consortium NORMOLIFE is on the development of new, highly effective multi-target analgesics which will interact with those opioid receptors which are expressed in inflamed and/or pathologically modified tissues.

We investigate the electrophysiological in vitro effects of newly developed peptides by comparing them with a substance database of a variety of well-characterized agonists and antagonists of the μ, κ, δ-opioid and other pain relevant receptor systems as references. We use primary murine frontal cortex and spinal cord networks on MEA neurochips to study the acute affects of these peptides on the electrical activity, regarding inhibition, excitability, synchrony, oscillation, and burst structure. The complex description of activity changes of neuronal networks co-cultured with glia allows a sophisticated approach to quantify their complex mode of actions. Our analyses provide multiparametric information on neuronal activity changes to assess the therapeutic or toxicological potential of neuroactive drugs. Through pattern recognition analyses and comparison with data of established analgesics drugs we obtain information on the physiological activity and potency of the new synthetic peptides and their potential as analgesic drugs.

## 1 New multi-target analgesics

Modern medicine can prolong the life expectancy of patients with advanced cancer. However, progressive pain that is associated with progression of the disease is the major factor that destructs the last span of life. The applications of oral (morphine) pills or transdermal patches with lipophilic analgesic drugs are the most common treatments of cancer pain. These compounds penetrating the central nervous system produce side effects to such extent that the pain treatment is often to be reduced by doctors or refused by the patients. Discoveries in recent years indicated changes in expressions of pro- and antinociceptive receptors in pathologically altered peripheral tissues as well as in the central nervous system. The concerted modulation of these receptors in combination with designed receptor ligands may block nociceptive signal formation and transmission more effectively than traditional monotherapies. The project NORMOLIFE which is supported by the FP6 of the European Union will yield basic data on structural requirements of analgesics for treatment of persistent cancer pain in advanced stages. The major goal is the chemical design of new multi-target molecules and the analysis of their pharmacological properties that will result in the selection of the best lead compounds for further clinical evaluation as possible new potent analgesics for multi-component cancer pain treatment. The approach in which compounds are designed to interact with a wide spectrum of targets involved in pain signal formation and transmission is a new and original therapeutic strategy, opposite to current strategies that use drugs which are as receptor-selective as possible. The approach involves three general complementary scientific objectives: chemistry, **in vitro** biopharmacology and **in vivo** pharmacology that will be accomplished by multidisciplinary teams integrated in the project.

The major prospective application of the results will be a more effective treatment of acute as well as chronic, neuropathic and inflammatory cancer pain of patients with advanced stages of the disease. The preclinical experimental data of a large number of newly developed compounds will allow for selection and proposition of new medicines for further clinical

evaluation. Compounds will be preselected in **in vitro** tests. The in vitro tests comprise receptor affinity evaluation and the here described functional screening assays. The selected compounds will be finally characterized in vivo in an animal model of cancer pain.
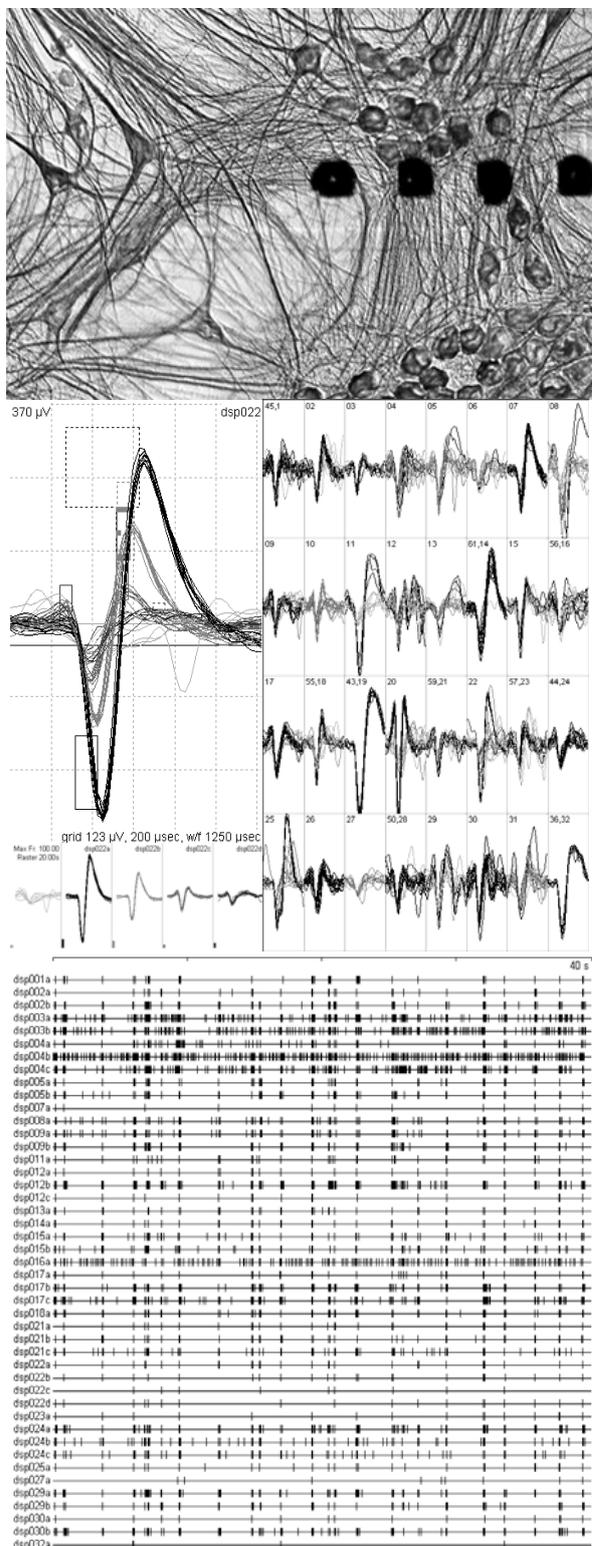


**Fig 1:** (Top) Frontal cortex network grown on a 64 electrode MEA 21 days *in vitro* (Staining: DAB against neurofilaments). (Center) Action potential recording from one electrode (left) and all active electrodes (Right). (Bottom) 40 seconds of spontaneous activity of 45 neurons of a frontal cortex culture.

## 2 "Fingerprinting" of substances – Multiparametric data analysis and pattern recognition

*In vitro* neuronal monolayer cultures are increasingly recognized as tools to study and characterize the functional response of neuronal networks to substances, bridging the gap between high-throughput approaches, genomics, and proteomics on the one side and animal tests on the other.

For our functional screening in vitro assay we used the microelectrode array (MEA) neurochip technology consisting of the MEAs (CNNS, UNT, Denton Texas, USA), the MEA workstation (Plexon, Inc., Dallas, TX, USA), and analyzing software (Plexon, Inc., and NeuroProof GmbH, Rostock, Germany) (Figure 1). By combining the measurement of single cell activities of neuronal networks on MEA-neurochips with optimized proprietary procedures for data analysis and pattern recognition we obtain high content results. The activity patterns of the neural networks are long-term stable [1], [5], [6] and change for substances specifically in a brain region characteristic manner [2], [3], [4]. With this functional screening, in particular multiple effect mechanisms, desired as well as unwanted, can be recognized and analyzed. Simultaneously they are systems which are complex enough to improve the predictability of drug effects in the tissue of origin. Unlike systems with neuronal stem cells or progenitor cells, primary cultures develop from a mixture of different types of neurons and glial cells. Glial cells have important auxiliary functions for metabolism, for supplying neurons with ions and nutrients, and they are necessary participants in the dialogue that neurons carry out at the synapses. Glial cells behave like additional targets of neuronal signals and respond to the synaptic release of neurotransmitters and neuromodulators. The concept of tripart synapses (pre-, postsynapse and glia) has been accepted to explain the contribution of glia in the synaptic transmission and information processing in the CNS.

The MEA technology allows an accelerated clarification of the mechanism of effects of neuro-active drugs. Modes of action of a substance can be visualized by dose-effect curves. Curve fitting yields $EC_{10}$ (10% effective concentration), $EC_{50}$, $EC_{90}$ and the Hill coefficients, nH. The Hill-coefficient as important parameter for Safety Pharmacology provides indications about how critical an incorrect dose could be in treat-

ment. The course of the dose-effect curve shows whether multiple mechanisms of action are involved.

Methods of spike train analysis are used to assess the activity patterns of neuronal networks. With the aid of the programs NEX (Plexon, Inc.), ANALYZER, GRAPHS and SQUID (NeuroProof GmbH) we can calculate more than 200 different spike train parameters. With these we mainly describe five fundamental categories of activity changes: general activity, burst structure, synchronicity, oscillatory behavior, and network connectivity.

The spike and burst rate, i.e. the number of spikes and bursts per unit of time, are two of the most important features. A further parameter in this category is the ratio of the spikes during the in bursting periods to all spikes. The burst structure is defined by parameters such as the mean frequency of spikes in bursts, describing the strength of the bursts; the number of spikes in bursts, the burst length and others. Tissue cultures obtained from different brain regions, e.g. from the frontal cortex and from the spinal cord, differ significantly in these features.

Action potentials occur with clearly periodic patterns. The regularity of these periodic patterns – the oscillatory behavior – is an additional characteristic of the network activity that may be changed by neuroactive substances. The influence of substances on the synchronicity is another very important characteristic phenomenon of activity patterns. Since the action potentials can be recorded from several neurons simultaneously with high precision in the microsecond range over a longer time, the analysis of the synchronicity is possible with a high temporal resolution.

Based on the 200 spike train features for an experimental episode, the changes of the activity patterns caused by a substance can be clearly identified, so that substances can be classified with respect to existing patterns. This documents the reproducibility of the observed activity patterns. In connection with our pattern recognition methods, we select the characteristic spike train features for each individual substance or group of substances that deliver dose-response curves with a high discriminative significance and informative value.

**DAMGO (μ-Agonist) — Classification with 40 best scoring features (L-Score)**

| ref. substance | main receptor | KB01 0.41 | KB02 0.42 | KB03 0.32 | KB04 0.40 | KB06 0.44 | KB07 0.37 | KB08 0.41 | KB12 0.39 | KB16 0.26 | KB21 0.38 | KB24 0.27 | KB25 0.45 |
|---|---|---|---|---|---|---|---|---|---|---|---|---|---|
| **DAMGO** | **μ-Agonist** | | | 97 | | | | | | | 99 | | |
| Endomorphin1 | μ-Agonist | | | | | | | | 0 | 14 | | | |
| Fentanyl | μ-Agonist, κ-Agonist | | | | 38 | | | | | | | | |
| Ultiva | μ-Agonist | | | | | 36 | 22 | 38 | | | | | 17 |
| Dynorphine | κ-Agonist | 28 | 22 | 1 | | | | | | | | | 17 |
| Nalorphine | κ-Agonist, μ-Agonist | | | | | | | 38 | 71 | | 1 | | |
| U50488 | κ-Agonist | | | | | 57 | 49 | 30 | | 28 | | | |
| 59 | δ-Agonist | 57 | | 1 | | | | | | | | | |
| DPDPE | δ-Agonist | | 51 | | | | 48 | | | 58 | | | 65 |
| 3280 3CD | SP-Antagonist | 16 | | | 6 | | | | | | 0 | | |
| AA2050 | SP-Antagonist | | | | | | | 25 | 29 | | | | |
| AA2080 | SP-Antagonist | | 28 | | 14 | | | | | | | | |

**DPDPE (δ-Agonist) — Classification with 40 best scoring features (L-Score)**

| ref. substance | main receptor | KB01 0.41 | KB02 0.42 | KB03 0.32 | KB04 0.40 | KB06 0.44 | KB07 0.37 | KB08 0.41 | KB12 0.39 | KB16 0.26 | KB21 0.38 | KB24 0.27 | KB25 0.45 |
|---|---|---|---|---|---|---|---|---|---|---|---|---|---|
| DAMGO | **μ-Agonist** | | | 40 | | | | | | | 53 | | |
| Endomorphin1 | μ-Agonist | | | | | | | | 5 | 1 | | | |
| Fentanyl | μ-Agonist, κ-Agonist | | | | 38 | | | | | | | | |
| Ultiva | μ-Agonist | | | | | 54 | 14 | 54 | | | | | 9 |
| Dynorphine | κ-Agonist | 38 | 4 | 38 | | | | | | | | | 2 |
| Nalorphine | κ-Agonist, μ-Agonist | | | | | | | 35 | 73 | | 33 | | |
| U50488 | κ-Agonist | | | | | 29 | 22 | 4 | | 6 | | | |
| 59 | δ-Agonist | 43 | | 21 | | | | | | | | | |
| **DPDPE** | **δ-Agonist** | | 95 | | | | 82 | | | 93 | 89 | | |
| 3280 3CD | SP-Antagonist | 20 | | | 32 | | | | | | 14 | | |
| AA2050 | SP-Antagonist | | | | | | | 11 | 21 | | | | |
| AA2080 | SP-Antagonist | | 2 | | 24 | | | | | | | | |

**Dynorphine A (κ-Agonist) — Classification with 40 best scoring features (L-Score)**

| ref. substance | main receptor | KB01 0.41 | KB02 0.42 | KB03 0.32 | KB04 0.40 | KB06 0.44 | KB07 0.37 | KB08 0.41 | KB12 0.39 | KB16 0.26 | KB21 0.38 | KB24 0.27 | KB25 0.45 |
|---|---|---|---|---|---|---|---|---|---|---|---|---|---|
| DAMGO | **μ-Agonist** | | | 1 | | | | | | | 19 | | |
| Endomorphin1 | μ-Agonist | | | | | | | | 28 | 61 | | | 0 |
| Fentanyl | μ-Agonist, κ-Agonist | | | | 32 | | | | | | | | |
| Ultiva | μ-Agonist | | | | | 48 | 64 | 33 | | | | | 3 |
| **Dynorphine** | **κ-Agonist** | 91 | 93 | 97 | | | | | | | | 94 | 99 |
| Nalorphine | κ-Agonist, μ-Agonist | | | | | | | 43 | 23 | | 42 | | |
| U50488 | κ-Agonist | | | | | 29 | 17 | 29 | | 28 | | | |
| 59 | δ-Agonist | 4 | | 1 | | | | | | | | | 1 |
| DPDPE | δ-Agonist | | 7 | | | | | 7 | | 12 | 3 | | |
| 3280 3CD | SP-Antagonist | 4 | | | 39 | | | | | | 39 | | |
| AA2050 | SP-Antagonist | | | | | | | 23 | 49 | | | | |
| AA2080 | SP-Antagonist | | | 0 | 35 | | | | | | | | |



**Fig 2:** Left: Cross validation experiments with feature selection for the μ-, κ-, and δ-opioid receptor agonists DAMGO, DPDPE, and Dynorphine A, respectively. Right: Related dose-response of electrical spike rate network activity to rising concentrations of DAMGO, DPDPE, and Dynorphine A. Values are expressed as mean ± SEM based on normalized activity (native=100%). Statistical analysis was based on Student's paired t-test comparing each concentration with the reference activity for spike or burst rate ($* p \leq 0.05$; $** p \leq 0.01$; $*** p \leq 0.001$).

# 3 Establishment and cross validation of a reference data base for the opioid receptor system

To characterize the electrophysiological properties of newly synthesized opioid-like peptides, we establish a data base of reference compounds acting at the opioid receptor system. Therefore we determined acute dose-response-curves to quantitatively describe the effects of known agonists and antagonists for the opioid receptor system and other pain relevant receptors (e.g. for NK1 and NPY). Fourteen standard reference substances were screened (e.g. DAMGO, Dermorphine, Endomorphine, DPDPE, Dynorphine A, Substance P, Neuropeptide Y) in frontal cortex and in spinal cord networks. The data showed brain region-specific responses of the activity to the different substances. For all substances tested on both tissues the dose-dependent effects were more distinct in spinal cord, revealed by lower $EC_{10}$, $EC_{50}$, and $EC_{90}$ values.

For the validation of the method, we performed cross validation experiments (Figure 2). We classified 3 substances for each classification experiment. Cross validation was performed with leaving out one experiment for each cross validation. Feature selection, a widely accepted method in bioinformatics [7], was performed and the 40 best discriminating features after L-Score computation were selected. Our classification results for the validation experiments revealed a total of correct prediction rates between 64% and 99%.

## 3.1 Screening of newly developed peptides

With the reference data base a precise assessment of the influence of new peptides is possible. So far 18 new peptides synthesized by project partners were tested and analyzed by pattern recognition methods. Classification studies revealed similarity of the electrophysiological behaviour between known opioid agonists and antagonists and most of the new synthetic peptides. This way we obtain information on the physiological activity and potency of new synthetic peptides and their potential as analgesic drugs. To further improve our classification results and prediction of involved modes of action for the new multi-target peptides we will include more references in the data base, and incorporate both tissues into the classification. Additional isobolographic studies will advance the data base. Together with data from binding studies and animal tests performed partners our results will form a base for the selection of lead substances for further preclinical and clinical testing.

## References

[1] Gramowski A, Jügelt K, Weiss DG, Gross GW. Substance identification by quantitative characterization of oscillatory activity in murine spinal cord networks on microelectrode arrays. Eur. J. Neurosci. 2004;19: 2815-2825

[2] Gramowski A, Jügelt K, Stüwe S, Schulze R, McGregor GP, Wartenberg-Demand A, Loock J, Schröder O, Weiss DG. Functional screening of traditional antidepressants with primary cortical neuronal networks grown on multielectrode neurochips. Eur.J.Neurosci. 2006; 24: 455-65

[3] Gross, GW, Norton, S, Gopal, K, Schiffmann, D, Gramowski, A. Nerve cell network in vitro: Applications to neurotoxicology, drug development, and biosensors. Cellular Engineering. 1997; 2: 138-147

[4] Gopal KV, Miller BR, Gross GW. Acute and sub-chronic functional neurotoxicity of methylphenidate on neural networks in vitro. J Neural Transm. 2007;114:1365-75

[5] Potter SM, DeMarse TB. A new approach to neural cell culture for long-term studies. J Neurosci Methods. 2001; 110:17-24.

[6] Wagenaar DA, Pine J, Potter SM. An extremely rich repertoire of bursting patterns during the development of cortical cultures. BMC Neurosci. 2006;7:11

[7] Guyon I, Elisseeff A. An introduction to variable and feature selection, J. Machine Learning Res.2003; 3: 1157-1182

# In vitro model for the peripheral nervous system

Agabi Oshiorenoya [1,2,3,*], Stefan Weigel[2] , Hansruedi Früh[2], Ruedi Stoop[3], Arie Bruinink[2,†]

1 Materials and Biology Interactions, Empa, Lerchenfeldstrasse 5, 9015 St. Gallen, Switzerland
2 Neuronics AG, Technoparkstrasse 1, 8005 Zürich, Switzerland
3 Institute of Neuroinformatics, UNI-ETH Zürich Winterthurerstrasse 190, 8057 Zürich, Switzerland
* Corresponding author. E-mail address: * osh.agabi@empa.ch, †arie.bruinink@empa.ch

Presently, only a single entity of the peripheral nervous system (PNS), e.g. motor neurons or DRG Neurons is used for investigating in vitro the effects of drugs and chemicals on the electrical activity of the PNS. A more holistic view could be obtained using a reduced model of neuromuscular system by co-culturing Motor Neurons and Muscle Cells. The MEA surface is functionalized to support contractile cells (muscle cells) and neural cells (Motor Neurons and dorsal root ganglia (DRG) neurons) also ensuring that recording and stimulation is not precluded by such functionalization.

## 1 Introduction

Current models for in vitro toxicity sensing revolve around single cell types or slices. However, one of the most studied systems, the neuromuscular junction provides ample space for observing a more system wide effects of drugs and other external factors on normal physiological functioning of biological systems.

In our experimental set up, we co-culture spinal cord neuron re-aggregates and myoblasts (which form myofibrils or muscle cells) on the same micro electrode array (MEA) chip. Therefore, the upper motor centres (i.e. motor cortex) are absent but the spinal cord neurons reorganize into circuits [1] that display typical regimes of activity as reported by others [2]. The myoblasts seeded on the chip form myobrils which display signals typical of $Ca^{2+}$ transients that could also be observed in vivo.

In addition, such systems also enable detailed view or understanding of the signal transduction between motor neurons and myofibrils on on hand and myofibrils and DRG neurons on the other hand. Knowledge obtained from our work could also prove beneficial in other applications like prosthesis and computation in vitro.

## 2 Methods

Owing to the contractile nature of the myobrils, a compliant surface should be designed such that the possibility of recording the field potentials of the myofibrils is not precluded. Collagen fibres are utilized as the elastic substrate however, the chip side of the collagen is subsequently treated with a combination of APTES and Glutaradehyde. The collagen fibres are covalently bonded to the silicon surface so that they are able to withstand the shear forces exerted by the myofibrils otherwise they are pulled on the chip surface. It is also noteworthy that the collagen matrix lasts for up to 14 days in vitro due to the functionalization.
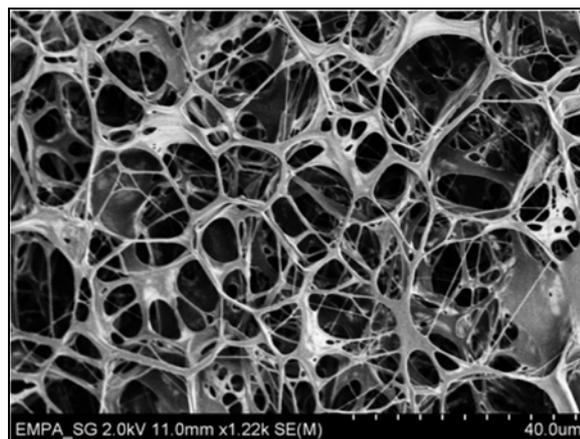


**Fig. 1.** SEM Image of collagen scaffold for muscle contractility.

Culture medium (Dubelco Modied Essential Medium (DMEM) ref. 41965 85.47% heat-inactivated horse serum, 8.55% Nutrient Concentrate N3, 0.85% chicken embryo extract, 4.27% Sodium Pyruvate (100mM) 85% and sterilized with a 0.45micron filter)

## 3 Results

For all 55 cultures observed with 5 different plating sessions a typical recording would begin show spiking activity both muscles and neurons on DIV 3. The muscle cells were separated from the neural cells, while being grown on a collagen sponge substrate, fig.-1. Typical signals obtained from the myofibrils show physiologically relevant signals i.e. the sharp efflux of $Ca^{2+}$ and the exponential re-absorption of same also called the calcium transient (Fig. 2). The Calcium transients last for approx. 10ms and maximum amplitude of approx. 20 micro volts.
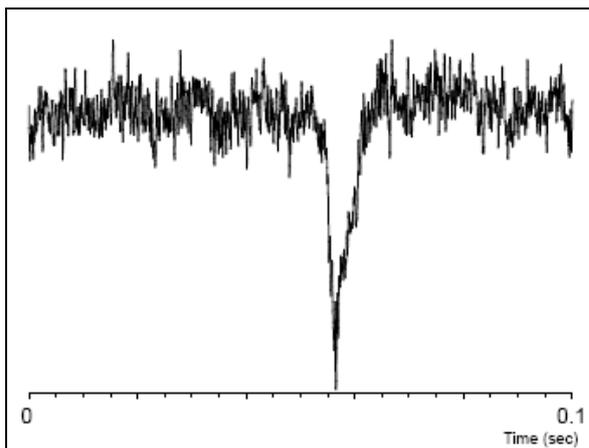
**Fig. 2.** Typical calcium transient.

We show the formation of functional neuromuscular junctions (should be referred to as neurites associated receptor patches NARPs as described in [3]) which is demonstrated by a co-localization of acetylcholine receptor (AChR) and neurites endings of the motor neurons. It could be also be observed that the contractile activity of the myofibrils is greatly increased in the presence of the neural cells as compared with myofibrils mono cultures.

The highest frequencies in myofibril activity were observed during the bursting regimes of the neural network as shown in fig. 3. The muscle cells are able to follow such bursting regimes faithfully but they lag behind the frequencies of spinal neurons.
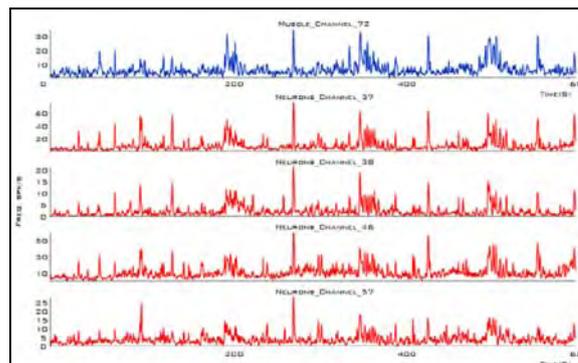


**Fig. 3.** The blue trace shows the frequencies of the myofibril while the red traces follow the activity of the spinal cord network.

## 4   Conclusion

We are able to effectively functionalize MEA chip surface in such a way that they support contractile cells for long periods without the attendant pull off of the collagen scaffold.

The formation of functional connections between the myofibrils and motor neurons is demonstrated. It is also shown that myofibrils achieve their highest frequencies during the bursting regime of the neural network.

**References**

[1]   P. B Armstrong and M T Armstrong. A role for  fibronectin in cell sorting. J Cell Sci, 69(1):179{197, 1984.

[2]   Jurg Streit, Anne Tscherter, Marc O. Heuschkel, and Philippe Renaud.The generation of rhythmic activity in dissociated cultures of rat spinal cord. European Journal of Neuroscience, 14(2):191

[3]   L W Role, D G Roufa, and G D Fischbach. The distribution of acetylcholine receptor clusters and sites of transmitter release along chick ciliary ganglion neurite-myotube contacts in culture. J. Cell Biol., 104(2):371{379, 1987.

# Influence of CSF from patients with cognitive decline on neuronal network activity: Blood-brain barrier permeability is correlated with neuronal network activity increase

Philipp Görtz[1], Christian Lange-Asschenfeldt[1], Frauke Otto[2], Jessica Opatz[2], Sebastian Illes[2], Tillmann Supprian[1], Mario Siebler[2]

1 Klin k für Psychiatrie und Psychotherapie, Heinrich-Heine-Universität, 40225 Düsseldorf
2 Neurologische Klinik; Heinrich-Heine-Universität, 40225 Düsseldorf

Cerebral spinal fluid (CSF) amyloid beta (1-42) concentration correlated well with cognitive scores in a sample of 20 patients with Alzheimer's disease and Mild Cognitive Impairment. Neither CSF amyloid beta (1-42) nor tau protein influenced neuronal network activity in vitro, though. However, patient CSF albumin index as a marker of blood brain barrier (BBB) dysfunction was associated with a significant increase in spike and burst activity. This possibly indicates an effect of other neuroactive substances that may cross the BBB under the conditions of this disorder.

## 1 Background

Alzheimer's disease (AD) is the most common reason for dementia in the elderly. Among the most reliable diagnostic parameters are the decrease of Aß(1-42) protein and the increase of tau protein in cerebrospinal fluid (CSF). The relevance of other CSF markers like chemokines or function of blood-brain barrier (BBB) is discussed controversially. In the present study, we investigated the influence of CSF of patients with AD and its precursor, amnestic mild cognitive impairment (aMCI), on neuronal network activity of rat cortical neurons cultured on multi electrode arrays (MEAs; Multi Channel Systems, Reutlingen, Germany).

## 2 Methods

CSF and serum samples of 20 individuals with AD or aMCI (MMST score ranged from 7/30 to 30/30) were analyzed for Aß(1-42) protein, tau protein and CSF albumin index (CSF-AI), a marker for the BBB permeability. A significant positive correlation was found between Aß(1-42) protein concentration and patients' MMST scores (r=0.65, p=0.006) underscoring the diagnostic validity of this parameter. To determine the influence of patients CSF on neuronal networks the basal neuronal network activity of cryopreserved embryonic rat cortical neurons (QBM Cell Science; Ottawa, Canada) on MEAs incubated with artificial CSF (NaCl 150 mM, MgCl 1 mM, KCl 1mM, Glucose 10 mM, HEPES 10 mM pH 7.4) was recorded (days in vitro 18-30). CSF was adjusted with HEPES buffer to pH 7.4 before application. Network activity was recorded after 15 minutes when a steady state of spontaneous activity was reached. Change in neuronal network activity was determined by calculating the relative change in overall spike activity, burst activity and burst duration (Spanner, Result, Tönisvorst, Germany). We found a significant correlation between CSF-AI and increase of spike activity (r=0.58, p=0.029), increase of burst activity (r=0.63 , p=0.044) and reduction of burst duration (r=-0.72, p=0.016). No correlation was detected between Aß(1-42) protein concentration and spike activity (r=0.32, p=0.41), burst activity (r=0.157, p=0.576) and burst duration (r=1.00, p=0.73). Also no significant correlation was found between tau protein concentration and spike activity (r=-0.304, p=0.2711), burst activity (r=-0.3, p=0.277) or burst duration (r=0.19, p=0.48).

## 3 Discussion

We found no influence of the typically seen tau-protein increase or Aß(1-42) protein decrease on neuronal network activity. Rather, activation of the neuronal network was correlated with an increased CSF-AI as a measure of BBB permeability. However, the enhanced network activity may not be ascribed to albumine itself but rather to other potentially harmful substances in the CSF that have crossed the BBB and impacted on neuronal network function by an unspecific ion-channel modulation. This effect could be relevant for patients with severe dysfunction or disruption of BBB.

# MEA supported cortical cultures as a novel tool in Alzheimer's research

Jochen F. Meyer[1*], Frits Kamp[3], Tim Bartels[3], Tiffany N. Kinney[1], Florian Ilchmann[2], Klaus Beyer[3], Bernhard Wolf[1,2]

1 Technische Universität München, Zentralinstitut für Medizintechnik Imetum, Garching, Germany
2 Technische Universität München, Heinz Nixdorf-Lehrstuhl für Medizinische Elektronik, Munich, Germany
3 Ludwig-Maximilians-Universität Munich, Adolf-Butenandt-Institute, Department Biochemistry, Laboratory for Neurodegenerative Disease Research, Munich, Germany
* Corresponding author. E-mail address: meyer@tum.de

The acute neurotoxic effects of several different aggregates of the amyloid ß peptide were investigated using primary neuronal networks from murine embryonic cortical tissue grown on multielectrode-arrays. Both monomer and oligomer aggregates were found to decrease spontaneous electrical activity in the sub-micromolar range. Specific antibodies could partially reverse this effect.

## 1 Background

Alzheimer's disease (AD) is characterized by the appearance of neuritic plaque deposits comprised primarily of fibrillar and ß-sheet rich aggregates of the amyloid ß peptide which is produced normally by the intramembranous proteolysis of APP, a protein of unknown function, throughout life. Different lines of evidence suggest that oligomer intermediates rather than the mature fibrillar deposits are responsible for the primary neurotoxic effects and memory loss in AD, probably by membrane incorporation and pore formation in neuronal membranes. Multi-Electrode-Arrays were used to characterize the neurotoxicity of different species of amyloid beta peptide on primary cultures of frontal cortex neurons.

## 2 Methods

We used an electrophysiological experimental setup similar to the one introduced by GW Gross et. Al. [1993] with custom made MEA glass plates (CNNS, University of North Texas, Denton, USA), a Plexon MEA-WS/64 Workstation (Plexon Inc., Dallas, USA) and data analysis software Neuroexplorer (Nex Technologies, Littleton, USA) as well as iBurst and Autoplots (CNNS).

Frontal cortex tissue was isolated from Balb/C embryonic mice (gestation: day 15). Networks reached maturity and developed spontaneous electrical activity after 3 weeks incubation time. Spontaneous activity of frontal cortex cultures always consisted of bursts, i. e. short sequences of at least 5 action potentials (APs) with repetition frequencies of typically 100-500 Hz.

Three different ß amyloid species were used: Monomers, oligomers and fibrils (F. Hoffmann-La Roche AG, Basel), as well as monomer-specific 2D8-antibodies and oligomer-specific A11-antibodies (LMU, Laboratory for Neurodegenerative Disease Research, Munich)

## 3 Results

### 3.1 Beta-amyloid toxicity

Beta-amyloid peptide appears to be acutely toxic in both monomer and oligomer aggregates in the sub-micromolar range. Dose-dependent behaviour was observed (see fig. 1). Oligomer species produced a stronger effect than monomers, but even fibrils caused a slight activity decrease. However, activity inhibition was not complete at these concentrations (fig. 2).
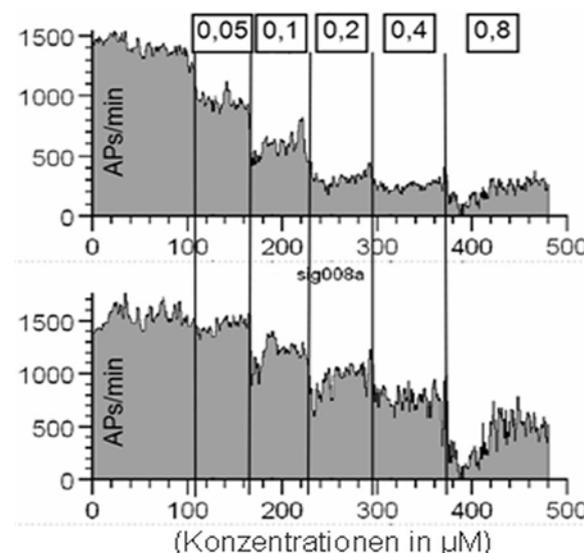


**Fig. 1.** Activity histograms of 2 individual neurons showing typical activity decrease during addition of ß-amyloid oligomers. Numbers denote concentrations in μM.
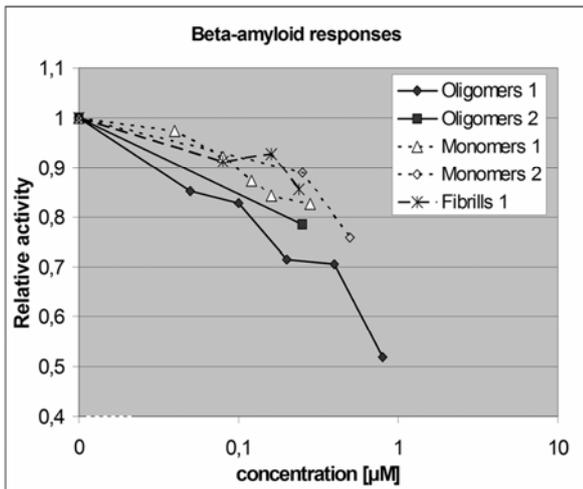
**Fig. 2.** Activity inhibition in 6 FC cultures under treatment with ß-amyloid oligomers, monomers and fibrils. Activity values were normalized with respect to the reference activity (value 1).

## 3.2 Interaction of specific antibodies

For recovery of activity suppression, the oligomer-specific A11-antibody was quite effective on oligomer-treated tissue (fig. 3). In one case ("B" in fig. 3), it granted partial protection from a second and third addition of 0.25 µM oligomers. The monomer-specific 2D8-antibodies had no beneficial effect on monomer-treated tissue.
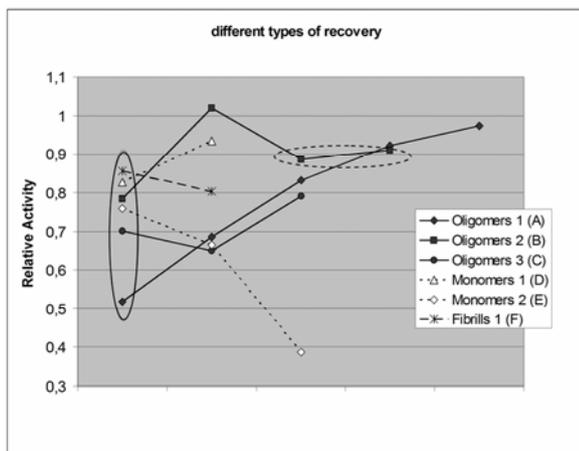


**Fig. 3.** Different approaches to achieving recovery of electrical activity: (A): native recovery over 8 hrs, (B): A11-antibodies, then addition of 2 x 0,25 µM oligomers (2 data points within dashed ellipse), (C): 2D8-antibodies, then A11-antibodies, (D): medium change, (E): A11-antibodies, then 2D8-antibodies, (F): A11-antibodies. The first point of each curve denotes the activity under maximum compound concentration (solid ellipse).

## 4 Discussion

Beta-amyloid peptides cause dose-dependent activity suppression in primary cortical cultures. In addition to confirming oligomer toxicity, our findings suggest that the established hypothesis that neither monomer nor fibrill species can be neurotoxic may

have to be revised, with regard to acute, functional toxicity. Whether there is a significant change in burst pattern dynamics must be analyzed in future studies. We are convinced that the proposed experimental setup will help shed light on electrophysiological effects of neurodegenerative proteins and possible rescue strategies using species-specific antibodies.

In future studies, we will be using a novel recording system that was built around a multi-well culture chamber with 24 separate MEA-plates and integrated sensors for pH and oxygen consumption (Fig. 4). Using a computer-controlled liquid handling robot, up to 24 experiments can be run simultaneously with high precision and under microscopic control.



**Fig. 4.** Automated screening setup with a) Till Photonics „iMIC" microscope, b) liquid handling robot, c) climate control chamber, d) control computer, and e) multi-well sensor plate

**References**

[1] G. W. Gross, B. K. Rhoades, D. L. Reust, F. U. Schwalm (1993): Stimulation of monolayer networks in culture through thin-film indium-tin oxide recording electrodes. *J. Neuroscience Methods, 50(2) 131-43*

# ARTEMIS Project - In Vitro 3D Neural Tissue System For Replacement Transgenic Animals With Memory/Learning Deficiencies.

Antonio Novellino[1,2*], Alessandro Maccione[1,2], Marcello Mulas[2], Angel Moreno[3], Eleni Nicodemou-Lena[3], Camillo Pizarro[3], Laura Lopez[3], Andrea Lanzara[3], Sara Cobena[3], Petros Lenas[3]

1 ETT S.r.l., Genoa, Italy
2 NBT - Department of Biophysical and Electronic Engineering, University of Genoa, Genoa, Italy
3 ARTEMIS Group - University Complutense of Madrid (UCM), Madrid, Spain
* Corresponding author. E-mail address: antonio.novellino@ettsolutions.com

The aim of this work is to present the preliminary result of a innovative three-dimensional neural tissue-like construct to replace the use of animals in experiments in transgenics and toxicology, on studies related with effects of genes, (transgenics) or chemicals, (toxicology), on neural tissue structure and function and in particular on studies related with memory and learning.

## 1 Introduction

The ARTEMIS project seeks to design, develop and optimize an in vitro system to replace the use of animals in transgenics and toxicology experiments, and in studies related to the effects of genes, chemicals, and neural tissue structure and function, such as memory and learning. From a scientific perspective, it targets the development of a three-dimensional neural tissue-like construct that is formed by the synaptic connections developed among neurons that are produced from mouse embryonic stem cells. For its operational goal, the project seeks to replace transgenic animals with memory and learning deficiencies with the in vitro developed neural tissues.

The in vitro tissue comes from embryonic cell lines that have the genes involved in memory and learning "switched off". The objective is to assess and compare the ability of the transgenic tissue to memorize electrical stimuli with that of the normal tissue.

Assessing the role of genes in memory and learning in vitro would provide preliminary information at tissue level, so as to determine the design of the transgenic animals towards the optimal ones with a higher probability of having altered phenotypes.

This would effectively reduce the number of transgenic animals that are currently produced by trial-and-error methods. The proposed in vitro system can effectively integrate biochemical damages to behavioral ones.

## 2 Material and Methods

### 2.1 The Cell Preparation

Mouse embryonic stem cells (ESC) are cultured inside a porous biomaterial that guide the network development. The tissue is interfaced at two opposite sides with multielectrode arrays for stimulating and recording purposes.

### 2.2 The Recording System

The recording/stimulation system is based on both commercially available devices (flexMEAs, MPA32I, PGA32 and STG1004 from Multi Channel Systems, Reutlingen, Germany) and ad hoc developed connections and software tools (Fig. 1).
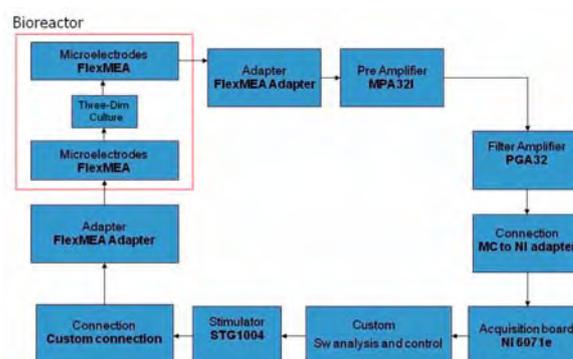


**Fig. 1**. The architectural overview of the system

In order to allow long-term monitoring of the system during differentiation and growth the recording system is fed into a Minucel-Minitissue bioreactor (Fig. 2).

**Fig. 2.** The recording system inside the incubator

The controlled complexity and easiness in biochemical analyses make this innovative in vitro system a suitable candidate for the replacement of the use of transgenic animals in memory/learning deficiencies studies and neurotoxicology tests.

## 3 Result and Conclusions

The innovative paradigm has been tests at both biochemical and electrophysiological level and here we report these primary results: Fig. 3 shows the plated stem cells during the differentiation process.



**Fig. 3.** Differentiated ESCs at 14 DIV

The neural cells form spheres from which neurons start spreading. The shown culture is still at an initial differentiation. Fig. 4 shows the recorded electrical activity in different channel.
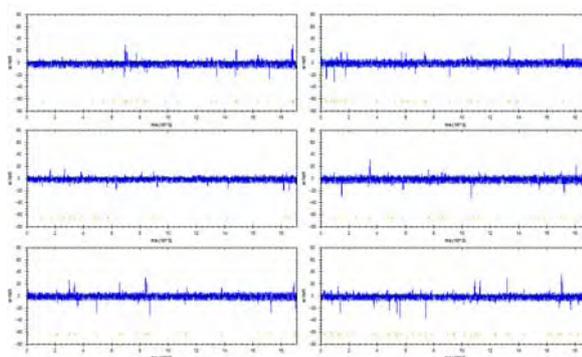


**Fig. 4.** Recording from the culture: at early age of the culture, the activity from different electrodes is not synchronous.

ESCs is an in vitro readily renewable cell source. In principle, these cell can be organized synaptically as in vivo, so that they could be used to replace animal tests related with simple cognitive functions like memory, (alternative instead of complementary), that are based on the topology of the synaptic network.

ESCs have been already used in the design of new in vitro alternatives and a test for embryotoxicity has been already validated [1]. However these in vitro systems are dedicated to studies at the cell level and they are not specifically designed to exhibit properties of the synaptic network, which is the main theme of our investigation.

Here we extent the design of the in vitro system with neurons arising from the differentiation of mouse ESCs to the development of the synaptic network providing a new design methodology which involves structural and functional guidance of in vitro development of the synaptic network in an in vivo-like manner.

### Acknowledgement

### References

[1] Bremer S and Hartung T. (2004) : The use of embryonic stem cells for regulatory developmental toxicity testing in vitro-The current status of tests development. *Current Pharmaceutical Design 10, 2733-2747*

# Store-Operated Calcium Entry Affects Neuronal Network Activity In Vivo And In Vitro

Jessica Opatz[1], Frauke Otto[1], Susanne Thomsen[1], Mario Siebler[1], Axel Methner[1*]

1 Heinrich-Heine University Düsseldorf, Department of Neurology, Düsseldorf, Germany
* Corresponding author. E-mail address: axel.methner@gmail.com

The mechanism of SOC-dependent calcium entry (SOCE) is an important means of maintaining cell calcium homeostasis, and activation of the SOCE key regulator Stromal interaction molecule 1 (Stim1) is tightly coupled to endoplasmic reticulum (ER) luminal store contents. Uncontrolled calcium entry following a sustained activation of Stim1 severely impairs neuronal activity both *in vitro* and *in vivo* and points to an important function of SOCE in the nervous system.

## 1   Background

Calcium-dependent signal transduction controls highly diverse biological functions such as electrical excitability and cell viability. Within the cell, Ca2+ is mainly stored in the ER and when depleted restored from the extracellular space by opening of store-operated channels (SOC) mediated by translocation of Stim1 from the ER to the plasma membrane. In this study, we investigated the impact of SOCE on neuronal network activity by uncoupling SOCE from luminal store content using a highly selective uncoupling peptide of Stim1 (SUP-1) and the SOC channel inhibitor 2-aminoethoxydiphenyl borate, 2-APB, in both in vivo and in vitro experiments.

## 2   Methods

Synchronously oscillating networks of cryopreserved rat cortical neurons were cultivated on multielectrode arrays. Recordings were simultaneously taken on 64 channels after 14-21 days in culture, and electrophysiological parameters of extracellular network activity were determined following application of SUP-1 or the control peptide C-SUP-1, with or without 2-APB pretreatment. Expression of Stim1 protein in brain was determined by quantitative PCR and immunoblotting. SOCE-dependent intracellular calcium elevation was fluorescently measured in both primary neurons and neuronal cell lines. In vitro data were corroborated by non-invasive recordings of cortical activity and electrical potential in mice via electroencephalograpy and direct current potential measurement following intraperitoneal administration of SUP-1 or C-SUP-1, respectively.

## 3   Results

In this study, we demonstrated that the SOCE key regulatory component Stim1 is expressed in rodent brain. Opening of SOC channels independently of store content transiently upregulated network activity of synchronized rat cortical neurons as characterized by an increase in spike rate and burst rate per minute, followed by a prolonged period of overall network inhibition. Downregulation of network activity by SUP-1-mediated uncoupling of Stim1/SOCE was significant, compared to the corresponding control peptide C-SUP-1, and was preceded by network desynchronization. Conversely, abrogation of calcium influx following application of 20 µM 2-APB led to a stabilization of network activity and was sufficient to inhibit SUP-1-mediated effects. Our findings hint to a SUP-1-induced deregulation of Stim1-dependent calcium homeostasis via plasma membrane channels as demonstrated by detection of calcium influx across the plasma membrane following SUP-1 treatment. Thereby, *in vitro* observations are in line with *in vivo* data where systemically administered SUP-1 leads to severe burst suppression in mice in a dose-dependent manner.

## 4   Conclusion

Our current investigations for the first time demonstrate the relevance of SOCE-mediated calcium entry on neuronal network activity both *in vivo* and *in vitro*. Uncoupling calcium entry from luminal calcium content by SUP-1-mediated permanent translocation of SOCE activator Stim1 evoked an uncontrolled and sustained calcium entry from the extracellular space in neuronal cultures. *In vitro* findings were punctuated by corresponding *in vivo* data of recordings of murine neuronal electrical activity. Therefore, our current investigation contributes to understanding the mechanism of SOCE-mediated regulation of cellular calcium homeostasis and further indicates the high relevance of SOCE for nervous system functional activity.

**Acknowledgement**

We thank QBM Cell Science, Canada, for kindly providing cryopreserved rat cortical neurons.

**References**

[1] Otto F. et al. (2003): Cryopreserved rat cortical cells develop functional neuronal networks on multielectrode arrays. Journal of Neuroscience Methods, 128, 173-181

# Desynchronisation Of Neuronal Network Activity In Traumatic Brain Injury

Frauke Otto[1*], Jessica Opatz[1], Philipp Görtz[2], Christian Lange-Asschenfeldt[2], Sebastian Illes[1], Marcel Dihné[1], Rudolf Hartmann[3], Dieter Willbold[3], Mario Siebler[1]

1 Heinrich-Heine University, Department of Neurology, Düsseldorf, Germany
2 Heinrich-Heine University, Department of Psychiatry, Düsseldorf, Germany
3 Forschungszentrum Jülich, Institute of Neuroscience and Biophysics, Jülich, Germany
* Corresponding author. E-mail address: Frauke.Otto@uni-duesseldorf.de

Cerebrospinal fluid from patients with traumatic brain injury modulates neuronal network activity and leads to inhibition and desynchronisation. Increased concentrations of glutamatergic substances in the cerebrospinal fluid and partial recovery of network changes after application of NMDA-antagonist APV indicates a relevant glutamatergic mode of action. Further detailed analysis might help in preventing and treating functional neuronal disturbances in traumatic brain injury.

## 1 Introduction

Traumatic brain injury (TBI) is the main cause for mortality and long-time disability in young adults. Apart from structural lesions release of neuroactive substances has been considered to cause functional neuronal disturbances. The composition of cerebrospinal fluid (CSF) from patients with TBI is often modified, but the functional impact of this modified CSF is still not fully investigated. We therefore tested the functional impact of physiologic and modified CSF on the electrophysiological parameters of neuronal networks.

## 2 Methods

CSF was obtained for diagnostic purpose from patients with TBI by external ventricular drain or from control subjects with other neurologic disease (OND) by lumbar puncture. Surplus CSF no longer required for standard diagnostics was centrifuged, aliquoted and stored at – 35 °C. Cryopreserved embryonic rat cortex neurons were thawed and plated on multielectrode arrays. Spontaneous extracellular network activity was sampled simultaneously from 60 planar microelectrodes. Recordings were started with a well-defined bath solution (artificial CSF: 150 mM NaCl, 1 mM $CaCl_2$, 3 mM KCl, 1 mM $MgCl$, 10 mM HEPES, 10 mM glucose). Content of CSF was analysed by NMR spectroscopy (Forschungszentrum Juelich).

## 3 Results

Within three weeks, cryopreserved embryonic neurons formed a neuritic network with a stable and synchronous spontaneous network activity in artificial CSF (ACSF). Application of pure human CSF is well tolerated by rat cryopreserved neurons. In comparison to ACSF, OND-CSF (pH 7.4-7.5) significantly enhanced network activity by increasing the spike rate per minute and burst rate per minute threefold without affecting the synchronicity (Figure A). TBI-CSF (pH 7.4-7.5) modulated network activity by means of inhibition and desynchronisation (Figure B). This effect could partly be reversed by adding NMDA-antagonist APV, indicating a relevant glutamatergic impact of TBI-CSF. TBI-CSF and OND-CSF differed in NMR spectroscopy in several spectra as well as in concentration of total protein and lactate, but not in concentration of electrolytes (sodium, calcium, magnesium and potassium).
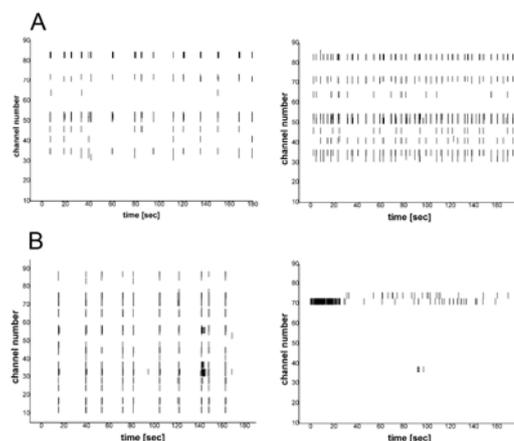


**Fig.** Spike raster plots: change of neuronal network activity after application of OND-CSF (A, right) or TBI-CSF (B, right) compared to artificial CSF (A and B, left).

## 4 Conclusion

Our study indicates that TBI-CSF contains several neuroactive substances rather than one active substance. One relevant electrophysiologic mode of action might be mediated via the NMDA receptor. Detailed analysis will determine the origin of these factors and might help in preventing and treating functional neuronal disturbances in TBI.

# Receptor-Cell-Transistor Sensor with Serotonin Receptor and K⁺ Channel

Peitz I, Fromherz P

Department of Membrane and Neurophysics, Max Planck Institute for Biochemistry
Martinsried / München, Germany

We report on the electrical interfacing of a ligand-gated ion channel to a field-effect transistor on the level of individual cells without an intracellular contact by a patch pipette. The ionotropic serotonin receptor 5-HT3A was overexpressed in HEK293 cells on a silicon chip. We contransfected the voltage-gated channel Kv1.3 to emulate the effect of voltage-clamp by a patch-pipette. When serotonin was applied, a biphasic transient of the extracellular voltage was recorded with an electrolyte-oxide-semiconductor transistor. By comparison with experiments under voltage-clamp and current clamp, the following mechanism was established: Upon application of serotonin, 5-HT3A channels open in the upper free membrane. The concomitant depolarization activates the Kv1.3 channels in the whole cell. Part of the potassium outward current flows through the attached membrane and along the cell-transistor junction and gives rise to a positive voltage. In a second phase, 5-HT3A channels open in the lower attached membrane with a delay due to diffusion of the agonist into the area of adhesion. Now, a net inward current flows through the attached membrane and along the cell-transistor junction and gives rise to a negative voltage. The coupling of an ionotropic receptor to a semiconductor device establishes a prototype for noninvasive receptor-cell-transistor sensorics that combines biochemical specificity with a direct electronic readout for applications in drug screening, diagnostics, and environmental analysis.

# Effects of SDF-1α and SDF-1-derived peptides on the electrophysiology of neuronal networks from rat cortex measured with Multielectrode Arrays (MEA)

Tom Wiegand[1], Birigit Hasse[2], Hans Werner Müller[1]

1 Department of Neurology, Heinrich-Heine-University Düsseldorf, Germany
2 NEURAXO Biopharmaceuticals GmbH
3 Molecular Neurobiology Laboratory, Heinrich-Heine-University, Düsseldorf, Germany

CXCR4 is a member of the G-protein-coupled receptor family and is expressed in neurons, astrocytes and microglia. Stromal cell-derived factor-1 (SDF-1α, CXCL12) is the only known ligand of CXCR4 and is expressed by astrocytes and neurons. SDF-1α dependent activation of CXCR4 was shown to affect cellular migration, regeneration and survival but can also modulate neuronal activity through regulation of intracellular calcium levels. In addition, CXCR4 can also serve as coreceptor for the entry of HIV-1 by enabling the major coat protein gp120 to attach to the target cell.

The aim of our work is to understand how SDF-1α affects the electrophysiology of a neuronal cell culture with a high proportion of glial cells and to investigate the effects of various SDF-1-derived peptides on network activity in comparison to the full length protein. We have synthesized eight SDF-1–derived peptides four of which were fusion peptides containing the CXCR4-binding domain. Applying immunocytochemistry we could demonstrate that the CXCR4 receptor is expressed in mixed cortical cell cultures (cryopreserved primary cortex cells from E18/19 rats) which generate functional cortical networks. We monitored the concentration-dependent effects of recombinant SDF-1α and the SDF-1-derived peptides to such neuronal networks grown on multielectrode arrays and determined their electrophysiological properties as a consequence of chemokine and peptide addition. The electrophysiological response of the cultures revealed to be complex and has, therefore, to be analysed with a defined and elaborated parameter set. Every channel has been classified individually with the following parameters: number of spikes, number of bursts, length of bursts, number of spikes in bursts, inter-burst-interval and frequency. In addition we have also applied compounds known to block SDF-1 dependent effects and substances known to modulate the second messenger cascade. For the SDF-1α – application, our results clearly demonstrate a general concentration dependent increase of network acivity. With the application of the different peptides we could show that some of them alter the network activity and others do not: therefore, the complete SDF-1α molecule is not needed to activate CXCR4. Our concomitant calcium-imaging-experiments further revealed that electrophysiology-modulating peptides alter the intracellular Calcium- and cAMP-level of the neurons.

In the next steps we will identify if these effects are direct effects on the neuronal cells mediated only through CXCR4 or if also other receptors are involved, e.g. RDC-1/CXCR7.

# Using the microelectrode array (MEA) to study hyperpolarising field potentials of non-excitable cells

Law JKY[2], Yeung CK[1*], Ingebrandt S[3], Rudd JA[1], Chan M[2]

1 Department of Pharmacology, Faculty of Medicine, The Chinese University of Hong Kong, Shatin, Hong Kong
2 Department of Electronic and Computer Engineering, The University of Science and Technology, Hong Kong.
3 Institute of Bio- and Nanosystems and CNI - Center of Nanoelectronic Systems for Information Technology, Forschungszentrum Jülich GmbH, D-52425 Jülich, Germany.
* Corresponding author. E-mail address: chi-kong_yeung@lycos.com

This study attempts to correlate the present findings with established knowledge of peritoneal mast cells under different physiological conditions, and we aim to demonstrate the applicability of the MEA to study electrophysiological changes, in terms of field potentials, of non-excitable cells (1).

## 1        Background

Mast cells are involved in type-1 allergic responses, typified by the release of histamine following immunological as well as non-immunological challenges (2). This release of histamine appears to be affected by cytoplasmic calcium concentration ($[Ca^{2+}]_i$) (3, 4). While $Ca^{2+}$ levels are obviously important in mast cell activation, ionic gradients of potassium ($K^+$) and chloride ($Cl^-$) are likely to also play important roles in secretory responses through their influence on membrane potential and thus $Ca^{2+}$ influx. In contrast to excitable cells, mast cell membrane hyperpolarisation is required to support $Ca^{2+}$ entry (5). Indeed, secretagogues, such as compound 48/80, have been shown to cause a fast hyperpolarisation and an increase in intracellular $Ca^{2+}$ levels (6).

## 2   Methods and Results

The present system detected a net gain of intracellular negative charge (with a positive field potential signal shape), which could either be due to an efflux of cations (e.g. K+) or an influx of anions (e.g. Cl-). In order to classify the recorded signal shapes were indeed primarily due to an efflux of K+, medium containing either high K+ (150mM), which disrupts K+ ionic gradient, or charybdotoxin (ChTX, 100nM), which blocks Ca2+-activated K+ channels, was used (Fig. 1). In both conditions, the latent periods; i.e. the time from the moment of drug application to the onset of response, were not significantly affected. The field potentials reduced to similar levels regardless of the concentration of compound 48/80 used (Fig. 1 and Fig. 2a). High $K^+$ buffer increased the temporal periods; i.e. *the duration of response*, while ChTX did not (Fig. 2b).

Because neither high K+ nor ChTX completely eliminated the cellular response to compound 48/80 at and below 0.3μg/ml of compound 48/80, it suggests that something other than K+ channel activation attributed to the potentials observed at these concentrations. Since another major factor that could have caused a net gain in the intracellular negative charge was Cl- influx, the concentration-response to compound 48/80 was repeated in cells exposed to Cl--free buffer containing ChTX. In this condition, only very negligible signals could be obtained, and the apparent potentials still detected at 1.0μg/ml in high K+ and ChTX experiments were no longer present suggesting that compound 48/80 has a significant Cl-channel activating action at concentrations close to 1.0μg/ml (Fig. 1). Although the involvement of Cl-channel was only marginal at ≤0.3μg/ml, it nonetheless contributed to the overall field potential. As such, the term hyperpolarising field potential (HFP) serves to better describe the combined effect of an efflux of K+ and an influx of Cl-.

The present study demonstrated, for the first time, the possibility of using MEA in the study of non-excitable cells, and that it could be of value in future pharmacological research

## References

[1] Yeung CK, Law JKL, Sam SW, Ingebrandt S, Lau AHY, Rudd JA, Chan M. (2008): The use of microelectrode array (MEA) in the study of rat peritoneal mast cell activation. *J Pharmacol Sci*. (*in press*).

[2] Metcalfe DD, Baram D, Mekori YA (1997): Mast cells. *Physiol*.;Rev., 77, 1033-1079.

[3] Nether E, Almers W (1986): Fast calcium transients in rat peritoneal mast cells are not sufficient to trigger exocytosis. *EMBO J*., 5, 51-53.

[4] White JR, Ishizaka T, Ishizaka K, Sha'afi R. (1984): Direct demonstration of increased intracellular concentration of free calcium as measured by quin-2 in stimulated rat peritoneal mast cell. *Proc Natl Acad Sci USA*, 81, 3978-3982.

[5]    Matthews G, Neher E, Penner R. (1989): Second messenger-activated calcium influx in rat peritoneal mast cells. *J Phyiol.*, 418, 105-130.

[6]    Cabado AG, Despa S, Botana MA, Vieytes MR, González M, Botana LM. (1999): Membrane potential changes associated with calcium signals in human lymphocytes and rat mast cells. *Life Sci.*, 64, 681-696.
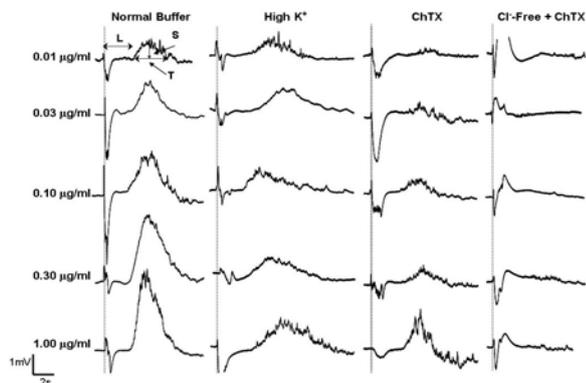
**Fig. 1:** Field potential recordings in the presence of compound 48/80 (0.01-1µg/ml) were compared with those obtained when cells were exposed to high extracellular $K^+$ (KCl, 150mM) or charybdotoxin (ChTX, 100nM). The latent period (L), spatial (S), and temporal (T) measurements are indicated. The large artefacts along the doted lines indicate the moment when compound 48/80 was added. The results show that the hyperpolarising potential was due to a combination of $K^+$ efflux and $Cl^-$-influx.

**Fig. 2:** Effects of compound 48/80 (log concentration, actual concentrations in parentheses, n = 3-7) on HFP (2a) and temporal measurements (2b) on mast cells cultured in high extracellular $K^+$ and ChTX-containing buffers. Significant reductions in HFPs were found in cells cultured in either condition with ChTX being more effective than high $K^+$ at reducing the effect of compound 48/80. The response time was substantially increased in cells cultured in high $K^+$ buffer but not when ChTX was used. The field potentials are expressed as mV ± SEM, and the temporal measurements are expressed as second ± SEM. (*P<0.05, **P<0.01, ***P<0.001, effects in normal vs High $K^+$ buffer; †P<0.05, ††P<0.01, †††P<0.001, effects in normal vs ChTX-containing buffer).
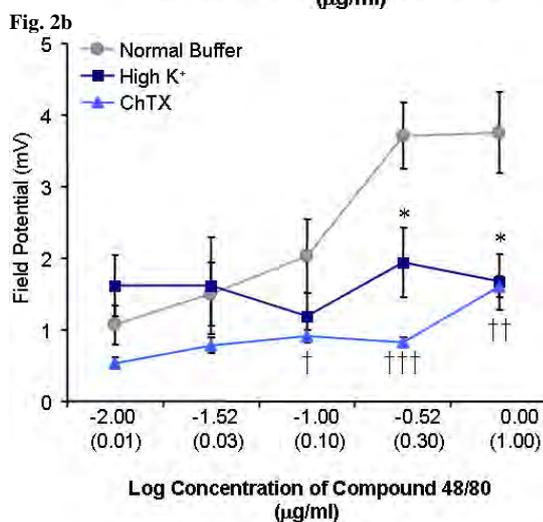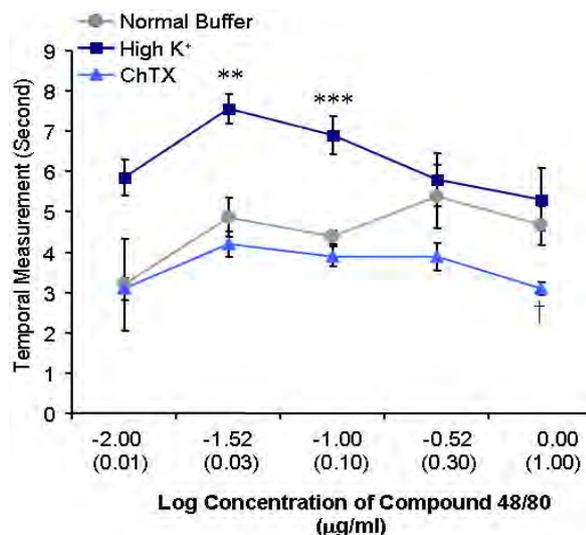


Fig. 2b



Fig. 2a

Technology

# CMOS-based array technology;
# Advances in culture, stimulaton and recording techniques

# CMOS-based Bioelectronics and Microelectrode Arrays

Andreas Hierlemann*, Urs Frey, Sadik Hafizovic, Flavio Heer

ETH Zürich, Bio Engineering Laboratory
Department Biosystems, Science and Engineering (BSSE), Mattenstrasse 26, CH-4058 Basel, Switzerland
* Corresponding author. E-mail address: andreas.hierlemann@bsse.ethz.ch

Microfabrication techniques and, in particular, CMOS technology are very powerful tools to devise bioelectronic and multielectrode microsystems. CMOS-based, fully integrated microelectrode arrays for bidirectional communication (stimulation and recording) with electrogenic cells are presented. These complex microsystems with integrated filter and amplification stages feature a high electrode density (3150 electrodes per mm$^2$) as well as low noise levels (5-6 $\mu V_{rms}$) in the recorded signals and are capable of monitoring relevant electrophysiological responses of cells to electrical stimuli or to pharmacological agents with prospective applications in the fields of neuroscience or pharmascreening.

## 1  Introduction

The two main advantages in using integrated-circuit (IC) or complementary metal oxide semiconductor (CMOS) technology include: (a) *connectivity*; larger numbers of transducers or electrodes can be addressed by on-chip multiplexing architectures, and (b) *signal quality*; the signal can be conditioned right at the electrode by means of dedicated circuitry units (filters, amplifiers) [1]. The use of CMOS technology (see Fig. 1) hence offers to realize - on a small-footprint system chip - a large number of electrodes that provide good signal quality owing to co-integrated circuitry units.

On-chip microelectronics as provided by the use of IC or CMOS technology translate into system capability: signal conditioning can be performed on-chip, ensuring that minute neural signals are faithfully recorded; a CMOS system also enables a bidirectional communication via the electrodes (stimulation and recording); smart switching schemes allow for stimulating the cell ensemble via an arbitrarily selectable set of electrodes, all while recording from other electrodes; on-chip analog-to-digital conversion means that such chip produces a robust signal that may be easily manipulated and transferred without compromising its information content. Moreover, the use of on-chip electronics allows for the monolithic integration of the complete system on a single chip, which leads to small system dimensions and low power consumption (no excess production of heat), which is a key requirement for, e.g., long-term culturing or implantable devices.

The use of multiplexers enables the integration of a large number of electrodes or transducers so that measurements at high spatiotemporal resolution be-come feasible. Traditional MEAs without multiplexers usually offer 64 electrodes with each electrode needing a connection to external circuitry, which adds parasitic capacitance and attenuates the small signals, whereas CMOS-based MEAs comprise up to 16'384 electrodes and the needed addressing circuitry on the same chip [2-4]. The high transducer density, which cannot be realized without on-chip multiplexers and addressing, simply since it is impossible to establish thousands of physical or electrical connections from a millimeter-size chip, is an important asset to, e.g., study the behavior of neural networks or other electrophysiologically relevant processes at cellular resolution.
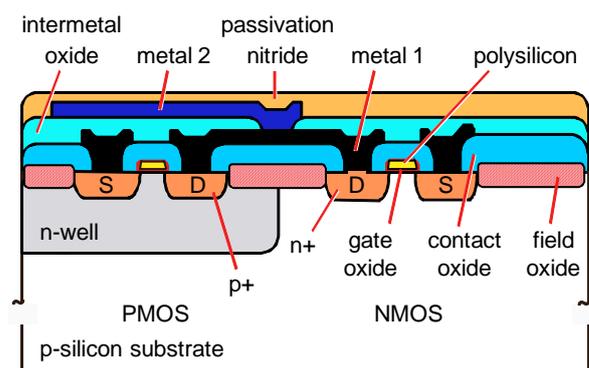


**Fig. 1.** Cross-sectional schematic of a CMOS chip showing the different functional layers and materials. The CMOS metals (metal 1 and metal 2) are aluminum.

A disadvantage of CMOS chips is that silicon is not transparent to visible light in contrast to standard cell culture substrates used in biology. Additionally, the chip or its components can corrode upon operation and long-term exposure to liquids (salt water). There-

fore, a good packaging solution is needed to, on the one hand, protect the chip against metabolism products and chemicals of the cell culture, and, on the other hand, to prevent the cells from being poisoned or disturbed by toxic materials released by the chip, such as the CMOS metal aluminum that dissolves in saline solution. For our chips we applied a technique to shift the electrodes away from the original CMOS Al contacts onto the chip silicon nitride passivation and to repassivate the whole chip with a stack of silicon oxide and nitride layers (see Fig. 2) [5]. Thereafter, the passivation is opened in the area of the final electrodes and leaves a metal Pt electrode exposed to the culture bath. This method was demonstrated to be effective and secure a chip life of several months under culture conditions.
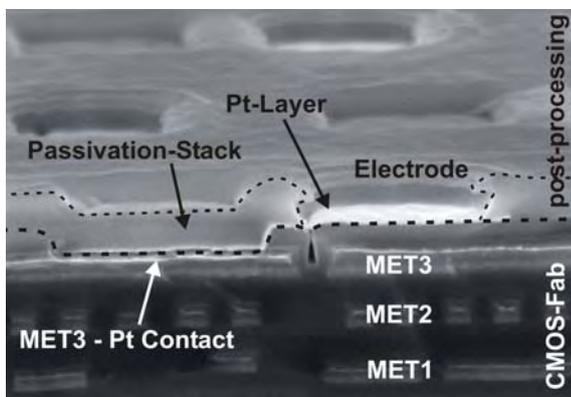


**Fig. 2.** Cross section of a CMOS chip showing the aluminum contacts (metal layer 3 of the CMOS chip) and the final Pt electrode shifted sideways after opening of the passivation .

## 2 Monolithic Chip Systems

### 2.1 Monolithic low-density-electrode system

The schematic of a monolithic 128-electrode CMOS microsystem is shown in Fig. 3. The 6.5 mm by 6.5 mm chip comprises 128 stimulation- and recording-capable electrodes in an 8x16 array. The system is structured in a modular design (Fig. 3) [5]. Each pixel of the micro-electrode array incorporates the signal-transducing electrode, a fully differential band-pass filter for immediate signal conditioning, a mode storage unit and a buffer for stimulation. The pitch of the pixel units is 250 µm. Electrode pitch, size and shape are very flexible, and the electrode material can be selected from a large variety of materials, since the electrodes are realized during the post-CMOS processing. A digital control unit is also integrated on the chip and controls the multiplexing, the electrode selection for stimulation, the reset of single electrodes, and it contains the successive-approximation registers of the A/D converters and the interface to the outside world. Implementing filters

and buffers at each electrode offers important advantages:

i. The signal is amplified and filtered in close proximity of the electrodes, which makes the design less sensitive to noise and interference picked up along connection lines;

ii. a buffer per electrode renders the stimulation signal independent of the number of activated electrodes;

iii. the high-pass filter removes offset and drift of the biochemical signals so that the signal can be amplified before it is multiplexed;

iv. the low-pass filter limits the noise bandwidth and works as an anti-aliasing filter for the multiplexing and for the subsequent A/D-conversion.
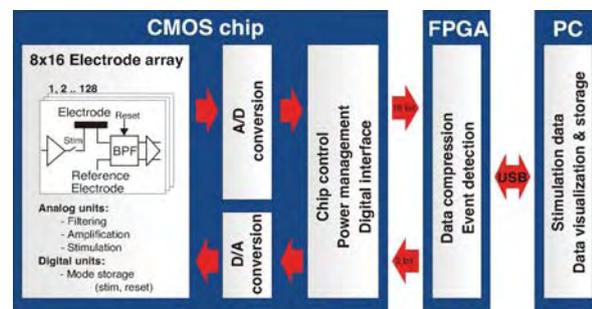


**Fig. 3.** Schematic of the setup for the 128-electrode CMOS microsystem: CMOS chip with 128 repeated analog units, analog-to-digital converters, a digital-to-analog converter, chip-control and power-management unit, and digital interface. A FPGA board for data compression and event detection is interfaced on the one hand to the chip, and, on the other hand, via USB to a computer for further data treatment, visualization and stimulus generation [5].

All in-pixel circuitry components have been optimized for low noise and small area. A total equivalent input noise of the pixel circuitry of 11.7 $\mu V_{RMS}$ (0.1 Hz to 100 kHz) has been measured. The electrodes are continuously read out at a sampling rate of 20 kHz per electrode. A gain of 1000 or 3000 can be selected. The overall power consumption of the chip is 120 mW at 5 V supply. An on-chip temperature sensor monitors the chip operating temperature. Operating the chip with liquid on the surface leads to a temperature rise of less than 1°C with respect to ambient temperature upon operation, so that additional cooling of the system is not required. Circuits operating at low frequency (down to 1 Hz) might be sensitive to leakage currents, the effect of which has been reduced by the fully differential design of the in-pixel readout circuitry. Furthermore, electromagnetic coupling is also generally reduced in a fully differential architecture. The electrode units also provide stimulation capabilities. Any arbitrary stimulation pattern (with a maximum sampling rate of 60 kHz and 8 bit resolution) can be applied to any subset of electrodes. The readout circuitry at each electrode can individually be reset to its operating point in order to suppress artifacts

evoked by the stimulation pulses from the stimulated electrode itself or from neighboring electrodes.

## 2.2 Monolithic high-density-electrode system

Considering the size of neurons, which range from below 10 µm in diameter for vertebrates up to 100 µm for invertebrates, it would be very interesting to conduct biological or electrophysiological experiments at cellular or subcellular resolution. Three different approaches have been realized so far; (i) constraining the cells with regard to the electrode positions, (ii) adapting the electrode layout to the biological structure or (iii) using high-density arrays that record from all electrodes simultaneously.
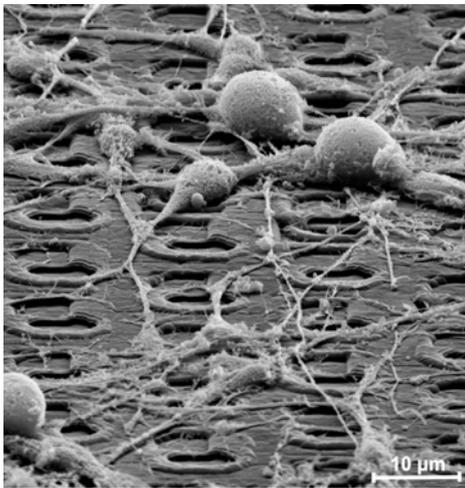


**Fig. 4.** Micrograph of chicken dorsal root ganglion neurons cultured 2 days on the high-density CMOS microsystem featuring 11.000 Pt electrodes.

Here, a CMOS-based microelectrode array with 11'016 metal electrodes and 126 on-chip channels, each of which includes recording and stimulation electronics for bidirectional communication with electrogenic cells (neurons or cardiomyocytes) was developed. The features of this chip include high spatial resolution with 3150 electrodes per mm$^2$ to attain cellular or subcellular resolution (electrode diameter 7 µm, pitch 18 µm, honeycomb pattern, see Fig. 4), great flexibility in routing the 126 readout channels to the 11'016 recording sites, and low noise levels in the recordings (5 µV$_{rms}$) so that single action potentials from mammalian cells can be monitored.

Instead of scanning the entire electrode array, the approach presented here provides a reconfigurable routing for an almost arbitrary set of electrodes to the readout channels. The 126 readout channels provide the signal conditioning with the amplification being programmable from 1 to 10'000 in 18 steps. A first-order high-pass filter cuts off at 0.3 Hz, a first low-pass filter is tunable to either 15 kHz or 50 kHz, and a second low pass to 4 kHz or 14 kHz. The signals are

sampled at 20 kHz and digitalized using an 8-bit AD converter. The digital core of the chip is split into two parts. The transmitter controls the 16 successive-approximation ADCs, the corresponding multiplexers, and sends the data off chip together with the chip status and a cyclic redundancy check (CRC) for transmission error detection. The receiver decodes commands sent to the chip such as array configuration, amplifier settings and stimulation signals. Electrical stimulation signals are generated via an 8-bit DAC and transmitted to buffers, which, in turn, can be connected to the electrodes through the same routing scheme that is used for the readout.

The flexibility in the electrode selection is attained by the use of an analog switch matrix integrated underneath the electrode array. The switch matrix consists of 13k SRAM cells and analog switches to define the routing from the electrode to the amplifiers as sketched in Fig. 5.
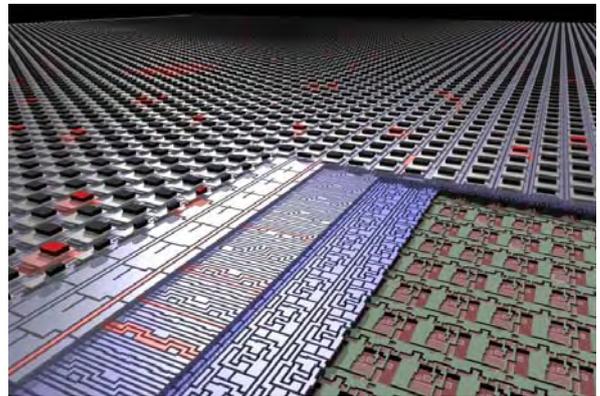


**Fig. 5.** Schematic of the chip layers with memory units and switches that allow for a flexible routing of a set (126) of almost arbitrarily selectable electrodes to the readout channels. Selected electrodes are marked in red.

To obtain the settings of the switches for a desired set of electrodes, the switch matrix is represented as a graph, and a modified "max-flow, min-cost" optimization problem is solved with an integer-linear program. The time required to reconfigure the array is on the order of milliseconds.

A data acquisition system consisting of a PCB that provides power supply and voltage references and a commercially available FPGA has been additionally developed. The FPGA provides data processing features, such as CRC error detection, digital filtering, event detection and data reduction/compression. The preprocessed data are sent to a PC for further data processing, visualization and storage.

# 3 Test Measurements

## 3.1 Recordings

Biological measurements obtained with the high-density MEA are shown in Fig. 6 to illustrate the broad range of applications. The top trace was obtained from neonatal rat cardiomyocytes cultured for 3 days in vitro (DIV). They form a confluent cell layer that beats at a regular frequency. The signal amplitudes are rather large. The middle trace stems from dissociated rat hippocampal neurons cultured for 16 DIV, which show bursts of network activity at that age. The two traces at the bottom are obtained from an acute parasagittal cerebellar slice from Long-Evans rats. The two electrodes have been located at a distance of 38µm (center-center). It is evident that signals from one of the neurons can be seen on several electrodes, which opens up new pathways and possibilities for neuronal signal processing.
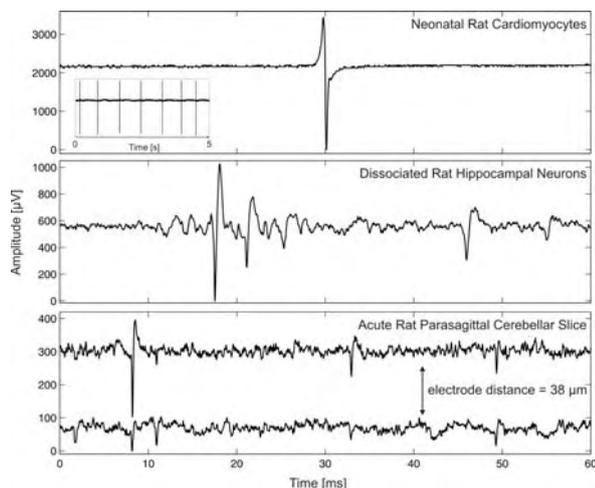


**Fig. 6.** Measurements obtained from rat cardiomyocytes (3 DIV), dissociated rat hippocampal neurons (16 DIV), and an acute cerebellar slice preparation from a Long-Evans rat.

## 3.1 Stimulation

Stimulation experiments have been carried out on the 128-electrode array using, e.g., cortical neurons from the rat brain as shown in Fig. 7. A successful excitation of spikes recorded at 250 µm distance from the stimulation site is shown. A single bipolar stimulation pulse of ±800 mV and 50 µs duration was used to stimulate the cells in this example. The inset shows the post-stimulus time histogram of this channel that includes the results of 142 stimulation pulses. The first event or neuronal signal generally occurs between two

and three milliseconds after the stimulation pulse with a very high probability of 96%.
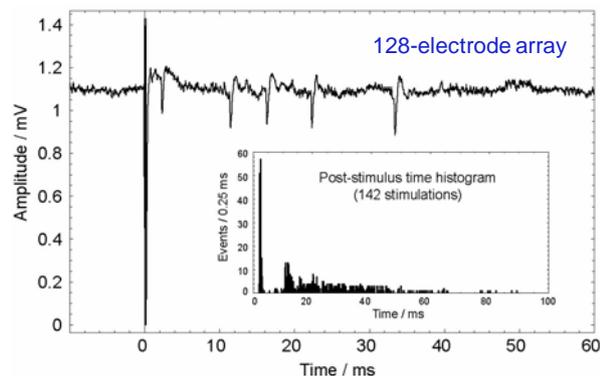


**Fig. 7.** Successful excitation of spikes in cortical neurons from rat brain at 250 µm distance from the stimulation site. A single bipolar stimulation pulse of ±800 mV and 50 µs duration was used to stimulate the cells in this example. The inset shows the post-stimulus time histogram of this channel based on 142 stimulation pulses.

**References**

[1] F. Heer, A. Hierlemann, "Integrated microelectrode arrays", in "CMOS Biotechnology", Editors: H. Lee, D. Ham, R.M. Westervelt, Springer Science & Business Media LLC, New York, USA, 2007, p. 207-258, ISBN 3-540-37315-2.

[2] L. Berdondini, P. D. van der Wal, O. Guenat, N. F. de Rooij, M. Koudelka-Hep, P. Seitz, R. Kaufmann, P. Metzler, N. Blanc, and S. Rohr, "High-density electrode array for imaging in vitro electrophysiological activity," *Biosens Bioelectron*, Vol. 21, 167-74, 2005.

[3] U. Frey, F. Heer, R. Pedron, S. Hafizovic, F. Greve, J. Sedivy, K-U. Kirstein, A. Hierlemann, '11k-Electrode, 126-Channel, High-Density Microelectrode Array to Interact with Electrogenic Cells'. *Digest of Technical Papers, ISSCC,* IEEE International Solid-State Circuits Conference, San Francisco, USA, 2007, p. 158-159, and 593 (ISSN 0193-6530).

[4] B. Eversmann, M. Jenkner, F. Hofmann, C. Paulus, R. Brederlow, B. Holzapfl, P. Fromherz, M. Merz, M. Brenner, M. Schreiter, R. Gabl, K. Plehnert, M. Steinhauser, G. Eckstein, D. Schmitt-Landsiedel, and R. Thewes, "A 128x128 CMOS biosensor array for extracellular recording of neural activity," *IEEE Journal of Solid-State Circuits*, vol. 38, pp. 2306-2317, 2003.

[5] F. Heer, S. Hafizovic, T. Ugniwenko, U. Frey, W. Franks, E. Perriard, J.-C. Perriard, A. Blau, C. Ziegler, A. Hierlemann, Single-chip microelectronic system to interface with living cells, *Biosens Bioelectron*, 2007, 22, 2546-2553.

# APS-MEA Platform for High Spatial and Temporal Resolution Recordings of In-Vitro Neuronal Networks Activity

Berdondini L.[1*], Imfeld K.[2], Gandolfo M.[3], Neukom S.[4], Tedesco M.[3], Maccione A.[3], Martinoia S.[3] and Koudelka-Hep M.[2]

1 Department of Neuroscience and Brain Technology, Italian Institute of Technology (IIT), Genova, Italy.
2 Institute of Microtechnology (IMT), Université de Neuchâtel, Neuchâtel, Switzerland.
3 Neuroengineering and Bio-nanoTechnologies Group (NBT), Department of Biophysical and Electronic Engineering (DIBE), University of Genova, Genova, Italy.
4 Centre Suisse d'Electronique et Microtechnique (CSEM), Zürich, Switzerland.
* Corresponding author. E-mail address: luca.berdondini@iit.it

The motivation of this work is to develop a MEA-based technology for in-vitro neurophysiology enabling to bridge the gap between local network activity recordings (at the population/cellular level) and overall network behaviour. To achieve this, a platform based on the Active Pixel Sensor (APS) concept was developed. The CMOS device integrates 4096 microelectrodes and provides spatial resolution of 20 μm and sampling rates ranging from 8kHz/channel (full array acquisitions) up to 120 kHz/channel (zoomed area acquisitions on 64 microelectrodes). Validation of the system was performed first with cardiomyocyte cultures and successively with different types of neuronal preparations with brain tissue from rat's E18 embryos. This presentation will describe the developed platform and present validation results achieved on hippocampal neuronal networks.

## 1  Introduction

The motivation of this work is to develop a MEA-based technology for in-vitro neurophysiology enabling to bridge the gap between local network activity recordings (at the population/cellular level) and overall network behaviour. To achieve this, high spatio-temporal resolutions have to be provided and the electrode density significantly increased. The integration of large active areas featuring dense electrode arrays (i.e. electrode separation down to cellular dimensions) requires an alternative enabling technology than the conventional thin-film approach. The Complementary Metal Oxide Semi-conductor (CMOS) technology provides the opportunity of integrating on-chip both signal conditioning circuitries and high-speed data read-out logic. Different approaches for implementing single-chip CMOS-MEAs based on Field-Effect-Transistors (FETs) (Hutzler et al., 2006), on MEAs (Hafizovic et al., 2007) or on the Active-Pixel-Sensor (APS) concept, i.e. APS-MEAs (Berdondini et al., 2002; Berdondini et al., 2005) are being investigated.

In this work the CMOS devices and the complete acquisition system were re-designed in order to provide both high spatial and temporal resolutions as well as a sufficiently low noise performance for detecting single spike events.

## 2  Materials and Methods

### 2.1 APS-MEA platform

The APS-MEA platform was designed in order to enable the recording of electrophysiological activities with spatial resolutions of 20 μm and sampling rates, ranging from 8kHz/channel (full array acquisitions on 4096 microelectrodes, 2.5 x 2.5 mm$^2$) up to 120 kHz/channel (zoomed area acquisitions on randomly chosen 64 microelectrodes). The applied methodology consists in implementing and adapting concepts from the image/video field at different levels of the system i.e. the CMOS device, the hardware interface and the acquisition / analysis tools (Imfeld et al., 2007).

The overall platform is shown in Fig. 1 and features *i*) on-chip amplification and high speed random addressing logic, *ii*) an FPGA-based interface for the device control and for the real-time data processing (e.g. filtering) and *iii*) a dedicated software application running on a host-PC for the hardware control, high-resolution data visualization and conventional MEAs data analysis (spike detection, mean-firing rate, etc.).

Devices were packaged by wire bonding and by gluing the chip on a printed-circuit-board interface and completed with a glass reservoir.
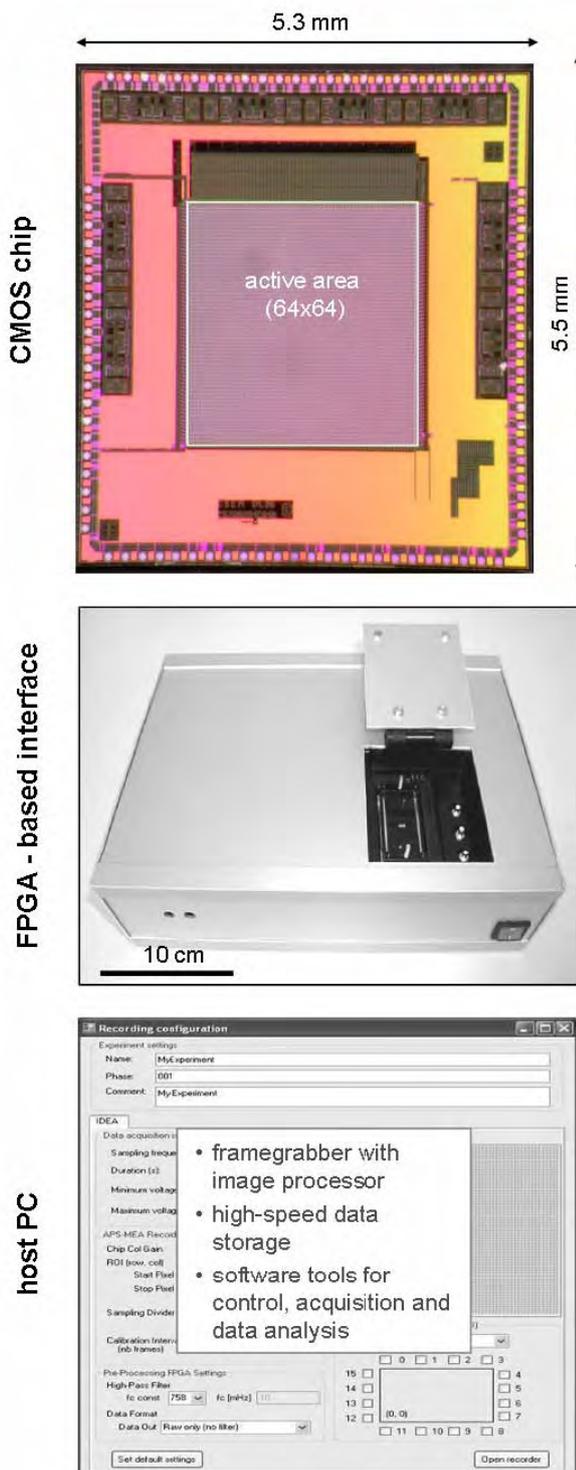
**Fig. 1.** Overview of the three main levels of the APS-MEA platform: (**top**) the CMOS chip level integrating an array of 64x64 microelectrodes with inter-electrode separation of 20 μm and the read-out electronics; (**middle**) the FPGA-based acquisition board implementing real-time data pre-processing tools and connected to an acquisition PC via a *CameraLink* interface; (**bottom**) the acquisition PC level equipped with a framegrabber for high speed data acquisition and high-speed data storage tools. A custom software application enables to control the overall setup, to perform data acquisitions and data analysis over 4096 electrode channels.

## 2.2 Hippocampal neuronal cultures

The APS-MEA devices were sterilized in ethanol 80% for 20 minutes, extensively rinsed in sterile water, dried under laminar flow and coated with laminin (3 hours) and poly-d-lysine (overnight).

Primary hippocampal cultures were obtained from brain tissue of Sprague Dawley rats at embryonic day 18 (E18) using standard protocols. Embryos were removed and dissected under sterile conditions and cortex pieces were separated, dissociated by enzymatic digestion in Trypsin 0.125% - 20 min at 37° C - and finally triturated with a fire-polished Pasteur pipette. Dissociated neurons were plated onto microelectrode arrays, in a 30 μl drop covering the active area (~ 600 cells/μl). Two hours later, when cells adhered to the substrate, 1 ml of medium was added in each device. The cells were incubated with 1% Glutamax, 2% B-27 supplemented Neurobasal Medium (Invitrogen), in a humidified atmosphere 5% CO2, 95% air at 37° C. 50% of the medium was changed every week. No antimitotic drug was used.

## 3 Results and Discussion

The validation of the platform under biological conditions was at first performed with cardiomyocyte cultures [6] and successively with different types of dissociated neuronal preparations. Here we present validation results achieved on hippocampal neuronal preparations.

The Fig. 2 shows a comparison of the mean firing rates (MFR) between hippocampal cultures of similar age (~30 DIVs) on a conventional MEA (Multichannel Systems) and on an APS-MEA. As shown, results are comparable allowing thus to validate the APS-MEA platforms with respect to the good cell culture viability as well as to the adequate signal-to-noise ratio performance for recording and detecting spiking activities.

An example of a whole array acquisition performed on a rat hippocampal neuronal preparation (31 DIVs) is presented in Fig. 3. A single channel raw data of the recorded, large amplitude spiking activity is shown in Fig. 3.a. and the overall array activity in Fig.3.b. This last image is one frame of the acquired activity movie displayed in a false colour map as the range of each channel computed over a time bin of 4.4 ms (35 frames). Spike-detection based statistical analysis was performed on these data with custom tools adapted to the large number of recording sites.

## 4 Conclusions

High spatial and temporal resolution recordings of hippocampal neuronal culture activities on the APS-MEA platform comprising 4096 microelectrodes are here demonstrated. It should be stressed that the resolution of the device enables to visualize local

spike propagations as well as whole network (bursting) activities. Such multi-level resolution (whole area or zoomed acquisitions) connecting cellular and network levels is a unique feature that will allow the understanding of the neuronal network dynamics to be enhanced.
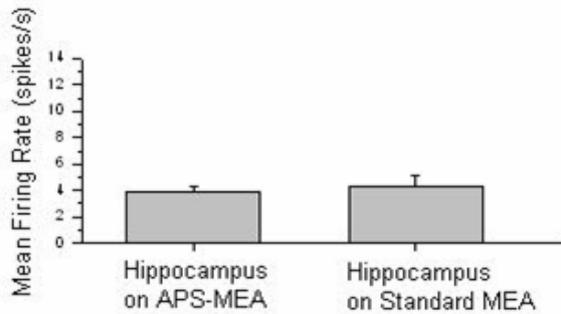


**Fig. 2.** Comparison of the Mean Firing Rates of a spontaneously active hippocampal neuronal cultures (~30 DIVs) grown on an APS-MEA and on a standard MEA (Multichannel Systems).
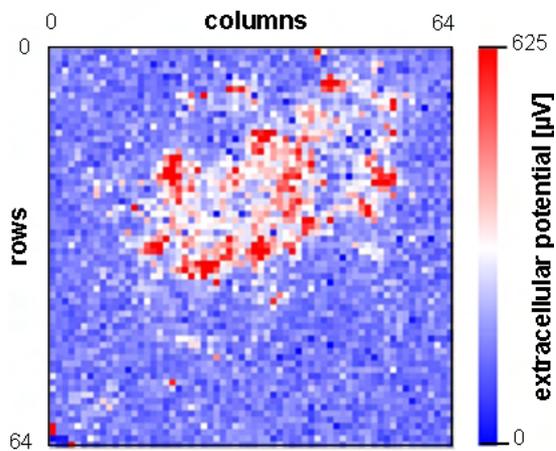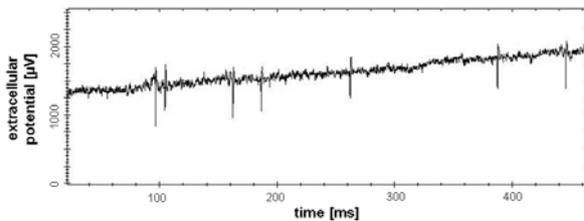


**Fig. 3.** APS-MEA recorded data from a rat hippocampal neuronal culture (31 DIVs, 8kHz sampling, from 4096 electrodes). (**top**) Single channel raw data showing the spontaneous spiking activity. (**bottom**) One frame of the 4096 microelectrode acquisition displayed as a video of the computed variance for each channel. The spatial distribution of a bursting event is clearly visible.

**References**

[1] Berdondini L, Overstolz T, de Rooij NF, Koudelka-Hep M, Martinoia S, Seitz P, Wäny M, Blanc N. High resolution electrophysiological activity imaging of in-vitro neuronal networks. IEEE-EMBS: Madison, Wisconsin, USA, 2002: 241-4.

[2] Berdondini L, van der Wal PD, Guenat O, de Rooij NF, Koudelka-Hep M, Seitz P, Kaufmann R, Metzler P, Blanc N, Rohr S. High-density electrode array for imaging in vitro electrophysiological activity. Biosensors & Bioelectronics, 2005; 21: 167-74.

[3] Hafizovic S, Heer F, Ugniwenko T, Frey U, Blau A, Ziegler C, Hierlemann A. A CMOS-based microelectrode array for interaction with neuronal cultures. Journal of Neuroscience Methods, 2007; 164: 93-106.

[4] Hutzler M, Lambacher A, Eversmann B, Jenkner M, Thewes R, Fromherz P. High-resolution multitransistor array recording of electrical field potentials in cultured brain slices. Journal of Neurophysiology, 2006; 96: 1638-45.

[5] Imfeld K, Garenne A, Martinoia S, Koudelka-Hep M, Berdondini L. Motivations and APS-based solution for high-resolution extracellular recording from in-vitro neuronal networks. 3rd International IEEE EMBS Conference on Neural Engineering (NER 2007). IEEE-EMBS: Kohala Coast, Hawaii, USA, 2007.

[6] Imfeld K, Neukom S, Maccione A, Bornat Y, Martinoia S, Farine PA, Koudelka-Hep M, Berdondini L. Large-Scale, High-Resolution Data Acquisition System for Extracellular Recording of Electrophysiological Activity. IEEE Transaction on Biomedical Engineering, in press.

# Characterization of Response Patterns Evoked by Light Addressed Electrical Stimulation in Cultured Neuronal Networks

Jun Suzurikawa[1*], Masayuki Nakao[2], Kanzaki Ryohei[1], Yasuhiko Jimbo[3], Hirokazu Takahashi[1]

1 Graduate School of Information Science and Technology, The University of Tokyo, Tokyo, Japan
2 School of Engineering, The University of Tokyo, Tokyo, Japan
3 Graduate School of Frontier Sciences, The University of Tokyo, Tokyo, Japan
* Corresponding author. E-mail address: suzuri@brain.imi.i.u-tokyo.ac.jp

Conventional microelectrode arrays have limitations of their electrode numbers and densities, resulting in low spatial resolutions of stimulation and recording. Here, to overcome this problem, we utilized light addressed stimulation and simultaneous $Ca^{2+}$ imaging and attempted to characterize evoked response patterns of local neuronal populations. These optical approaches turned out to enable dense monitoring and stimulation at any locations of electrode substrates. By probing local neuronal populations with this setup, we found a functional structure with an exponential distribution of synaptic connectivity topology, which implies presence of a small-world network property.

## 1 Introduction

In studies on cultured neuronal networks, microelectrode arrays (MEAs) have been widely utilized for electrophysiological recording and stimulation [1]. However, the electrode density of MEA is too sparse as compared with those of neurons on the substrates. This lack of electrode density can be a disadvantage particularly when probing local neuronal populations. To overcome this problem, we have developed a novel experimental system for light addressed electrical stimulation and simultaneous $Ca^{2+}$ imaging [2, 3]. These optical approaches are expected to enable dense monitoring and stimulation at any locations on culturing substrates. Here, we evaluated this novel method as a tool for probing local neuronal populations. Then, with the method, we also attempted to characterize neuronal response patterns evoked by the light addressed stimulation and to reveal functional structure in local neuronal populations, which the conventional MEAs have not been able to access due to the lack of spatial resolution.

## 2 Light Addressable Electrode

Light addressing technique was originally proposed as a light addressable potentiometric sensor (LAPS) for pH measurement of electrolyte with silicon wafer [4]. Focal light illumination to the photoconductive substrate induces a localized increase of substrate conductivity and thus generates a virtual electrode for potential measurement and control at the substrate-electrolyte interface. To the present, many applications of LAPS have been proposed, including electrical stimulation to neurons [5, 6] and extracellular measurement of membrane potentials [7]. Recently, hydrogenated amorphous silicon (a-Si:H) was introduced for the same objective [8, 9] and proved to contribute to improvement of spatial resolution in addressing [10]. One large problem in use of a-Si:H is that a-Si:H can be deteriorated by weak alkaline culture medium and requires a complicated passivation structure [8].
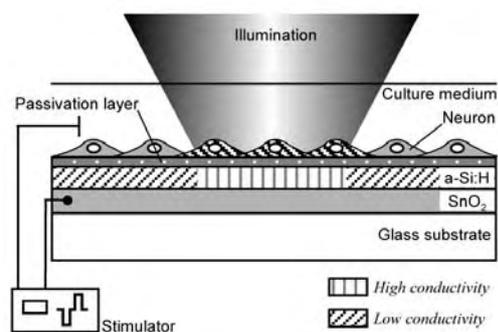


Fig. 1. Schematic diagram of the light-addressable electrode. Illumination to the electrode increases the conductivity of a-Si:H layer and addresses a stimulating site.

Considering these backgrounds, we have developed a novel light addressable electrode [2]. As shown in Fig. 1, the electrode substrate has a three-layer-laminated simple structure, namely, a SnO2 transparent metal thin film, a-Si:H photoconductive layer and low conductive passivation layer deposited on a glass substrate. Low conductive thin film serves as anisotropic conductor and prevents diffusion of photocurrent in the in-plane direction without lateral insulation structures.

# 3 Experimental

## 3.1 Optical configuration

Figure 2 describes an optical setup for addressing illumination and simultaneous $Ca^{2+}$ imaging. Light illumination from a mercury lamp was collimated and projected to the electrode substrate through a digital micro-mirror device (DMD; Texas Instruments, ). The DMD serves as a reflective active photo-mask and generates desired illumination patterns for addressing. For $Ca^{2+}$ imaging, a fluorescence upright microscope (Olympus, BX51WI) was utilized with an attached cooled charge-coupled device (CCD) camera (Hamamatsu Photonics, C9100-02).

## 3.2 Cell culturing

Dissociated cortical neurons from rat E18 embryos were plated and incubated on poly-D-lysine- and laminin-coated electrode substrates. During the first 24 h, neurobasal/B-27 medium (Gibco) with 0.5 mM L-glutamine was used as culture medium. Dulbecco's modified Eagle's medium (Gibco) with 5 % horse serum, 5 % fetal bovine serum, 2.5 μg/ml of insulin and 1 % antibiotics [1] were then added to the dishes. Half of the medium was exchanged twice a week. Experiments were performed during 15-45 days in vitro (DIV).
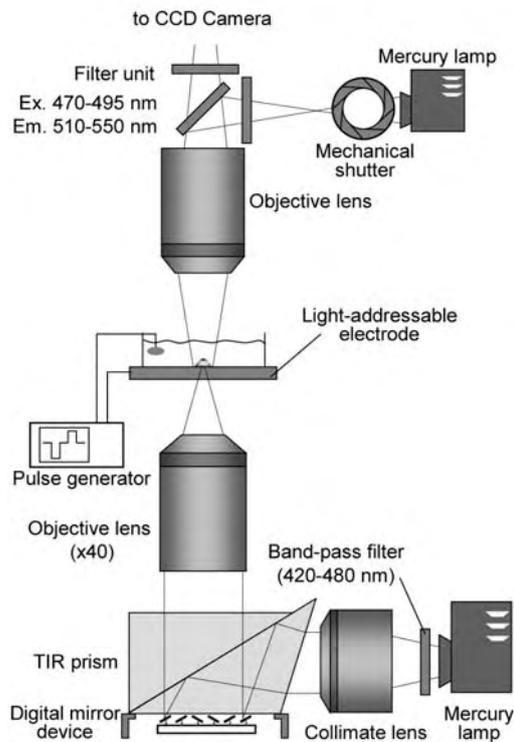
## 3.3 $Ca^{2+}$ imaging

As calcium indicator, fluo-4 (Molecular Probes) was loaded to cells before experiments at 10 M. Fluorescence images were obtained by the cooled CCD camera at the frame rate of 5 frames per second with the exposure time of 40 ms per frame. Electrical simulation consisted of voltage-controlled negative-first biphasic pulses with pulse duration of 1 ms and voltage amplitude of 3-3.5 V. In experiments, solution of the following composition was used as the external medium: NaCl 149 mM; KCl 2.8 mM; $CaCl2$ 2 mM; $MgCl2$ 1 mM; HEPES 10mM; glucose 10 mM, pH 7.2. For blockade of excitatory synaptic transmission, APV and CNQX were added to external medium at 50 and 10 M.

# 4 Results and Discussion

## 4.1 Neuronal activity patterns evoked by light addressed stimulation

Figure 3 shows a typical result of light addressed stimulation to a 15 DIV culture.
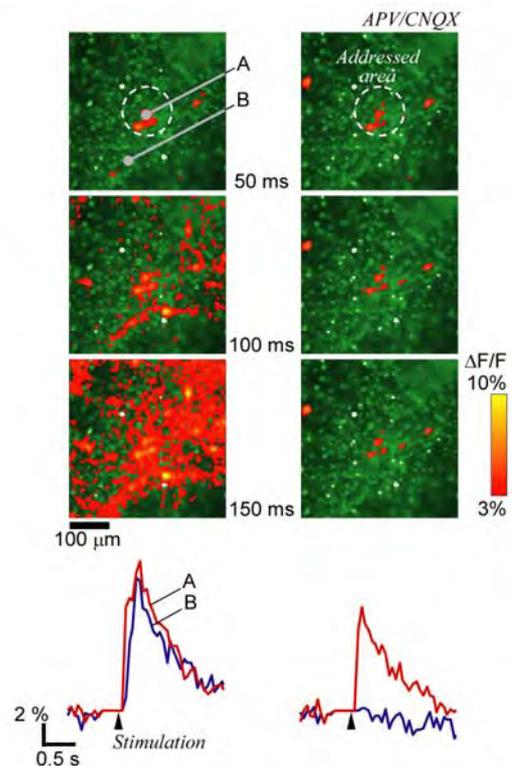


**Fig. 3.** Evoked response patterns and fluorescence transients with and without synaptic blockade (15DIV). Fractional changes of fluorescence intensities above 3 % are color-coded and imposed on the raw fluorescence images.



**Fig. 2.** Experimental setup for light addressed stimulation and simultaneous $Ca^{2+}$ imaging.
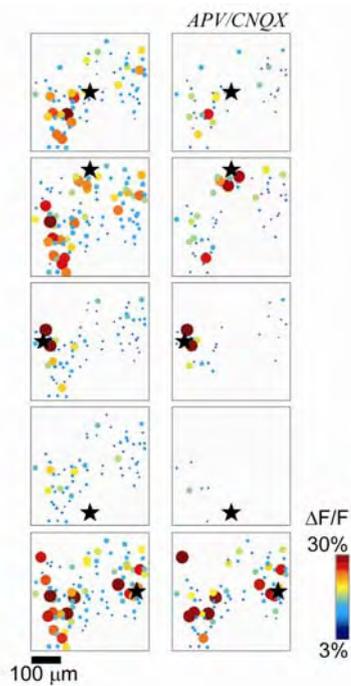
**Fig. 4.** Spatial response patterns evoked by light addressed stimuli to five different locations with and without synaptic blockade (45DIV). Response amplitudes at 100 ms post-stimulus were extracted from 110 neurons. Circle positions and colors correspond with cell positions and their response amplitudes, respectively. A star in each panel indicates a addressed location.

tion can be used as probing input even to local and mature neuronal populations.



**Fig. 5.** Correlation coefficients between response patterns evoked by different stimuli (mean for 5 dishes). (a) Under synaptic blockade, response patterns were differentiated. Error bars show standard deviations (n = 50). (b) Under synaptic blockade, correlation coefficients negatively correlate with distance between the stimulation sites. Error bars show standard errors (n = 20, 20, 10).

Fluorescence transients of individual cell bodies showed steep rise and subsequent immediate fall derived from neuronal spiking. This result successfully demonstrated the feasibility of our experimental setup for light addressed stimulation and simultaneous Ca2+ imaging. Activated cells were clearly localized to the addressed area under synaptic blockade, whereas, without synaptic blockade, neural excitation propagated beyond the addressed area via synaptic transmission.

In more mature cultures, however, spatial resolution of light addressed stimulation degraded because activation through neuronal processes became dominant. Figure 4 shows that even under synaptic blockade, there were activated neurons at more than 200 m from the addressed spot. This observation is consistent with the previous study, which strongly suggested that axons, rather than somas, are the primary sites of stmulation [6].

To quantify how much difference can be achieved in response patterns of local neuronal population in a mature culture by different stimuli, correlation coefficients between response patterns evoked by stimuli to five locations were calculated as shown in Fig. 5. As a result, correlation coefficients under synaptic blockade turned out to be significantly smaller than those without blockade (a). Moreover, under synaptic blockade, the correlation coefficients negatively correlated with distance between stimulated sites (b). These results indicate that the light addressed stimula-

## 4.2 Functional structure in local neuronal populations

In order to reveal functional structure in local neuronal populations, then, we characterized heterogeneity of response patterns evoked by the five different stimuli. Figure 6(a) shows five post-stimulus response amplitudes normalized in individual neurons. Focusing attention on which stimulation evoked the maximum amplitude in responses of each cell, one or two stimuli turned out to dominantly evoke the maximum-amplitude responses in many neurons. In Fig. 6(b), averaged ratios of the neurons exhibiting maximum-amplitude responses were plotted against the five sorted stimulation sites (n = 4). Without synaptic blockade, the ratio distribution displayed an exponential decay, which suggests that the local neuronal population did not have complete randomness but had some heterogeneous topology in synaptic connectivity. It is also noteworthy that the stimulation site which evoked maximum-amplitude responses in the most neurons under synaptic blockade did not always do so without synaptic blockade. In fact, there were no cases where the first-order stimulation coincided between control and APV/CNQX trials (data not shown). This investigation suggests that the minor neuronal population activated by not-first-order stimuli had nonlinearly large influence on local neuronal circuit.
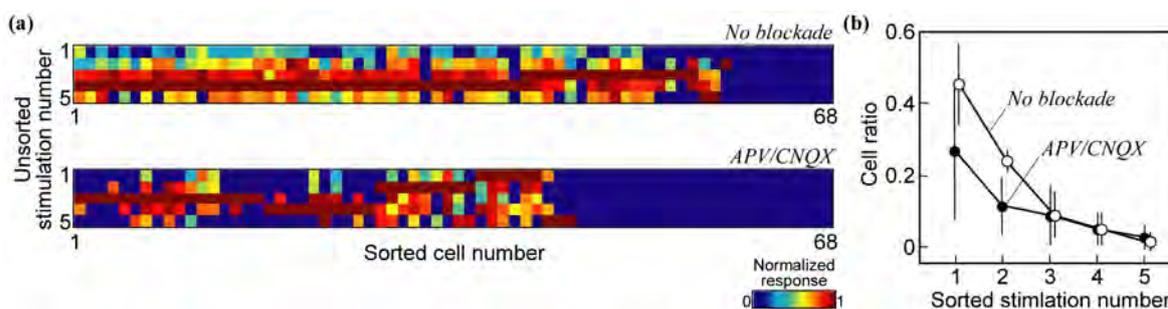
**Fig. 6.** Small world network property revealed in local neuronal populations. (a) Response amplitudes evoked by five different light addressed stimuli (as shown in Fig. 4 and 5) without (top) and under (bottom) synaptic blockade. Response amplitudes are normalized in individual neurons. (b) Cell ratio distributions of the neurons whose maximum-amplitude were evoked are plotted against the sorted stimulation numbers. Distributions for individual trials were sorted and averaged for 4 dishes. Error bars show standard deviations.

Recent studies revealed a small-world network property in network morphology and topology of dissociated neuronal cultures, where the functional or anatomical network connectivity topologies followed an exponential distribution [12-14]. Then, the observed heterogeneity in the response patterns of local neuronal population also seems to support the presence of such a small world network property.

## 5 Conclusion

In this study, we evaluated an experimental setup for light addressed stimulation and simultaneous $Ca^{2+}$ imaging as a tool of probing local neuronal populations. And then, with the setup, we attempted to characterize evoked neuronal response patterns and reveal a functional structure in local neuronal populations. In mature cultures, activation through densely packed neuronal fibers became dominant and degraded stimulus spatial resolution. However, we demonstrated that, under synaptic blockade, the evoked response patterns were sufficiently differentiated by light addressed stimuli to different sites. By investigating the heterogeneity in the neuronal response patterns, we found a functional structure with an exponential distribution of synaptic connectivity, which implies presence of a small world network property in local neuronal populations.

## References

[1] Jimbo Y, Robinson HPC, Kawana A (1298): Simultaneous measurement of intracellular calcium and electrical activity from patterned neural networks in culture. *IEEE Trans. Biomed. Eng., 40, 804-810*

[2] Suzurikawa J, Takahashi H, Kanzaki R, Nakao M, Takayama Y, Jimbo Y (2007): Light-addressable electrode with hydrogenated amorphous silicon and low-conductive passivation layer for stimulation of cultured neurons. *Appl. Phys. Lett., 90, 093901*

[3] Suzurikawa J, Nakao M, Kanzaki R, Jimbo Y, Takahashi H (2007): Light-Addressed Stimulation and Simultaneous Calcium Imaging for Probing Spatio-Temporal Activity of Cultured Neural Network. *Proceedings of the 3rd International IEEE EMBS Conference on Neural Engineering, 57-60*

[4] Hafeman DG, Parce JW, McConnell HM (1988): Light-addressable potentiometric sensor for biochemical systems. *Science, 240, 1182-1185*

[5] Colicos MA, Collins BE, Sailor MJ, Goda Y (2001): Remodeling of synaptic actin induced by photoconductive stimulation. *Cell, 107, 605-616*

[6] Starovoytov A, Choi J, Seung HS (2004): Light-directed electrical stimulation of neurons cultured on silicon wafers. *J. Neurophysiol., 93, 1090-1098*

[7] Stein B, George M, Gaub HE, Parak WJ (2004): Extracellular measurements of averaged ionic currents with the light-addressable potentiometric sensor (LAPS). *Sens. Actuators B, 98, 299-304*

[8] Bucher V, Brunner B, Leibrock C, Schubert M, Nisch W (2001): Electrical properties of a light-addressable microelectrode chip with high electrode density for extracellular stimulation and recording of excitable cells. *Biosens. Bioelectron., 16, 205-210*

[9] Bucher V, Schubert M, Kern D, Nisch W (2001): Light-addressed sub-µm electrodes for extracellular recording and stimulation of excitable cells. *Microelectron. Eng., 57-58, 705-712*

[10] Moriz W, Yoshinobu Y, Finger F, Krause S, Fernandez MM, Schoning MJ (2004): High resolution LAPS using amorphous silicon as the semiconductor material. *Sens. Actuators B, 103, 436-441*

[11] Watts DJ, Strogatz SH (1998): Collective dynamics of 'small-world' networks. *Nature, 393, 440-442*

[12] Shefi O, Golding I, Segev R, Ben-Jacob E, Ayali A (2002): Morphological characterization of *in vitro* neuronal networks. *Phys. Rev. E, 66, 021905*

[13] Bettencourt LM, Stephens GJ, Ham MI, Gross GW (2007): Functional structure of cortical neuronal networks grown *in vitro. Phys. Rev. E, 75, 021915*

[14] Kudoh SN, Kiyohara A, Taguchi T (2007): The heterogeneous distribution of the functional synaptic connections in a rat hippocampal dissociated neurons. *IEEJ Trans. EIS, 127, 1611-1618*

# Impedance Spectroscopy with Field-Effect Transistor Arrays as Novel Tool for Probing Cellular Adhesion, Viability, and Motility

Sven Ingebrandt[*], Susanne Schäfer, Thomas Dufaux, Günter Wrobel, Stefan Eick, Boris Hofmann, Regina Stockmann, Andreas Offenhäusser

Institute of Bio- and Nanosystems (IBN2) and CNI- Center of Nanoelectronic Systems for Information Technology, Forschungszentrum Jülich, Germany
* Corresponding author. E-mail address: s.ingebrandt@fz-juelich.de

We describe a novel method for the non-invasive, electronic monitoring of the cell-substrate adhesion. We utilize open-gate field-effect transistor (FET) chips for our adhesion measurements. These chips were developed, fabricated, and previously used for the extracellular recording from electrogenic cells. We developed a miniaturized and portable 16-channel amplifier system, which monitors the transistor transfer function (TTF) of the devices. We present cellular adhesion and time-dependent detachment measurements of HEK 293 cells on an individual cell level.

## 1 Introduction

Cellular adhesion plays a major role in inflammation, wound healing, and metastasis. In recent years an Electric Cell-substrate Impedance Sensing (ECIS) system has been established (www.biophysics.com) and its feasibility for pharmacological studies was already successfully demonstrated [1-3]. However, because of high input impedance these metal microelectrodes are usually larger than 25 µm in diameter. Therefore the ECIS bioassays are restricted to cells, which form larger syncytia and responses from many cells in parallel are monitored (e.g. MDCK epithelial cell line). The improvement of the ECIS method down to a single cell level (sensor size < 10 µm) has been an issue in the past. In this article we report about the use of small, open-gate field-effect transistor (FET) arrays together with recently developed impedance equipment [4] for cellular adhesion measurements [5].

## 2 Materials and Methods

### 2.1 FET devices

For first experiments we used standard 16-channel open-gate FET devices [6]. These chips were fabricated in the cleanroom facilities of IBN at the Forschungszentrum Jülich. The 16 transistors (4×4) in the arrays had a pitch of 200 µm in the center of a 5×5 mm$^2$ silicon chip. Gate sizes of 5×25 µm$^2$ (channel length times width) or smaller were used to enable single-cell adhesion with one cell covering the whole transistor gate. The gate oxide consisted of thermally grown SiO$_2$ with a thickness of 10 nm.
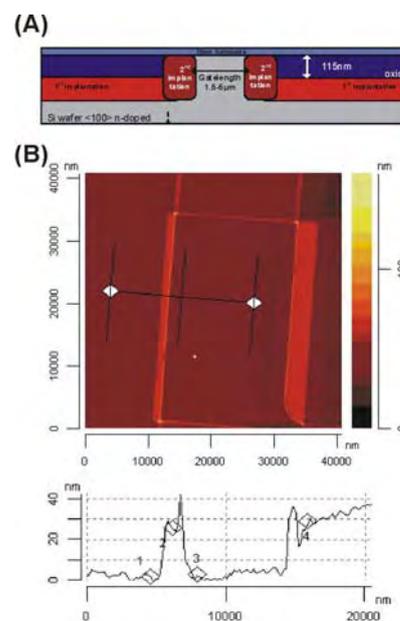


**Fig. 1.** (A) Schematical cross-section through a gate area of the ultraflat FET chip. (B) AFM image with line scan of a gate area. Largest feature sizes are bird beaks of only 30 nm height.

A sandwich layer stack of oxide-nitride-oxide for the passivation of the FET contact lines was found to be stable for repeated usage of the devices. However, due to the fabrication process, the topographical features on the chip surface were up to 800 nm in step height. In this case cells usually tend to adhere on etches or grooves of the chips surface.

In a second process we introduced an additional planarization step to fabricate new sensors with ultra-flat surfaces having maximum topographical features of only 30 nm (Fig. 1) [7]. Gate lengths of 3 to 5 µm and gate widths of 6, 12, or 25 µm were used for this

design. Contact lines were passivated by a sufficiently thick layer of thermal oxide, raising the gate area onto a plateau. Those planar FETs are mandatory to monitor cellular migration under minimized topographical influence.

## 2.2 Cell culture

The FET chips were cleaned and coated with poly(L)lysine. For the basic adhesion measurements we cultured HEK cells that expressed a voltage-gated $K^+$ channel as previously described [8]. In short, the cells were grown in minimal essential medium (M2279, Sigma), supplemented with 2 mM glutamine, 1% non-essential amino acids, 100 units ml$^{-1}$ penicillin, 10% FBS and 0.1 mg ml$^{-1}$streptomycin (all from Invitrogen). The cells were plated onto the substrates at densities of 40–200 cells mm$^{-1}$ and kept for 3–5 days at 37°C and 5% $CO_2$.

## 2.3 Chemicals

Trypsin was purchased from Sigma and used without dilution. For the TTF measurements the cell culture medium was exchanged to an extracellular patch-clamp solution: 5 mM KCl, 140 mM NaCl, 1 mM $CaCl_2$, 10 mM HEPES, 5 mM glucose, adjusted to pH 7.4 with NaOH [8]. The cell culture container on the chips offered a volume of 500 µl. To induce the detachment of cells, 200 µl extracellular patch-clamp solutions were exchanged by 200 µl of trypsin resulting in a concentration of 0.4 v/v. All experiments were performed at 37°C by temperature control of the chip and pre-warming of the solutions.

## 2.4 Readout system

For signal recording a miniaturized 16-channel amplifier system was developed [5]. The portable amplifier offered electronic characterization of the FETs and recordings in potentiometric and impedimetric mode. The whole amplifier unit was operated by a microprocessor and the data were transferred via an USB connection to the PC. The read-out software was implemented in Delphi® 5.0 (Borland Software Corporation). For all experiments, we used an Ag/AgCl wire as reference electrode.

In the potentiometric readout mode, the FETs were operated in the constant-voltage mode. By applying a constant drain-source voltage $V_{DS}$ and a constant gate-source voltage $V_{GS}$, the working point of the device was set. At the first operational amplifier (OP), changes in the drain-source current $\Delta I_{DS}$ were converted into an output voltage $v_{out}$.

In our latest amplifier version for impedimetric readout, 16 independent, frequency-selective amplifiers were additionally included into the system. This allowed simultaneous operation of all 16 readout channels. The scan of the transfer function can be done by feeding a sinodal test signal $V_{mod}$ with 10 mV amplitude and varying frequency from 1 Hz – 1 MHz to the reference electrode (Fig. 3a). The FETs were operated in the same working point as for the *dc-*readout. Test signals of exact amplitude, frequency and phase were provided by a direct-digital-synthesis device. Frequency-selective amplification was performed via a frequency multiplier, which was built-in into a capacitive de-coupled amplification cascade. By a right selection of stimulation voltage and sampling frequency for the data, a simultaneous readout of impedimetric and potentiometric signals is possible.
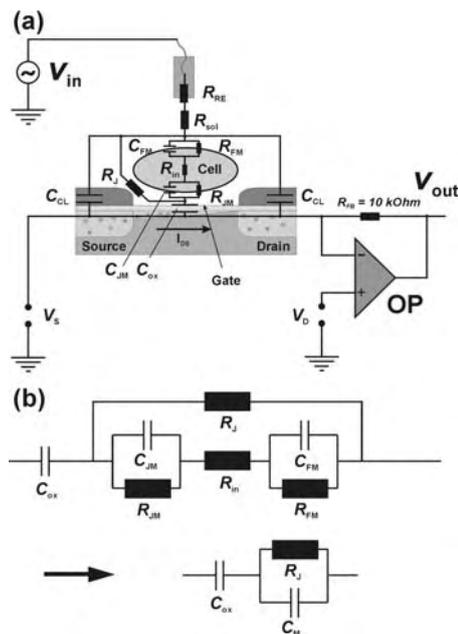


**Fig. 3.** (a) Equivalent electrical circuit for the attachment of an individual cell to an FET. Active ion-channels and electrochemistry of the solid-liquid interface are not included. In (b) the elements for the contact of the cell to the gate are shown with free and attached membrane, internal resistance $R_{in}$ and the seal resistance formed in the membrane-surface junction $R_J$. This circuit can be simplified to an element comprising gate oxide capacitance $C_{ox}$, seal resistance $R_J$, and total membrane capacitance $C_M$ [9].

## 2.5 Electrical equivalent model

As a first, simple model the attachment of an individual cell to a transistor gate can be described by an extension of the standard point-contact model [10]. For the description of the cell-transistor impedance, the sheet-contact model has to be utilized [11]. For adhesion experiments, we additionally need to take reference electrode impedance, solution resistance, FET parasitic and the transfer characteristics of the first amplifier stage into account. In Fig. 3a, the experimental configuration is shown including all passive elements in an electrically equivalent circuit (EEC). Such a circuit can be well described by a transfer function $H(j\omega)$. It is defined by the ratio of the input $v_{in}$ and the output voltage $v_{out}$ of the amplifier:

$$H(j\omega) = \frac{v_{out}}{v_{in}} = |H(j\omega)| \cdot e^{j\varphi(\omega)} \quad (1)$$

$H(j\omega)$ is dimensionless and simply describes the attenuation of the system at a specific frequency. It can be separated into the magnitude $|H(j\omega)|$ and its phase component $\varphi(\omega)$. To calculate the passive elements, the EEC of the cell-transistor contact can be simplified to a large extent (Fig. 3b). This simplification was previously used to model cell transfer functions [9]. Since the cell membrane is a very good insulator, the resistances $R_{JM}$ and $R_{FM}$ can be neglected. The internal resistance $R_{in}$ is relatively small and can be neglected, too. Thus the remaining membrane capacitances can be combined to the total membrane capacitance $C_M = (C_{JM} \cdot C_{FM})/((C_{JM} + C_{FM})$. By using this simplification the gate input is reduced to the oxide capacitance $C_{ox}$ plus the seal resistor $R_J$ and the total membrane capacitance $C_M$ in parallel. The cell sensor contact is then equivalent to what was described before for a membrane [12], glucose oxidase [13], or DNA [4] attached to an FET gate.

Using this simplification, it is possible to exactly calculate the elements of the normalized transfer function of the EEC for a given set of time constants [14]. For the derivation of this analytical solution assumptions are necessary, which require certain magnitude ranges of the circuit elements. For the following set of parameters, the transfer-function term can be factorized: ($R_J$ ($\Omega$) in the order of $10^6 \gg R_{acc} = (R_{EL} + R_{sol})$ ($\Omega$) $10^3 \gg g_m$ (S) $10^{-5} \gg C_{CL}$ (F) $10^{-10} \gg C_{ox}$, $C_M$ $10^{-12}$-$10^{-13}$). The resulting transfer function is:

$$H(j\omega) = R_{FB} \cdot g_m \cdot \frac{1 + j\omega \cdot 2\zeta\tau_{n1} - \omega^2\tau_{n1}^2}{(1 + j\omega\tau_{p1}) \cdot (1 + j\omega\tau_{p2})} \quad (3)$$

The respective time constants for the pole $\tau_{p1}$, $\tau_{p2}$ and zero point $\tau_{n1}$ are:

$$\tau_{n1} = \sqrt{\frac{1}{g_m} \cdot R_J C_{CL}(C_M + C_{ox})} \quad (4)$$

$$\zeta = \frac{g_m C_M R_J + C_{CL}}{2 \cdot \sqrt{g_m R_J C_{CL} + (C_M + C_{ox})}}$$

$$\tau_{p1} = R_J \cdot (C_M + C_{ox})$$

$$\tau_{p2} = 2R_{acc} \cdot C_{CL}$$

The included elements are the feedback resistor of the first amplifier stage $R_{FB}$, the device transconductance $g_m$, the seal resistor $R_J$, the contact line capacitance $C_{CL}$, and the access resistance $R_{acc}$ combining the electrode resistance $R_{EL}$ and the solution resistance $R_{sol}$ with $R_{acc} = (R_{EL} + R_{sol})$. The cell's parameter

influenced in our experiments are the seal resistance $R_J$ and the membrane capacitance $C_M$. In general, for the TTF characteristics an increase in $R_J$ leads to a shift of the cutoff frequency of the low pass to lower frequencies, whereas a reduced cell membrane capacitance $C_M$ leads to steeper band-stop characteristics at a fixed frequency. A more detailed description of this model with an analytic solution of the transfer characteristics is provided elsewhere [7, 14].

# 3 Results and Discussion

By means of the TTF method it was possible to determine, if a cell was adhered to the gate area of a single transistor. Fig. 4 shows two normalized transfer functions of the same transistor as a function of the frequency. After subsequent removal of the individual cell from the gate using a patch-clamp pipette the transfer function changed drastically.
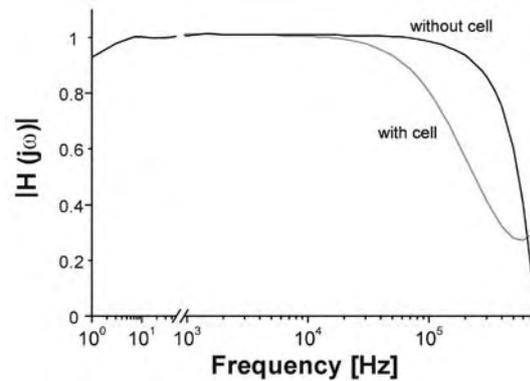


**Fig. 4.** Comparison of the transfer functions for one FET with an adhered HEK cell and after subsequent removal of the cell with a patch-clamp pipette.

The single cell reduced the normalized transfer function in a frequency range above 10 kHz. With this technique the action of i.e. anti cancer drugs on cells can now be followed.

To exemplarily demonstrate the possibility of such an assay, we monitored the trypsin-induced cellular detachment of individual HEK 293 cells with our system. For these assay we work at a fixed frequency of the amplifier and follow the change in transfer-function time-dependently. The addition of trypsin caused the cells to detach from the chip surface and adapt a round morphology. This immediately induced a significant increase in the readout signal, which was followed over time (Fig. 5). Different kinetics of the detachment processes of the different cells was visible. We recently presented a viability measurement with our system [5], where the signals from a single cell look similar to what was presented previously using a colony of cells on the ECIS system [1]. Similar to assays done with this system, our flat FET design enabled migration studies on the single cell level using fibroblast cells [7].
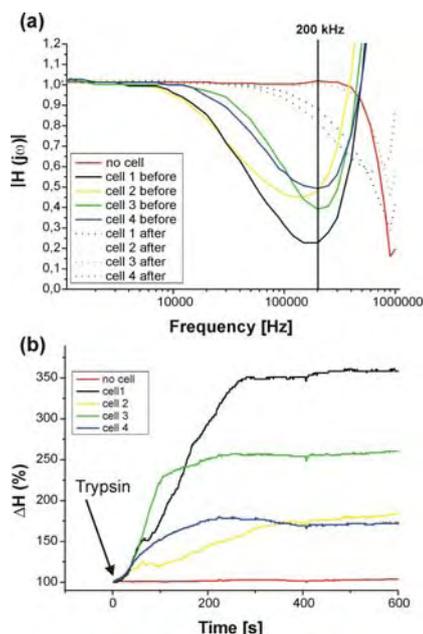
**Fig. 5.** Example of a trypsin assay at an individual cell level. (a) Transfer functions of the FETs with attached HEK 293 cells before (solid lines) and after (dotted lines) administration of trypsin. (b) Time-dependent evolution of the detachment signals of the 4 individual cells at 200 kHz (red line is shown as reference) [15].

## 4   Conclusion and Outlook

We developed a system utilizing the transistor-transfer function method to electronically observe cell-substrate binding events to the gate structure of 16-channel FET chips. Our system can be used to record a full TTF spectrum out of which passive elements of the electronically equivalent circuit of the cell-transistor contact can be extracted. However, for pharmacological or biomedical applications, it is most of the time favorable to observe binding events in a time-dependent form at a fixed frequency of the *ac* input signal. Since a lock-in based readout is used the system offers a very high signal-to-noise ratio, where even small variations of the adhesion properties can be detected. With this proof-of-principle study we demonstrate that it is possible to observe individual binding events of cell types, which usually do not form gap junctions or confluent tissue. Therefore our approach can be applied to various cell types including neurons for toxicology studies. In addition, the use of silicon semiconductor devices offers the possibility to fabricate large arrays with multiple sensor spots on a single device for applications in high-throughput screening for pharmacology.

However, with the current chip design one drawback is that the passive components of cells and chip are always combined in the different time constants and cannot be extracted individually.

In future we intent to develop chip designs, which can be used to detect the cellular components more efficiently and which offer many more readout channels. Additionally, we will apply our method to many different biomedical assays utilizing other cell types such as neurons in toxicology studies.

### References

[1] Giaever, I. and Keese, C. R. (1991): Micromotion of Mammalian-Cells Measured Electrically. Proc. Natl. Acad. Sci. U. S. A., 17, 7896-7900

[2] Lo, C. M., Keese, C. R. and Giaever, I. (1995): Impedance analysis of MDCK cells measured by electric cell-substrate impedance sensing. Biophys. J., 6, 2800-2807

[3] Giaever, I. and Keese, C. R. (1993): A Morphological Biosensor for Mammalian-Cells. Nature, 6455, 591-592

[4] Ingebrandt, S., Han, Y., Nakamura, F., et al. (2007): Label-free detection of single nucleotide polymorphisms utilizing the differential transfer function of field-effect transistors. Biosens. Bioelectron., 12, 2834-2840

[5] Ingebrandt, S., Wrobel, G., Eick, S., et al.: in TRANSDUCERS 07 and EUROSENSORS XXI, The 14th International Conference on Solid-State Sensors, Actuators and Microsystems,, Lyon, France, (2007), 803-806.

[6] Offenhäusser, A., Sprössler, C., Matsuzawa, M., et al. (1997): Field-effect transistor array for monitoring electrical activity from mammalian neurons in culture. Biosens. Bioelectron., 8, 819-826

[7] Schäfer, S. (diploma thesis - 2008): Electrical Characterization of the Cell-Sensor Adhesion with Transistor Transfer Function Measurements, Mathematisch-naturwissenschaftliche Fakultät, Universität zu Köln, (in english).

[8] Wrobel, G., Seifert, R., Ingebrandt, S., et al. (2005): Cell-transistor coupling: Investigation of potassium currents recorded with p- and n-channel FETs. Biophys. J., 5, 3628-3638

[9] Morgan, H., Sun, T., Holmes, D., et al. (2007): Single cell dielectric spectroscopy. J. Phys. D-Appl. Phys., 1, 61-70

[10] Regehr, W. G., Pine, J., Cohan, C. S., et al. (1989): Sealing Cultured Invertebrate Neurons to Embedded Dish Electrodes Facilitates Long-Term Stimulation and Recording. J. Neurosci. Methods, 2, 91-106

[11] Fromherz, P., Kiessling, V., Kottig, K., et al. (1999): Membrane transistor with giant lipid vesicle touching a silicon chip. Appl. Phys. A-Mater. Sci. Process., 5, 571-576

[12] Antonisse, M. M. G., Snellink-Ruel, B. H. M., Lugtenberg, R. J. W., et al. (2000): Membrane characterization of anion-selective CHEMFETs by impedance spectroscopy. Anal. Chem., 2, 343-348

[13] Kharitonov, A. B., Wasserman, J., Katz, E., et al. (2001): The use of impedance spectroscopy for the characterization of protein-modified ISFET devices: Application of the method for the analysis of biorecognition processes. J. Phys. Chem. B, 19, 4205-4213

[14] Dufaux, T. (diploma-thesis - 2008): Design and development of amplifier electronics for silicon-nanowire biosensors, Fakultät für Elektrotechnik und Informationstechnik, RWTH Aachen, (in english).

[15] Schäfer, S., Eick, S., Hofmann, B., et al. (2008): Time-dependent observation of individual cellular binding events to field-effect transistors. submitte

# Carbon Nanotube Based MEA for Retinal Interfacing Applications

David-Pur M[1], Adams C[2], Sernagor E[2], Sorkin R[1], Greenbaum A[1], Shein M[1], Ben-Jacob E[3], and Hanein Y[1*]

1 School of electrical engineering, Tel-Aviv University, Tel-Aviv, Israel
2 Institute of Neuroscience, Medical School, Newcastle University, UK,
3 Schools of Physics, Tel-Aviv University, Tel-Aviv, Israel
* Corresponding author. E-mail address: Hanein@eng.tau.ac.il

A newly developed, fully functional carbon nanotube (CNT) based MEA device for neuronal interfacing applications is presented. The CNT coated electrodes have very large surface area which contributes to high specific capacitance and good electrode performances. Additionally, the roughness of the coated electrodes facilitates effective cell attachment and proliferation of dissociated cells. The potential use of these electrodes for retinal interfacing application is discussed and preliminary recording and stimulation results are described.

## 1 Introduction

One of the key issues determining the performances of MEA devices is the nature of the interface between the electrode and the biological tissue. High quality electrode surfaces are reflected by good electrical recording and stimulation performance as well as strong cell adhesion and proliferation. For optimal electrical coupling, the electrode surface has to be as rough as possible so that it effectively enlarges the surface area. Independently, to achieve good biological coupling, the surface has to be cell adhesive. Interestingly, these two requirements can be attained concurrently if extremely rough and conducting surfaces are used [1, 2]. Such surfaces can function both as excellent electro-chemical electrodes and substrates for neuronal growth. Using this novel approach it is possible to directly interface with neurons in an unmediated fashion.

A most suitable interface material for the application described above is carbon nanotube (CNT). CNTs are chemically inert and robust against mechanical damage. In addition, high density CNTs coated surfaces are distinguished by possessing extremely high surface area. Most interestingly, CNTs appear to encourage neuronal growth. Since CNTs are good electrical conductors, they may also function as very effective electro-chemical electrodes. As a result of this unique combination of properties, CNT electrodes offer exciting new opportunities as an interface material for neuronal applications. Indeed, several recent studies have provided extensive evidence for the potential of CNT coated surfaces as neuronal interfaces [1-6].

One application that may benefit from this technology is retinal implants. Indeed, vision loss due to retinal degeneration (e.g. retinitis pigmentosa, macular degeneration) is a major impairment in ageing populations and it has devastating consequences, often leading to complete blindness. Several projects are currently exploring the possibilities for developing retinal prostheses that could functionally replace lost vision and the results achieved are indicative of the viability of MEA stimulation, although this technology is very much in its infancy (e.g. [7,8]).

The present limited success arises from many technical challenges, ranging from biocompatibility and intraocular implant stability, to problems of stimulation efficacy and restriction of current spread across the retina following focal stimulation. Whilst an optimal device would have a 1:1 ratio of electrode to retinal ganglion cells (RGCs), most of the devices currently under development comprise arrays of as few as 12-16 electrodes, each with diameters of several hundred micrometers, thereby covering large retinal areas. Recent studies indicate significant improvement in spatial resolution (MEAs comprising 61 ITO electrodes; spacing 60μm-diameters 6-25 μm) [9,10]. It is estimated that an array of 625 electrodes with centre-centre spacing of 20 μm would restore enough visual acuity to enable the patient to navigate their surroundings without additional external aids.

It is evident that a key challenge in developing better MEAs for retinal implant devices is to achieve better coupling between the electrodes and the tissue. This, in turn, will allow the reduction of the electrode size and increase the electrode density on the device.

In this paper we examine the suitability and the possible advantages of CNT MEAs for retinal implant applications. We first review the fabrication scheme of these electrodes. Next the electrochemical and bio-

logical properties are highlighted. And finally, preliminary electrophysiological tests with mouse retinal wholemounts are described.
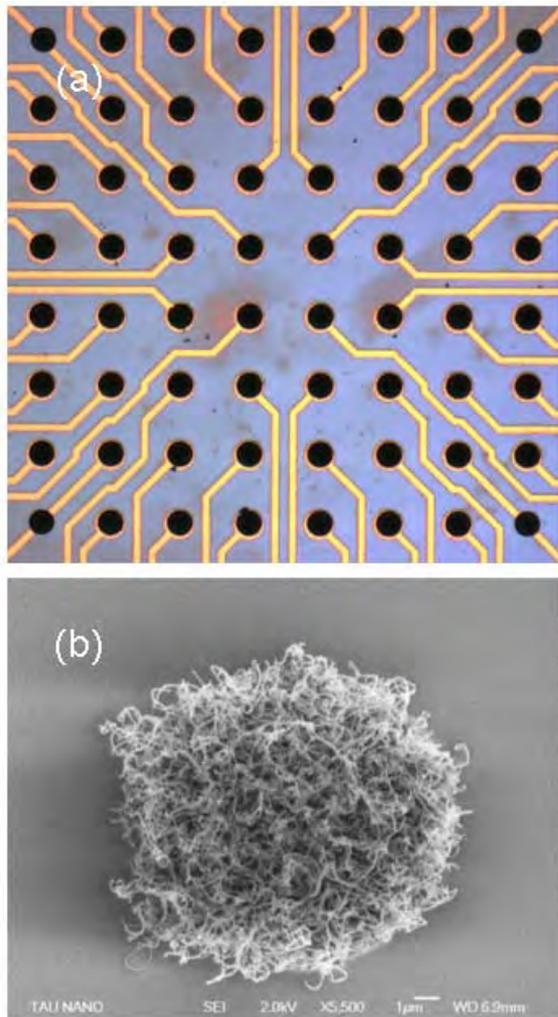


**Fig. 1.** The CNT based neuro-chip (a). The CNT based multi electrode array is fabricated using standard optical lithography combined with chemical vapor deposition process to grow the CNTs. The resulting chip includes passivated interconnecting TiN lines (bright thin lines) and CNT coated electrodes (dark disks). Electrode diameter is 80 μm. (b) A high resolution scanning electron microscope (HRSEM) image of an isolated 20 μm CNT island revealing the extremely rough morphology of the surface.

## 2 Fabrication Methodology

An important advantage of CNTs is their compatibility

with micro-fabrication processes. The process of integrating CNTs with micro-fabrication is not standard and had to be tailored to accommodate the various fabrication and material challenges such as high process temperature during the CNT growth, biocompatibility, durability in ionic solutions for very prolong times, to name several. A robust procedure, satisfying all the challenges mentioned above, was

developed at Tel-Aviv University over the last several years and is described in detail in reference [1].

The CNT MEAs are fabricated using a combination of micro and nano fabrication techniques. The micro-fabrication consists of photolithography and thin film deposition to pattern and passivate conducting tracks. Titanium nitride (TiN) lines are used as conducting tracks as well as support for the catalyst for the CNT growth. $Si_3N_4$ (Silicon Nitiride) layer is used for passivation. Nickel (Ni) islands act as a catalyst layer and define the CNT electrode area. Ni islands are patterned directly at desired location through holes etched in the passivation layer. Their dimensions and position define the geometry and position of the CNT islands. A CNT chemical vapor deposition (CVD) growth concludes the fabrication.

The final packaging consists of a PCB setup which was designed and developed to be fully compatible with the MEA60 recording system from Multichannel Systems.

The thermal CVD CNT growth yields extremely rough and three dimensional surfaces (figure 1b) deposited directly onto conducting tracks. Since the CNTs are electrically conducting, the resulting CNT islands are in fact perfectly functional electrochemical electrodes. Electrochemical characterization validate that the CNT electrodes are marked by very high specific capacitance (10 mF•cm$^{-2}$) [1] coupled with high charge injection limit of $2\times10^{-3}$ C/cm$^2$. This limit is measured by applying a current pulse between a CNT electrode (working electrode) and a counter electrode while validating that the potential build-up between the working electrode and a reference electrode remains within the safe boundaries for the electrode. These boundaries are determined from a standard cyclic voltammetry measurement. Figure 2 shows the results of such a test with a 2 μA pulse applied for 50 ms yielding a charge injection of $Q=I\times t=1\times10^{-7}$ C.

## 3 The use of CNT MEAs for dissociated neuronal cultures

The biological properties of the electrodes were explored by culturing dissociated neurons on CNT MEAs. Neurons adhere extremely well to the electrode surface. Moreover, neurons form a very intimate contact with the CNT surface (figure 3a, b). Therefore, the first advantage of the CNT electrodes over other electrode materials is their ability to allure the cells to adhere strongly to their surface without the need for any chemical modification. This ensures a direct and tight coupling between the electrodes and the cells.
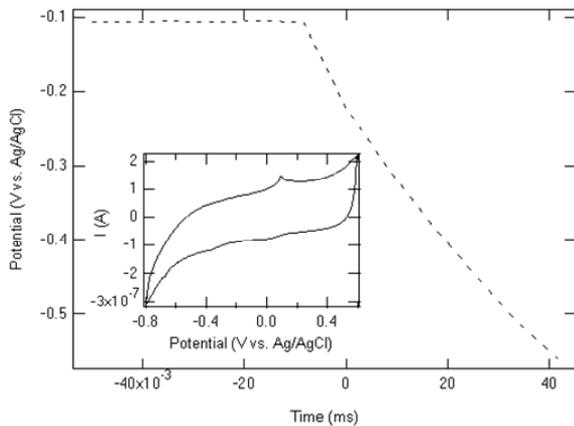
**Fig. 2.** Charge injection limit test using 2 A pulse for 50 ms. Inset: CV measurement of an 80 m CNT electrtode. Test were carried out in PBS.
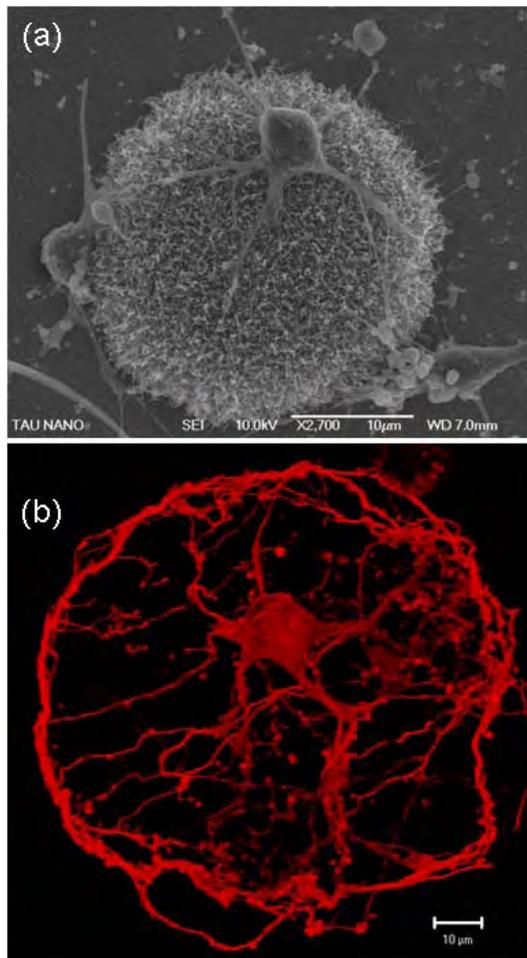


**Fig. 3.** Dissociated cortical neuronal cells on CNT islands. (a) HRSEM image of fixated cells. (b) Confocal florescence image of a neuron.

In addition, the strong affinity of the cells to the CNT electrodes facilitate a unique arrangement in which very compact and well ordered neural networks are formed [2]. Electrical recordings from such networks are marked by high-fidelity signals corresponding to single cell spiking as well as synchronized bursting across several cells. Electrical stimulation has also been demonstrated.

## 4 The use of CNT MEAs for *in vitro* studies of retinal function

The high affinity of neural cells to CNTs, the electrical stability of the latter as well as their high surface area (resulting in high charge injection capacity), make the use of CNTs particularly attractive for long-term bio-implantable electrical devices, in particular retinal prosthetic applications. Indeed, the intimate contact between the retinal tissue and the CNT surface offers great potential for retinal implant applications where the gap between the electrode surface and the tissue hinders high resolution targeting of cells.

To validate the potential of these electrodes for retinal implant applications, we have placed mouse retinal wholemounts (from the cone rod homeobox knockout mouse, an animal model of retinal degeneration) onto CNT MEAs, with RGCs (the output cells of the retina) in direct contact with the electrodes. Spontaneous bursts of neural impulses (figure 4) as well as slow oscillatory activity were routinely recorded, indicating the viability of these electrodes for recording from intact neural tissue.
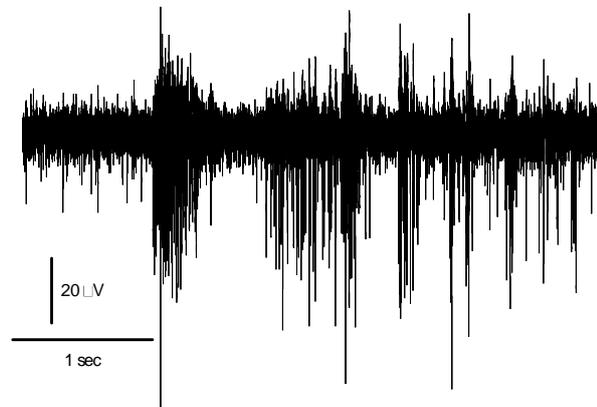


**Fig. 4.** Typical electrical recording trace

We have also investigated the suitability of CNT electrodes as an appropriate interface for retinal neural stimulation. Using the 8-channel STG stimulating system from MultiChannel Systems, we have stimulated individual electrodes on the MEA and recorded evoked spikes on neighboring electrodes. The stimulus applied were cathodic charge-balanced bi-phasic square current waveforms of various amplitudes and durations ranging from 50-700 A and 60-100 s per phase respectively. At 480 A, a 60 s pulse (corresponding to 28 nC) yielded responses in 16% of trials. For 80 s pulses (38 nC), responses were elicited in

75% of trials, and finally, responses were obtained in 100% trials for 100 s pulses (48nC). Figure 5A illustrates a single spike (marked by the asterisk) and figure 4B a burst of spikes (first spike marked by an asterisk) following 48 nC stimulation of a neighboring electrode (bursts were observed both with 38 and 48 nC pulses).
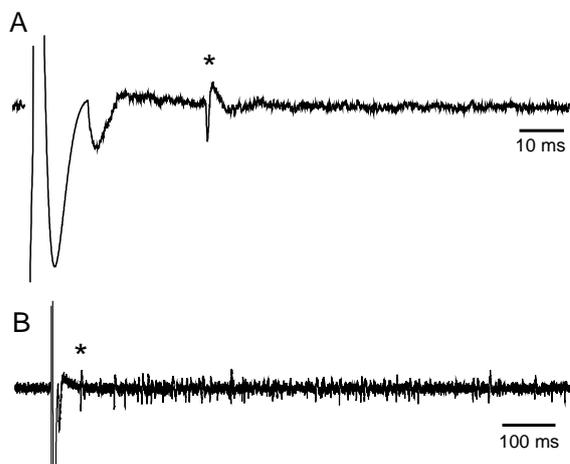


**Fig 5.** Retinal ganglion cell responses to CNT electrode stimulation

## 5 Discussion

Overall, CNT-MEA technology offers excellent electrochemical properties (in terms of current requirements for effective stimulation), which would potentially make this material the ideal choice for long-term in vivo implantation.

The enhanced electrochemical properties of the electrodes, their flexible and simple micro-fabrication procedure as well as their bio-compatibility and durability suggest that CNT electrodes are a promising platform for high resolution neuronal interfacing.

## References

[1] T. Gabay, et al. (2007): Electro-chemical and biological properties of carbon nanotube based multi-electrode arrays, *Nanotechnology, 18, 035201-035206*

[2] Raya Sorkin, Tamir Gabay, Pablo Blinder, Danny Baranes, Eshel Ben-Jacob and Yael Hanein *(2006)* Compact self-wiring in cultured neural networks, *Journal of Neural Engineering, 3, 95-101*

[3] Malarkey EB, Parpura V. (2007) Applications of carbon nanotubes in neurobiology. *Neurodegenerative Diseases* ;4:292-9.

[4] Mattson MP, Haddon RC, Rao AM. (2000) Molecular functionalization of carbon nanotubes and use as substrates for neuronal growth. *J Mol Neurosci* ;14:175-182.

[5] Hu H, Ni YC, Mandal SK, Montana V, Zhao N, Haddon RC et al. (2005) Polyethyleneimine functionalized single-walled carbon nanotubes as a substrate for neuronal growth. *J Phys Chem* B;109:4285-9.

[6] Hu H, Ni YC, Montana V, Haddon RC, Parpura V. (2004) Chemically functionalized carbon nanotubes as substrates for neuronal growth. *Nano Lett*; 4:507-511.

[7] Rizzo JF 3rd, Wyatt J, Loewenstein J, Kelly S, Shire D (2003) Methods and perceptual thresholds for short-term electrical stimulation of human retina with microelectrode arrays. *Invest Ophthalmol Vis Sci.* 44:5355-61.

[8] Mahadevappa M, Weiland JD, Yanai D, Fine I, Greenberg RJ, Humayun MS (2005) Perceptual thresholds and electrode impedance in three retinal prosthesis subjects. *IEEE Trans Neural Syst Rehabil Eng* 13:201-6.

[9] Sekirnjak C, Hottowy P, Sher A, Dabrowski W, Litke AM, Chichilnisky EJ (2006) Electrical stimulation of mammalian retinal ganglion cells with multielectrode arrays. *J Neurophysiol* 95: 3311-3327.

[10] Gunning D, Adams C, Cunningham W, Mathieson K, O'Shea V, Smith KM, Chichilnisky EJ, Litke AM, Rahman M (2005) 30 μm spacing 519-electrode arrays for in vitro retinal studies.

*Nucl Instr Meth Phys Res A* 546: 158-153.

# Micronail-structured micro electrode arrays for selective local stimulation of excitable cells

Dries Braeken[1,2*], Danny Jans[1,2], Danielle Rand[2], Bart Van Meerbergen[2], Roeland Huys[2], Josine Loo[2], Geert Callewaert[1], Gustaaf Borghs[2,3] and Carmen Bartic[2,3]

1 K.U.Leuven, Laboratory Of Physiology, O&N Herestraat 49, 3000 Leuven, Belgium
2 IMEC vzw, Kapeldreef 75, 3001 Leuven, Belgium
3 K.U.Leuven, Department of Physics and Astronomy, Celest jnenlaan 200D, 3001 Heverlee, Belgium
* Corresponding author. E-mail address: dries.braeken@imec.be

Micro Electrode Arrays (MEAs) consisting of either passive electrodes or active circuitry allow to investigate activities of numerous electrogenic cells simultaneously. The use of microchip technology makes fast readout and high throughput feasible, thus it could provide tools suitable for pharmacological research. Nevertheless high signal-to-noise ratio recordings from vertebrate cells with extracellular electrodes still remain challenging. Towards the optimization of the electrical signal transfer between a cell and an electronic device, we have developed micronail-structured electrodes. Due to their particular configuration, the nails are strongly engulfed by the cellular membrane. In this paper, we demonstrate the feasibility of selective extracellular electrical stimulation at the (sub)cellular level in dissociated cultured cells. By measuring the calcium signals, we found that electrical stimulation via the micronails activates the cell locally, with very low applied currents. The results suggest the applicability of the device in pharmacological and/or signal propagation studies.

## 1 Introduction

The electrical activity of excitable cells such as neuronal and cardiac cells [1,2] or tissue slices [3] can be studied by monitoring the extracellular field potentials (FPs), which correlate with the action potentials in activated cells. Micro Electrode Arrays (MEAs) consisting of either passive electrodes or active circuitry allow to investigate FPs of numerous cells simultaneously [4-7]. The use of microchip technology makes fast readout and high throughput feasible, because of higher spatial resolution and improved scaling. Nevertheless, high signal-to-noise ratio extracellular recordings from mammalian cells, particularly at single cell level, still remain challenging.

Towards the optimization of the electrical signal transfer between a cell and an electronic device, we have developed micronail-structured electrodes. The tight junction between the cell membrane and the sensor surface increases the seal resistance between cells and electrodes as compared to planar electrodes (as shown in Figure 2). Immunocytochemical stainings combined with fluorescence imaging as well as electron microscopy were used to investigate the coupling.

Beside recordings, these electrodes can also be used for local specific stimulation of cells using low injected charge densities. In this paper, we report results illustrating the highly specific stimulation demonstrated on rat cardiomyocyte cells. Changes in the relative intensity of the fluorescent calcium indicator

Fluo4 recorded from stimulated cells can provide an effective measure of the stimulation efficacy. The combination of localized electrical stimulation and calcium imaging may offer a relevant tool for basic cardiac or neuronal electrophysiology, pharmacological studies and cell pacing [8,9].

## 2 Materials and Methods

### 2.1 Device Fabrication

Micronail-based electrodes were fabricated using a CMOS-compatible process-flow as described elsewhere [10]. The structure of such a micronail is shown in Figure 1C.

Briefly, metal structures defining the electrodes, bondpads and conductor lines were embedded in $SiO_2$ and fabricated using a Cu damascene process. A metal diffusion barrier layer made of 50 nm SiC and 50 nm $Si_3N_4$ was deposited onto the metal followed by the deposition of a 1.4 μm layer of $SiO_2$. In order to define the metal core of the nail, via holes with diameters ranging from 250 nm to 1 μm aligned with the metal underneath were formed by deep-reactive ion etching, selective to the Cu metal. We have used either Cu electroplating or tungsten chemical vapor deposition in order to fill the vias and form the nail shaft. After metal deposition and chemical-mechanical polishing, an additional lithography step was used to define the nail structures by etching the $SiO_2$ around the nail shaft (~1 μm deep). A thin oxide layer of ~200 nm was left around the metal core to protect the nail

against corrosion and reduce the parasitic capacitance between the metal nail and the medium. Finally, the tip of the nail was covered either by a thin layer of electroplated Au (in the case of Cu nails) or by 100 nm sputtered TiN layer (in the case of the W nails).

After dicing, the individual chips were flip chip bonded onto epoxy PCBs on which a culture chamber has been created by gluing a glass ring (Figure 1).



**Fig. 1.** Photograph of a packaged chip with a culture chamber on top.

## 2.2 Embryonic Cardiomyocytes Culture

Hearts of 16-day old embryos of Wistar rats were removed under sterile conditions and placed in $Ca^{2+}/Mg^{2+}$-free HBSS solution as described previously [11]. The hearts were minced in 1 $mm^2$ pieces. Trypsin-EDTA (0.05%, Sigma) was added and after 8 minutes of incubation at 37°C, the supernatant was discarded. The enzymatical dissociation was done by adding DNAse Type II (10,000 units/ml, Sigma) and incubated for 3 minutes at 23°C. Then, trypsin-EDTA solution was added and incubated for 8 minutes. The supernatant was collected and added to Ham's F10 (Invitrogen) containing 0.5% ITS (Gibco) and 33% FCS (Gibco) and kept on ice. The collected cells were then centrifuged for 10 minutes at 4°C at 200g and resuspended in Ham's F10, containing 0.5% ITS and 5% FCS. The collected cell suspensions were seeded in 30 mm culture dishes and incubated for 70 minutes at 37°C, 5% $CO_2$ for differential adhesion. Afterwards, the cells were collected and centrifuged for 10 minutes at 200g. The cells were plated on uncoated, ethanol-sterilized devices at cell densities of 40000 cells/ml. The medium was replaced every other day. Cells were typically used for experiments after 2-6 days *in vitro*.

## 2.3 Calcium Imaging

For calcium imaging experiments, Fluo4 AM (Invitrogen) was dissolved in DMSO containing 20% (w/v) Pluronic (Invitrogen) to obtain a final concen-

tration of 5 μM Fluo4. For ester loading of the Fluo4, cells were transferred to $Ca^{2+}$-free KREBS solution (135 mM NaCl; 5.9 mM KCl; 2 mM EGTA; 1.2 mM $MgCl_2\cdot6H_2O$; 11.6 mM HEPES; 11.5 mM glucose; pH 7.3) for 30 minutes at 37°C. The working buffer was a 1.5 mM $Ca^{2+}$ KREBS solution (135 mM NaCl; 5.9 mM KCl; 1.5 mM $CaCl_2$; 1.2 mM $MgCl_2\cdot6H_2O$; 11.6 mM HEPES; 11.5 mM glucose; pH 7.3). Cells were excited at 488 nm using a CellR Live Imaging system coupled to an upright microscope (BX51, Olympus) at 2 frames/s. Data were processed using the CellR software.

## 2.4 Immunocytochemical Stainings

Cells were fixated and permeabilized in PBS containing 0.5% TX-100 for 5 min. After washing, cells were blocked overnight at 4°C followed by 1.5 h incubation at 23°C in the same blocking solution containing the first antibody. After washing, immunoreactivity was revealed by incubation (1 h, 23°C) with Alexa488 conjugated secondary antibodies (Invitrogen). To label actin filaments, Alexa488 conjugated phalloidin was included in the incubation mix. The cells were then washed with PBS and water. The substrates were examined using an Axioskop FS2 Mot (Zeiss) equipped with a Pascal LSM5 confocal scanning unit.

## 2.5 Electrical Stimulation Set-up

For the electrical stimulation of the cells, rectangular biphasic current pulses with amplitudes ranging from 100 nA to 1 μA and a total pulse width of 2 ms were used. The pulses were applied using a DS8000 digital stimulator (WPI) and a DLS100 stimulus isolator (WPI). The cathode and anode of the DLS100 were connected to an electrode covered by a cell body and an uncovered electrode, respectively, thus forming a bipolar stimulation set-up. The liquid was grounded using an Ag/AgCl reference electrode.

## 3   Results and Discussion

### 3.1 Cellular attachment on micronails

Primary cardiomyocyte cells were grown on nail beds with a pitch of 3 μm between individual nails. Cells were stained with phalloidin to reveal the actin filaments and imaged using confocal microscopy. We observed strong engulfment of the nail structures by the cell membrane. As shown in Figure 3, immunostaining demonstrates an accumulation of actin fibers around the micronails, indicating an intimate contact of the cell membrane with the nail. Moreover, the nail structures seem to promote cell spreading and adhesion to the surface.

**Fig. 3**. Actin filament staining of cardiomyocytes on nail bed structures with electrodes spaced 3 μm apart.

## 3.2 Local Stimulation of Cardiomyocytes

Typically 2-6 days after the plating of cardiomyocyte cells on passive nail electrode chips, stimulation experiments were performed. Local and selective stimulation of a single cardiomyocyte is demonstrated in Figure 4. Initially, the cell was triggered using a bipolar stimulus, creating a charge transfer of $6 \times 10^{-10}$ C between two electrodes with micronails, spaced 6 μm apart. Upon this stimulus, the relative intracellular calcium level increases (region 1 on the graph in Figure 4). Applying the same stimulus yields an additional calcium increase (region 2), while a third stimu-

**Fig. 2.** Schematic illustration of the main differences between (A) flat and (B) nail-structured surfaces for MEA applications. The seal resistance, $R_s$ is increased by the stronger coupling between cell membrane and the electrode. (C) SEM photograph of a nail bed structure.

lus with higher intensity ($10 \times 10^{-10}$ C) induces a faster and stronger increase in the calcium concentration (region 3), showing stimulus dependency of the cell response. A final stimulus ($16 \times 10^{-10}$ C) saturates the calcium level detectable with Fluo4. This experiment showed dose-dependent behaviour of the intracellular calcium signal upon stimulation. Moreover, we showed that subcellular regions of the cell could be stimulated without stimulation of the entire cell, suggesting the local impact of the stimulation on the cell.

## 4 Conclusion

Strong engulfment of sub-micrometer probes by the cellular membrane can be used in order to optimize the electrical signal transfer between the cell and an electronic device. Such coupling results in efficient stimulation of cardiac cells at low injected currents in a localized way. Selective stimulation of the cells shows dose-dependent increase of the free intracellular calcium concentration.

In this paper, we showed that these nail-like structured MEAs can be used for pharmacological screening on subcellular level. Moreover, the response of ion channels in the cell membrane upon local stimulation can be investigated.

**Fig. 4.** Selective and local stimulation of a single cardiomyocyte positioned on top of the micronail. Bipolar pulses of 2 ms width are applied between two electrodes, one of which is underneath the cell. The cell response is shown as the change in intracellular calcium ($\Delta F/F_0$).

**References**

[1]  R. H. Whittington, L. Giovangrandi and G. T. A. Kovacs, (2005): A closed loop electrical stimulation system for cardiac cell cultures, IEEE Trans. Biomed. Eng., 52 (7); 1261-70.

[2]  D. A. Wagenaar, J. Pine, S. M. Potter, (2004): Effective parameters for stimulation of dissociated cultures using multi-electrode arrays, *J. Neurosci. Meth.*, 138: 27-37.

[3]  D. Echevarria, K. Albus, (2000): Activity-dependent development of spontaneous bioelectric activity in organotypic cultures of rat occipital cortex, *Dev Brain Res* 123(2):151–64.

[4]  S. M. Potter, T. B. DeMarse, (2001): A new approach to neural cell culture for long-term studies, *J Neurosci Methods* 110(1/2):17–24.

[5]  J. Pine, (1980): Recording action potentials from cultured neurons with extracellular microcircuit electrodes, *J. Neurosci. Meth.* 2: 19-31.

[6]  M. Hutzler, A. Lambacher, B. Eversmann *et al.* (2006): High-resolution multitransistor array recording of electrical field potentials in cultured brain slices', *J. Neurophysiol.*, 96: 1638-1645.

[7]  . Fromherz, A. Offenhausser *et al.*, (1991): A neuron-silicon junction: A Retzius cell of the leech on an insulated-gate field effect transistor', *Science,* 252: 1290-93.

[8]  M. Reppel, P. Igelmund, U. Egert *et al.*, (2007): Effect of cardioactive drugs on action potential generation and propagation in embryonic stem cell-derived cardiomyocytes, Cellular *Physiology and Biochemistry*, 19 (5-6): 213-224.

[9]  M. Reppel, F. Pillekarnp, Z.J. Lu *et al.*, (2004): Microelectrode arrays: A new tool to measure embryonic heart activity, *Journal of Electrocardiology*, 37: 104-+ Suppl..

[10]  R. Huys, D. Braeken, B. Van Meerbergen *et al.*, (2008): Novel concepts for improved communication between nerve cells and silicon electronic devices, *Solid-State Electron*, 52 (4): 533-539.

[11]  M.C.T. Denyer, M. Riehle, J. Hayashi *et al.*, (1999): Bioassay development: the implications of cardiac myocyte motility in vitro, *In Vitro Cell. Dev. Biol.-Animal* 35, pp. 352–356.

# An MEA-based System for Multichannel, Low Artifact Stimulation and Recording of Neural Activity

Pawel Hottowy[1,2*], Władysław Dąbrowski[1], Sergei Kachiguine[2], Andrzej Skoczeń[1], Tomasz Fiutowski[1], Alexander Sher[2], Przemysław Rydygier[1], Alexander A. Grillo[2], Alan M. Litke[2]

1 AGH University of Science and Technology, Faculty of Physics and Applied Computer Science, Krakow, Poland
2 Santa Cruz Institute for Particle Physics, University of California, Santa Cruz, CA, USA
* Corresponding author. E-mail address: pawel@scipp.ucsc.edu

We present a design and preliminary test results of an MEA-based system for the spatio-temporal distributed stimulation and low-artifact recording of neural activity. The custom-made MEA includes 61 microelectrodes with 60 μm spacing and 5 μm diameter. The stimulation and recording are realized by a pair of 64-channel Application Specific Integrated Circuits. In the preliminary tests, using a triphasic current pulse shape for the stimulation of mouse retinal ganglion cells, we recorded the evoked spikes as soon as 55 μs after the stimulation pulse, even on the same electrodes that were used for stimulation.

## 1 Introduction

The aim of our project is to develop an MEA-based system able to stimulate individual neurons in a general spatio-temporal pattern, with simultaneous recording of the elicited activity with minimal stimulus artifacts. We plan to use the system to investigate the mechanisms of information processing in brain tissue, and to develop stimulation techniques for future generations of high-resolution neural prostheses.

## 2 System overview

The system presented here is based on a custom-made high-density MEA [1] and two multichannel Application Specific Integrated Circuits (ASICs). The Stimchip [2] generates the electrical stimulation signals independently on each electrode and the Neuroplat chip [3] simultaneously records the neural activity.

The system is controlled by a PC running a Labview application, which generates the stimulation signals in real-time and continuously records the neuronal activity on all the electrodes. The recorded data are analyzed off-line with custom software developed in Java and Matlab.

### 2.1 Multielectrode array

The MEA consists of 61 microelectrodes arranged in a hexagonal pattern, with 60 μm inter-electrode spacing. All the electrodes have a diameter of 5 μm and are electroplated with platinum before the experiment in order to minimize their impedance. Arrays of the same type have been used previously for electrical stimulation of retinal ganglion cells in ro-

dents [4] and primates [5], however, with stimulation electronics with much more limited functionality.

### 2.2 Stimchip

The block diagram of the Stimchip is shown in Fig. 1. The chip comprises 64 independent stimulation channels with active artifact suppression circuits, circuitry for generating the internal bias voltages, and a logic block that controls the operation of each channel based on digital commands sent from the control PC.
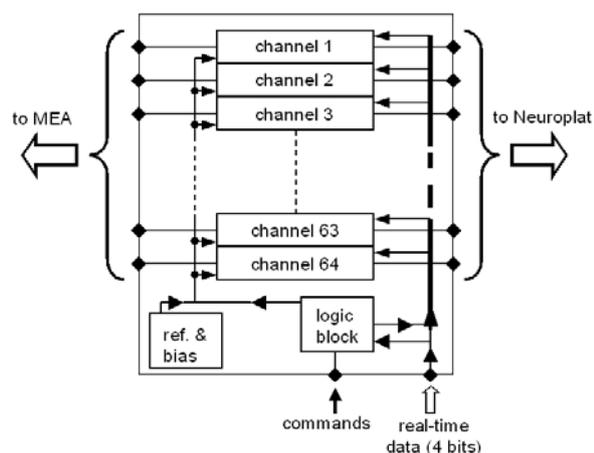


**Fig. 1.** Block diagram of the Stimchip.

The functional diagram of a single channel of the Stimchip is shown in Fig. 2. Each channel comprises a programmable generator of arbitrary current waveforms, a current-to-voltage converter, and artifact suppression circuitry. The waveform generator is built from an 8-bit digital-to-analog converter (DAC) and includes eight selectable output current buffers with maximum current values of 60 nA, 250 nA, 1 μA, 4

μA, 16 μA, 65 μA, 250 μA or 1 mA. The generated current signal can be sent directly to the electrode, or via the current-to-voltage converter when the voltage stimulation mode is selected. The output voltage of the stimulation circuitry is limited to +/-1.5V. The current range and stimulation mode are set independently for each channel by an external command.
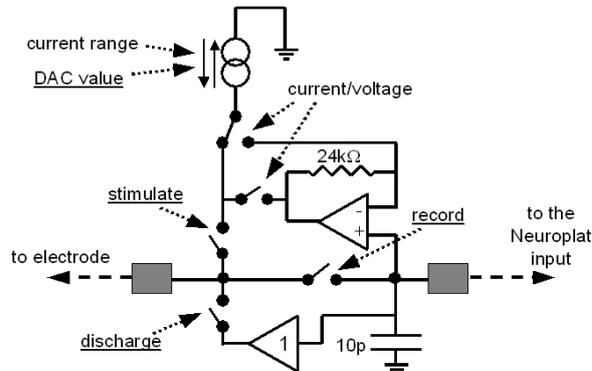


**Fig. 2.** Functional diagram of a Stimchip channel. The real-time control signal names are underlined.

During signal recording, the electrode is connected to the input of the external amplifier (in our case, a Neuroplat channel) through the *record* switch (Fig. 2). In order to avoid sat

uration of the amplifier by the large voltage signal generated by the stimulation pulse, the amplifier input can be disconnected from the electrode prior to the stimulation pulse and held at the potential equal to the electrode DC level. If necessary, the electrode-electrolyte interface can be actively discharged via a voltage follower before the electrode is reconnected to the amplifier input.

The states of all the switches in the circuit as well as the shape of the stimulation signal are controlled with a time resolution of 50 μs, independently for each channel, by a stream of real time data (~15 Mb/sec) sent from the control computer.

## 2.3 Neuroplat chip

The Neuroplat chip comprises 64 independent recording channels, an analog multiplexer, control logic and bias circuitry. Each channel includes an AC-coupled amplifier, a band-pass filter, and a sample-and-hold circuit. Both the gain of the amplifier and the band-pass frequency range of the filter can be set with digital commands. The output signals on all the channels are sampled with a frequency of 20 kHz, multiplexed, and sent to the control computer for digitization and storage.

## 3  Preliminary tests

To evaluate the performance of the system we stimulated and recorded from the retinal ganglion cells of adult mice. In the following we discuss briefly the

stimulation protocol and present some examples of the test results.

## 3.1 Stimulation protocol

All the experiments reported below were done with stimulation pulses generated in the current mode. We used a charge-balanced stimulation pulse shape with three phases (positive-negative-positive sequence, as shown in Fig. 3). The duration of each phase was set at 100 μs and the ratio of amplitudes of the first and the third phase (A1/A3) was optimized for minimal stimulus artifact.

For this pulse shape, with A1/A3=2, we were able, in most cases, to connect the stimulating electrode back to the recording amplifier and record the elicited spike as soon as 55 μs after the stimulation pulse, with no necessity for active discharge. The signals on the neighboring electrodes of the array could be recorded typically with 5 μs latency with respect to the end of the stimulus pulse. For comparison, when a standard charge-balanced pulse with two phases (A1=0) was used, the active discharge of the stimulating electrode for at least several hundred microseconds was required before the elicited spikes could be recorded effectively.

In the tests discussed below we used one nearby electrode to stimulate a given neuron. The gain of the Neruoplat chip was always set to 800 and the passband was 45-2000 Hz. For all the plots, except Fig. 9, the stimulation current was applied between t=0.05 ms and t=0.35 ms. The pulse amplitude always refers to the amplitude of the negative pulse phase.

## 3.2 Results

Figure 3 shows 150 overlaid responses to 0.43 μA stimulation pulses, recorded on the stimulating electrode. We classified 130 of the recorded waveforms as the superpositions of stimulation artifacts and the elicited neuronal spikes (red), and 20 as the artifacts only (black). Although the amplifier input was disconnected from the electrode for the period from t=0.005 ms to t=0.405 ms for each pulse, there are visible artifacts recorded during that period due to crosstalk between the electrode and the amplifier input through the parasitic capacitances of the open CMOS switch. The optimized shape of the stimulation current waveform results in a minimal residual charge left on the electrode-electrolyte interface so that we observe a low-amplitude artifact after reconnecting the amplifier input to the electrode.
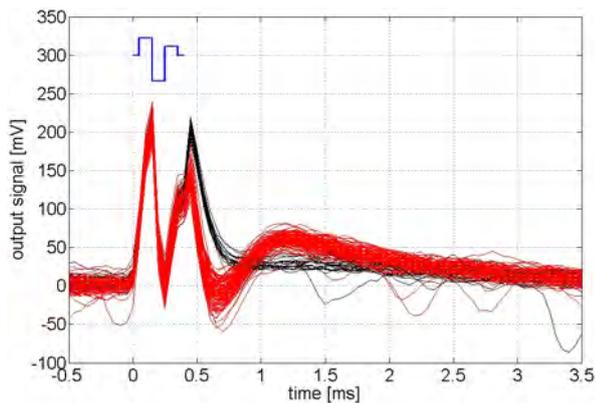
**Fig. 3.** 150 responses to 0.43 µA stimulation pulses recorded on the stimulating electrode. The artifact-only responses are shown in black and the responses including spikes are shown in red. The blue trace illustrates the shape and timing of the stimulation pulse.

The amplitudes of the recorded artifacts are within the same range as the typical amplitudes of the neuronal spikes and well below the amplifier limit for linearity (+/-1 mV for the gain set to 800). This suggests that the system can record the evoked spikes with similar quality as the spontaneous activity. To verify this, we averaged the traces within each of the two classes shown in Fig. 3 and subtracted the obtained average waveforms to find the average shape of the recorded elicited spike [4]. The same procedure has been applied also to the electrodes adjacent to the one used for stimulation. The elicited waveforms match very well the averaged waveforms generated by the same neuron spiking spontaneously (Fig. 4), indicating that the system is capable of recording the elicited spikes with minimal distortions, even on the electrodes used for stimulation.
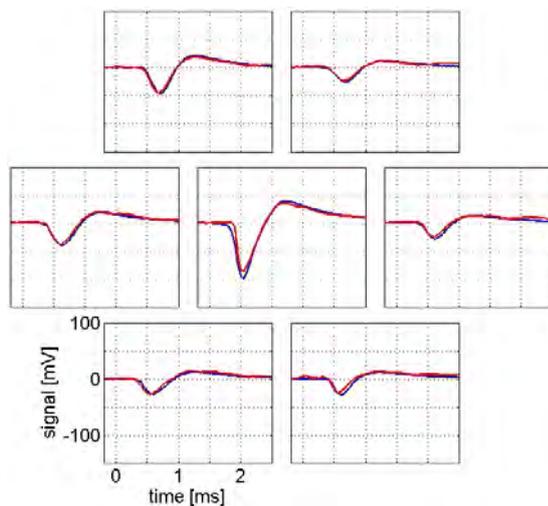


**Fig. 4.** Comparison of signals generated on seven electrodes by the same neuron spiking spontaneously (blue traces) and in response to electrical stimulation (red traces, shown after artifact subtraction). The relative position of each plot in the figure follows the position of the corresponding electrode on the MEA layout. Both vertical and horizontal scales are the same for each plot. The 0.43 µA stimulation pulse was applied to the center electrode.
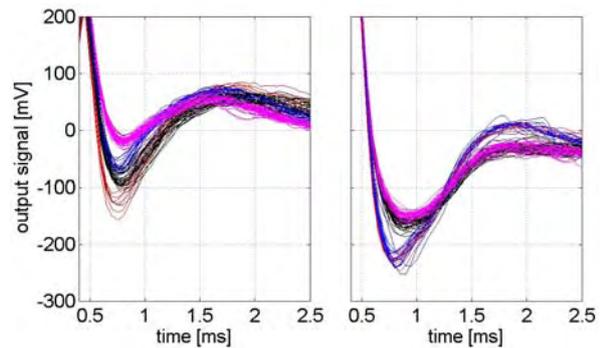


**Fig. 5.** 98 overlaid responses to 0.65 µA stimulation pulses recorded on the stimulating electrode (left) and the neighboring electrode (right). The vertical scale range is the same for both plots. The waveforms include the responses from three neurons (1-3), stimulated with efficiencies of 100%, 23%, and 38%, respectively. All the waveforms include the stimulus artifact. Pink traces: signal from neuron 1. Blue traces: combined signal from neurons 1 and 2. Black traces: combined signal from neurons 1 and 3. Red traces: combined signal from all three neurons.

By increasing the amplitude of the stimulation current, we usually could stimulate several neurons with the same electrode. Figure 5 shows 98 overlaid responses, recorded on the stimulating electrode (left) and on one of the neighboring electrodes (right). The displayed waveforms divide into four classes, separated very well in the Principal Components Analysis space (Fig. 6). These four clusters originate from the spiking activity of three independent neurons (1-3), responding to the 0.65 µA stimulation pulse with efficiencies of 100%, 23% and 38%, respectively. The signal from neuron 1 contributes equally to each of the displayed waveforms (as does the stimulus artifact). Identification of neuron 1 was possible with analysis of the data for lower stimulation currents (data not shown).
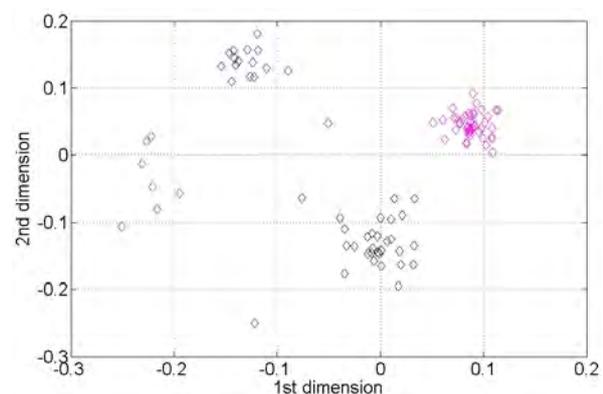


**Fig. 6.** Scatter plot of the two most significant Principal Components Analysis variables for the waveforms presented in Fig. 5. The color of each symbol is identical to the color of the corresponding waveform in Fig. 5.

We associate the four waveform clusters (a-d) with: (a) the stimulus artifact plus the signal from neuron 1 (45 pink traces in Fig. 5); (b) the artifact plus the signals from neurons 1 and 2 (16 blue traces); (c) the artifact plus the signals from neurons 1 and 3 (30

black traces); and (d) the artifact plus the signals from all three neurons (7 red traces).

If our interpretation of the four clusters is correct, the signal shape for neuron 2 can be estimated in two independent ways: as a difference between the averaged waveforms in clusters b and a, or as a difference between clusters d and c. These two estimates, as shown in Fig. 7, match well on both the stimulating (left) and neighboring (right) electrodes. Similarly, as also shown in Fig. 7, the neuron 3 signal shape can be estimated from clusters c and a, or independently from clusters d and b. These results indicate that the signal recorded from multiple neurons activated simultaneously is a linear superposition of the signals generated by these neurons spiking separately.
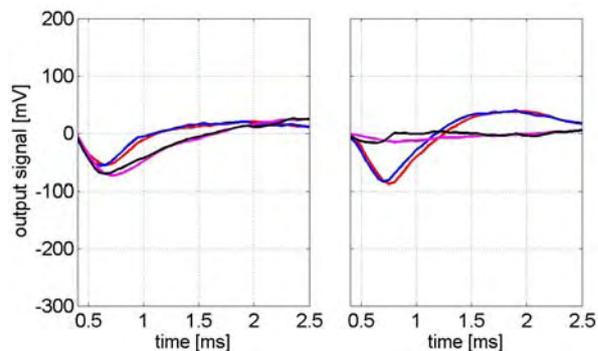


**Fig. 7.** The calculated difference between the averaged waveforms for clusters b and a (red), between clusters d and c (blue), between clusters c and a (pink) and between clusters d and b (black). The red and blue traces correspond to neuron 2 and the pink and black traces correspond to neuron 3. The left and right plots show, respectively, the results for the stimulating and neighboring electrodes. The vertical scale is the same for both plots.

One of the future goals of our project is to use the developed system to stimulate complex patterns of activity in a collection of neurons. A simple example of pattern stimulation is presented in Figs. 8 and 9. We independently stimulated two near-by RGCs by sending pulse trains through two electrodes. These two pulse trains generated well-separated response waveform classes, indicating that two different neurons were independently activated by each of the two electrodes.

## 4 Summary

We have developed a system based on a custom-made MEA and VLSI electronics that is capable of stimulating a population of neurons with an arbitrarily defined, spatio-temporal distributed pattern of stimulation currents, with simultaneous recording of the elicited activity. Using this system and optimized stimulation protocol, we are able to stimulate the RGCs in adult mice and record the evoked low-latency spikes with minimal distortions, even on the electrodes used for stimulation. In the near future, we

plan to build a large-scale system, based on an array with 512 electrodes and the same electronics.
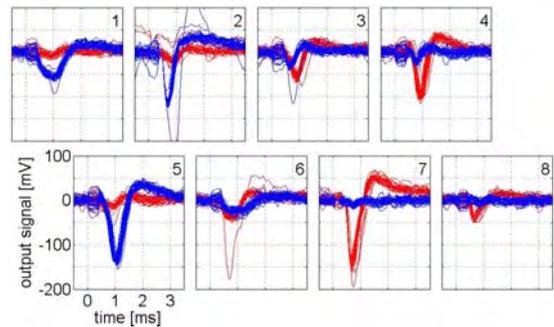


**Fig. 8.** Responses to 50 stimulation pulses sent through electrode 2 (blue traces) and to 50 pulses sent through electrode 7 (red traces). The relative position of each plot in the figure follows the position of the corresponding electrode on the MEA layout. Each electrode produced a pulse every 20 ms, with a 10 ms shift between pulses on different electrodes (compare Fig. 9). The pulse amplitudes were 0.50 µA for electrode 2 and 0.30 µA for electrode 7. All the traces are shown after artifact subtraction.
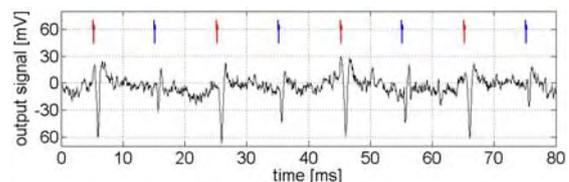


**Fig. 9.** Signal recorded at electrode 3 (the same data as in Fig. 8) shown after artifact subtraction. The blue and red marker positions correspond to the timing of stimulation pulses on electrodes 2 and 7, respectively.

## References

[1] Litke AM: (1999): The Retinal Readout System: a status report. *Nuclear Instruments and Methods in Physics Research A*, vol. 435, 242-249.

[2] Hottowy P, Dabrowski W, Skoczen A, Wiacek P: (2008): An integrated multichannel waveform generator for large-scale spatio-temporal stimulation of neural tissue. *Analog Integrated Circuits and Signal Processing*, vol. 55 (3), 239-248.

[3] Grybos P, Dabrowski W, Hottowy P, Fiutowski T, Bielewicz B: (2006): Neuroplat64 – low noise CMOS integrated circuit for neural recording applications. *Proceedings of the 5th International Meeting on Substrate-Integrated Micro Electrode Arrays*, 208-209.

[4] Sekirnjak C, Hottowy P, Sher A, Dabrowski W, Litke AM, Chichilnisky EJ: (2006): Electrical stimulation of mammalian retinal ganglion cells with multielectrode arrays. *Journal of Neurophysiology*, vol. 95 (17), 3311-3327.

[5] Sekirnjak C, Hottowy P, Sher A, Dabrowski W, Litke AM, Chichilnisky EJ: (2008): High-resolution electrical stimulation

of primate retina for epiretinal implant design. *Journal of Neuroscience*, vol. 28 (17), 4446-4456.

# Chemical stimulation of cells – microsystem, experiment & modelling

Susanne Zibek, Britta Hagmeyer, Alfred Stett, Martin Stelzle[*]

NMI Natural and Medical Sciences Institute, Reutlingen, Germany
* Corresponding author. E-mail address: martin.stelzle@nmi.de

The objective of this study was to explore the feasibility of microfluidic devices and methods for chemical stimulation of cells with the ultimate goal of achieving cell selective stimulation as is not available by common electrostimulation methods. Cells were cultivated on nanoporous membranes with various pore sizes. An inkjet printhead was used to apply approximately 20 pl droplets of the chemical stimulant, namely calcein AM and acetylcholine, to the bottom face of these membranes. $Ca^{2+}$ imaging was employed to visualize cellular response upon acetylcholine stimulation by fluorescence microscopy. Application of calcein AM results in a continuous uptake by cells depending on local concentration. Modelling of transport phenomena taking into account contributions from diffusion, flow and evaporation revealed a pronounced influence of pore size on stimulation kinetics.

## 1 Motivation & Objectives

While electrical stimulation will inevitably cause all cells in the vicinity of the electrode to be addressed, the application of chemical stimulants holds the promise of a more cell type specific stimulation. This could lead to devices providing higher spatial resolution and/or additional functionality. Microfabrication technology may yield devices for uses in neuroprosthetics, drug delivery, and substance screening [1-4].

The goal of this research therefore was to devise methods for the localized chemical stimulation of cells, for the quantitative modelling of the spatio-temporal distribution of stimulant, and for the comparison of experimental with modelling results.

## 2 Materials & Methods

### 2.1 Experimental Setup

An inkjet print head was used to deposit approximately 20 pl droplets of the stimulant across an "air gap" onto the bottom face of the membrane [5] (Fig.1). Commercially available Nucleopore® track-etched membranes with different pore sizes were glued to glass rings to form cell culture vessels. $Ca^{2+}$imaging was employed to record the excitation patterns developing after application of acetylcholine.

### 2.2 Cell culture

TE 671 cells expressing acetylcholine receptors were cultivated in homemade cell culture dishes comprising nanoporous membranes on their bottom (Fig.1). Membranes were treated in air plasma and functionalized with laminin prior to seeding of cells.
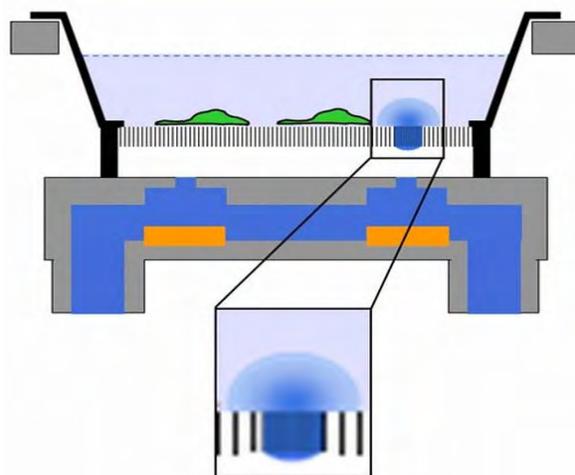


**Fig. 1.** Experimental setup: chemical stimulation of cells growing on a nanoporous membrane using an inkjet print head to deliver droplets of the stimulant via an "air gap" to the bottom face of the membrane.

### 2.3 Modelling and Simulation

Modelling of transport phenomena considering diffusion, pressure driven flow through pores due to surface tension in the droplet, convection, and evaporation was performed (Fig.2). The equations were implemented in the software package FlexPDE®.and the model was simulated As a result, the concentration of any stimulant, c(r,t) could be calculated at any location within the cell culture chamber and could be compared to experimentally observed stimulus related cellular responses.
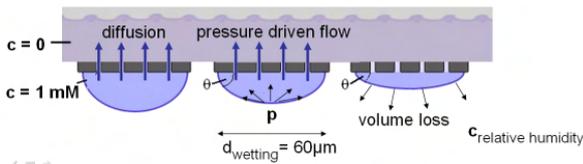
**Fig. 2:** Modelling of transport phenomena: graphs depict physical effects considered (from left to right): diffusion due to concentration gradient across membrane between droplet and medium, pressure driven flow through nanopores due to surface tension in droplet and change in droplet volume and related pressure due to evaporation.

# 3. Results & Discussion

## 3.1 Calcein AM as stimulant

A mixture of calcein AM and eosin Y (0,25 mM / 0,1 mM) was applied to the bottom face of the membrane on which TE 671 cells were cultured (Fig.4A). Eosin Y was added in order to visualize the application spot, since calcein AM is non-fluorescent. Eosin Y does not stain the cells but diffuses freely in the medium and fluorescence from this dye therefore decays over time. Calcein AM in contrast is taken up by the cells at a rate that should be proportional to the concentration at the cell surface and subsequently is converted enzymatically into fluorescent calcein. Since calcein is retained within the cells, the resulting fluorescence signal of a particular cell corresponds to the integral dose received by that cell.
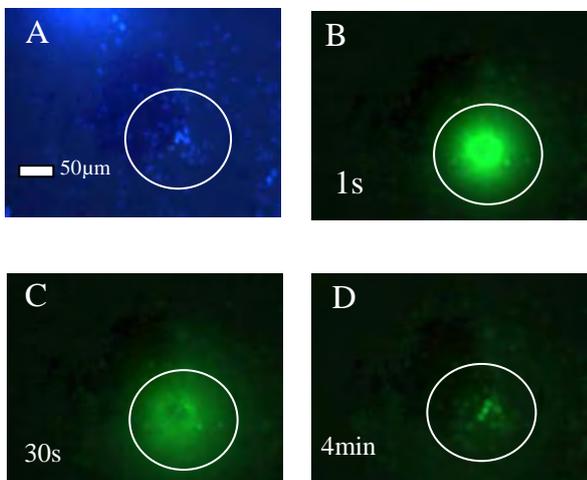


**Fig. 4.** TE 671 cells on nanoporous membrane prior to (A) and after (B – D) application of 5 droplets of calcein AM / eosin Y. A :Nucleus staining shows the loci of the cells prior to stimulation. B: Immediately after application of the droplet, eosin Y fluorescence is dominant and indicates the stimulation spot. C: 30 s after application, eosin Y is already significantly diluted by diffusion. D: 4 min after stimulation, no eosin Y fluorescence is visible but cells in the vicinity of the application spot show calcein fluorescence, whose intensity decreases with increasing distance from the application spot.

## 3.2 Acetylcholine as stimulant

Application of approximately 20 pl droplets allowed for localized stimulation on spots with a diameter of approximately 60μm (Fig.5). TE 671 cells showed dose related excitation upon stimulation by acetylcholine [6]. Slope and amplitude of fluorescence intensity signals measured by $Ca^{2+}$ imaging were shown to depend on the concentration of neurotransmitter present at the site of a particular cell (Fig.6). Pore size and porosity of the membrane determine kinetics of stimulant delivery as well as the maximum concentration achieved. Delivery of stimulant across the membrane competes with transport processes (diffusion and convective flow) in the culture dish. These findings are in general agreement with results obtained from simulation as discussed below.
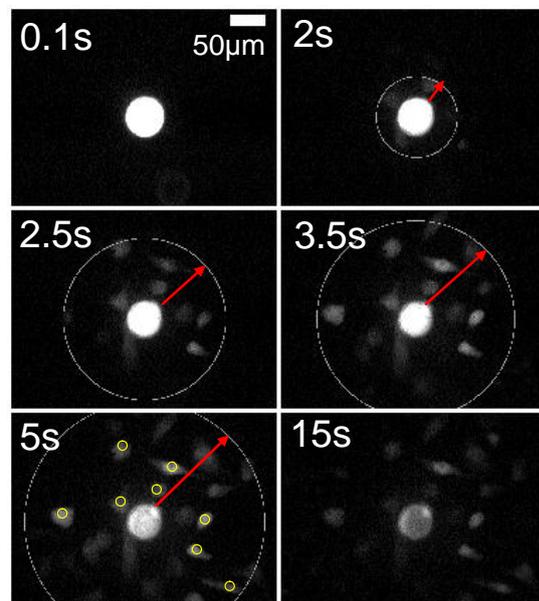


**Fig. 5.** Panel of micrographs showing the application of a single droplet of acetylcholine (1 mM) / eosin Y (10 μM). Dilution of eosin Y is a result of diffusion. The spatio-temporal development of an excitation pattern in the cell layer is visualized by $Ca^{2+}$ imaging. The small circles in the graph at t=5s indicate the location of cells whose fluorescence intensity is quantitatively evaluated.

## 3.3 Simulation Results

Fig. 7 shows a colour coded cross-section through the cell chamber in the x, y=0, z - plane at two different times after application of a stimulant and displays the concentration of the stimulant.

From data as these, the concentration at any particular cell site, i.e. c(x, y, z=0, t) may be retrieved and compared to the experimentally observed cellular response. In the case of the results shown in Fig. 7, 8, transport through a membrane with a pore diameter of 50 nm, porosity of ~1% and a thickness of 6 μm was simulated.

A



B
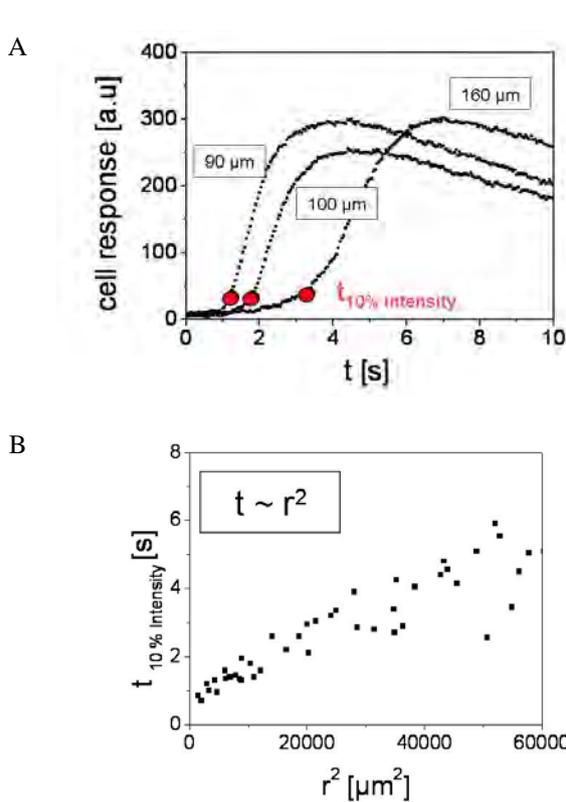


**Fig. 6:** Cell response after application of a single droplet acetylcholine (100 µM).A:Fluorescence intensity integrated over region of interest within the respective cell (circles in Fig.5) as a function of time. B: Delay between application of droplet and onset of fluorescence signal as a function of diffusion time.



**Fig. 7.** Calculation of spatio-temporal distribution profiles. Diffusion, pressure driven flow due to surface tension of droplet, convection and evaporation effects were considered. Membrane parameters were: pore diameter 50 nm, porosity ~1 %, membrane thickness 6 µm. Application of a single droplet (20 pl) of acetylcholine (100 µM) was calculated.

## 3.4 Experiment vs. simulation

As a preliminary result, it appears as if the onset of the cellular response of cells at various distances from the application spot coincides with the concentration at the respective location (Fig.9). We observed a threshold concentration < 0,1 µM acetylcholine at which cell response starts (measured as 10% of its main amplitude). However, further experiments have to be performed to confirm whether increasing rate of acetylcholine correlates with cell responding rate (slope).

## 4  Conclusion

Feasibility of chemical stimulation of cells was demonstrated and quantitative results were obtained from a joint evaluation of experiment and simulation. These findings are considered a first step towards a rational design of application specific chemical stimulation devices.



**Fig.8.** Concentration as a function of time at different distances from the centre of the application spot calculated for the following membrane parameters: pore diameter 50 nm, porosity ~1 %, membrane thickness 6 µm. and application of single droplet (20 pl) of acetylcholine (100 µM).
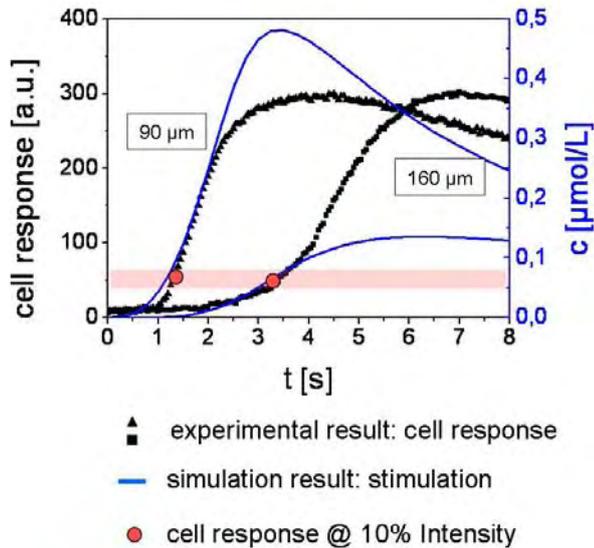
**Fig. 9:** The black curves are experimentally measured fluorescence traces obtained from cells located at 90 μm and 160 μm distance from the centre of the application spot. The blue curves show the numerically calculated concentration of the stimulant at these locations. From results as these it appears as if the onset of the cellular response coincides with a certain level of acetylcholine concentration. Red bar shows the threshold concentration < 0,1 μM acetylcholine where cell response starts (measured as 10% of its main amplitude).Calculation was performed using the following membrane parameters: pore diameter 50 nm, porosity ~1 %, membrane thickness 6 μm. and application of a single droplet (20 pl) of acetylcholine (100 μM).

.

## References

[1] Fishman, H. A.; Peterman, M. C.; Leng, T.; Huie, P.; Lee, C. J.; Bloom, D. M.; Sanislo, S. R.; Marmor, M. F.; Bent, S. F.; Blumenkranz, M. S. The Artificial Synapse Chip: A Novel Interface for a Retinal Prosthesis based on Neurotransmitter Stimulation and Nerve Regeneration. Proceedings of the ARVO 2002.

[2] Noolandi, J.; Peterman, M. C.; Huie, P.; Lee, C.; Blumenkranz, M. S.; Fishman, H. A. Towards a Neurotransmitter-Based Retinal Prosthesis Using an Inkjet Print-head. Biomedical Microdevices 2003, 5, 195.

[3] Peterman, M. C.; Bloom, D. M.; Lee, C.; Bent, S. F.; Marmor, M. F.; Blumenkranz, M. S.; Fishman, H. A. Localized Neurotransmitter Release for Use in a Prototype Retinal Interface. Investigative Ophthalmology & Visual Science 2003, 44, 3144.

[4] Peterman, M. C.; Noolandi, J.; Blumenkranz, M. S.; Fishman, H. A. Localized chemical release from an artificial synapse chip. Proc. Natl. Acad. Sci 2004, 101, 9951.

[5] Hu, M.; Lindemann, T.; Gottsche, T.; Kohnle, J.; Zengerle, R.; Koltay, P. Discrete Chemical Release from a Microfluidic Chip. J. Microelectromechanical Systems 2007, 16, 786.

[6] Zibek, S.; Stett, A.; Koltay, P.; Hu, M.; Zengerle, R.; Nisch, W.; Stelzle, M. Localized functional chemical stimulation of te 671 cells cultured on nanoporous membrane by calcein and acetylcholine. Biophys J 2007, 92, L04

# Extracellular Recording from Mass-produced Small Neuronal Networks using Mobile Metal Microelectrodes

Hiroyuki Moriguchi[*], Yuzo Takayama, Kiyoshi Kotani, Yasuhiko Jimbo

Graduate School of Frontier Sciences, University of Tokyo, Japan
* Corresponding author. E-mail address: mhendrix@cronos.ocn.ne.jp

We have developed a series of practical experimental methods to mass-produce small neuronal networks consisted of a single to several tens of neurons and glial cells in culture, and record extracellular potential from microscopically selected constituent cells, by means of spraying or ink-jet printing of poly-D-lysin solution onto agarose-gel-coated culture surfaces and fine tungsten wires. As the result of recording from neurons in culture for 2 weeks or longer, slow, oscillatory transition was observed in the temporal patterns of spontaneous activity in cycles of several minutes' duration, not only in the timing but also in the magnitude of spikes, and equivalent temporal patterns were also observed in the spontaneous firings of smaller neuronal networks even in the minimum networks made each of a single neuron. These results indicate that the spike magnitude reflect some sort of physiologic state of a cell, which can oscillate slowly and intrinsically in cultured neurons with recurrent network topology.

## 1 Introduction

Extracellular recording from patterned neuronal networks with defined topology using microelectrode arrays (MEAs) is a valid bottom-up approach to the understanding and utilization of the cellular- and network-level phenomena and functions of nervous systems [1-4]. There remains, however, a practical problem in the experiments: throughput of recording from spatially sparse neurons in patterned neuronal networks. One solution for this problem is the stabilization of the positional relation between electrodes and neural cells or fibers [4-6], and another is complemental utilization of mobilized microelectrodes which are accessible to any cells in microscopic fields. In addition, these mobile microelectrodes can also be applicable to recording from neurons grown on general, non-functionalized surfaces with non-invasive manner. In this context, this time, a large number of small neuronal networks, on which the entire construction can be microscopically defined, were prepared by means of spraying or ink-jet printing of cell-adhesive substrate, and their electrical activity was recorded with mobilized metal microelectrodes.

## 2 Materials and Methods

### 2.1 Micropatterning

The culture surfaces for the mass production of small neuronal networks were prepared by putting drops of poly-D-lysin (PDL) solution (100 μg/ml) on the bottom-serfaces of 35-mm culture dishes (cell-culture-treated, Corning). The bottom serfaces were preveously coated with agarose-gel (2 % (w/v), low-melting point, Wako) and dried in room temperature. The drops were produced and distributed randomly by spraying or set in array by ink-jet printing apparatus (IJK-200s, Microjet, Inc.) in combination with a motorized XY stage (BIOS-201T, Sigma-Koki). The tipical diameter of the cell-adhesive spots formed by spraying were around 150 μm. As for the ink-jet printing, the size, shape and alignment of the spots are controllable. In this study, arrays of 50 x 50 spots (diameter: 90 μm, interval: 150 μm center-to-center) were printed one-by-one on the agarose-gel-coated bottom surfaces of culture dishes. Patterned dishes were washed three times with deionized water and re-dried prior to use. Neuronal cells were derived from E18 rat hippocampus and distributed on the patterned surface (from 20000 to 100000 cells/dish), and cultured in 5 % carbon dioxide for up to 6 weeks in astrocyte-conditioned Neurobasal/B27 serum-free medium (Invitrogen). This procedure enables production of thousands of small networks in a dish with a simple procedure. Figure 1 shows some examples of cultured small neuronal networks formed on randomely (a) or precisely (b) patterned surfaces.

### 2.2 Microelectrodes

Microelectrodes were fabricated by inserting a metal wire into a glass micropipettes (inner dameter: 50 μm at the tip). The tip area of a metal wire was a tungsten wire (length: 5 mm, diameter: 10 μm,

Nilaco), which was connected to a thicker copper wire (length: 50 mm, diameter: 200 µm, Nilaco) with electrically conductive glue (Dotaito, Fujikura-Kasei) and had a exposed region of about 500 µm in length out of the glass pipette (Fig. 2 A). Each metal wire was fixed on the glass pipette with Araldite at the both side of glass pipette, and the tip of the tungsten wires were electrochemically sharpened and plated with platinum black according to an established procedure [7] (Fig. 2 B bellow).
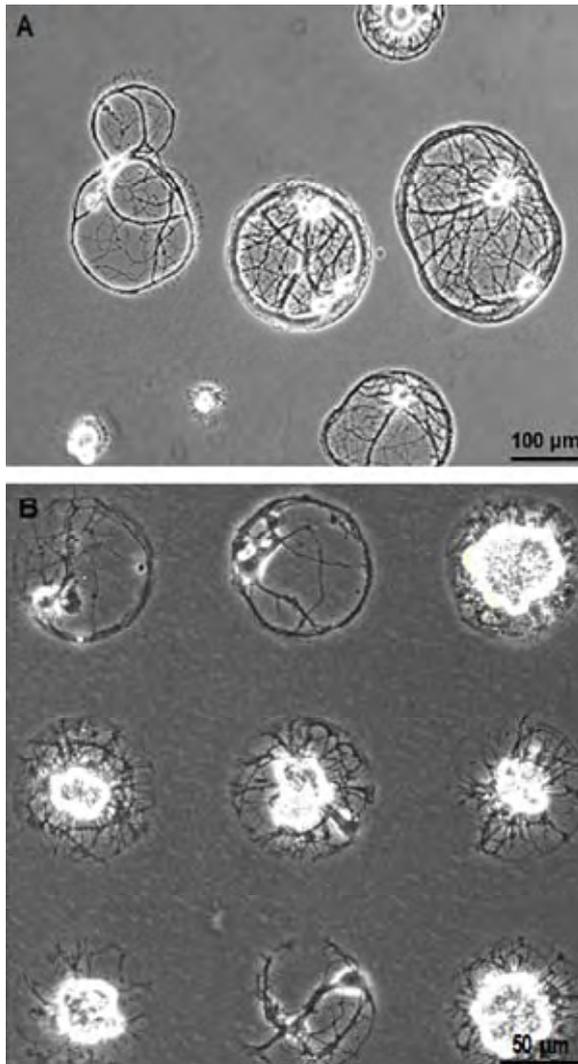


**Fig.1.** Small neuronal networks formed on cell-adhesive spots printed on agarose-gel by spraying (A: 28 DIV) or ink-jet printing (B: 18 DIV)

## 2.3 Recording and stimulation

The extracellular potential was recorded in reference to a platinum coil soaked in the same culture media by positioning the tip of a recording microelectrode close to the cell body of a selected neuron under microscopic field (distance from the surface of cell bodies < 5 µm) with a micromanipulator (Fig. 2 B). Analogue voltage signals were filtered (100 - 2000 Hz), amplified (total gain: 2000 – 20000 fold), converted into digital signals and recorded on a hard disc

of a PC through a National Instrument DAQ cards driven by the Labview software (sampling rate: 25 kHz). At the same time, analogue signals were simultaneously recorded on thermal paper for the real-time monitoring of the long-term changes in the spike patterns. As for the stimulation, voltage signals were generated with a pulse generator (NF corp.) and applied to the same microelectrode that is used in the recording through a switching circuit, which allows rapid switching of the microelectrode between stimulation and recording electrode in 1.2 ms [8].
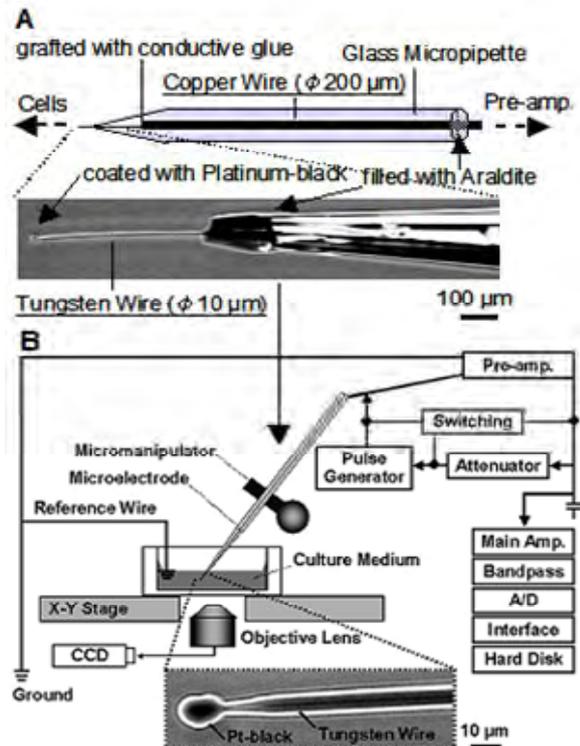


**Fig. 2.** A schematic of our handmade metal microelectrode and a micrograph of its apical part (A), and a schematic of the setup for the recording and stimulation on cultured cells.(B).

## 3 Result and Discussion

### 3.1 Extracellular recording from neurons in dissociated cultures

The ability of our microelectrodes to detect electrical activity extracellularly from cultured neurons was tested by moving the tip closer to a cell body of neurons in dispersed low-density cultures. Figure 3 shows an example of the recordings. As shown in the figures, single-unit spikes were successfully detected from the top side of neurons grown on culture surfaces. Additionally, continuous changes and oscillation was observed in both the magnitude and frequency of the spikes. The cycles were typically several minutes. This result indicates that the spike magnitude reflect some sort of physiologic state of cultured neurons.
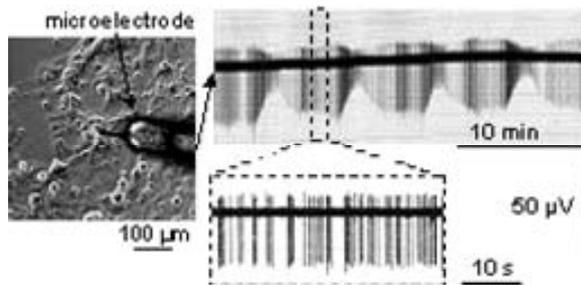
**Fig. 3.** A micrograph of recording from a single neuron in a dissociated culture of hippocampal cells (A: 28 DIV) and the temporal pattern of the recorded spikes (B: above: recorded on a thermal paper. below: recorded on a hard disc and magnified.). Note that the magnitude and frequency of spikes changes continuously and oscillates in the top right recording over about 30 minutes in cycles of about 7 minutes' duration.

## 3.2 Recording and stimulation on small neuronal networks

Signals of spontaneous firings were detected from neurons grown in small networks even in the case of minimum networks made of a single neuron (autapse) or small numbers of neurons, and many of them showed periodicity on several minutes cycle (Fig. 4-6) in a similar fashion with larger networks. These periodic patterns were constructed from groups of fast oscillatory spike patterns (1-3 Hz) (Fig. 5), and similar oscillatory spike patterns were also found in the evoked activity (Fig. 4 B). These results indicate that the physiologic state, which is reflected by the spike magnitude, can oscillate intrinsically in single neurons with recurrent network topology.

## 3.3 Multisite recording with mobile microelectrodes

By placing multiple electrodes on a small neuronal network, spontaneous activity of different groups of cells in a small neuronal network was simultaneously recorded. In the activity, two different patterns were observed: "local bursts" and "synchronous firings". The local bursts had periodical patterns both in the short (~ 1 Hz) and long (~1 mHz) time scale. The synchronous firings were simultaneously detected (timing difference < 1 ms) at the three sites in a network with larger magnitude than the local bursts. This result suggests that the synchrony in the firings of neurons provide the summation of the transitory potential change of the extracellular spaces of each firing neurons, which result in the increase in the magnitude of detected signals.
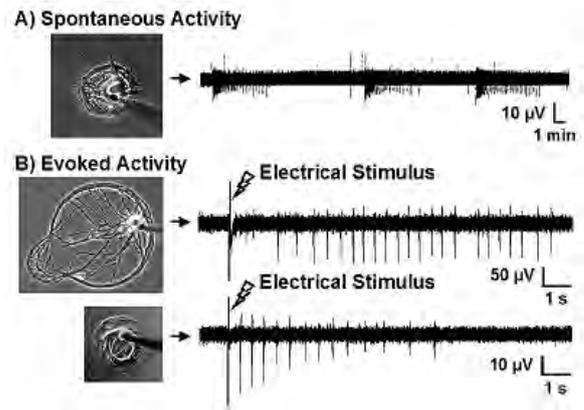


**Fig. 4.** Signals from autapse neurons recorded with mobile metal microelectrodes (28 DIV).
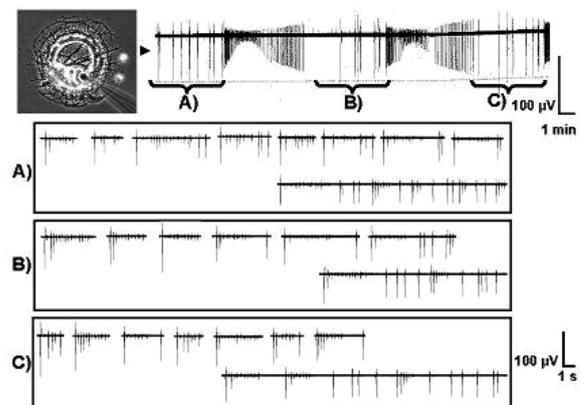


**Fig. 5.** Periodic spontaneous activity of a small neuronal network made of 3 neurons (28 DIV).
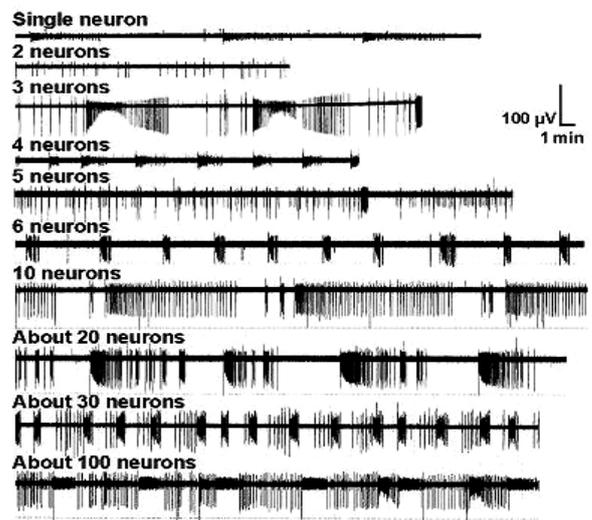


**Fig. 6.** Spontaneous activity of small neuronal networks made of a varied number of cells (28 DIV).
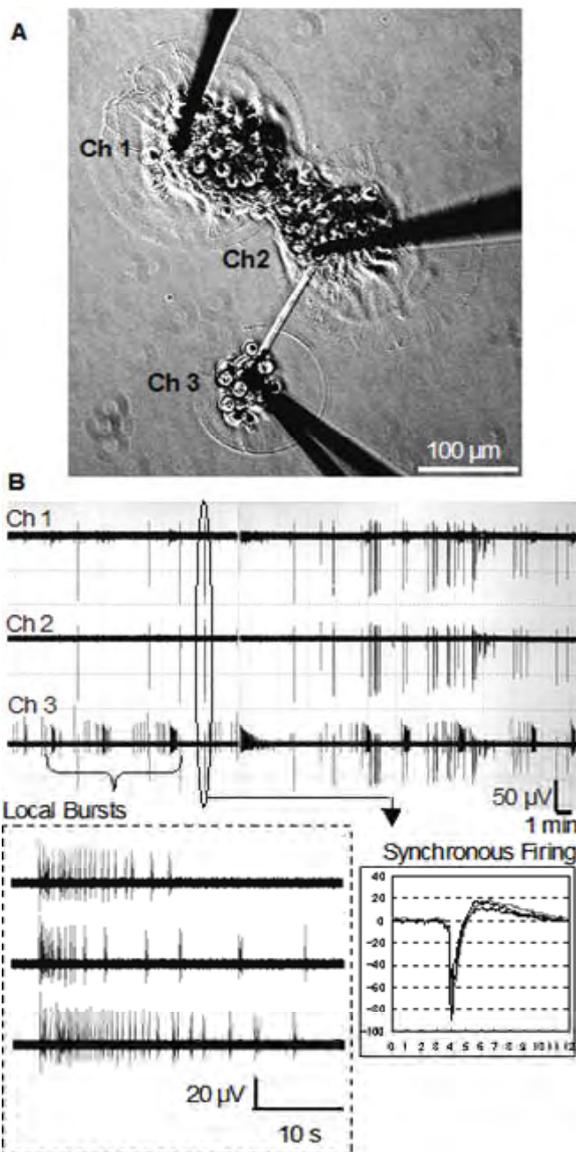
**Fig.7.** An example of multi-site recording from a small neuronal network with three mobile microelectrodes (A), and a time course of the extracellular potential recorded from the three recording sites (B, above) and its partial magnifications (B, below).

## 4 Summary

By mobilizing the metal microelectrodes, electrical activity of specific neurons in cultures was selectively stimulated and recorded with non-invasive manner. The spontaneous and evoked activity of these neurons was characterized respectively by oscillative phase-transition in both the frequency and the magnitude of spikes, and oscillatory firings at the frequency of 1-3 Hz. Mobile metal microelectrodes could also be used for the multi-site recording from cultured neuronal networks or supplemental recording sites for MEA.**Acknowledgement**

**References**
[1] J. C. Chang G. J. Brewer and B. C. Wheeler (2006) Neuronal network structuring induces greater neuronal activity through enhanced astroglial development, J. Neural Eng. 3, 217-226
[2] Y. Jimbo, H. P. C. Robinson and A. Kawana (1993) Simultaneous Measurement of Intracellular Calcium and Electrical Activity from Patterned Neural Networks in Culture. IEEE Trans. Biomed. Eng., 40, 804-810
[3] M. Merz and P. Fromherz (2005) Silicon chip interfaced with a geometrically defined net of snail neurons, Adv. Funct. Mater., 15, 739-744
[4] I. Suzuki and K. Yasuda (2007) Detection of tetanus-induced effects in linearly lined-up micropatterned neuronal networks: Application of a nulti-electrode array chip combined with agarose microstructures, Biochem. Biophys. Res. Commun. 356, 470-475
[5] J. Erickson, G. Chow, A. Tooker, Y-C. Tai and J. Pine (2006) Progress on the Caged-Neuron MEA Project, Proceedings of the 5th international Meeting on Substrate-Integrated Micro Electrode Arrays, 192-193
[6] G. J. Brewer, M. D. Boehler and B. C. Wheeler (2006) Higher activitywith increased connections in patterned hippocampal neurons, Proceedings of the 5th international Meeting on Substrate-Integrated Micro Electrode Arrays, 190-191
[7] J. Millar (1992) Extracellular singleand multiple unit recording with microelectrodes, Monitoring Neuronal Activity (edit. J. A. Stamford) , 1-27
[8] Y. Jimbo, N. Kawana, K. Torimitsu T. Tateno and H. P. C. Robinson (2003) A System for MEA-based Multisite Stimulation, IEEE Trans. Biomed. Eng. 50, 241-248

# A new Principle for intracellular Potential Measurements of adherently growing Cells

Philipp Julian Koester[1], Carsten Tautorat[1], Angela Podssun[1], Jan Gimsa[1], Ludwig Jonas[2], and Werner Baumann[1*]

1 University of Rostock, Chair of Biophysics, Rostock, Germany
2 University of Rostock, Electron Microscopy Center, Medical Faculty, Rostock, Germany
* Corresponding author. E-mail: werner.baumann@uni-rostock.de

The investigation of cellular reactions in living cell cultures gets increasingly into focus of drug development and environmental monitoring. Existing classical methods for intracellular measurements are time-consuming and complex. Existing Patch-on-chip systems are limited to the investigation of suspended single cells. Nevertheless, most cells in the human body are adherently growing. To address this problem, we are developing a new chip system with 64 micro-structured needle electrodes arranged within a measuring area of 1 mm$^2$. We believe that the intracellular investigation of electro-chemical properties and processes in adherently growing cells will become possible with our new analytical chip.

## 1 Introduction

The biological cell represents the smallest living unit. The basic structure of the cell membrane is a phospholipid double layer, a variety of functional proteins and other bound molecules [1]. Active and passive ion transports as well as leak fluxes through the membrane generate a potential difference between the extra- and intracellular space.

The physiological transmembrane potential $V_m$ is described by the Goldman equation [3]:

$$V_m = \frac{RT}{F} \ln \frac{\sum P_C c_C{}^e + \sum P_A c_A{}^i}{\sum P_C c_C{}^i + \sum P_A c_A{}^e}$$

$R$ = gas constant, $T$ = absolute temperature, $F$ = Faraday constant, $P$ = ion permeability, $c$ = ion concentration, e = extracellular, i = intracellular, C = cations, A = anions

Strong external electrical fields may induce membrane pores. Their size depends on pulse shape and electric cell parameters [2]. Extracellular compounds may cross the membrane via these pores affecting cell metabolism. In living cells, typical Vm values vary around -65 mV, depending on organism and cell type. Measurement of Vm is a complex problem, even with penetrating electrodes. Up to now, voltage changes in adherently growing single cells can only be examined by the classical Patch-Clamp technique [4]. Patch-on-chip methods are limited to cell suspensions [5]. Nevertheless, most cell types of the human body are adherently growing on biological surfaces (e.g. other cells), in artificial systems on biocompatible matrices (e.g. polystyrene) (Fig.1).
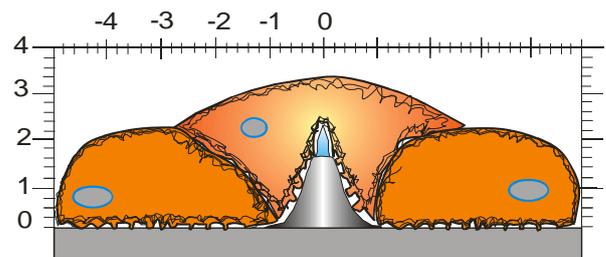


**Fig. 1.** Schematic cross-sectional view of a model cell over-growing a MNE. Scaling in μm.

However, all these methods, except for the patch clamp technique in whole cell configuration, are mainly used to investigate ion channel currents. In the following, we present a new method for the Vm measurement with Micro-structured Needle Electrodes (MNE) after Local Electroporation (LEP) of single cells growing on silicon chips.
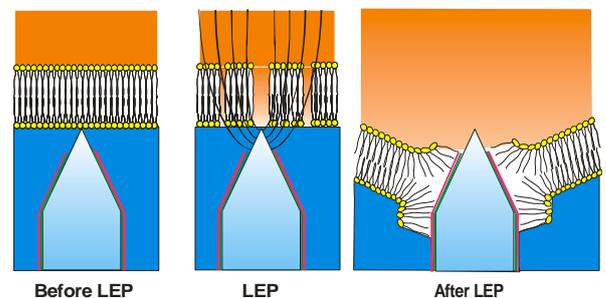


Fig. 2. Schematic cross-sectional view of LEP and the resulting MNE-penetration through the membrane.

The aim of our Local Micro-Invasive Needle Electroporation (LOMINE) system is to detect alterations of Vm induced by pharmacological test substances or drugs. The patented LOMINE method [11, 12] combines LEP with a Patch-on-chip system. The

LOMINE technique uses voltage pulses applied to single MNEs (Fig.2). This allows for a local electroporation of the membrane of a single attached cell. In contrast, the classical setup of suspension cell electroporation leads to the formation of many membrane pores due to increased transmembrane voltages. During LOMINE, the very high local electrical field at the tip of the MNE alters the lipid structure of the membrane, i.e. the binding forces (dipole-dipole and hydrophobic interactions, van der Waals forces, etc.) are overcome allowing for a reassembling of the phospholipids (Fig.2). Like in the classical electroporation, the pore size depends on the applied field strength at the MNE, molecular membrane composition, pulse characteristics (length, rate and shape), medium properties, etc. Depending on these conditions, pores can reseal or enlarge until the membrane is torn apart and the cell dies [13]. At low voltages (<1 V) of the LEP-pulse, electroporation of the cell membrane was observed only directly above the MNE. This successful membrane penetration by the MNE is the first step towards the detection of Vm changes.

## 2 Material and methods

A 68-Pin *ceramic leadless chip carrier* (CLCC) carries a silicon chip comprising 64 MNEs arranged in an 8x8-MEA. Electrode tips are fabricated in silicon technology; chip layout and production were adapted to the requirements imposed by the LEP [6-8]. The chip is completed by a plastic trough glued to the silicon chip and the CLCC. The setup allows for long-term culture of adherently growing cells, LEP of independently selectable single MNEs and the measurement of intracellular potentials. Cells are attracted by dielectrophoresis electrodes. A guided growth of the cells is possible by silicon surface coating with cell attracting polymers. Coating and cell positioning [10] by dielectrophoresis electrodes are described by our project partners [19]. All images were captured by means of an Olympus BX-51 WI microscope equipped with a water immersion objective (40x). Experiments were accomplished using a special *Electroporation Buffer* (EB; KCl 25 mM, $KH_2PO_4$ 0.3 mM, $K_2HPO_4$ 0.85 mM, myo-Inositol 280 mOsmol/kg, pH 7.2 ±0.1, conductivity = 3.5 mS/cm ±10% at 25°C). Experiments with primary neurons suspended over 6 hours in EB show cell survival. Seeded cells are healthy and build branching processes.

## 3 Results

## 3.1 Reflected light microscopy

First electroporation experiments are promising. An opening of the cell membrane by LEP was proven in fibroblasts of the mouse sarcoma cell line L929 by using vital dye staining (trypan blue, TB, Fig.3) [14]. TB stains dead cells dark-blue. The dye was added to the EB prior to LEP pulses to prove that the MNEs are individually controllable. After a strong LEP pulse (±2 V), the TB diffused into the electroporated cells inducing a change in cell color (Fig.3).
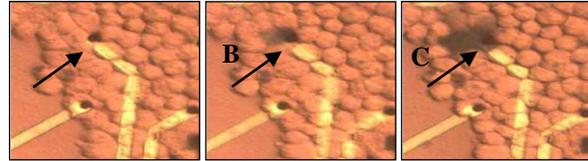


**Fig. 3.** LEP of a L929 fibroblast with one selected MNE. A: before, B: 30 s after, C: 360 s after LEP. Fibroblast vital staining with TB. Electrode pitch 50 µm, one LEP pulse: ±2 V, 20 Hz.

Additionally, LEP experiments in cell free chips were accomplished [18]. The observed potential alterations depend on the pulse characteristics, reference electrode properties etc.

## 3.2 Epifluorescence microscopy

We could successfully grow primary neurons of the frontal cortex (for protocol see [15]) and fibroblasts on the tip of the MNEs as shown in the Focused Ion Beam (FIB) SEM image in Fig.8 [16]. In order to establish a sensitive test for the LEP of primary nerve cells, different experiments were accomplished by using propidium iodide (PI, 40 µM in EB), a fluorescent RNA/DNA binding dye. We also used rhodamine phalloidine (RP, 2 µM in EB, Fig.5) that binds to actin. PI and RP do not cross the intact cell membrane; however, they can cross membranes of dead cells or through the artificially produced membrane pores by LEP. Pore size, diffusion and fluorescence signal are directly dependent on the LEP parameters (frequency, amplitude, MNE characteristics, etc.) and the membrane characteristics. Dead, PI-penetrated cells already show strong fluorescent signals at the beginning of the experiment (Fig.4, upper left). In contrast, the fluorescence of the living "target cell" strongly increases above the MNE (see white arrow) only after LEP. In order to proof that the used LEP is tolerated by living cells, vitality tests of electroporated cells were accomplished. For this, cell chips were treated as described and stored for one day in the incubator. On the following day, again vitality staining with TB was conducted. Fig.6 demonstrates that white-circled electroporated electrodes did not show blue-stained dead cells, meaning that the LOMINE parameters used did not kill the cells. Some blue-stained cells are recognizable throughout the chip, which is however a common observation in every cell culture.
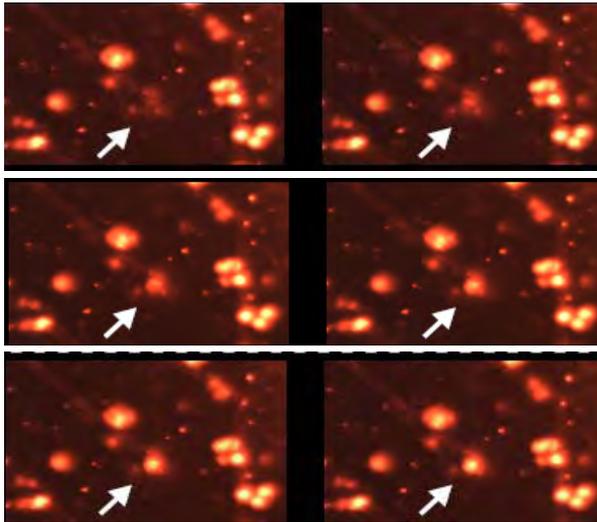
**Fig. 4.** LOMINE sequence of a primary mouse neuron. PI staining, 40x. LEP pulse parameters: 2x ±1 V and 1 x ±2 V, pulse frequency = 100 kHz, pulse train length = 30 ms.
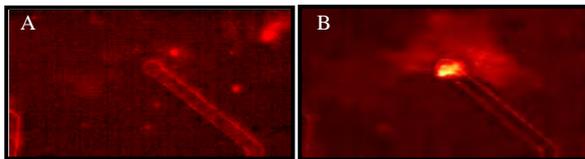


**Fig. 5** LOMINE with a human skin fibroblast. A: before, B: 30 s after fluorescent staining with RP, 40x. LEP pulse parameters: 5x ±1.5 V, pulse frequency = 100 kHz, pulse train length = 30 ms and 5x ±1.5 V, pulse frequency = 10 kHz, pulse train length = 300 ms.
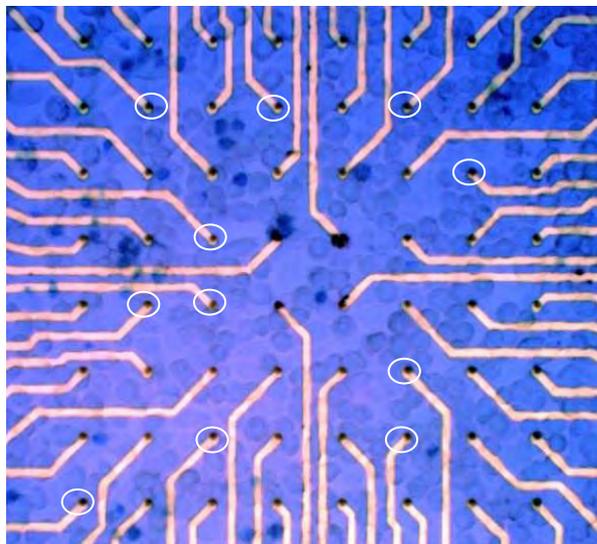


**Fig. 6** Vital staining of L929 fibroblasts one day after LOMINE.

### 3.3 FIB-SEM examinations

The FIB-SEM technique allows crosscutting through hard (metal etc.) and soft matters (cells) [16]. With this technique, we could demonstrate the penetration of cells by the MNEs. Chips, treated with LOMINE were examined with the FIB-SEM technique. Fig.7 is digitally stained. It shows a human skin

fibroblast overgrowing a MNE. Fig.8 is a FIB-SEM of an electroporated L929 mouse sarcoma fibroblast.
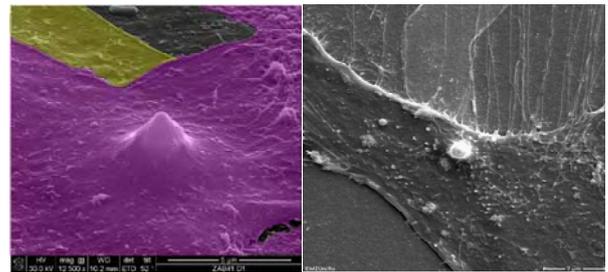


**Fig. 7** A human skin fibroblast entirely overgrowing a MNE. Left: tilt angle = 52°, 12500x. Digital staining: yellow = needle conductor, magenta = fibroblast. Right: top view, 3000x.
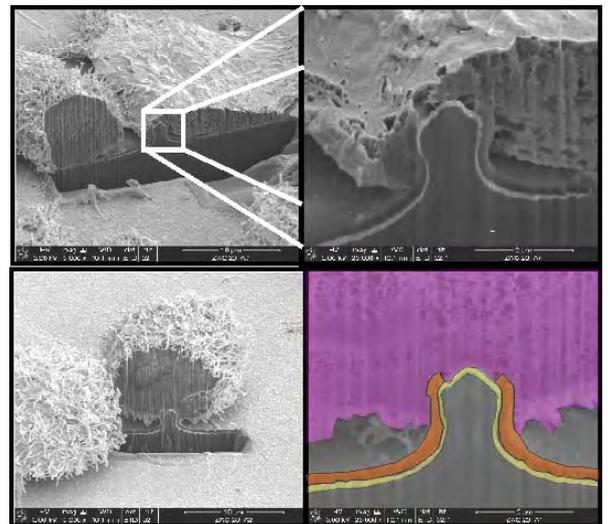


**Fig. 8.** Electroporated L929 mouse sarcoma fibroblasts overgrow MNEs. The FIB cuts show membrane penetration by LOMINE. Cells do not show any disruption or dispersion. Digital staining: magenta = fibroblast, orange = needle passivation, yellow = MNE tip metallization, needle conductor.

### 3.4 Intracellular potentials

Up to now, potential measurements after LOMINE are dominated by electrochemical effects causing electrode potential alterations. This is due to the electrochemical properties of the used tip metal etc. [18]. Currently, the authors work on the minimization of software control times. [17, 18] give a short overview of the influence of the metal type on the measured potential. Platinum electrode tips show instable electrode potentials. Until now, this hinders measurements of absolute membrane potentials. We believe that the use of electrode material, exhibiting stable potentials, will make intracellular measurements feasible.

### 4 Outlook

Fluorescent and vital staining showed successful LEP in adherently growing cells on MNEs. A stable Gigaseal between the cell membrane and the MNE

will be facilitated with a special bio-polymer-layer. Further, we will improve the LOMINE parameters for other cell types. In future, four voltage-clamp channels will be used to test the Gigaseal quality. A smooth electroporation of the cells will be achieved by the use of multiple short pulses of small amplitude [13]. Our goal is to optimize the stability of the electrode potentials and to compensate the influence of electrode effects on the measuring signals. In order to improve the observed long-term behavior of the MNE potentials, different reference electrodes and MNE materials will be tested. In future, LOMINE will provide a new, easy to use intracellular measuring technique for the analysis of drugs and other chemicals in different adherently growing cell types.

## Acknowledgement

## References

[1]  S. Singer, J. Nicolson, L. Garth (1972): The Fluid Mosaic Model of the Structure of Cell Membranes. *Science, 175, 720-731*

[2]  J. Olofsson, K. Nolkrantz, F. Ryttsén, B. A. Lambie, S. G. Weber, O. Orwar (2003): Single-cell electroporation. *Curr Opin Biotechnol, 14, 1, 29-34*

[3]  D.E. Goldman (1943): Potential, impedance, and rectification in membranes. *J Gen Physiol, 27, 37-60*

[4]  O.P. Hamil., A. Marty, E. Neher, B. Sakmann, F.J. Sigworth (1981): Improved patch-clamp techniques for high-resolution current recording from cells and cellfree membrane patches. *Eur J Physiol, 406, 73-82*

[5]  P. van Stiphout, T. Knott, T. Danker, A. Stett (2005): 3D Microfluidic Chip for Automated Patch-Clamping. *MST-Congress 2005, 435-438*

[6]  A. Trautmann, P. Ruther, W. Baumann, M. Lehmann, O. Paul (2004): Fabrication of Out-of-Plane Electrodes for Intracellular Potential Measurements on Living Adherent Cells. *in Confer-ence Proceedings of the 4th International Meeting on Sub-strate-Integrated Micro Electrode Arrays, 2004, Reutlingen, Germany*

[7]  J. Held, J. Gaspar, P. Ruther, O. Paul (2007): Characterization of the DRIE Fabrication of Cell-Penetrating Microneedles. *in Proceedings Mikrosystemtechnik Kongress 2007, October 15-17, Dresden, VDE VERLAG GMBH, Berlin-Offenbach, 845-849*

[8]  J. Held, J. Gaspar, P.J. Koester, C. Tautorat, A. Cismak, A. Heilmann, W. Baumann, A. Trautmann, P. Ruther, and O. Paul (2008): Microneedle arrays for intracellular recording applications, *MEMS 2008, 268-271*

[9]  J. Rühe, N. Knoll (2002): Functional polymer brushes. *J Macromol Sci-Pol Rev, C42, 91-138*

[10]  P.J. Koester, C. Tautorat, A. Podssun, J. Gimsa, and W. Baumann (2008): Dielectrophoretic Positioning Of Cells For The Measurement Of Intracellular Potentials Using Kidney-Shaped Electrodes, *in Conference Proceedings of the 6th International Meeting on Substrate-Integrated Micro Electrode Arrays, July 8-11, 2008, Reutlingen, Germany*

[11]  W. Baumann, R. Ehret, M. Lehmann, G. Igel, H.-J. Gahle, B. Wolf, U. Sieben, I. Freund, M. Brischwein (1998a): Verfahren und Vorrichtung zur Messung eines Zellpotentiales. *Patent DE 19827957A1*

[12]  W. Baumann, R. Ehret, M. Lehmann, G. Igel, H.-J. Gahle, B. Wolf, U. Sieben, I. Freund, M. Brischwein (1998b): Verfahren und Vorrichtung zur intrazellulären Manipulation einer biologischen Zelle. *Patent DE19841337C1*

[13]  M.-P. Rols, J. Teissié (1998): Electropermeabilization of cells to macromolecules, *Biophys J, 75, 1415-1423*

[14]  P.J. Koester, C. Tautorat, A. Podssun, J. Gimsa, Baumann W. (2007): Analytikchip zur Erfassung intrazellulärer Potentiale adhärent wachsenden Zellen nach lokaler Elektroporation: Einleitung – Biologische Aspekte, *in Proceedings Mikrosystemtechnik Kongress 2007, October 15-17, Dresden, VDE VERLAG GMBH, Berlin-Offenbach, 433-437*

[15]  P. Koester, J. Sakowski, W. Baumann, H.-W. Glock, J. Gimsa (2007): A new exposure system for the in vitro detection of GHz field effects on neuronal networks. *Bioelectrochem., 70, 1, 104-114*

[16]  A. Heilmann, F. Altmann, A. Cismak, W. Baumann, M. Lehmann (2007): Investigation of Cell-Sensor Hybrid Structures by Focused Ion Beam (FIB) Technology, *mrs proceedings, 0983-LL03-03*

[17]  C. Tautorat, P.J. Koester, A. Podssun, J. Gimsa, W. Baumann (2007): Analytikchip zur Erfassung intrazellulärer Potentiale adhärent wachsenden Zellen nach lokaler Elektroporation: Einleitung – Elektrotechnische Aspekte. *in Proceedings Mikrosystemtechnik Kongress 2007, October 15-17, Dresden, VDE VERLAG GMBH, Berlin-Offenbach, 975-979*

[18]  C. Tautorat, P.J. Koester, A. Podssun, J. Gimsa, L. Jonas and W. Baumann (2008): Local Micro-Invasive Needle Electroporation – A Technical Challenge, *in Conference Proceedings of the 6th International Meeting on Substrate-Integrated Micro Electrode Arrays, July 8-11, 2008, Reutlingen, Germany*

[19]  J. Held, J. Gaspar, P. Ruther, and O. Paul (2008): Microneedle Arrays Electrode With Dielectrophoretic Electrodes For Intra-cellular Recording Applications, *in Conference Proceedings of the 6th International Meeting on Substrate-Integrated Micro Electrode Arrays, July 8-11, 2008, Reutlingen, Germany*

# Neuronal Cells Electrical Activity Recorded by Hydrogen Terminated Diamond Electrode

Ariano P[1*], Lo Giudice A, Marcantoni A[3], Vittone E[2], Carbone E[3], Lovisolo D[1]

1 Department of Animal and Human Biology, NIS Center, University of Torino, Torino, Italy
2 Department of Experimental Physics, NIS Center, University of Torino, Italy
3 Department of Neuroscience, NIS Center, University of Torino, Torino, Italy
* Corresponding author. E-mail address: paolo.ariano@unito.it

The paper reports for the first time the use of a hydrogen terminated diamond electrode for the recording of electrical activity from cultured neurons. Diamond is emerging as a most promising substrate for the development of molecular biosensors, but direct evidence that it can be successfully interfaced with living excitable cells is still missing.

## 1 Introduction

In the field of diamond based biosensors, up to now the emphasis has been on the development of diamond-enzyme interfaces exploiting electron transfer mechanisms [1,2] and of electrodes for electrochemical measurements from cells and tissues [3]. These examples highlight the feasibility of building molecular biosensors: a significant biotechnological breakthrough would be however to develop diamond based cellular sensors to record electrical and optical activity from cultured cells. In a previous paper [4] employing primary neurons, we have shown that it is possible to exploit the optical properties of diamond to record neuronal activity by means of fluorescent probes. Up to now, however, what was lacking was the last and key step, i.e. evidence that conductive hydrogen terminated diamond can be successfully employed in the fabrication of electrodes for recording cellular electrical activity.

To achieve this goal, we used a commercially available (Sumitomo Electric Industries, Japan) high purity (IIa type) 5 µm thick diamond layer epitaxially grown onto a Ib type HPHT (high pressure high temperature) diamond substrate, with (100) orientation and (3x3x0.5) mm$^3$ dimensions. The homoepitaxial layer showed a surface roughness at the nanoscale (root mean square roughness below 3 nm) as observed by 20x20 µm$^2$ non contact AFM maps.

## 2 Materials and Methods

**Preparation of the hydrogen terminated diamond electrode**

The diamond sample was oxidised in a sulfochromic mixture at 170°C and in a boiling solution of $H_2O_2$:$NH_4OH$, in order to remove contaminants and to oxygen terminate the surface; after this treatment the surface was hydrophilic and the sheet resistance, was higher than $10^9$ Ohm per square ($\Omega$/sq). The oxidised sample was annealed for 1 hour at 900 °C and $10^{-5}$ Pa to induce desorption of oxygen and residual adsorbates. The surface hydrogenation was carried out in a hot filament CVD reactor through two Ta hot (2100 °C) filaments and using purified hydrogen gas. The high hydrophobicity of the surface (wetting angle around 90°) and a sheet resistance of 23±1 k$\Omega$/sq confirmed the hydrogen termination of the homoepitaxial layer.

Assuming a hole mobility of 60 cm$^2$ V$^{-1}$ s$^{-1}$, the sheet hole concentration relevant to a sheet resistance of 23 k$\Omega$/sq of the hydrogen terminated surface, is about 5 $10^{12}$ cm$^{-2}$, in good agreement with experimental data available in literature [5].

**Electrode mounting**

The diamond was attached to a high resistance printed circuit board shaped to fit the inverted microscope stage. Two conductive copper pathways were connected respectively to the diamond surface by means of a 20 m gold wire and a silver paste bond and to a silver chloride reference electrode placed in the extracellular medium. The electrical insulation of conductors, interconnects and bondwires from the electrolyte was ensured by a silicone elastomer (Sylgard 184, Dow Cornig, USA) passivation layer. The fraction of the diamond surface acting as recording area was about 1 mm$^2$.

**Signal recording**

Electrical signals from cells cultured on the diamond surface were fed into a low noise (<5 V$_{RMS}$) amplification (G=$10^4$) and filtering (bandwidth: 0.02-24 kHz) custom stage before signal digitalization and recording [6]. Signal acquisition and analysis were performed by means of a Digidata 1440 board and pClamp10 software (Molecular Devices, Toronto, Canada).

**Cell cultures**

GT1-7 cells represent an appropriate model of differentiated, electrically excitable and autorhytmic neuronal cells, that can be grown at high density [7].

For the recordings, cells were plated on poly-L-lisin (PL) coated hydrogen terminated diamond in the presence of B27 medium supplement (Invitrogen) and cultured for 5-7 days . During the recordings, the medium was replaced with standard Tyrode solution.
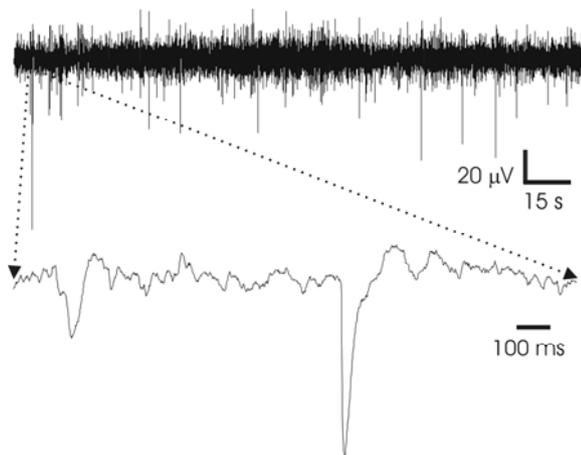


**Fig. 1.** A typical recording of electrical activity lasting several minutes from GT1-7 cells. The inset shows a stretch from at an expanded time scale.

## 3  Results and Discussion

In five experiments, electrical activity could be recorded from GT1-7 cells plated at high density on the fraction (1 mm$^2$) of the HTD surface free of the silicone insulating layer covering interconnections and bond pads. Consistently with previous observations by other groups [7], electrical activity was episodic, with bursts separated by silent intervals. Occasionally, trains of fast (a few ms) spikes could be observed; more often, the recorded activity consisted of slower spikes, lasting some tens of ms and of different amplitude (Fig. 1). While the former could be ascribed to the firing of isolated neurons, the latter were likely the result of the synchronized activity of clusters of cells.

Since clusterization is a prerequisite for the emergence of spontaneous electrical activity [7], and since we were recording the collective behaviour of a population of densely packed cells plated on a single macro-electrode, it is quite reasonable that slow signals were the most common.

The uniformity in time courses can be interpreted as evidence that the events are due to similar numbers of synchronously firing cells; the differences in amplitude are likely related to different degrees of adhesion – and therefore of electrical coupling – of different units to the diamond substrate.

Further tests will be carried out with a commercially available multielectrode array (MEA1060, Multichannel System GmbH, Germany).

**References**

[1] Haertl, A. et al. Protein-modified nanocrystalline diamond thin films for biosensor applications. Nature Mater. 3, 736-42 (2004).

[2] Zhao W., Xu J. J., Qiu Q.Q., Chen H. Y. Nanocrystalline diamond modified gold electrode for glucose biosensing. Biosens. Bioelectron. 22, 649-55 (2006) .

[3] Martinez-Huitle, C. Diamond microelectrodes and their applications in biological studies. Small 3, 1474-1476 (2007) .

[4] Ariano, P. et al. Cellular adhesion and neuronal excitability on functionalised diamond surfaces. Diam. Rel. Mater. 14, 669-674.

[5] Gan L., Baskin E., Saguy C., Kalish R. Quantization of 2D hole gas in conductive hydrogenated diamond surfaces observed by electron field emission. Phys. Rev. Lett. 96, 196808 (2006) .

[6] Obeid I., Nicolelis M. A. L., Wolf P. D. A low power multichannel analog front end for portable neural signal recordings. J. Neurosci. Methods 133, 27-32 (2004).

[7] Funabashi T. et al. Immortalized Gonadotropin-Releasing Hormone Neurons (GT1-7 Cells) Exhibit Synchronous Bursts of Action Potentials. Neuroendocrinology 73, 157-165 (2001).

# About MEA impedance measurement and analysis

Guillaume Becq[1], Guillaume Bienkowski[2], Jean Paul Diard[3], and Catherine Villard[2]

1 Department Image and Signal, Gipsa-lab CNRS, Grenoble, France
2 LEPMI, UMR 5631, BP 46, F-38402, St Martin d'Hères, France
3 Institut Néel, CNRS-UJF, BP166, 38042 Grenoble, France
* Corresponding author. E-mail address: catherine.villard@grenoble.cnrs.fr

The electrode impedance Z is an important parameter for the MEA detection of neural activity. Beside the commonly admitted fact that a low Z at 1 kHz increases the signal to noise ratio, the knowledge of the Z(f) variation inside a larger frequency range is essential to simulate realistic extra-cellular data suitable for validation of spike sorting algorithms. We have thus built an experimental set-up allowing an automated MEA impedance spectroscopy. It appears clearly that Z cannot be simply described by classical electrical circuits : electrochemical circuits including for example Warburg impedance show better concordance with experimental data. Lastly, great care must be taken when giving a Z value, as it is for example strongly time dependent.

## 1 Experimental

The automated set-up dedicated to MEA impedance spectroscopy we have developed is shown in Fig. 1. Jointly, an electronic interface that enable MEA connection with a commercial potentiostat has been designed in order to validate our automated set-up (not shown). Calibration electrical circuits have also been designed (Fig. 2) in order to determine the cut-off frequency associated to our electronics.
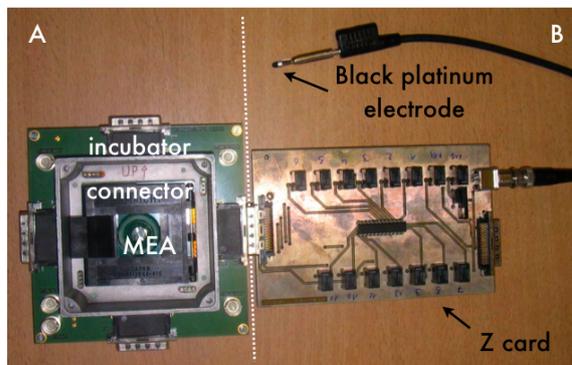


**Fig. 1.** Set-up for automated impedance spectroscopy. Part A is common with the experiment dedicated to neuronal signal recording while part B is the specific impedance electronic card ("Z card") developed for this study. Switches corresponding to each electrode (13 per card, 8 available positions) are seen.
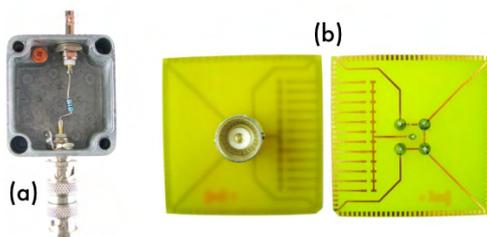


**Fig. 2.** Calibration electrical circuit. (a) Box with electrical components. (b) "Test MEA" built from a yellow printed circuit board.

It appears clearly that Z cannot be simply described by electrical RC parallel circuits [1] as the experimental Z(f) slope is far from the expected -1 value (Fig.3). Equivalent circuits built from four elements including resistance, capacitance and Warburg impedance [2] fit our data and can show good concordance with the physical and geometrical properties of the electrochemical system. In some cases however, we found equivalent circuits that match no evident physical interpretation, although their good description of experimental data make them useful for extra-cellular data simulations. This is the case using PBS medium, unlike concentrated KCl.
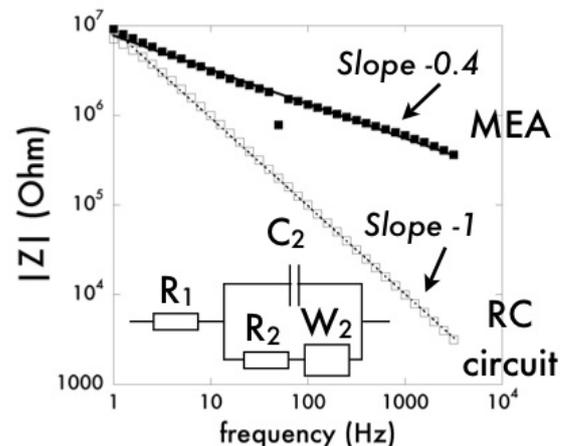


**Fig. 3.** Z(f) data obtained from the electrode marked in red in Fig.4(a) 30 min after the addition of a KCl 3M medium, compared to Z of a theoretical RC// circuit with R=10 MΩ and C=100nF. The equivalent electrochemical circuit fitting MEA Z(f) data is represented ($R_1 \approx 200$ kΩ, $R_2 \approx 500$ kΩ, $C_2 \approx 200$ pF, $W_2 \approx 15$ MΩ).

## 2 Trends in impedance measurements

Although correct measurements implies a three electrodes configuration, a two electrodes set-up like

our automated one provides accurate measurements if the surface of the counter electrode exceeds that of the working electrode by several order of magnitude. Ag/AgCl reference electrodes are useless, and an electrical plug covered by a thick black platinum layer has been used in our study. The differences observed between a commercial potensiostat and our electronic set-up (Fig.4) are negligeable compared to the effect of time.
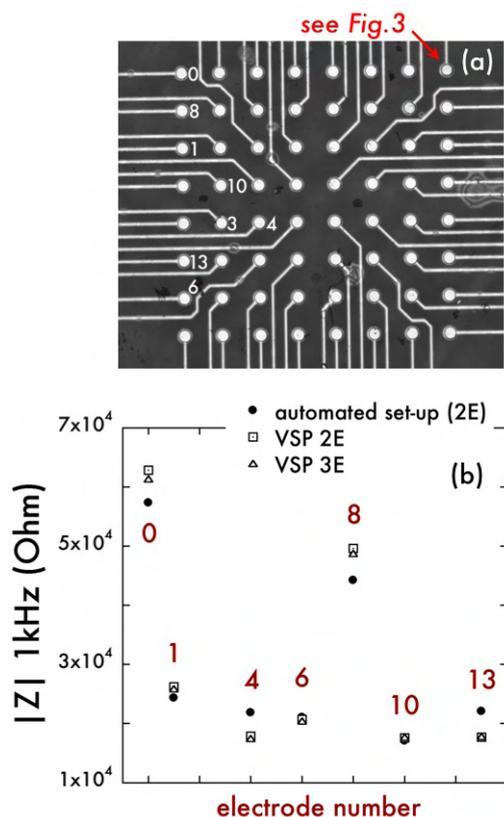


**Fig. 4.** (a) Picture of the MEA (purchased from Ayanda GmbH [3]). The electrodes concerned by impedance measurements are labeled. (b) Z modulus measurements performed in PBS liquid medium. Values are obtained at 1 kHz according three different experimental conditions : (i) use of the commercial Bio-Logic VSP set-up with either a 2 (2E) or a 3 (3E) electrodes configuration, the third electrode in the latter case being the MEA ground electrode, (ii) use of our automated set-up (two electrode configuration : the working micro-electrode and the plunging black platinum electrode, which behave as the reference electrode in the 3E configuration).

Impedance values at 1 kHz can indeed vary by 80%, mostly within the first minutes before stabilization, with a time constant of about 30 min using an usual medium like PBS (Fig. 5). This figure shows that the reference starting time is given by the liquid medium introduction.

Beside, the choice of the liquid medium strongly influences Z value at 1 kHz, with for example a factor three difference between PBS and saturated KCl after achieving the steady state (not shown).
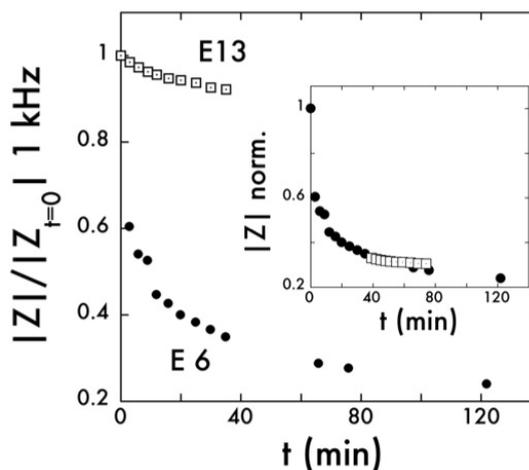


**Fig. 5.** Impedance kinetic on electrodes 6 (E6) and 13 (E13). For E6, the measurement started immediately after PBS medium introduction, while E13 began to be tested 39 min after E6. The normalization of the impedance has been done using the effective starting time of each experiment (main figure) or using the absolute time since the PBS introduction (inset : the E13 impedance has been normalized by the factor $\frac{1}{Z_{V13,39'}}\frac{Z_{V6,39'}}{Z_{V6,0'}}$ , where $Z_{VX,\,Y'}$ corresponds to the impedance of the $X^{th}$ electrode measured at the $Y^{th}$ minute, Y=0' being the PBS introduction time). This kinetic is clearly related to the contact between the metallic surface of the micro-electrode and the medium, as shown by the continuity between the E6 and E13 data versus time.

## 3 Conclusion

Impedance values are time (and medium) dependent. Thus, great care must be taken when giving micro-electrode impedance values at 1 kHz for example.

The modelisation of Z(f) variations requires electrochemical components whose significance is strongly medium dependent. The modelisation of a metal/liquid interface, fundamental for extra-cellular recording, is a difficult task for which a link between the macroscopic electrochemical description and the microscopic physical one is highly desirable, but still missing.

**Acknowledgement**

**References**
[1] Martinoia, S., Massobrio, P., Bove, M., and Massobrio, G. (2004). Cultured neurons coupled to microelectrode arrays: circuit models, simulations and experimental data. IEEE Transactions on Biomedical Engineering, 51(5):859–864.
[2] http://www.bio-logic.info/potentiostat/notes.html
[3] http://www.ayanda-biosys.com/

# NbActiv4™, a Novel Improvement to Neurobasal/B27™ Medium, Increases Activity in Neuronal Networks by Promoting Synaptogenesis

Brewer G[1, 2*], Boehler M[1], Jones T[1], Wheeler B[3]

1 Medical Microbiology, Immunology and Cell Biology,
2 Neurology, Southern Illinois University School of Medicine, Springfield, IL USA
3 Bioengineering Department and Beckman Institute, University of Illinois at Urbana-Champaign, Beckman Institute, Urbana, IL USA
*Corresponding author. Email gbrewer@siumed.edu

Neurobasal/B27™ is a serum-free, defined medium optimized for rat hippocampal neuron survival after 4 days in culture. For cultures of neuron networks, neurons on microelectrode arrays (MEA) may benefit from the ability of this medium to inhibit astroglial growth, which can undermine the close proximity of neurons to microelectrodes. However, spontaneous activity of networks on MEA after 3 weeks was only 0.5 Hz, lower than cultures in serum-based media and offering an opportunity for improvement. NbActiv4™ was formulated by the optimized addition of 3 components to Neurobasal/B27™ which synergistically increased spike activity and percentage of active electrodes correlating with an increase in synaptic puncta (1). Development of synapses in neuron cultures promotes the most interesting aspect of these cells, cell to cell communication by action potentials or spikes. We find low spike rates for rat embryonic hippocampal neurons cultured in Neurobasal/B27™ can be improved 4 to 8-fold with certain optimized additions to this classic medium including: cholesterol, shown to promote synaptogenesis (2,3); estrogen, to control better handling of the calcium influx (4,5); and creatine as an energy precursor for phosphocreatine to empower greater spike rates (6) and as a possible inducer of more inhibitory synapses (7). The resulting optimized medium, NbActiv4™, appears to promote higher spike rates by a mechanism involving greater synaptogenesis.

## 1  Methods

NbActiv4™ (BrainBits LLC) was formulated at proprietary concentrations by addition to the ingredients in Neurobasal/B27™ and Glutamax (Invitrogen). The primary hippocampal neurons were isolated from E18 rat embryos and cultured at 37°C in an atmosphere of 5% $CO_2$, 9% $O_2$ on substrates coated with poly-D-lysine. For measurement of electrical activity, neurons were cultured at 500 cells/mm$^2$ on multi-electrode arrays. Signals were acquired through an MEA 1060-BC amplifier (gain 1100, filtered at 8-3000Hz, sampled at 25 kHz) and MCRack software (Multichannel Systems). Those signals were also analyzed with PCLAMP 9.0 software. At 3 weeks after plating, in the same culture conditions, spontaneous spike activity was detected in a one-minute recording period as the number of spikes with amplitude exceeding five times the standard deviation of the baseline noise. Cultures of E18 hippocampal neurons were plated at 160 cells/mm$^2$ on glass slips for immunostaining. One-half medium changes every 4-5 days were performed. Recordings were collected at day 22-28 or immunostains performed at day 22.

## 2  Results

NbActiv4™ increases activity 8-fold and more than doubles percent active electrodes compared to Neurobasal/B27™ (Fig. 1). Mean astroglia are not significantly different (n=12 fields of 0.145 mm2). NbActiv4™ also produced more neurites/cell after 4 days in low density cultures. The increased activity with NbActiv4™ correlated with a 2-fold increase in immunoreactive synaptophysin bright puncta and GluR1 total puncta (Fig 2). Total synaptophysin puncta increased 1.5-fold. Characteristic of synaptic scaling, immunoreactive $GABA_{A\beta}$ puncta also increased 1.5-fold and bright NMDA-R1 puncta increased 1.8-fold (Fig 3). Resting respiration was more efficient with cultures in NbActiv4™, while maximum respiration was similar between cultures in NbActiv4™ and Neurobasal/B27™. NbActiv4™ produced cell survival rates equal to Neurobasal/B27™ with consistent 70% to 90% survival at 8 days. Shelf life at 4°C for 90% of original survival extended to at least sixteen weeks.
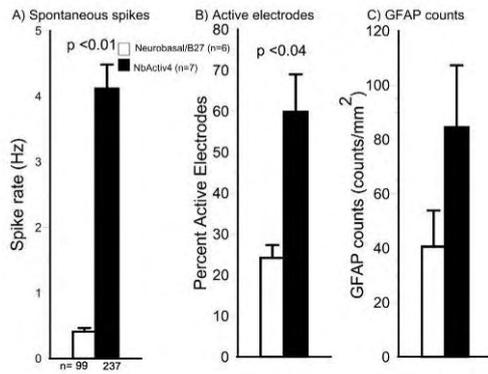
**Fig. 1**. NbActiv4 increases electrical activity, the percentage of active electrodes, but not astroglial density compared to cultures in Neurobasal/B27. (A) Mean spontaneous spike rates of electrodes with activity above 0.03 Hz ($n = 6$–7 cultures). (B) Percentage active electrodes with activity above 0.03 Hz ($n = 6$–7 cultures). (C) Mean astroglia counts are not significantly different ($n = 12$ fields of 0.145mm2 from two cultures).



**Fig. 3.** NbActiv4 (black bar) increases bright NR1 puncta 100% and total GABA puncta 40% compared to neurons cultured in Neurobasal/B27 (clear bar). ($n$=16 fields of 0.016mm2 from two cultures).

## 3 Conclusions

Overall, these results show that NbActiv4TM is a serum-free improvement to Neurobasal/B27TM for cultured networks with an increased density of synapses and transmitter receptors which produces higher spontaneous spike rates in neuron networks.

**Fig 2.** NbActiv4 (black bar) increases bright synaptophysin puncta twofold and total Glu-R1 puncta twofold compared to neurons cultured in Neurobasal/B27 (clear bar). ($n = 16$ fields of 0.016mm2 from two cultures).

**References**
1. Brewer, G., M. Boehler, T. Jones, B. Wheeler. 2008. NbActiv4TM, a Novel Improvement to Neurobasal/B27TM Medium, Increases Activity in Neuronal Networks by Promoting Synaptogenesis. J. Neurosci. Meth., In Press.
2. Pfrieger,F.W. and B.A.Barres. 1997. Synaptic efficacy enhanced by glial cells in vitro. Science 277:1684-1687.
3. Goritz,C., D.H.Mauch, and F.W.Pfrieger. 2005. Multiple mechanisms mediate cholesterol-induced synaptogenesis in a CNS neuron. Mol. Cell. Neurosci. 29:190-201.
4. Kumar,A. and T.C.Foster. 2002. 17beta-estradiol benzoate decreases the AHP amplitude in CA1 pyramidal neurons. J. Neurophysiol. 88:621-626.
5. Brewer,G.J., J.D.Reichensperger, and R.D.Brinton. 2006. Prevention of age-related dysregulation of calcium dynamics by estrogen in neurons. Neurobiol. Aging 27:306-317.
6. Brewer,G.J. and T.W.Wallimann. 2000. Protective effect of the energy precursor creatine against toxicity of glutamate and beta-amyloid in rat hippocampal neurons. J. Neurochem. 74:1968-1978.
7. Ducray,A.D., R.Qualls, U.Schlattner, R.H.Andres, E.Dreher, R.W.Seiler, T.Wallimann, and H.R.Widmer. 2007. Creatine promotes the GABAergic phenotype in human fetal spinal cord cultures. Brain Res. 1137:50-57.

# Embryonic Hippocampal Cultures in NbActiv4™ Surpass Spiking Activity of Embryonic Cortical Cultures in either Serum Medium or NbActiv4™

Brewer G[1, 2*], Boehler M[1], Wheeler B[3]

1 Medical Microbiology, Immunology and Cell Biology,
2 Neurology, Southern Illinois University School of Medicine, Springfield, IL USA
3 Bioengineering Department and Beckman Institute, University of Illinois at Urbana-Champaign, Beckman Institute, Urbana, IL USA
* Corresponding author. Email gbrewer@siumed.edu

We have shown that NbActiv4™ is a serum-free improvement to Neurobasal/B27™ for cultured networks with an increased density of synapses and transmitter receptors which produces up to an 8-fold increase in spontaneous spike rates (1). Other studies have used dense cortical cell cultures in DMEM/Serum media and reported high levels of spontaneous spike rates (2). To determine whether the nutrients in NbActiv4™ were sufficient to produce high spike rates and whether cortical neurons were capable of higher spike rates, we compared networks of cortical cultures on MEAs in serum containing medium with NbActiv4™, then compared this data to our hippocampal culture data in Neurobasal/B27™ and NbActiv4™.

## 1 Methods

NbActiv4™ (BrainBits LLC) was formulated at proprietary concentrations by addition of estrogen, cholesterol, and creatine to the ingredients in Neurobasal/B27™ and Glutamax (Invitrogen). The primary hippocampal and cortical neurons were isolated from E18 rat embryos and cultured at 37°C in an atmosphere of 5% $CO_2$, 9% $O_2$ on substrates coated with poly-D-lysine.

For cortical cultures in serum medium, initial plating was in Neurobasal/B27™/10% horse serum for 24h, then switched to DMEM/10% horse serum until day of recording.

For measurement of electrical activity, neurons were cultured at 500 cells/mm$^2$ on multi-electrode arrays. Signals were acquired through an MEA 1060-BC amplifier (gain 1100, filtered at 8-3000Hz, sampled at 25 kHz) and MCRack software (Multichannel Systems). Signals were also analyzed with PCLAMP 9.0 software. At 3 weeks after plating, in the same culture conditions, spontaneous spike activity was detected in a one-minute recording period as the number of spikes with amplitude exceeding five times the standard deviation of the baseline noise. Cultures of E18 hippocampal neurons were plated at 160 cells/mm$^2$ on glass slips for immunostaining. One-half medium changes every 4-5 days were performed. Recordings were collected at day 22-28 or immunostains performed at day 22.

## 2 Results

Cortical cultures in NbActiv4™ or serum media did not have significantly different spontaneous spike rates, but both rates were up to 4-fold higher than spike rates seen with hippocampal cultures in Neurobasal/B27™ (Fig. 1). Hippocampal cultures in NbActiv4™ produced significantly higher spontaneous spike rates over cortical neurons in either medium. Cortical cell cultures in DMEM/Serum had significantly higher counts of glia and significantly lower counts of neurons when compared to cortical cultures in NbActiv4™ (Fig. 2). Area of individual glia between the two media did not differ. The synaptic markers SYN, Glu-R1, GABA$_{AB}$, and NR-1 were also compared with no significant differences seen between the two media (data not shown)

## 3 Conclusions

Our studies show that for optimal activity with neuronal networks on MEAs, hippocampal cultures in NbActiv4™ provide the highest spontaneous spike rates over cortical cultures in serum-containing medium or NbActiv4™. Plating cortical cultures in NbActiv4™ seems more advantageous than plating in a serum medium despite similar spike rates because cultures in NbActiv4™ are less overgrown with glia and contain more neurons.
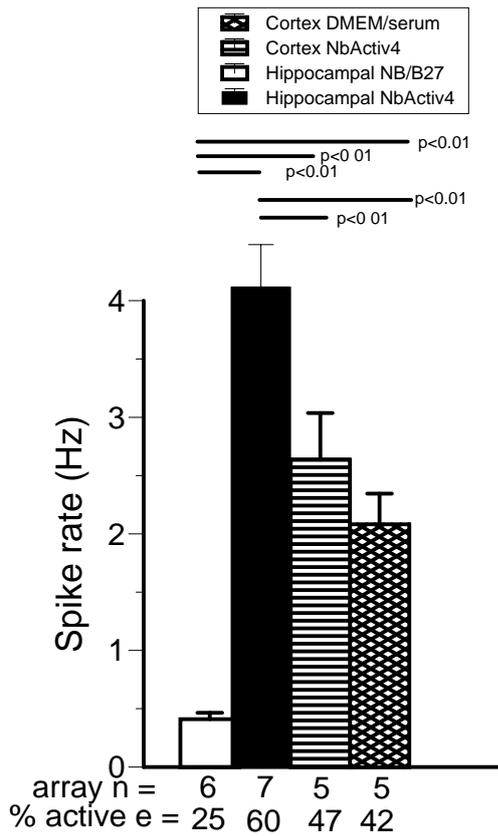
**Fig. 1.** Spontaneous spike rates increase 8-fold for hippocampal cultures in NbActiv4TM (solid) compared to cultures in Neurobasal/B27TM (clear). Hippocampal cultures in NbActiv4TM have higher spontaneous spike rates than cortical cultures in NbActiv4TM (horizontal lines) and cortical cultures in DMEM/Serum (hatched). Both cortical cultures have higher spontaneous spike activity than hippocampal cultures in Neurobasal/B27TM.
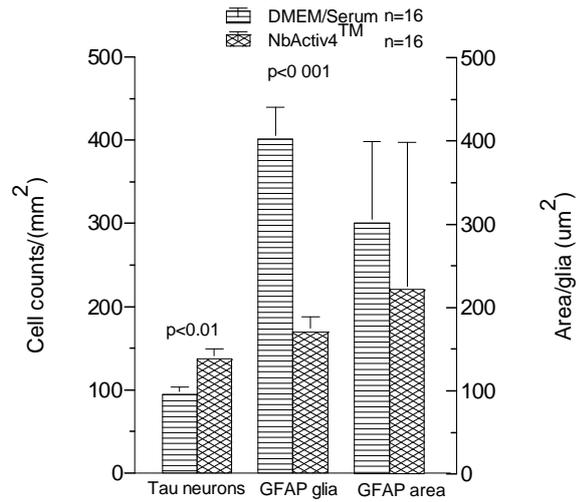


**Fig 2.** Cortical cultures in NbActiv4[TM] have more neurons and less glia than cortical cultures in DMEM/Serum after 22 DIV. Areas of individual glia between cultures do not differ.

## References

[1] Brewer, G., M. Boehler, T. Jones, and B. Wheeler. 2008. NbActiv4TM, a Novel Improvement to Neurobasal/B27TM Medium, Increases Activity in Neuronal Networks by Promoting Synaptogenesis. J. Neurosci. Meth., In Press.

[2] Madhaven, R., Z. Chao, and S. Potter. 2007. Plasticity of recurring spatiotemporal activity patterns in cortical networks. Phys. Biol. 4: 181-193

.

# BioMEA<sup>TM</sup>: A 256-channel microelectrode array (MEA) system with integrated electronics for recording and stimulation of neural networks

Charvet G[1*], Billoint O[1] , Colin M[4] , Fanet H[1], Gharbi S[1] , Goy F[3] , Guillemaud R[1], Joucla S[5], Mercier B[2], Meyrand P[5], Rostaing JP[1], Rousseau L[2], Trevisiol M.,  Yvert B[5]

1 CEA-LETI MINATEC, Grenoble, France;
2 Université Paris EST, ESIEE, Noisy-le-Grand, France;
3 Bio-Logic SAS, Claix, France;
4 Memscap, Crolles, France;
5 CNIC-CNRS & Univ Bordeaux1&2, UMR5228, Talence, France
* Corresponding author. E-mail address: guillaume.charvet@cea.fr

To understand the dynamics of large neural networks, one of today's challenges is to successfully record the simultaneous activity of as many cells or groups of cells as possible. This is made possible with microelectrodes arrays (MEAs) positioned in contact with the neural tissue. With microelectronics' microfabrication technologies, it now becomes possible to build high density MEAs containing several hundreds of microelectrodes. However, achieving dense arrays of 3D needle electrodes and increasing the number of electrodes using conventional electronics are difficult to achieve. Moreover, high density devices addressing all channels independently for simultaneous recording and stimulation are not readily available. Here, we present a 256-channel *in-vitro* MEA system with dense 3D-electrode arrays and integrated electronics allowing simultaneous recording and stimulation of neural networks.

## 1 Introduction

Microelectrode arrays (MEAs) provide an elegant way to probe the neural code distributed over large populations of neurons either *in-vitro* or *in-vivo* [1]. MEAs also offer the possibility to deliver electrical stimulation to neural networks, making it a promising technology to study activity-dependent plasticity and to build neural prosthesis [2].

This paper presents a new 256-channel recording/stimulation system named BioMEA™. In this system, dense 256-3D-electrode arrays are interconnected to four 64-channel analog ASICs dedicated to amplification and multiplexing of neural signals and stimulation. Each ASIC includes one amplification stage and one current generator per channel, and has the capability to rapidly switch between recording and stimulation. The realization of high-density MEA systems with integrated electronics offers new possibilities for both *in-vitro* and *in-vivo* studies of large neural network [3].

## 2 Electrode Arrays

In order to be as close to neurons as possible, the microelectrodes of *in-vitro* systems may be shaped as 3D needles. Pioneering techniques use classic isotropic etching, (either plasma or wet etching). However, these isotropic processes prevent the fabrication of dense 3D electrode arrays with large aspect ratios (the electrode pitch cannot be smaller than twice the electrode height). This limitation has been overcome using Deep Reactive Ion Etching (DRIE). A specific microfabrication process in which silicon substrate is etched anisotropically in order to obtain high aspect ratio microneedles, has been developed. Pitches down to 50 μm could be achieved with electrodes 80 μm in height (Fig. 1). This process offers the possibility to manufacture various shapes of electrodes on silicon or glass substrate.
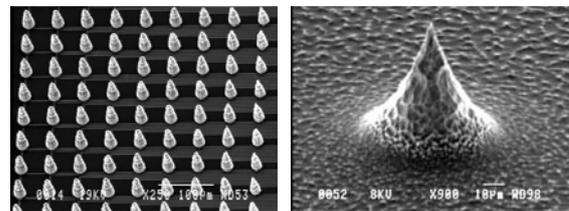


**Fig. 1.** 256 Electrode array

## 3 BioMEA<sup>TM</sup>: 256 Channel system

The BioMEA™ system manages 256 Electrodes and performs both measurement and stimulation. This system uses four 64-channels ASICs mounted on a mechanical support allowing electrical interconnections with a 256-channel array, and a PC running a specific firmware and providing a user interface (fig 2). The modular BioMEATM system allows the connection of different types of MEA (64 or 128 or 256 electrodes) to different numbers of analog ASICs. The

system is compatible with MultiChannelSystems and Ayanda Biosystems 60-channel MEA chips. Each ASIC includes one amplification stage (maximum gain of 750) and one current generator per channel (+/- 400µA peak max), and one serial output for multiplexed 64 channels data input. A user friendly software allows real time visualization, data storage of 256 channels and configuration of stimulation parameters.
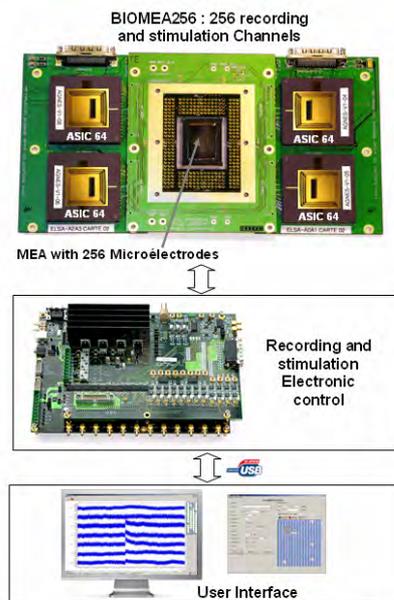


**Fig. 2.** BioMEATM System Setup

## 4 Biological Tests

We have performed validations of the BioMEA[TM] system. First, the noise level of the system was determined, and was found to be comparable to that of the MCS system. Second, we used the BioMEA[TM] system to successfully record both LFP and spike activity in a whole mouse embryonic hindbrain-spinal cord preparation (Fig 3), a developing network expressing waves of spontaneous activity travelling through the entire network once every 2-5 minutes [4,5]. Third, we could use the BioMEA system to trigger bursts of activity using electrical microstimulation.

## 5 Conclusion

High density MEA systems with integrated electronics, such as the BioMEATM system, will offer new possibilities for in-vitro studies of large neural networks. This modular system can also be adapted to various MEAs for in vitro or in vivo studies. It will be distributed by Bio-Logic SAS (http://www.bio-logic.info) in conjunction with 256-channel MEA biochips from Ayanda biosystems SA (http://www.ayanda-biosys.com).
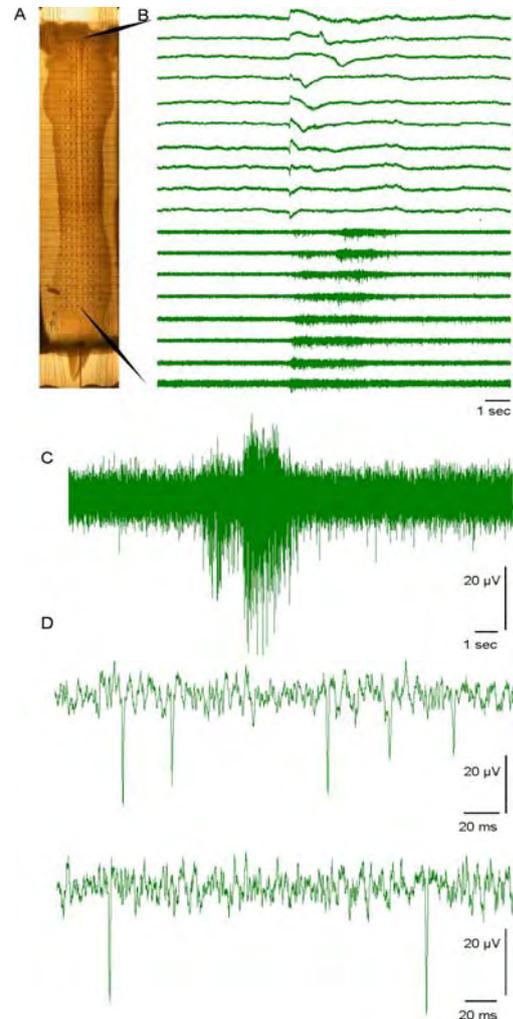
**Fig. 3.** A) Whole embryonic hindbrain-spinal cord on a 256-MEA. B) Single spontaneous wave showing both LFPs and bursts of spikes. C) Detail of a burst. D) Samples of isolated spikes.

**References**
[1] Nicolelis, M.A, et al. Reconstructing the engram: simultaneous, multisite, many single neuron recordings. Neuron 18:529-537, 1997.
[2] Jackson, A., et al. Long-term motor cortex plasticity induced by an electronic neural implant. Nature 444:56-60, 2006.
[3] Blum, R.A. et al. A Custom Multielectrode Array with Integrated Low-Noise Preamplifier IEEE EMBS Proceedings, 2003, pp. 3396-3399.
[4] Yvert, B., et al. Multiple Spontaneous Rhythmic Activity Patterns Generated by the Embryonic Mouse Spinal Cord Occur Within a Specific Developmental Time Window. J. Neurophysiol., vol. 91, pp. 2101-2109, 2004.
[5] Yvert B, et al. Mechanical control of spontaneous rhythmic activity in the embryonic hindbrain-spinal cord neural networks by the flow of perfusion over the fourth ventricle. Soc Neurosci Abstr 132.25, 2007

# Enhanced Extracellular Recordings from Axons Patterned through PDMS Microtunnels in a Neuronal Culture

Bradley J Dworak[1,2*] and Bruce C Wheeler[1,2]

1 Department of Bioengineering, University of Illinois at Urbana-Champaign, Urbana, Illinois, USA
2 Beckman Institute, University of Illinois at Urbana-Champaign, Urbana, Illinois, USA
* Corresponding author e-mail address: bdworak@illinois.edu

This study investigated an approach to sustain long-term recordings of axonal action potentials using a multi-electrode-array (MEA) device. We successfully grew neurons in culture so that only axons extended through narrow (10 µm wide by 3 µm high) and long (750 µm) microtunnels under which electrodes were integrated. This permitted the recording of relatively large (up to 200 µV) signals. The electrode impedance was measured and biophysical models of action potentials were revisited to support these readily observed and enhanced signal amplitudes.

## 1 Introduction

Spiking activity of neuronal cultures recorded from planar multielectrode arrays (MEAs) generally arise from cell bodies, rather than axons [1] because the signal attributed to currents generated is proportional to local surface area. Addition of the ability to record signals more reliably from axons, as well as to control their position, would substantially aid in-vitro research in understanding the functional connectivity among small networks of neurons. For instance, the directionality of the pre- and post-synaptic connections between neurons could be more easily identified.

Here we report the integration of three technologies: MEAs for electrical recording, PDMS chambers to separate populations of cells, and Campenot [2] chamber type microtunnels to select and guide axonal growth. Demonstrated is a reusable prototype capable of recording enhanced amplitudes of axonal action potentials by the microtunnels. These criteria permitted the recording of many signals with minimal effort simply by maintaining and growing the cell culture.

## 2 Methods

### 2.1 Design and Fabrication

A configuration of five 1.5-mm culture wells in a grid formation was designed (one center well and four on each side; see Fig. 1). The microstructure was fabricated with polydimethylsiloxane (PDMS) material (50 µm in height) bonded to a glass surface. Connecting the wells are 4 groups of 11 microtunnels, each 750 µm in length, 10 µm in width and 3 µm in height. The cross-sectional dimensions prevented cell bodies
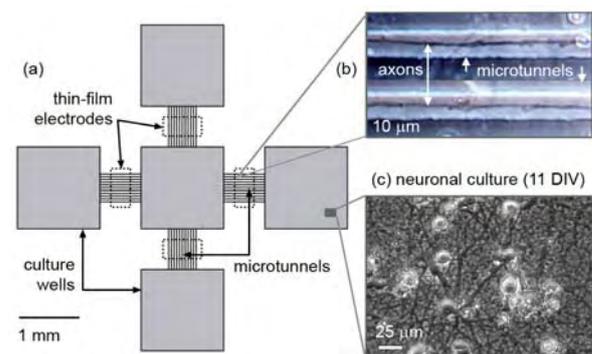


**Fig. 1**. (a) Schematic of design configuration. (b) Phase-contrast image of axonal growth inside microtunnels. (c) Healthy neuronal growth inside culture well.

from entering the tunnels. The MEA was composed of chromium (20 Å) and gold (500 Å) evaporated on 49-mm square glass substrates of 1-mm thickness. Thin film electrodes were patterned onto the surface so as to lie at the bottom of each group of microtunnels (see Fig. 2).
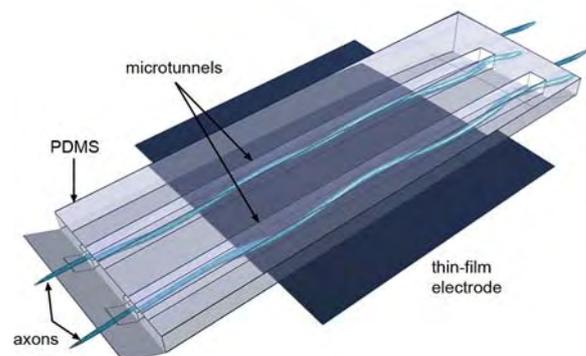


**Fig. 2.** (a) Pictorial representation of microtunnel architecture, electrode position and neuronal growth. Axonal growth runs perpendicular to each electrode and is physically guided by the long and narrow microtunnels.

## 2.2 Surface/Culture preparation

The surfaces were cleaned by piranha etching for 10 min followed by ashing at 55W for 30 sec. Next, poly-D-lysine (PDL) solution (100 µg/ml) was physisorbed onto the surface overnight and rinsed. Cortical tissue from embryonic day 18 (E18) rats was re-suspended in Neurobasal™/B27/GlutaMAX™ growth medium and plated at 600 cells/mm$^2$.

## 2.3 Data acquisition/analysis

Cultures on arrays were placed in the holder of a commercial data-acquisition system (MultiChannelSystems, Inc.). At 10-14 DIV, the raw electrode signals were recorded using MC Rack software. Next, the MCS data files were directly imported into Offline Sorter v2 software (Plexon, Inc.) for analysis.

## 3    Results/Discussion

Four electrode impedance measurements were taken, each measurement from a different set of microtunnels (10 mV @ 1 kHz). Impedance values for two MEAs were 507±18 kΩ, 7±1° and 424±36 kΩ, 9±4°. These values are close to the theoretical value of the spreading resistance as modelled by a circuit composed of 11 resistive parallel paths, estimated to be 355 kΩ. Furthermore, the results show that resistances from electrodes to the ends of an individual microtunnel are in the MΩ range.

The small phase angle of 6 to 12° implies that the impedance is largely resistive, unlike electrodes from conventional MEAs. The dominant impedance component is the resistance within the long and narrow microtunnel, whereas most microelectrodes are dominated by the more capacitive electrode-electrolyte interface coupled with a smaller spreading resistance.

A total of 31 MEAs were tested, 25 of them were healthy and survived for 3 to 6 weeks. Axons freely extended into the microtunnels as early as 48 hours after plating. Of the 25 healthy cultures 21 were electrically active. Spike rates between 3 and 22 Hz were recorded (11 microtunnels to each electrode) from at least one microtunnel group. The background noise of the electrodes ranged from 10 to 50 µV P-P.

Spike amplitude typically peaked between 100 and 200 µV, with a maximum of 220 µV (see Fig. 3). These voltages were significantly larger than expected, since spike amplitudes measured from somas from MEAs are most often in the range of 10-100 µV. Cultures exhibited synchronous bursting activity from all active electrodes, indicating that all culture wells were synaptically interconnected.

We sought to ascertain if these enhanced signals are plausible from a biophysics model. Thus, we downscaled the dimensions and hence results from

Clark and Plonsey on the squid giant axon [3]. For the present case, a 1-µm diameter axon would have a 100-µm long active region and a net current of 0.8 nA. If inserted into the 3-MΩ resistance from the centre of the tunnel, the signal would be 2.4 mV, which would be reduced to 220 µV over the 11 parallel electrodes. Thus, amplitudes in the range of up to 200 µV appear reasonable.
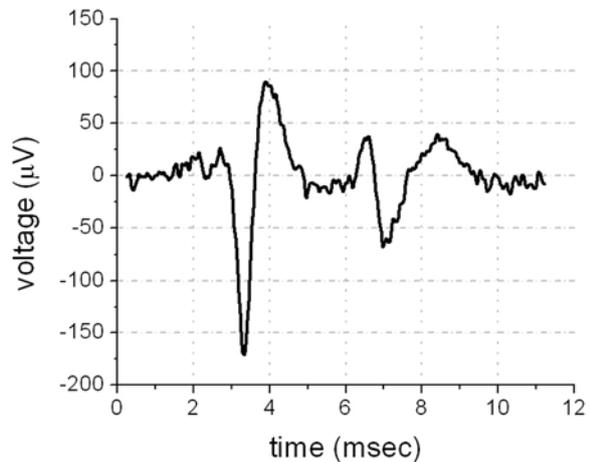


**Fig. 3** Extracellular recording of two axonal action potentials inside a microtunnel. The background noise level is 15 µV P-P.

## 4    Conclusion

This device is a powerful research tool to investigate localized network activity and the development and growth of axons and their connections. Moreover, with compartmentalized culture growth, we anticipate further experimentation to study how extending axons would interact with cultures of different cells or subpopulations and environments. By plating cells at different times, we propose that a certain degree of connective polarization is possible. The flexibility and robustness of the clustering, microtunnel and electrode configurations will provide numerous opportunities for further study of neuronal network behaviour.

**References**
[1]    J. van Pelt, P. Wolters, M. Corner, W. Rutten and G. Ramakers (2004): Long-term characterization of firing dynamics of spontaneous bursts in cultured neural networks. *Biomedical Engineering, IEEE Transactions on,* 51, 2051-2062.
[2]    R. Campenot (1994): NGF and the local control of nerve terminal growth. *Jounal of Neurobiology,* 25(6), 599-611.

Technology

[3]   J. Clark and R. Plonsey (1968): Extracellular Potential Field of Single Active Nerve Fiber in a Volume Conductor. *Biophysical Journal,* 8(7), 842-864.

# First Network Studies With the Caged -Neuron Multielectrode Array

Jon Erickson[1*], Angela Tooker[2], Yu-Chong Tai[2], and Jerry Pine[3]

1. Department of Bioengineering
2. Department of Electrical Engineering
3. Department of Physics, California Institute of Technology, Pasadena, California, USA
* Corresponding author. E-mail address: Erickson@caltech.edu

## 1  Background

We have fabricated 16-electrode 4 x 4 arrays on silicon with parylene plastic cages to contain the neurons near the electrodes. We call these "neurochips". A Nomarski photo of a neurochip culture, which has grown for eight days in vitro, is shown in Figure 1. The distance between cages is 110 microns. There are many more fine processes than can be seen in the Nomarski picture. The growth is the same as for mass low density ($200/mm^2$) cultures grown in Petri dishes. We have measured neuron survival over time and the average after three weeks is 55%, which mirrors conventional low density mass cultures grown in Petri dishes.
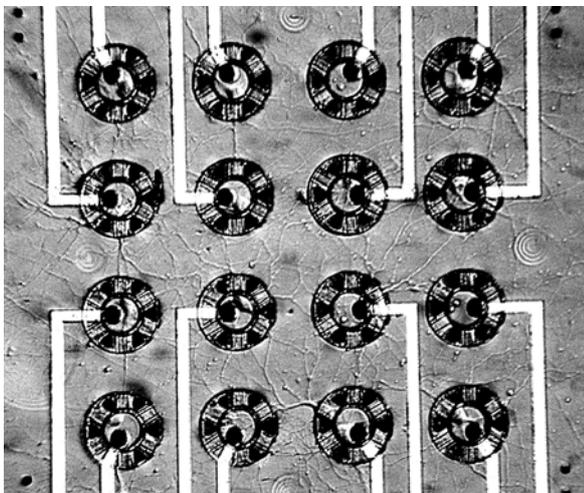


**Fig. 1.** An eight day old neurochip culture

We have determined the neurochip stimulation and recording capabilities. We have used a voltage sensitive dye, Di4ANNEPDHQ, to record from neurons when a current stimulus was applied to its neighboring electrode and determined that at least 90% are stimulated with a bipolar current of less than 20 microamperes and 400 microseconds per phase. (The dye recording is free of interference from the stimulus artifact.) We have recorded from caged neurons with good signal to noise ratios of 5 to 20.

## 2  Methods

The cages are fabricated by depositing parylene from the gas phase on a form made of photoresist and aluminum, which is dissolved away. The neurons are placed in from above, with a suction pipette, and dendrites and axons grow out of tunnels. Custom Labview software provides control of bipolar current stimulation and recording with digitizing at 20 khz. Figure 2 below shows the recorded signals of traces in fifteen cages when one is stimulated. Figure 3 shows a raster of the results of ten successive stimuli, with spike timings derived from the traces. The rasters are the raw material for analysis of culture development.
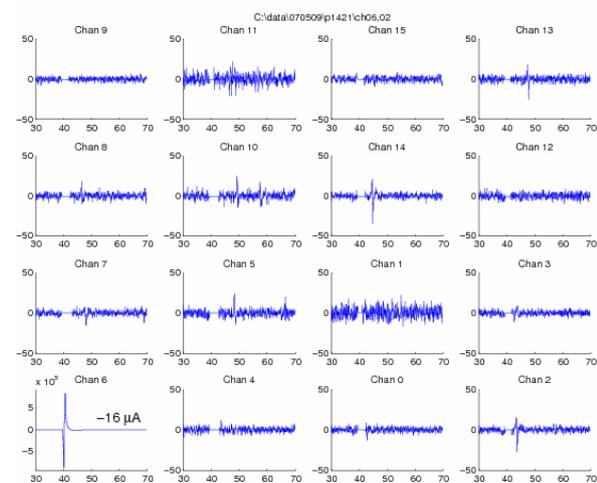


**Fig. 2.** Digitized traces after stimulation at lower left.

## 3  Results

To begin with, we have made networks of dissociated hippocampal pyramidal cells from eighteen day embryos, primarily CA1 and CA3 neurons. The cells are loaded into the neurochips by picking them up with a suction electrode from a non-adhesive surface and carrying them to the cages. The results of preliminary experiments with these cultures, including the software that has been developed, is the substance of this poster. Culture development has been studied in experiments which have examined the connectivity, the response delays, and the response strengths over

time for four weeks in culture. The networks had 6-14 neurons. Figure 4 shows the development of connectivity for a typical culture.
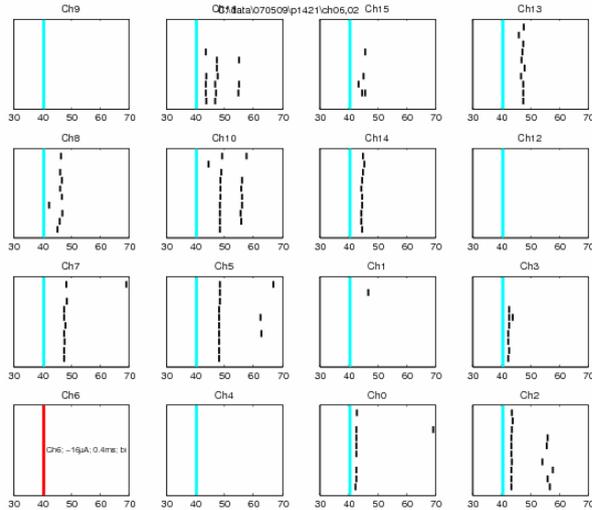


**Fig. 3.** Raster plot for stimulation of cage at lower left, at 40 msec.
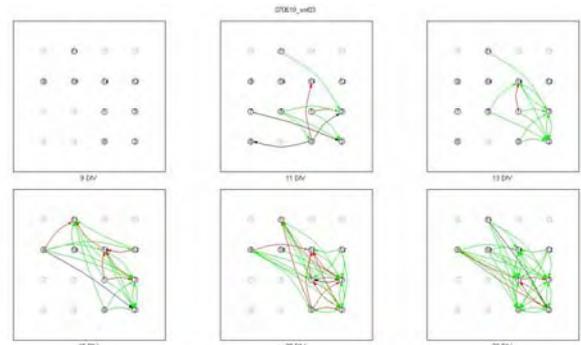


**Fig. 4.** Evolution of connectivity of a typical culture. Red lines are <5 msec delay, and green ones are 5-20 msec.

## 4 Conclusion/Summary

The neurochip offers powerful new opportunities for studying network development and plasticity. Planned work includes studies of:

1. Networks of one cell type, and the patterns of connectivity they create over time

2. Networks of different cell types, and the specificity of connections, such as CA1-CA3.

3. Activity-dependent effects of chronic general stimulation and of spike-timing- dependent plasticity.

# MEMS based examination platform for neuro-muscular communication in a co-culture system coupled to a multi-electrode-array

U. Fernekorn[1*], M. Fischer[1], M. Klett[1], D. Hein[1], C. Augspurger[1], B. Hiebl[2], A. Schober[1]

1 MacroNano® Center for Innovation Competence, Dept. for Microfluidics and Biosensors,Technische Universität Ilmenau, Ilmenau, Germany
2 Forschungszentrum Karlsruhe, Eggenstein- Leopoldshafen, Germany
* Corresponding author. E-mail address: uta.fernekorn@tu-ilmenau.de

Development of a sensor-connected in vitro neuromuscular co-culture system may provide a useful tool for interpreting mutual signal transfers between the cell species and for future applications in drug screening. A glass-based, autoclavable, micro fluidic culturing system consisting of two chambers connected by micro capillaries was designed. The co-culture system was combined with a commercially available multi electrode array. This setup allows stimulation of adherent neuronal cells in one chamber and measurement of action potentials induced in myotubes derived from C2C12 cells in the other. Neuronal processes growing through micro capillaries were detected by immuno-fluorescence stainings.

## 1 Introduction

Many aspects about the factors facilitating the interplay between motoneurons and muscle fibers have been unravelled by studying different types of co-culture models [1-3]. Our system intends to generate motorical end plates derived from cell lines.
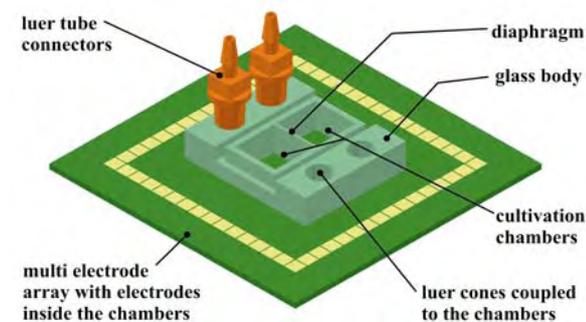


**Fig.1**: Scheme of the co-culture system

Their interactions shall be surveyed on multielectrode arrays. In the system presented here (Fig. 1), a commercially available pMEA has been combined to a co-culture system that facilitates separated growth of monolayers of neuronal and myogeneic species. Stimulation of the adherent cells and subsequent recording of the extracellular signals will be sought.

## 2 Technological Setup

To obtain a chamber volume of about 300 µl at lateral geometries defined by the MEA, a minimum chamber height of 5 mm is necessary. A 100 mm wafer-formatted borofloat glass substrate with a thickness of 5 mm was used to be compatible with standard MEMS technologies. As technological approaches, Reactive Ion Etching (RIE) versus SU8-lithography was tested to manufacture the lateral micro capillaries. However, autoclaving tests showed that the glass body is de-bonding using the first method. So it was necessary to verify the second technological approach because the overall system is designed for multiple uses. For simultaneous creation of the 5-µm capillaries as well as the intermediate bond layer SU-8, an epoxy based photoresist is used. This resist is commonly used for micro electro mechanical systems (MEMS) with high aspect ratios as well as high chemical and thermal stability. The 49 mm x 49 mm glass substrate with electrodes and a passivation layer is coated with 5-µm thick SU8-2005 layer and patterned by a modified lithography step. After a cleaning step including plasma treatment, a single co-culture glass body is aligned and pressed to the MEA glass carrier. Using a heating press a very stable bonding between glass body and MEA system is achieved during the post exposure bake of the resist at 110°C.

## 3 Cell based Applications

### 3.1. Cell Culture

Undifferentiated NG108-15 cells or C2C12 cells were cultured in DMEM supplemented with 10% FCS, Penicillin /Streptomycin + L-Glutamine. To induce differentiation, medium was changed to serum free DMEM + Penicillin/Streptomycin + diButyryl-cAMP. Upon changing medium to DMEM + 2% horse serum, differentiation to myotubes was initiated. MEA dishes were coated with 0.02% gelatine. $2.5 \times 10^4$ un-

differentiated C2C12 cells were plated to one chamber of the co-culture system and cultured for 9 days. Undifferentiated NG108-15 cells were added to the other chamber. Both cell species were maintained in DMEM + 2% horse serum.

## 3.2 Transfection

NG108-15 cells were transiently transfected with the pDsRed-Express-C1. For this process, the Lipofectamine 2000 Kit was used according to the protocol provided by the supplier. The plasmid contained a G418- resistant gene. G418 stable cell lines were selected in medium containing 400µg/ml G418 and tested for expression of pDsRed. Successfully transfected were sorted using a Partec CyFlow®space flow cytometer connected to a Cell Sorter.

## 3.3 Immunohistochemistry

Neuronal processes were stained with antibodies directed against microtubule-associated protein 2a, growth- associated protein 43 or neurofilament 200, respectively. Cells were washed and fixed with ethanol. Nonspecific binding was blocked using 10 % normal goat serum in PBS. Cells were incubated with primary antibodies at 4°C overnight. Cells were exposed to Texas Red labelled donkey anti goat IgG or goat anti-mouse IgG.

## 4 Results and Discussion

We combined pMEAs to our glass co-culture system consisting of two cultivation chambers interconnected by micro channels of 5µm width and 50µm length. This arrangement enables neuronal processes to grow through the channels. As the system is autoclavable, it is suitable for repeated measurement approaches. The electrodes are directly located beside the diaphragm. The co-culture system may be connected to a perfusion system, thus allowing both static and fluidic cultivation conditions. We established a co-culture of the neuroblastoma x glioma cell line NG108-15 and mouse myoblast cell line C2C12 cells. NG108-15 cells have been reported to resemble motoneurons as they are able to synthesize acetylcholine, agrin and neuregulin [4,5].

These cells are capable of generating functional synapses with myotubes including induction of AChR clusters. Moreover, twitching of myotubes cocultured with NG108-15 cells has also been described [5]. C2C12 cells provide a well established system to cultivate myotubes and produce nAChR. Some neurological disorders are correlated with a defective signal transmission between the innervating motoneuron and muscle fibers. Thus, we are seeking to further understand the electrophysiology of the neuromuscular interface. Our MEA- based co-culture system may provide a new setup for electrophysiological recordings of cell culture derived end plate potentials.
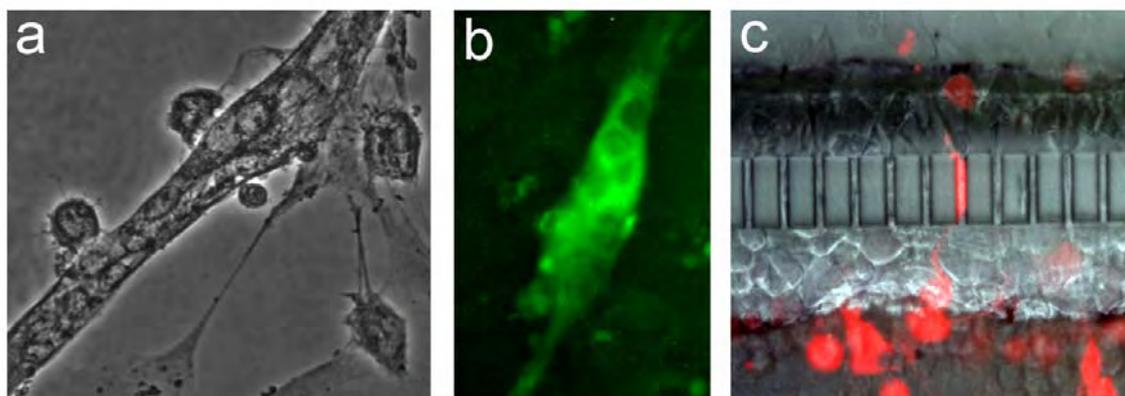


**Fig.2:** NG108-15 cells form neurites binding to C2C12 myotubes (a). IF staining with FITC conjugated α-bungarotoxin demonstrates the presence of nAChR (b) in C2C12 myotubes. Neurites growing through microchannels separating the cultivation chambers (c).

**References**
[1]   M. Das et al. (2007): Embryonic motoneuron-skeletal muscle co-culture in a defined system. *Neuroscience, 146, 481-488*

[2]   T.F. Kosar et al. (2006): A nanofabricated planar aperture as a mimic of the nerve–muscle contact during synaptogenesis. *Lab on a Chip, 6,632-638*
[3]   J.X.S. Jiang et al. (2003): Muscle Induces Neuronal Expression of Acetylcholinesterase in Neuron-Muscle Co-culture. *J. Biol. Chem., 278; 46 ,45435-45444*
[4]   N.R. Cashman et al. (1992): Neuroblastoma x Spinal Cord (NSC) Hybrid Cell Lines Resemble Developing Motor Neurons. *Dev. Dyn., 194, 209-221*
[5]   N.A. Busis et al. (1984): Three cholinergic neuroblastoma hybrid cell lines that form few synapses on myotubes are deficient in acetylcholine receptor aggregation molecules and large dense core vesicles. *Brain Res. 324, 201-210*

# High-Resolution CMOS-based Microelectrode Array and its Application to Acute Slice Preparations

U. Frey[1*], U. Egert[2], J. Sedivy[1], F. Heer[1], S. Hafizovic[1], A. Hierlemann[1]

1 ETH Zurich, Department of Biosystems, Science and Engineering, Basel, Switzerland
2 University of Freiburg, IMTEK Biomicrotechnology, Freiburg, Germany
* Corresponding author. E-mail address: urs.frey@bsse.ethz.ch

Recordings have been performed using a CMOS-based microelectrode array (MEA) featuring 11'016 metal electrodes and 126 channels, each of which comprises recording and stimulation electronics for extracellular, bidirectional communication with electrogenic cells. The important features of the device include (i) high spatial resolution at (sub)cellular level with 3'150 electrodes per $mm^2$ (diameter: 7 μm, pitch: 18 μm), (ii) a reconfigurable routing of the electrodes to the 126 channels, and (iii) low noise levels. Signals from neurons in an acute cerebellar slice preparation are presented.

## 1  Introduction

In many experiments with living tissue, it is desirable to adapt the locations of the recording sites with regard to the biological structure. One possibility is to simultaneously record from all electrodes of a high-density array [1, 2], which results in rather high noise levels due to the limited pixel area available for circuitry implementation. Instead of scanning the entire electrode array, the approach presented here provides a reconfigurable routing for an almost arbitrary set of electrodes to the readout channels, and enables low-noise signal amplification and filtering with the front-end circuitry placed outside the array.

Acute sagittal cerebellar slices have been used to assess the performance of the device. In these preparations, predominantly Purkinje cells are spontaneously active. The Purkinje cells are effectively disconnected from each other as the parallel fibers have been cut. Their electrical fields hence can be considered to be independent, which facilitates spike sorting and eases waveform interpretations.
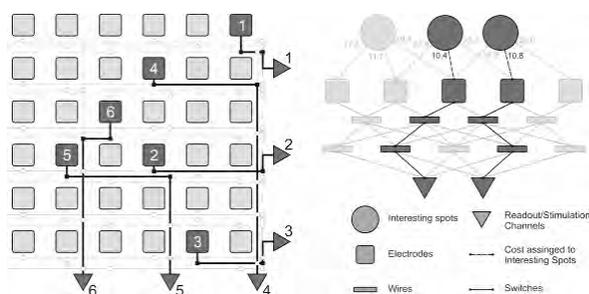


**Fig. 1.** Array wiring and routing scheme.

## 2  Results

The recorded signals are amplified and filtered in three stages. The gain is programmable via the digital interface from 0 to 80 dB.

The first stage provides a first-order high-pass-filter featuring a low cut-off frequency of 0.3 Hz. ADCs sample the signals at 20 kHz and 8 bit resolution. The stimulation capability is provided through an 8-bit flash DAC and stimulation buffers [3].

The equivalent-input noise of only the amplifiers is 2.4 μV$_{rms}$ (1 Hz-100 kHz), it is 3.9 μV$_{rms}$ for bare Pt-electrodes in physiological saline, and 3.0 μV$_{rms}$ for dendritic Pt-black electrodes in physiological saline (+0.5 LSB quantization noise). The flexibility in electrode selection is attained by use of an analog switch matrix integrated underneath the electrode array. The switch matrix consists of 13k SRAM cells and analog switches to define the routing from the electrodes to the amplifiers as illustrated in Fig 1. The measurement setup, that includes an FPGA for data preprocessing, such as digital filtering and data compression/reduction is depicted in Fig 2. The fabricated chip is shown in Fig 3.

Measurements of spike activity in acute brain slices have been performed. The data shown in Fig 4 were obtained from a cerebellar slice of a Long-Evans rat shown in Fig 5. The preparation was performed at room temperature, as described in [4]. In the figure, six exemplary recordings from adjacent electrodes are shown: action potentials of single cells are visible on several neighboring electrodes.
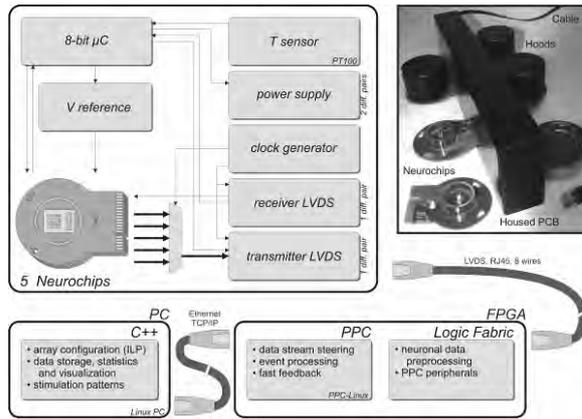
**Fig. 2.** Measurement setup.
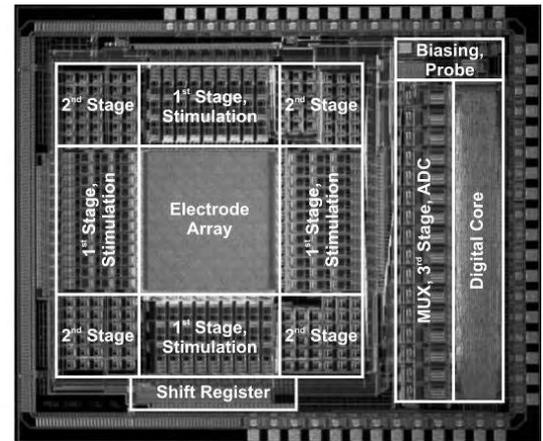


**Fig. 3.** Micrograph of the CMOS HD-MEA.
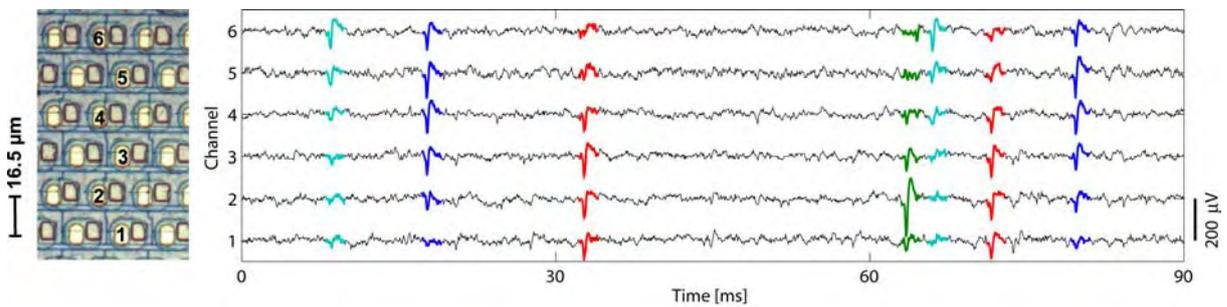


**Fig.4.** Recordings from an acute sagittal cerebellar slice of a Long-Evans rat.
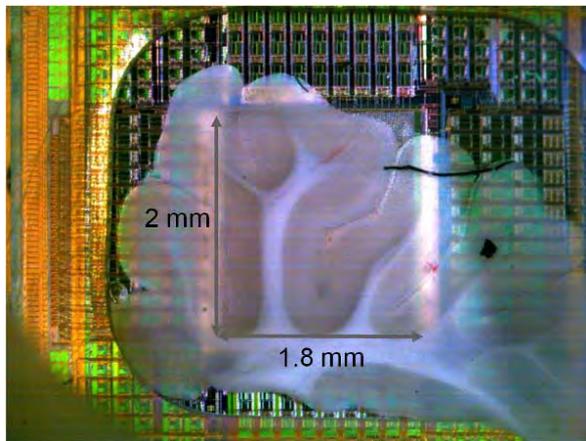


**Fig. 5.** HD-MEA with an acute cerebellar

## 3 Conclusion

We developed a CMOS-based microelectrode array with 11'016 metal electrodes and 126 on-chip channels. Each channel includes recording and stimulation electronics for bidirectional communication with electrogenic cells, such as neurons or cardiomyocytes. The new features of this chip include the possibility to perform high spatial resolution recordings with 3'150 electrodes per mm$^2$ at cellular or subcellular resolution (electrode diameter 7 μm, pitch 18 μm), a great flexibility in routing the 126 channels to the 11'016 recording sites, and low noise levels, since the large front-end amplifiers have been placed outside the electrode array.

Spike sorting allows for identifying single action potentials in the multi-unit recordings obtained from the acute cerebellar slices.

## References

[1] B. Eversmann et al., "A 128 x 128 CMOS Biosensor Array for Extracellular Recording of Neural Activity," *IEEE J. Solid-State Circuits*, pp. 2306-2317, Dec., 2003.

[2] L. Berdondini et al., "High-density Electrode Array for Imaging in Vitro Electrophysiological Activity," *Biosensors and Bioelectronics*, vol. 21, Issue 1, pp. 167-174, 2005.

[3] U. Frey et al., "An 11k-Electrode 126-Channel High-Density Microelectrode Array to Interact with Electrogenic Cells," in **ISSCC 2007**, San Francisco, February 2007, pp. 158 – 159.

[4] U. Egert et al., "Two-dimensional monitoring of spiking networks in acute brain slices," *Experimental Brain Research*, vol. 142, pp. 268–274, 2002.

# Robust Methodology For The Study Of Cultured Neuronal Networks on MEAs.

Hammond M.W.[1,2], Marshall S.[1], Downes J.H.[2], Xydas D.[2], Nasuto S.J.[2], Becerra V.M.[2], Warwick K.[2], Whalley B.J[1]

1 School of Pharmacy, Reading University, Reading, RG6 6AJ, England
2 School of Systems Engineering, Reading University, Reading, RG6 6AJ, England

In order to conduct consistent experiments using cultured neuronal networks, environmental stability and preparation repeatability must be tightly controlled. Here we describe considerations and low cost, simple methods permitting restriction of culture growth to within the recording horizon of standard multi-electrode arrays (MEAs) and reduction of culture media evaporation via simple adaptations to standard Potter rings, thereby increasing stable recording time. We also present data confirming the importance of a rest period prior to recordings due to observed movement-induced activity.

## 1 Introduction

The production, maintenance and recording from cultures grown on MEAs are affected by numerous factors that may cause significant experimental variability [1]. These fall into two principal categories: culture area and environmental stability.

Given that the active area represents ~9% of a typical MEA (8x8 array of 60 titanium nitride electrodes with a diameter of 30 μm and 200 μm spacing, Multi Channel Systems, Reutlingen, Germany), unrestricted seeding carries the risk that ~91% of neurones will lie outside of the recording horizon and will therefore be unaccounted for when describing network dynamics. Here we present a simple, effective and low cost method for the restriction of cells using a circular inverse template.

Moreover, primary cortical cultures require maintenance at $37^oC/5\%$ $CO_2$ in a humidified environment. Potter rings [2] allow recording to take place in non-humidified electrical equipment-friendly environments, increasing culture lifespan due to reduced evaporation and increased sterility. However despite this 'sealed' environment, a gradual drop in spiking levels is observed as a result of fluid loss and associated osmolarity changes. Here we raise the consideration of environmental humidity and present an adaptation to extend recording time.

Finally, consistent with Wagenaar *et al* [3] we present data supporting the effects of physical movement on neuronal activity that should be accounted for in any given experiment.

## 2 Methods

Cortical cells were dissociated from E18 Wistar rats and plated onto MEAs at 1 million cells/ml (see [4] for details). Cells were restricted to the active area using a circular inverse Sellotape template cut by hollow metal tube, the diameter of which was equal to the width of the MEA active area. Templates were positioned on the MEA before autoclaving and application of 100 μl PDL (sterile filtered, washed after 20 mins). Finally, prepared MEAs were UV treated overnight. Cells were found to adhere to the coated MEA surface ~1 hour after seeding, at which point templates were gently removed.

Potter rings were modified by application of adhesive tape around the ring and subsequently silicone sealant between the O-ring and the tape.

Cells were maintained in a humidified incubator at $37^oC/5\%$ $CO_2$ whilst recordings were made in a non-humidified $37^oC/5\%$ $CO_2$ incubator. Media changes (50%) were performed 3 times per week. Recordings were undertaken in MEABench and analysed using custom written Matlab code.

## 3 Results

### Seeding & Restriction

Whilst dense ($1-7x10^6$ cells/ml ) networks are attractive as a correlate to *in vivo* cell densities, they present several difficulties. Firstly, higher densities result in greater migration across the MEA surface. Secondly, very dense cultures result in cells forming a 3D structure that separates from the electrodes by DIV 14. Animal age also influenced final cell density (at DIV 7) as the presence of progenitor cells in <E18 tissue causes post-seeding proliferation. Optimal densities were between $5x10^4$-$1x10^6$ cells/ml.

Initial cell restriction attempts comprised of seeding active area-sized cell suspension droplets, however this resulted in osmolarity changes and widespread cell death (n=60), even at very short settling times (~20 mins). Selective PDL coating the active area alone in cells that settled outside of the active

area and later developed into glia providing a substrate upon which neurones could migrate away from the active area whilst retaining strong connections to those within. The most effective solution was to apply a circular inverse template (1.96 mm$^2$) around the active area that was removed once cells had settled. This method resulted in no cells outside of the active area at early DIVs and only limited migration to within ~100 μm of the recording horizon at later DIVs (>25; Fig. 1).
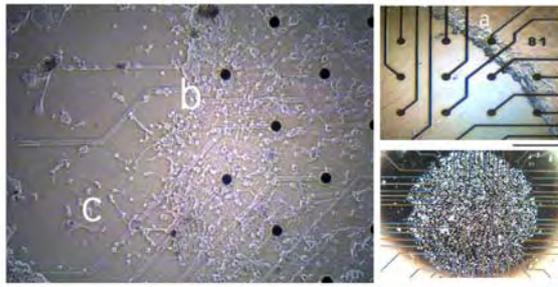


**Fig.1.** Top right: Edge of template prior to seeding (a). Bottom right: DIV 1 cells localised to active area. Left: original border (b) and relatively isolated cells surviving outside recording horizon (c), DIV 40. Scale bars represent 200 μm

### Environment

Simple low cost modifications to Potter rings (Fig. 2) resulted in a significant reduction in water loss (Fig. 3) and a slower decline in array wide spike detection rate (ADSR) vs unmodified rings (Fig. 2). However variability was still observed as a result of variation in ambient environmental humidity; both modified and unmodified showed very little loss of activity at >90% humidity however activity was often reduced to zero at < 70% humidity after 5 hours. Such osmolarity-related loss of activity should considered when performing long experiments in non humidified incubators.
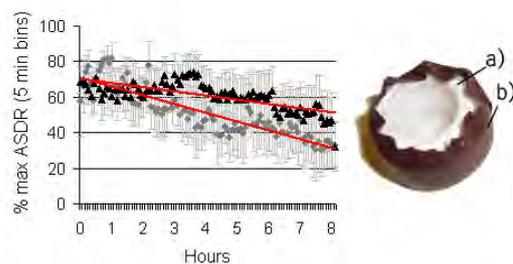


**Fig.2.** Left: Mean decline in ADSR over extended periods of recording due to water loss: modified Potter rings (black triangles) showed a shallower decline activity than unmodified rings (grey circles). Error bars represent SEM, n=3 unmodified, n=7 modified. Right: modified Potter ring showing silicone sealant (a) between 0-ring and tape (b).
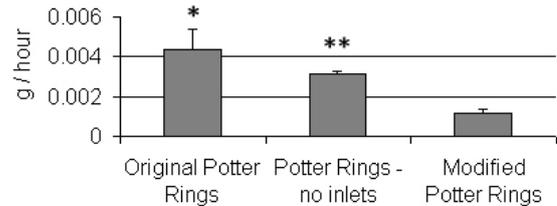


**Fig.3.** Comparison of water loss from standard, purfusionless and modified rings during a 1-hour period. Error bars show SEM. Significance; $*P < 0.01$, $**P < 0.0001$ vs modified rings.

### Movement Induced Activity

In support of Potter's group's findings we provide data that supports the necessity of a rest period of 10 minutes before recording to avoid artificially high activity-induced by movement (Fig. 4).
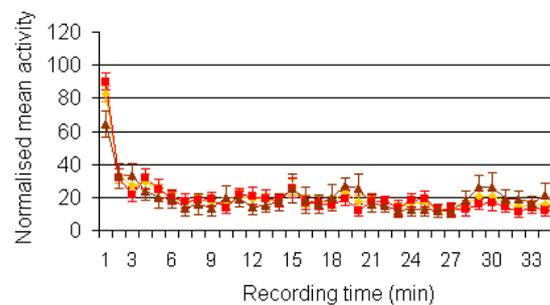


**Fig.4.** Effect of physical movement on activity. Red: bursting activity DIV 10-15. Brown: tonic spiking DIV 6-10. Yellow, combined DIV 6-15. Mean ADSR $2.7 \pm 3.7\%$ during the first minute dropping to $17.6 \pm 3.4\%$ by the 6th minute (Mean ± SEM) which persisted for the remainder of the recording; min: 13.3 % max: 19.3%

## 4   Conclusions

We have described a simple set of easy-to-implement, low cost adaptations and considerations that significantly reduce experimental variability and allow increases to both viable recording time and the information gained about a given neuronal network Stable, repeatable experiments may be achieved using E18 tissue seeded at $1 \times 10^6$ cells/ml restricted to the active area using an inverse template and sealed using adapted Potter rings with due consideration given to environmental humidity.

### References

[1] WAGENAAR, D. A., PINE, J. & POTTER, S. M. (2006) *J Negat Results Biomed,* 5**,** 16.

[2] POTTER, S. M. & DEMARSE, T. B. (2001) *Journal of Neuroscience Methods,* 110**,** 17-24.

[3] WAGENAAR, D. A., PINE, J. & POTTER, S. M. (2006) *BMC Neurosci,* 7**,** 11.

[4] SHAHAF, G., MAROM, S. (2001) Journal of Neuroscience, 21(22), 8782-8788.

# Microneedle Electrode Arrays with Dielectrophoresis Electrodes for Intracellular Recording Applications

Jochen Held[*], Joao Gaspar, Patrick Ruther, and Oliver Paul

Department of Microsystems Engineering (IMTEK), Microsystems Materials Laboratory, University of Freiburg, Germany
* Corresponding author. heldj@imtek.de

This paper reports on the fabrication of microneedle-based electrodes for the electroporation of adherent cells and intracellular recording applications with focus on the study of the influence of external factors in the cell metabolism. Classical methods such as the patch-clamp method have been mostly applied to single cells in suspension. However, in the human body the majority of cells are adherent cells, which motivated the development of the new microneedle-based chip design. The chip comprises an array of 64 microneedles, each combined with two kidney-shaped electrodes to position cells towards the needle electrodes using dielectrophoresis. The array occupies a total area of approximately 1 mm2. The microneedles are fabricated using dry etching of silicon, followed by insulation, two metallization and two passivation layers. The passivation layer is opened at the tip of the needles in order to expose the metal for cell positioning via dielectrophoresis, as well as electroporation and intracellular recording. Various needles with diameters as small as 1 µm and a height smaller than 10 µm were fabricated. Preliminary investigations have shown that heart muscle cells, fibroblasts, and primary cells of mice and rats grow on these structures and can be moved by dielectrophoresis and electroporated using the micro-needle electrodes.

## 1 Introduction

Electrical recording of cell response to an external stimulus in living cell cultures is a fundamental method of uncontested importance for disease studies and drug development. Absolute values of the transmembrane potential $V_m$ between -20 mV and -200 mV are accessible in living cells, depending on organism and cell type [1]. Available classical patch-clamp method used for intracellular measurements of cells in suspension are typically time-consuming and require experienced labor [2]. On the other hand, highly parallel measurements using patch-on-chip systems are limited to the investigation of individual suspended cells [3]. None of these methods use adherent cells in a biological matrix attached to artificial biocompatible materials on which they can firmly grow.

These facts motivated the development of a novel research tool which enables cell positioning close to microneedle-based electrodes, introduction of these electrodes into the cell body using electroporation and respective intracellular recordings. Preliminary investigations have shown that heart muscle cells, fibroblasts, and primary cells of mice and rats can be cultured on the technical surfaces of these electrode arrays and that the cells could successfully be electroporated [1].

## 2 Fabrication

The fabrication process of the microneedle electrodes is schematically shown in Fig. 1. The three-
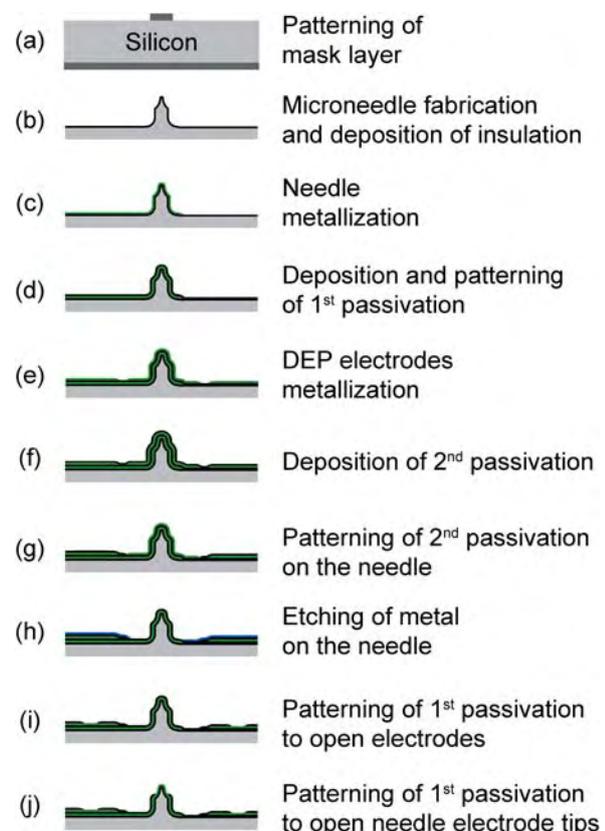


**Fig. 1.** Schematic representation of the stepwise isotropic–anisotropic-isotropic fabrication process of microneedle arrays with DEP electrodes for intracellular recording applications.

dimensional definition of the microneedles comprises
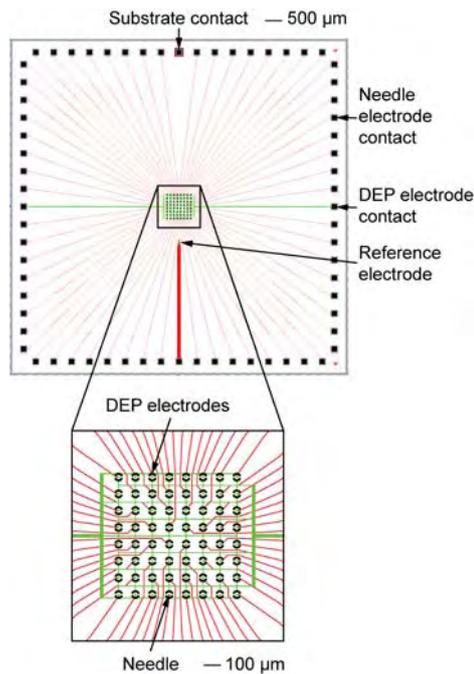
**Fig. 2.** Chip layout of the electrode array used for intracellular recording fabricated using a seven masks process.

three dry etching steps, namely: isotropic, anisotropic and isotropic silicon etching. The first step creates the tip of the microneedle, the anisotropic etching step adjusts its height, and the final isotropic step thins the needle and sharpens its tip {Fig. 1 (b)}. By varying the etch mask diameter and process parameters, different needle profiles can be realized [5]. After dry etching, an insulation layer, a first metal layer {needle metallization, Fig. 1 (c)}, a first passivation layer {Fig. 1 (d)}, a second metal layer {DEP electrodes metallization, Fig. 1 (e)} and a second passivation layer are deposited {Fig. 1 (f)}. The second passivation layer is completely removed around the needle {Fig. 1 (g)}, with the second metal layer used as etch stop. After the second passivation layer has been etched, the DEP electrode metallization is patterned {Fig. 1 (h)} using wet etching. Then the second passivation layer is pattern by RIE to open the electrodes {Fig. 1 (i)}. Finally, the first passivation layer at the needle tip is removed by a photoresist etch-back and subsequent RIE {Fig. 1 (j)}. Figures 2 and 3 schematically show the layout of the fabricated chip an present SEM micrographs of realized microelectrode needles, respectively.
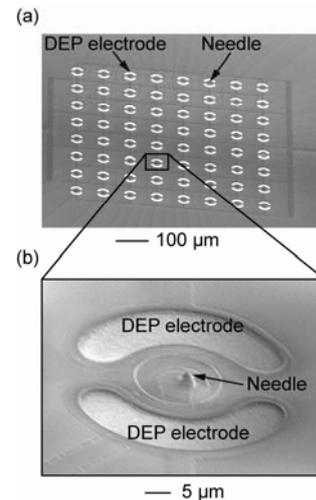


**Fig. 3.** SEM graphs of microneedle array with DEP electrodes; (a) overview and (b) close-up of microneedle with DEP electrodes

## 3 Conclusions

This paper focuses on the fabrication of micro-needle based electrode arrays. Successful electroporation tests with such needle systems have been demonstrated previously [1] and the working principle and effectiveness of the DEP electrodes will be demonstrated by collaboration partners [6].

**References**

[1] D.E. Goldman, "Potential, impedance, and rectification in membranes," J Gen Physiol, 1943, Vol. 27, pp. 37-60.

[2] O.P. Hamil, A. Marty, E. Neher, B. Sakmann, F.J. Sigworth, "Improved patch-clamp techniques for high-resolution current recording from cells and cell-free membranes patches," Eur J Physiol, 1981, Vol. 406, pp. 73-82.

[3] P. van Stiphout, T. Knott, T. Danker, A. Stett, "3D Microfluidic Chip for Automated Patch-Clamping," MST-Kongress, 2005, ISBN 3-8007-2926-1, pp. 435-438.

[4] J. Held, J. Gaspar, P.J. Koester, C. Tautorat, A. Cismak, A. Heilmann, W. Baumann, A. Trautmann, P. Ruther, and O. Paul, "Microneedle arrays for intraceIlular recording applications," Dig. Tech. Papers IEEE MEMS Conf. 2008, pp. 268-271.

[5] J. Held, J. Gaspar, P. Ruther, M. Hagner, A. Cismak, A. Heilmann, O. Paul, "Systematic characterization of DRIE-based fabrication process of silicon microneedles," in Mat. Res. Soc. Symp. Proc, 2007, 1052-DD07-07.

[6] P. J. Koester, C. Tautorat, A. Podssun, J. Gisma, W. Baumann, "Dielectrophoretic positioning of cells with kidney-shaped electrodes for the measurement of intracellular potentials," 6th Int. Meeting on Substrate-Integrated Microelectrodes 2008, in press.

# Functional Analysis Of Cultured Hippocampal Slices With Multi-Transistor Array At High Resolution

Hermann CC[1], Zeitler R[1], Thewes R[2], Fromherz P[1*]

1 Max Planck Institute of Biochemistry, Membrane and Neurophysics, Munich, Germany
2 Infineon Technologies, Corporate Research, Munich, Germany
* Corresponding author. E-mail address: fromherz@biochem.mpg.de

We report on the two-dimensional extracellular recording of organotypic brain slices with a spatial resolution of 7.8μm. The recording site consist of a multi-transistor array (MTA) with 16384 sensor pixels on 1 mm^2. The CMOS chip has a reduced noise of 70 microV rms and a higher sampling rate of 6 kHz as compared to a previous MTA [1]. Stable signals were recorded over several hours. We stimulated at different locations in CA3 and CA1 with conventional electrodes. Detailed maps of evoked field potentials were recorded in several sets of experiments: (i) The fiber volley along the Schaffer collaterals could be traced due to the higher sampling rate and the lower noise. (ii) We observed all steps of the trisynaptic circuit from the mossy fibers to the alveus. The recorded pEPSPs had amplitude of 2-3 mV. (iii) Complex patterns due to interneuron activity were recorded. In particular an outward current occurred at the border of stratum radiatum/lacunosum-moleculare with a sharp onset 4 ms after the pspike in CA1. (iv) The effect of LTP was found to be rather homogeneously distributed along the cornu ammonis, but modulated across the layers. (v) During the postsynaptic field potential we were able to record action potentials of individual neurons.

## References

[1] M. Hutzler, A. Lambacher, et al (2006): High-Resolution Multitransistor Array Recording of Electrical Field Potentials in Culutred Brain Slices. J. Neurphysiol. 96, 1638-1645

# The OptoMEA Platform: a New Tool Combining Local Chemical Stimulation with Distributed Multi-Electrode Array Recordings

Marc Heuschkel[1*], Diego Ghezzi[2], Andrea Menegon[3,4], Alessandra Pedrocchi[2], Sara Matero[2], Solomzi Makohliso[1], Flavia Valtorta[3,4], and Giancarlo Ferrigno[2]

1 Ayanda Biosystems SA, Lausanne, Switzerland
2 Politecnico di Milano, Milano, Italy
3 San Raffaele Scientific Institute and "Vita-Salute" University, Milano, Italy
4 Unit of Molecular Neuroscience, The Italian Institute of Technology, Milano, Italy
* Corresponding author. E-mail address: marc.heuschkel@ayanda-biosys.com

We present a novel OptoMEA platform that combines multisite electrical recording with local chemical stimulation. Applying UV light pulses through an array of optical fibres aligned to transparent indium-tin oxide electrodes of an MEA biochip leads to local compound uncaging (e.g. glutamate), thereby stimulating only the tissue/cells around the electrode vicinity. Experimental results obtained using the OptoMEA platform demonstrate its capability to uncage chemical compounds and to locally stimulate neuronal networks, thus providing a significant improvement in spatial control of chemical stimulation. It is expected that this methodology will be useful in facilitating studies of neuronal network systems, and may also find applications in drug screening.

Micro-Electrode Array (MEA) biochips have been exploited as devices providing distributed information about learning, memory and information processing in tissue slices and cultured neuronal networks. MEA biochips represent a growing technology for the study of the functional activity of neuronal networks providing the possibility to gain information about the spatio-temporal dynamics of the network and to allow recordings of electrical activity over periods of time not compatible with conventional electrodes at several sites in parallel. The presence of large stimulus artefacts and the poorly controlled spread of electrical stimuli in the culture medium limit the applicability of MEA biochips for neuronal stimulation. Although the problem of artefacts has been recently solved using blanking circuits, the problem of electrical signals spreading is inherent to the use of electrical stimulations in a conductive volume. Moreover, due to natural interconnection of neurons in complex networks, electrical stimuli applied to a region of the network may activate neurons of that region and also fibres of passage coming from neurons of other regions. To overcome these limitations, an optical method for local neuronal stimulation has been developed, via the local optical activation of caged compounds.
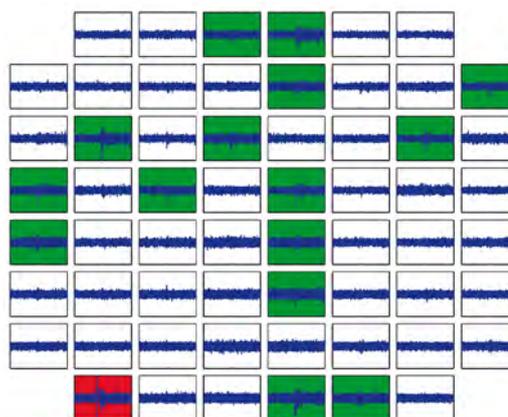


**Fig. 1.** Activity recorded from the entire network. The red box highlights the local stimulation site. Electrodes showing biological response to the local chemical stimulation are highlighted by green boxes.
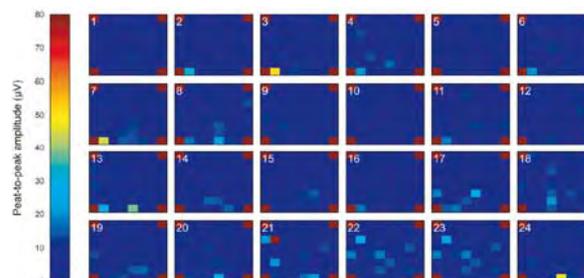


**Fig. 2.** Graphical representation of the spreading of the electrical activity in the network after the optical pulse. Every frame, acquired with a sample rate of 1kHz, represents a measure of the activity at every site. The colour map represents a colour representation of the peak-to-peak amplitude at every recorded site.

We present a novel OptoMEA platform that combines multisite electrical recording with local chemical stimulation. Applying UV light pulses through an array of optical fibres aligned to transparent indium-tin oxide electrodes of an MEA biochip leads to local compound uncaging (e.g. glutamate), thereby stimulating only the tissue/cells around the electrode vicinity. Experimental results obtained using the OptoMEA platform demonstrate its capability to uncage chemical compounds and to locally stimulate neuronal networks, thus providing a significant improvement in spatial control of chemical stimulation. It is expected that this methodology will be useful in facilitating studies of neuronal network systems, and may also find applications in drug screening.

# Laser Micro-Patterning of Neuronal Network on Multi-Electrode Arrays

Chie Hosokawa[1,2*], Suguru N. Kudoh[1], Ai Kiyohara[1,3], Yoichiroh Hosokawa[4], Kazunori Okano[4], Hiroshi Masuhara[4], Takahisa Taguchi[1,3,5]

1 Research Institute for Cell Engineering, National Institute of Advanced Industrial Science and Technology, Osaka, Japan
2 PRESTO, Japan Science and Technology Agency, Saitama, Japan
3 Graduate School of Science, Osaka University, Osaka, Japan
4 Graduate School of Materials Science, Nara Institute of Science and Technology, Nara, Japan
5 Neuroscience Research Institute, National Institute of Advanced Industrial Science and Technology, Tsukuba, Japan
* Corresponding author. E-mail address: chie-hosokawa@aist.go.jp

A femtosecond laser microprocessing technique was utilized for patterning neurons on multi-electrode arrays (MEAs). The neuronal cells cultured on a source substrate were transferred onto an electrode of MEAs in solution by a femtosecond laser-induced impulsive force and a pattern of neuronal cells were formed on the MEAs. The cellular activity of the detached neurons was supported that neurites could be regenerated around the electrodes. The present method is applicable to artificial construction of living neuronal network.

## 1 Introduction

The spatio-temporal structure of electrical activity in neuronal networks has been widely studied using multi-electrode arrays (MEAs) [1]. Resent studies have investigated organization and connectivity in functional network of dissociated neurons, and interaction of biomodeling system [2, 3]. Since dissociated neurons are randomly organized and overlapped with their neurites, MEA analysis of neuronal network is extremely difficult to clarify the spatio-temporal structure of neuronal network. Now, our attention is directed to invent a new approach for artificial control of the neuronal network at the single cell level.

Femtosecond laser pulses make it possible to cut various kinds of biological materials precisely and in three-dimensions due to an effective multiphoton absorption process. In earlier work, we have demonstrated the direct cutting of neuronal network using the femtosecond laser and found that resynchronization gradually occurred as the neurons regenerated although synchrony in the neuronal network decreased after laser cutting [4, 5]. Furthermore, isolation and patterning of animal cells has been performed using an amplified femtosecond laser-induced impulsive force [6, 7]. The precise patterning can be applicable for artificial modification and reconstruction of neuronal network for MEAs analysis. In this work, we present laser micro-patterning method of neurons. The neuronal cells were patterned on the single electrode of MEAs using an impulsive force generated by the amplified femtosecond laser.

## 2 Methods

Hippocampal neurons of Wister rat embryos (embryonic day 18) were prepared by a method reported previously [3, 4]. The dissociated neurons were plated at a density of $2.6 \times 10^5$ cells/cm$^2$ in a poly-L-lysin-coated slide glass, whose area was 12 x 2 mm. Neurons were maintained at 37$^o$C in air containing 5% $CO_2$ and cultured for 1-3 days in Neurobasal medium containing 50 U/ml penicillin, 50 μg/ml streptomycin, 10 μg/ml insulin, and B27 supplement. As a target substrate for micro-patterning, a poly(ethyleneimine)-coated MEA dish (MED-P545A, Alpha MED Sciences), which consisted of 64 planar microelectrodes with area of $50 \times 50$ μm was used. A silicon rubber spacer with a thickness of 50 μm was plated between the sample slide glass and the substrate of the MEAs.
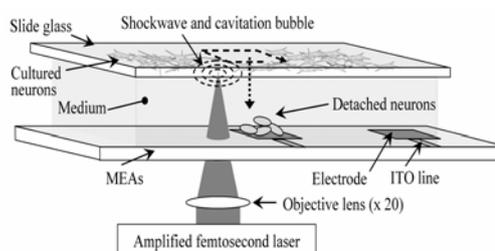


**Fig.1.** Experimental procedure of micro-patterning of neurons on MEAs.

The experimental setup for laser micro-patterning system was described in previous report [7]. Femtosecond laser pulses generated by a regeneratively amplified Ti:sapphire laser system (Hurricane, Spectra-Physics), with a center wavelength 800 nm, pulse du-

ration of 120 fs, and repetition rate of 1 kHz) was introduced into an inverted microscope (IX-71, Olympus) and focused on the neurons over the slide glass by a 20 × objective lens (N. A. 0.46).

## 3 Results and Discussion

The patterning of neurons on MEAs by an amplified femtosecond laser was performed according to procedure in [7]. Briefly, the upside-down sample was set above intact MEAs, as shown in Fig. 1. The femtosecond laser with the pulse energy of 700 nJ/pulse was focused into the neurons on the slide glass as a source substrate and horizontally scanned on it. The neuronal cells had been already cultured on the slide glass for 3 days and formed the network with elongating the neurites (Fig. 2(a)). When the femtosecond laser was irradiated into the neurons on the slide glass, the neuronal cells were cut along the scanning line and disconnected from the surrounding neurons (Fig. 2(b)). By scanning the laser along a square corresponding to the circumference of single electrode in MEAs, the cut area of neurons was detached from a source substrate and fell down on the top of electrodes. The detachment of neurons is due to femtosecond laser-induced impulsive force generated by shockwave and cavitation bubble [7].

As the neuronal cells were detached from the slide glass, they disappeared at the focal point of the CCD camera, as shown in Fig. 2(c). When the camera focus was set on MEAs, the cluster of neuronal cells came on an electrode in MEAs in a few sec (Fig. 2(d)). This indicates that the detached cells are transferred to the electrode and deposited on it, namely, sank in the culture medium due to its gravity. Since the platinum black on the electrode has strong absorption even in the visible and near-infrared regions, it is impossible to manipulate cells on the top of the electrode by the direct laser irradiation such as optical trapping. Thus, by using the femtosecond laser-induced impulsive force, we have succeeded in patterning of neurons on the electrode.

The cells deposited on an electrode through the femtosecond laser patterning changed to the spherical shape, since the neurites of neuronal cells were disrupted in the process. Figures 2 (e) and 2(f) show the deposited cells forming neuronal network on an electrode at 2 days after the laser patterning. As they elongated their neurites on the surrounding of the electrode, it is reasonable to consider that they retained their activity and the neuronal regeneration proceeded within 2 days. It is surprising that the femtosecond laser-induced impulsive force derived from shockwave and cavitation bubble generations scarcely loses the viability of the detached neurons and the deposited neurons proceed the regeneration on the electrode with elongating the neurites after being affected by the

impulsive force. Electrodes, conducting lines, and a substrate in MEAs did not show any etching after the laser irradiation under the present condition. The present patterning method allows us to arrange the isolated cells with single cell resolution in principle [6], while a cluster of the cells was patterned in the present experiment on the electrode.
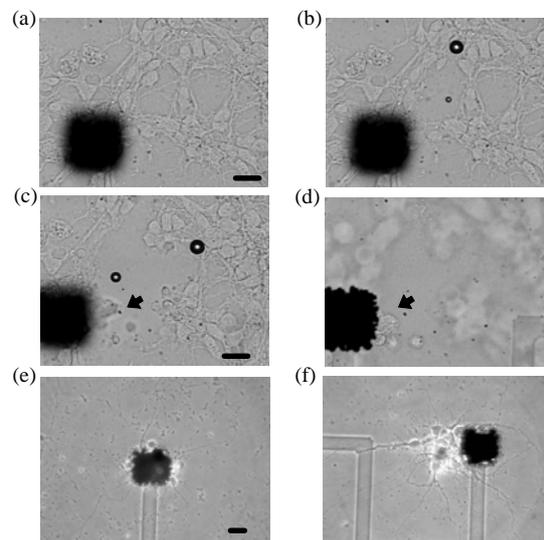


**Fig. 2.** Microphotographs of hippocampal neurons. Neurons cultured for 3 days on a slide glass before the laser irradiation (a) and immediately after the laser irradiation (b). Detached neurons on the slide glass after the laser scanning (c) and ones on an electrode (d) at 19 s later. The black arrow indicates a cluster of detached neurons. (e, f) Representative images of neurons deposited on the electrode at 2 days after the laser patterning. The black square is an electrode with area of 50 × 50 μm and the scale bar is 20 μm.

In conclusion, patterning of neuronal cells on MEAs was performed by using femtosecond laser-induced impulsive force. This femtosecond laser micro-patterning has high potential to study functional connections in the neuronal network.

### Acknowledgement

### References

[1] G. W. Gross, E. Rieske, G. W. Kreutzberg, A. Meyer. (1977): *Neurosci. Lett., 6, 101-106*

[2] J-P. Eckmann, O. Feinerman, L. Gruendlinger, E. Moses, J. Soriano, T. Tlusty. (2007): *Phys. Rep., 449, 54-76*

[3] S. N. Kudoh, C. Hosokawa, A. Kiyohara, T. Taguchi, I. Hayashi. (2007): *J. Robot. Mech., 19, 592-600*

[4] C. Hosokawa, S. N. Kudoh, A. Kiyohara, T. Taguchi. (2008): *NeuroReport, 19, 771-775*

[5] C. Hosokawa, S. N. Kudoh, A. Kiyohara, Y. Hosokawa, K. Okano, H. Masuhara, T. Taguchi. (2008): *Appl. Phys. A, in press*

[6] Y. Hosokawa, J. Takabayashi, S. Miura, C. Shukunami, Y. Hiraki, H. Masuhara. (2004): *Appl. Phys. A, 79, 795-798*

[7] T. Kaji, S. Ito, H. Miyasaka, Y. Hosokawa, H. Masuhara, C. Shukunami, Y. Hiraki. (2007): *Appl. Phys. Lett., 91, 023904-1-3*

# Automated multiparametric 24 Well Neuro Screening system

Florian Ilchmann[1*], Jochen Meyer[2], Volker Lob[1], Chen Zhang[1], Helmut Grothe[1], Bernhard Wolf[1,2]

1 Heinz Nixdorf-Lehrstuhl für Medizinische Elektronik, Technische Universität München, Arcisstr.21, 80290 München, Germany
2 IMETUM - Zentralinstitut für Medizintechnik, Technische Universität München, Boltzmannstr. 11, 85748 Garching, Germany
* Corresponding author. E-mail address: ilchmann@tum.de

Pharmacological research requires screening systems capable of performing parallel analyses to deliver a high quantity of comparable data for statistical evaluation. The NeuroPlate handles 24 separated cell cultures on disposable glass chips with integrated sensors for extracellular cell recordings, i.e. a microelectrode array, a sensor to measure changes in dissolved oxygen and a pH sensor. Together with an automated microscope and a liquid handling robot, the NeuroPlate allows comprehensive studies and convenient handling.

## 1  Biochemical background

The utilization of cultured neuronal networks grown on sensor chips with MEAs for pharmacological studies is a well established method and has yielded extensive knowledge in neurological research. The functional properties of cells can best be examined by intelligent incubation methods that combine two requirements: First to cultivate cells in a quasi in-vivo physiological environment and second to read out their metabolic signals automatically in real time.

However, parallel recordings have always been difficult to achieve due to signal interference and the need for large electronics. The newly introduced system integrates 24 separate cell cultures on the area of a standard multiwell plate together with the detection and amplification circuitry for both metabolic and MEA sensors. In combination with the automated robotic fluidic and sampling system and a microscope, a highly sophisticated system for high-throughput laboratory screenings is presented (Fig. 1 + 3).

## 2  Automated parallel recording of electrophysiological activity and metabolic parameters for up to 24 culture wells

### 2.1 NeuroPlate sensor chip system

The core of the NeuroPlate recording system is comprised of 24 interchangeable glass sensor chips (Fig 2). Each disposable chip includes its own culture well with up to 750 µl of culture medium. Through 32 thin film Au microelectrodes on an area of 1 mm², neuro-electrical signals can be monitored. A special sandwich type coating ensures high impedance of the signal deflecting electrodes.

For measuring the pH-value and the oxygen concentration, optical sensor spots have been integrated. The chip is designed to withstand humidity for up to three month in an incubator for cell growth or extended studies.



**Fig. 1.** NeuroPlate: i) baseplate with inserted sensor chips and electronic module, ii) enlargement of amplifier section, iii) sensor chip
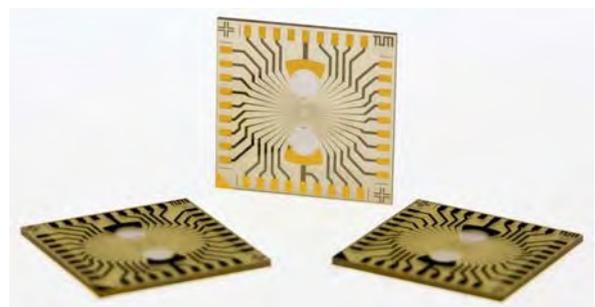


**Fig. 2.** Glass sensor chip without culture vessel

## 2.2 NeuroPlate

The NeuroPlate itself is reusable and can carry up to 24 sensor chips. As the user selects the cell culture chip individually, a huge variety of experimental setups is possible. For example, different cell age groups or tissues can be selected and compared in parallel.

Highly integrated variable gain amplifiers and active filters allow precise amplification of up to 20,000 V/V in a range from 150 Hz to 8 kHz. All 768 (24 wells x 32 electrodes) channels can be addressed individually for different gain factors and customized readout. As the digitizing circuit is part of the NeuroPlate, there is no need for extensive wiring. The digital signal is processed on FPGAs providing digital filters and further signal processing. Special shielding technology is implemented to make low-noise recording possible. A single high-speed USB interface connects the NeuroPlate to an ordinary computer for activity and micro-environmental condition analysis.

## 2.3 Intelligent Microplate Reader for automated experimental setups

Once the NeuroPlate is populated with 24 selected cell culture chips, the plate is inserted into the Intelligent Microplate Reader (IMR) (Fig. 3, right).



**Fig. 3.** NeuroPlate inside the Intelligent Microplate Reader

The concept of the IMR pursues a modular configuration. Consisting of a robotic liquid handling sys-

tem and an automated microscope, long time monitoring of living cell cultures becomes a manageable task. The robot moves between seven user-programmable positions and transports culture media and drug solutions to / from the desired vessels of the NeuroPlate. Besides the described setup, the system can handle standard 24 and 96 microwell plates for different experimental configurations. A fully controlled climatic chamber guarantees life-supporting conditions for extended measurement periods.

In addition to the electrical MEA signal recording, the current configuration allows optical readout of the pH-value and the oxygen concentration. The built-in automated fluorescence microscope enables the user to acquire cell culture images at any time of the experiment, making documentation and interpretation of the results much easier and more reliable.

## 3  Conclusions

Studies conducted utilizing the NeuroPlate and the IMR system showed excellent multiparametric recordings for up to four days with parallel documentation of vital parameters and cell culture images. All parameters are obtained marker-free, so cells do not need to be labelled. No matter if high throughput or redundancy is desired, the presented system is an ideal basis for further studies on metabolism dependent activity in pharmacological research.

**References**

[1]  F. Ilchmann, V. Lob, J. Wiest, B. Wolf (2008): Automated Cell Analytics, Application on Sensor Chips. Screening - trends in drug discovery, Volume 9, 21-23

[2]  F. Ilchmann, V. Lob, B. Wolf (2008): Zell-Chipsysteme - Mikrosensorarrays für die biologische Grundlagenforschung und Diagnostik, GIT Laborfachzeitschrift, Volume 52, 285-260

[3]  V. Lob, T. Geisler, M. Brischwein, J. Ressler, B. Wolf: Multiparametric automated screening system based on a 24-Well-Microplate for living cells and tissues. World Congress on Medical Physics and Biomedical Engineering Seoul, Korea (2006)

[4]  J. Wiest, M. Brischwein, J. Ressler, H. Grothe, B. Wolf: Cellular Assays with Multiparametric Bioelectronic Sensor Chips. CHIMIA, Volume 59, No. 5, 243-246

# Multiparametric NeuroLab recording chamber with MEA and integrated metabolic sensors

Florian Ilchmann[1*], Jochen Meyer[2], Johann Ressler[1], Helmut Grothe[1], Bernhard Wolf[1,2]

1 Heinz Nixdorf-Lehrstuhl für Medizinische Elektronik, Technische Universität München, Arcisstr.21, 80290 München, Germany
2 IMETUM - Zentralinstitut für Medizintechnik, Technische Universität München, Boltzmannstr. 11, 85748 Garching, Germany
* Corresponding author. E-mail address: ilchmann@tum.de

The NeuroLab offers the possibility to handle different metabolic sensors and provides accurate temperature control of both sensor chip and medium. The integrated recording chamber is designed for multiparametric sensor chips without need for external sensors, facilitating process sterility outside laminar flow benches. It contains a glass sensor chip integrating different sensors for extracellular cell recordings, i.e. a microelectrode array, an amperometric sensor to measure changes in dissolved oxygen, a pH sensor and a temperature sensor. By including all necessary circuits for easy computer readout and temperature control, the NeuroLab allows convenient handling.

## 1 Biochemical background

The utilization of cultured neuronal networks grown on sensor chips with MEAs for toxicological studies is a well established method and has yielded extensive knowledge in neurological research. Stable culturing of neuronal networks over long periods of time requires strict control over biochemical parameters of the culture medium. Therefore, the quantitative analysis of micro-environmental conditions and cell metabolic rates is essential in interpreting the changing patterns of electrophysiological activity. Changes in spontaneous spike production and oxygen consumption measured at the site of the network monolayer can provide rapid indications of metabolic disturbances.

## 2 Combined recording of electrophysiological activity and metabolic parameters

### 2.1 NeuroChip

The core of the NeuroLab is a glass sensor chip with an array of 64 microelectrodes recording neuroelectrical signals (Fig. 1). In addition to the obvious benefit for microscope inspection from both sides, glass-based sensor chips with metal oxide pH sensors need no silicon MOS technology. Glass chips are therefore not sensitive to electrostatic discharge, resulting in easier handling precaution. In addition, manufacturing costs are much lower for small quantities of large area chips, making them ideally suited for one-time use.

To monitor the microenvironmental parameters of the living cell culture, three sensors were placed in immediate vicinity of the 8x8 microelectrode array,

resulting in accurate detection of the cellular parameters.

For measuring the pH-value, a ruthenium oxide (RuO2) spot is applied on the surface of the sensor chip. Together with a reference electrode integrated inside the recording chamber, pH measurement of the culture medium is possible. Combined with the use of ultra high impedance amplifiers of the NeuroLab, precise monitoring over the entire lifespan of the cell culture can be carried out.

Changes in the oxygen concentration can be monitored with a planar amperometric oxygen sensor. It consists of three electrodes (working-, quasi-reference- and auxiliary-electrode) without the need for membrane structures. The electrically adjustable working potential is -600 mV, with the option of periodically cleaning the sensor spot without operation interruption through impression of a reversed voltage between the sensor electrodes.
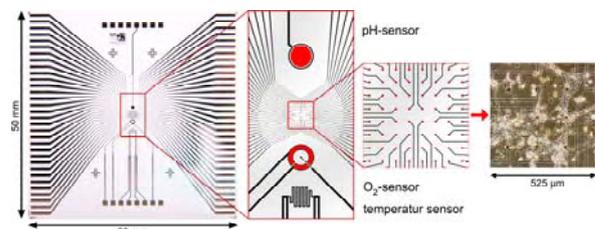


**Fig. 1.** Multiparametric NeuroChip with stepwise magnification

### 2.2 NeuroLab recording chamber

For multiparametric measurements with the sensor chip, a recording chamber called NeuroLab has been developed (Fig. 2). It is made of biocompatible plastics and includes a micro-fluidic system that supports the cell culture with fresh culture media supplied by an external syringe pump. A cut-out underneath the

chip allows various types of microscopic monitoring of the sensor chip at any time.

Within the NeuroLab, all measured parameters are directly amplified, converted and stored until they are read out via USB. High-precision preamplifiers are used to process the neuronal impulses before submitting them to the Plexon digitizing circuitry. For better protection against electromagnetic interferences, the amplifiers are placed inside a shielded enclosure underneath the printed circuit board.
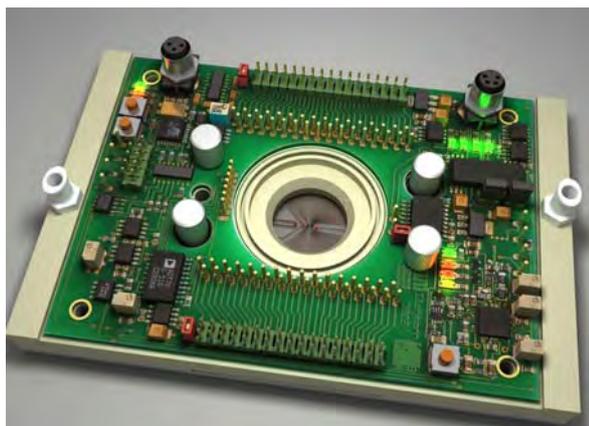


**Fig. 2.** NeuroLab with inserted sensor chip. For better understanding, the picture shows an encapsulated version.

To allow work outside an incubator, a PID controlled heating surrounds the sensor chip and preheats the medium inside the fluidic system next to the cell culture. Several sensors ensure operation within the predefined temperature limits. An optional heated glass plate on top of the culture vessel protects the culture from contamination. All parts in contact with the cell medium can be fully autoclaved, as they can easily be separated from the module carrying the electronic components.

The NeuroLab comes with housing which has been removed for the picture above. It protects the system from spill out of culture media, making it a robust yet high-precision tool for everyday work in any laboratory.

## 2.3 NeuroLab software

For easy interpretation of micro-environmental condition changes, an analysis software has been developed. It is capable of controlling the external life support systems for the cell culture as well as recording all measured parameters. Scalable graphical plots allow both real-time and long-term monitoring.

Using Plexon's MEA Workstation data acquisition software, activity can be easily analyzed (Fig. 3).



**Fig. 3.** Typical recording done with Plexon's MEA Workstation data acquisition software

## 3 Conclusions

Studies conducted utilizing the NeuroLab showed excellent multiparametric recordings for up to nine days with parallel documentation of vital parameters. Currently, the NeuroLab serves for two experimental settings: First, to measure effects of electromagnetic pulses similar to those used in Transcranial Magnetic Stimulation (TMS), and second, to examine neurodegenerative proteins contributing to Alzheimer's and Parkinsons's disease. The measured data provide an ideal basis for further studies on metabolism dependent activity. The compact design allows integration in any laboratory environment.

**References**
[1] F. Ilchmann, V. Lob, J. Wiest, B. Wolf (2008): Automated Cell Analytics, Application on Sensor Chips. Screening - trends in drug discovery, Volume 9, 21-23
[2] F. Ilchmann, V. Lob, B. Wolf (2008): Zell-Chipsysteme - Mikrosensorarrays für die biologische Grundlagenforschung und Diagnostik, GIT Laborfachzeitschrift, Volume 52, 285-260
[3] J. Wiest, M. Brischwein, J. Ressler, H. Grothe, B. Wolf: Cellular Assays with Multiparametric Bioelectronic Sensor Chips. CHIMIA, Volume 59, No. 5, 243-246

# Hardware-Based Real-Time Signal Processing for High-Density MEA Systems

Kilian Imfeld[1*], Luca Berdondini[2], Alessandro Maccione[3], Sergio Martinoia[3], Pierre-André Farine[1], Milena Koudelka-Hep[1]

1 Institute of Microtechnology (IMT), Université de Neuchâtel, Neuchâtel, Switzerland
2 Department of Neuroscience and Brain Technology, Italian Institute of Technology, Genova, Italy
3 Neuroengineering and Bio-nano Technology Group, Department of Biophysical and Electronic Engineering (DIBE), University of Genova, Genova, Italy
* Corresponding author. E-mail address: kilian.imfeld@unine.ch

High-density MEA systems with thousands of electrodes generate high-speed data streams that require large computational power for signal analysis. We adopted a new real-time signal processing strategy based on hardware-implemented functions. In that sense, we demonstrate a Discrete Wavelet Transform (DWT) for neurophysiological signal analysis on a Field Programmable Gate Array (FPGA).

## 1 Introduction

To fully exploit the recordings capabilities of large-scale high-density MEA systems with thousands of electrodes [1], generating data streams in the order of several hundreds of Mbits/s, new strategies of signal processing and data handling have to be implemented. One interesting approach to speed up the analysis of electrophysiological signals is to implement real-time spike detection and analysis in hardware. We presented recently a high-density MEA system architecture allowing to handle and process a large amount of data in real-time [2].

Here we report on further enhancing the real-time signal processing capacity of this system by implementing a Discrete Wavelet Transform (DWT) on an FPGA. We show that the DWT provides an alternative approach for neuronal signal detection and spike analysis of in-vitro electrophysiological cultures recorded with high-density MEAs. As an example, the mapping of activity of a neuronal network using the Wavelet Transform Modulus Maxima (WTMM) is presented.

## 2 DWT and Singularity Detection

The Continuous Wavelet Transform (CWT) is defined as

$$(1) \quad WT(u,s) = \frac{1}{\sqrt{s}} \int_{-\infty}^{\infty} f(t) \cdot \psi^* \left( \frac{t-u}{s} \right) \cdot dt$$

which can be interpreted as the degree of similarity of a signal f(t) and the analyzing wavelet $\psi$ at the translation $u$ and dilation $s$ [3]. For real-time computing, the CWT has to be discretized. The Discrete Wavelet Transform (DWT) of a function f(t) is defined as

$$(2) \quad f(t) = \sum_k c_j(k) \cdot 2^{j/2} \rho(2^j t - k) + \sum_k d_j(k) 2^{j/2} \varphi(2^j t - k)$$

with $c_j$ the approximation coefficients, $d_j$ the detail coefficients, $\rho(t)$ the scaling function and $\varphi(t)$ the wavelet function. The DWT coefficients $c_j$ and $d_j$ at each scale can be obtained by a simple filter bank structure that enables an efficient computation of the wavelet coefficients with O(N) operations. The filter bank structure is therefore well suited for a real-time implementation.

Singularities of a signal often carry important information and are essential for identifying spikes and bursts. They can be found at the points of convergence of the wavelet transform modulus maxima (WTMM) as it was shown in [4]. The WTMM is defined at the point $(u_0, s_0)$ where

$$(3) \quad \frac{\partial \left| WT(f)(u_0, s_0) \right|}{\partial u} = 0$$

and WT(f) corresponds to the CWT of f(t), u is the translation variable and s is the scale variable.

An example of the WTMM can be seen in fig. 1. The retained coefficients are used to localize the individual singularities of the signal. For practical purposes, we bin the number of WTMM coefficient in order to get a measure of mean activity.

## 3 Results

The filter bank (fig.2a) was implemented on an Altera Cyclone FPGA (20 kLogicElements) connected to an external $2^{18}$ x 32 bit SRAM. 255 electrodes make up one frame in the Wavelet Mode. The wavelet coefficients of the next scale are computed during the arrivals of two subsequent frames by a low-pass filter g(n) and a high-pass filter h(n) followed by a subsampling of 2. The individual frame schedule for all levels

is shown in fig. 2b. We opted for a serial architecture of both high-pass and low-pass filter (fig. 2c) and implemented a filter order of 14 (e.g Symlet 7) at a frame rate of 18 kHz. The SRAM is used to store the 14 past samples of each electrode and at each scale of the DWT.

To validate this method, the DWT and the WTMM were implemented in Matlab and used to analyze the recordings performed on dissociated neuronal cultures (23 DIV). Fig. 3 shows an analysis over the entire array of 4096 electrodes. Each image displays the number of WTMM events per bin of 100 frames.
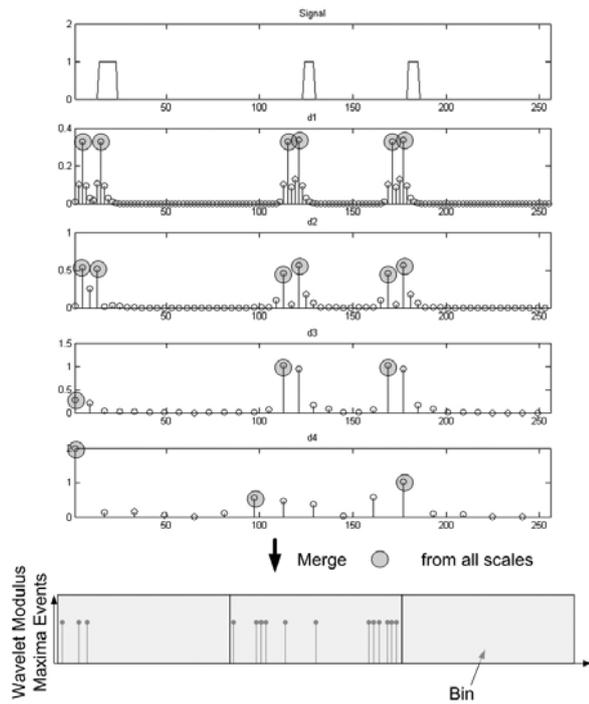


**Fig. 1.** Binning of WTMM across scales

## 4  Conclusion

Outsourcing of data analysis to hardware is an interesting approach to handle the large amount of data from high-density MEA systems. In this work we implemented a real-time DWT of 255 electrodes on the embedded FPGA of our high-density MEA acquisition system. We also showed that spike activity can be detected by the DWT. Combining the DWT with its efficient hardware implementation potentially enables further real-time data processing, from spike sorting and spike classification to high compression of raw data.

### Acknowledgement
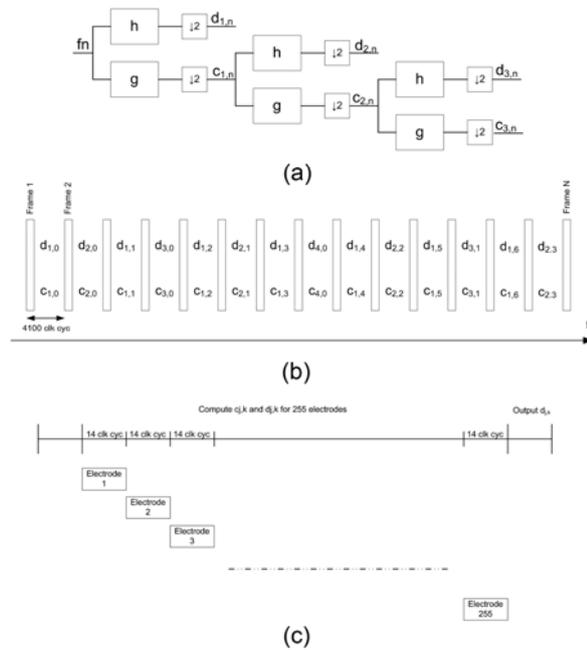
**Fig. 2.** Implemented filter structure (a), frame scheduling (b) and serialized architecture (c)
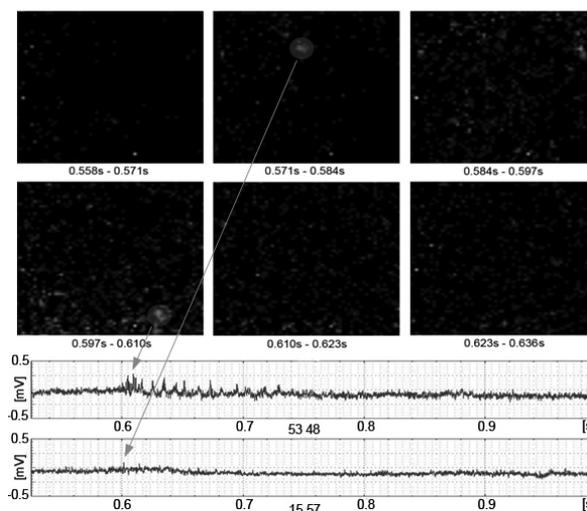


**Fig. 3.** Detected activity patterns of cortical cultures using WTMM. Each activity frame corresponds to a bin that contains 100 temporal frames (top). Two individual active channels, (53, 48) and (15, 57), are displayed (bottom).

### References

[1]  L. Berdondini, et al. (2001): High-density microelectrode arrays for electrophysiological activity imaging of neuronal networks. *ICECS, the 8th IEEE International Conference on Electronics, Circuits and Systems*

[2]  K. Imfeld, et al. (2008): Large-Scale, High-Resolution Data Acquisition System for Extracellular Recording of Electrophysiological Activity. *Accepted in IEEE Trans. Biomed. Eng.*

[3]  S. Mallat (2001): A wavelet tour of signal processing. *New York, Academic Press*

[4]  S. Mallat, et al. (1992): Singularity detection and processing with wavelets. *IEEE Trans. on Information Theory, vol. 38, pp. 617-641*

# Modular MEA-System with Selective Local Agent Injection Utilizing Enhanced Microfluidics

Martin Jäger[1*], Frank Sonntag[2], Niels Schilling[2], Alexandra Bussek[3], Jens Müller[1], Ursula Ravens[3], Rüdiger Poll[1]

1 Dresden University of Technology, Institute of Biomedical Engineering, Germany
2 Fraunhofer Institute for Material and Beam Technology IWS, Dresden, Germany
3 Dresden University of Technology, Department of Pharmacology and Toxicology, Germany
* Corresponding author. E-mail address: martin.jaeger@tu-dresden.de

A new biosensor system for electrophysiological characterization of adherent cells and tissue slices is described. Adapted microfluidics and sensor structures enable selective local injection of agents in defined areas of interest. The sensor system facilitates reproducible comparing measurements of treated and untreated areas of the samples with different sensor types. The main advantage is the direct comparability of the respective samples and references due to identical ambient conditions.

## 1 Introduction

Cell and tissue based biosensors are of growing importance in several fields of research. Two of the main difficulties are the reproducibility of the examinations and the preparation of suitable reference samples [1]. Here a new biosensor system for the electrophysiological characterization of adherent cells and tissue slices is introduced. The technical innovation consists of adapted microfluidics and sensor structures, which enable the selective local injection of agents in defined areas of interest. Certain areas within one sample remain under initial conditions, whereas others can be exposed to the agent under investigation. The modular design of the sensor system facilitates a quick and easy use under laboratory conditions. Standardized multiwell plate dimensions assure the use in commercial mountings (Fig. 1). The electrode design was adapted to the special needs of the carried out electrophysiological studies.



**Fig. 1.** Developed modular sensor system

## 2 Materials and Methods

Alternative methods to conventional lithography were established in sensor production. Polystyrene and glass slides were locally coated using ion beam sputtering technique in combination with laser-cut deposition masks. The electrodes consist of 450 nm indium tin oxide, isolated by a layer of 200 nm titan oxide and 20 nm silicon dioxide. Another sensor type with integrated micro fluidic was developed using low temperature co-fired ceramic (LTCC) multilayer technology. The electrodes consist of 500 nm gold and a ceramic isolation layer. All sensors are manufactured in commercial slide dimensions (Fig. 2).
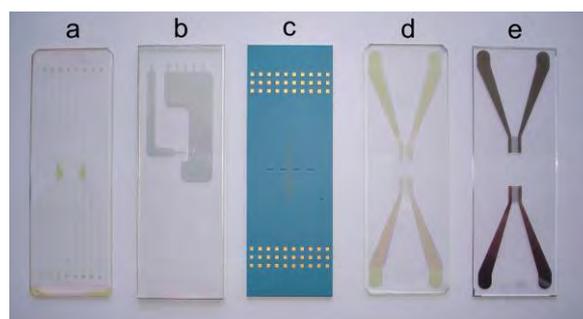


**Fig. 2.** Different types of sensors are manufactored in standardized slide dimensions; **a, b:** micro electrode array sensors; **c:** LTCC-multilayer micro electrode array; **d, e:** impedance sensors

The modular sensor system consists of a casing and a cast polydimethylsiloxane flow chamber with integrated microfluidics. Pharmacological compounds are injected into the main flow near the cells via an injection port. The compounds are flushed by the main flow through a defined part of the chamber [2]. A suitable amplifier for extracellular signals with up to 64 channels has been developed. It can be read out by commercial A/D converters (e.g. the MC_Card from Multi Channel Systems, Reutlingen).

Electrophysiological studies on excitation and propagation under different conditions in isolated mouse atria and neonatal mouse cardiomyocytes (NCM) were carried out with the micro electrode array sensors. All experiments adhered to the guidelines of the German animal welfare regulation.

1–3 days old mice (male C57black6) were used for neonatal cardiomyocytes isolation. The isolation was carried out as previously described [3]. The sensor was coated with fibronectin (20µg/ml PBS) [4]. A concentration-response curve was recorded to investigate the effect of isoprenaline (ISO) on the beating frequency of the NCM culture.

For electrophysiological experiments on spontaneous active mouse atrium male C57black6 mice (mean weight $28.98 \pm 0.7$ g) were used as well. After cervical dislocation, the mice hearts were removed immediately. The heart was placed into ice cold gassed (carbogen) tyrode solution (mmol/L): NaCl 124, $NaH_2PO_4$ 1.25, $NaHCO_3$ 26, KCl 4, $CaCl_2$ 2, $MgCl_2$ 2, Glucose 10 (pH 7.4). Afterwards, the atrium was separated and stored in gassed tyrode solution at room temperature. Field potentials (FP) have been recorded under the influence of ISO ($10^{-6}$ M).

## 3 Results

The application of ISO caused a concentration dependent increase of beating frequency in NCM culture (Fig. 3). After application of 10nM almost the maximum effect was achieved. ISO increased the frequency from $133 \pm 8.5$ (control) to $221.5 \pm 3.75$ (10nM) (n=2).
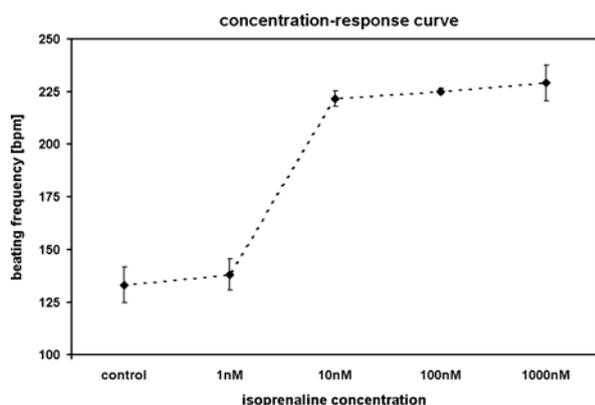


**Fig. 3.** Effect of isoprenaline on the beating frequency of NCM culture (concentration-response curve)

Comparable results were obtained in the spontaneous active mouse atrium experiments. After application of ISO, the beating frequency increased from 100 bpm to approximately 300 bpm (Fig. 4).
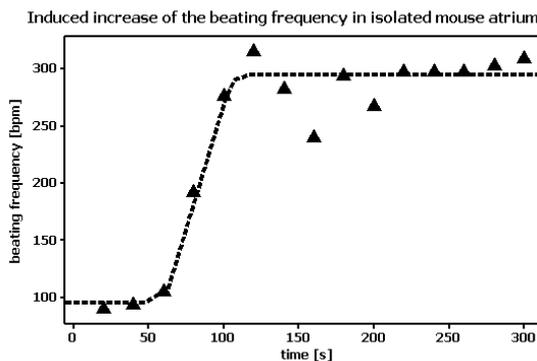


**Fig. 4.** Induced beating frequency increase in isolated mouse atrium

Isoprenaline is known as a β-adrenergic agonist and increases the force of contraction and the beating frequency of the heart. This is demonstrated by the presented results of our experiments.

## 4 Discussion and Conclusion

A new modular sensor system for electrophysiological characterization of adherent cells and tissue slices was developed. By means of enhanced microfluidics with a selective local agent injection and different adapted sensor designs, several approaches to enhance the reliability of cell-based tests were put into practice. Elementary experiments with mouse neonatal ventricular cardiomyocytes and spontaneous active mouse atrium were carried out successfully to validate the sensor system. Extended studies on excitation and propagation in NCM cultures are the focus of prospective investigations. Changes in propagation velocity caused by different sodium channel blockers will be examined.

**References**
[1]  Mohanty, S.P., Kougianos, E., IEEE Potentials 25 (2), 35-40 (2006)
[2]  Schilling, N., Ott, J., Jäger, M., Lipfert, S., Sonntag, F., Dresdner Beiträge zur Sensorik 29, 183 (2007)
[3]  Shiraishi, I. et al, J Mol Cell Cardiol. 29(8), 2041-2052 (1997)
[4]  Borg K. et al, Divelopmantal Biology 104, 86-96 (1984)

# Three-Dimensional Silicon-based MEA with High Spatial Resolution

Neil Joye[*], Alexandre Schmid, Yusuf Leblebici

Microelectronic Systems Laboratory (LSM), Ecole Polytechnique Fédérale de Lausanne (EPFL), Lausanne, Switzerland
* Corresponding author. E-mail address: neil.joye@epfl.ch

A new approach based on three-dimensional tip electrodes has been developed as a way to increase the electrical coupling between the neural cells and the individual sensors in a microelectrode array (MEA). With respect to standard planar electrodes, the electrical coupling between an electrode and a neural cell is improved as benefit of an increased cell-electrode contact area. Thus using a custom fabrication process, three-dimensional MEAs exhibiting a higher spatial resolution than classical integrated MEA systems have been manufactured on a silicon wafer. These MEAs have an electrode diameter of 3-4 $\mu$m, a height of 1.75 $\mu$m, and a pitch dimension of 5-6 $\mu$m. *In-vitro* electrical measurements and electrophysiological experiments using standard planar electrodes as well as the proposed three-dimension electrodes are currently performed.

## 1 Introduction

Microelectrode arrays have become an essential tool both in fundamental and applied electrophysiology research, enabling stepping from the observation of the electrical behaviour of single neurons toward the simultaneous analysis of populations of neural cells [1]. However, one of the main limitations of MEAs is related to their low spatial resolution. Currently, MEAs have typical inter-electrode spacings of 18-100 $\mu$m [2]-[5]. These dimensions are much larger than the 10 $\mu$m typical size of prenatal hippocampal rat cells used in *in-vitro* electrophysiological experiments. Therefore, a new approach based on three-dimensional electrodes has been developed as a way to increase the electrical coupling between the cells and the individual sensors. Using this technique, MEAs with higher spatial resolution are fabricated, thus eluding the under-sampling limitation of classical MEAs.

## 2 Three-dimensional Tip Electrode Array

Arrays of three-dimensional tip electrodes with a height of 1-2 $\mu$m and a pitch of 4-6 $\mu$m have been considered in order to guarantee that every neuron is in electrical contact with several electrodes. The cell membrane is expected to adapt to the surface topology as depicted in Fig. 1. In this case, the electrical coupling between an electrode and a neuron is improved as a benefit of an increased cell-electrode contact area.
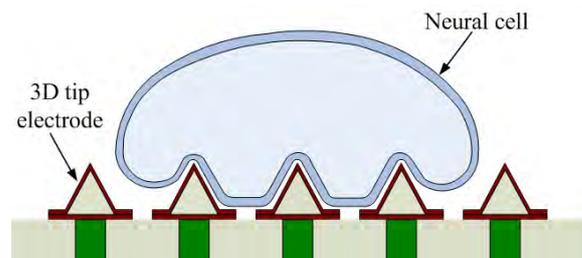


**Fig. 1.** Conceptual cross-section of a neural cell lying on the tips of a three-dimensional MEA with the attached membrane adapting to the surface topology.

The fabrication process for the three-dimensional tip electrode array has been established as follows. First, a 1.75 $\mu$m thick layer of Silicon Dioxide is sputtered on top of Platinum planar electrodes, as depicted in Fig. 2(a). The thickness of this layer sets the height of the electrodes. Then an isotropic etching in BHF is performed in order to create the tips, as depicted in Fig. 2(b). The Silicon Nitride layer is used as an etching stop. Metallization of the electrodes is conducted in a further step by evaporating a 10 nm thick Titanium adhesion layer, followed by a 100 nm thick Platinum layer. Finally, a 300 nm thick Silicon Dioxide passivation layer is sputtered on the surface of the chip. The final cross section of the MEA is depicted in Fig. 2(c).
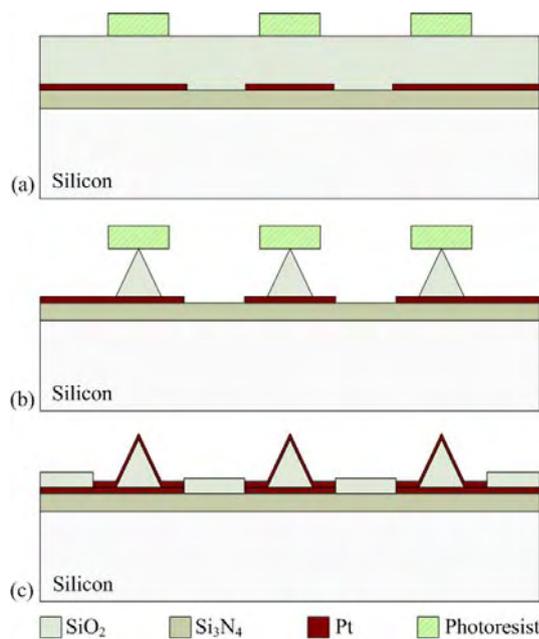
**Fig. 2.** Schematic view of the cross-section of selected steps of the three-dimensional tip electrodes fabrication process.

## 3 Results

Three-dimensional MEAs with an electrode diameter of 3-4 μm, a height of 1.75 μm, and a pitch dimension of 5-6 μm have been manufactured. The minimum tip diameter that has been obtained is approximately 0.5 μm, as depicted in Fig. 3. Ongoing experiments are conducted to determine whether this dimension is satisfactory. Nevertheless, work is already being performed in order to sharpen these tips.
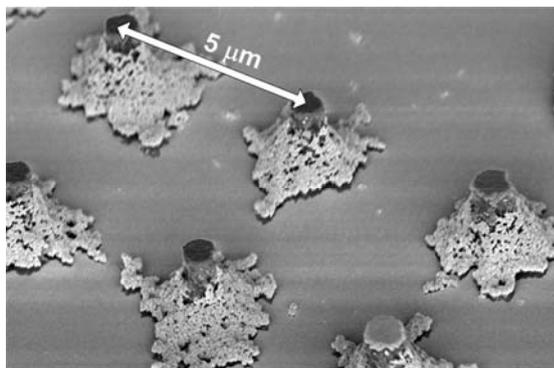


**Fig. 3.** SEM photograph of a three-dimensional tip MEA with a tip height of 1.75 μm, a pitch of 5 μm, and a tip size of around 0.5 μm.

Finally, the MEAs have been packaged as described in Fig. 4 and Fig. 5. In-vitro electrical measurements and electrophysiological experiments using standard planar electrodes as well as the proposed three-dimensional electrodes are currently performed. The results are expected to confirm the superiority of the three-dimensional MEAs in terms of electrical coupling, as numerical simulations carried out using a finite element solver have established.
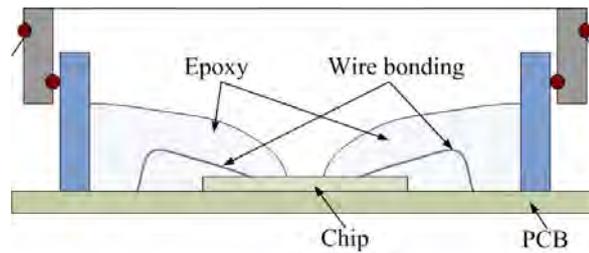


**Fig. 4.** Schematic cross-section of the final MEA system.
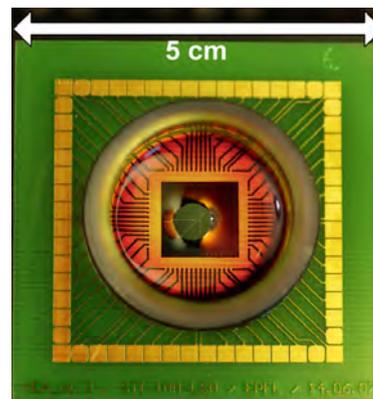


**Fig. 5.** Packaged MEA. The system is fully compatible with commercial signal acquisition system from multi Channel Systems MCS GmbH (Reutlingen, Germany).

## 4 Conclusion

A new approach based on three-dimensional tip MEAs has been developed as a way to increase the electrical coupling between the neurons and the electrodes. Moreover, the fabrication of very dense arrays of microelectrodes has been demonstrated as a post-fabrication step to be performed on standard CMOS ICs. Electrical characterization is currently performed.

**References**

[1] S. Marom and G. Shahaf (2002): Development, learning and memory in large random networks of cortical neurons: lessons beyond anatomy. *Quarterly Reviews of Biophysics, 35, 63-87.*

[2] U. Frey, F. Heer, R. Pedron, S. Hafizovic, F. Greve, J. Sedivy, K-U. Kirstein, and A. Hierlemann (2007): An 11k-electrode 126-channel high-density microelectrode array to interact with electrogenic cells. *Proceedings of IEEE ISSCC, 153-593.*

[3] L. Berdondini, P. D. van der Wal, O. Guenat, N. F. de Rooij, M. Koudelka-Hep, P. Seitz, R. Kaufmann, P. Metzler, N. Blanc, and S. Rohr (2005): High-density electrode array for imaging in vitro electrophysiological activity. *Biosensors and Bioelectronics, 21, 167-174.*

[4] Y. Jimbo, N. Kasai, K. Torimitsu, T. Tateno, and H. P. C. Robinson (2003): A system for MEA-based multisite stimulation. *IEEE Transactions on Biomedical Engineering, 50, 241-248.*

Technology

[5]   Multi Channel Systems MCS GmbH,
      http://www.multichannelsystems.com

# In-vitro compartmented neurofluidic system for studying neural networks

Thirukumaran T. Kanagasabapathi[1], Ke Wang[1], Ger J.A. Ramakers[2] and Michel M.J. Decré[1]

1 Healthcare Devices and Instrumentation Department, Philips Research Laboratories Eindhoven, High Tech Campus 4(01), 5656 AE Eindhoven, The Netherlands.
2 Netherlands Institute for Neurosciences, 1105 AZ Amsterdam, The Netherlands.

In-vitro neural network models are promising tools for gaining insight into many chronic brain diseases and their treatment options. As a first step to build such in-vitro neural network models, we demonstrate a dual compartment neurofluidic system with inter-connected microchannels to connect neurons from their respective compartments on a planar microelectrode arrays (MEAs). Design and development of the compartmented microfluidic device for neuronal culture, axonal growth through microchannels, preliminary MEA recordings of network activity in the compartments and challenges involved in sustaining long-term cultures are presented in this work.

## 1  Introduction

Dissociated primary neuronal cell cultures provide easy access to individual neurons for electrophysiological recording, electrical/chemical stimulation and possibly a better understanding of the neuronal network. *In vivo* access to neuronal networks relevant for brain diseases is severely restricted, and organotypic brain slices are unable to capture enough of the three-dimensional pathways (e.g. Parkinson's disease motor pathways [1]).

On the other hand, microfluidic devices show promise in the study of cell cultures and constructing *in vitro* models that more accurately reproduce the natural environment of neurons [2-4]. Such techniques will allow to better control the in-vitro assembly of neuronal networks involved in the brain or neurodegenerative diseases. In this work, soft lithographic techniques are used to fabricate Polydimethylsiloxane (PDMS) based multi-compartmented devices that allow neurons to grow for few months and form controlled neural networks. Microelectrode arrays (MEAs) were integrated in the device to record and stimulate long-term cultured neuronal networks.

We present long term neuronal cell culture in PDMS based dual-compartment microfluidic devices attached to the MEAs. Neural network formation through the microchannels connecting the compartments are demonstrated and preliminary results of electrophysiological recording from the compartmented cultures are presented. Improvements to the existing microfluidic system used for neuronal cell culture and protocols for successfully maintaining cultures of dissociated rat cortical neurons in such devices are discussed. Particular attention is devoted to characterize inter-compartment growth and connectivity. In the future we envisage demonstrating the effects of electrical and chemical stimulation in the compartmented network and culturing several neuron types belonging to the basal ganglia motor pathways involved in Parkinson's disease.

## 2  Materials and Methods

### 2.1 Device Preparation

Polydimethylsiloxane (PDMS) stamps were produced by conventional soft lithography techniques reported elsewhere [5]. As shown in the figure (Fig. 1), the resultant PDMS device has 2 microfluidic compartments ('A' & 'B') of 100μm height and 8mm length interconnected with microchannels of 10μm height, 3μm width and 150μm in length. The microchannels prevent the movement of cells between compartments [6]. These fabricated PDMS stamps were rinsed thoroughly in an ultrasonic bath, stored in Milli-Q water for 24h and decontaminated in a 70% ethanol bath for 1 min. The PDMS device was then sterilized in a dry oven at 165° C for 5 min and placed on cover-slips with the microchannels facing downwards for oxygen-plasma treatment. This treatment renders the microfluidic compartment and the microchannels hydrophilic, while preserving hydrophobicity of the contact surface, thereby preventing leakage. The PDMS devices were then aligned and bonded to planar Micro Electro Arrays (MEAs) sterilized in vacuum oven and coated overnight with a solution of Polyethylenimine (PEI) (Sigma-Aldrich, stock solution at 50% w/v in water, Ca. No.P3143) at a concentration of 40 μg/ml in Sterile Tissue Grade water (GIBCO, Invitrogen, Ca. No. 15230).
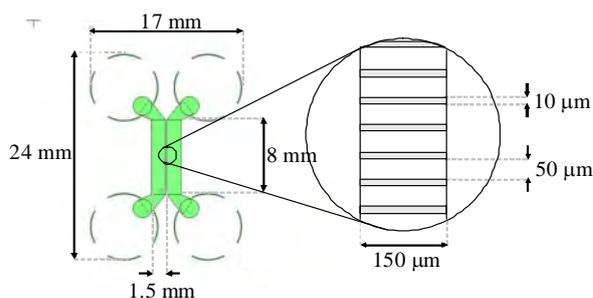
**Fig. 1.** Schematic representation of the PDMS based microfluidic device used for the in-vitro neural network studies.

## 2.2 Cell Culture and Platting

Primary cultures of Rat embryonic cortical neurons were prepared by Trypsine digestion of day-18 embryonic rat whole cortices, as per the approved protocols for the care and use of lab animals in the Netherlands. The dissociated cells were cultured in neurobasal medium supplemented with 1% fresh, stable L-Glutamine (GlutaMAX™ 100x, GIBCO, Invitrogen, Ca. No. 35050-038), 1% Penicillin-Streptomycin Solution (GIBCO, Invitrogen, Ca. No. 15140-122), 2% B27 Supplement™ (GIBCO, Invitrogen, 17504-044) and 10nM Triiodo thyronine. The cultured cells were plated on PEI coated MEAs substrates at a concentration of ~ 25 x $10^6$ cells / ml. The devices were then incubated in a humidified incubator at 37° C supplied with 5% $CO_2$. The culture is checked at regular intervals and required quantity of medium was added to compensate for the evaporation losses.
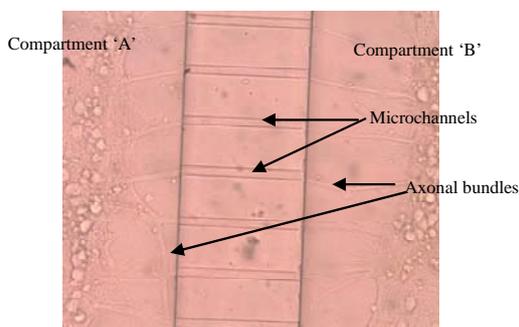


**Fig. 2.** Formation of axonal bundles through the microchannels. Axonal bundles navigate through the 10μm wide microchannels connecting cells between compartments 'A' and 'B'.

## 3 Results and Discussion

The cultured cells were actively networked within their respective compartments by DIV 3 and eventually connected with cells in the adjacent compartment through the microchannels as shown in Fig. 2. MEA60-1-1060 recording system (Multi Channel Systems, Ge) for inverted microscope was used for data acquisition from the cultured neuron network in the devices. Cultures were observed to be electrically active by DIV 13 and recordings were continued at regular intervals for 3 weeks until an infection affected the culture during a recording procedure. The raw data from the recording system was sampled at 25 kHz and analyzed using custom built MatLab programs. Spontaneous activity of one such culture is shown in Fig.3. In the figure, each dot represents an action potential recorded by one of the multi-electrode array channels.

Although the task is challenging, we are convinced that multi-compartmental neural networks on devices will prove to be a valuable tool in understanding neural network pathways and the intricacies involved in network formation. The preliminary results reported in this work are encouraging towards achieving this goal.
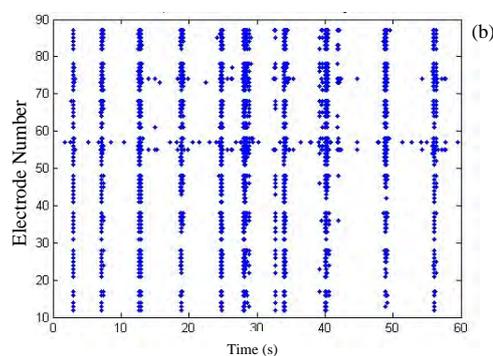


**Fig. 3.** Spontaneous activity of a culture on DIV 14 and DIV 20 (60s time interval) (a) Electrode activity on DIV 14, (b) Electrode activity on DIV 20

**References**

[1] Olanow, C.W., The scientific basis for the current treatment of Parkinson's disease. Annual Review of Medicine, 2004. 55: p. 41-60.
[2] Dittrich, P.S., K. Tachikawa, and A. Manz, Micro total analysis systems. Latest advancements and trends. Analytical Chemistry, 2006. 78(12): p. 3887-3907.
[3] Thiebaud, P., et al., PDMS device for patterned application of microfluids to neuronal cells arranged by microcontact printing. Biosensors & Bioelectronics, 2002. 17(1-2): p. 87-93.
[4] Berdondini, L., et al., A microelectrode array (MEA) integrated with clustering structures for investigating in vitro neurodynamics in confined interconnected sub-populations of neurons. Sensors and Actuators B-Chemical, 2006. 114(1): p. 530-541.
[5] Rhee, S.W., et al., Patterned cell culture inside microfluidic devices. Lab on a Chip, 2005. 5(1): p. 102-107.
[6] Taylor, A.M., et al., Microfluidic multicompartment device for neuroscience research. Langmuir, 2003. 19(5): p. 1551-1556

# Modifying metal electrodes with carbon nanotubes

Edward Keefer[1*], Guenter W. Gross[2]

1 UTSW Medical School, USA
2 University of North Texas
* Corresponding author. E-mail address: edward.keefer@utsouthwestern.edu

The quality of neuronal recording is heavily dependent upon the type electrode used; an electrode designed to record single-unit firing is generally less than optimal for passing electrical stimulation current. Similarly, an efficient stimulating electrode usually does not have the selectivity to record spiking neurons.

Neural prosthetics are currently used in treating a variety of pathologies such as Parkinson disease, hearing loss, macular degeneration, depression, chronic pain, and limb amputation. These techniques will ultimately be widely adopted only if bi-directional neuron-electrode interfaces can be established and maintained for long periods of time.

Sharpened metal microwires have been the primary tool of the electrophysiologist for at least 50 years; attempts to modify and improve the metal electrode surface started shortly thereafter. Nearly all modifications aim to lower the electrode impedance, either to enhance electrode sensitivity, or to increase the amount of electrical charge a given electrode can safely pass when used for stimulation. Recently, carbon nanotubes (CNTs) have been used to construct electrodes for a variety of purposes; batteries, electrochemical detection, supercapacitors, and neural interfaces among them. CNTs are extremely conductive electrically and have intrinsically large surface areas, implying that a CNT-coated electrode will have low impedance and large capacitance.

We devised techniques for coating metal electrodes with CNTs, and tested the function of the CNT-coated electrodes for both recording and stimulating neurons in three different preparations; multi-electrode arrays, the motor cortex of anesthetized rats, and area V4 of rhesus macaques performing a visual task. We used MEAs produced by Guenter Gross at the Center for Network Neuroscience in Denton, TX to develop the coating methodology, and to test the recording and stimulus efficacy of CNT-coated electrodes. MEAs proved to be ideal platforms for such research, allowing different coating methods to be tested on adjacent electrodes, and the direct comparison of CNT-coated to non-coated electrode recording and stimulating performance with the same neuronal network.

CNT coatings lowered the impedance of MEA electrodes by nearly 100-fold at 1 kHz, and increased the charge transfer capacity by up to 1600-fold when applied in combination with conductive polymers. CNT-coated electrodes recorded 4 times more single units than controls, and the threshold for neuronal activation using both voltage and current-controlled stimulation was decreased by 80% with CNT deposition. Electrodes coated with CNTs were broad-band neuronal sensors, able to simultaneously record field potentials, multi-unit activity and single units without the use of noise filters.

These findings have direct application in the neural prosthetic field, where the ability to both record and stimulate neurons may be essential. Neuronal physiology research will also be facilitated by these versatile tools.

# A New Glass Chip System Acquiring Electric Activity and Physiological Parameters of Stem Cell Derived Cells

Philipp Julian Koester, Sebastian Buehler, Carsten Tautorat, Jan Sakowski, René Schrott, Werner Baumann, and Jan Gimsa*

University of Rostock, Chair of Biophysics, Rostock, Germany
* Corresponding author. E-mail: jan.gimsa@uni-rostock.de

The EU chemical policy REACH regulates the registration, evaluation and authorization of chemicals. Investigations on the effects of neurotoxic and developmental-neurotoxic substances are required by European and US-American test guidelines. However, until now these tests are based on animal experiments contradicting society claims to abolish animal experiments and to implement the 3R-principle. The acquisition of electrophysiological signals of cultivated nerve or muscle cells differentiated from stem cells on a glass chip is a novel method for the reduction of animal experiments. Our Modular Glass Chip System (MOGS) has the potential to become a compact and versatile test system for producers of pharmaceutical, HCS applications as well as bioanalytical substances.

## 1 Introduction

A new EU chemical policy for the registration, evaluation and authorization of chemicals (REACH) has been effective since June 2007. Further, European and US-American test guidelines require investigations on the effects of neurotoxic and developmental-neurotoxic substances. However, these tests are still based on animal experiments, contradicting the 3R-principle and society claims to abolish animal experiments. Our *Modular Glass Chip System* (MOGS) may become a compact and versatile tool for producers of pharmaceuticals, high content screening applications as well as for the bio-analysis of substances. MOGS allows for the acquisition of electrophysiological signals of cultivated nerve or muscle cells [1]. MOGS can also be used in basic scientific research as a test system for the differentiation of stem cells, to correlate the electric activity and structure of neuronal networks or e.g. to test methods of neuronal regeneration to fight degenerative diseases.

## 2 Material and methods

The main sensor of MOGS is an array of 52 micro-electrodes for the detection of electric cell activity. An integrated Interdigitated Electrode Structure (IDES) allows for the impedance detection of cell adhesion as a measure for the viability of adherently growing cells. A temperature sensor is integrated in direct proximity to the cells. A thermostatic system regulates the chip temperature. State-of-the-art fiberglass sensors (Presens GmbH, Germany) for the measurement

of metabolic parameters will be integrated in the near future. In a flow-through cap allowing for the measurement of pH and O2, two modified Luer-adapters (MINSTAC, The Lee Company, USA; Fig.1) are integrated allowing for medium exchange.



**Fig. 1.** Center: Glass chip with platinum coated glass ring. Right: Flow-through cap with in- and outflow connectors.
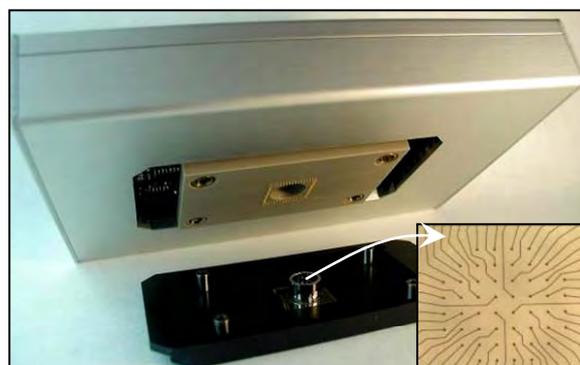


**Fig. 2.** Open MOGS. Zoom: MEA on glass chip.

The use of stem cells will improve the sustainability by avoiding animal experiments (stem cells) or reducing the number of required donor organisms for primary cells. The differentiation of mouse stem cells

into electrically active neurons is currently in progress.

## 3  Results

Details of the glass chip are shown in Figs. 1 and 2. Preliminary experimental results are shown in figures 3-6. Primary cortex neurons build branched networks on the glass chip (Fig.3). IDES, temperature sensor and the logo are overgrown with primary neurons (Fig.4). The cell culture protocol is used after [3]. Figs. 5 and 6 demonstrate the success of our stem cell protocol. Fluorescent staining of differentiated stem cells (murine stem cell line D3) with a neuronal marker (beta-3-tubulin, green stain) is a fundamental step towards stem cell derived neurons. However, the stem cell differentiation protocol must further be optimized to an electrical activity of the derived neuronal networks. Up to now, we were not successful in inducing an electrical activity in the stem cell derived neuronal network.
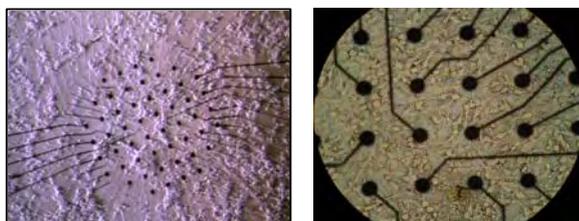


**Fig. 3.** Left: primary mouse cortex cells overgrowing the chip surface and building a branched neuronal network, 4x. Right: zoom of the neuronal network spanning the MEA electrodes, 20x.



**Fig. 4.** Primary cortex cells overgrowing different chip structures (IDES, temperature sensor, logo).



**Fig. 5.** Stem cell derived neurons cells overgrowing the chip surface. Left: IDES. Center: MEA electrodes. Right: Si3N4-surface.
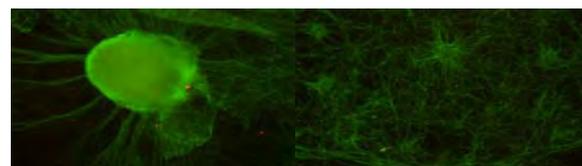


**Fig. 6.** Stem cell derived neuron culture. Left: neuronal network. Right: neurosphere. Green = beta-3-tubulin-staining.

## 4  Outlook

In the future, we will apply MOGS in basic scientific research as a test system for the differentiation of stem cells, to correlate the electric activity and structure of neuronal networks differentiated from primary and stem cells, to test methods of neuronal regeneration, to fight degenerative diseases, to improve the signal characteristics for the stimulation of neurons, etc. In summary, MOGS is a very versatile system, providing optimal culture conditions for primary and stem cells for days until months in combination with the microscopic observability (cp. [2]). In comparison to other commercial systems, MOGS has a significantly smaller cell culture area. The system can be applied for testing the toxicity of substances in the clinical, environment, and food areas, as well as in the development and analysis of chemical substances, e.g. fertilizers, food, household chemicals and consumer goods.

**References**

[1] S. Illesa, W. Fleischer, M. Sieblera, H.-P. Hartung, and M. Dihné (2007): Development and pharmacological modulation of embryonic stem cell-derived neuronal network activity. *doi 10.1016/j.expneurol.2007.05.020*

[2] A. Stett, U. Egert, E. Guenther, F. Hofmann, T. Meyer, W. Nisch, and H. Haemmerle (2003): Biological application of microelectrode arrays in drug discovery and basic research. *Anal Bioanal Chem  377, 486–495*

[3] P. Koester, J. Sakowski, W. Baumann, H.-W. Glock, J. Gimsa (2007): A new exposure system for the in vitro detection of GHz field effects on neuronal networks. *Bioelectrochem, 70, 1, 104-114*

# Dielectrophoretic Positioning of Cells for the Measurement of intracellular Potentials using Kidney-Shaped Electrodes

Philipp Julian Koester[1], Carsten Tautorat[1], Angela Podssun[1], Jan Gimsa[1], Ludwig Jonas[2], and Werner Baumann[1*]

[1] University of Rostock, Chair of Biophysics, Rostock, Germany

[2] University of Rostock, Electron Microscopy Center, Medical Faculty, Rostock, Germany

* Corresponding author. E-mail: werner.baumann@uni-rostock.de

The combination of cell culture with new technical measuring principles leads to a number of problems, e.g. the positioning of specific cells at sites of interest, such as micro-electrodes. Additionally, a high number of cells hinder the measurement of single cell signals. Both problems can be tackled combining active dielectrophoretic positioning of cells at desired chip locations and by long-term fixation of cells by biopolymer coatings.

## 1 Introduction

The use of *dielectrophoresis (DP)* [1] as well as cell attracting polymers [2, 3] can help positioning single cells at specific sites of a biochip. DP forces can be punctually applied with micro-needle electrodes leading to very high AC field strengths at the tip of the electrode and cell stress (for details, see [5]). To reduce cell stress, specific DP-electrodes were integrated. We present a first application of DP in a new silicon chip with an array of micro-needle electrodes designed for the measurement of intracellular potentials [4-8]. The additional DP-electrodes are kidney-shaped and located around the measuring needle electrodes. The kidney-shaped electrodes are designated for rough cell positioning. For the final allocation smaller field strength are applied between the micro-needle and the kidney-shaped electrodes.

## 2 Material and methods

128 additional kidney-shaped DP-electrodes were integrated into a silicon sensor chip containing 64 *micro-structured needle electrodes (MNE)* [5, 6]. Two DP-electrodes confine each measuring MNE. The DP-electrode distance is 30 μm [7]. The measuring area (1 mm$^2$) was patterned with the cell-adhesives poly-l-lysine and laminin. Fig. 1 shows a microscopic image of the MEA. The setup was microscopically controlled and cooled with freezer packs to approx. 12 °C. No neuronal cell survival was observed without cooling the setup. Cell positioning as well as cell adhesion was subsequently examined by SEM. In our future chips, defined patterns of adhesive molecules will guide the cell growth and inhibit migration of the positioned cells (Fig.2).
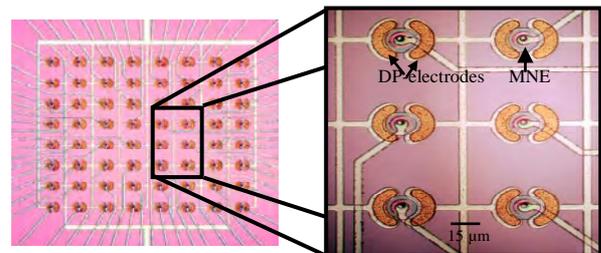


**Fig. 1.** MNE-chip with kidney-shaped DP-electrodes.
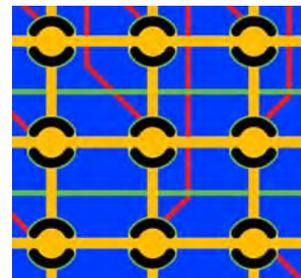


**Fig. 2.** CAD sketch of defined cell-attractive and cell-repellent polymer stripes on the chip surface. Blue: cell repelling layer, yellow: cell adhesive layer, black: DP-electrodes, red & green: conductors.

## 3 Results

Primary cells of prenatal (glia, neurons) and postnatal mice (data not shown), L929 tumor cells and human skin fibroblasts (data not shown) can be positioned in the proximity of the MNE and may adhere. However, cells tend to migrate after some time (see Fig.3). Different DP-electrode arrangements were tested (cp. Figs.3&4).

**Prenatal mouse neurons after DP-allocation and after 2 days**
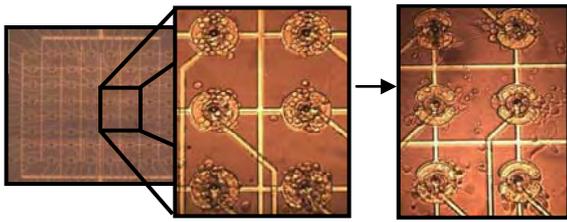


**L929 tumor cells**
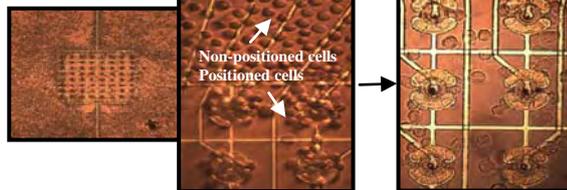


**Fig. 3.** Attraction of different cell types by the DP-electrodes.
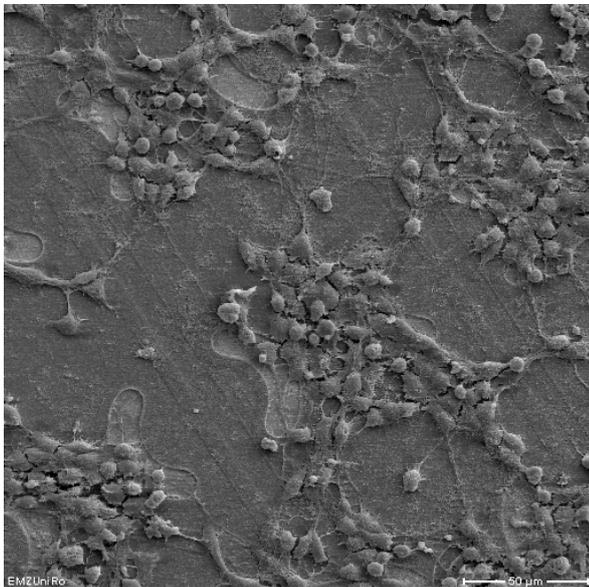


**Fig. 4.** SEM image of DP-allocated primary neurons of frontal cortex (DIV 1, mouse, E15) on silicon chip MEA.

## 4  Outlook

The presented method allows for direct allocation of different cell types by DP-allocation with kidney-shaped electrodes. Allocation is a prerequisite for the exact and reproducible Local Micro-Invasive Needle Electroporation (LOMINE) [4-8], opening new ways for intracellular measurement and bioanalytics of pharmacological or xenobiotical compounds with adherently growing cells in culture. Our new chips allow for fast and parallel intracellular potential measurements of 64 MNE. The silicon surface of our new chip will be polymer-pattern coated providing additional cell guiding structures [2, 3]. Our aim is to prevent cells from migrating away from the electrodes and to increase the probability of a successful positioning on the MNEs.

## 5  Acknowledgement

## 6  References

[1]  J. Gimsa (2001): Characterization of particles and biological cells by AC-electrokinetics, in: A.V. Delgado (ed.) Interfacial Electrokinetics and Electrophoresis. Marcel Dekker Inc., New York, 369-400

[2]  G. Baaken, M. Sondermann, O. Prucker, J.C. Behrends, and J. Rühe (2007): Planares Patch-Clamping für Hochdurchsatz-Untersuchungen an biologischen Membrankanälen, in: Proceedings Mikrosystemtechnik Kongress 2007, October 15-17, Dresden, VDE VERLAG GMBH, Berlin-Offenbach, 441-445

[3]  A. Wörz, B. Berchtold, S. Kandler, O. Prucker, U. Egert, A. Aertsen, and J. Rühe (2007): Tailormade surfaces for a guided adhesion and outgrowth of cells, in: Proceedings Mikrosystemtechnik Kongress 2007, October 15-17, Dresden, VDE VERLAG GMBH, Berlin-Offenbach, 979-983

[4]  P J. Koester, C. Tautorat, A. Podssun, J. Gimsa, L. Jonas and W. Baumann (2008): A New Principle For Intracellular Potential Measurements Of Adherently Growing Cells, in: Conference Proceedings of the 6th International Meeting on Substrate-Integrated Micro Electrode Arrays, July 8-11, 2008, Reutlingen, Germany

[5]  J. Held, J. Gaspar, P J. Koester, C. Tautorat, A. Cismak, A. Heilmann, W. Baumann, A. Trautmann, P. Ruther, and O. Paul (2008): Microneedle arrays for intracellular recording applications, MEMS 2008, 268-271

[6]  J. Held, J. Gaspar, P. Ruther, and O. Paul (2007): Characterization of the DRIE Fabrication of Cell-Penetrating Microneedles, in: Proceedings Mikrosystemtechnik Kongress 2007, October 15-17, Dresden, VDE VERLAG GMBH, Berlin-Offenbach, 845-849

[7]  J. Held, J. Gaspar, P. Ruther, and O. Paul (2008): Microneedle Arrays Electrode With Dielectrophoretic Electrodes For Intracellular Recording Applications in: Conference Proceedings of the 6th International Meeting on Substrate-Integrated Micro Electrode Arrays, July 8-11, 2008, Reutlingen, Germany

[8]  P J. Koester, C. Tautorat, A. Podssun, J. Gimsa, and W. Baumann (2007): Analytikchip zur Erfassung intrazellulärer Potentiale adhärent wachsender Zellen nach lokaler Elektroporation: Einleitung – Biologische Aspekte. in: Proceedings Mikrosystemtechnik Kongress 2007, October 15-17, Dresden, VDE VERLAG GMBH, Berlin-Offenbach, 433-437

# Dielectrophoretic Neuron Positioning on MEAs in Semiconductor Chips for the Extracellular Detection of the Neuronal Network Activity

Philipp Julian Koester, Carsten Tautorat, Jan Sakowski, Werner Baumann, and Jan Gimsa*

University of Rostock, Chair of Biophysics, Rostock, Germany
* Corresponding author. E-mail: jan.gimsa@uni-rostock.de

Biological cells are more or less homogeneously distributed when seeded on a sensor chip. Different methods can be applied when artificial substrates are used to stimulate cell growth in a predetermined way. Such methods are applied to single cells, cell aggregates or cell networks. One can use photolithography or, more easily, dielectrophoresis to allocate cells to specific adhesive sites or to electrically conducting structures. Here, we present silicon chips containing an array of plane microelectrodes for the measurement of extracellular potentials from neurons. The same electrodes are used for dielectrophoretic cell allocation.

## 1 Introduction

When cells are seeded on a sensor chip, they are more or less homogeneously distributed on the chip surface. Additional methods have to be applied if single cells, cell aggregates or networks shall be cultured in a predetermined way. Photolithography [1] and dielectrophoresis [2-7] to allocate cells to a specific adhesive site or to electrically conducting chip structures. Uncharged particles can be moved by *dielectrophoresis (DP)* due to their polarization induced in a non-uniform AC field [4]. Practically, DP is easily applicable because the same electrodes are simultaneously used for allocation and measurement. In this paper, we apply positive DP on a silicon sensor chip to increase the number of neurons on the electrodes in order to improve the signal yield. Unfortunately, neurons tend to migrate, which lowers the cell number on the electrodes after DP-allocation. In future, we plan to immobilize cell attractive polymers only on the electrodes, in order to keep the surrounding silicon surface cell-free.

DP is defined as the translational motion of uncharged particles due to their polarization induced by non-uniform electric fields. For cells, it was first described by Pohl [5]. The cell membrane consists of a manifold of different charged and uncharged molecules. The electric field induced dipole moment leads to a net movement of the whole cell to the attracting electrodes. The movement depends on parameters like e.g. cell shape, cell parameters, and medium conductivity [6]. The *dielectrophoretic force* ($F_{DP}$) of a spherical cell is given by:

$$F_{DP} = \frac{2}{3}\pi \cdot \varepsilon_0 \cdot \varepsilon_e \cdot r^3 \cdot \mathrm{Re}(K) \cdot \nabla E^2$$

[4]

here $\varepsilon_0$, $\varepsilon_e$, $r$ stand for the dielectric constant of vacuum, the relative dielectric constant of the surrounding medium and the radius of the cell, respectively. Re($K$) and E stand for the real part of the Clausius-Mossotti-Factor and the electric field, respectively [4]. For *positive DP (pDP)* the cells move towards regions of higher field, i.e. towards the electrodes. Accordingly, *negative DP (nDP)* is the repulsion of the cells from the electrodes, following the minimum of the field strength [4]. The choice of buffer is important for successful pDP; the conductivity must be lower than that of the cytoplasm for pDP, and higher for nDP, respectively, in our frequency range. Accordingly, higher voltage must be applied for larger electrodes and/or electrode distances. However, higher voltages and/or lower frequencies may cause severe cell damages. The parameters must be adequately adjusted in order to obtain a reproducible dielectrophoretic movement and maintain cell viability.

## 2 Material and methods

Our silicon neurochip features a passive MEA of 58 microelectrodes for the acquisition of action potentials. MEA coating and preparation of cortex tissue from mouse embryo was carried out in saline buffer under sterile conditions (for details see [8]). Neuronal signal quality depends on the neuron-electrode coupling properties. Each chip [9] quality was controlled by a function generator signal before use. Then the chip was filled with cell/buffer solution. The DP voltage was applied instantaneously to prevent cell attachment at undesired locations. The used cell solution volume corresponded to approx. 2x103 neuronal cells on the MEA. After pDP and cell attachment, the underlying buffer was removed by a pipette and carefully substituted with supplemented DMEM. Snap-

shots of DP-allocated cells are shown in figures 1 and 2.

## 3 Results

Localization of the suspended cells to the attracting electrodes is clearly visible. Cells build star-like pearl chains around the electrodes (Fig.1). However, cells tend to migrate and to move away from the electrodes after some days (Fig.2). Figure 3 shows the electrophysiological signal acquisition of successfully treated chips.
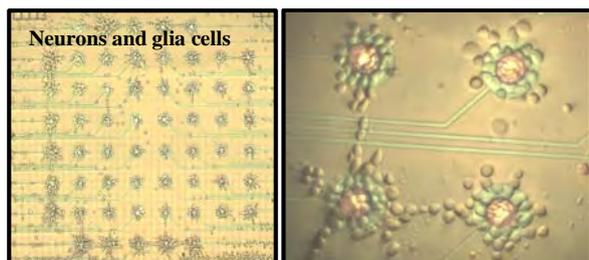


**Fig. 1.** Dielectrophoretic positioned primary neurons on the neurochip. Cells build star-like pearl chains due to "antenna effects" of each cell.
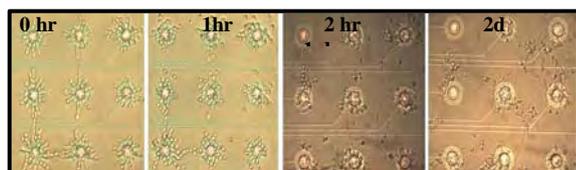


**Fig. 2**. Time course of positioned and cultured cells over 2 days. Cells tend to migrate away from the electrodes.
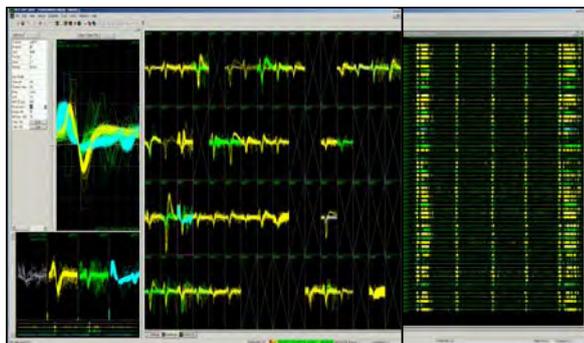


**Fig. 3.** Electrophysiological measurement of neuronal signals (DIV 30, mouse embryo E15), recorded with Plexon© software.

## 4 Outlook

DP on silicon sensor chips is a simple method to increase the number of cells (see also [10]). The method allows for a significant improvement of the signal yield. However, the tendency of the neurons to migrate after sedimentation and attachment complicates the situation. Cell immobilization after allocation may further improve the yield. For that, further investigations are necessary.

**References**

[1]    C. Wyart, C. Ybert, C. Douarche, C. Herr, D. Chateney, and L. Bourdieu (2005): A New Technique to Control the Architecture of Neuronal Networks in vitro" in: P. Poindron, P. Piguet, E. Förster (eds.): New Methods for Culturing Cells from Nervous Tissues. BioValley Monogr. Basel, Karger, vol 1, 23-57

[2]    N. Lautemann, T. Künzel, S. Ingebrandt , S. Böcker-Meffert, A. Offenhäuser, and P. Bräunig (2006): Bionic approach to defined networks on MEAs, in: Conference Proceedings of the 5th International Meeting on Substrate-Integrated Micro Electrode Arrays, July 4-7, Reutlingen, Germany, 198-199

[3]    S. Prasad, M. Yang, X. Zhang, C. S. Ozkan, and M. Ozkan (2003): Electric Field Assisted Patterning of Neuronal Networks for the Study of Brain Functions, Biomedical Microdevices, vol 5 (2), 125-137

[4]    J. Gimsa (2001): Characterization of particles and biological cells by AC-electrokinetics, in: A.V. Delgado (ed.) Interfacial Electrokinetics and Electrophoresis. Marcel Dekker Inc., New York, ISBN: 0-8247-0603-X, 369-400

[5]    H.A. Pohl, (1951): The Motion and Precipitation of Suspensoids in Divergent Electric Fields, J. Appl. Phys. 22(7), 869–871

[6]    J. Gimsa (1991): Dielectrophoresis and electrorotation of neurospora slime and murine myeloma cells. Biophys J, 60, 749-760

[7]    T. Heida (2003): Electric field-induced effects on neuronal cell biology accompanying dielectrophoretic trapping. Adv Anat Embryol Cell Biol.,173:III-IX, 1-77javascript:PopUpMenu2_Set(Menu12901336);

[8]    P. Koester, J. Sakowski, W. Baumann, H.-W. Glock, J. Gimsa (2007): A new exposure system for the in vitro detection of GHz field effects on neuronal networks. Bioelectrochem, 70, 1, 104-114

[9]    W.H. Baumann, E. Schreiber, G. Krause, A. Podssun, S. Homma, R. Schrott, R. Ehret, I. Freund and M. Lehmann (2004): Cell monitoring system with multiparametric CMOS sensorchips, in: Proceedings µ-TAS, Malmö, Sept. 2004, Vol. II, 554-556

[10]  P J. Koester, C. Tautorat, A. Podssun, J. Gimsa, and W. Baumann (2008): Dielectrophoretic Positioning Of Cells For The Measurement Of Intracellular Potentials Using Kidney-Shaped Electrodes, in: Conference Proceedings of the 6th International Meeting on Substrate-Integrated Micro Electrode Arrays, July 8-11, 2008, Reutlingen, Germany

# A Low Cost High Resolution Fabrication Process for Disposable MEAs

Niall MacCarthy[1*], Marcella Burke[1], John Alderman[1]

1 Tyndall National Institute, Cork, Ireland
* Corresponding author. E-mail address: niall.maccarthy@tyndall.ie

As part of a project aiming to investigate novel electrode geometries and improved electrode coatings a need was identified for a low cost alternative to commercial Multielectrode Arrays (MEAs) to allow for economical evaluation and testing. Large numbers were required to achieve the desired statistical significance levels and avoid the possibilities of contamination or degradation which might occur with cyclic use. This paper will discuss the development of a process for the fabrication of fine geometry arrays on an inexpensive platform providing devices which can be used a few times or disposed of after a single use.

## 1   Introduction

To achieve the high numbers of MEAs required at a low cost the MEA was separated into two parts consisting of the high resolution electrode region and the low resolution routing region. The electrode region was fabricated as a 4 x 4 mm$^2$ chip using integrated circuit fabrication techniques. The chip was interconnected to PCB routing layer as detailed in Fig. 2. The large yield of the process (376 chips per wafer) makes it economical to include special designs tailored to particular experiments. On each wafer we included many layouts and electrode geometries as well as variants with varying electrode size and pitch totalling nearly 40 separate designs which were repeated ~ 9 times each to cover the wafer area.

## 2   Fabrication

The number of MEAs produced per batch was limited by the metallisation step to 13 wafers due to limited space in the metal evaporator carousel. Since this is the most expensive fabrication step it is most economical to produce batches of 4,888 MEAs.

The Pyrex wafer surface is roughened by plasma cleaning (300W, 5 min). A 500 nm $SiO_2$ layer is deposited on the wafer to facilitate metallisation patterning by a lift-off process. An imaging resist S1813 (Shipley) is applied and patterned by photolithography (i-line, 75 mJ cm$^{-2}$). The resist is then wet etched using MF319 (Shipley) developer for 3 min. The developer also etches though the $SiO_2$ layer leading to an undercut profile.

Ti (10 nm) and Pt (200 nm) are deposited on the wafer by evaporation. The Ti layer enhances metal adhesion to the Pyrex. An insulation layer of $Si_3N_4$ (400 nm) is deposited by PECVD.

The final step of creating vias to the electrode surfaces and connector pads is achieved using an RIE etch step through an imaging resist mask (Shipley S1813).

## 3   Packaging

To provide for microscope access the chips were embedded into a hole in the PCB. In an unconventional step the chips were secured to the PCB along their edges using Ablebond 2025 ND (Ablestick). The chips were held in place by Kapton tape during the die attach cure. The tape also protects the chip connector pads from contamination by the die attach adhesive.

Encapsulating the wirebonds whilst maintaining an open area around the electrode array proved especially difficult. AMICON 50300 HT (Emerson and Cumming) which has a very low degree of flow out after dispense and which also appears to be non-cytotoxic form our studies was selected as the encapsulant material. A computer controlled dispense instrument (Camalot) was used to pattern the encapsulant over the wirebonds. The dispense pattern was adaptively controlled by modifying the margin to achieve the desired window opening (see Fig. 3).

## 4   Results

To test the functionality of the fabricated arrays HL-1 cells were cultured on the MEAs. The extracellular field potentials were successfully recorded. The signal to noise ratio of recordings with the bare Platinum microelectrodes which have been tested thus far is of a lesser quality compared to commercial Titanium Nitride (TiN) microelectrodes. This is not unexpected as the choice of Platinum as an electrode material was based on compatibility with the coating de-

velopment process rather than optimisation for recording.
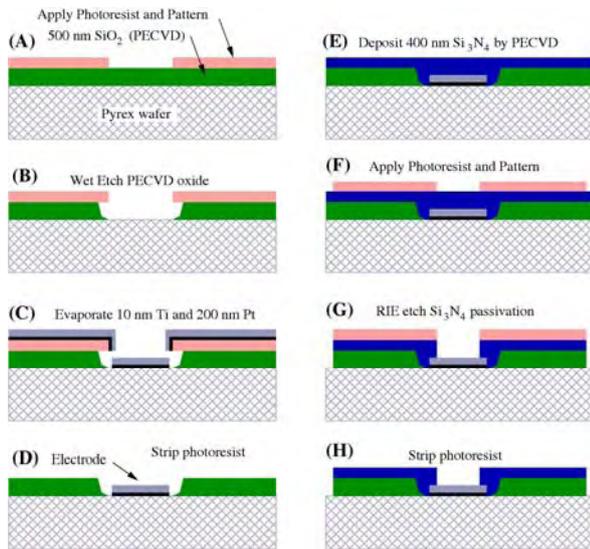


**Fig.1.** MEA chip fabrication Process

# 5 Summary

Because of the high yield of MEAs from the fabrication process the cost per MEA chip is reduced to only a few euros. The packaging cost does not scale with chip size but nevertheless the overall package can be produced at a mere fraction of the cost of commercial MEAs. This provides for units which can be disposed of after just a few experiments or even after just a single experiment. Since there is space for a large number of die per wafer a library of designs can be produced from a single lithography mask.

For future designs a larger chip size of perhaps 6 mm per side would be considered to increase the available contact area for cells/tissue and to increase the process window for the encapsulation step. Our preliminary tests have shown that these low cost arrays do provide a suitable platform for the development, testing and evaluation of novel MEAs. They are also ideally suited to applications where disposability and low cost are driving factors.



**Fig.2.** MEA packaging process

preliminary studies have shown that the MEA package withstands auto-clave sterilisation, plasma cleaning and permits successful culturing of HL-1 cells over a 3 day period.
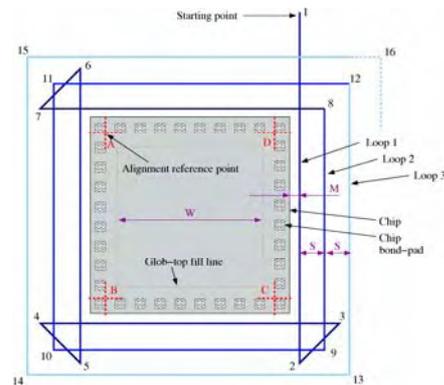


**Fig. 3.** Illustration of encapsulation dispense pattern used to isolate the wirebonds whilst keeping the electrodes uncovered. The window opening (W) is the target parameter. The dispense line spacing (S) is fixed. The margin (M) is adaptively varied to achieve the desired window opening.



**Fig. 3.** Photograph of a MEA package (a glass chamber is attached in a subsequent step)

# High-Density Microelectrode Arrays on Flexible Substrates

Keith Mathieson[1*], Alan Moodie[2], Derek Murdoch[1], James D. Morrison[2]

1 Department of Physics and Astronomy, University of Glasgow, Glasgow G12 8QQ, Scotland
2 Faculty of Biomedical and Life Sciences, University of Glasgow, Glasgow G12 8QQ, Scotland
* Corresponding author. E-mail address: k.mathieson@physics.gla.ac.uk

In order to understand how populations of neurons signal in a concerted manner, small electrodes covering a large area are required. This necessitates a high-density coverage of microelectrodes. We report on the development of an array of microelectrodes for recording and stimulating extracellular signals from retinal ganglion cells. The array consists of 61 platinum electrodes of 5 $\mu$m diameter, spaced at 60 $\mu$m and connected by 8 $\mu$m wide gold tracks all encased in a flexible polyimide substrate. As well as determination of the electrical characteristics of our electrodes, we have tested them on a biological preparation in the form of the exposed frog retina. The quality of electrode contact with the retinal surface was attested to by the recording of ganglion cell action potentials at different electrodes.

## 1 Introduction

Microelectrode arrays (MEAs), formed by microfabrication techniques, have found application in recording and stimulating neural tissue [1][2]. They also form a critical component of a viable retinal prosthesis to repair some forms of retinal blindness [3]. This application requires high-density, biocompatible MEAs capable of interfacing with hundreds of neurons. Here we present a scalable technology on that has the potential to be extended to hundreds of microelectrodes.

## 2 Methods

### 2.1 Microelectrode array fabrication

The arrays were fabricated from polyimide (HDmicrosystems PI2545). A first layer of polyimide was applied by spin coating the liquid form onto 525 $\mu$m thick 4-inch silicon wafers to a thickness of 2.4 $\mu$m and "soft-baked" to effect a partial removal of the solvent. Five layers were successively applied in this manner, with intermediate $O_2$ plasma treatments at 100W RF power to improve layer adhesion. These layers were then fully cured at 350$^o$C in a nitrogen environment. A layer of titanium (20nm) and of gold (130nm) were deposited using a Plassys electron-beam evaporator and Shipley S1818 photoresist was used to pattern the titanium/gold layer using UV exposure under a Karl Suss MA6 mask aligner. Extraneous gold was removed using a 10-second potassium iodide and iodine (32g potassium iodide, 200ml water, 8g iodine) wet etch and extraneous titanium removed using a silicon tetrachloride plasma etch in a reactive-ion etcher, which allowed the demarcation of electrodes tracks of very high resolution. In order to passivate the top surface of the electrode array, a final layer of polyimide was applied achieving a total thickness of ~15 $\mu$m. A $C_2F_6/O_2$ plasma etch was further used to expose the electrode sites and bond pads using a photo-resist mask (AZ4562) to protect the rest of the array. The photo-resist was then cleaned-off through an n-butyl acetate rinse after which the silicon wafer was removed. To form platinum electrodes an aqueous solution of 1.00% platinic chloride and 0.08% lead acetate was deposited on the region above the electrode array. A platinum wire was placed in this solution and kept at a positive potential with respect to the electrodes. Each electrode was supplied with a current density of 4nA/$\mu$m$^2$. The electrodes were platinised for approximately 15s in order to form 5 $\mu$m diameter platinum electrodes. The finished device is shown in Fig. 1(a).
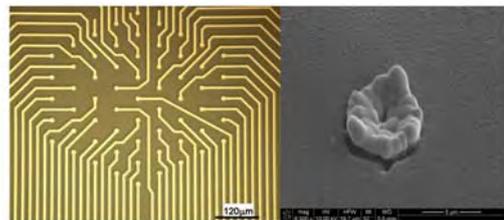


**Fig. 1.** Left: A 61-electrode microelectrode array on a flexible polyimide substrate. Right: A scanning electron micrograph of a platinised microelectrode.

### 2.2 Electrical characteristics

To measure the electrode impedances, the array area was immersed in 0.1M NaCl solution and a platinum wire electrode was used to supply an AC voltage of 100mV peak to peak. An LCR meter was used to

vary the frequency of the AC voltage signal and record the impedance of the electrode. Each electrode was measured 5 times and the averaged reading taken over the range of test frequencies of 100Hz to 100kHz. A typical value was ~300kΩ at 1kHz frequency. Inter-electrode resistances typically exceeded 100GΩ, and shorted channels were ~10kΩ. Inter-electrode capacitance was less than 1pF. RMS noise was measured with the electrodes in contact with the frog retina preparation and was 13μV.

## 2.3 Physiological preparation

The physiological preparation used to test the electrode arrays was the frog retina in situ. The retina was exposed under dim red illumination. After resection of the upper and lower eyelids, the cornea was pierced with a fine needle to relieve the intraocular pressure and was resected at the limbus. The aqueous humour was soaked up with filter paper and the iris was retracted with strips of filter paper which also served to remove the last traces of aqueous humour. The lens was gripped by its anterior capsule, lifted so as to expose the suspensory ligaments which were parted with fine scissors. The lens and attached vitreous body were then lifted from the eyecup to expose the surface of the retina. This preparation which involves minimal disturbance to the retina remains viable at room temperature for 8-10 hr.

## 3   Results

## 3.1 Light-evoked Recordings

The crucial test of the utility of the electrode array is to record bursts of action potentials which are different at the different electrodes in terms of their timings and number of spikes in order to confirm they had been recorded from different ganglion cells, rather than as a common signal transmitted through the extracellular fluid space overlying the retina. This has been confirmed by the recordings in response to a range of light intensities from the different array electrodes (Fig. 2).
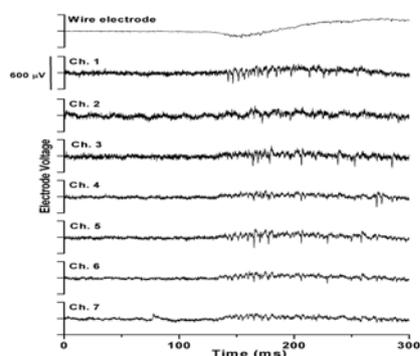


**Fig. 2.** Light-evoked retinal ganglion cell action potentials. Top channel is from a Pt wire electrode, with the lower traces from the MEA. Light stimulus intensity was 0.03μW/mm².

The form of the light-evoked ganglion cell response was a discrete burst of action potentials at either the onset (ON response) or termination (OFF response) or both onset and termination of light (ON-OFF response). With increasing light intensities, there was a shortening of the response latency with an increase in ERG amplitude.

## 3.2 Electrically evoked recordings

Square wave cathodal pulses of pulse widths 0.2 ms, 0.5ms, 1.0ms, 2.0ms and 5.0ms of voltages 200 mV to 2V in 200mV steps were delivered to a specified electrode while recordings were made from the adjacent electrodes on the array. The recordings showed action potentials generated on the decay phase of the positive overshoot following differentiation of the square-wave stimulus waveform. The threshold voltage was observed to decrease with increasing pulse width as shown in Fig. 3 which showed a significant hyperbolic relation between the two variables for threshold action potential generation. The data shown in Fig. 5 give a voltage "rheobase" of 0.8 +/- 0.06 V and a chronaxie of 288 +/- 54 μs.
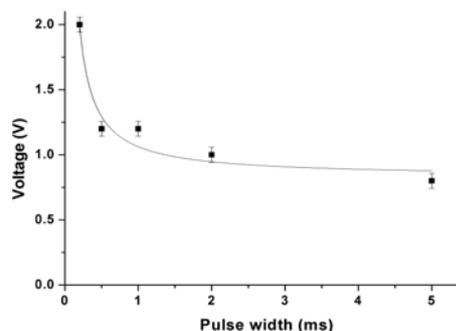


**Fig. 3.** Relationship between stimulation voltage at the electrode as a function of pulse width for threshold generation of action potentials. The data are described by equation y = 0.8(1+ 0.00029/x).

## 4.  Conclusions

We have fabricated a high-density array of microelectrodes on a flexible substrate and demonstrated the feasibility of using them to record from and to stimulate the small retinal ganglion cells of the frog retina.

**References**
[1]   K. Mathieson et al.(2004): IEEE Trans Nucl Sci 51, 2027-2031
[2]   T. Stieglitz et al.(2005), IEEE EMB Magazine 24 (5), 58-65
[3]   E. Zrenner et al. (2002): Science 295, 1022-1025

Technology

# Towards Interruptionless Experiments on MEAs

Jarno E. Mikkonen[1,2*], Steffen Kandler[2], Samora Okujeni[2], Oliver Weihberger[2], Ulrich Egert[2,3]

1 Regea Institute for Regenerative Medicine, University of Tampere, Tampere, Finland
2 Bernstein Center for Computational Neuroscience, Albert-Ludwigs-University, Freiburg, Germany
3 Biomicrotechnology, Dept. of Microsystems Engineering, Albert-Ludwigs-University Freiburg, Germany
* Corresponding author. E-mail address: jarno.mikkonen@regea.fi

Microelectrode array (MEA) systems are widely used to explore neuronal cells and their interactions in culture. They are suitable for long term cellular experiments and sustainable over months or even years. However, routine maintenance of the cultures introduces artificial disturbances, a human-made rhythmicity, to the cultures. We propose to circumvent or reduce the artificial break-points in culturing by providing a continuous maintenance system for the neurons cultured on MEAs.

## 1 Introduction

Neurons grown on MEAs offer a practical platform to explore small-scale biological networks. These networks maintain the essential features of brain-bound networks, but are recordable over weeks and can be influenced by extensive pharmacological or electrical manipulations [1]. For example, isolated cortical neurons plated on a MEA form monosynaptic connections within first week after plating, and a mature bursting network within four weeks [2, 3]. However, the state of the network, and thereby its response to electrical stimuli or pharmacological treatments, is strongly affected by any systematic changes. Typical changes are mechanical disturbances, i.e. moving of the MEA, heat induction through the measurement setup, $CO_2$ level fluctuations, and the exchange of the neuronal culture medium. We present here an approach towards interruption-free recordings of the neuronal culture.

## 2 Methods

Recordable cultures should reside in the MEA amplifier inside a dry incubator. Generally, the amplifier produces heat that damages the culture, if the incubator is operated at 37°C. One could lower the temperature of the incubator to compensate for the heat production of the amplifier. However, this is not feasible, since it limits other usage of the incubator. Therefore, we propose to couple the amplifier with a cooling body with water circulation which transfers the excess heat from the amplifier to a radiator outside of the incubator. With the above described setup the recording time of the cultures is limited only by the medium exchange. An additional coupling with a continuous perfusion system consisting of a peristaltic perfusion pump provides the culture continuous replacement of culture medium, and, in principle, enables temporally unlimited recordings. Most perfusion

systems can be set to slow (20 to 100 µl/h) rates, thus providing the same daily volumes as bolus exchange thus circumventing the need to recalibrate the osmolarity and pH of the culture medium. In order to minimize the risk of over-floating the MEA, there must be a bias favouring medium suction over pumping of the fresh medium. This causes drying of the MEA and therefore the micro-climate of the MEA should be humidified. The incubator itself must be kept dry to protect the electrical equipment and to avoid contamination.
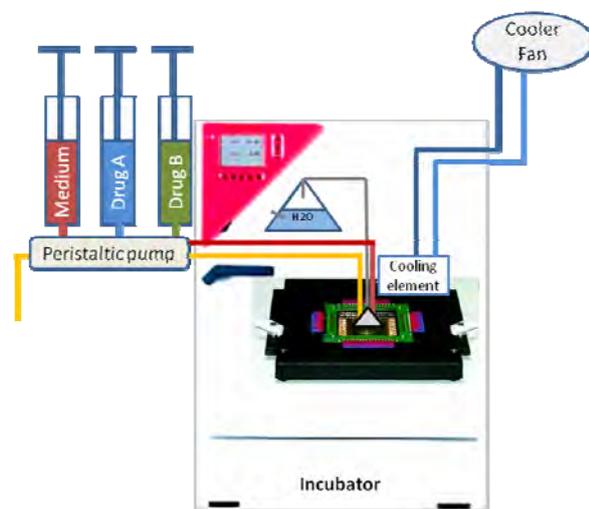


**Fig. 1.** Schematic illustration of the incubator embedded recording system, including water-based cooling system, air humidification for the culture and perfusion system with peristaltic syringe pump

## 3 Results and conclusion

We present here a system that enables recording and stimulation without involuntary stimulation to the neuronal culture. Furthermore, such a system could include slow infusion of pharmacological agents at rates resembling the situation *in vivo*. Our approach

enables the design of long term experiments with repetitive stimulations or adaptations beyond artificial experiment endpoints.

**References**

[1]  S. Marom, & G. Shahaf (2002): Development, learning and memory in large random networks of cortical neurons: Lessons beyond anatomy. *Q Rev Biophys, 35,63-87*

[2]  H. Kamioka, E. Maeda, Y. Jimbo, H. P. C. Robinson, & A. Kawana (1996): Spontaneous periodic synchronized bursting during formation of mature patterns of connections in cortical cultures. *Neurosci. Lett., 206 109-112*

[3]  D. A. Wagenaar, J. Pine, & S. M. Potter (2006): An extremely rich repertoire of bursting patterns during the development of cortical cultures. *BMC Neurosci 7 11*

# Microfabricated biointerface for high density microelectrode arrays

Mohssen Moridi[1*], Steve Tanner[1], Pierre-André Farine[1], Stephan Rohr[2]

1 University of Neuchâtel, Institute of Microtechnology, Neuchâtel, Switzerland
2 University of Bern, Department of Physiology, Bern, Switzerland
* Corresponding author. E-mail address: mohssen.moridi@unine.ch

We present the concept and microfabrication steps of a new bio-interface for active MEAs. Unlike standard approaches using post-processing of the integrated circuit to deposit the MEA electrodes, the proposed structure relies on the microfabrication of platinum electrodes into a glass interface, which is then connected to the IC with high density bumps. The concept offers high density electrodes, a potentially higher biocompatibility, and the possibility to implement, on the same glass device, other kinds of detectors, allowing multi-parameter, long-term measurement of biological preparations.

## 1  Introduction

Presently, there exist two types of extracellular electrical recording systems: the first is based on passive multi-electrode arrays (MEAs) which exhibit high biocompatibility but poor spatial resolution due to signal routing constraints. The second is based on active integrated MEAs which offer high spatial resolution due to the fact that amplifiers are integrated under each electrode. In active MEAs, the interface between integrated circuits (ICs) and the biological material is produced using a post-process on the surface of the IC to deposit biocompatible electrodes and inert layers. While straightforward, this approach has several limitations such as process compatibility with the IC, constraints on sterilization and mechanical cleaning, and the necessity of wafer-level processing.



**Fig. 1.** Cross-section of the proposed device. Quartz is used as substrate and traversing electrodes connect the IC to the cells.

To overcome these limitations, we present a new concept of a highly biocompatible biointerface which offers high spatial resolution (64 x 64 electrodes, pitch of 60 μm) and is suited to be connected to amplification ICs using high density bump interconnections. Fig. 1 shows an overview of the proposed system

## 2  Methods

### 2.1 Fabrication process

The fabrication steps are as follows: First, glass is dry etched (bottom side) with an opening aperture of 20 x 20 μm, a depth of 50 μm and a pitch of 60 μm in order to form holes for electrode deposition. As shown in Fig. 2, good results have been obtained using quartz wafers as substrates and $C_4F_8$ as etching gas (vertical walls with more than 85° of angle). Subsequently, titanium as an adhesive layer and platinum as electrode are sputtered inside the holes. In order to obtain massive electrodes, the holes are filled by copper electroplating up to the aperture. The surface is then flattened with CMP (Chemical Mechanical Processing). Finally, the electrodes are separated by wet etching of copper in $HFeNS_2O_8+H_2SO_4$ and dry etching of platinum/titanium layers by using $Cl_2$-Ar and $Cl_2$-$BCl_3$ as etching gas respectively. A thin layer of Ti/Ni/Au, used as UBM (Under Bump Metallization), is deposited by a lift-off method on the back of each electrode, followed by a thick patterned photo-resist used as a mold to define the bumps. Then, indium bumps are deposited by evaporation up to 4 μm thickness on top of UBM layers. After plasma treatment to remove native oxide, a thermal annealing at 200°C for 10 min under $H_2$ atmosphere is done to create the bumps.

**Fig. 2.** SEM image of array holes on quartz obtained by deep dry etching by $C_4F_8$ with a depth etch of 50 um,.

In the regions of the electrodes, the glass is chemically back-etched (top side) inside concentrated HF to reduce its thickness from 500 to ~50 μm so as to expose the electrodes. For this, a 3 μm LPCVD poly-Silicon layer is used as mask to protect the top side, and a special chuck is used to protect the back side of the device. Fig.3 shows an optical profile measurement of the surface. The surface roughness amounts to a few microns which is sufficiently small for our application.
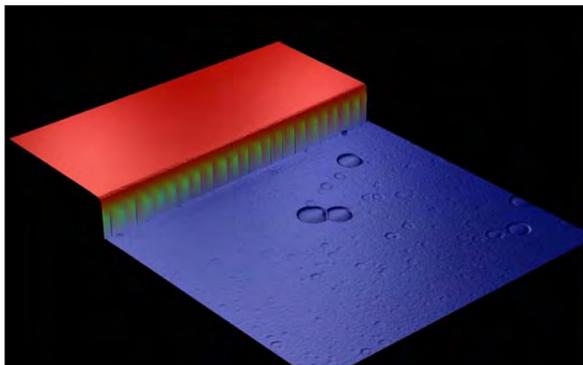


**Fig.3.** Optical profile of deep quartz etching by HF. Surface roughness is around some microns.

## 2.2 Packaging

The proposed bio-interface is then connected to the amplification integrated circuit. For this, it is optically aligned with the CMOS die, and pressed to it at a temperature of 150°C. A PCB is fixed to the glass with epoxy resin, serving as mechanical support. Under bump metallization is used to connect the pads of the IC to the PCB via wire bonding. A glass container is finally fixed to the system to form the culture chamber. Fig. 4 shows an overall view of the packaged system.
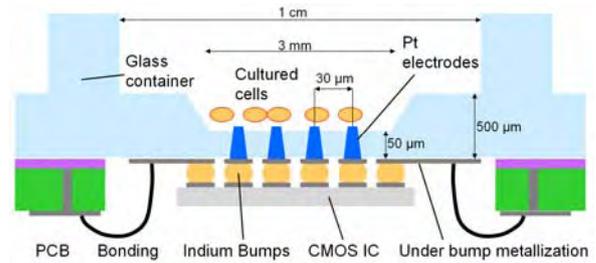


**Fig. 4.** Schematic cross-section of packaged system.

Fig. 5 shows the final PCB of a similar system developed in our institute [1] used to connect the MEA to a data acquisition platform for real time processing.
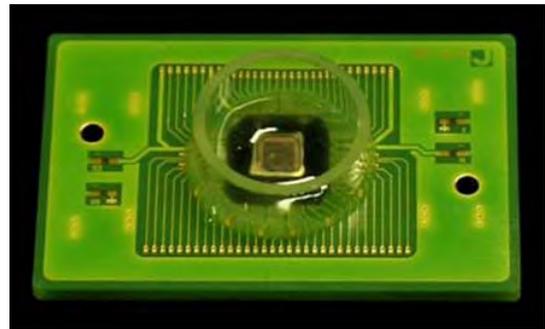


**Fig. 5.** Entire package module.

## 3 Results

The critical steps of the proposed fabrication methods have been validated and a prototype is currently under fabrication.

## 4 Conclusion

We present the concept and key fabrication steps of a new bio-interface for high-density MEAs, offering 64 x 64 Ti/Pt electrodes at a pitch of 60 μm, integrated on a quartz substrate connected to the MEA IC through high density bumps. This hybrid MEA approach prevents the sensitive CMOS electronic circuits from critical post-processing steps, and allows for potentially better biocompatibility. Furthermore, other kinds of sensor can be implemented into the glass interface through patterned growth techniques, thereby expanding the range of possible applications of the device.

**References**

[1] K. Imfeld, A. Garenne, S. Neukom, A. Maccione, S. Martinoia, M. Koudelka-Hep, L. Berdondini, "High-resolution MEA platform for in-vitro electrogenic cell networks imaging", *proc. of the 29th Annual International Conference of the IEEE EMBS, Lyon, France, August 23-26, 2007*.

# Replica-molded polymer microelectrode arrays (polyMEAs)

Angelika Murr[1], Christiane Ziegler[1], Fabio Benfenati[2], Axel Blau[2*]

1 University of Kaiserslautern, Dept. of Physics and Biophysics, Erwin-Schroedinger-Str. 46, 67663 Kaiserslautern, Germany
2 The Italian Institute of Technology, Dept. of Neuroscience and Brain Technologies, via Morego 30, 16163 Genoa, Italy
* Corresponding author. E-mail address: axel.blau@iit.it

We present a prototype of a multielectrode array (MEA) made entirely out of polymers. It consists of thin conductive polymer leads embedded in an insulating and partially micro-structured, replica-molded polydimethylsiloxane (PDMS) substrate sandwich. The passive device is suited for the recording of bioelectrical signals from electrogenic cells. The presented *polyMEA* design is compatible to the 60-channel recording setup made by Multi Channel Systems, but may be adapted to any other geometry. The electrical characteristics have been investigated by impedance spectroscopy and recordings from cardiomyocytes from embryonic chicken (E8).

## 1 Introduction

Passive multi-microelectrode arrays (MEAs) or plates (MMEPs) for non-invasive electrophysiological *in vitro* studies have been around for several decades. Most common fabrication strategies resort to photolithography and the evaporation, etching or electroplating of metallic conductors to generate electrode structures on predominantly rigid substrates [1]. In alternative approaches, metal electrodes and leads are embedded into more flexible polymeric substrates [2]. The aim of the presented design study was the development of inexpensive and mass-producible passive and mostly transparent MEAs made entirely out of polymers.

## 2 Methods

### *polyMEA* fabrication

The *polyMEAs* were fabricated in three steps. Firstly, cavities for the electrodes, leads and contact pads were molded into a thin ($\leq 500\ \mu m$) PDMS top layer. The geometries of these cavities were defined by a SU 8 molding master on top of a 4" silicon wafer. Its two-level design ensured that the electrode and pad features extended through the entire top layer while the interconnection channels for the electrode leads stayed covered by PDMS. Secondly, the cured PDMS was peeled from the master and hydrophilized. Its cavities were then filled with a conducting polymer and tempered (Fig. 1). In a last step, the back side of the top layer was electrically insulated by a PDMS bottom layer. The rigidity of such *polyMEA* sandwich with a thickness below 1.5 mm could be increased by bonding it to a glass carrier.

### *polyMEA* characterization

Impedance measurements from 100 mHz to 5 kHz were performed on differently treated and reused *polyMEAs* in phosphate buffered saline (PBS) using a potentiostat (EG&G Applied Research, model BES with PowerSuite software). An Ag/AgCl wire served as the reference electrode, a Pt sheet as the counter electrode. Noise levels on individual electrodes were evaluated using a 60-channel recording station (MEA60, Multi Channel Systems).

### *polyMEA* recordings

Bioelectrical signals from embryonic chicken (E8) were recorded using acute heart muscle cell preparations. Biocompatibility and biostability of *polyMEAs* were evaluated for a period of two weeks with cultures from dissociated cortical chicken neurons (E10) using standard cell culturing protocols.

## 3 Results

The impedance of the mostly transparent polymer electrodes with diameters of about 80 µm (Fig. 2) were almost constant and below 1 MOhm over the range of 0.1 Hz to 5 kHz with an average of $145 \pm 10$ kOhm. For different electrodes, RMS noise varied between $\pm 9\ \mu V$ to $\pm 50\ \mu V$. It is hypothesized that differences in impedance and noise may be attributed to the non-uniformity of the different conducting path geometries and to artefacts resulting from manual fabrication of the prototypes. Electrical characteristics were not affected by normal use (autoclavation, several weeks of cell culturing under standard cell culturing conditions: 5% $CO_2$ in a humidified incubator at 37° C).
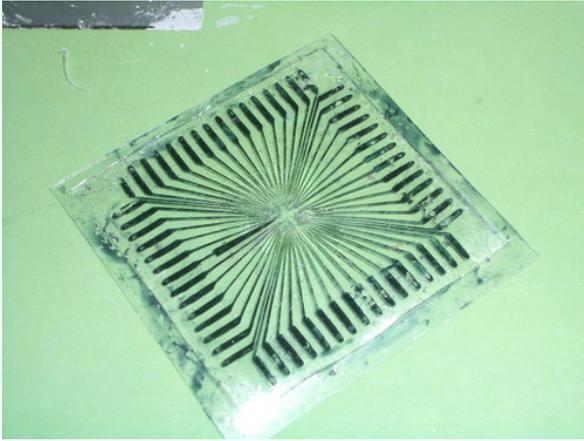
**Fig. 1**. Backside of a sample *polyMEA* (temporarily resting on a carrier polymer foil) before its cleaning and sealing with a second layer of PDMS. Outer *polyMEA* dimensions are 4,9 * 4,9 cm$^2$.
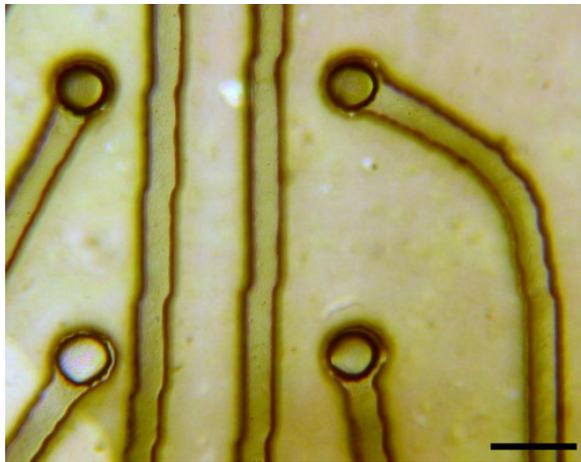


**Fig. 2**. Zoom onto four mostly transparent polymer electrodes and leads embedded into the PDMS of a *polyMEA* (without any biological tissue). Bar represents 100 µm.

## 4 Conclusion

Prototypes of replica-molded polymer MEAs with rather large diameter (80 µm) polymer electrodes have favorable impedance characteristics over a wide frequency spectrum. This allowed the recording of myocardiograms from acute cardiomyocyte preparations. Low-frequency components of the bioelectric signals (P, Q, R, S and T deflections) were clearly visible. The devices are not only biocompatible and optically transparent for inverse light microscopy, but tolerate standard sterilization procedures (e.g., auto-clavation, 70% ethanol) without noticeable deterioration. *polyMEAs* may thus become inexpensive and discardable devices for the study of bioelectrical signals from *in vitro* preparations of electrogenic cells. In a follow-up study electrode dimensions will be scaled down to match those of currently available MEAs. Electrode charge transfer characteristics for stimulating cells with different voltage or current protocols will be evaluated. A translation of the design to the fabrication of passive *in vivo* probes may be envisioned. Furthermore, the replica molding strategy may be exploited for other applications such as the fabrication of micro-channel MEA overlays for cell placement and axon guidance or in microfluidics.

### Acknowledgement

### References

1] Taketani M, Baudry M (eds). Advances in Network Electrophysiology: Using Multi-Electrode Arrays Springer US; 2006.
[2] Boppart SA, Wheeler BC, Wallace CS. A flexible perforated microelectrode array for extended neural recordings. IEEE Trans Biomed Eng 1992; 39: 37-42.

# Three-Dimensional Microelectrode Array for Recording Dissociated Neuronal Cultures

Katherine Musick[1*], Bruce Wheeler[2]

1 Department of Electrical and Computer Engineering, University of Illinois at Urbana-Champaign
2 Department of Bioengineering, University of Illinois at Urbana-Champaign
* Corresponding author. E-mail address: kmusick@uiuc.edu

Presently, *in vitro* studies of neural networks are done with two-dimensional monolayers of cells even though three-dimensional cultures are more like *in vivo* correlates in both structure and response to stimuli. This project aims to advance knowledge of neural networks through the development of a device that permits in-depth study of three-dimensional neural cultures *in vitro*. Here we present the first demonstration of signals collected from an *in vitro* neural culture grown within this 3D scaffolding system.

## 1  Introduction

The device described here, a three-dimensional microelectrode array (3D MEA), is designed as a stack of individually-patterned thin films. Electrodes and microfluidic channels are created on these thin films prior to stacking (Fig. 1). The purpose of the microfluidics is to provide an artificial vasculature for nutrient supply and aeration, and to permit dissociated neurons to be loaded into the structure. Once the neurons grow and establish electrical activity, the embedded electrodes allow for recording and stimulation. The goal is to allow the collective properties of 3D neural networks to be observed and manipulated with a level of control not possible in living animals.

## 2  Methods/Statistics

The device is fabricated out of biocompatible materials and is subjected to extensive soaking and rinsing to ensure all chemical residues from processing have been fully removed. A coating of PDL is applied to give a favorable surface for neural adhesion, growth, and long-term survival. E18 rat cortical cells are mechanically dissociated, diluted to a concentration of 800,000 cells in 250 μL of media, and loaded into the device with the fluidic channel. The devices are placed into an incubator, and a constant flow of 2 μL/hr is withdrawn through the chamber. The fluid is replaced with fresh media every 2 days. After approximately 18 days in vitro (DIV), spontaneous and stimulated recordings can be obtained from the devices. Activity is recorded and analyzed in terms of number of active electrodes and spike rate.
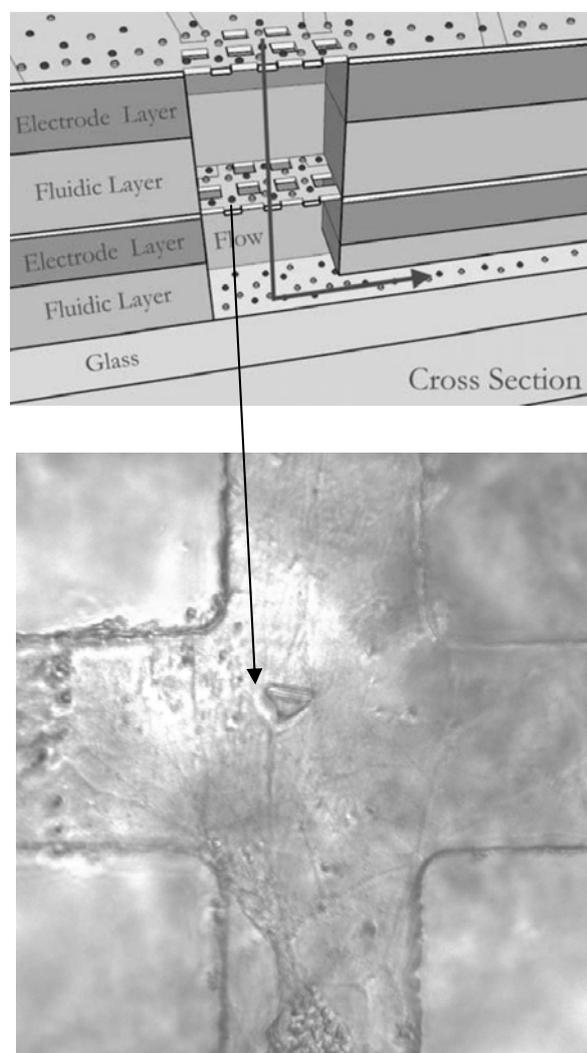


**Fig. 1.** 3D MEA. (top) Cross section of a three-level prototype. The fluidic layers are made of PDMS, and the electrode layers are made of thin silicon with a suspended SU-8 grid that contains the Ti/Au electrodes. (bottom) Growth on the middle layer of the device at 28 DIV.

## 3  Results

Spontaneous recordings have been made on two devices. At 26 DIV, the first device had 65% active electrodes with an average spike rate of 0.5 Hz. The second device had 77% active electrodes with an average spike rate of 1.0 Hz. Activity was most reliably detected on the bottom layer of these devices.

To obtain concrete evidence of interlayer growth within a device at 28 DIV, active electrodes were serially stimulated to elicit responses from other levels. The pulse train consisted of a biphasic voltage pulse (200 ms per phase, positive phase first) with stimuli delivered at a rate of 1 Hz. There were 10 pulses at each level of $\pm 0.6$ V, $\pm 0.8$ V, $\pm 1.0$ V, and $\pm 1.2$ V. A channel located on the top layer of the device was stimulated and responses were recorded from a channel located on the middle layer of the device. The perievent raster plots from these results are shown in Fig. 2. Also shown are the spike waveforms recorded on these electrodes to give further evidence that the events are neural spikes instead of electronic artifacts. A time-locked response that occurred approximately 10 ms after the stimulus is seen on this channel. This suggests a multi-neuron but direct pathway from the channel on the top layer to the channel on the middle layer of the device.

## 4  Conclusion/Summary

This work is the first demonstration of signals collected from an *in vitro* neural culture grown within a 3D scaffolding system. The most notable accomplishments are 1) fabrication of a 3D MEA, 2) proof of biocompatibility and capability of sustaining long-term *in vitro* neuronal cultures, and 3) acquisition of spontaneous and evoked neural signals.
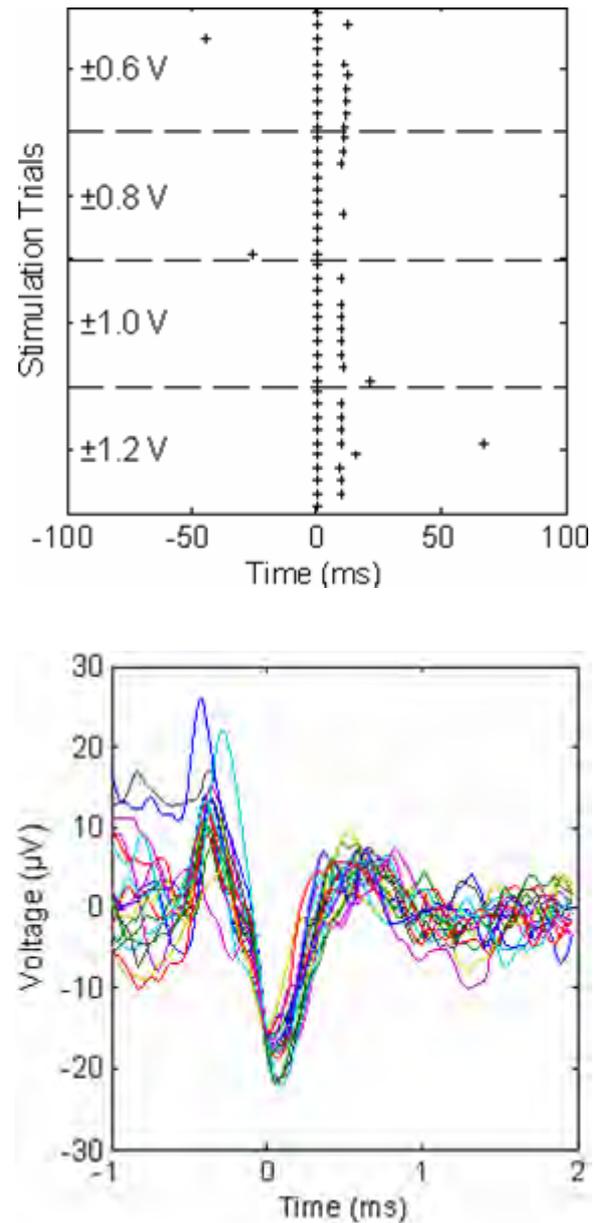


**Fig. 2.** Perievent raster plot from the stimulation trials and corresponding spike waveforms from a device at 28 DIV. These spike events were recorded from a channel on the middle layer of the device while the stimulus was delivered to the top layer of the device, providing evidence of interlayer connections.

# Planar NCD microelectrodes for detecting quantal release of catecholamines from chromaffin cells

Alberto Pasquarelli[1*], Michele Dipalo[1], Erhard Kohn[1], Andrea Marcantoni[2], Valentina Carabelli[2] and Emilio Carbone[2]

1 Dept. of Electronic Devices & Circuits, University of Ulm, D-89069 Ulm (Germany)
2 Dept. of Neuroscience, NIS Center, CNISM, University of Torino, I-10125 Torino (Italy)
* Corresponding author. E-mail address: alberto.pasquarelli@uni-ulm.de

Quantal release of catecholamines is commonly detected from single chromaffin cells as amperometric currents by means of carbon-fiber microelectrodes, with a ms temporal resolution and high sensitivity, but with low spatial resolution (~30 µm2). To overcome these limitations, we designed a new planar device of boron-doped (B-doped) nanocrystalline diamond (NCD) with four separate recording areas in a circular region of 25 µm diameter. Early results are presented.

## 1 Introduction

Neurotransmitter and hormone release are key steps for controlling synaptic plasticity and vital body functions (blood pressure, heart beats and pulmonary ventilation). Release occurs in quantal packages of molecules ($10^3$-$10^4$) loaded in small vesicles (or granules) of 50 to 300 nm diameter either concentrated in specialized presynaptic regions of neuronal terminals (active zones) or homogeneously distributed along the plasma membrane in neuroendocrine cells.

Neurotransmitter release is a strictly $Ca^{2+}$-dependent event triggered by membrane depolarization and opening of voltage-gated $Ca^{2+}$ channels: these in turn elevate intracellular $Ca^{2+}$ levels and initiate vesicle fusion and neurotransmitter release. Presently, the most used technique to resolve single secretory events is the amperometric detection of catecholamines using carbon-fiber microelectrodes [1], having a typical diameter of 5 µm and a diagonal cut, placed closely to the cell [2]. carbon fibers electrodes should be polarized to +650-800 mV to detect catecholamines by electrochemical oxidation. Amperometric burst-signals consisting of current spikes of tens to hundreds of pA, lasting tens of milliseconds, can be recorded for seconds or minutes depending on the stimulus. Each spike monitors the fusion of single vesicles. Despite having several advantages: 1) high time resolution (ms rising phase), 2) high-sensitivity (detection of several thousand molecules) and 3) not being invasive, carbon fibers have serious drawbacks. Their use is limited to single cells, have low spatial resolution (~30 $µm^2$) and can be hardly used in combination with a lateral glass-pipette microelectrode for simultaneous amperometric and patch-clamp recordings.

A new approach, based on planar platinum electrodes [3, 4] could significantly improve the measuring tech- nique, but the use of platinum restricts the transparent observable area and limit the range of detectable re- dox reactions to the hydrolysis potential window of platinum (approx 1.8 Volt)

## 2 Materials and Methods

With the idea of overcoming these limitations, we designed a planar B-doped nanocrystalline diamond (NCD) with four separate recording areas included in a circular area of 25 µm diameter (Fig. 1).
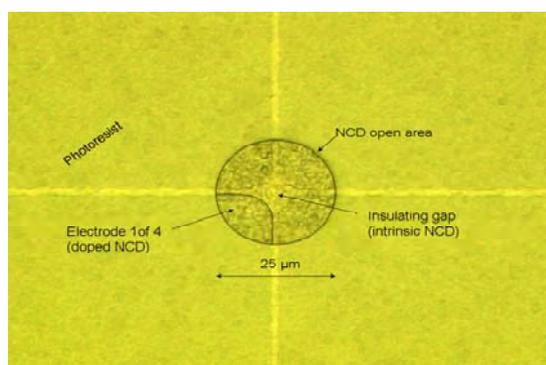


**Fig. 1**. Microphotograph showing the active area of the NCD Microelectrodes device

The quadruple electrode was made of nanocrystalline diamond grown on a silicon wafer. First was deposited a 3µm thick layer of intrinsic diamond as insulating buffer, on top of which was grown a 180 nm thick boron-doped NCD layer with a boron concentration of approx 1020 cm-3, thus achieving a quasi-metallic conductivity and a sheet resistance of 600 Ohm/square. The upper conductive layer was then processed by means of lithographic and dry chemical techniques to obtain four independent electrodes forming a quadrupolar array with a 2µm wide gap. On the back side of the chip, we opened a circular win-

dow of 3 mm in diameter by means of an Inductive Coupled Plasma (ICP) Bosch process, (deep vertical etching of silicon), thus leaving a transparent diamond membrane for convenient work under the inverted microscope. The active sensing area of the quadrupole was delimited by means of a Photoresist in which we opened by lithography a window of 25 μm in diameter. Finally we provided ohmic contacts for the electrodes at the corners of the chip by deposition of gold-over-titanium pads in our electron-beam evaporator. The chip was then processed in oxygen plasma to enhance the cell adhesion on the surface without the use of biological substrates (laminin, polylysine, collagene etc.), which may adversely affect the operation of the planar electrodes. The very last step consisted in gluing a glass ring (2 mm high and 8 mm inner diameter) to provide a 100μl perfusion chamber.

## 3 Results and Discussion

We performed a series of cyclic-voltammetry measurements to detect the oxidation activity of adrenaline on our NCD-electrodes starting at 400 mV, peaking around 650 mV (Fig. 2).
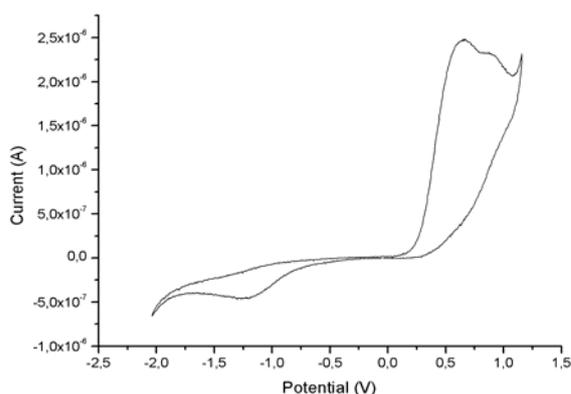


**Fig.2.** Cyclic-voltammetry of 1 mM adrenaline in Tyrode physiologic solution, performed with the NCD-Electrodes. The NCD device shows a hydrolysis potential window of approximately 3 Volts.

We then performed preliminary tests in the absence of cells to evaluate the transient's response to adrenaline. These experiments showed that the B-doped NCD quadrupole had a peculiarly high polarization current which settled very slowly when one of the four electrodes was polarized to +650 mV (20-40 min to reach 1-2 nA). This behaviour clearly indicates

the presence of amorphous carbon and graphite at the grain boundaries, which causes a background current much larger than in the case of diamond single crystals. We are dealing with this issue in the current development of the next device generation. The NCD-quadrupole was nevertheless highly sensitive to adrenaline, furnishing amperometric responses of 1-18 nA following the application of microliter amounts of 1 mM adrenaline (Fig. 3). The rising phase of the response was fast and limited by the diffusion time of adrenaline application. Control solutions with no catecholamines gave no responses while lower concentrations gave smaller amperometric signals.

Our preliminary data indicate that B-doped diamond devices are promising tools for detecting amperometric signals associated to the release of quantal amounts of catecholamine molecules from living cells.
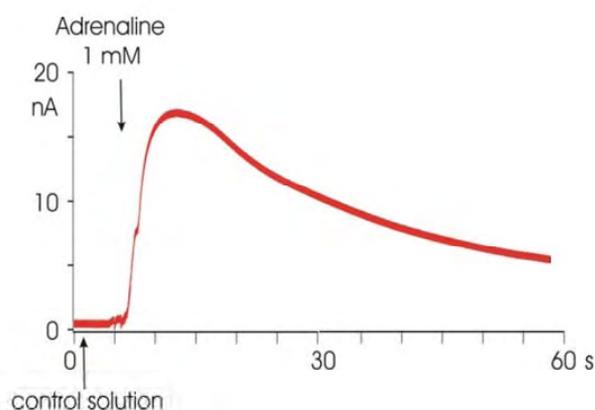


**Fig. 3.** Amperometric transient response following the application of 20 μl adrenaline, 1 mM

### References
[1]  Kawagoe et al. 1991. Anal Chem. **63**: 1589-1594
[2]  Chow et al. 1992. Nature **356**: 60-63
[3]  Dias et al 2002. Nanotechnology, 3: 285.
[4]  Hafez et al 2005. Proc Natl Acad Sci USA. 102(39): 13879-84.

# A Low-Cost System for Simultaneous Recording and Stimulation with Multi-microelectrode Arrays

John D. Rolston[1,2*], Robert E. Gross[2], Steve M. Potter[1]

1 Laboratory for Neuroengineering, Coulter Department of Biomedical Engineering, Georgia Institute of Technology, Atlanta, Georgia, USA
2 Department of Neurosurgery, Emory University School of Medicine, Atlanta, Georgia, USA
* Corresponding author. E-mail address: jrolston@neuro.gatech.edu

Both electrical recording and stimulation of neural tissue have been used extensively to improve our understanding of the brain, and to provide therapy for neurological and psychiatric disorders. Few systems exist, however, that can perform both of these essential tasks simultaneously. To this end, we have developed an inexpensive and easy-to-use *in vivo* system, capable of multi-channel, multi-scale recording (local field potentials, multi-unit activity, and action potentials), stimulation on all channels, and rapid recovery from stimulation artifact, even on stimulating electrodes.

## 1 Introduction

Electrical stimulation of the nervous system is a routine therapy for many neurological and psychiatric disorders and, recently, clinical trials have shown improved therapeutic efficacy when recorded neural signals are used as stimulation feedback. We previously developed software and hardware to enable closed-loop stimulation and recording of MEAs *in vitro* [1-5].

Such real-time, closed-loop systems are not only useful for basic research, but will ultimately enable new feedback-based neurostimulation treatments. For widespread adoption of the closed-loop paradigm, in the lab or the clinic, it is important to lower the cost of such systems and improve their ease of use. We present here a completely new, easy-to-use, and inexpensive stimulation/recording system. A 64 channel version of our system costs less than US$10,000, compared to existing MEA systems ranging from $50,000-$100,000 that cannot simultaneously stimulate and record.

## 2 Methods

Our system was designed for our MEA work in behaving animals, but can be adapted to *in vitro* applications (Fig. 1). The system comprises two 100× gain preamps/headstages (Triangle Biosystems, US$1,800) for use with two 16-wire MEAs (various manufacturers, US$150-300), a 32-channel 16-bit 1-MHz data acquisition card (PCI-6259, National Instruments, US$1,349), a conventional desktop computer, custom-made interface printed circuit boards (PCBs; PCBExpress, US$200) and a miniature custom-made stimulation switching circuit (ExpressPCB, US$200).

Stimulation, recording, filtering and visualization are controlled by our software, NeuroRighter™, a graphical multi-threaded Windows application written in Visual C#. Matlab routines are provided for offline analysis. Software, circuit schematics, and layouts are freely available upon request.
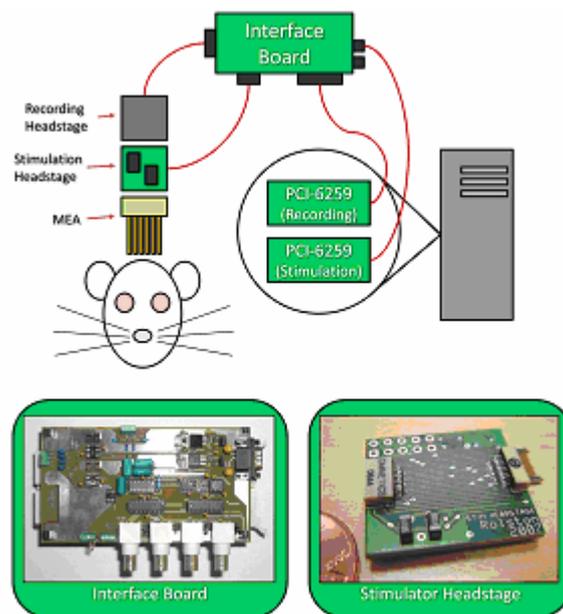


**Fig. 1.** Schematic overview of system, with images of custom-made components.

### 2.1 Analog input

Signals from chronically implanted MEAs are amplified in the 100× gain headstages. These signals pass to an interface PCB. Interface circuitry consists of power supply filtering, two-pole high-pass active filtering for all analog channels, and one-pole passive low-pass filtering. Active filtering provides an additional 1.6× gain. The filters' -3 dB points can be adjusted by changing capacitor and resistor values.

## 2.2 Stimulation

Stimulation pulses of arbitrary waveform shape and duration are generated with 10 µs resolution by a D/A card (National Instruments, PCI-6259). Current or voltage control is specified in software, which controls solid-state analog switches on our stimulation interface board. These switches direct D/A output to the appropriate op-amps for conversion to current- or voltage-controlled waveforms. Additionally, the instantaneous current of voltage-controlled pulses and instantaneous voltage of current-controlled pulses is monitored, buffered, and sent to board test-points. These traces can be monitored on an oscilloscope for diagnostic purposes, or captured by the software for later experimental analysis. Additionally, monitoring of instantaneous current/voltage traces allows the software to calculate electrode impedance spectra, using either voltage- or current-controlled test signals (by monitoring the instantaneous current or voltage delivered, respectively).

## 3 Results

### 3.1 Recording

Thirty-two analog channels are digitized at up to 32,500 Hz, providing minimum resolutions of 325 nV and 30.8 µs. Broadband signals (1 to 9000 Hz) or spike waveforms are displayed with a 4 Hz refresh rate for all channels. Online digital filtering divides the data into two streams with independent sampling rates and filters for simultaneous field potential and spike analysis. Several spike detection methods are available, with thresholds dynamically updated as frequently as each sample. Data are saved as 1) spike times and clipped waveforms, 2) filtered and down-sampled field potentials, and/or 3) broadband unfiltered data. The broadband RMS electrode-referred noise of the system is 6.2 µV, which is identical to the headstage manufacturer's noise specification, implying that our interface and stimulation circuitry introduce no appreciable noise. When restricted to >300 Hz (the range used to detect action potentials), the noise is 3.9 µV, compared to 3.4 µV for our Plexon *in vivo* recording system (>300 Hz high-pass), and 2.9 µV for typical MEA recordings from the Multichannel Systems MEA1060+MCCard (>200 Hz) [6].

### 3.2 Stimulation

High-speed solid state switches on a lightweight stimulation headstage deliver voltage- or current-controlled pulses of arbitrary waveform to any recording electrode. Stimulation causes saturation of non-stimulating and stimulating channels only for the duration of the stimulus (<1 ms). Polarizable microelectrodes suffer from a baseline shift lasting several ms, which can be subtracted in real-time with digital filtering, such as our SALPA algorithm [4] (Fig. 2).
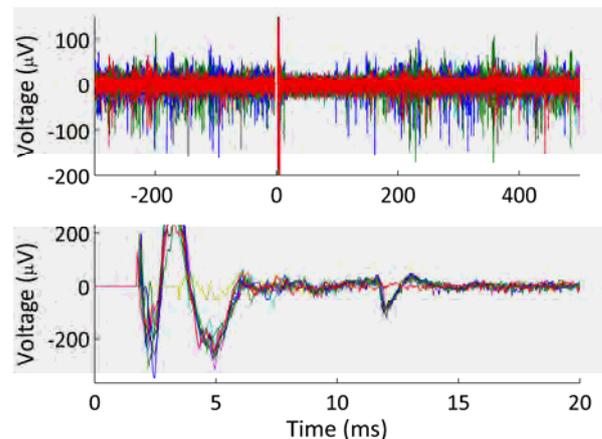


**Fig. 2.** Example stimulation data, recorded from a 16-channel array (33 micron diameter tungsten; TDT) chronically implanted in the hippocampal CA3 region of a male Sprague-Dawley rat. Responses to a 10 µA biphasic (400 µs/phase) cathodal-first stimulation pulse are shown. Ten trials are displayed in different colors, overlaid. Stimulation begins at 0 ms. The top panel shows a large number of action potentials before stimulation, followed by a post-stimulus inhibition, as observed in neocortical neurons [7]. The bottom panel shows a detail of the 20 ms immediately after stimulation, with a precisely timed action potential at 12 ms occurring in 9/10 trials. The large oscillation after the stimulation pulse is likely physiological, as it is not present when arrays are stimulated in saline, is inhomogeneous across electrodes, and does not occur in deeply anesthetized or post-mortem rats (John D. Long, personal communication).

## References

[1] Potter SM, Wagenaar DA, DeMarse TB. Closing the Loop: Stimulation Feedback Systems for Embodied MEA Cultures. In: Taketani M, Baudry M, eds. Advances in Network Electrophysiology Using Multi-Electrode Arrays. New York: Springer 2006.

[2] Wagenaar DA, DeMarse TB, Potter SM. MeaBench: A toolset for multielectrode data acquisition and on-line analysis IEEE EMBS Conference on Neural Engineering; 2005; Arlington, VA: IEEE; 2005. p. 518-21.

[3] Wagenaar DA, Pine J, Potter SM. Effective parameters for stimulation of dissociated cultures using multi-electrode arrays. J Neurosci Methods. 2004 Sep 30;138(1-2):27-37.

[4] Wagenaar DA, Potter SM. Real-time multi-channel stimulus artifact suppression by local curve fitting. J Neurosci Methods. 2002 Oct 30;120(2):113-20.

[5] Wagenaar DA, Potter SM. A versatile all-channel stimulator for electrode arrays, with real-time control. J Neural Eng. 2004 Mar;1(1):39-45.

[6] Nam Y, Branch DW, Wheeler BC. Epoxy-silane linking of biomolecules is simple and effective for patterning neuronal cultures. Biosensors and Bioelectronics. 2006;22(5):589-97.

[7] Butovas S, Schwarz C. Spatiotemporal effects of microstimulation in rat neocortex: a parametric study using multielectrode recordings. J Neurophysiol. 2003 Nov;90(5):3024-39.

# Function Principle of a CMOS Pixel Array for Bi-directional Communication with Individual Cells

U.Yegin[1], M. Schindler[1], S. Ingebrandt[1], S. Eick[1], S.K. Kim[3], C.S. Hwang[3], C. Schindler[2], A. Offenhäusser[1]*

1 Institute of Bio- and Nanosystems 2 (IBN-2) and CNI – Center of Nanoelectronic Systems for Information Technology, Forschungszentrum Jülich GmbH, D-52425 Jülich, Germany
2 Institute of Solid State Research (IFF-6) and CNI – Center of Nanoelectronic Systems for Information Technology, Forschungszentrum Jülich GmbH, D-52425, Germany
3 Department of Materials Science and Engineering, College of Engineering, Seoul National University, Seoul, South Korea
* Corresponding author. E-mail address: a.offenhaeusser@fz-juelich.de

We introduce a 64x64 array of CMOS FG-FET's capable of bi-directional communication with electrogenic cells. Apart from stimulation, recording, and on-chip signal amplification, calibration of pixels is enabled. The chip features a biocompatible high-k dielectric as passivation layer against the electrolyte solution.

## 1 Introduction

Creating bi-directional communication between CMOS chips and individual electrogenic cells is a challenge for many research groups worldwide. Based on a previously published design [1], we developed a chip with a 64x64 sensor array consisting of floating-gate field-effect transistors (FG-FET) fabricated using an industrial 3-metal 2-poly CMOS process, with on-chip decoder, amplifier, and buffer circuitry (Fig. 1A). A FG-FET consists of a regular MOS-FET with a sensing capacitor connected to its gate [2, 3]. Our circuit design connected to the individual pixels allows a bi-directional communication between the cells and the chip, while the small pitch of 12.5 μm between these pixels greatly increases the probability of a cell being in contact with a sensing capacitor. After fabrication, the chips were post-processed to create a high-k dielectric passivation layer on top of the sensing areas.

## 2 Chip Structure

### 2.1 Pixel Circuitry

Since extracellular recordings of signals from electrogenic cells are only a few millivolts in amplitude and the variation of threshold voltages of the transistors on a single chip is greater then 4 millivolts, a calibration procedure [1] needed to be implemented in order to achieve reproducible results. Fig. 2 shows the circuitry that forms a pixel of the array and performs the calibration, recording, and stimulation. The calibration of the pixel is done by forcing a constant current through M1 and closing the switch S2, while S1 and S3 are open. The stimulation voltage can be applied to the sensing capacitor if S1 is closed and S2 and S3 are opened. An extracellular potential change due to cell activity would change the current through M1, which can be recorded and amplified if S3 is closed.



**Fig.1.** Optical microscopy image of the 64x64 FG-FET CMOS chip (A), and electron microscopy close-up of the sensor-array (B).
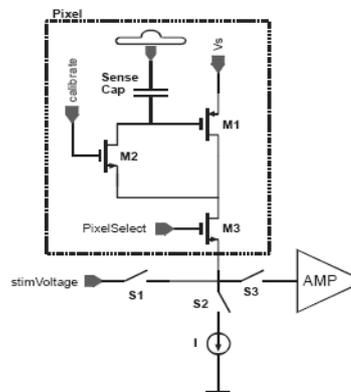


**Fig.2.** Calibration, recording and stimulation circuitry of an individual pixel of the 64×64 channel sensor array

## 2.2 Technology Cross-Section

Fig. 3 shows the cross-section of a single pixel of the sensor array. The sensing transistor M1 in Fig. 2 is buried underneath metal, polysilicon, silicon oxide and nitride layers. The metal layer 3 serves as the bottom electrode of the sensing capacitor, which is connected to the gate of M1. The high-k dielectric is deposited on the whole chip surface and is removed from the bond pads subsequent to its deposition.
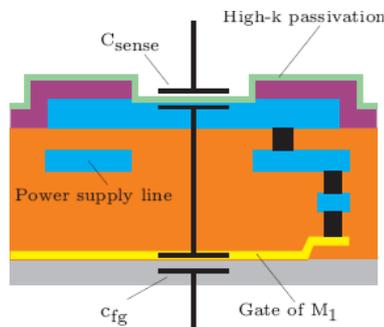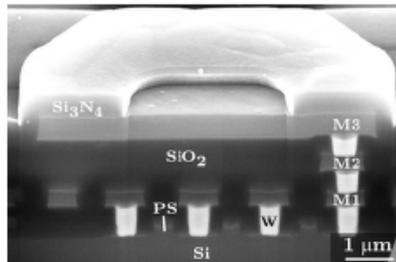




**Fig. 3.** Cross section (focussed ion beam etching) through a pixel of the array (A) and FG-FET schematics (B).

## 3   Results

## 2.1 Post-Processing

To improve the signal-to-noise ratio during recording, the sensing capacitance must be maximized while guaranteeing minimum leakage currents. Choosing dielectric materials with a high-k value and a low deposition thickness is a way of increasing this capacitance. We performed several characterization experiments with alternative high-k materials as the final passivation layer for the CMOS chips. The best result of k=11.3 so far was achieved with a only 50 nm thick double stack of $HfO_2$ and $Al_2O_3$ layers [4]. Cyclovoltammetry measurements of this passivation system were performed on 1cm×1cm highly doped silicon test substrates. Chips were metalized on the front- and on the backside and the $Al_2O_3/HfO_2$ stack was deposited on their front side in a low temperature atomic layer deposition process. As the results in Fig. 4 indicate, the passivation stack resisted bias voltages up to 5V with only a minor change of leak current density. This stack has also proven to be biocompati-

ble as it can be seen in Fig. 5. Further experiments utilizing other high-k materials are still in progress.
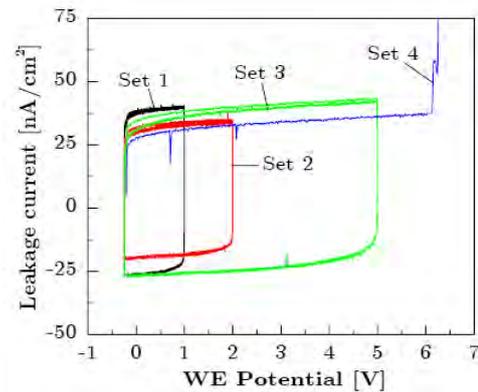


**Fig. 4.** J-V curve of a 50nm $Al_2O_3/HfO_2$ stack on a test substrate with Al back contacting
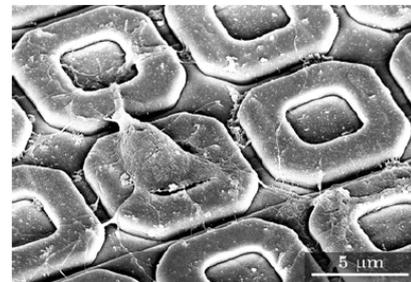


**Fig. 5.** Embryonic rat cortex neuron cultured on a post-processed chip.

## 4   Conclusion and Outlook

We developed a 64x64 FG FET sensor array for bidirectional communication with calibration, recording and stimulation capabilities. The electronic functioning of the chip was already proven and an ALD deposited high-k stack was sufficient for first characterization measurements in liquid environment. In future this passivation needs to be improved in terms of capacitance. The chip will then be used in bioassays with different cell systems.

**References**

[1]   Björn Eversmann et al. „A 128x128 CMOS Biosensor Array for Extracellular Recording of neural activity" IEEE JOURNAL OF SOLID-STATE CIRCUITS, VOL. 38, NO. 12, DECEMBER 2003

[2]   Andreas Offenhausser, Jurgen Ruhe, Wolfgang Knoll, "Neuronal Cells cultured on modified microelectronic device surfaces", J. Vac. Sci. Technol. A, 13, pp., 2606-2612, 1995

[3]   Sven Meyburg et al., "N-Channel field-effect transistors with floating gates for extracellular recordings", Biosensors and Bioelectronics, 21, pp. 1037, 2006

[4]   M. Schindler, S. K. Kim, C. S. Hwang, C. Schindler, A. Offenhäusser, S. Ingebrandr*, „Novel post-process for the passivation of a CMOS biosensor, phys. Stat. sol. (RRL), 2008, 2, No. 1, 4-6

# Multi-transistor array recording of field potentials in acute hippocampal slices at high spatial resolution

Christian Stangl, Peter Fromherz[*]

Max Planck Institute of Biochemistry, Department of Membrane and Neurophysics, Martinsried/Munich
* Corresponding author. E-mail address: fromherz@biochem.mpg.de

Exploring epileptiform signals and oscillations in acute brain slices, simultaneos extracellular recordings have to be considered at different sites. Planar metal electrode arrays (MEA) were used to probe the CA3 region of hippocampal slices at a resolution of 100um [1]. To investigate network dynamics in its complexity it is desirable to record 2D maps of field potentials at higher spatial resolution.

It was shown that cultured slices on CMOS fabricated multitransistor arrays (MTA) allow recordings of field potentials at very high resolution [2]. Within an area of 1mm² the sensors of the chip provide a spacing of 7.8um. In this study we applied this chip to record extracellular field potentials simultaneously in acute brain slices for mapping their neuronal signals.

Firstly hippocampal slices of mice and rats were coupled to simple field effect transistor (FET) chips to understand the principle of the interfacing of acute brain slice and chip. We found that the FET recordings were identical to micropipette electrode signals. In spite of inactive cells caused by cutting processes the recorded signals at the bottom of the slice were about 40% of their maximum in the center of the tissue [3].

Further on we used MTAs and performed following experiments: (i) After stimulation by an tungsten electrode the pathways mossy fibres–CA3 and Schaffer collaterals–CA1 could be mapped at high resolution on a wide area. (ii) Epileptiform signals were evoked by application of Mg(2+) -free medium as well as bicuculline to resolve 2D maps of field oscillatory activity. Sharp wave complexes and phase-locked fast ripples in CA3 could be monitored in space and time. (iii) Fast field oscillations near the principal cells were observed. Carbachol is applied to record also field oscillations in the gamma and theta range.

## References

[1] Mann EO, Suckling JM, Hajos N, Greenfield SA, Paulsen O. (2005): Perisomatic feedback inhibition underlies cholinergically induced fast network oscillations in the rat hippocampus in vitro. *Neuron 45,1, 105-117*

[2] Hutzler M, Lambacher A, Eversmann B, Jenkner M, Thewes R, Fromherz P. (2006): High-resolution multitransistor array recording of electrical field potentials in cultured brain slices. *Journal of Neurophysiology 96, 1638-1645*

[3] Stangl C, Fromherz P. (2008): Neuronal field potential in acute hippocampus slice recorded with transistor and micropipette electrode. *European Journal of Neuroscience 27, 958-964*

# Local Micro-Invasive Needle Electroporation – A Technical Challenge

Carsten Tautorat[1], Philipp Julian Koester[1], Angela Podssun[1], Helmut Beikirch[2], Jan Gimsa[1], Ludwig Jonas[3], and Werner Baumann[1*]

1 University of Rostock, Chair of Biophysics, Rostock, Germany
2 University of Rostock, Institute of Electronic Appliances and Circuits, Rostock, Germany
3 University of Rostock, Electron Microscopy Center, Medical Faculty, Rostock, Germany
* Corresponding author. E-mail address: werner.baumann@uni-rostock.de

In our paper, we present a new sensor chip system for intracellular potential measurements of adherently growing cells using the novel technique of *Local Micro-Invasive Needle Electroporation* (LOMINE). LOMINE enables the electrical connection between cytoplasm and the needle-shaped measuring electrode. The silicon sensor chips comprise 64 micro-structured needle electrodes arranged in 8×8 arrays for parallel intracellular measurements. Existing techniques for intracellular investigations are more time-consuming and usually limited to the analysis of suspended cells.

## 1 Introduction

The *Local Micro-Invasive Needle Electroporation* (LOMINE) technique offers intracellular potential investigations due to *Local Electroporation* (LEP). By applying an electrical field to the *Micro-structured Needle Electrode* (MNE), LOMINE gently opens the thin cell membrane for introducing this electrode into the cytoplasm. The MNE is then used to detect the intracellular potential. Therefore, our electrodes combine sensory as well as actuating functionalities.

The sensor chip contains 64 platinum MNEs arranged in an 8×8 array with a pitch of 100 μm. MNEs have diameters as small as 1 μm and heights below 5 μm [1]. Their fabrication technology is described in [2-4].

## 2 Material and Methods

We developed a preliminary test system with 16 electrode channels for the proof of principle. Nevertheless, chip rotation by 90° allows sequential signal recordings from all 64 MNEs.
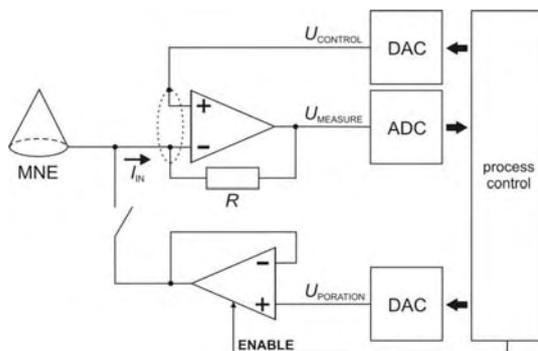


**Fig. 1.** Electrode channel circuitry (simplified)

Each electrode channel features electronic circuitry for cell manipulation (LOMINE and stimulation) as well as intracellular potential measurements, as shown in Fig.1. Four channels offer the possibility for voltage clamping (cf. Fig.1), while the other channels possess voltage followers for signal acquisition. Defined intracellular long-term measurements are only feasible when leakage currents etc. are avoided. Therefore, we use ultra-low bias current operational amplifiers, high insulation reed relays for signal switching, active guarding structures on the circuit board, etc. Our modular design allows for a complete system cleaning and sanitizing.

Fig.2 shows the closed test system. The aluminum housing provides electromagnetic shielding and temperature control.
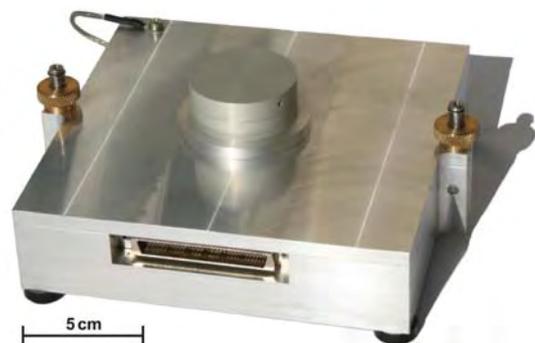


**Fig. 2.** Test system with 16 electrode channels

A data acquisition card (NI PCI-6221) is used for signal digitization and system control. A Graphical User Interface (GUI) and the fully automated process control are programmed in LabVIEW®. The GUI features a multichannel display, oscilloscope functions, data recording, LEP settings etc. The LEP settings (e. g. pulse frequency, amplitude and duty cycle) are

adjustable in a wide range to investigate best parameters for LOMINE. Currently, pulses up to 300 kHz with amplitudes up to ±4 V can be generated for cell manipulation.

## 3 Results

First LEP experiments were accomplished and the results were checked by Focused Ion Beam - Scanning Electron Microscopy (FIB-SEM) [5] as well as fluorescence microscopy. The results are described in detail in [6]. The preliminary LEP experiments using fluorescence microscopy require intense electric field parameters for clear staining results. However, these high field strengths can cause undesired electrode potential alterations of up to 200 mV depending on the electroporation buffer [6] as well as the electrode properties (material, design etc.). As a matter of course, tests with silver-coated needle electrodes produced significantly better results than the chemically inert platinum MNEs. Fig.3 exemplifies this context with six MNEs on a single cell-free chip. After sequential LEP (cf. Fig.3, 800-801 min), the potentials of the uncoated Pt MNEs converge slower to their start values (cf. Fig.3, 796-800 min).
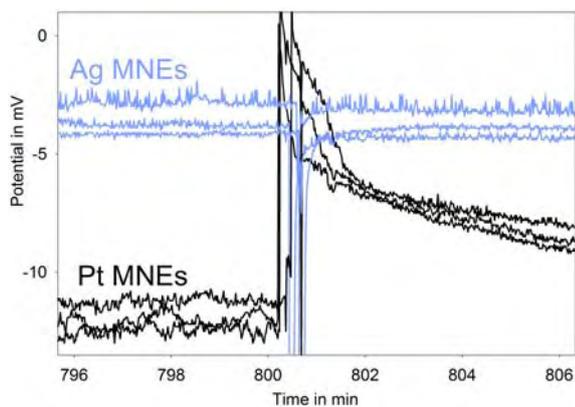


**Fig. 3.** Electroporation experiments with cell-free chip.
Long-time measuring; 50% of the MNEs were silver-coated; Ag/AgCl reference electrode; phosphate buffered saline; LEP parameters: start at t ≈ 800 min, ±1.5 V, pulse train length = 10 ms, pulse frequency = 100 kHz, duty cycle = 50%.

## 4 Outlook

The presented LOMINE technique opens new ways for fast and parallel intracellular measurements with adherently growing cells. Nevertheless, we believe that it is essential to know the LOMINE system characteristics with and without cells for defined potential measurements. Presently, we redesign the test system for an improved LOMINE sequence using a faster hardware-timed process control. In the new design, the time constants for the pre- as well as the post processing phases of the LOMINE signals at the individual MNE will be reduced by at least one order of magnitude.

Our project partners are testing different needle materials and shapes as a prerequisite for well defined long-term measurements.

**References**

[1] J. Held, J. Gaspar, P. Ruther, M. Hagner, A. Cismak, A. Heilmann, and O. Paul (2007): Systematic Characterization of DRIE-based Fabrication Process of Silicon Microneedles. Mat. Res. Soc. Symp. Proc., 1052-DD07-07

[2] J. Held, J. Gaspar, P. Ruther, and O. Paul (2008): Microneedle Arrays Electrode With Dielectrophoretic Electrodes For Intracellular Recording Applications. in: Conference Proceedings of the 6th International Meeting on Substrate-Integrated Micro Electrode Arrays, 2008, Reutlingen, Germany

[3] J. Held, J. Gaspar, P J. Koester, C. Tautorat, A. Cismak, A. Heilmann, W. Baumann, A. Trautmann, P. Ruther, and O. Paul (2008): Microneedle Arrays for Intracellular Recording Applications. MEMS 2008, 268-271

[4] A. Trautmann, P. Ruther, W. Baumann, M. Lehmann, and O. Paul (2004): Fabrication of Out-of-Plane Electrodes for Intracellular Potential Measurements on Living Adherent Cells. in: Conference Proceedings of the 4th International Meeting on Substrate-Integrated Micro Electrode Arrays, 2004, Reutlingen, Germany

[5] A. Heilmann, F. Altmann, A. Cismak, W. Baumann, and M. Lehmann (2007): Investigation of Cell-Sensor Hybrid Structures by Focused Ion Beam (FIB) Technology. in: Mat. Res. Soc. Symp. Proc., 0983-LL03-03

[6] P J. Koester, C. Tautorat, A. Podssun, J. Gimsa, L. Jonas, and W. Baumann (2008): A New Principle For Intracellular Potential Measurements Of Adherently Growing Cells. in: Conference Proceedings of the 6th International Meeting on Substrate-Integrated Micro Electrode Arrays, 2008, Reutlingen, Germany

# Electrical Recording of Mammalian Neurons by Multi-Transistor Array (MTA).

V. Vitzthum[1], M. Eickenscheidt[1], R. Zeitler[1], A. Lambacher[1], A. Kunze[1], B. Eversmann[2], R. Thewes[2], and P. Fromherz[1]

1 Max Planck Institute for Biochemistry, Department of Membrane and Neurophysics, Martinsried/München, Germany
2 Infineon Technologies, Corporate Research, München, Germany

We show that Multi-Transistor Array (MTA) recording is suitable to record the electrical activity of individual mammalian neurons as well as of neuronal networks with a spatial resolution of 7.8 µm and a sampling frequency of 6 kHz on a total area of 1 mm2. The chips were fabricated by an extended CMOS process as described before [1]. Improvements of the chip design, of the electronic control circuits and of the read-out lead to a reduction of noise and to an enhancement of time resolution as compared to a previous setup [2, 3]. The chip was electrically insulated by a thin layer of titaniumdioxide/zirconiumdioxide. The individual sensor transistors were adjusted to their operating point by a reset circuit and calibrated in terms of a change in the electrolyte potential by applying voltages to a Ag/AgCl electrode in the bath.

We cultured neurons from rat hippocampus in serum free medium for 21 days and recorded the response of the MTA to spontaneous activity. Most signals of individual sensor transistors were negative with amplitudes up to 4 mV, typically in the range of 1 mV. There were also biphasic waveforms positive/negative and negative/positive and also purely positive signals. During the measurement phases of several seconds, the signals on the same sensor transistor were almost invariant. Frequently, several sensor transistors probed the same cell as indicated by a perfect coincidence of the signals. The coincident signals were used to construct a coupling map of individual neurons. In particular they could be used to identify individual neurons in a firing network. By this approach, correlations of network activity could be observed.

## References

[1] Eversmann, B., et al. (2003) IEEE J. Solid State Circ. 38, 2306.
[2] Lambacher, A., et al. (2004) Appl. Phys. A 79, 1607.
[3] Hutzler, M., et al. (2006) J. Neurophysiol., 96, 1638.

# Guided Adhesion and Outgrowth of a Constrained Network on Tailormade Surfaces

Anke Wörz[1,2], Steffen Kandler[2,3], Oswald Prucker[1,2], Ulrich Egert[2,4], and Jürgen Rühe[1,2*]

1 Chemistry and Physics of Interfaces, Depart. of Microsystems Engineering, Albert-Ludwigs-University of Freiburg, Germany
2 Bernstein Center for Computational Neuroscience, Albert-Ludwigs-University of Freiburg, Germany
3 Neurobiology and Biophysics, Institute of Biology III, Albert-Ludwigs-University of Freiburg, Germany
4 Biomicrotechnology, Depart. of Microsystems Engineering, Albert-Ludwigs-University of Freiburg, Germany
* Corresponding author. E-mail address: ruehe@imtek.de

Planar micro-electrode arrays (MEAs) have been used for some time to investigate the activity dynamics and response of neural networks to electrical or chemical stimuli. Constructing defined connectivity statistics under conditions that allow the maturation of the neuronal networks has thus far not been achieved. Such networks would be useful to understand the influence of the composition, connectivity statistics, and plasticity in a neuronal network on the dynamics of electrical activity. The key issue is the control over microscale, spatial and long-term stability of cell adhesion and neurite outgrowth by physicochemical surface modifications under cell culture conditions that allow long-term maintenance of these networks. We report a simple way to tailor the surface-chemistry using a photochemical approach, leading to the covalent attachment of polymer layers to glass and MEA surfaces. We examined the biocompatibility of polymer layers with different properties, such as hydrophilicity and charge, and their potential to promote or inhibit neuronal cell adhesion. Finally, patterns with cell attractive domains were obtained using pin printing or μ-contact printing (μ-CP) of polymer solutions. These patterns were able to guide neuronal cells in a constrained network and were stable over several weeks in a serum containing cell culture medium.

## 1 Biocompatibility of covalently attached polymer layers

To tailor the surface chemistry of glass slides and MEAs we used a surface-immobilized benzophenone derivative, which can be attached to any alkyl group photo-chemically (Figure 1) [1]. These surfaces were modified by attaching hydrophilic (poly(dimethyl acrylamide) - PDMAAm), hydrophobic (poly(methyl methacrylate) - PMMA, polystyrene - PS), ultra-hydrophobic (fluoropolymer - FP), and positively charged (poly(ethylene imine) - PEI) polymers (for
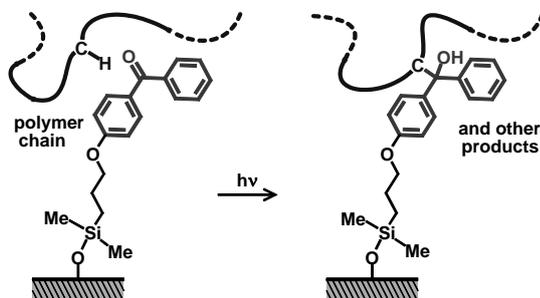


**Fig. 1.** Schematic illustration of the photo-chemical attachment of polymers via benzophenone units. Image taken from [1].

detailed polymer synthesis see [2]). Adhesion and outgrowth of neurons were studied in a serum containing medium. Dissociated neuronal cells from neonatal rat cortex (for details see [3]) were seeded onto the polymer coatings and incubated for several weeks. The number of adherent cells was reduced and the neuronal network morphology was degraded on the FP, PMMA, and PS coatings (indicated by clustering of cell somata). PEI (Figure 2, A) supported the initial adhesion of neurons forming a uniform neuronal network within three days in vitro. In contrast, neurons never adhered on PDMAAm (Figure 2, B).
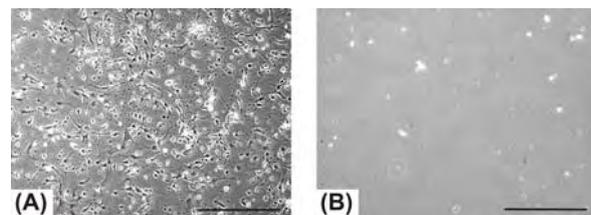


**Fig. 2.** Dissociated neurons from neonatal rat cortex grown on surface-attached PEI (A) and PDMAA (B) after two weeks of incubation in serum-containing medium. Scale bar 200 μm.

## 2 Guidance of neuronal cells on patterned polymer layers

To guide neuronal cells, long-term stable patterns of two polymers on a single substrate (MEA or cover slip) were developed. These polymers were chosen specifically such that the neurons should adhere to only one of the polymers but be repelled by the other. As described previously, PEI coatings were found to be cell attractive. PDMAAm, on the other hand, was

cell repellent even after several weeks of incubation in serum-containing medium.

A grid like pattern with a minimum line-width of 100 µm was developed by a contact pin-printer, which deposited the cell attractive polymer on the cell repellent background. This structured substrate led to a patterned initial adhesion of neuronal cells. Even after incubation over a period of four weeks in serum-containing medium, neurons were confined to the PEI surface and formed a highly interconnected network (Figure 3, A). Since the grid resolution of 100 µm was insufficient for the detailed control of the network structure and the analysis of the neuronal network dynamics we used micro-contact printing (µ-CP) [4], where a silicone rubber stamp created a comparable pattern with smaller dimensions. After incubation with a neuronal cell suspension, the µ-CP patterns showed similar results (Figure 3, B). Neuronal cell bodies preferred to adhere on the circular area of the pattern (diameter 40 µm) and after several days of incubation, a network was formed along the patterned lines (width 5 µm).
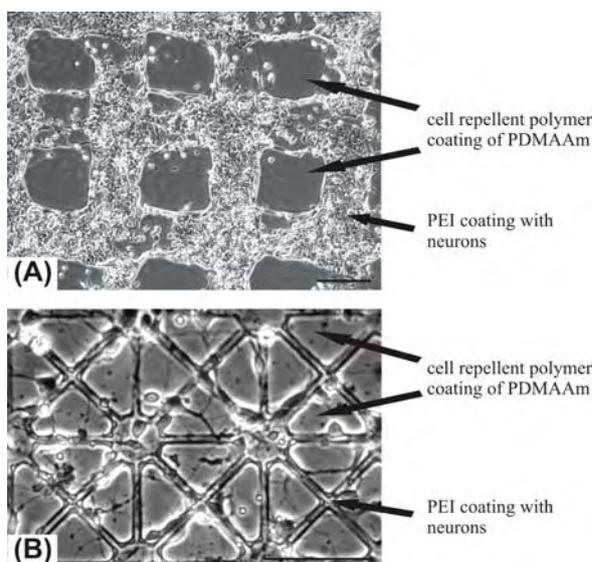


**Fig. 3.** Neurons grown on (A) printed or (B) stamped PEI on a PDMAAm background after incubation for (A) 32 days and (B) 2 days. Scale bar 100 µm.

Nevertheless it should be noted that the patterning techniques revealed specific limitations. Minute quantities of PEI, e.g. when washing off excess PEI, will firmly adhered to the PDMAAm surface outside the attachment regions. Ultimately, this led to neuronal growth violating the parent pattern. It appears that PEI physisorbs rather strongly to PDMAAm, which in many cases prohibits a quantitative removal of PEI through simple washing procedures.

## 3 Conclusions

We have shown that versatile surface coatings can be obtained with covalent attachment of polymers to solid substrates via a photochemical approach. Furthermore, a qualitative study of cell adhesion on certain polymer surfaces revealed the biocompatibility of these coatings. PEI and PDMAAm were found to induce initial neuronal cell adhesion with further network formation and no adhesion, respectively. The cells conform on patterns developed with the combination of these two polymers for several weeks in serum-containing medium.

**References**
[1] Prucker, O.; Naumann, C.A.; Rühe, J.; Knoll, W.; Frank, C.W. (1999). *J. Am. Chem. Soc. 121, 8766.*
[2] Berchtold, B. (2006), *PhD thesis, University Freiburg.*
[3] Shahaf, G.; Marom, S. (2001). *J. Neurosci.* 21, 8782.
[4] Vogt, A.K.; Wrobel, G.; Meyer W.; Knoll, W.; Offenhäusser, A. (2005). *Biomaterials 26, 2549.*

# List of Authors

Adams C
Aisa R
Aldermann J
Amblard PO
Amodei D
Andrieux A
Annie A
Ariano P
Augspurger C
Austin J
Bading H
Bakkum DJ
Baldelli P
Baljon PL
Bamberg E
Baranauskas G
Bartels T
Bartic C
Baumann W
Baumgartner W
Becerra VM
Bêche J
Becq G
Beikirch H
Bellostas ED
Benfenati F
Bengtson CP
Ben-Jacob E
Berdondini L
Berry M
Beverra V M
Beyer K
Bienkowski G
Billoint O
Blau A
Boehler M
Boido D
Bologna LL
Bonnet S
Borghs G
Boven, KH
Bräunig P
Breaken D
Bressand K
Brewer G
Brewer GJ
Broadbent S
Bruinink A
Brussard AB
Bryant S
Buehler S
Bull L
Burke M

Bussek A
Callewart G
Carabelli V
Carbone E
Casagrande S
Chan M
Chang KP
Chang WP
Chao ZC
Charvet G
Chiappalone M
Cobena S
Colin M
Comunanza V
Corinne R
Dabrowski W
David-Pur M
Decré M
Defontaine A
DeMaris A
Demmon J
Diard J P
Diaz C
Didier J
Dihne M
Dipalo M
Downes J
Downes JH
Dufaux T
Dworak BJ
Echtermeyer C
Egert U
Eglen S
Eick S
Eickenscheidt M
Erickson J
Escola R
Esposti F
Eversmann B
Eytan D
Fanet H
Farine PA
Farisello P
Fernekorn U
Ferrigno G
Fischer M
Fiutowski T
Fletcher M
Freitag HE
Frey U
Fromherz P
Früh H
Fussenegger M

Gal A
Gandolfo M
Garofalo M
Gaspar J
Gasteier P
Gavello D
Geoffrey R
Gepstein L
Gerhardt M
Gharbi S
Ghezzi D
Ghirardi M
Giachello C
Gibson F
Gimsa J
Gintautas V
Göbbels K
Gohara K
Goo YS
Görtz P
Goy F
Gramowski A
Greenbaum A
Grillo A
Gritsun T
Groll J
Gross GW
Gross RE
Grothe H
Guenther E
Guillemaud R
Gullo F
Hafizovic S
Hagmeyer B
Ham M
Hammond M
Hanein Y
Hartmann R
Hasse B
Hayashi I
Hayashi J
Heal R
Heer F
Heikkilä T
Hein D
Held J
Heli S
Hermann CC
Herrmann T
Hesse M
Heuschkel M
Hiebl B
Hierlemann A

Hofmann B
Hofmann F
Holy T
Hosokawa C
Hosokawa Y
Hottowy P
Huys R
Hwang CS
Hyttinen J
Ide AN
Ilchmann F
Illes S
Imfeld K
Ingebrandt S
Ingram C
Inyushkin AN
Ito D
Ivert B
Jackson T
Jäger M
Jalonen TO
Jans D
Jari H
Jarno T
Jessop M
Jianguo S
Jie L
Jimbo Y
Jina N
Job D
Jonas L
Jones T
Joucla S
Joye N
Jügelt K
Kachiguine S
Kaiser M
Kamp F
Kanagasabapthi TT
Kandler S
Kang G
Kanzaki R
Karine B
Karnas D
Keefer E
Kelm J
Kempter R
Kern P
Khatami D
Kim SK
Kinney TN
Kiyohara A
Klett M
Klisch C
Knoll A
Knowles A
Koester JP

Kohn E
Kolomiets B
Kotani K
Kotiadis W
Koudelka-Hep M
Krause T
Kraushaar U
Kretzberg J
Kudoh SN
Kunze A
Künzel T
Kuokkanen P
Laganá K
Lamanna J
Lambacher A
Lange-Asschenfeldt C
Lanzara A
Lappalainen R
Laura YO
Lautemann N
Law JKY
Le Feber J
Leblebici Y
Lee CM
Lenas P
Lévi T
Li M
Li X
Liang B
Linne ML
Linpeng W
Lipkowski A
Litke A
Lo Giudice A
Lob V
Loo J
Lopez L
Lord P
Lovisolo D
Luo Q
Lyakhov V
MacCarthy N
Maccione A
Madhavan R
Maffezzoli A
Makohliso S
Marani E
Marcantoni A
Marom S
Marshall S
Martiniuc A
Martinoia S
Masayuki N
Massobrio P
Masuhara H
Matero S
Mathieson K

Matteoli M
Meffert S
Meissl H
Menegon A
Menna E
Mercier B
Methner A
Meyer J
Meyer JF
Meyer T
Meyrand P
Mikkonen JE
Misicka-Kesik A
Möller M
Moodie A
Moreno M
Moridi M
Moriguchi H
Morrison J D
Mulas M
Müller HW
Müller J
Murdoch D
Murr A
Musick K
Nagayama M
Nagel J
Nakao M
Nam Y
Narkilahti S
Nasuto S
Neukom S
Nicodemou-Lena E
Nicol S
Nicoletti M
Nieus T
Nieus T
Novellino A
Offenhäusser A
Okano K
Okujeni S
Opatz J
Oshiorenoya A
Otto F
Palmer R
Park JH
Parsons A
Pasquale V
Pasquarelli A
Paul O
Paz LMJ
Pearson, R
Pedrocchi A
Peitz I
Pekkanen-Mattila M
Periorellis P
Pettinen A

| | | |
|---|---|---|
| Pévet P | Shahaf G | van Ooyen A |
| Pham P | Shahid S | van Pelt J |
| Picaud S | Shein M | Villard C |
| Pine J | Sher A | Vittone E |
| Ping F | Shin JA | Vitzthum V |
| Pitsilis G | Shyu BC | Volman |
| Pizarro C | Siebler M | Wagner H |
| Podssun A | Signorini MG | Wallys J |
| Poll R | Simonotto J | Wallys J |
| Potter SM | Simonutti M | Wang K |
| Prucker O | Skoczeń A | Wanke E |
| Rabosio A | Skottman H | Warwick K |
| Raichman N | Smith LS | Watson P |
| Ramakers G | Sobanski T | Weigel S |
| Rand D | Sommerhage F | Weihberger O |
| Ravens U | Son MS | Weislogel J |
| Reska A | Sonntag F | Weiss DG |
| Ressler J | Sorkin R | Weyh T |
| Riika L | Spinelli A | Whalley BJ |
| Riita S | Stangl C | Wheeler B |
| Rohr S | Stegenga J | Wheeler BC |
| Rojo-Ruiz J | Stelzle M | Wiegand T |
| Rolston JD | Stett A | Wiemhöfer M |
| Rostaing JP | Stockmann R | Willbold D |
| Roucard C | Stoop R | Wolf B |
| Rousseau L | Stürzl W | Wörz A |
| Rudd JA | Supprian T | Wrobel G |
| Rühe J | Susanna N | Wu JS |
| Ruther P | Suuronen R | Wyllie C |
| Rutten WLC | Suzuki I | Xiaoqing Z |
| Rydygier P | Suzurikawa J | Xydas D |
| Ryohei K | Taguchi T | Yan H |
| Sahel JA | Tai YC | Yan M |
| Saito A | Takahashi H | Yang SR |
| Sakowski J | Takayama Y | Yasuda K |
| Sarkanen JR | Tamate H | Yasuhiko J |
| Schäfer S | Tanner S | Ye JH |
| Scheidt K | Tanskanen J | Yegin U |
| Schilling N | Tautorat C | Yeung CK |
| Schindler C | Tedesco M | Ylä-Outinen L |
| Schindler M | Teemu H | Yuemei H |
| Schmid A | Teichmann C | YuJun G |
| Schnakenberg U | Teppola H | Yvert B |
| Schober A | Thewes R | Zeck G |
| Schoen F | Thomsen S | Zeitler R |
| Schröder O | Tokuda N | Zeng S |
| Schroeder OHU | Tooker A | Zhang C |
| Schrott R | Trevisol M | Zhou W |
| Schulte P | Uchida T | Zibek S |
| Schwartz G | Uroukov IS | Ziegler C |
| Sedivy J | Väisänen J | Zrenner C |
| Selinummi J | Vajda I | |
| Serangor E | Valtorta F | |
| Sernagor E | van Meerbergen B | |

# Imprint

NMI Natural and Medical Sciences Institute at the University of Tuebingen

BIOPRO Baden-Württemberg GmbH

Multi Channel Systems MCS GmbH

City of Reutlingen

www.bio-pro.de